THE UNIVERSITY OF CHICAGO

SYNTHESIS AND REACTIVITY OF GROUP 10 METAL OLEFIN POLYMERIZATION CATALYSTS BEARING α-DIIMINE ANCILLARY LIGANDS

A DISSERTATION SUBMITTED TO

THE FACULTY OF THE DIVISION OF THE PHYSICAL SCIENCES

IN CANDIDACY FOR THE DEGREE OF

DOCTOR OF PHILOSOPHY

DEPARTMENT OF CHEMISTRY

BY

FENG ZHAI

CHICAGO, ILLINOIS

MARCH 2017

TABLE OF CONTENTS

LIST OF TABLES

LIST OF FIGURES

LIST OF SCHEMES

LIST OF CHARTS

ACKNOWLEDGEMENTS

First, I thank my advisor Prof. Richard Jordan for his invaluable guidance and instruction through the entire graduate school. I also thank the other members of my thesis committee, Profs. Anderson and Lewis, for their time and helpful discussion.

I am grateful to the current and former Jordan group members for providing scientific insights and friendship. I would like to thank Drs. Meagan Evans, Ben Petro and Ryan Zarkesh for teaching me the glovebox and Schlenk techniques during my initial stage of graduate school. I also thank Dr. Nathan Contrella, Dr. Ge Feng, Dr. Ka Cheong Lau, Dr. Qian Liu, Dr. Frank Olechnowicz, Dr. Jia Wei, Rebecca Black, Erik Reinhart, Alison Johnson, Shinji Wada, Dr. Hiroshi Terao, Dr. Mingfang Zheng and Dr. Biyun Su for their assistance with lab work and for creating an enjoyable working atmosphere. I give special thanks to the UofC undergraduates Naomi Clayman, Joseph Solomon and Kelsey Brown for their research work related to this thesis.

I would like to thank Profs. Hillhouse, Hopkins, Talapin, He and Snyder for having inspiring conversations at different stages of my graduate school. Also, I would thank Profs. Yuguo Ma and Dahui Zhao at Peking University for providing me an opportunity for chemical research.

The completion of this thesis heavily relies on the support from the department facility managers. I thank Dr. Ian Steele and Dr. Alexander Filatov for the assistance with X-ray crystallography, Dr. Antoni Jurkiewicz for the assistance with NMR spectroscopy, and Dr. C.-Jin Qin for the assistance with mass spectroscopy. I also thank Vera Dragisich, Melinda Moore and Laura Baker for their assistance with administrative work and Valerie Keller for her instruction on teaching skills.

I would thank all my friends in the Department for always being available for discussion.

Last but not the least, I would thank Lili Wang and my family for their love and support throughout my graduate studies.

ABSTRACT

This thesis describes the synthesis and reactivity of α-diimine group 10 metal catalysts that contain hydrogen-bonding (H-bonding) groups in the second coordination sphere and the effect of H-bonding groups on the copolymerization of ethylene with polar monomers.

Chapter One provides a brief introduction to ethylene polymerization and the copolymerization of ethylene with polar monomers using α-diimine Pd catalysts. The relationship between ligand structure and reactivity of ethylene/polar-monomer copolymerization was discussed, and the main challenges of (α-diimine)Pd-catalyzed ethylene/polar-monomer copolymerization were mentioned. This chapter includes a summary of the objectives of this thesis.

Chapter Two describes the synthesis, coordination chemistry, and reactivity of a class of (Ar-N=CMeCMe=N-Ar')Pd complexes that contain *ortho*-amide substituents on the N-aryl (Ar and Ar') rings. H-bonding interactions involving the amide groups influence the structures, isomer distributions, and ligand coordination behavior of these compounds.

Chapter Three describes the synthesis of second-generation amide-functionalized (α-diimine)Pd catalysts [{2,6-$(CHPh_2)_2$-4-Me-Ph}-N=CMeCMe=N-(2-CONHMe-6-^{i}Pr-Ph)]PdMeCl (**1d**,**d'**) and [{2,6-$(CHPh_2)_2$-4-Me-Ph}-N=CMeCMe=N-(2-$CONMe_2$-6-^{i}Pr-Ph)]PdMeCl (**1e**,**e'**). Replacement of two isopropyl groups of the first-generation catalysts {(2,6-$^i Pr_2$-Ph)-N=CMeCMe=N-(2-CONHMe-6-^{i}Pr-Ph)}PdMeCl (**1a**,**a'**) and {(2,6-$^i Pr_2$-Ph)-N=CMeCMe=N-(2-$CONMe_2$-6-^{i}Pr-Ph)}PdMeCl (**1b**,**b'**) with the more steric demanding benzhydryl (-$CHPh_2$) groups in **1d**,**d'** and **1e**,**e'** was expected to significantly improve ethylene polymerization performance. Activation of **1d**,**d'** and **1e**,**e'** by NaB{3,5-$(CF_3)_2C_6H_3$}$_4$ generates active ethylene polymerization catalysts that produce highly branched (77-81 br/1000C) polyethylenes with a moderate MW (M_n ca. 26-60 kDa). The replacement of two isopropyl units in the catalysts **1a**,**a'** and **1b**,**b'** with

benzhydryl groups leads to a significant improvement on the overall homopolymerization performance. The H-bonding catalyst **1d**,**d'** is capable of incorporating ca. 2 times as much methyl acrylate and ca. 3 times as much acrylic acid as the non-H-bonding catalyst [{2,6-$(CHPh_2)_2$-4-Me-Ph}-N=CMeCMe=N-(2,6-$^{i}Pr_2$-Ph)]PdMeCl (**1f**,**f'**) in the copolymerization with ethylene. The reactions of **1a**,**a'** and **1b**,**b'** with metal salts that contain weakly coordinating anions lead to extrusion of CH_4 and the formation of μ-CH_2 complexes, in which the amide carbonyl O-atoms coordinate to Pd centers.

Chapter Four describes the coordination chemistry and ethylene polymerization behavior of amide-functionalized (α-diimine)Ni complexes. The α-diimine ligands (2,6-$^{i}Pr_2$-Ph)-N=CMeCMe=N-(2-^{i}Pr-6-$CONMe_2$-Ph) (**L1**) and (2,6-$^{i}Pr_2$-Ph)-N=CMeCMe=N-[2,6-$(CONMe_2)_2$-Ph] (**L2**) react with (dme)$NiBr_2$ to form the five-coordinate paramagnetic complexes (**L1**)$NiBr_2$ (**1**) and (**L2**)$NiBr_2$ (**2**), in which one amide oxygen atom and the two imine nitrogen atoms of **L1** and **L2** coordinate to the Ni center. **L1** reacts with $(py)_2NiMe_2$ to form the diamagnetic, square planar 4-coordinate complex (**L1**)$NiMe_2$ (**3**). Activation of **1** with Et_2AlCl generates an ethylene polymerization catalyst that produces semicrystalline polyethylene with a broad molecular-weight (MW) distribution.

Chapter Five describes the synthesis of 2,3-dihydroquinazolin-4(1*H*)-one compounds **4a**, **5a** and **6a**, and their facile C-C cleavage reactions triggered by autoxidation. 2-Acyl-2,3-dihydroquinazolin-4(1*H*)-one compounds **4a** and **5a** undergo facile C-C cleavage reactions with O_2 by a radical mechanism. The reaction pathway is dependent on the structure of substrate. The strained spirocyclic **4a** undergoes ring expansion by 1,2-acyl migration to form a C-based radical followed by trapping with O_2. Compound **5a**, in which the 2-acetyl is not part of a cyclic structure, undergoes fragmentation to generate acetyl radical, which is trapped by O_2 to form peracetic acid.

Bis(dihydroquinazolinone) **6a** undergoes C-C cleavage and formal dehydrogenation by O_2.

Chapter Six describes the synthesis and structure of an unusual Pd complex that contains the α-aminoimine ligand 6-Me-4-^{i}Pr-6-(dippN=C(Me))-6,11-dihydro-5*H*-indolo[3,2-*c*]quinoline (**6**). Ligand **6** coordinates in a κ^2-C=*N*,*N*H fashion in the square planar complex **(6)PdCl$_2$**.

Chapter Seven describes the synthesis, coordination chemistry, and conformational isomerism and dynamics of chiral menthyl-substituted α-diimine ligands *N,N'*-(2-Men-4-Me-Ph)-BIAN (**L1**, BIAN = bis(imino)acenaphthene) and *N,N'*-(2-Men-4,6-Me$_2$-Ph)-BIAN (**L2**). The *syn* conformation, in which the two menthyl groups face each other on the same side of N=C-C=N plane, is favored for **L1**, **L2** and square planar complexes of these ligands, possibly due to attractive dispersion interactions between the two menthyl groups. In contrast, the *anti* conformation is favored for tetrahedral complexes of **L1** and **L2**, and both menthyl ^{i}Pr units point to the acenaphthene backbone. The *anti,syn* isomerization of square planar complexes **(L1)Ni(acac)-*anti*,*syn*** is facile at room temperature. Square planar complexes **(L2)Ni(acac)-*anti*,*syn*** are kinetically stable at room temperature, and the *syn* isomer produces polyethylene with a higher MW and branching level than the *anti* isomer. The *syn* isomer also produces poly(1-hexene) with less branches and a higher degree of chain-straightening compared to the *anti* isomer. These differences in polymerization behavior are attributed to the significantly different steric profiles of the two isomers.

PREFACE

Each chapter has an independent numbering system for compounds. A given compound may have a different number in different chapters. For each chapter, the relevant experimental information, references, and notes are provided at the end of the chapter.

CHAPTER ONE

Introduction to (α-Diimine)Pd Olefin Polymerization Catalysts

1.1 Introduction

Brookhart and coworkers reported that the (α-diimine)PdR^+ species **A** catalyzes the homopolymerization of ethylene to produce highly branched polyethylene (ca. 100 br/1000C),[1] and also catalyzes the copolymerization of ethylene with methyl acrylate (MA) up to 12 mol% incorporation of MA through an insertion mechanism (Scheme 1.1). The MA unit are incorporated predominantly at the end of branches.[2] The steric bulk of the α-diimine ligand strongly influences the activity, the microstructures of resulting polymer, and the incorporation of polar monomer (PM). (α-diimine)PdR^+ species can also copolymerize ethylene with several other types of PMs, including methyl vinyl ketone,[2] acrolein dimethyl acetal,[3] *N*-pentenylcarbazole,[4] vinyl silyl ethers,[5] vinyltrialkoxysilanes[6] and olefinic monomers with remote polar groups (Chart 1.1).[7] The incorporation of PMs into polyethylene may enhance the surface physical properties, including adhesion, dyeability, printability and compatibility.[8]

Scheme 1.1

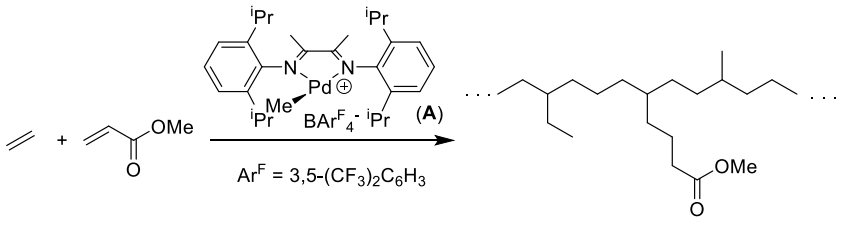

Chart 1.1. Polar Monomers Incorporated by (α-Diimine)Pd-Catalyzed Copolymerization with Ethylene

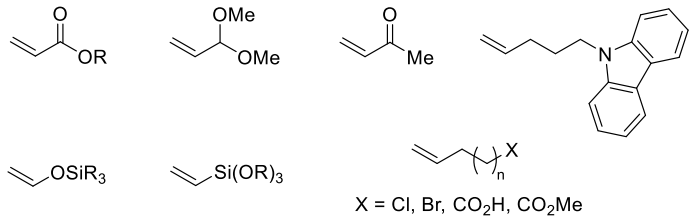

Besides the benchmark catalyst **A**, many other (α-diimine)Pd catalysts that exhibit different types of steric bulk were developed. These catalysts are able to control the microstructure of polyethylene in a broad range and exhibit different reactivity in ethylene/PM copolymerization. A few structural modifications that are promising in ethylene/PM copolymerization are shown in Chart 1.2. The ^{i}Pr-substituted catalysts (**B**) that contain *para*-electron-donating groups (R = NMe_2, OMe, Me) on the N-aryl rings, can incorporate MA in higher levels than the catalyst **A**.[9] Guan and coworkers reported the cyclophane Pd catalyst **C**, which produced highly branched polyethylene (110 br/1000C).[10] **C** exhibited high incorporation of MA (up to 21.8 mol%),[11] and mechanistic studies showed that the cyclophane structure strongly inhibited associative olefin exchange on (α-diimine)PdR(olefin)$^+$ species, and thus the selectivity in monomer binding was dominated by the relative kinetic trapping rate of β-agostic (α-diimine)PdR^+ species rather than fast olefin exchange equilibrium.[12] Daugulis and coworkers reported the 8-(*p*-tolyl)-1-naphthyl "sandwich"-type catalyst **D**, which produced very highly branched polyethylene (100-120 br/1000C)[13] and can incorporate MA up to 13.8 mol% and vinyltriethoxysilane up to 2.03 mol%.[6, 13] Chen and coworkers reported the benzhydryl-substituted catalyst **E**, which produced low branching polyethylene (25-30 br/1000C) and exhibited high activity and thermal stability. **E** can incorporate MA up to 3.3 mol%.[14] Catalyst **F** is more sterically bulky than **E** and has been shown to exhibit even higher activity and produce lower branched polyethylene (20 br/1000C). While **F** is less

capable for incorporating MA compared to **E** due to increased steric bulk, **F** can incorporate vinyl monomers with remote polar functionalities to form low branching copolymers.[15] Takeuchi and coworkers reported the macrocyclic dipalladium catalyst **G**, which can incorporate MA up to 9.3 mol% with predominantly main-chain incorporation.[16]

Chart 1.2. (α-Diimine)Pd Catalysts for Ethylene/PM Copolymerization

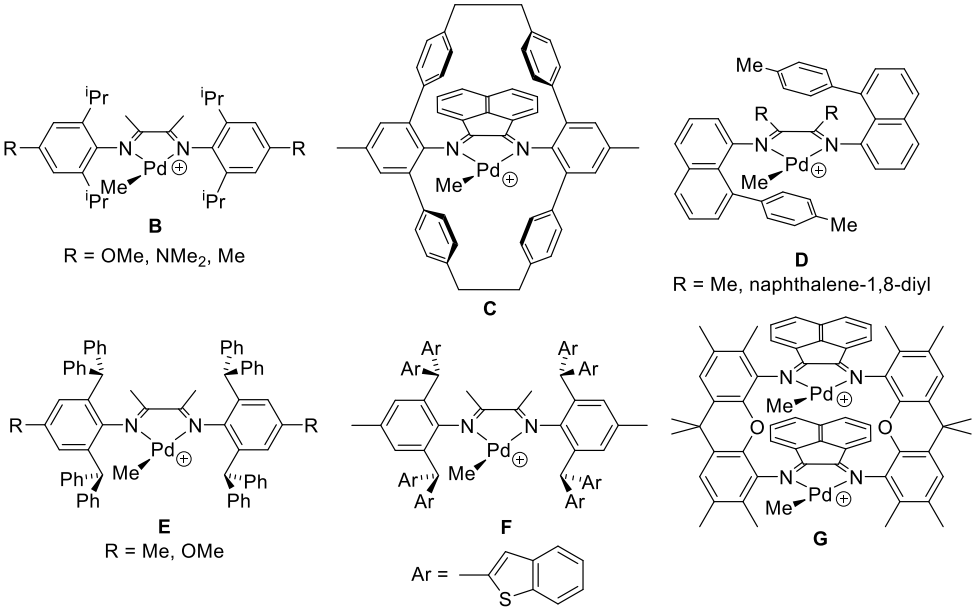

(α-Diimine)Pd-catalyzed ethylene/PM copolymerization has major challenges, including low PM incorporation and retardation of copolymerization by chelate formation following the insertion.[17-18] Mechanistic studies showed that electron-deficient PMs bound much more weakly than ethylene to Pd center, resulting in low PM incorporation.[17]

Hydrogen bonding (H-bonding) interactions in the second coordination sphere can strongly influence the structures and ligand binding preferences of coordination and organometallic compounds, and their reactivity in transition metal-catalyzed transformations.[19-22] The presence of Lewis basic, H-bond-accepting heteroatoms in the structure of PMs inspired us to investigate how H-bonding interaction may influence the copolymerization of ethylene with PMs.

1.2 Objectives

The objective of this thesis is to synthesize α-diimine group 10 metal catalysts that contain hydrogen bonding groups in the second coordination sphere and to study their effect on the copolymerization of ethylene with polar monomers.

Chapter Two describes the synthesis, coordination chemistry, and reactivity of a class of (Ar-N=CMeCMe=N-Ar')Pd complexes that contain *ortho*-amide substituents on the N-aryl (Ar and Ar') rings. Hydrogen bonding interactions involving the amide groups influence the structures, isomer distributions, and ligand coordination behavior of these compounds.

Chapter Three describes the synthesis of second-generation amide-functionalized (α-diimine)Pd catalysts [{2,6-$(CHPh_2)_2$-4-Me-Ph}-N=CMeCMe=N-(2-CONHMe-6-^{i}Pr-Ph)]PdMeCl (**1d**,**d'**) and [{2,6-$(CHPh_2)_2$-4-Me-Ph}-N=CMeCMe=N-(2-$CONMe_2$-6-^{i}Pr-Ph)]PdMeCl (**1e**,**e'**). Replacement of two isopropyl groups of the first-generation catalysts {(2,6-$^i Pr_2$-Ph)-N=CMeCMe=N-(2-CONHMe-6-^{i}Pr-Ph)}PdMeCl (**1a**,**a'**) and {(2,6-$^i Pr_2$-Ph)-N=CMeCMe=N-(2-$CONMe_2$-6-^{i}Pr-Ph)}PdMeCl (**1b**,**b'**) with the more steric demanding benzhydryl (-$CHPh_2$) groups in **1d**,**d'** and **1e**,**e'** was expected to significantly improve ethylene polymerization performance. Activation of **1d**,**d'** and **1e**,**e'** by NaB{3,5-$(CF_3)_2C_6H_3$}$_4$ generates active ethylene polymerization catalysts that produce highly branched (77-81 br/1000C) polyethylenes with a moderate MW (M_n ca. 26-60 kDa). The replacement of two isopropyl units in the catalysts **1a**,**a'** and **1b**,**b'** with benzhydryl groups leads to a significant improvement on the overall homopolymerization performance. The H-bonding catalyst **1d**,**d'** is capable of incorporating ca. 2 times as much methyl acrylate and ca. 3 times as much acrylic acid as the non-H-bonding catalyst [{2,6-$(CHPh_2)_2$-4-Me-Ph}-N=CMeCMe=N-(2,6-$^i Pr_2$-Ph)]PdMeCl (**1f**,**f'**) in the copolymerization with ethylene. The reactions of **1a**,**a'** and **1b**,**b'** with metal salts that contain weakly coordinating anions lead to

extrusion of CH_4 and the formation of μ-CH_2 complexes, in which the amide carbonyl O-atoms coordinate to Pd centers.

Chapter Four describes the coordination chemistry and ethylene polymerization behavior of amide-functionalized (α-diimine)Ni complexes. The α-diimine ligands (2,6-$^{i}Pr_2$-Ph)-N=CMeCMe=N-(2-^{i}Pr-6-$CONMe_2$-Ph) (**L1**) and (2,6-$^{i}Pr_2$-Ph)-N=CMeCMe=N-[2,6-$(CONMe_2)_2$-Ph] (**L2**) react with (dme)$NiBr_2$ to form the five-coordinate paramagnetic complexes (**L1**)$NiBr_2$ (**1**) and (**L2**)$NiBr_2$ (**2**), in which one amide oxygen atom and the two imine nitrogen atoms of **L1** and **L2** coordinate to the Ni center. **L1** reacts with $(py)_2NiMe_2$ to form the diamagnetic, square planar 4-coordinate complex (**L1**)$NiMe_2$ (**3**). Activation of **1** with Et_2AlCl generates an ethylene polymerization catalyst that produces semicrystalline polyethylene with a broad molecular-weight (MW) distribution.

Chapter Five describes the synthesis of 2,3-dihydroquinazolin-4(1*H*)-one compounds **4a**, **5a** and **6a**, and their facile C-C cleavage reactions triggered by autoxidation. 2-Acyl-2,3-dihydroquinazolin-4(1*H*)-one compounds **4a** and **5a** undergo facile C-C cleavage reactions with O_2 by a radical mechanism. The reaction pathway is dependent on the structure of substrate. The strained spirocyclic **4a** undergoes ring expansion by 1,2-acyl migration to form a C-based radical followed by trapping with O_2. Compound **5a**, in which the 2-acetyl is not part of a cyclic structure, undergoes fragmentation to generate acetyl radical, which is trapped by O_2 to form peracetic acid. Bis(dihydroquinazolinone) **6a** undergoes C-C cleavage and formal dehydrogenation by O_2.

Chapter Six describes the synthesis and structure of an unusual Pd complex that contains the α-aminoimine ligand 6-Me-4-^{i}Pr-6-(dippN=C(Me))-6,11-dihydro-5*H*-indolo[3,2-*c*]quinoline (**6**). Ligand **6** coordinates in a κ^2-C=*N*,*N*H fashion in the square planar complex **(6)$PdCl_2$**.

Chapter Seven describes the synthesis, coordination chemistry, and conformational isomerism and dynamics of chiral menthyl-substituted α-diimine ligands *N,N'*-(2-Men-4-Me-Ph)-BIAN (**L1**, BIAN = bis(imino)acenaphthene) and *N,N'*-(2-Men-4,6-Me_2-Ph)-BIAN (**L2**). The *syn* conformation, in which the two menthyl groups face each other on the same side of N=C-C=N plane, is favored for **L1**, **L2** and square planar complexes of these ligands, possibly due to attractive dispersion interactions between the two menthyl groups. In contrast, the *anti* conformation is favored for tetrahedral complexes of **L1** and **L2**, and both menthyl ^{i}Pr units point to the acenaphthene backbone. The *anti*,*syn* isomerization of square planar complexes **(L1)Ni(acac)-*anti*,*syn*** is facile at room temperature. Square planar complexes **(L2)Ni(acac)-*anti*,*syn*** are kinetically stable at room temperature, and the *syn* isomer produces polyethylene with a higher MW and branching level than the *anti* isomer. The *syn* isomer also produces poly(1-hexene) with less branches and a higher degree of chain-straightening compared to the *anti* isomer. These differences in polymerization behavior are attributed to the significantly different steric profiles of the two isomers.

1.3 References

(1) Johnson, L. K.; Killian, C. M.; Brookhart, M. S. *J. Am. Chem. Soc.* **1995**, *117*, 6414.

(2) Johnson, L. K.; Mecking, S.; Brookhart, M. S. *J. Am. Chem. Soc.* **1996**, *118*, 267.

(3) Li, W.; Zhang, X.; Meetsma, A.; Hessen, B. *J. Am. Chem. Soc.* **2004**, *126*, 12246.

(4) Li, W.; Zhang, X.; Meetsma, A.; Hessen, B. *Organometallics* **2008**, *27*, 2052.

(5) Luo, S.; Jordan, R. F. *J. Am. Chem. Soc.* **2006**, *128*, 12072.

(6) Chen, Z.; Liu, W.; Daugulis, O.; Brookhart, M. *J. Am. Chem. Soc.* **2016**, *138*, 16120.

(7) Chen, G.; Ma, X. S.; Guan, Z. *J. Am. Chem. Soc.* **2003**, *125*, 6697.

(8) Nakamura, A.; Ito, S.; Nozaki, K. *Chem. Rev.* **2009**, *109*, 5215.

(9) Popeney, C. S.; Guan, Z. *Organometallics* **2005**, *24*, 1145.

(10) Camacho, D. H.; Salo, E. V.; Ziller, J. W.; Guan, Z. *Angew. Chem., Int. Ed.* **2004**, *43*, 1821.

(11) Popeney, C. S.; Camacho, D. H.; Guan, Z. *J. Am. Chem. Soc.* **2007**, *129*, 10062.

(12) Popeney, C. S.; Guan, Z. *J. Am. Chem. Soc.* **2009**, *131*, 12384.

(13) Allen, K. E.; Campos, J.; Daugulis, O.; Brookhart, M. S. *ACS Catal.* **2014**, 456.

(14) Dai, S.; Sui, X.; Chen, C. *Angew. Chem., Int. Ed.* **2015**, *54*, 9948.

(15) Dai, S.; Chen, C. *Angew. Chem., Int. Ed.* **2016**, *55*, 13281.

(16) Takano, S.; Takeuchi, D.; Osakada, K.; Akamatsu, N.; Shishido, A. *Angew. Chem., Int. Ed.* **2014**, *53*, 9246.

(17) Mecking, S.; Johnson, L. K.; Wang, L.; Brookhart, M. S. *J. Am. Chem. Soc.* **1998**, *120*, 888.

(18) Williams, B. S.; Leatherman, M. D.; White, P. S.; Brookhart, M. S. *J. Am. Chem. Soc.* **2005**, *127*, 5132.

(19) Davis, H.; Phipps, R. J. *Chem. Sci.* **2017**, doi: 10.1039/C6SC04157D.

(20) Raynal, M.; Ballester, P.; Vidal-Ferran, A.; van Leeuwen, P. W. N. M. *Chem. Soc. Rev.* **2014**, *43*, 1660.

(21) Dydio, P.; Reek, J. N. H. *Chem. Sci.* **2014**, *5*, 2135.

(22) Crabtree, R. H. *New J. Chem.* **2011**, *35*, 18.

CHAPTER TWO

Hydrogen Bonding Behavior of Amide-Functionalized α-Diimine Palladium Complexes

2.1 Introduction

Hydrogen bonding interactions[1] can strongly influence the structures and ligand binding preferences of coordination and organometallic compounds, and provide a potentially versatile tool for controlling their reactivity. The incorporation of hydrogen bonding units in the ancillary ligands of metal complexes provides a means to stabilize high energy species,[2] control molecular recognition,[3] activate chemical bonds, mediate proton transfer, enable new reactivity modes, and influence selectivity in catalytic reactions.[4] For example, molecular recognition through hydrogen bonding in the second coordination sphere enables highly regio- and/or stereoselective catalytic organic transformations, including sp^3 C–H oxidation,[5] C–H amination,[6] sulfoxidation of sulfides,[7] alkene epoxidation,[8] alkene hydroformylation,[4d,9] and allylation of indoles.[10] Second-sphere hydrogen bond donor groups play an important role in substrate activation in the catalytic hydrogenation and transfer hydrogenation of carbonyl compounds, imines, and nitriles[4c,11] and the hydrogenation of CO_2.[12] Hydrogen bonding groups also provide critical proton relay pathways in electrocatalytic H_2 oxidation and production,[13] O_2 reduction,[14] and CO_2 reduction.[15]

Pd complexes that contain ancillary α-diimine ligands have been used as catalysts for reactions, including olefin polymerization,[16] copolymerization of olefins with polar comonomers,[17] olefin/CO copolymerization,[18] cationic polymerization of vinyl ethers,[19] dimerization of vinyl ethers to acetals,[20] oligomerization and functionalization of alkynes,[21] selective hydrogenation of alkynes to *Z*-alkenes,[22] and other reactions.[23] (α-Diimine)Pd complexes have also been used in the stoichiometric activation of aliphatic,[24] aryl,[25] and indenyl C–H bonds[26]

and the C–N bond in nitromethane.[27]

Many structural modifications of α-diimine ligands have been explored to manipulate their electronic and steric properties. Additionally, multifunctional α-diimine ligands have been designed to enable hemilabile coordination of pendant donors, external control of reactivity, and modulation of selectivity through secondary interactions. Representative examples of multifunctional (α-diimine)Pd species are shown in Chart 1. Coordination of the pendant ether and thiophene units was observed in **A** and **B**.[24,28] A cyclophane-type (α-diimine)Pd catalyst with a *trans*-azobenzene unit (**C**) exhibited excellent activity and stereoselectivity in the polymerization of diallylmalonate, whereas photoisomerization to the *cis*-azobenzene isomer significantly diminished both properties.[29] Hemilabile F···Pd interactions in **D**[30] and binding of Al cocatalysts to the pyridine unit of **E**[31] are believed to strongly influence the molecular weights (MWs) and branching densities in polyethylene produced by these catalysts. The *m*-pyridyl units enabled coordination of zinc(II) salphen complexes in trinuclear species **F**, and the (α-diimine)$PdMe^+$ cation derived from **F** yielded high-MW syndiotactic copolymer in catalytic CO/4-*tert*-butylstyrene copolymerization.[32]

Here we describe the syntheses, structures, and dynamics of several (α-diimine)PdRX and (α-diimine)$PdRL^+$ complexes that contain amide functional groups in the α-diimine ligand. The amide carbonyl group behaves as a hydrogen bond acceptor, and the (secondary) amide NH unit behaves as a hydrogen bond donor. Intramolecular hydrogen bonding in the second coordination sphere is an important feature of these complexes and strongly influences their structures and ligand binding affinities.

Chart 2.1. Representative Multifunctional (α-Diimine)Pd Complexes.

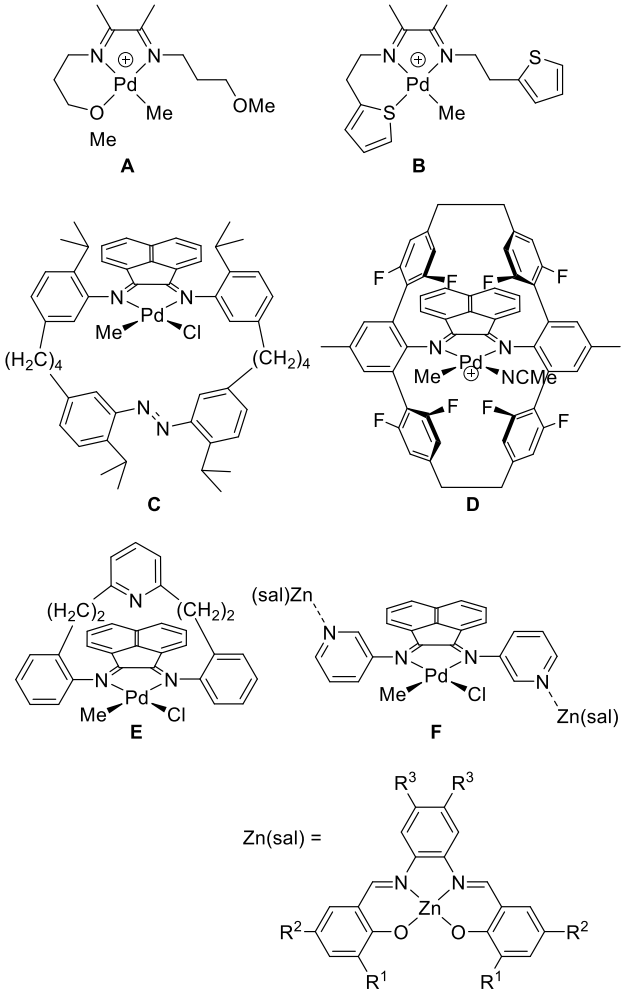

2.2 Results and Discussion

Tertiary Amide-Functionalized α-Diimine Ligands. The monoamide-functionalized α-diimine (2,6-^{i}Pr$_2$-Ph)N=CMeCMe=N(2-C(=O)NMe$_2$-6-^{i}Pr-Ph) (**4a**) was synthesized by the route in Scheme 2.1 starting from 3-isopropylanthranilic acid (**1**).[33] The reaction of **1** with thionyl chloride to generate the corresponding acyl chloride in situ, followed by reaction with aqueous dimethylamine afforded *o*-aminobenzamide **2a**. Acid-catalyzed condensation of **2a** and α-ketaimine **3** yielded **4a**.[34] The ^{1}H NMR spectrum of **4a** at room temperature contains 3 sets of isopropyl resonances, which implies that rotation around the C$_{aryl}$–N bonds is slow on NMR time

scale. The ^{1}H NMR spectrum also contains two NMe resonances, consistent with the expected slow rotation around the amide OC–NMe_2 bond.

Scheme 2.1

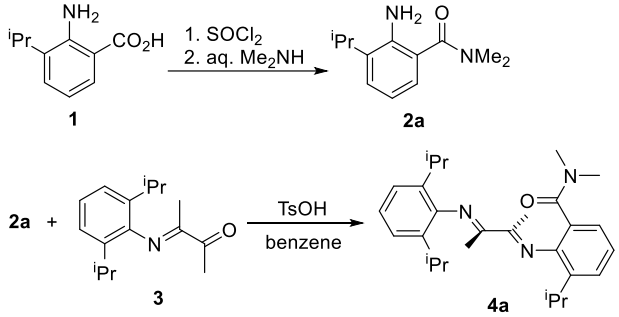

The unsymmetrical bisamide-functionalized α-diimine (2,6-^{i}Pr$_2$-Ph)N=CMeCMe=N(2,6-(C(=O)NMe_2)$_2$-Ph) (**4b**), which contains two dimethylamide groups on the same aryl ring, was prepared by condensation of aniline **2b**[35] and α-ketaimine **3** (Scheme 2.2). The room temperature ^{1}H NMR spectrum of **4b** is consistent with the expected C_s symmetry. The spectrum contains two ^{i}Pr doublets, corresponding to the inequivalent Me groups within each ^{i}Pr unit, and two singlets for the –NMe_2 groups due to restricted rotation around the amide OC–NMe_2 bonds. Warming the sample to 70 °C results in coalescence of two NMe signals. The free energy barrier for amide NMe exchange is $\Delta G^{\ddagger}$ = 16.5(4) kcal mol^{-1}, which is within the normal range for *N*,*N*-dialkylamides.[36]

Scheme 2.2

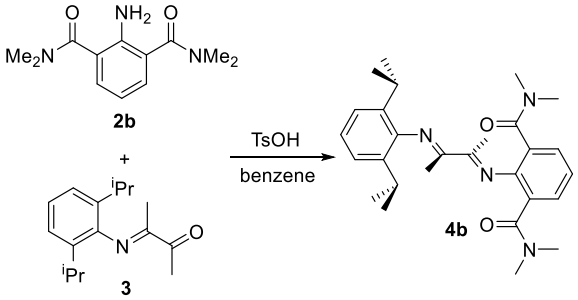

The isomeric bisamide-functionalized α-diimine (2-C(=O)NMe$_2$-6-^{i}Pr-Ph)N=CMeCMe=N(2-C(=O)NMe$_2$-6-^{i}Pr-Ph) (**4c**), which contains one amide group on each N-aryl unit, was prepared by condensation of 2,3-butanedione with 2 equiv of aniline **2a** (Scheme 2.3). The ^{1}H NMR spectra of **4c** in $CDCl_3$, CD_2Cl_2, and toluene-d_8 at room temperature contain two complete sets of resonances, indicating the presence of two C_2-symmetric isomers in a ca. 1.4/1 ratio. The two species were assigned to be the syn and anti isomers that result from restricted rotation around the C_{aryl}–N bonds.[37] **4c-*anti*** was isolated by crystallization from a CH_2Cl_2/hexanes solution of the **4c-*anti*/4c-*syn*** mixture and characterized by X-ray diffraction (Figure 2.1). The N=CMeCMe=N unit is planar and adopts an *s-trans* conformation. The N-aryl groups are nearly perpendicular to the N=CMeCMe=N plane (dihedral angle C8–C9–N2–C13 = –74.2(3) deg), and the amide groups are rotated ca. 65 deg out of the plane of adjacent aryl ring (dihedral angle C9–C8–C10–O1 = 114.5(3) deg).

Scheme 2.3

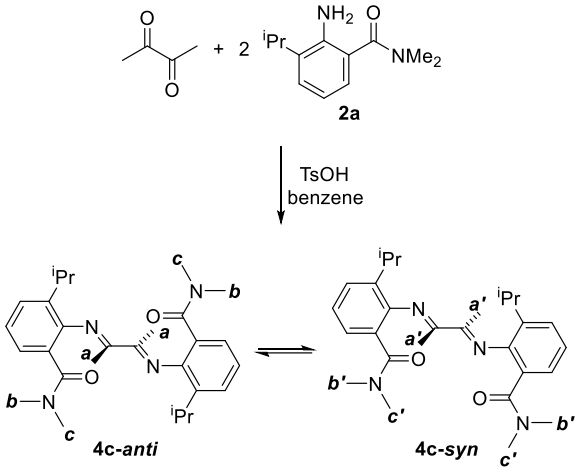

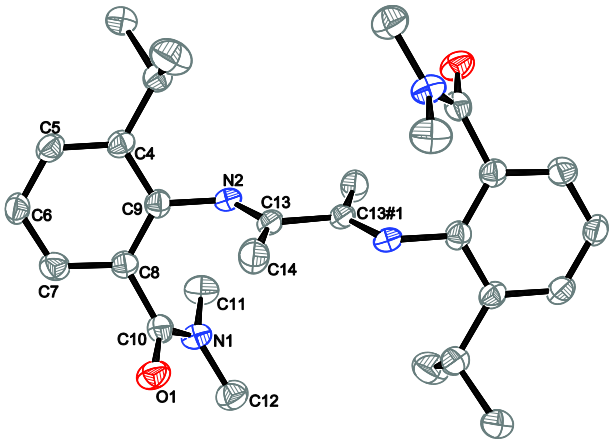

Figure 2.1. Molecular structure of **4c-*anti***. Hydrogen atoms are omitted. Selected bond lengths (Å) and angles (deg): C13–N2 1.273(3), C13–C13#1 1.489(5), C9–N2 1.407(3), C10–O1 1.229(3), C10–N1 1.329(3); N2–C13–C13#1 115.7(3), C13–N2–C9 121.6(2), O1–C10–N1 121.4(2), C10–N1–C12 119.7(2).

Two dynamic processes are observed for **4c** in solution by ^{1}H NMR spectroscopy in the temperature range 20 to 90 °C: rotation around the C_{aryl}–N bonds, which interconverts **4c-*syn*** and **4c-*anti***, and rotation around the amide OC–NMe_2 bonds, which permutes the two NMe groups within a given amide unit. With reference to the labeling scheme for the methyl groups in Scheme 2.3, **4c-*anti*/4c-*syn*** interconversion results in *a*/*a'*, *b*/*b'*, and *c*/*c'* exchange, while amide OC–NMe_2 bond rotation results in *b*/*c* and *b'*/*c'* exchange. Free energies of activation for these processes were determined by total line shape analysis (Figure 2.2); $\Delta G^{\ddagger}_{syn\rightarrow anti,20°C}$ = 16.4(11) kcal mol^{-1}; $\Delta G^{\ddagger}_{b/c,20°C}$ = 18.0(11) kcal mol^{-1}, $\Delta G^{\ddagger}_{b'/c',20°C}$ = 17.6(8) kcal mol^{-1}.

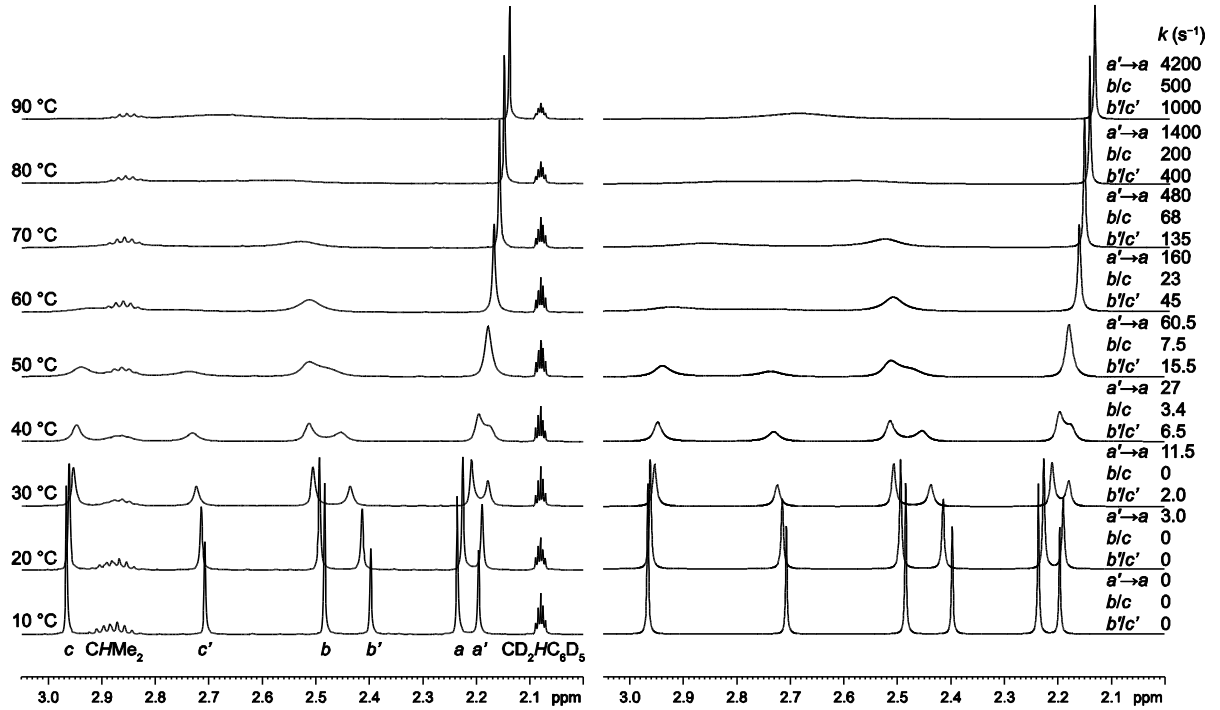

Figure 2.2. Variable temperature ^{1}H NMR spectra of **4c** in toluene-d_8 (10 to 90 °C, 500 MHz). The δ 3.05–2.00 region is shown. Left: experimental spectra. Right: simulated spectra (gNMR). The labeling scheme is given in Scheme 2.3. First-order rate constants (s^{-1}) determined by simulation are shown for each temperature.

Pd Complexes of 4a and 4b. The reaction of α-diimine ligands **4a** and **4b** with (cod)PdMeCl in Et_2O yields the corresponding square planar (α-diimine)PdMeCl complexes **5a**,**a'** and **5b**,**b'** (Scheme 2.4). Complex **5a**,**a'** was isolated as an 8.7/1 mixture of isomers by crystallization from CH_2Cl_2/hexanes at –40 °C; this mixture equilibrates to a 4.5/1 mixture in CD_2Cl_2 at room temperature. Similarly, **5b**,**b'** was isolated as a 6.5/1 isomer mixture, which equilibrates to a 17/1 mixture at room temperature. For these square planar (α-diimine)PdMeCl complexes, two isomers that differ in the orientation (trans/cis) of the Pd–Me ligand and the amide-substituted arylimine unit are possible.[38] The NOESY spectrum of **5a**,**a'** exhibits correlations between the Pd–Me resonance of the major isomer **5a** and *two* isopropyl methyl resonances, which establishes that the Pd–Me group of this isomer is cis to the *N*-(2,6-$^{i}Pr_2$-Ph) imine unit and trans to the amide-substituted arylimine unit. The NOESY spectrum of **5b**,**b'** exhibits Pd–Me/^{i}Pr

correlations for the major isomer **5b**, which establishes that the Pd–Me ligand is also cis to the *N*-2,6-$^{i}Pr_2$-Ph imine unit and trans to the amide-substituted arylimine unit. The equilibrium isomer ratios reflect the preference for the strong donor Pd–Me group to be positioned trans to the imine unit which is the weaker donor.

Scheme 2.4

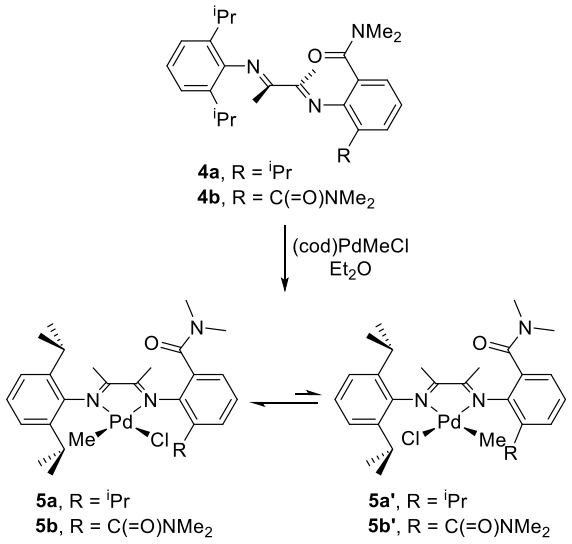

Pd Complexes of 4c. The reaction of **4c** (1.4/1 anti/syn mixture) with $(MeCN)_2PdCl_2$ in CH_2Cl_2 at room temperature yields a 1/1.7 mixture of isomeric (α-diimine)$PdCl_2$ complexes **6c-*anti*** and **6c-*syn*** (Scheme 2.5). Heating a $CDCl_2CDCl_2$ solution of the product mixture at 110 °C for 1 h produces a 5.7/1 equilibrium mixture of **6c-*anti***/**6c-*syn***. The thermodynamically more stable isomer **6c-*anti*** was selectively crystallized as the solvate **6c-*anti***·$3CH_2Cl_2$ from CH_2Cl_2/hexanes and identified by X-ray diffraction. The solid state structure of **6c-*anti***·$3CH_2Cl_2$ is shown in Figure 2.3. The Pd center exhibits square planar geometry and the two N-aryl groups are perpendicular to the Pd plane. The amide oxygen atoms (O1, O2) are directed toward the α-diimine side of the molecule, and do not interact with Pd (O1···Pd1, O2···Pd1 distances > 4 Å). However, each oxygen atom forms a hydrogen bond with a CH_2Cl_2 molecule.[39] The two N-aryl

units show noticeable bowing to the side of O1, as quantified by the deviations of the C1 (0.264(6) Å) and C17 (0.186(6) Å) atoms from the N1-Pd1-N3 least-squares plane.

^{1}H NMR analysis of pure **6c-*anti*** enabled assignment of the NMR spectra of both isomers. The kinetically favored isomer **6c-*syn*** was isolated in pure form by recrystallization of the 1/1.7 kinetic anti/syn isomer mixture. The barrier for isomerization of **6c-*syn*** to **6c-*anti*** is $\Delta G^{\ddagger}$ = 29.1(3) kcal mol^{-1} at 80(1) °C.

Scheme 2.5

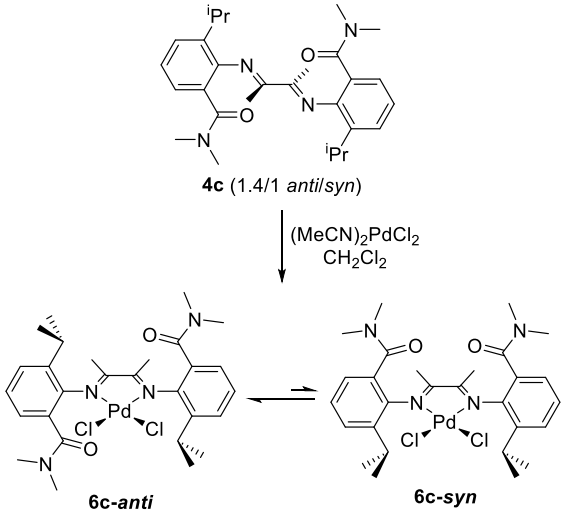

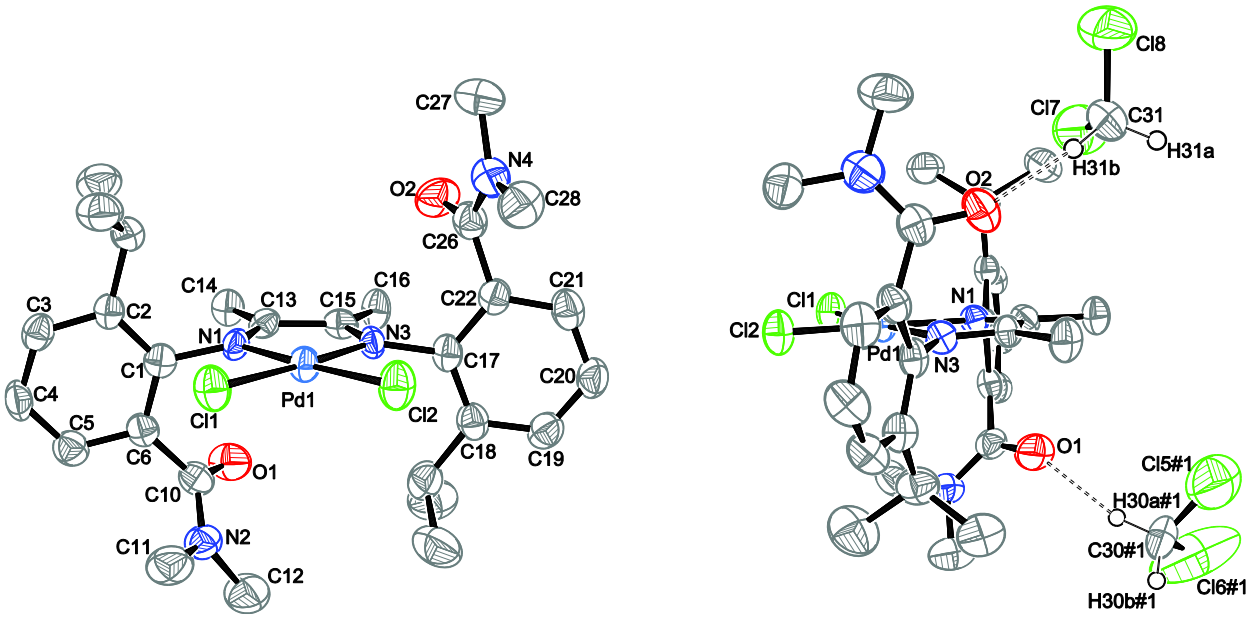

Figure 2.3. Molecular structure of **6c-*anti*** in **6c-*anti*·3CH$_2$Cl$_2$**. Left: Front view. Hydrogen atoms and solvent molecules are omitted. Right: Side view, which shows the O1···H30a#1–C30#1 and O2···H31b–C31 hydrogen bonds. The C29 CH_2Cl_2 molecule is omitted. Selected bond lengths (Å) and angles (deg): N1–Pd1 1.984(4), N3–Pd1 2.002(4), Cl1–Pd1 2.2565(16), Cl2–Pd1 2.2436(16), C13–N1 1.280(6), C15–N3 1.284(6), C13–C15 1.463(8), C1–N1 1.439(7), C17–N3 1.416(7), C10–O1 1.212(7), C26–O2 1.217(7), C10–N2 1.326(7), C26–N4 1.337(8); N1–Pd1–N3, 79.18(18), N1–Pd1–Cl2 174.71(13), N3–Pd1–Cl2 95.55(13), N1–Pd1–Cl1 95.29(13), N3–Pd1–Cl1 174.47(13), Cl2–Pd1–Cl1 89.98(6), O1–C10–N2 122.3(6), O2–C26–C22 118.7(6).

The reaction of **4c** (1.4/1 anti/syn mixture) with (cod)PdMeCl in Et_2O yields a 5.2/1 mixture of isomeric (α-diimine)PdMeCl complexes **5c-*anti*** and **5c-*syn*** (Scheme 2.6). In CD_2Cl_2, anti/syn isomerization produces a 4.6/1 equilibrium mixture of **5c-*anti*** and **5c-*syn*** in a few hours at room temperature. Crystallization of a 5.2/1 isomer mixture at –40 °C from CH_2Cl_2/hexanes yields crystals of the bis-CH_2Cl_2 solvate of the minor isomer, **5c-*syn*·**2CH_2Cl_2, which was characterized by X-ray diffraction (Figure 2.4). The Pd1–N2 bond is ca. 0.11 Å longer than the Pd1–N1 bond, which is attributed to the stronger trans influence of the Pd–Me ligand versus the chloride ligand. One CH_2Cl_2 molecule is hydrogen bonded to the O2 atom.[40]

Scheme 2.6

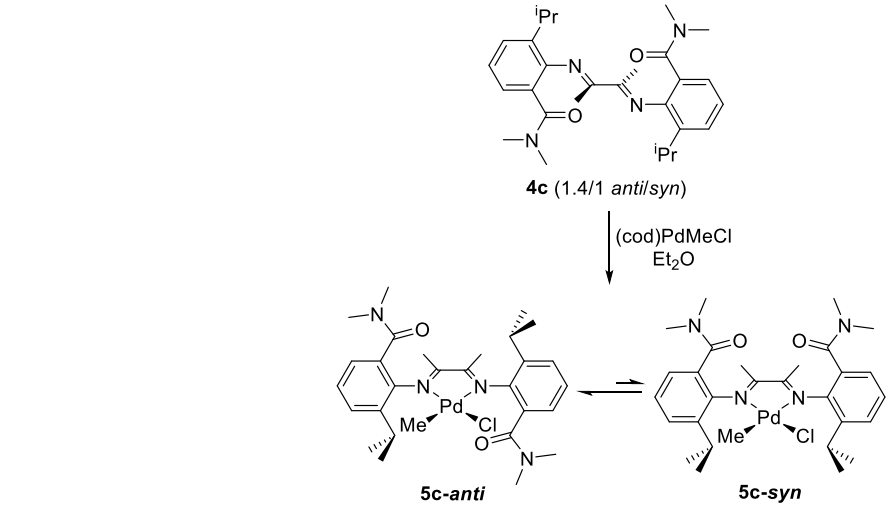

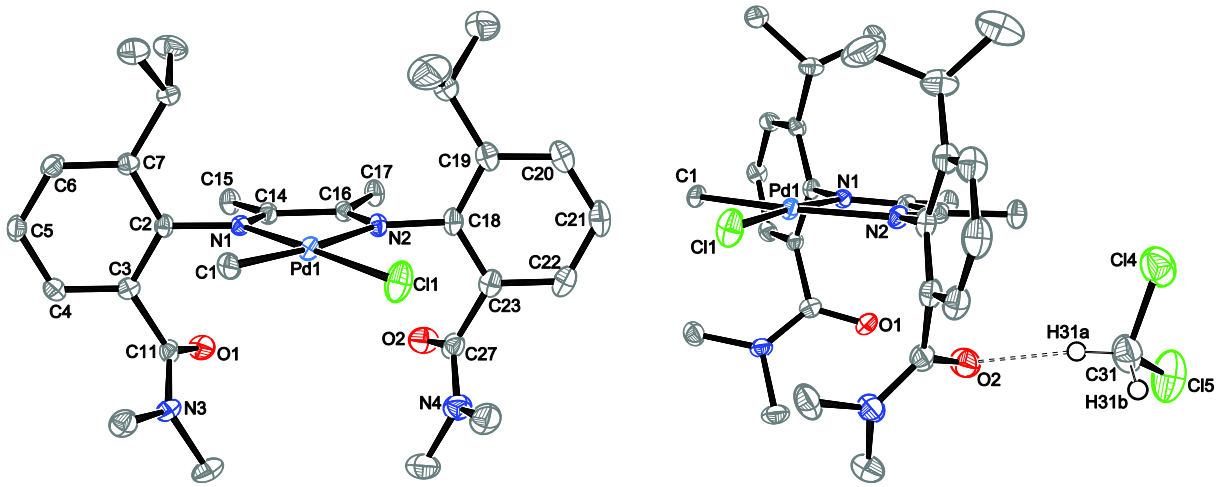

Figure 2.4. Molecular structure of **5c-*syn*** in **5c-*syn*·2CH$_2$Cl$_2$**. Left: Front view. Hydrogen atoms and solvent molecules are omitted. Right: Side view, which shows the O2···H31a–C31 hydrogen bond. The C30/C30X CH_2Cl_2 molecule is omitted. Selected bond lengths (Å) and angles (deg): N1–Pd1 2.0455(15), N2–Pd1 2.1560(16), Cl1–Pd1 2.2855(5), C1–Pd1 2.0288(18), C14–N1 1.288(2), C16–N2 1.285(2), C14–C16 1.501(3), C2–N1 1.442(2), C18–N2 1.435(2), C11–O1 1.230(2), C27–O2 1.230(3), C11–N3 1.344(3), C27–N4 1.342(3); N1–Pd1–N2 77.03(6), N1–Pd1–Cl1 176.04(4), N2–Pd1–Cl1 100.04(4), C1–Pd1–N1 96.42(7), C1–Pd1–N2 173.11(7), C1–Pd1–Cl1 86.60(6), O1–C11–N3 122.72(18), O2–C27–N4 122.4(2).

The interconversion of the anti and syn isomers of **5c** and **6c** requires net rotation around one (or both) N–C_{aryl} bonds, and the rate of this process is probably determined by steric factors.[41] The Pd1–N2 bond in **5c-*syn***, which is trans to the Pd–Me group, is ca. 0.16 Å longer than the Pd–

N bonds in **6c-*anti***, due to the trans influence of the Pd–Me ligand. The C18–C23 aryl group that is bonded to N2 in **5c-*syn*** is thus less crowded than the aryl groups in **6c-*anti*** and may experience a lower barrier to rotation, which would explain the faster anti/syn isomerization of **5c** (hours at room temperature) versus **6c** (hours at 80 °C).[42]

Secondary-Amide-Functionalized (α-Diimine)Pd Chloride Complexes. The α-diimine (2,6-$^{i}Pr_2$-Ph)N=CMeCMe=N(2-C(=O)NHMe-6-^{i}Pr-Ph) (**4d**, Scheme 2.7), which contains a secondary amide group as the key structural feature, was targeted as a ligand for Pd(II) complexes. The secondary *o*-aminobenzamide 2-NH_2-3-^{i}Pr-PhC(=O)NHMe (**2d**) was prepared analogously to **2a**. Acid-catalyzed condensation of **2d** with α-ketaimine **3** yields dihydroquinazolinone derivative **4d'** instead of the α-diimine **4d**, via imine condensation to form **4d** and subsequent ring closure between the secondary amide group and the adjacent imine C=N unit. The structure of **4d'** was established by X-ray diffraction and is shown in Figure 2.5. Two independent molecules are present in the asymmetric unit, which are linked by intermolecular N–H···O hydrogen bonds to form infinite chains. The C15–N2 (1.440(5) Å) and C15–N3 (1.445(5) Å) bond lengths establish that both of these bonds are single bonds. The ^{1}H NMR spectrum of **4d'** in $CDCl_3$ contains a broad singlet at δ 5.11 for the NH unit and a sharp singlet at δ 3.28 for the NMe group. The absence of $J_{NH–NMe}$-coupling shows that **4d'** does not undergo ring opening to form α-diimine **4d** in solution. The ^{13}C NMR resonance for the aminal carbon C15 appears at δ 76.7. **4d** was not observed as an intermediate or a co-product in Scheme 2.7.

Scheme 2.7

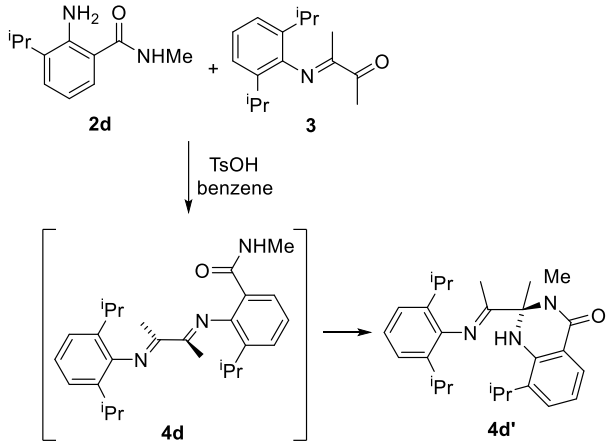

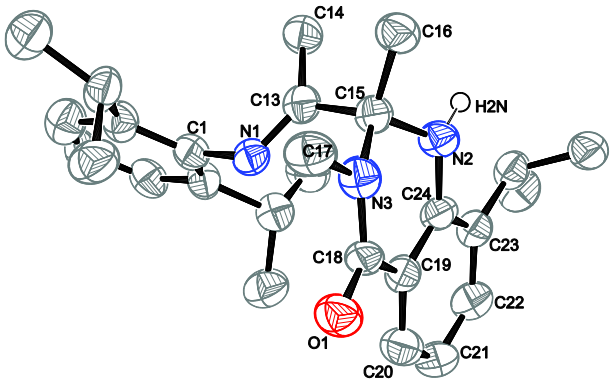

Figure 2.5. Molecular structure of one independent molecule of **4d'**. The structure of the other independent molecule is similar. Hydrogen atoms are omitted except H2N. Selected bond lengths (Å) and angles (deg): C13–N1 1.248(5), C13–C15 1.536(6), C18–O1 1.222(5), C18–N3 1.342(5), N2–H2N 0.98(3); N1–C13–C15 117.4(5), N2–C15–C13 108.9(4), N3–C15–C13 110.8(4), N2–C15–N3 107.8(4), O1–C18–N3 121.5(5).

The reaction between pro-ligand **4d'** and $(MeCN)_2PdCl_2$ in CD_2Cl_2 for 3 d at room temperature or 1 d at 40 °C results in heterocycle opening and formation of the α-diimine complex (**4d**)$PdCl_2$ (**6d**, Scheme 2.8). This reaction may proceed by initial κ^2-C=*N*,*N*H-coordination of **4d'** to Pd, which induces the ring-opening of **4d'**. The α-diimine structure of **6d** is stabilized by chelation to Pd(II).[43]

The structure of **6d** was confirmed by X-ray diffraction and is shown in Figure 2.6. The secondary amide N–H bond points toward a chloride ligand, and the associated N3···Cl1 (3.436(3)

Å) and H3N···Cl1 (2.68(6) Å) distances are consistent with an N–H···Cl hydrogen bonding interaction.[44] The Pd1–Cl2 bond is ca. 0.02 Å shorter than the Pd1–Cl1 bond, which may reflect the weaker donor ability and trans influence of the *N*-(2-C(=O)NHMe-6-^{i}Pr-Ph) imine unit compared to the *N*-(2,6-^{i}Pr$_2$-Ph) imine unit. It is also possible that the H3N···Cl1 hydrogen bond contributes to the lengthening of the Pd1–Cl1 bond.

Scheme 2.8

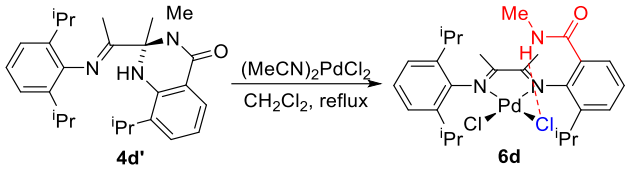

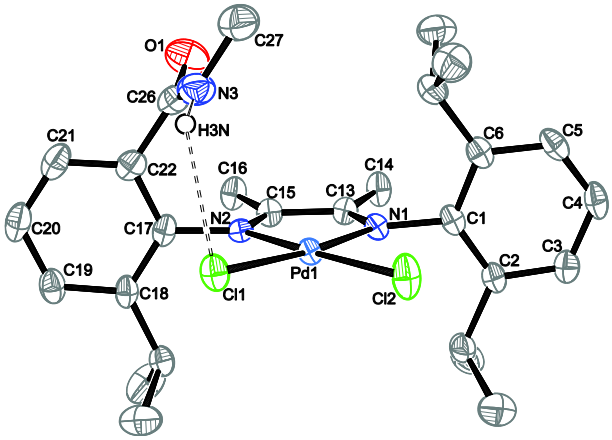

Figure 2.6. Molecular structure of complex **6d**. Hydrogen atoms are omitted except H3N. Selected bond lengths (Å) and angles (deg): N1–Pd1 2.018(3), N2–Pd1 2.019(3), Cl1–Pd1 2.2929(8), Cl2–Pd1 2.2701(9), N3–H3N 0.91(6); N1–Pd1–N2 79.15(11), N1–Pd1–Cl2 94.71(8), N2–Pd1–Cl2 173.79(8), N1–Pd1–Cl1 172.56(8), N2–Pd1–Cl1 94.12(8), Cl2–Pd1–Cl1 92.06(3), N3–H3N···Cl1 141(4), H3N···Cl1–Pd1 82.8(11).

The ^{1}H NMR spectrum of **6d** in CD_2Cl_2 contains a doublet at δ 3.03 (J = 4.9 Hz) for the amide NMe group, which is coupled to the amide NH resonance (br q, J = 4.9 Hz) at δ 6.75. The solid state IR spectrum of **6d** exhibits a ν_{N-H} stretching band at 3330 cm^{-1}, which is consistent with the intramolecular N–H···Cl hydrogen bond observed in the crystal structure.[45]

4d' does not react with (cod)PdMeCl in Et_2O at room temperature. However, **6d** reacts with $SnMe_4$ in CH_2Cl_2 at room temperature to yield a 16/1 equilibrium mixture of (**4d**)PdMeCl complexes **5d** and **5d'**, which differ in the relative positions of the Pd–Me group and the amide-substituted arylimine unit (**5d** trans, **5d'** cis, Scheme 2.9). The major isomer **5d** was selectively crystallized from CH_2Cl_2/hexanes at –40 °C, and identified by X-ray diffraction. Isomer **5d** is stable in CD_2Cl_2 at –40 °C, but isomerizes to the equilibrium **5d**,**d'** mixture within 5 min at room temperature.

The structure of **5d** is shown in Figure 2.7. The secondary amide group is hydrogen bonded to the Pd–Cl ligand in a manner similar to that observed for **6d**. The N3···Cl1 (3.345(4) Å) and H3N···Cl1 (2.53(3) Å) distances are 0.09 and ca. 0.15 Å shorter, and the N3–H3N···Cl1 angle (172(3) deg) is 31 deg larger, than the corresponding values for **6d**. The Pd1–N2 bond is ca. 0.10 Å longer than the Pd1–N1 bond due to the stronger trans influence of the Pd–Me ligand compared to chloride.

Scheme 2.9

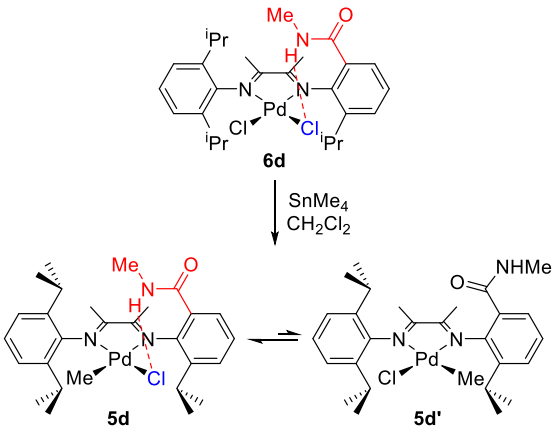

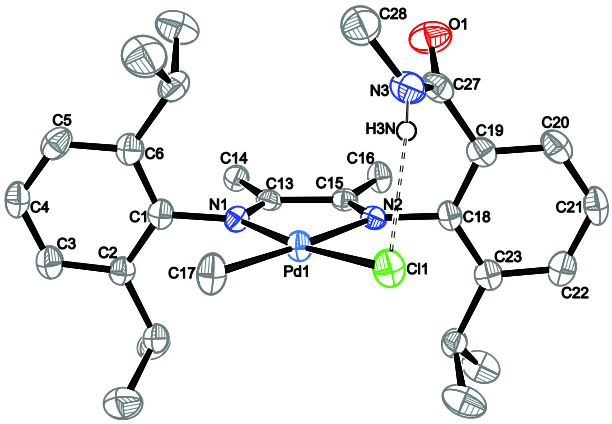

Figure 2.7. Molecular structure of complex **5d**. Hydrogen atoms are omitted except H3N. Selected bond lengths (Å) and angles (deg): N1–Pd1 2.026(3), N2–Pd1 2.121(3), C17–Pd1 2.021(3), Cl1–Pd1 2.2979(12), N3–H3N 0.82(3); C17–Pd1–N1 95.92(12), C17–Pd1–N2 173.44(12), N1–Pd1–N2 77.54(10), C17–Pd1–Cl1 90.03(10), N1–Pd1–Cl1 172.83(7), N2–Pd1–Cl1 96.54(8), H3N···Cl1–Pd1 75.0(7).

The amide ^{1}H NMR NH resonance for **5d** in CD_2Cl_2 solution appears as a broad signal at δ 7.48, which overlaps an aromatic hydrogen resonance. This assignment was confirmed by the COSY spectrum, which exhibits a correlation between the amide NH signal and the amide NMe signal at δ 2.92 (d, J = 4.9 Hz). The amide NH signal of **5d'** appears at δ 6.29. The 1.19 ppm downfield shift of the amide NH resonance of **5d** versus **5d'** is due to the intramolecular hydrogen bond in the former species. The IR spectrum of **5d** (thin film) contains a ν_{N-H} stretching band at 3302 cm^{-1}.

The equilibrium **5d**/**5d'** ratio is significantly greater than the equilibrium **5a**/**5a'** ratio despite their similarity in the steric and electronic properties of the α-diimine ligands in these compounds. The additional stabilization in **5d** by the intramolecular hydrogen bond is most likely responsible for this effect. The difference between ratios **5d**/**5d'** and **5a**/**5a'** corresponds to an additional stabilization in **5d** by $\Delta\Delta G$ = 0.7 kcal mol^{-1}, which is a measurement of the strength of intramolecular N–H···Cl hydrogen bond in **5d**.

The structural and spectroscopic data discussed above establish that **5d** has a stronger

intramolecular hydrogen bond than **6d**. In particular, the N3···Cl1 distance of **5d** is 0.09 Å shorter than that of **6d**, the amide ^{1}H NMR NH resonance of **5d** is 0.73 ppm downfield versus that of **6d**, and the IR ν_{N-H} value for **5d** is 28 cm^{-1} lower than the value for **6d**. This difference is ascribed to higher basicity of the chloride ligand in **5d** versus those in **6d**, which results from the stronger donor ability of the Pd–Me group of **5d** versus the Pd–Cl groups in **6d**.

Secondary-Amide-Functionalized (α-Diimine)Pd Acetate Complex. The salt metathesis reaction of **5d**,**d'** and AgOAc yields (**4d**)PdMe(OAc) (**7d**, Scheme 2.10), which exists as a single isomer in CD_2Cl_2 solution. The structure of **7d** was confirmed by X-ray crystallography (Figure 2.8). The acetate ligand is coordinated to Pd in a κ^1-fashion, lies perpendicular to the Pd square plane, and is cis to the amide-functionalized arylimine donor. The non-Pd-bound acetate oxygen O2 is directed toward the amide NH unit, and the N3···O2 (2.866(2) Å) and H3N···O2 (2.06(2) Å) distances are indicative of an N–H···O hydrogen bond.[46]

Scheme 2.10

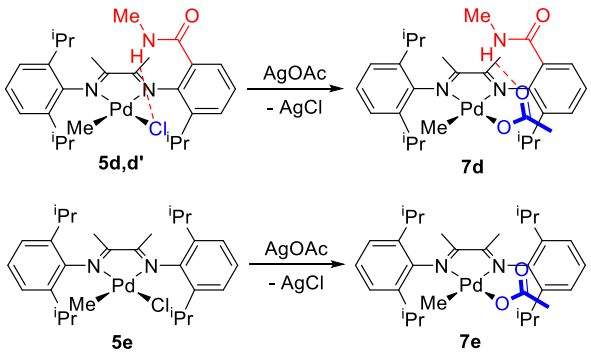

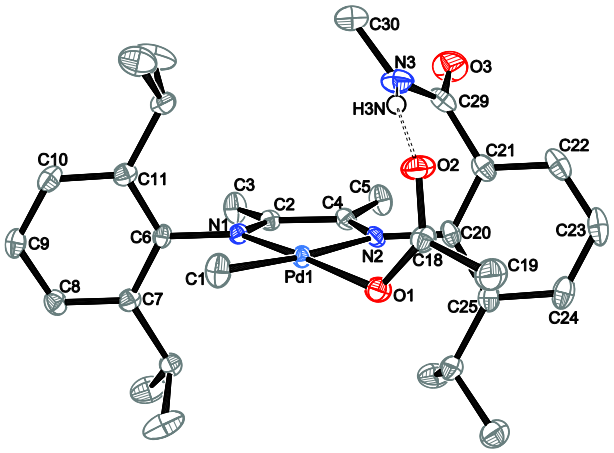

Figure 2.8. Molecular structure of complex **7d**. Hydrogen atoms are omitted except H3N. Selected bond lengths (Å) and angles (deg): N1–Pd1 2.0176(14), N2–Pd1 2.1233(14), C1–Pd1 2.0158(17), O1–Pd1 2.0247(12), C18–O2 1.231(2), C18–O1 1.278(2), C18–C19 1.512(2), N3–H3N 0.82(2); C1–Pd1–N1 97.43(6), C1–Pd1–O1 87.24(6), N1–Pd1–O1 173.58(5), C1–Pd1–N2 174.35(6), N1–Pd1–N2 77.49(5), O1–Pd1–N2 98.02(5), C18–O1–Pd1 120.25(11), O2–C18–O1 125.83(16), O2–C18–C19 120.05(16), O1–C18–C19 114.11(15), N3–H3N···O2 168(2), H3N···O2–C18 133.5(6).

The ^{1}H NMR resonance for the amide NH unit of **7d** in CD_2Cl_2 solution appears at low field (δ 9.43), and the IR ν_{N-H} stretching band appears at 3213 cm^{-1} in the solid state. These data confirm the presence of hydrogen bonding. The IR spectrum of **7d** also exhibits asymmetric and symmetric acetate ν_{OCO} stretching bands at 1590 and 1329 cm^{-1}, which shift to 1557 and 1317 cm^{-1} respectively when the carboxyl carbon is ^{13}C-labeled. The difference between the $\nu_{OCO,asym}$ and $\nu_{OCO,sym}$ values ($\Delta\nu_{OCO}$ = 261 cm^{-1}) is characteristic of a highly unsymmetrically bound acetate ligand.[47] The $\Delta\nu_{OCO}$ value for **7d** is 32 cm^{-1} lower than that for the model complex {(2,6-^{i}Pr$_2$-Ph)N=CMeCMe=N(2,6-^{i}Pr$_2$-Ph)}PdMe(OAc) (**7e**, $\Delta\nu_{OCO}$ = 293 cm^{-1}, Scheme 2.10) which lacks the amide group, due to the presence of the hydrogen bond. For comparison, the $\Delta\nu_{OCO}$ value for the intramolecularly N–H···O hydrogen-bonded Ir(III) κ^1-formate compound κ^3-*P,N,P'*-(^{i}Pr$_2$P(CH$_2$)$_2$NH(CH$_2$)$_2$P^{i}Pr$_2$)Ir(H)$_2$(O$_2$CH) reported by Hazari and Crabtree is 265 cm^{-1}.[12a]

The isomer of **7d** in which the acetate ligand is trans to the amide-functionalized arylimine unit was not observed and is likely disfavored relative to **7d** because its geometry would preclude

strong intramolecular N–H···O hydrogen bonding.

Amide-Functionalized (α-Diimine)Pd Pyrazole Complexes. The reaction of **5a**,**a'** or **5d**,**d'** with $AgSbF_6$ in the presence of pyrazole yields pyrazole adducts **8a** and **8d**, respectively (Scheme 2.11). Pyrazole adduct **8e** derived from α-diimine complex **5e** that lacks an amide group was prepared in the same manner. Complexes **8a** and **8d** exist as single isomers in CD_2Cl_2 solution. The solid state structure of **8d** is shown in Figure 2.9 and features an N–H···O hydrogen bond between the pyrazole ligand and the amide oxygen (N4···O1 2.815(4) Å, H4N···O1 2.02(4) Å, N4–H4N···O1 166(4) deg). The secondary amide NH unit does not participate in intramolecular or intermolecular hydrogen bonding in solid state.

Scheme 2.11

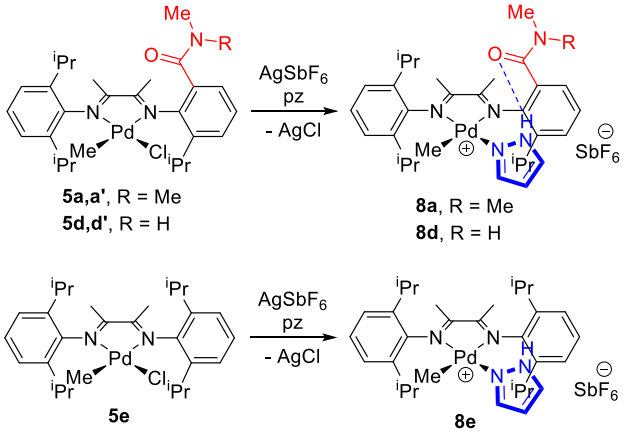

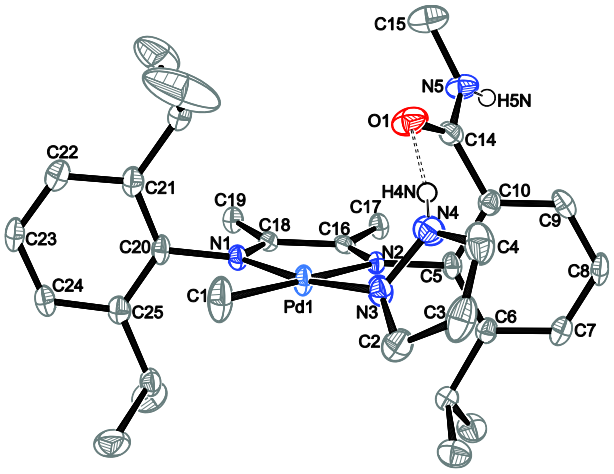

Figure 2.9. Molecular structure of **8d**. Hydrogen atoms are omitted except H4N and H5N. The SbF_6^- anion is omitted. Selected bond lengths (Å) and angles (deg): N1–Pd1 2.029(3), N2–Pd1 2.142(2), N3–N4 1.348(4), N3–Pd1 2.016(3), C1–Pd1 2.019(3), C14–O1 1.229(4); N3–Pd1–C1 86.94(13), N3–Pd1–N1 172.32(11), C1–Pd1–N1 96.80(12), N3–Pd1–N2 98.56(10), C1–Pd1–N2 174.42(13), N1–Pd1–N2 77.85(10), H4N···O1–C14 112.6(12).

In the solid state, the pyrazole IR ν_{N-H} stretching bands for **8a** and **8d** appear at 3135 and 3137 cm^{-1}, shifted ca. 230 cm^{-1} to lower frequency versus the ν_{N-H} band for **8e** (3364 cm^{-1}) due to the N–H···O hydrogen bonding in **8a**,**d**. Comparison of the ^{1}H NMR data for **8a**,**d**,**e** provides strong evidence that the pyrazole-amide hydrogen bonding is maintained in CD_2Cl_2 solution for **8a**,**d**. The pyrazole ^{1}H NMR NH resonances for **8a**,**d** appear at $\delta > 14$, ca. 4 ppm downfield from the pyrazole NH resonance for **8e**.

These (α-diimine)PdMe(pz)$^+$ complexes undergo partial dissociation of the pyrazole ligand in CD_3CN solution (Scheme 2.12). Complex **8a**, which bears the unsymmetrical α-diimine ligand **4a**, reacts in CD_3CN to generate an equilibrium mixture of free pyrazole and isomeric CD_3CN adducts (**4a**)PdMe(CD_3CN)$^+SbF_6^-$ (**9a**,**a'**, equilibrium ratio 1.3/1). Analogously, the secondary amide-functionalized α-diimine complex **8d** generates isomeric CD_3CN adducts **9d**,**d'** (equilibrium ratio 1.1/1) in CD_3CN. The model compound **8e** also dissociates pyrazole to yield **9e** in CD_3CN.

The equilibrium constants for pyrazole dissociation, K_{eq} = [(α-

diimine)PdMe(CD_3CN)$^+$][pz][(α-diimine)PdMe(pz)$^+$]$^{-1}$, were measured by ^{1}H NMR and are listed in Table 2.1. These values vary in the order **8e** > **8d** > **8a** and span more than a factor of 50. The lower values of K_{eq} for **8a**,**d** reflect the intramolecular hydrogen bonding between the pyrazole NH and amide carbonyl units, which enhances pyrazole binding. The lower value of K_{eq} for **8a** versus **8d** reflects the higher basicity of the tertiary amide in **8a** versus the secondary amide in **8d**.

Scheme 2.12

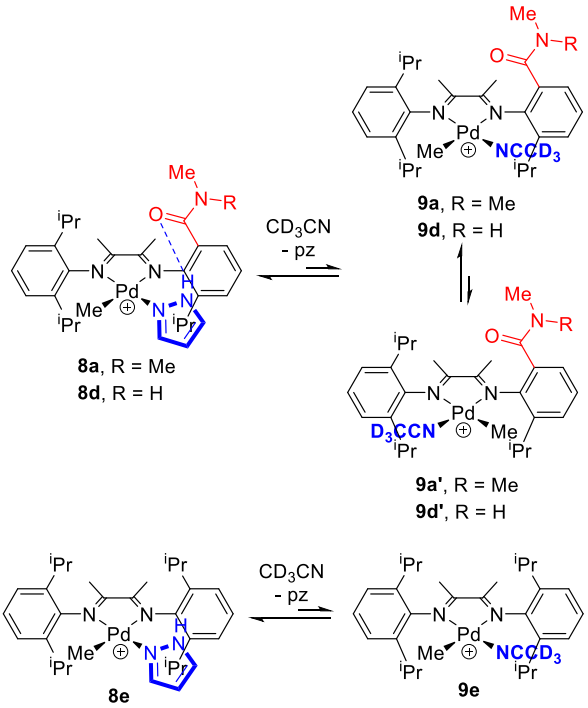

Table 2.1. Equilibrium Constants of Pyrazole Dissociation of (α-Diimine)PdMe(pz)$^+$ Complexes in CD_3CN

Reaction[a,b]	K_{eq} / M[c]
8a ⇌ **9a**/**9a'** + pz	7.7(3) × 10^{-5}
8c-*anti*/**8c-*syn*** ⇌ **9c-*anti***/**9c-*syn*** + pz	3.3(4) × 10^{-5}
8d ⇌ **9d**/**9d'** + pz	3.7(1) × 10^{-4}
8e ⇌ **9e** + pz	4.1(2) × 10^{-3}

[a]Conditions: CD_3CN solvent, room temperature. [b]Isomer ratios at equilibrium are as follows: **9a**/**9a'** = 1.3/1; **8c-*anti***/**8c-*syn*** = 2.0/1; **9c-*anti***/**9c-*syn*** = 1.6/1; **9d**/**9d'** = 1.1/1. [c]Average values from three independent measurements.

Because **9a**,**a'** and **9d**,**d'** exist in two isomeric forms, there is an extra entropic contribution that favors pyrazole dissociation from **8a**,**d** that is not present for **8e**. To circumvent this issue, pyrazole complexes **8c-*anti*,*syn*** were studied (Scheme 2.13). The reaction of pure **5c-*anti*** with $AgSbF_6$ and pyrazole in CD_2Cl_2 at room temperature yields a 13/1 kinetic mixture of isomeric pyrazole adducts **8c-*anti*** and **8c-*syn*** in 5 min, which equilibrates to a 1.5/1 isomer mixture within a few hours. The pyrazole ^{1}H NMR NH resonances (δ 14.42, broad singlet, **8c-*anti*** and **8c-*syn***, CD_2Cl_2 solvent) and thin-film IR ν_{N-H} stretching band (3131 cm^{-1}) of the **8c-*anti*/8c-*syn*** mixture establish the presence of intramolecular N–H···O hydrogen bond. **8c-*anti*,*syn*** undergoes partial pyrazole dissociation in CD_3CN to yield a mixture of CD_3CN adduct **9c-*anti*** and **9c-*syn*** (Scheme 2.14; equilibrium ratio 1.6/1) and a mixture of **8c-*anti*** and **8c-*syn*** (equilibrium ratio 2.0/1). The apparent pyrazole dissociation constant for **8c**, K_{eq} = [**9c-*anti*,*syn***][pz][**8c-*anti*,*syn***]$^{-1}$, was measured by ^{1}H NMR (Table 2.1) and is decreased by a factor of 2 compared to the K_{eq} value for **8a**. The lower value of K_{eq} for **8c** versus **8a** reflects the fact that both **8c** and its pyrazole dissociation product **9c** exist as two isomers, so that the entropic factor that contributes to the K_{eq} for pyrazole dissociation from **8a** is absent. The intramolecular hydrogen bonding in **8c** strengthens pyrazole binding by a factor of ca. 120 (i.e., $\Delta\Delta G$ = 2.8(1) kcal mol^{-1}) relative to the case of **8e**.

Scheme 2.13

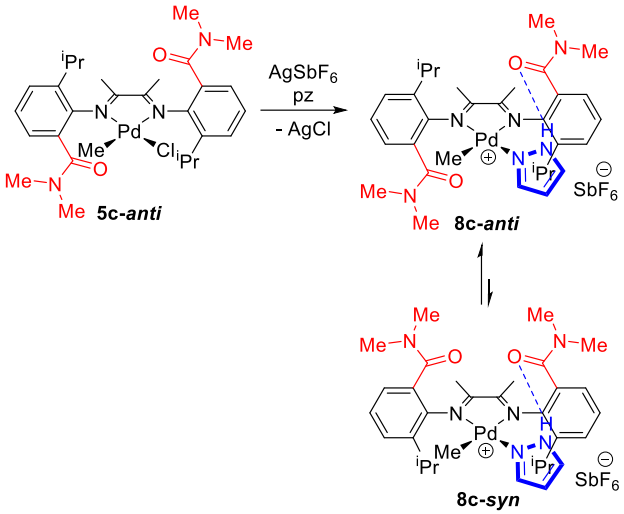

Scheme 2.14. Anion = SbF_6^-.

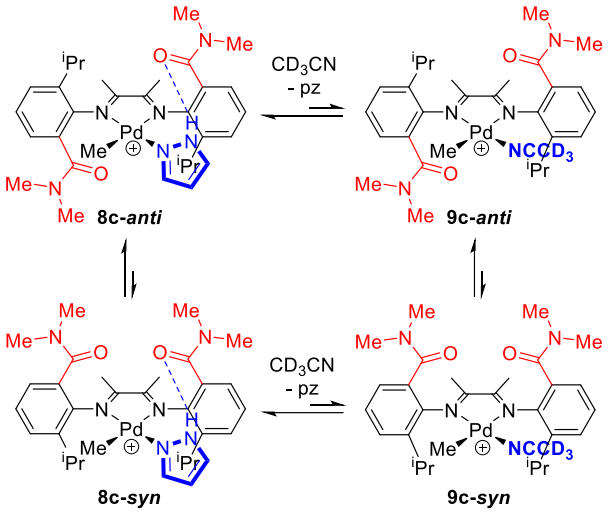

2.3 Conclusions

Hydrogen bonding interactions involving amide substituents on the N-aryl rings of (*N,N'*-diaryl-α-diimine)Pd complexes strongly influence the structures and ligand coordination behavior of (*N,N'*-diaryl-α-diimine)PdMeX and (*N,N'*-diaryl-α-diimine)PdMeL$^+$ complexes. The tertiary amide –C(=O)NMe_2 group is a good hydrogen bond acceptor, whereas the secondary amide –

C(=O)NHMe group behaves as an acceptor or a donor. In the solid state, the amide oxygen atoms in **6c-*anti*** and **5c-*syn*** engage in hydrogen bonding with co-crystallized CH_2Cl_2 solvent molecules. Intramolecular hydrogen bonding influences the equilibrium isomer ratios of unsymmetrical (α-diimine)PdMeX and (α-diimine)PdMeL$^+$ complexes due to selective stabilization of the isomer that can engage in hydrogen bonding, and leads to the greater ratio for **5d**/**5d'** versus the non-hydrogen bonded **5a**/**5a'** and the observation of a single isomer for the cases of acetate **7d** and pyrazole complexes **8a**,**d**. The pyrazole dissociation constants in CD_3CN, K_{eq} = [(α-diimine)PdMe(CD_3CN)$^+$][pz][(α-diimine)PdMe(pz)$^+$]$^{-1}$, vary in the order **8e** > **8d** > **8a** > **8c**, span more than two orders of magnitude, and reflect the enhancement of pyrazole binding in **8a**,**c**,**d** by amide-pyrazole hydrogen bonding. The intramolecular hydrogen bonding in **8c** strengthens pyrazole binding by a factor of ca. 120 (i.e., $\Delta\Delta G$ = 2.8(1) kcal mol^{-1}) relative to the case of **8e**. Future studies will explore the influence of hydrogen bonding on the behavior of amide-functionalized (*N,N'*-diaryl-α-diimine)Pd complexes in olefin polymerization and other catalytic reactions.

2.4 Experimental Section

General Procedures. All manipulations of organometallic compounds were performed under nitrogen or vacuum using Schlenk or high-vacuum techniques or in a nitrogen-filled drybox unless otherwise indicated. Nitrogen was purified by passage through activated molecular sieves and Q–5 oxygen scavenger. Hexanes, benzene, and toluene were purified by passage through activated alumina and BASF R3–11 oxygen scavenger. THF, CH_2Cl_2, and Et_2O were purified by passage through activated alumina. All workup and purification procedures for organic compounds were carried out with reagent grade solvents in air. $CDCl_3$ and CD_2Cl_2 were distilled from P_2O_5

and stored under vacuum. $CDCl_2CDCl_2$ was distilled from P_2O_5 and stored under N_2. CD_3CN was distilled from CaH_2 and stored under N_2. Toluene-d_8 was purchased from Cambridge Isotope Laboratories and used as received. 3-Isopropylanthranilic acid (**1**),[33] *N,N,N',N'*-tetramethyl-2-nitroisophthalamide,[35] α-ketaimine **3**,[34] (cod)PdMeCl (cod = 1,5-cyclooctadiene),[48] complex **5e**,[49] and $AgO_2{}^{13}CCH_3$[50] were synthesized by literature procedures or modifications thereof.

NMR spectra were recorded on a Bruker DRX-500 spectrometer in Teflon-valved tubes at ambient temperature unless otherwise indicated. ^1H and ^{13}C chemical shifts are reported relative to $SiMe_4$ and were determined by reference to the residual ^1H and ^{13}C solvent resonances. ^{19}F NMR spectra were referenced externally to $CFCl_3$ (δ 0). Coupling constants are given in hertz (Hz). NMR assignments were made with the aid of COSY, NOESY, HMQC, and HMBC experiments. For all compounds containing *N*,*N*-dimethylbenzamide groups, the ^{13}C NMR resonances at δ ca. 39.5 and 35.0 were assigned to the amide N–Me groups that are trans and cis to O, respectively.[51]

Elemental analyses were performed by Robertson Microlit Laboratories (Ledgewood, NJ) or Columbia Analytical Services (Tucson, AZ). Infrared spectra were recorded on thin-film solid samples on NaCl plates using a Nicolet NEXUS 470 FT-IR spectrometer. Mass spectrometry was performed on an Agilent 6130 LC-mass spectrometer (low resolution) or an Agilent 6224 Tof-mass spectrometer (high resolution). The listed *m*/*z* value corresponds to the most intense peak in the isotope pattern.

2-Amino-3-isopropyl-*N*,*N*-dimethylbenzamide (2-NH_2-3-^{i}Pr-PhC(=O)NMe_2, 2a). A 500 mL round bottom flask was charged with 3-isopropylanthranilic acid (**1**, 9.45 g, 52.7 mmol), benzene (120 mL) and thionyl chloride (20 mL). The yellow suspension was refluxed for 19 h under air to give an orange solution. The volatiles were removed under vacuum to form the crude acyl chloride as a red oil. The oil was dissolved in dry THF (100 mL) and added dropwise to an

aqueous Me_2NH solution (28 mL, 40 wt. %, 4.2 equiv) at 0 °C. The mixture was warmed to room temperature, stirred for additional 40 min and quenched with water (ca. 100 mL). The THF was removed on a rotovap. The aqueous residue was extracted with EtOAc. The organic phase was washed with aqueous $NaHCO_3$ solution and brine, dried with anhydrous $MgSO_4$, filtered, and concentrated to give a dark red oil. The residue was subjected to flash column chromatography (silica, hexanes/EtOAc/Et_3N = 82/14/5 to 71/24/5 by volume) and concentrated to give an orange oil, which crystallized at –30 °C after 1 day. The resultant solid was washed with hexanes to yield a pale yellow powder (7.04 g, 64%). ^{1}H NMR (500 MHz, $CDCl_3$): δ 7.16 (dd, *J* = 7.7, 1.4, 1H, Ar), 6.96 (dd, *J* = 7.6, 1.5, 1H, Ar), 6.74 (t, *J* = 7.6, 1H, Ar), 4.38 (br s, 2H, NH_2), 3.06 (br s, 6H, amide NMe), 2.90 (septet, *J* = 6.8, 1H, ^{i}Pr), 1.27 (d, *J* = 6.8, 6H, ^{i}Pr). ^{13}C{^{1}H} NMR (126 MHz, $CDCl_3$): δ 171.6 (C=O), 142.2, 133.5, 126.4, 125.3, 120.4, 117.2 (Ar), 39.4 (br, amide NMe), 34.9 (br, amide NMe), 27.5 (^{i}Pr methine), 22.2 (^{i}Pr methyl). IR (cm^{-1}): $\nu_{N–H}$, 3459, 3364; $\nu_{C=O}$, 1611. HRMS (APCI-TOF, positive ion, *m*/*z*): Calc. 207.1497 ([M + H]$^+$), found 207.1497.

(a)

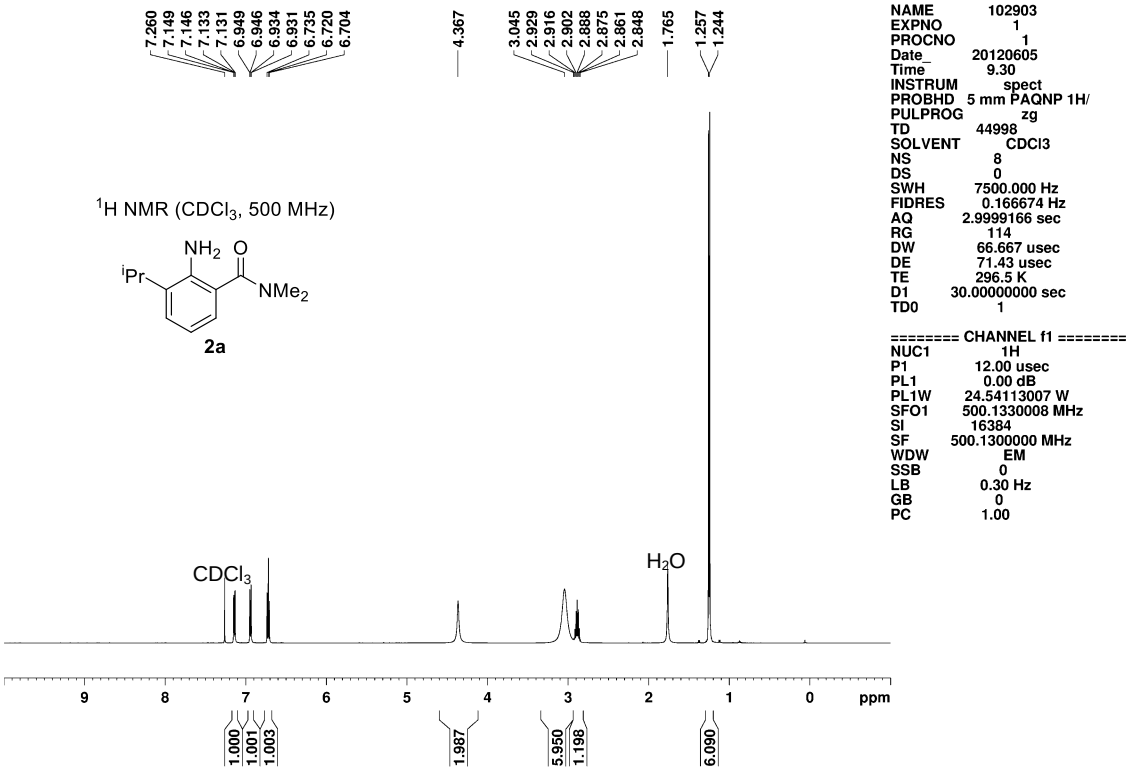

(b)

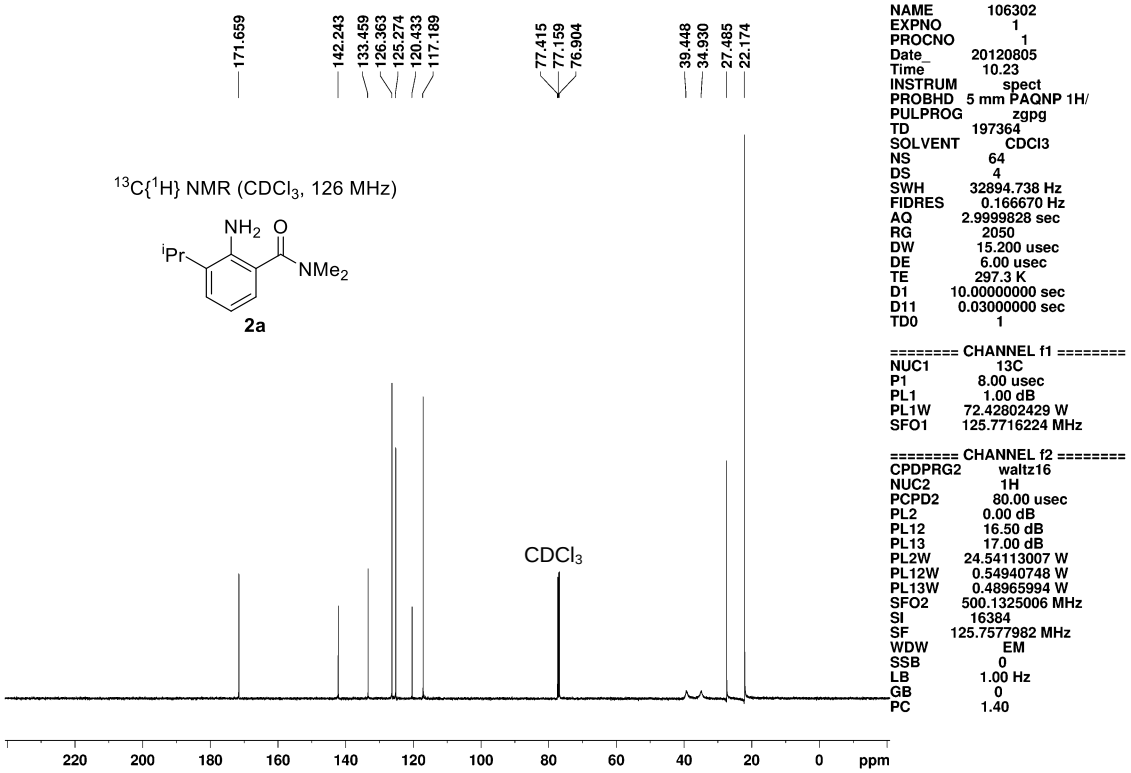

Figure 2.10. NMR spectra of **2a**.

2-Amino-*N,N,N',N'*-tetramethylisophthalamide (2b).[35] *N,N,N',N'*-Tetramethyl-2-nitroisophthalamide (5.47 g, 20.6 mmol) and iron powder (4.14 g, 3.6 equiv) were suspended in ^{i}PrOH (30 mL), and the mixture was heated to reflux under air. An aqueous NH_4Cl solution (1.23 g in 20 mL water, 1.1 equiv) was added to the reaction mixture during reflux. The mixture turned rust-colored instantly and was refluxed for additional 22.5 h. The mixture was vacuum-filtered through a Büchner funnel to remove most of the iron powder. The ^{i}PrOH were removed on a rotovap. The remaining aqueous fraction was then filtered through a pad of Celite to give a yellow solution. The solution was diluted to 300 mL, treated with Na_2CO_3, and extracted with CH_2Cl_2. The organic phase was washed with brine, dried with anhydrous $MgSO_4$, filtered, and concentrated to give white microcrystals (3.21 g, 66%). ^{1}H NMR (500 MHz, $CDCl_3$): δ 7.12 (d, J = 7.6, 2H, Ar), 6.70 (t, J = 7.6, 1H, Ar), 4.37 (br s, 2H, NH_2), 3.05 (br s, 12H, amide NMe). ^{13}C{^{1}H} NMR (126 MHz, $CDCl_3$): δ 170.5 (C=O), 143.5, 129.4, 122.0, 116.6 (Ar), 39.5 (br, amide NMe), 35.4 (br, amide NMe). IR (cm^{-1}): ν_{N-H}, 3481, 3370; $\nu_{C=O}$, 1622. HRMS (ESI-TOF, positive ion, *m*/*z*): Calc. 236.1399 ($[M + H]^+$), found 236.1400.

(a)

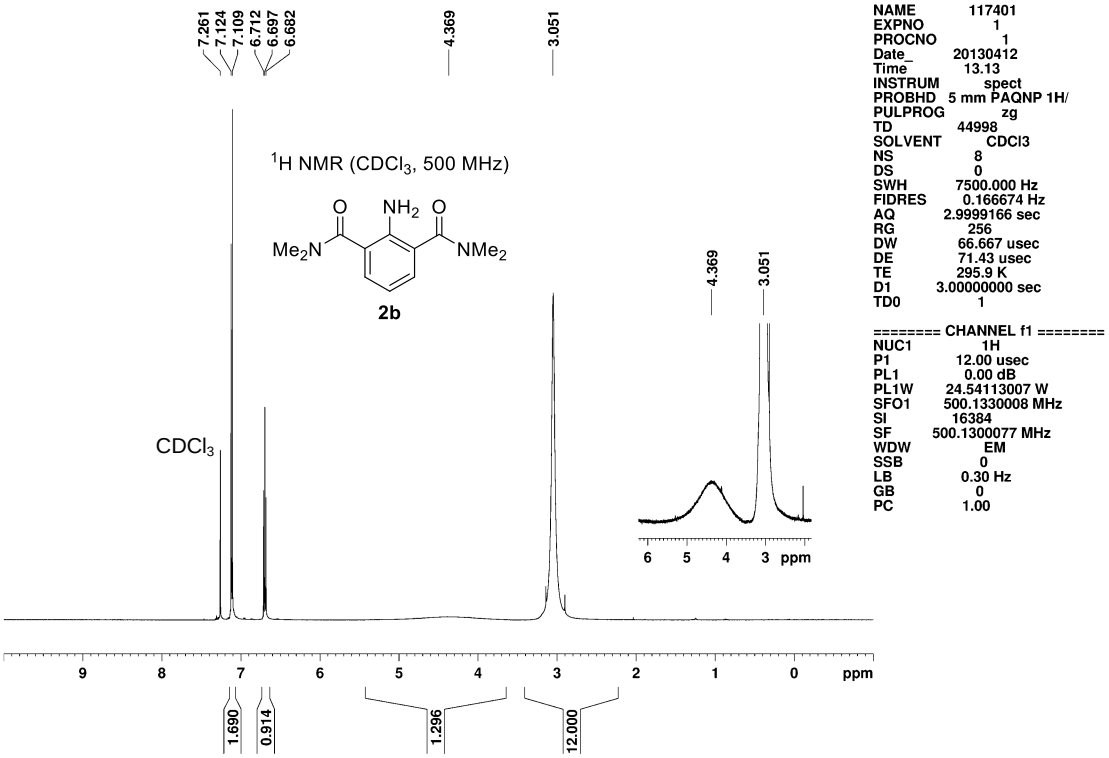

(b)

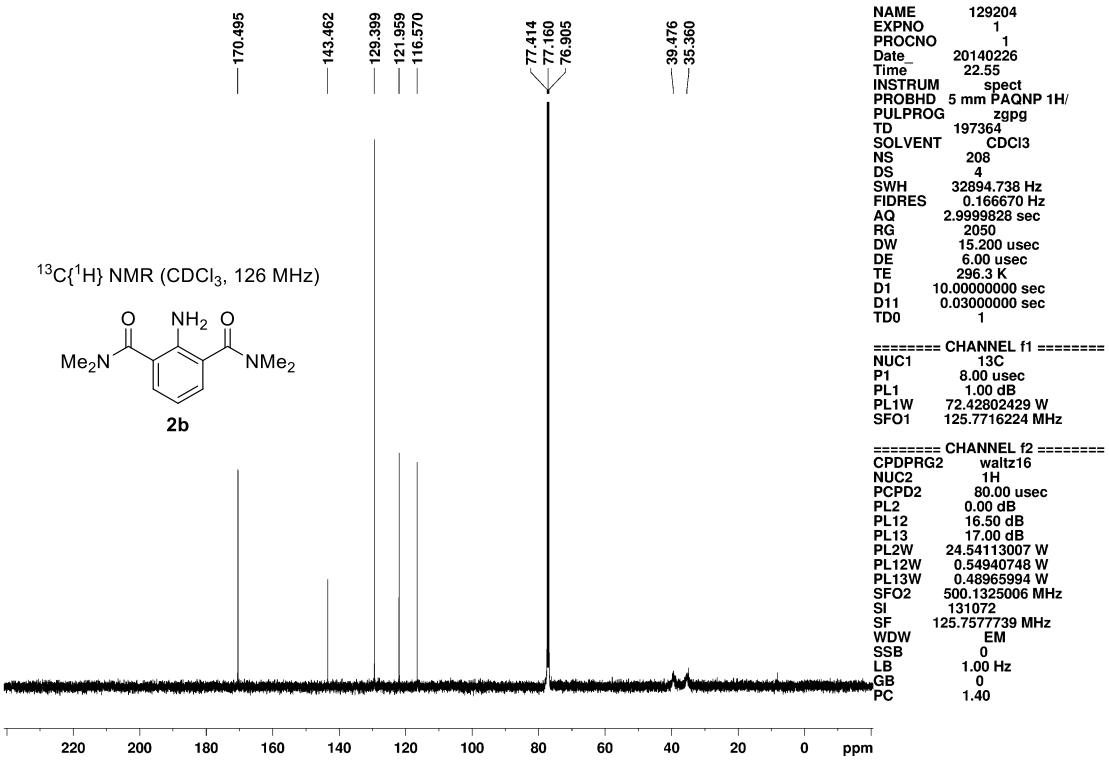

Figure 2.11. NMR spectra of **2b**.

2-Amino-3-isopropyl-*N*-methylbenzamide (2-NH_2-3-^{i}Pr-PhC(=O)NHMe, 2d). A 500 mL round bottom flask was charged with 3-isopropylanthranilic acid (**1**, 10.0 g, 55.8 mmol), benzene (150 mL), and thionyl chloride (25 mL). The yellow suspension was refluxed for 2.5 h under air to give an orange solution. The volatiles were removed under vacuum to yield the crude acyl chloride as a red oil. The oil was dissolved in dry THF (100 mL) and added dropwise to a mixture of $MeNH_2$ solution in THF (60 mL, 2.0 M, 2.2 equiv) and Et_3N (16.7 mL, 2.15 equiv) at 0 °C. The mixture was stirred at 0 °C for additional 10 min and at room temperature for 20 min and quenched with water (ca. 100 mL). The THF was removed on a rotovap. The aqueous residue was extracted with EtOAc. The organic phase was washed with brine, dried with anhydrous $MgSO_4$, filtered, and concentrated to give an orange oil. The residue was subjected to flash column chromatography (silica, hexanes/EtOAc/Et_3N = 82/14/5 by volume), concentrated, and washed with hexanes to yield pale yellow needles (7.48 g, 70%). ^{1}H NMR (500 MHz, $CDCl_3$): δ 7.21 (dd, *J* = 7.6, 1.1, 1H, Ar), 7.18 (dd, *J* = 7.8, 1.3, 1H, Ar), 6.67 (t, *J* = 7.7, 1H, Ar), 6.03 (br s, 1H, amide NH), 5.68 (br s, 2H, NH_2), 2.97 (d, *J* = 4.9, 3H, amide NMe), 2.90 (septet, *J* = 6.8, 1H, ^{i}Pr), 1.26 (d, *J* = 6.8, 6H, ^{i}Pr). ^{13}C{^{1}H} NMR (126 MHz, $CDCl_3$): δ 170.9 (C=O), 145.5, 133.7, 128.1, 124.9, 116.7, 116.4 (Ar), 27.3 (^{i}Pr methine), 26.6 (amide NMe), 22.1 (^{i}Pr methyl). IR (cm^{-1}): ν_{N-H}, 3454, 3348; $\nu_{C=O}$, 1610. HRMS (ESI-TOF, positive ion, *m*/*z*): Calc. 193.1341 ([M + H]$^+$), found 193.1312.

(a)

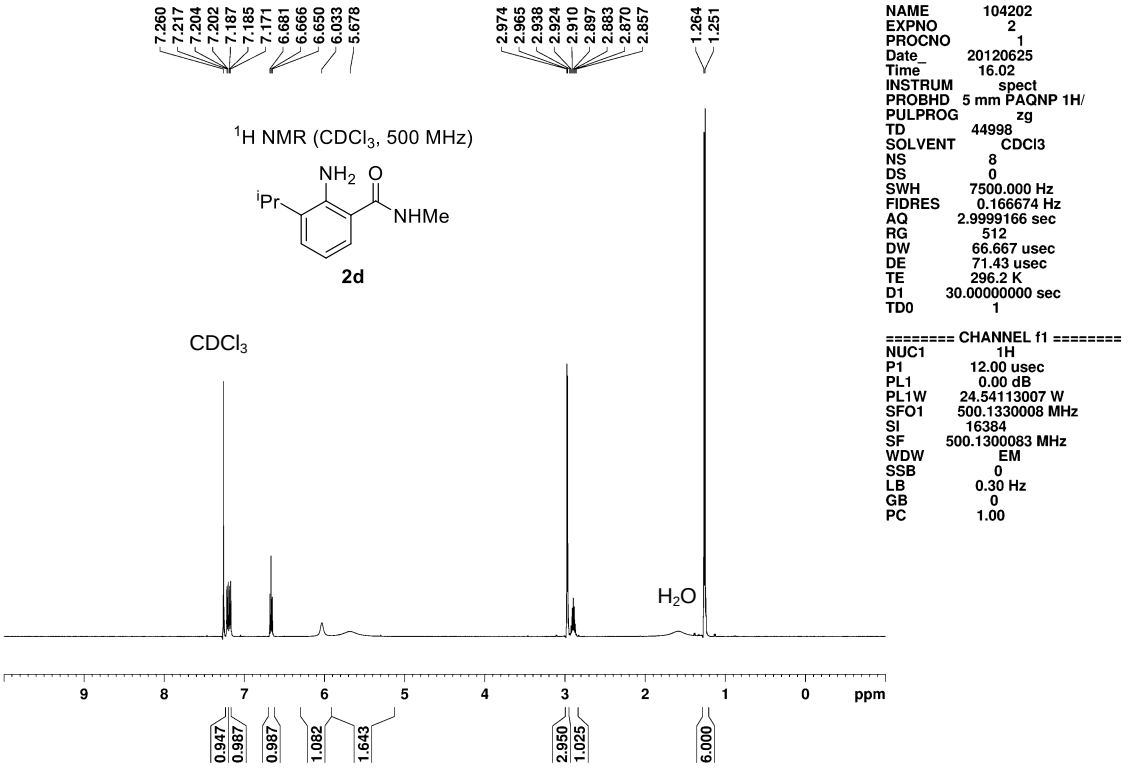

(b)

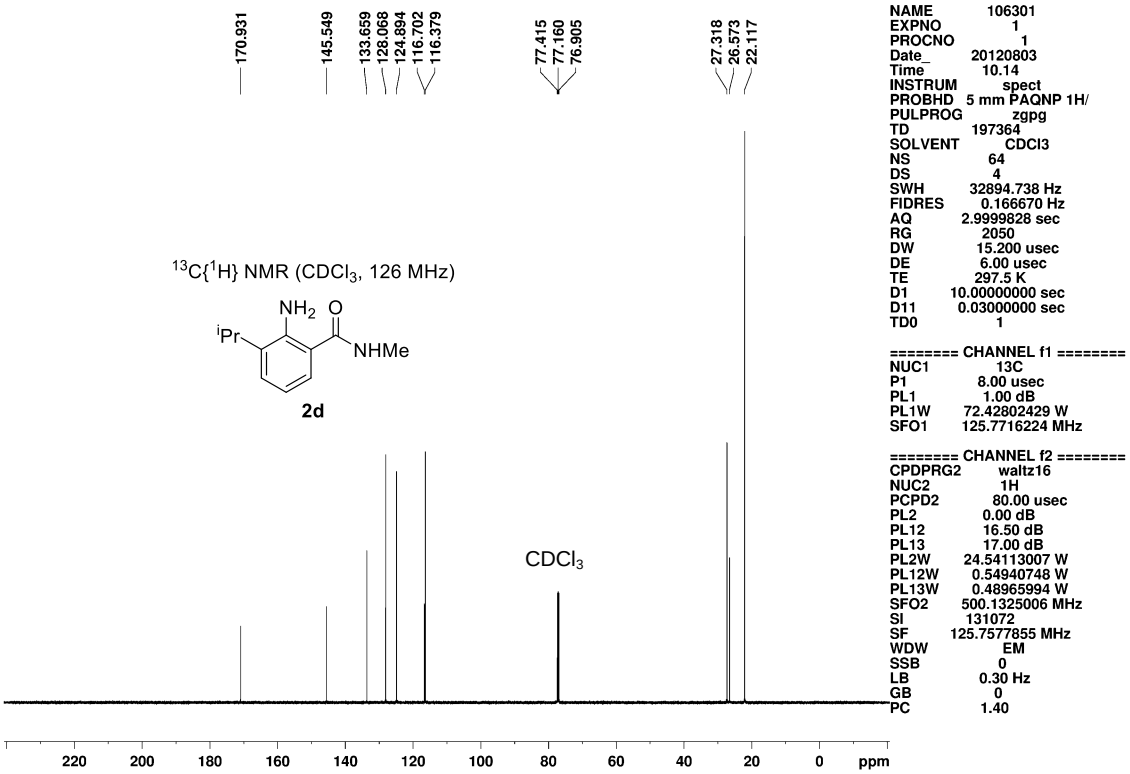

Figure 2.12. NMR spectra of **2d**.

(2,6-^{i}Pr$_2$-Ph)N=CMeCMe=N(2-C(=O)NMe$_2$-6-^{i}Pr-Ph) (4a). A Schlenk flask was charged with **3** (2.45 g, 10.0 mmol), **2a** (2.17 g, 10.5 mmol, 1.05 equiv), a small amount of anhydrous TsOH (ca. 100 mg), and benzene (100 mL) under nitrogen. The flask was equipped with a Dean-Stark trap filled with 3 Å molecular sieves and a water condenser. The mixture was refluxed under nitrogen for 40 h, then cooled to room temperature, and quenched with Et_3N (ca. 5 mL). The volatiles were removed under vacuum to give a brown oil. The oil was subjected to flash column chromatography (silica, hexanes/CH_2Cl_2/Et_3N = 80/20/0.5 by volume) and concentrated to give a yellow oil, which crystallized at –30 °C to give yellow granular crystals. Yield: 1.65 g (53%). ^{1}H NMR (500 MHz, CD_2Cl_2): δ 7.37–7.33 (m, 1H, Ar), 7.16–7.13 (m, 4H, Ar), 7.07 (dd, *J* = 8.0, 7.3, 1H, Ar), 2.94 (s, 3H, H^7), 2.83 (s, 3H, H^6), 2.83 (septet, *J* = 6.8, 1H, ^{i}Pr methine), 2.67 (septet, *J* = 6.8, 1H, ^{i}Pr methine), 2.62 (septet, *J* = 6.8, 1H, ^{i}Pr methine), 2.07 (s, 3H, H^1), 1.96 (s, 3H, H^2), 1.22 (d, *J* = 6.8, 3H, ^{i}Pr), 1.18 (d, *J* = 6.8, 3H, ^{i}Pr), 1.17 (d, *J* = 6.8, 6H, ^{i}Pr), 1.14 (d, *J* = 6.8, 6H, ^{i}Pr). ^{13}C{^{1}H} NMR (126 MHz, CD_2Cl_2): δ 170.3 (C^4), 169.9 (C^3), 168.1 (C^5), 146.5, 145.0, 137.0, 135.40, 135.36, 126.6, 126.5, 125.0, 124.4, 124.2, 123.4, 123.3 (Ar), 38.1 (C^6), 34.6 (C^7), 29.0, 28.9, 28.7 (^{i}Pr methine), 23.4, 23.2, 23.0, 22.8 (2C), 22.7 (^{i}Pr methyl), 17.2 (C^1), 16.6 (C^2). IR (cm^{-1}): $\nu_{C=N+C=O}$, 1645. HRMS (ESI-TOF, positive ion, *m*/*z*): Calc. 456.2991 ([M + Na]$^+$), found 456.3014.

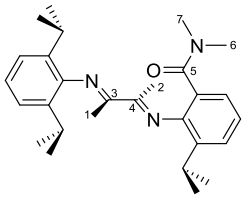

(a)

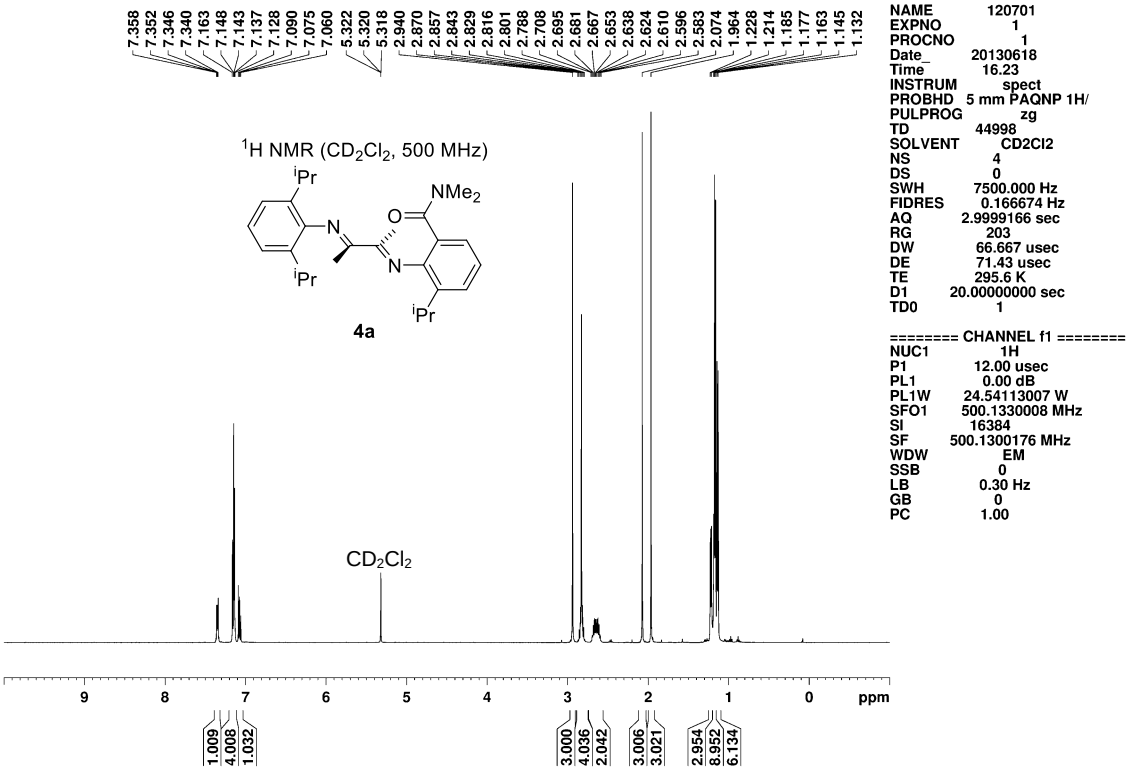

(b)

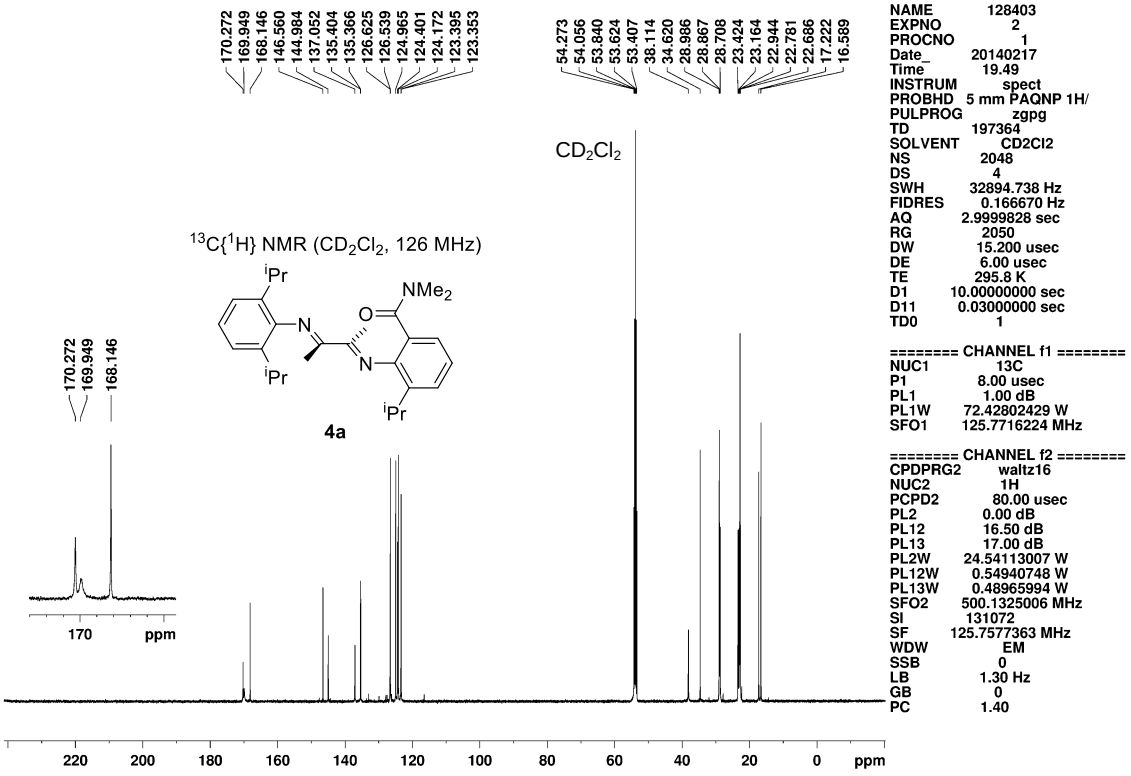

Figure 2.13. NMR spectra of **4a**.

(2,6-^{i}Pr$_2$-Ph)N=CMeCMe=N(2,6-(C(=O)NMe$_2$)$_2$-Ph) (4b). A 100 mL Schlenk flask was charged with **3** (1.37 g, 55.9 mmol), **2b** (1.43 g, 60.9 mmol, 1.1 equiv), a small amount of TsOH·H_2O (ca. 50 mg), and benzene (40 mL) under nitrogen. The flask was equipped with a Dean-Stark trap containing 3 Å molecular sieves and a water condenser. The mixture was refluxed under nitrogen for 20 h, then cooled to room temperature, and quenched with Et_3N (ca. 5 mL). The solvent was removed under vacuum to afford a dark oil. The oil was subjected to flash column chromatography (silica, hexanes/CH_2Cl_2/Et_3N = 49/49/1 by volume) and concentrated to give a yellow powder (1.69 g, 65%). ^{1}H NMR (500 MHz, CD_2Cl_2): δ 7.36 (d, *J* = 7.6, 2H, Ar), 7.23 (t, *J* = 7.6, 1H, Ar), 7.15 (d, *J* = 7.4, 2H, Ar), 7.08 (dd, *J* = 8.4, 6.9, 1H, Ar), 2.97 (s, 6H, H^7), 2.88 (s, 6H, H^6), 2.60 (septet, *J* = 6.9, 2H, ^{i}Pr methine), 2.11 (s, 3H, H^1), 1.88 (s, 3H, H^2), 1.15 (d, *J* = 6.9, 6H, ^{i}Pr), 1.13 (d, *J* = 6.8, 6H, ^{i}Pr). ^{13}C{^{1}H} NMR (126 MHz, CD_2Cl_2): δ 171.4 (C^3), 169.1 (C^5), 167.8 (C^4), 146.3, 143.4, 135.3, 128.1, 127.6, 124.7, 124.3, 123.4 (Ar), 38.1 (C^6), 34.6 (C^7), 28.7 (^{i}Pr methine), 23.3, 22.9 (^{i}Pr methyl), 17.5 (C^1), 16.6 (C^2). Key ^{1}H–^{13}C HMQC correlations (CD_2Cl_2): δ/δ 2.97/34.6 (H^7/C^7), 2.88/38.1 (H^6/C^6), 2.11/17.5 (H^1/C^1), 1.88/16.6 (H^2/C^2). IR (cm^{-1}): $\nu_{C=N+C=O}$, 1645. HRMS (ESI-TOF, positive ion, *m*/*z*): Calc. 463.3073 ([M + H]$^+$), found 463.3044.

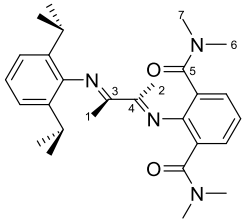

(a)

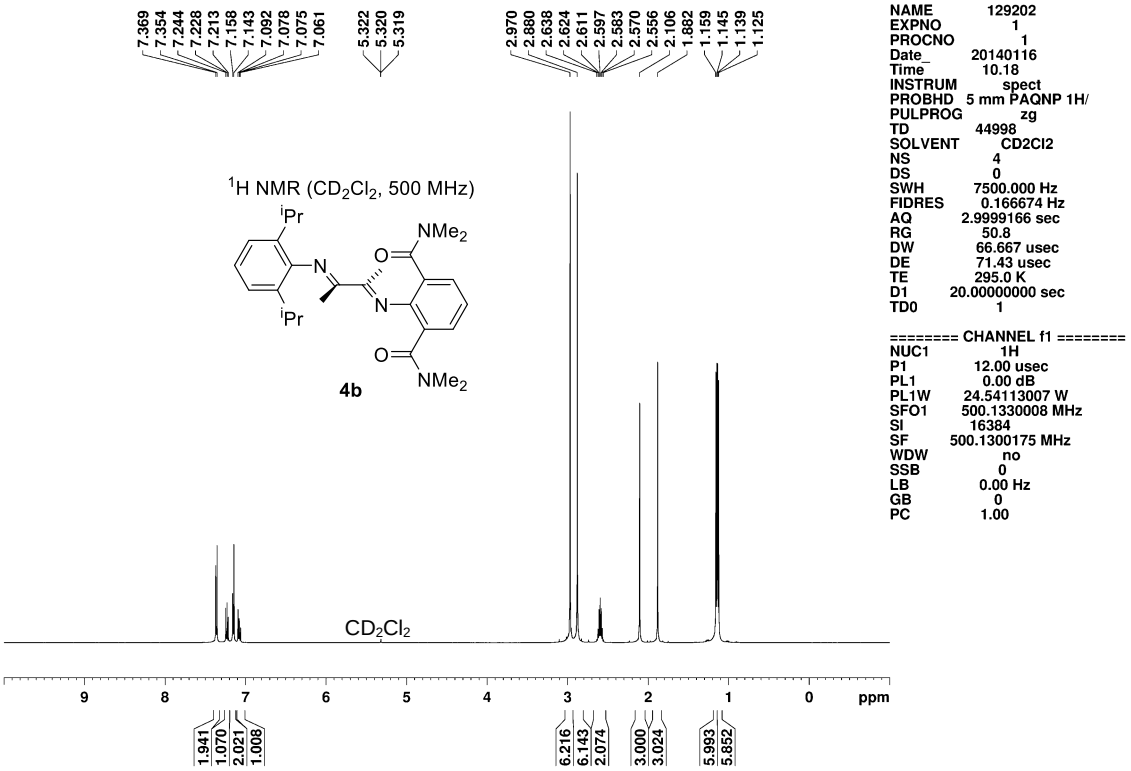

(b)

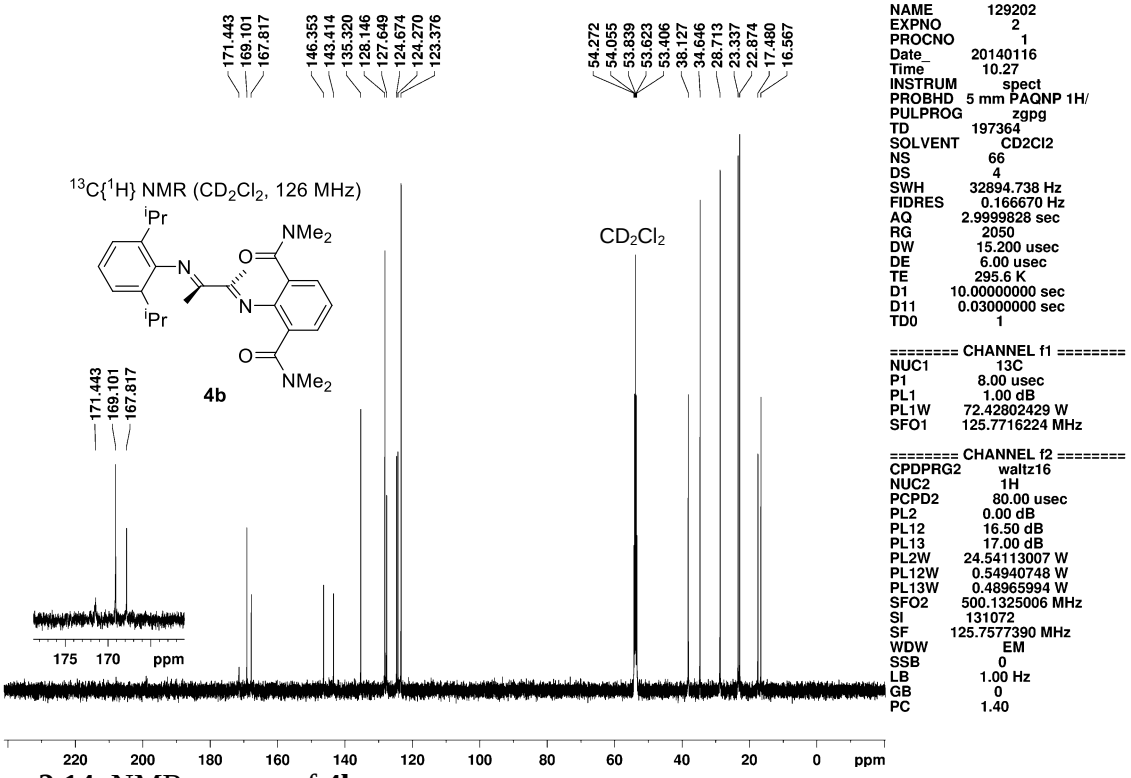

Figure 2.14. NMR spectra of **4b**.

Dynamics of Amide NMe Exchange of 4b. A J. Young NMR tube was charged with **4b** (9 mg) and toluene-d_8 (0.5 mL) under nitrogen to give a pale yellow homogeneous solution. The tube was sealed and subjected to variable temperature ^{1}H NMR. Spectra are shown in Figure 2.15.

Scheme 2.15. **Labeling for Amide NMe Permutation of 4b**

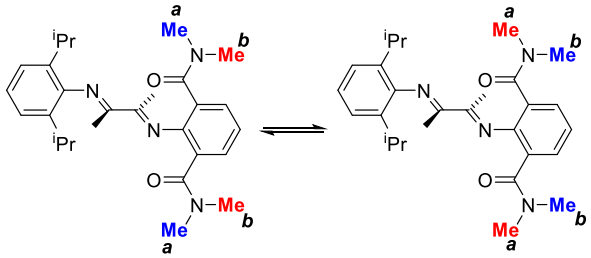

NMR spectral simulations were performed using gNMR v.5.0.6. Simulations of the amide N*Me* resonances of **4b** were performed as follows. The chemical shifts observed in the slow exchange limit (10 °C) were used to set up the spin system. The natural line width in the absence of exchange, 1.2 Hz, was measured at 10 °C for the N*Me* resonance at δ 2.74 and confirmed by observation of the same line width at 0 °C. The septet for ^{i}Pr methine hydrogens at δ 2.7 was excluded from the simulations. The exchange rate constants and the chemical shifts were varied to get the best fit for the amide N*Me* resonances between the simulated and the experimental spectra. Above 60 °C, the chemical shifts were estimated by linear extrapolation using data from 30 to 50 °C. The Eyring plot for this dynamic process is shown in Figure 2.16. The activation parameters are: $\Delta H^{\ddagger}$ = 18.4(3) kcal mol^{-1}; $\Delta S^{\ddagger}$ = 6.4(10) eu; $\Delta G^{\ddagger}_{20°C}$ = 16.5(4) kcal mol^{-1}.

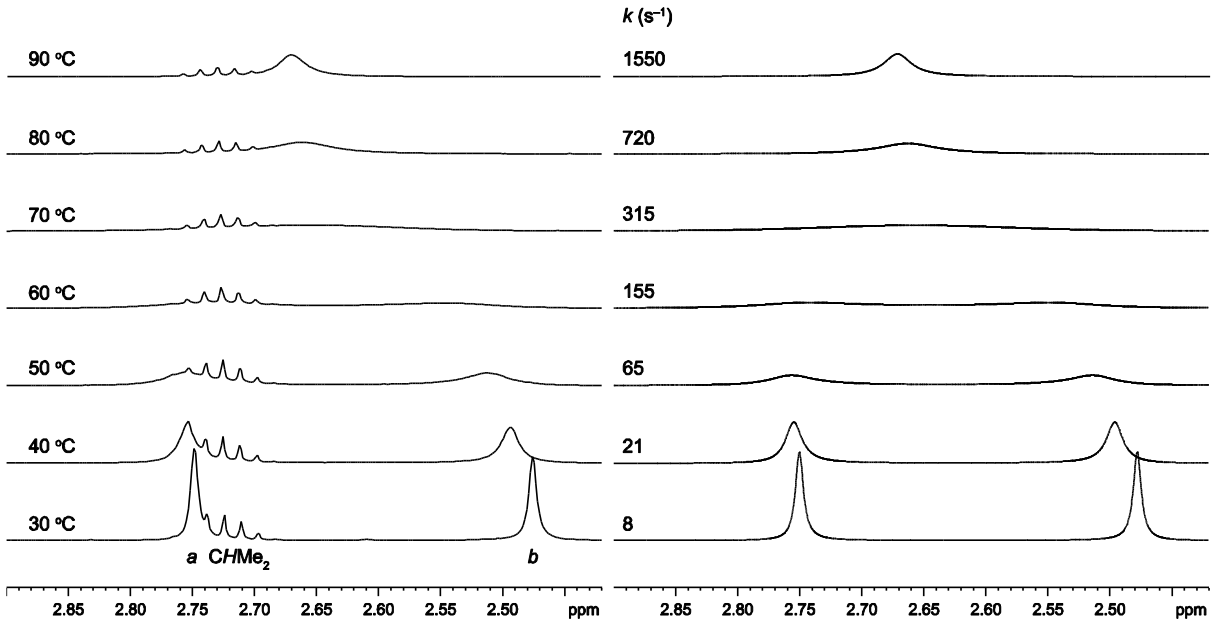

Figure 2.15. Variable temperature ^{1}H NMR spectra of **4b** in toluene-d_8 (30 to 90 °C, 500 MHz). The δ 2.90–2.35 region is shown. Left: experimental spectra. Right: simulated spectra (gNMR). The labeling scheme is shown in Scheme 2.15. First-order rate constants (s^{-1}) determined by simulation are shown for each temperature.

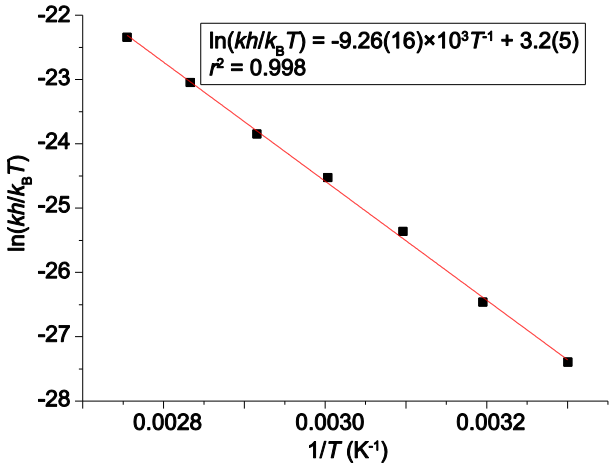

Figure 2.16. Eyring plot of amide N*Me* exchange of **4b** in toluene-d_8.

(2-C(=O)NMe$_2$-6-^{i}Pr-Ph)N=CMeCMe=N(2-C(=O)NMe$_2$-6-^{i}Pr-Ph) (4c-*anti*,*syn*). A Schlenk flask was charged with 2,3-butanedione (1.7 mL, 19 mmol), **2a** (8.38 g, 40.6 mmol, 2.1 equiv), TsOH·H_2O (250 mg), and benzene (150 mL) under nitrogen. The flask was equipped with a Dean-Stark trap containing 3 Å molecular sieves and a water condenser. The mixture was refluxed under nitrogen for 65 h. The mixture was cooled to room temperature and quenched with Et_3N (ca. 5 mL). The volatiles were removed under vacuum to give a brown solid. The solid was recrystallized from hexanes/CH_2Cl_2 to give yellow brownish microcrystals. The crystals were collected by vacuum filtration, washed with cold acetone and dried under vacuum to give light yellow crystals. Yield: 3.80 g (43%). The equilibrium **4c-*anti***/**4c-*syn*** ratio in CD_2Cl_2, $CDCl_3$, and toluene-d_8 solution at room temperature is 1.4/1. **4c-*anti***: ^{1}H NMR (500 MHz, CD_2Cl_2): δ 7.34–7.33 (br m, 2H, Ar), 7.16–7.10 (br m, 4H, Ar), 2.92 (br s, 6H, H^5), 2.81 (br s, 6H, H^4), 2.77 (septet, *J* = 6.9, 2H, ^{i}Pr methine), 2.00 (br s, 6H, H^1), 1.22–1.19 (br m, 6H, ^{i}Pr), 1.17–1.14 (br m, 6H, ^{i}Pr). ^{13}C{^{1}H} NMR (126 MHz, CD_2Cl_2): δ 170.4 (C^2), 169.6 (C^3), 144.3, 136.7, 126.4, 126.0, 124.8, 124.5 (Ar), 38.1 (C^4), 34.7 (C^5), 28.5 (^{i}Pr methine), 22.8, 22.7 (^{i}Pr methyl), 17.2 (C^1). **4c-*syn***: ^{1}H NMR (500 MHz, CD_2Cl_2): δ 2.99 (br s, 6H, H^5), 2.81 (br s, 6H, H^4), 2.00 (br s, 6H, H^1). ^{13}C{^{1}H} NMR (126 MHz, CD_2Cl_2): δ 170.2 (C^2), 169.6 (C^3), 144.7, 136.3, 126.3, 126.2, 124.6, 124.4 (Ar), 38.1 (C^4), 34.9 (C^5), 28.7 (^{i}Pr methine), 23.1, 22.8 (^{i}Pr methyl), 17.1 (C^1). IR (cm^{-1}): $\nu_{C=N+C=O}$, 1641. Anal. Calcd. for $C_{28}H_{38}N_4O_2$, %: C, 72.69; H, 8.28; N, 12.11. Found: C, 72.61; H, 7.94; N, 11.76. ESI-MS (1:1 CH_2Cl_2:MeOH, positive ion scan, *m*/*z*): 463.2 ([M + H]$^+$).

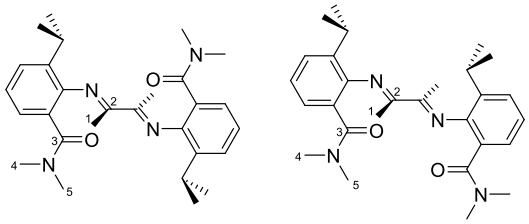

(a)

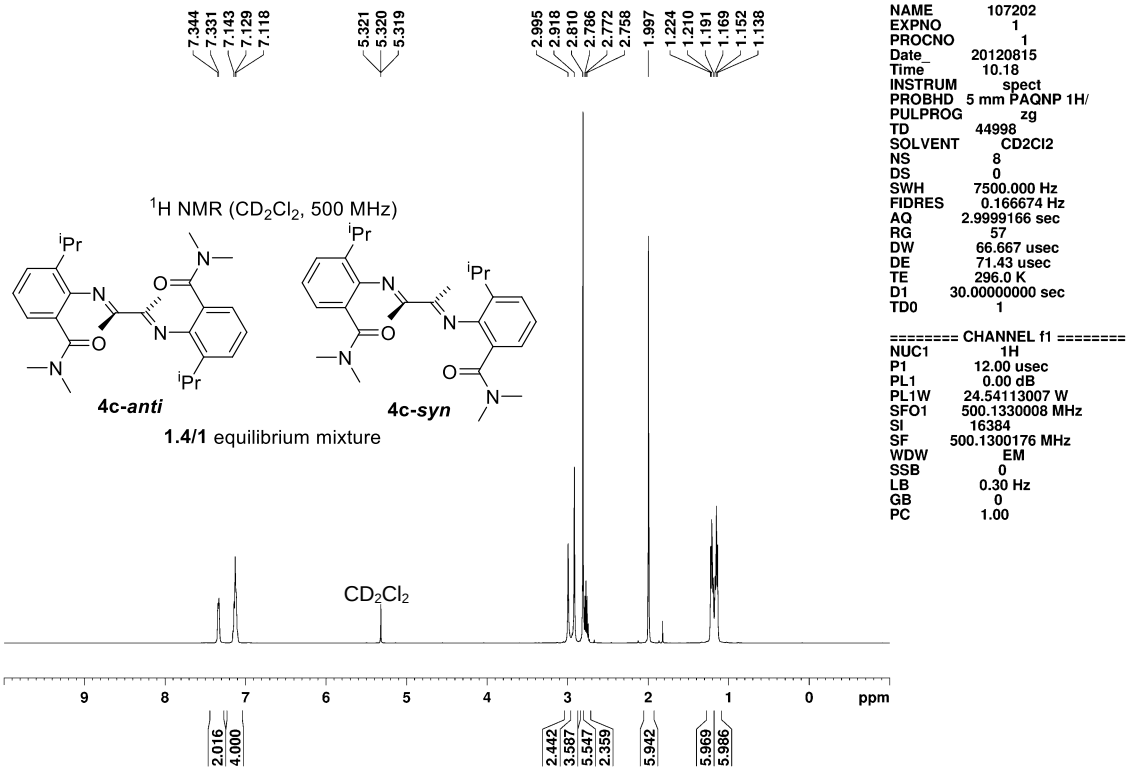

(b)

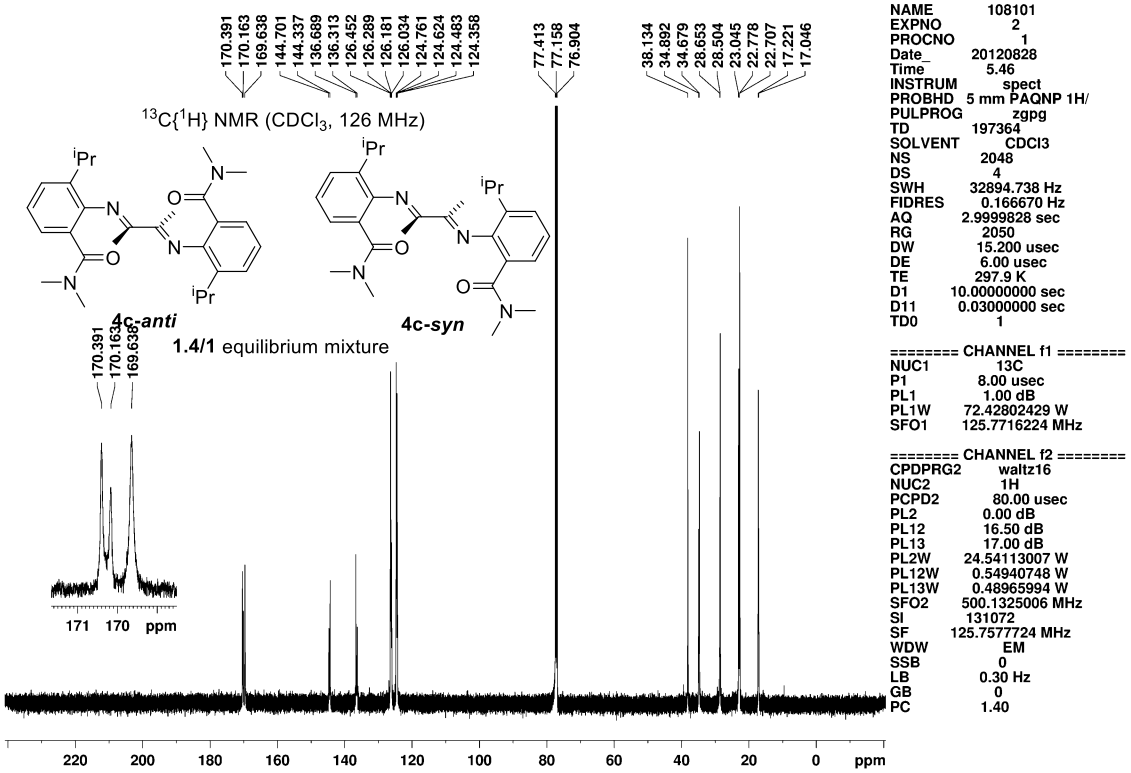

Figure 2.17. NMR spectra of **4c-*anti,syn***.

Dynamics of 4c. A J. Young NMR tube was charged with **4c** (8 mg) and toluene-d_8 (0.5 mL) under nitrogen to give a light yellow homogeneous solution. The tube was sealed and subjected to variable temperature ^{1}H NMR. Spectra are shown in Figure 2.2.

Simulations of the amide N*Me* and *Me*C=N resonances were performed as follows. The chemical shifts observed in the slow exchange limit (10 °C) were used to set up the spin systems for both isomers, and the relative population ratio was fixed at 1.4/1 (concentration of the major isomer = 1.4; concentration of the minor isomer = 1). The natural line width in the absence of exchange, 1.5 Hz, was measured at 10 °C and confirmed by observation of the same line width at 0 °C. The ^{i}Pr methine resonances at ca. δ 2.9 were excluded from the simulations. Below 40 °C, the isomerization rate and the chemical shifts were varied to get the best fit for the *Me*C=N signals (*a*/*a'*) between the simulated and the experimental spectra. The amide N*Me* resonances in the experimental spectra showed more broadening than those simulated by only anti/syn isomerization. Then, the amide N*Me* permutations (*b*/*c* and *b'*/*c'*) were set up and their rates were varied to get the best fit for the amide N*Me* resonances. Above 50 °C, the chemical shifts were estimated by linear extrapolation using data from 10 to 40 °C. The rate constants were calculated from the simulated rates and the concentrations. Eyring plots are shown in Figures 2.18-2.20..

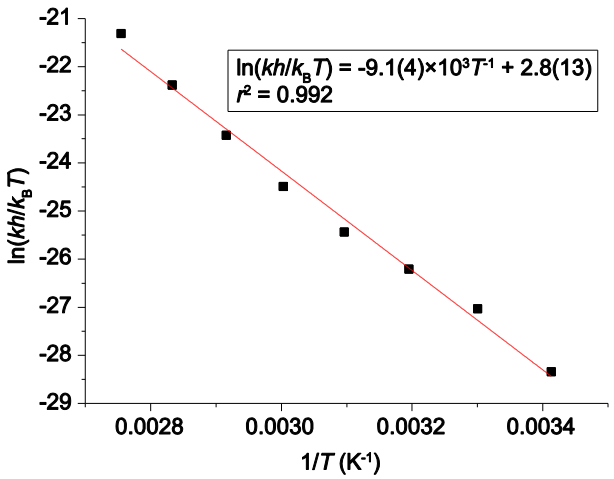

Figure 2.18. Eyring plot for anti/syn isomerization (*a*/*a'* exchange) of **4c** in toluene-d_8. The activation parameters are: $\Delta H^{\ddagger}$ = 18.1(8) kcal mol^{-1}; $\Delta S^{\ddagger}$ = 6(3) eu; $\Delta G^{\ddagger}_{\text{syn}\rightarrow\text{anti},20^{\circ}\text{C}}$ = 16.4(11) kcal mol^{-1}.

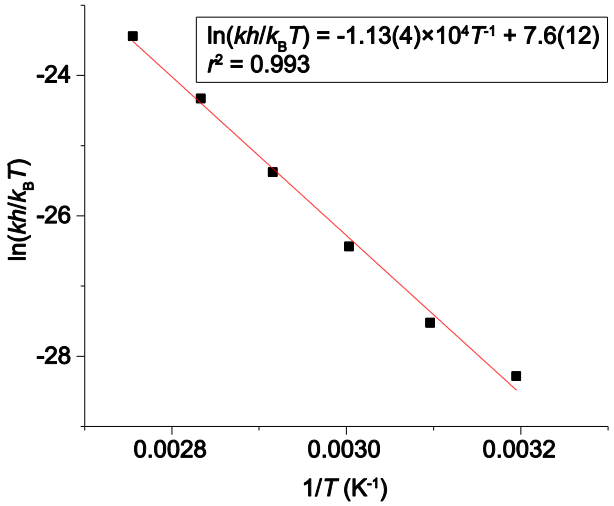

Figure 2.19. Eyring plot for amide N*Me* exchange of **4c-*anti*** (*b*/*c* exchange) in toluene-d_8. The activation parameters are: $\Delta H^{\ddagger}$ = 22.5(8) kcal mol^{-1}; $\Delta S^{\ddagger}$ = 15(2) eu; $\Delta G^{\ddagger}_{b/c,20^{\circ}\text{C}}$ = 18.0(11) kcal mol^{-1}.

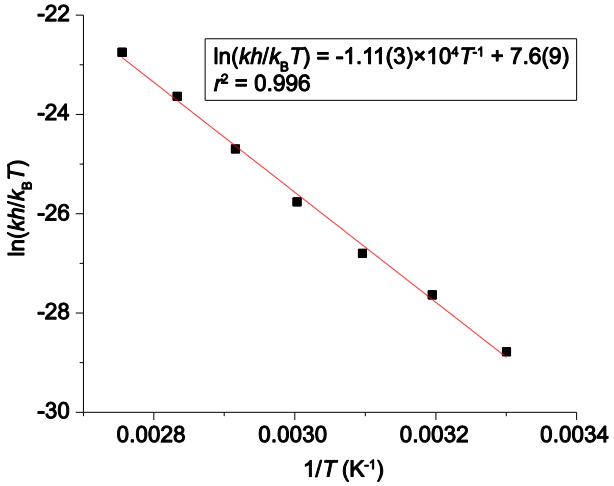

Figure 2.20. Eyring plot for amide N*Me* exchange of **4c**-***syn*** (*b'/c'* exchange) in toluene-d_8. The activation parameters are: $\Delta H^{\ddagger}$ = 22.1(6) kcal mol^{-1}; $\Delta S^{\ddagger}$ = 15(2) eu; $\Delta G^{\ddagger}_{b'/c',20°C}$ = 17.6(8) kcal mol^{-1}.

4d'. A Schlenk flask was charged with **2d** (1.99 g, 9.55 mmol), **3** (3.52 g, 14.3 mmol, 1.5 equiv), and TsOH·H_2O (99 mg, 0.06 equiv) under nitrogen. Benzene (50 mL) was added via cannula. The flask was equipped with a Dean-Stark trap containing 3 Å molecular sieves and a water condenser. The mixture was refluxed under nitrogen for 19.5 h. The mixture was cooled to room temperature and quenched with Et_3N (ca. 5 mL). The volatiles were removed under vacuum to give a brown oil. The oil was triturated with acetone (20 mL), leading to formation of white crystals. The mixture was kept at –30 °C for 2 days and filtered. The crystals were washed with cold acetone and Et_2O. Yield: 1.81 g (46%, 2 crops). ^{1}H NMR (500 MHz, $CDCl_3$): δ 7.83 (dd, *J* = 7.8, 1.1, 1H, Ar), 7.28 (dd, *J* = 7.6, 1.1, 1H, Ar), 7.03–6.97 (m, 3H, Ar), 6.90 (t, *J* = 7.7, 1H, Ar), 5.01 (br, 1H, amine NH), 3.28 (s, 3H, amide NMe), 2.94 (septet, *J* = 6.8, 1H, ^{i}Pr methine), 2.27 (septet, *J* = 6.9, 1H, ^{i}Pr methine), 1.93 (septet, *J* = 6.9, 1H, ^{i}Pr methine), 1.91 (s, 3H, *Me*C=N), 1.68 (s, 3H, C*Me*(N)(N)), 1.26 (d, *J* = 6.8, 3H, ^{i}Pr), 1.24 (d, *J* = 6.8, 3H, ^{i}Pr), 1.01 (d, *J* = 6.8, 3H, ^{i}Pr), 0.95 (d, *J* = 6.9, 3H, ^{i}Pr), 0.87 (d, *J* = 6.8, 3H, ^{i}Pr), 0.81 (d, *J* = 6.9, 3H, ^{i}Pr). ^{13}C{^{1}H NMR

(126 MHz, $CDCl_3$): δ 173.4 (C=N), 164.7 (C=O), 144.8, 142.8, 136.2, 135.8, 133.3, 129.5, 126.6, 123.9, 123.1, 122.9, 120.0, 117.2 (Ar), 76.7 (*C*Me(NH)(NMe)), 29.9 (NMe), 28.1, 27.8, 27.1 (^{i}Pr methine), 25.3 (C*Me*(NH)(NMe)), 23.54, 23.45, 23.35, 22.8, 22.6, 22.3 (^{i}Pr methyl), 16.9 (*Me*C=N). IR (cm^{-1}): ν_{N-H}, 3340; $\nu_{C=N+C=O}$, 1633. HRMS (ESI-TOF, positive ion, *m*/*z*): Calc. 420.3015 ($[M + H]^+$), found 420.3012.

(a)

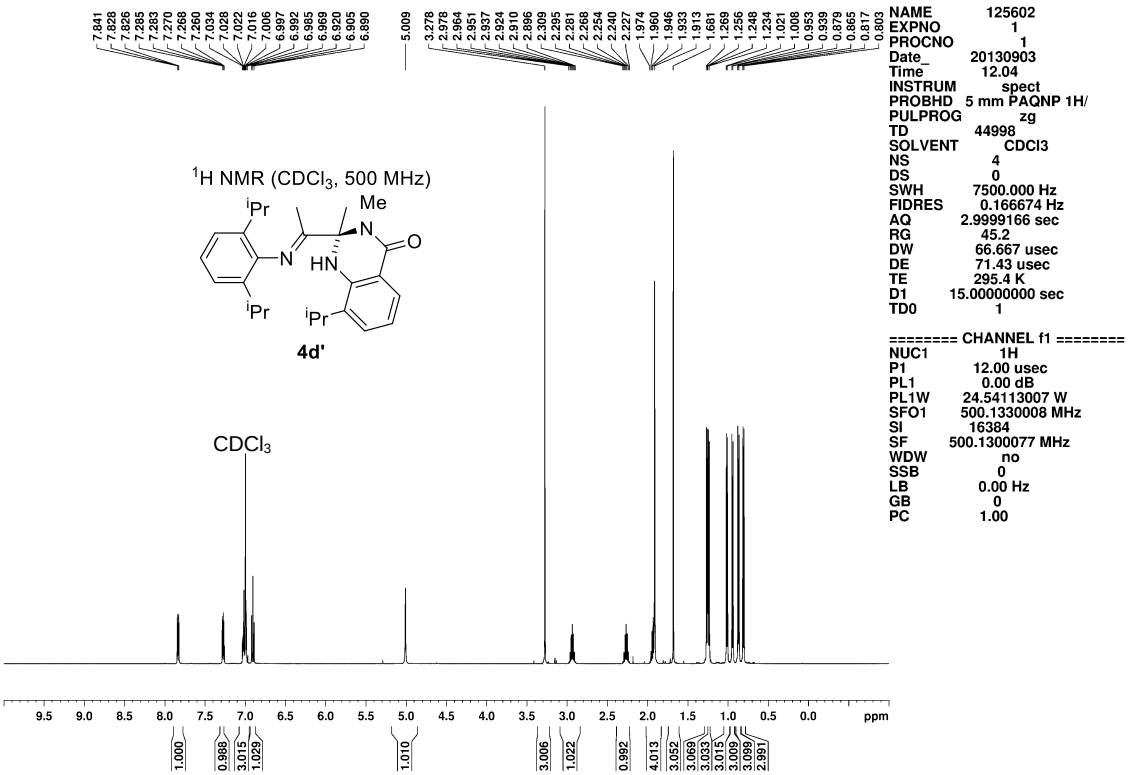

Figure 2.21. NMR spectra of **4d'**.

(b)

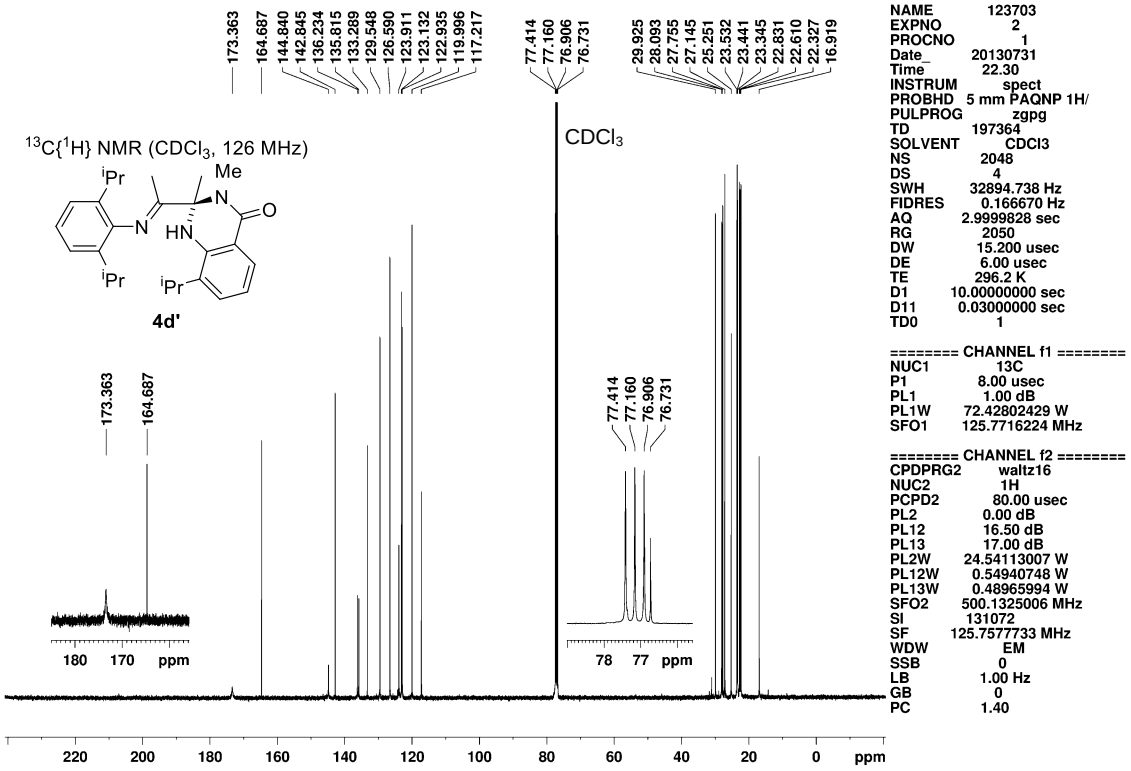

Figure 2.21, continued. NMR spectra of **4d'**.

W5a,a'. A Schlenk flask was charged with **4a** (98 mg, 0.23 mmol), (cod)PdMeCl (59 mg, 0.22 mmol, 1.0 equiv), and Et_2O (8 mL). The mixture was stirred at room temperature for 24 h to give an orange suspension. The yellow solid was collected by vacuum filtration. Yield: 80.0 mg (65%). The equilibrium isomer ratio **5a**/**5a'** is ca. 4.5/1 in CD_2Cl_2 at room temperature based on integration of the Pd–Me resonances. **5a**: ^{1}H NMR (500 MHz, CD_2Cl_2): δ 7.45 (dd, J = 7.9, 1.1, 1H, Ar), 7.31–7.27 (m, 4H, Ar), 7.11 (dd, J = 7.5, 1.3, 1H, Ar), 3.25 (septet, J = 6.9, 1H, H^{10}), 3.09 (s, 3H, H^6), 3.03 (s, 3H, H^7), 3.00 (septet, J = 6.9, 1H, $H^{13\text{ or }16}$), 2.95 (septet, J = 6.9, 1H, $H^{13\text{ or }16}$), 2.16 (s, 3H, H^2), 2.00 (s, 3H, H^1), 1.44 (d, J = 6.8, 3H, H^8), 1.34 (d, J = 6.8, 3H, $H^{11\text{ or }14}$), 1.31 (d, J = 6.8, 3H, $H^{11\text{ or }14}$), 1.18–1.16 (m, 6H, H^{12} + H^{15}), 1.14 (d, J = 6.9, 3H, H^9), 0.32 (s, 3H, Pd–Me). ^{13}C{^{1}H} NMR (126 MHz, CD_2Cl_2): δ 175.6 (C^3), 172.9 (C^4), 169.1 (C^5), 142.0, 141.7, 140.4, 139.1, 138.8, 128.2, 128.0, 126.7, 126.6, 124.4, 124.3, 124.2 (Ar), 40.7 (C^6), 34.9 (C^7), 29.3 (C^{10}), 28.7

($C^{13\text{ or }16}$), 28.4 ($C^{13\text{ or }16}$), 24.2 ($C^{9\text{ or }12\text{ or }15}$), 24.1 ($C^{9\text{ or }12\text{ or }15}$), 24.0 ($C^{9\text{ or }12\text{ or }15}$), 23.43 ($C^{11\text{ or }14}$), 23.41 ($C^{11\text{ or }14}$), 23.1 ($C^{8}$), 21.9 ($C^{2}$), 21.4 ($C^{1}$), 2.2 (Pd–Me). Key ^{1}H–^{1}H NOESY correlations (CD_2Cl_2): δ/δ 1.34/0.32, 1.31/0.32 (H^{11}/Pd–Me + H^{14}/Pd–Me), 1.18–1.16/2.00 (H^{12}/H^{1} + H^{15}/H^{1}), 1.14/2.16 (H^{9}/H^{2}). Key ^{1}H–^{13}C HMQC correlations (CD_2Cl_2): δ/δ 3.09/40.7 (H^{6}/C^{6}), 3.03/34.9 (H^{7}/C^{7}). **5a'**: ^{1}H NMR (500 MHz, CD_2Cl_2): δ 7.50 (dd, *J* = 8.0, 1.3, 1H, Ar), 7.35 (t, *J* = 7.8, 1H, Ar), 7.25–7.21 (m, 3H, Ar), 7.18 (dd, *J* = 7.5, 1.3, 1H, Ar), 3.19 (septet, *J* = 6.9, 1H, ^{i}Pr methine), 3.06 (s, 3H, H^{7}), 2.99 (s, 3H, H^{6}), 2.13 (s, 3H, H^{2}), 2.00 (s, 3H, H^{1}), 1.37 (d, *J* = 6.9, 6H, ^{i}Pr), 1.35 (d, *J* = 6.9, 3H, ^{i}Pr), 0.38 (s, 3H, Pd–Me). ^{13}C{^{1}H} NMR (126 MHz, CD_2Cl_2): δ 178.4 (C^{4}), 170.8 (C^{3}), 168.2 (C^{5}), 142.4, 142.2, 140.8, 138.7, 138.3, 128.4, 127.4, 127.2, 127.0, 125.3, 123.6, 123.5 (Ar), 39.6 (C^{6}), 35.0 (C^{7}), 29.1, 28.8, 28.7 (^{i}Pr methine), 23.9, 23.8, 23.6, 23.2, 20.0 (^{i}Pr methyl + *Me*C=N), 1.3 (Pd–Me). The other ^{1}H NMR and ^{13}C{^{1}H} NMR resonances overlap with resonances for **5a** and are not listed. Key ^{1}H–^{13}C HMQC correlations (CD_2Cl_2): δ/δ 2.99/39.6 (H^{6}/C^{6}). IR (cm^{-1}): $\nu_{C=O}$, 1634. Anal. Calcd. for $C_{27}H_{37}ClN_3OPd$, %: C, 58.98; H, 7.17; N, 7.12. Found: C, 58.80; H, 6.98; N, 6.98. ESI-MS (1:1 MeOH:H_2O, positive ion scan, *m*/*z*): 554.2 ($[M - Cl]^{+}$).

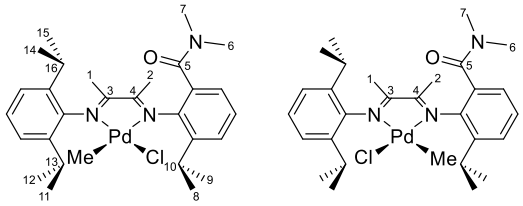

(a)

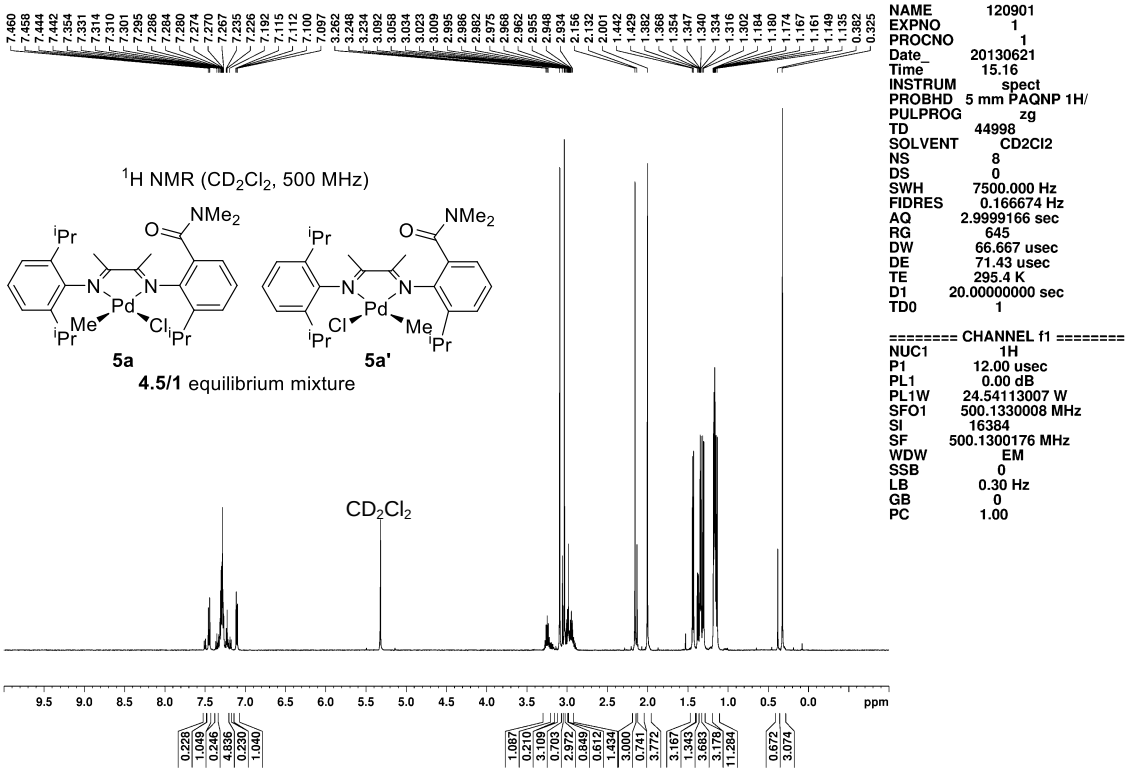

(b)

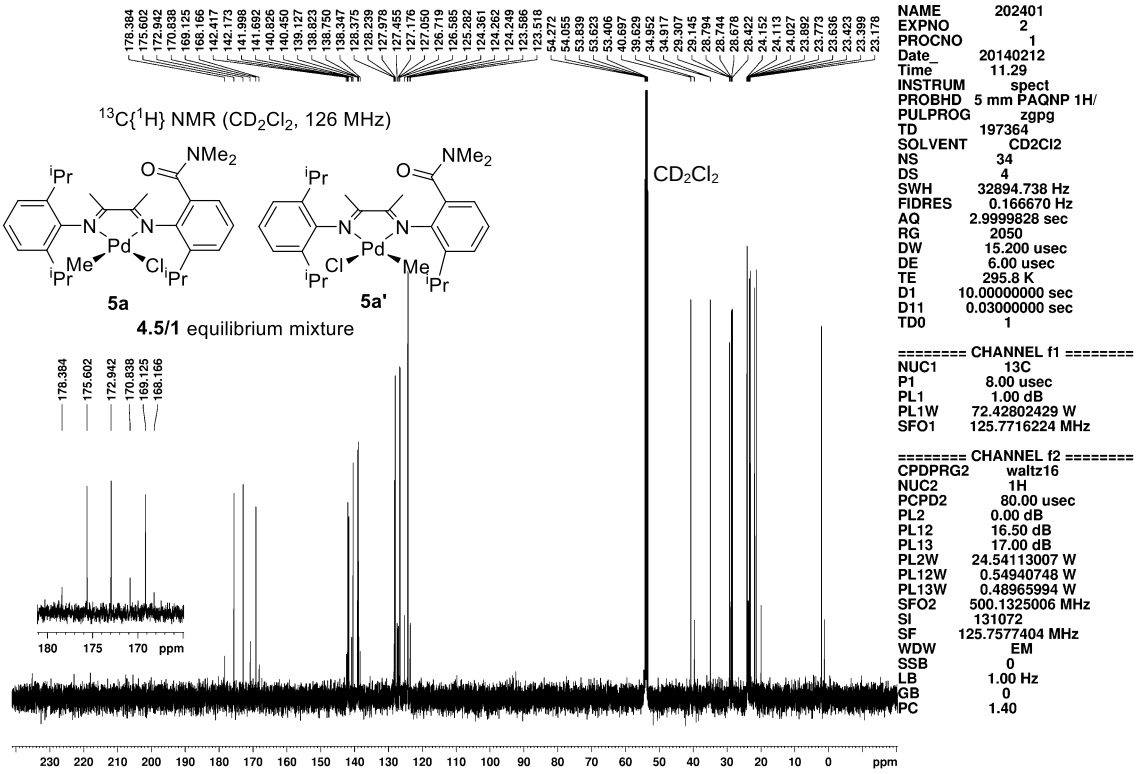

Figure 2.22. NMR spectra of **5a,a'**.

(c)

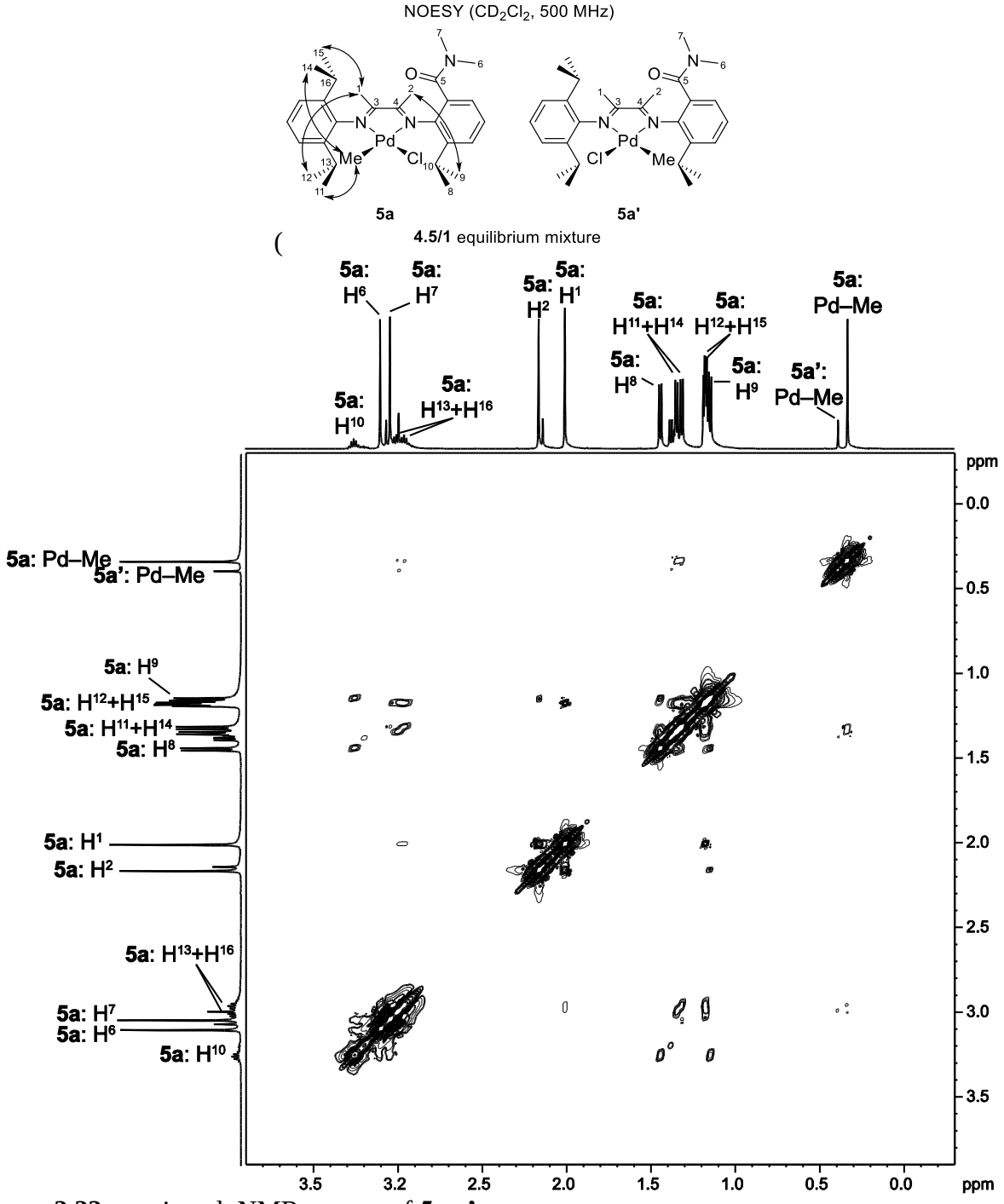

Figure 2.22, continued. NMR spectra of **5a,a'**.

Isomerization Equilibrium of 5a,a'. An 8.7/1 mixture of **5a**/**5a'** was obtained by recrystallization of **5a**,**a'** from CH_2Cl_2/hexanes at –40 °C. This mixture (4 mg) was added to a J. Young NMR tube, and CD_2Cl_2 was transferred in under vacuum at –196 °C. The NMR tube was sealed, and the sample was thawed at –78 °C and transferred to a precooled NMR probe at –40 °C. The isomerization was monitored by gradually warming the sample, collecting ^{1}H NMR spectra at various temperatures (Figure 2.23), and calculating the integral ratio of the Pd–Me resonances. No change in the **5a**/**5a'** ratio was observed at –20 °C after 30 min. At 20 °C, the mixture reached equilibrium (**5a**/**5a'** = 4.5/1) within 20 min.

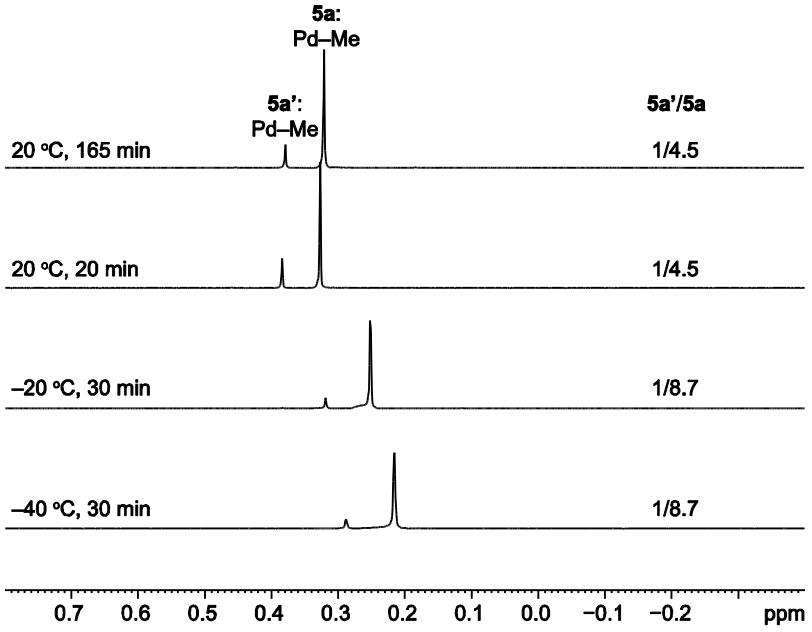

Figure 2.23. Low temperature ^{1}H NMR spectra of **5a,a'** in CD_2Cl_2 (500 MHz). The δ 0.8 to –0.4 region is shown. Temperature and equilibration time are noted for each spectrum.

5b,b'. A Schlenk tube was charged with (cod)PdMeCl (0.265 g, 1.00 mmol) and **4b** (0.449 g, 0.0972 mmol). Et_2O (5 mL) was added, and the mixture was stirred overnight to afford an orange suspension. The orange solid residue was isolated by cannula filtration and washed twice with Et_2O. The resulting orange powder was recrystallized by layering hexanes onto a CH_2Cl_2 solution at room temperature to afford an orange powder (0.570 g, 95%). The equilibrium isomer ratio **5b**/**5b'** is ca. 17/1 in CD_2Cl_2 at room temperature based on integration of the Pd–Me resonances. **5b**: ^{1}H NMR (500 MHz, CD_2Cl_2): δ 7.34–7.24 (m, 6H, Ar), 3.18 (s, 6H, H^6), 3.05 (s, 6H, H^7), 2.95 (septet, J = 6.8, 2H, H^{10}), 2.22 (s, 3H, H^2), 1.99 (s, 3H, H^1), 1.30 (d, J = 6.8, 6H, H^8), 1.16 (d, J = 6.9, 6H, H^9), 0.24 (s, 3H, Pd–Me). ^{13}C{^{1}H} NMR (126 MHz, CD_2Cl_2): δ 175.8 (C^3), 175.0 (C^4), 167.9 (C^5), 143.4, 142.2, 138.9, 129.2, 127.8, 127.4, 125.2, 124.2 (Ar), 40.9 (C^6), 35.1 (C^7), 28.5 (C^{10}), 24.0 (C^9), 23.2 (C^8), 22.7 (C^2), 21.3 (C^1), 2.1 (Pd–Me). Key ^{1}H–^{1}H NOESY correlations (CD_2Cl_2): δ/δ 1.30/0.24 (H^8/Pd–Me), 1.16/1.99 (H^9/H^1). **5b'**: ^{1}H NMR (500 MHz, CD_2Cl_2): δ 3.07 (s, 6H, $H^{6\text{ or }7}$), 3.06 (s, 6H, $H^{6\text{ or }7}$), 2.91 (septet, J = 6.8, 2H, H^{10}), 2.20 (s, 3H, H^2), 1.99 (s, 3H, H^1), 1.34 (d, J = 6.8, 6H, H^8), 1.15 (d, J = 6.8, 6H, H^9), 0.37 (s, 3H, Pd–Me). Several ^{1}H NMR resonances overlap with resonances for **5b** and are not listed. IR (cm^{-1}): $\nu_{C=O}$, 1636. Anal. Calcd. for $C_{29}H_{41}ClN_4O_2Pd$, %: C, 56.22; H, 6,67; N, 9.04. Found: C, 55.97; H, 6.40; N, 8.85. ESI-MS (1:1 MeOH:H_2O, positive ion scan, m/z): 583.1 ($[M - Cl]^+$).

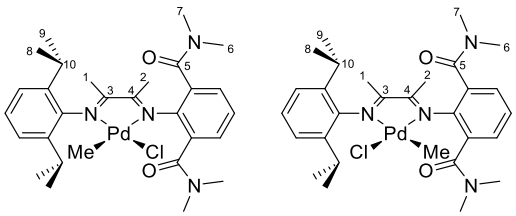

(a)

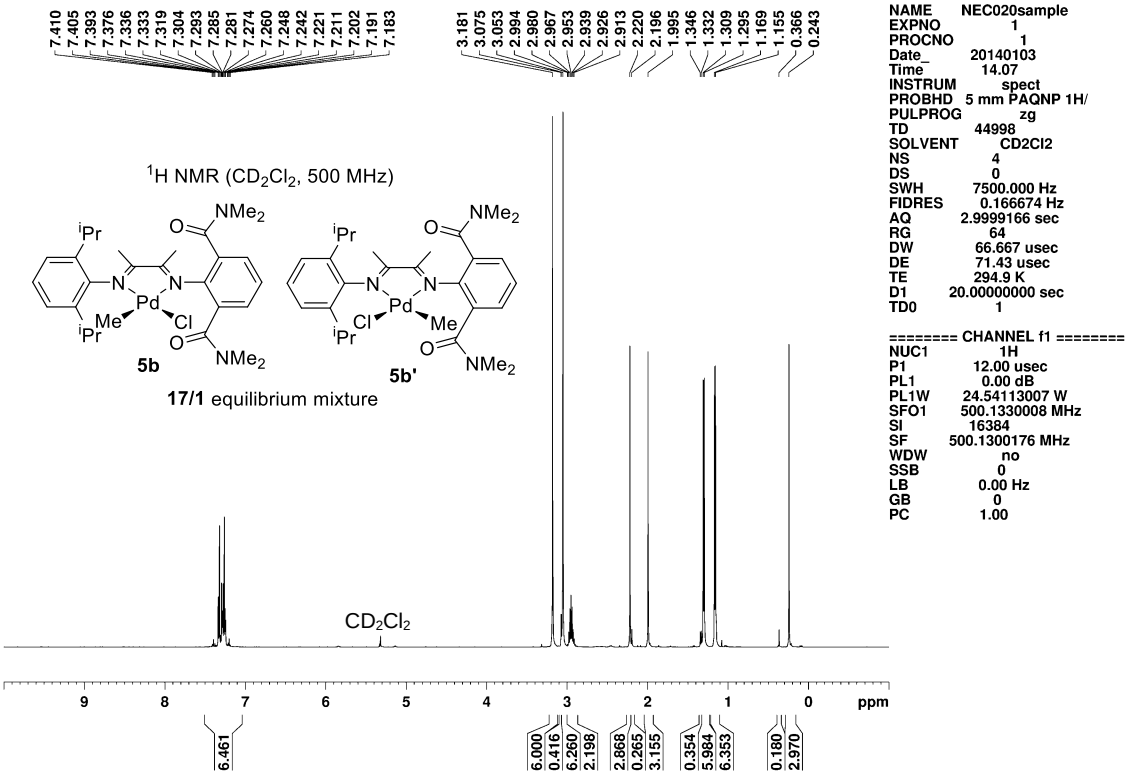

(b)

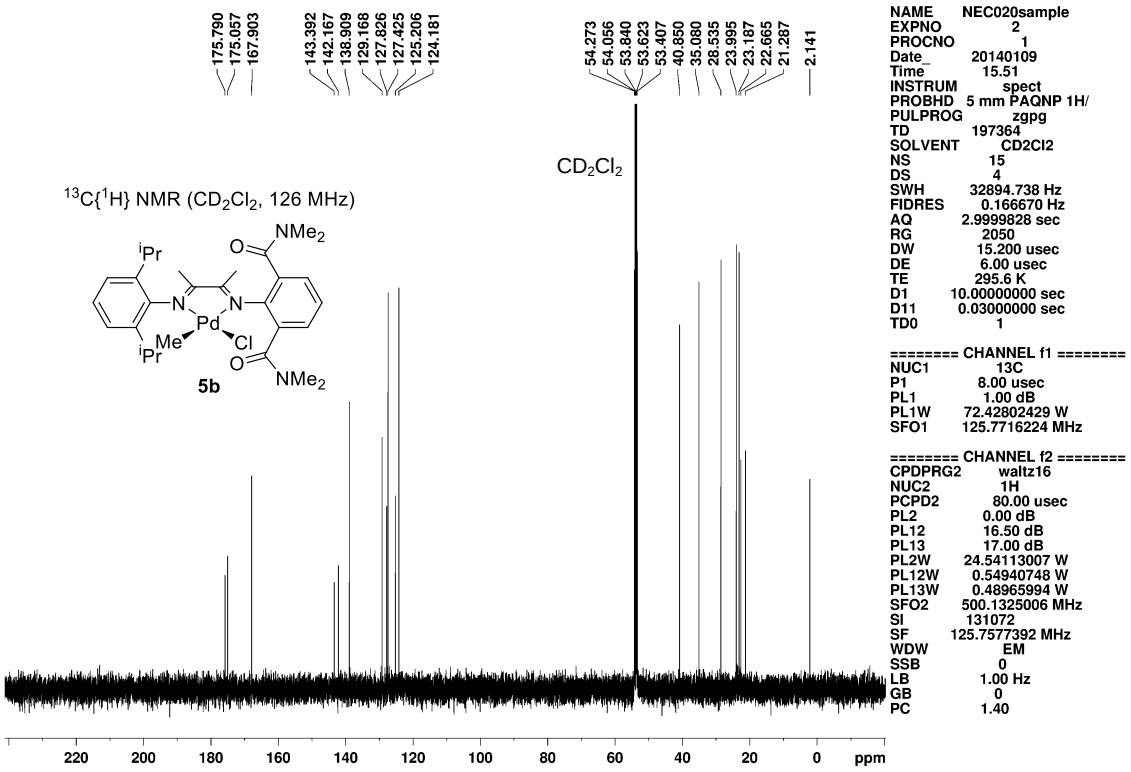

Figure 2.24. NMR spectra of **5b,b'**.

(c)

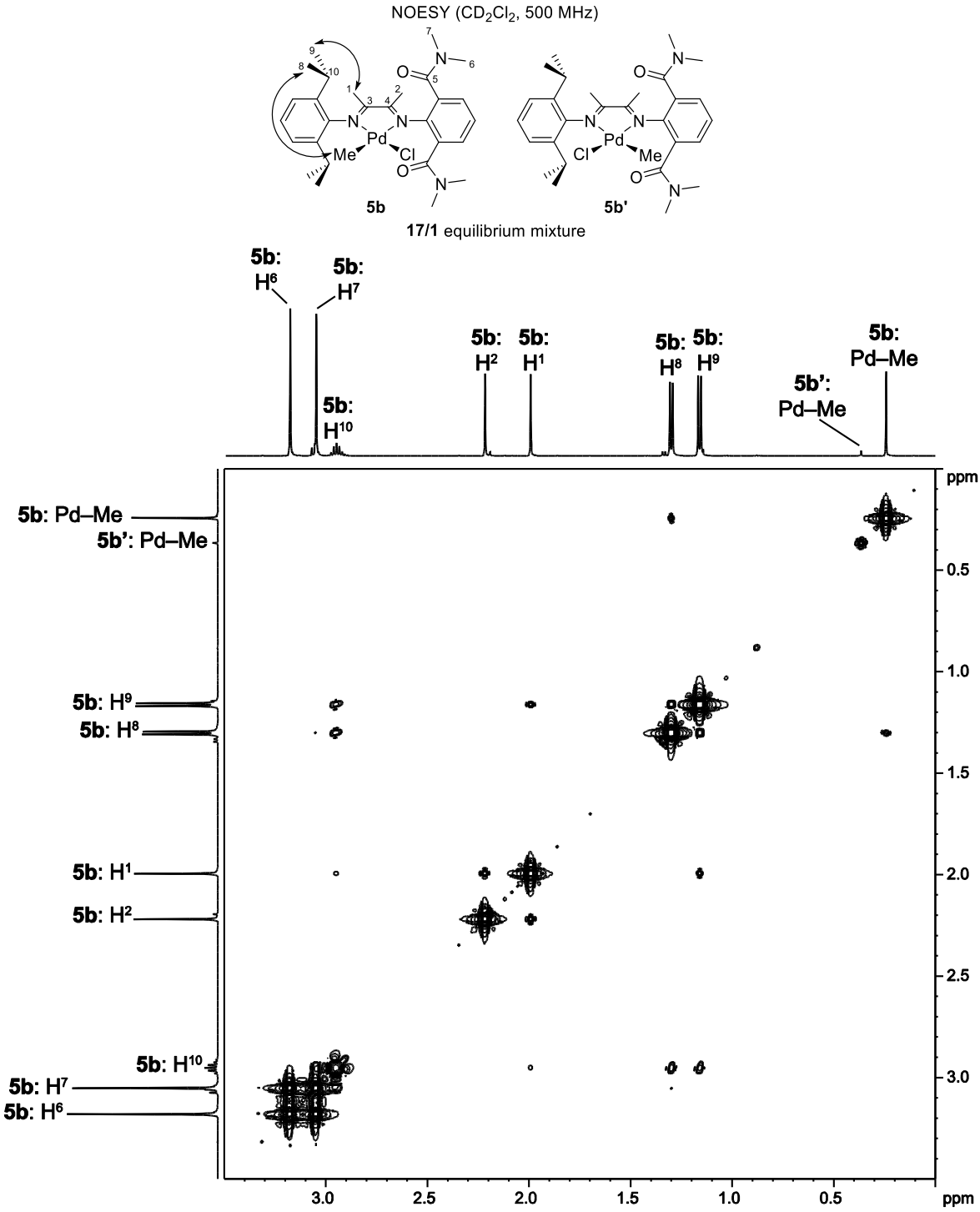

Figure 2.24, continued. NMR spectra of **5b,b'**.

Isomerization Equilibrium of 5b,b'. A 6.5/1 mixture of **5b**/**5b'** was obtained by recrystallization of **5b**,**b'** from CH_2Cl_2/hexanes at –40 °C. This mixture (4 mg) was added to a J. Young NMR tube, and CD_2Cl_2 was transferred in under vacuum at –196 °C. The NMR tube was sealed, and the sample was thawed at –78 °C and transferred to a precooled NMR probe at –40 °C. The isomerization was monitored by gradually warming the sample, collecting ^{1}H NMR spectra at various temperatures (Figure 2.25), and calculating the integral ratio of the Pd–Me resonances. Change in the **5b**/**5b'** ratio was observed as a slow process at –20 °C within 30 min. At 0 °C, the mixture reached equilibrium (**5b**/**5b'** = 17/1) within 10 min.

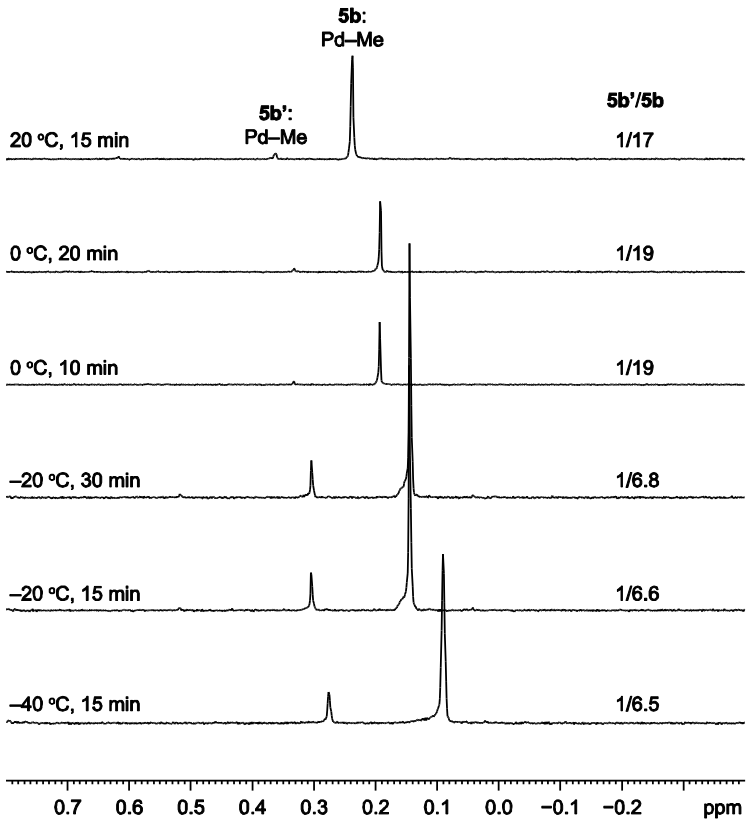

Figure 2.25. Low temperature ^{1}H NMR spectra of **5b,b'** in CD_2Cl_2 (500 MHz). The δ 0.8 to –0.4 region is shown. Temperature and equilibration time are noted for each spectrum.

5c-*anti,syn*. A Schlenk flask was charged with α-diimine **4c** (231 mg, 0.500 mmol), (cod)PdMeCl (132 mg, 0.500 mmol), and Et_2O (10 mL). The mixture was stirred at room temperature for 28 h to give an orange suspension. The orange solid was collected by vacuum filtration, washed with Et_2O and dried under vacuum. Yield: 265 mg (85%). This solid is a 5.2/1 mixture of anti and syn isomers, as determined by ^{1}H NMR at –30 °C based on the integrals of the Pd–Me resonances. The isomer mixture was recrystallized by layering hexanes onto a dilute CH_2Cl_2 solution of the 5.2/1 isomer mixture at –30 °C to give pure major isomer (**5c-*anti***) as orange needles. A similar recrystallization from a concentrated solution of the isomer mixture gave a mixture of orange needles and orange granular crystals. A granular crystal was subjected to X-ray analysis and identified as **5c-*syn***·$2CH_2Cl_2$. The ^{1}H NMR spectrum of a crystalline sample of **5c-*syn***·$2CH_2Cl_2$ in CD_2Cl_2 at –30 °C confirmed that **5c-*syn*** is the minor isomer in the equilibrium mixture. Anti/syn isomerization affords a 4.6/1 equilibrium **5c-*anti*/5c-*syn*** mixture within a few hours at room temperature in CD_2Cl_2. **5c-*anti***: ^{1}H NMR (500 MHz, CD_2Cl_2): δ 7.47 (dd, *J* = 7.9, 1.2, 1H, Ar), 7.42 (dd, *J* = 7.9, 1.1, 1H, Ar), 7.37 (t, *J* = 7.7, 1H, Ar), 7.31 (t, *J* = 7.8, 1H, Ar), 7.17 (dd, *J* = 7.5, 1.3, 1H, Ar), 7.09 (dd, *J* = 7.5, 1.3, 1H, Ar), 3.15 (septet, *J* = 6.9, 1H, H^{16}), 3.10 (s, 3H, H^9), 3.07 (septet, *J* = 6.9, 1H, H^{13}), 3.04 (s, 3H, H^7), 3.02 (s, 3H, H^{10}), 2.99 (s, 3H, H^6), 2.12 (s, 3H, H^2), 2.10 (s, 3H, H^1), 1.40 (d, *J* = 6.8, 3H, H^{14}), 1.34 (d, *J* = 6.8, 3H, H^{11}), 1.16 (d, *J* = 6.9, 3H, H^{12}), 1.12 (d, *J* = 6.9, 3H, H^{15}), 0.34 (s, 3H, Pd–Me). ^{1}H NMR (500 MHz, CD_2Cl_2, –30 °C): δ 7.45 (dd, *J* = 7.9, 1.2, 1H, Ar), 7.40 (dd, *J* = 7.9, 1.1, 1H, Ar), 7.32 (t, *J* = 7.7, 1H, Ar), 7.27 (t, *J* = 7.7, 1H, Ar), 7.16 (dd, *J* = 7.5, 1.3, 1H, Ar), 7.08 (dd, *J* = 7.5, 1.3, 1H, Ar), 3.12 (septet, *J* = 6.8, 1H, H^{16}), 3.06 (s, 3H, H^9), 3.00 (s, 3H, H^7), 3.00 (septet, *J* = 6.8, 1H, H^{13}), 2.99 (s, 3H, H^{10}), 2.95 (s, 3H, H^6), 2.10 (s, 3H, H^2), 2.08 (s, 3H, H^1), 1.34 (d, *J* = 6.7, 3H, H^{14}), 1.28 (d, *J* = 6.8, 3H, H^{11}), 1.10 (d, *J* = 6.9, 3H, H^{12}), 1.05 (d, *J* = 6.9, 3H, H^{15}), 0.27 (s, 3H, Pd–Me). ^{13}C{^{1}H} NMR (126

MHz, CD_2Cl_2): δ 178.8 (C^3), 173.3 (C^4), 169.0 (C^8), 168.0 (C^5), 142.4, 141.7, 140.7, 140.5, 128.3, 128.2, 127.3, 127.1, 126.6, 126.5, 125.1, 124.1 (Ar), 40.8 (C^9), 39.7 (C^6), 34.94 ($C^{7 \text{ or } 10}$), 34.90 ($C^{7 \text{ or } 10}$), 29.2 (C^{16}), 28.6 (C^{13}), 24.0 (2C, C^{12} + C^{15}), 23.1 (2C, C^2 + C^{14}), 22.9 (C^{11}), 21.8 (C^1), 1.6 (Pd–Me). Key ^1H–^1H NOESY correlations (CD_2Cl_2): δ/δ 1.28/0.27 (H^{11}/Pd–Me), 2.95/0.27 (H^6/Pd–Me), 1.10/2.08 (H^{12}/H^1), 1.05/2.10 (H^{15}/H^2). Key ^1H–^{13}C HMQC correlations (CD_2Cl_2): δ/δ 3.06/40.8 (H^9/C^9), 3.00/34.9 (H^7/C^7), 2.99/34.9 (H^{10}/C^{10}), 2.95/39.7 (H^6/C^6). Key ^1H–^{13}C HMBC correlations (CD_2Cl_2): δ/δ 3.06/169.0 (H^9/C^8), 3.00/168.0 (H^7/C^5), 2.99/169.0 (H^{10}/C^8), 2.95/168.0 (H^6/C^5). **5c-*syn***: ^1H NMR (500 MHz, CD_2Cl_2): δ 7.50 (dd, *J* = 7.9, 1.3, 1H, Ar), 7.44 (dd, *J* = 7.9, 1.3, 1H, Ar), 7.34 (t, *J* = 7.8, 1H, Ar), 7.29 (t, *J* = 7.8, 1H, Ar), 7.21 (dd, *J* = 7.5, 1.4, 1H, Ar), 7.13 (dd, *J* = 7.5, 1.3, 1H, Ar), 3.48 (septet, *J* = 6.9, 1H, H^{16}), 3.21 (septet, *J* = 6.9, 1H, H^{13}), 3.11 (s, 3H, $H^{6 \text{ or } 7 \text{ or } 9 \text{ or } 10}$), 3.082 (s, 3H, $H^{6 \text{ or } 7 \text{ or } 9 \text{ or } 10}$), 3.077 (s, 3H, $H^{6 \text{ or } 7 \text{ or } 9 \text{ or } 10}$), 2.99 (s, 3H, $H^{6 \text{ or } 7 \text{ or } 9 \text{ or } 10}$), 2.12 (s, 3H, H^2), 2.07 (s, 3H, H^1), 1.44 (d, *J* = 6.8, 3H, H^{14}), 1.37 (d, *J* = 6.8, 3H, H^{11}), 1.14 (d, *J* = 7.0, 3H, H^{12}), 1.08 (d, *J* = 7.0, 3H, H^{15}), 0.37 (s, 3H, Pd–Me). ^1H NMR (500 MHz, CD_2Cl_2, –30 °C): δ 7.48 (d, *J* = 7.8, 1H, Ar), 7.42 (d, *J* = 8.0, 1H, Ar), 7.33 (t, *J* = 7.7, 1H, Ar), 7.29 (t, *J* = 7.7, 1H, Ar), 7.19 (d, *J* = 7.5, 1H, Ar), 7.14 (d, *J* = 7.6, 1H, Ar), 3.48 (septet, *J* = 6.9, 1H, H^{16}), 3.08 (septet, *J* = 6.9, 1H, H^{13}), 3.08 (s, 3H, $H^{6 \text{ or } 7 \text{ or } 9 \text{ or } 10}$), 3.06 (s, 3H, $H^{6 \text{ or } 7 \text{ or } 9 \text{ or } 10}$), 3.04 (s, 3H, $H^{6 \text{ or } 7 \text{ or } 9 \text{ or } 10}$), 2.94 (s, 3H, $H^{6 \text{ or } 7 \text{ or } 9 \text{ or } 10}$), 2.09 (s, 3H, H^2), 2.03 (s, 3H, H^1), 1.38 (d, *J* = 6.7, 3H, H^{14}), 1.31 (d, *J* = 6.7, 3H, H^{11}), 1.09 (d, *J* = 6.8, 3H, H^{12}), 0.99 (d, *J* = 6.9, 3H, H^{15}), 0.29 (s, 3H, Pd–Me). $^{13}C\{^1H\}$ NMR (126 MHz, CD_2Cl_2): δ 178.5 (C^3), 172.8 (C^4), 169.0 (C^8), 167.9 (C^5), 142.6, 141.1, 140.7 (2C), 128.5, 127.72, 127.70, 127.0, 126.7, 126.6, 125.8, 124.9 (Ar), 40.7 (C^9), 39.8 (C^6), 35.4 ($C^{7 \text{ or } 10}$), 35.2 ($C^{7 \text{ or } 10}$), 29.6 (C^{16}), 28.7 (C^{13}), 24.0, 23.8, 22.93, 22.86, 22.7 (^{i}Pr methyl + *Me*C=N), 1.3 (Pd–Me). One aliphatic carbon signal overlaps with a resonance of **5c-*anti***. Key ^1H–^1H NOESY correlations (CD_2Cl_2): δ/δ 1.31/0.29 (H^{11}/Pd–Me), 1.09/2.03

(H^{12}/H^{1}). IR (cm^{-1}): $\nu_{C=O}$, 1631. Anal. Calcd. for $C_{29}H_{41}ClN_4O_2Pd$, %: C, 56.22; H, 6.67; N, 9.04. Found: C, 55.95; H, 6.62; N, 8.82. ESI-MS (1:1 MeOH:H_2O, positive ion scan, *m*/*z*): 583.2 ([M – Cl]$^+$).

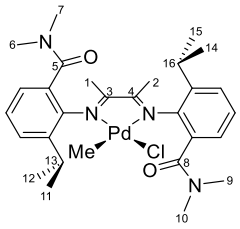

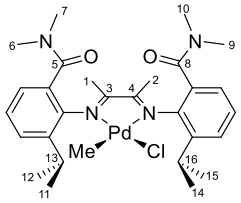

(a)

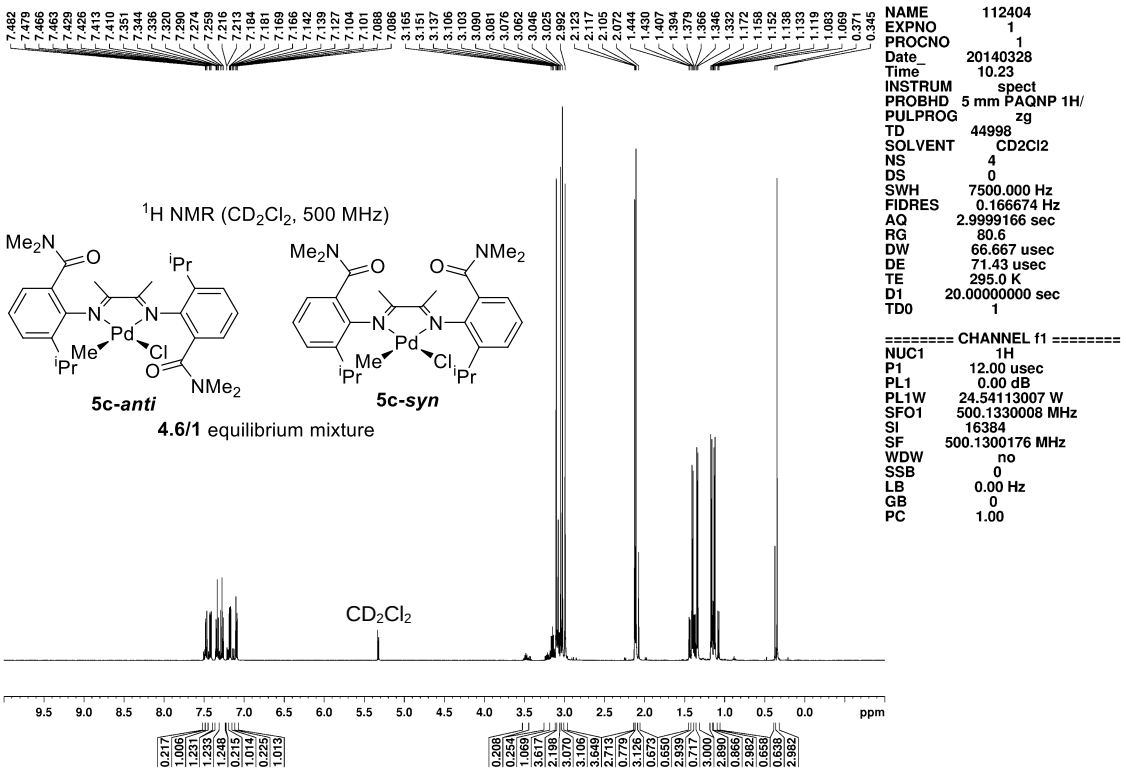

(b)

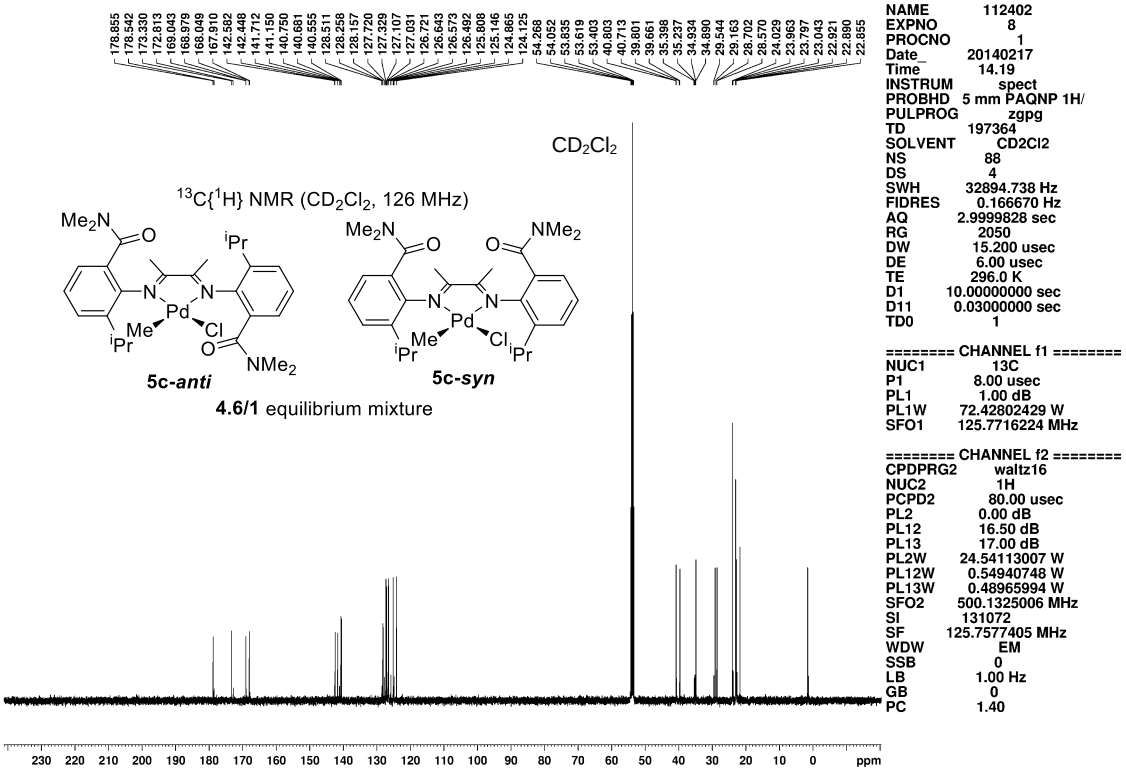

Figure 2.26. NMR spectra of **5c-*anti,syn***.

(c)

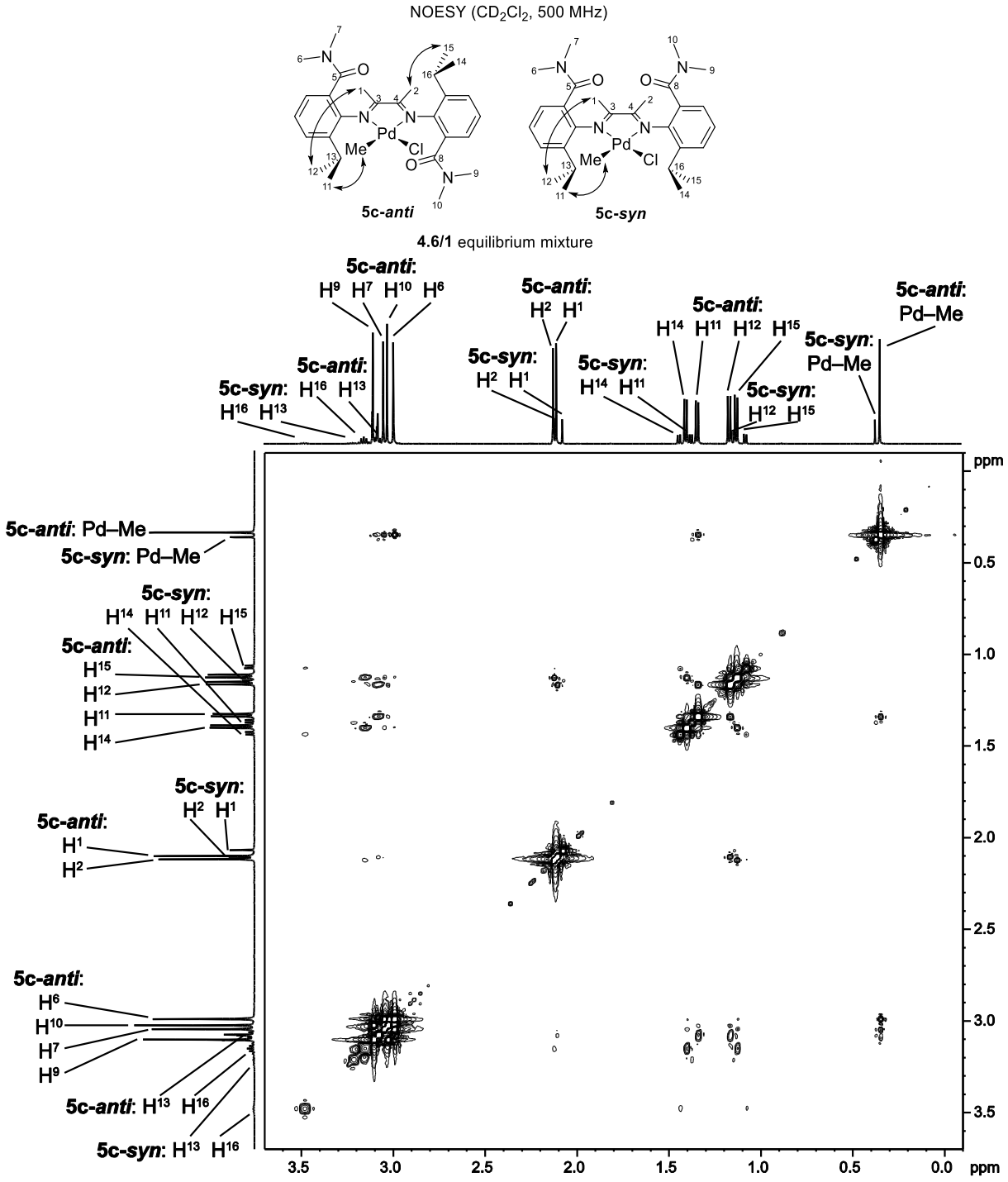

Figure 2.26, continued. NMR spectra of **5c-*anti*,*syn***.

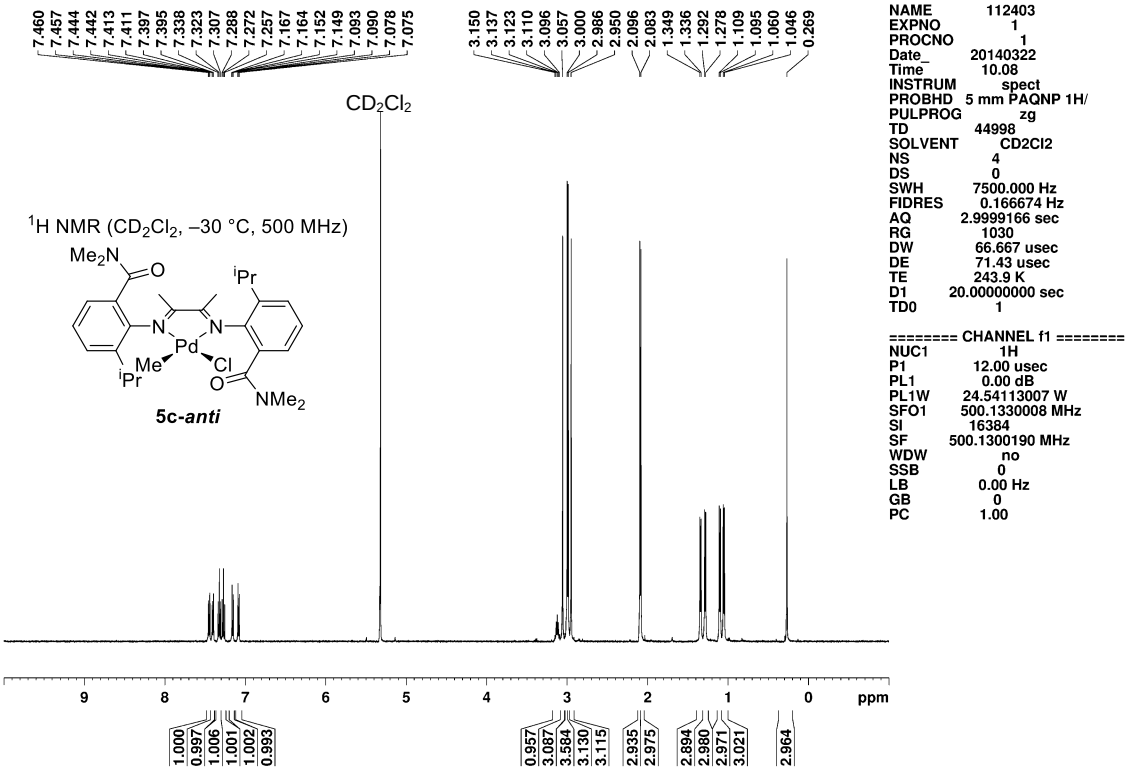

Figure 2.27. ^{1}H NMR spectrum of **5c-*anti*** at -30 °C.

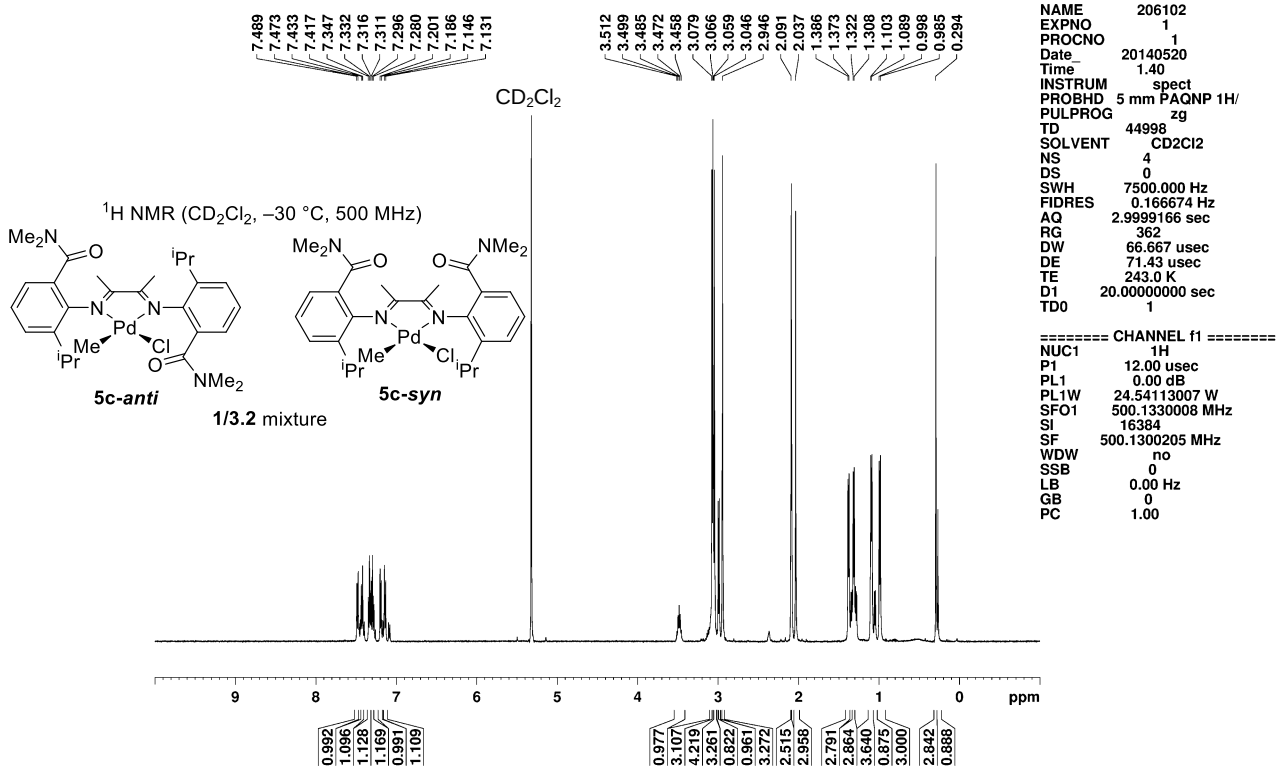

Figure 2.28. ^{1}H NMR spectrum of **5c-*anti,syn*** (1:3.2 mixture) at -30 °C.

Isomerization Equilibrium of 5c-*anti*,*syn*. A J. Young NMR tube was charged with a solid mixture of **5c-*syn*** and **5c-*anti*** (8 mg), and CD_2Cl_2 (0.5 mL) was transferred in under vacuum at –196 °C. The tube was sealed, and the sample was warmed to room temperature to yield an orange solution. The sample was then transferred to NMR probe at room temperature, and ^1H NMR spectra were collected periodically (Figure 2.29). The mixture reached equilibrium (**5c-*anti*/5c-*syn*** = 4.6/1) within 180 min.

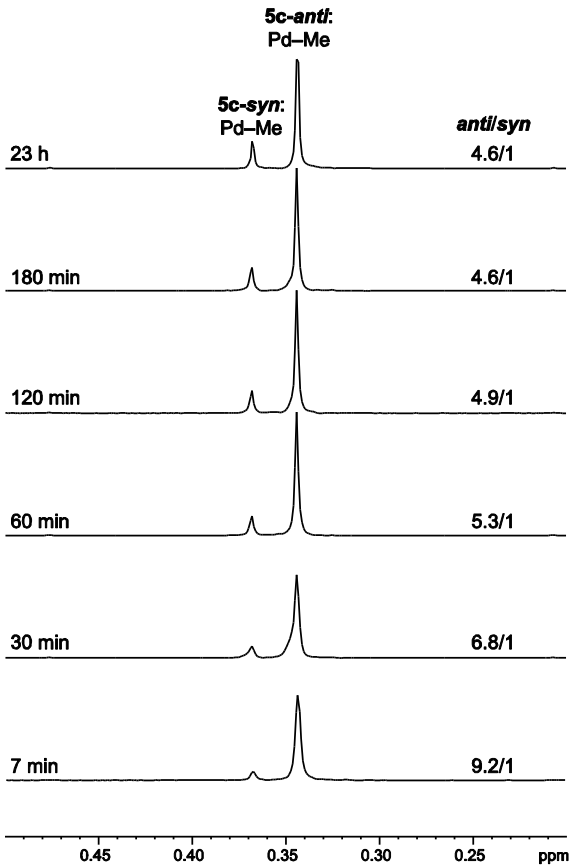

Figure 2.29. Stacked ^1H NMR spectra showing the isomerization of **5c-*anti*** to **5c-*syn*** in CD_2Cl_2 at room temperature (500 MHz). The Pd–Me region (δ 0.50–0.20) is shown.

5d,d'. A glass vial was equipped with a stir bar and charged with **6d** (473 mg, 0.793 mmol), CH_2Cl_2 (3 mL), and $SnMe_4$ (425 mg, 2.38 mmol, 3.0 equiv, 0.8 M). The vial was covered with foil, and the mixture was stirred at room temperature for 29 h, giving a dark red solution and Pd mirror. The solution was filtered through a pad of Celite, and the filtrate was concentrated under vacuum to 0.5 mL. Et_2O (20 mL) was added in one portion, and orange microcrystals formed in a few minutes. The crystals were collected by vacuum filtration, washed with Et_2O, and dried under vacuum. The product was stored in a –40 °C freezer. Yield: 406 mg (89%). The equilibrium **5d**/**5d'** ratio is ca. 16/1 at room temperature in CD_2Cl_2 based on the integration of the Pd–Me resonances. **5d**: ^{1}H NMR (500 MHz, CD_2Cl_2) : δ 7.48 (br, 1H, amide NH), 7.46 (dd, *J* = 6.9, 2.2, 1H, Ar), 7.35–7.28 (m, 5H, Ar), 3.04 (septet, *J* = 6.9, 1H, $H^{12\text{ or }15}$), 2.98 (septet, *J* = 6.9, 1H, H^9), 2.92 (d, *J* = 4.9, 3H, H^6), 2.92 (septet, *J* = 6.8, 1H, $H^{12\text{ or }15}$), 2.08 (s, 3H, H^2), 2.03 (s, 3H, H^1), 1.43 (d, *J* = 6.8, 3H, H^7), 1.36 (d, *J* = 6.8, 3H, $H^{10\text{ or }13}$), 1.30 (d, *J* = 6.8, 3H, $H^{10\text{ or }13}$), 1.20 (d, *J* = 6.8, 3H, H^8), 1.19 (d, *J* = 6.8, 3H, $H^{11\text{ or }14}$), 1.15 (d, *J* = 6.9, 3H, $H^{11\text{ or }14}$), 0.40 (s, 3H, Pd–Me). ^{13}C{^{1}H} NMR (126 MHz, CD_2Cl_2): δ 175.5 (C^3), 171.8 (C^4), 168.9 (C^5), 141.8, 141.0, 138.9, 138.8, 138.7, 130.1, 128.2, 127.4, 127.2, 125.2, 124.4, 124.3 (Ar), 29.1 (C^9), 29.0 ($C^{12\text{ or }15}$), 28.6 ($C^{12\text{ or }15}$), 26.2 (C^6), 24.1 ($C^{11\text{ or }14}$), 23.8 ($C^{11\text{ or }14}$), 23.5 ($C^{10\text{ or }13}$), 23.4 (C^7), 23.2 (C^8), 22.9 ($C^{10\text{ or }13}$), 21.4 (C^1), 20.1 (C^2), 2.8 (Pd–Me). Key ^{1}H–^{1}H COSY correlations (CD_2Cl_2): δ/δ 7.48/2.92 (amide NH/H^6). Key ^{1}H–^{1}H NOESY correlations (CD_2Cl_2): δ/δ 1.36/0.40, 1.30/0.40 (H^{10}/Pd–Me + H^{13}/Pd–Me), 1.19/2.03, 1.15/2.03 (H^{11}/H^1 + H^{14}/H^1), 1.20/2.08 (H^8/H^2). **5d'**: ^{1}H NMR (500 MHz, CD_2Cl_2): δ 7.55 (dd, *J* = 7.8, 1.4, 1H, Ar), 6.29 (br, 1H, amide NH), 3.17 (septet, *J* = 6.9, 1H, ^{i}Pr methine), 2.10 (s, 3H, H^2), 2.04 (s, 3H, H^1), 1.38 (d, *J* = 6.8, 6H, ^{i}Pr), 0.29 (s, 3H, Pd–Me). Several ^{1}H NMR resonances overlap with resonances for **5d** and are not listed. IR (cm^{-1}): ν_{N-H}, 3302; $\nu_{C=O}$, 1664. Anal. Calcd. for $C_{28}H_{40}ClN_3OPd$, %: C, 58.33; H, 6.99; N, 7.29. Found: C, 58.19; H, 6.75; N, 7.12.

ESI-MS (1:1 MeOH:H_2O, positive ion scan, *m*/*z*): 524.1 ($[M - Cl - CH_4]^+$), 540.2 ($[M - Cl]^+$).

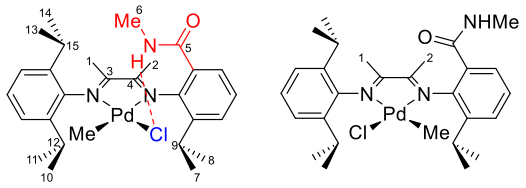

(a)

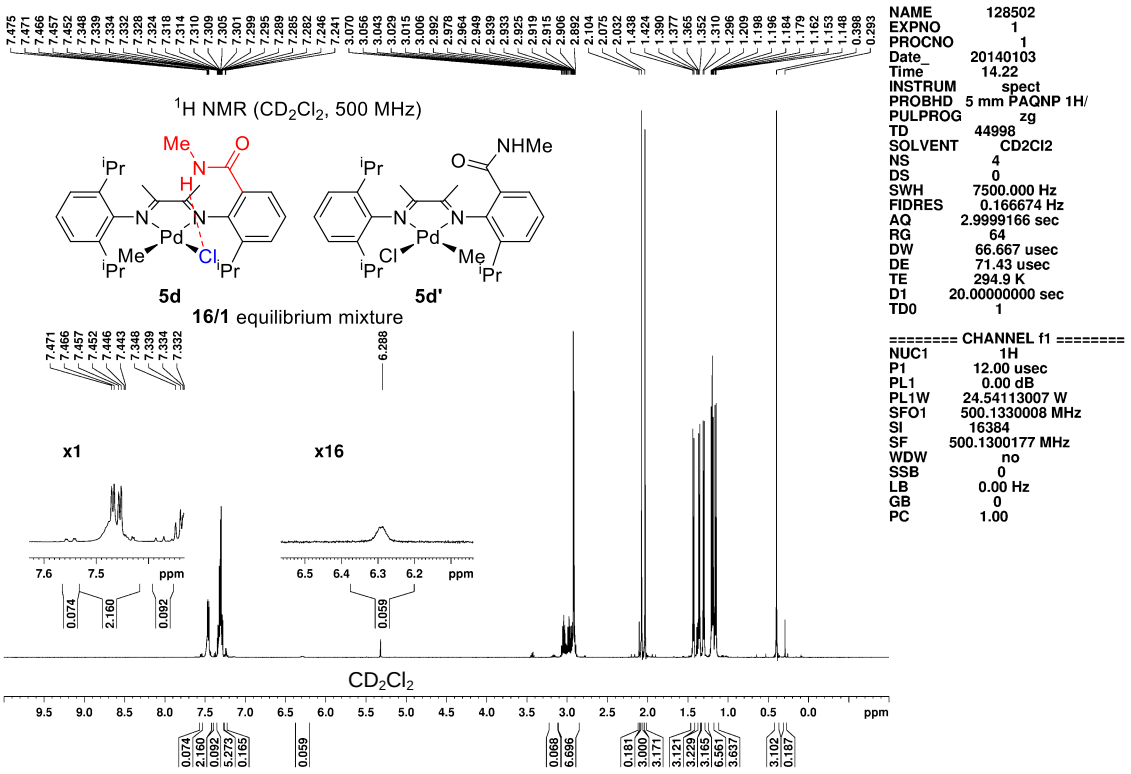

(b)

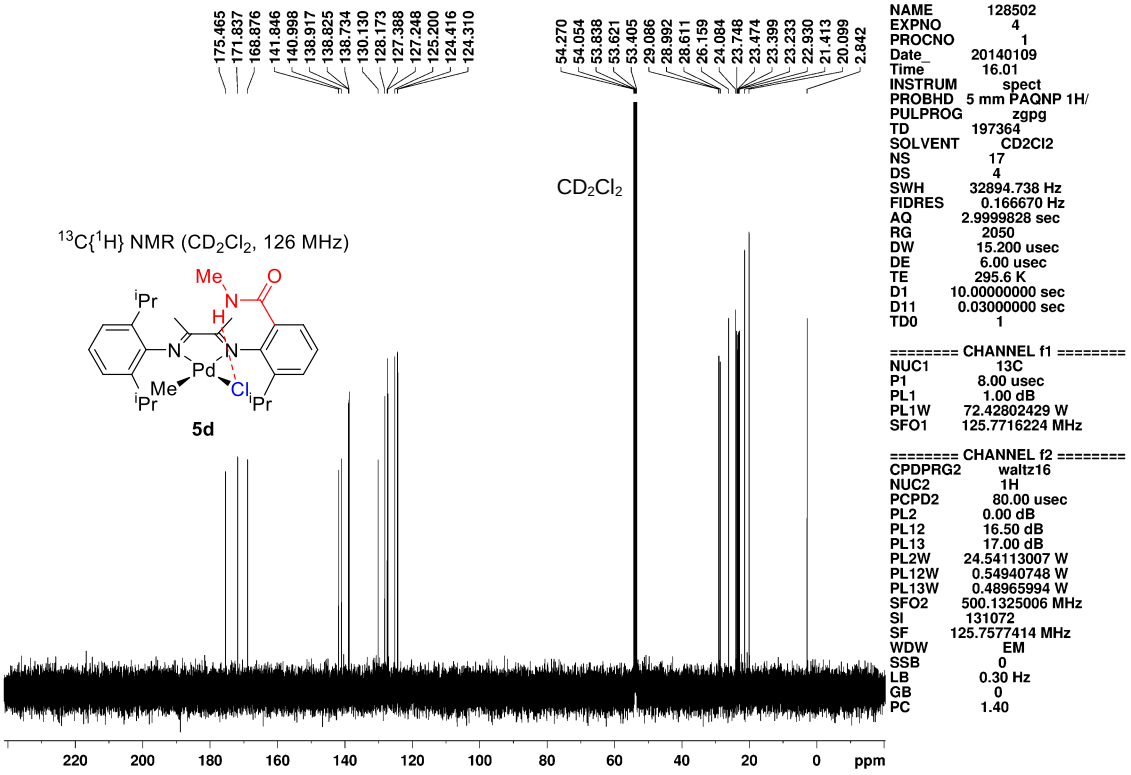

Figure 2.30. NMR spectra of **5d,d'**.

(c)

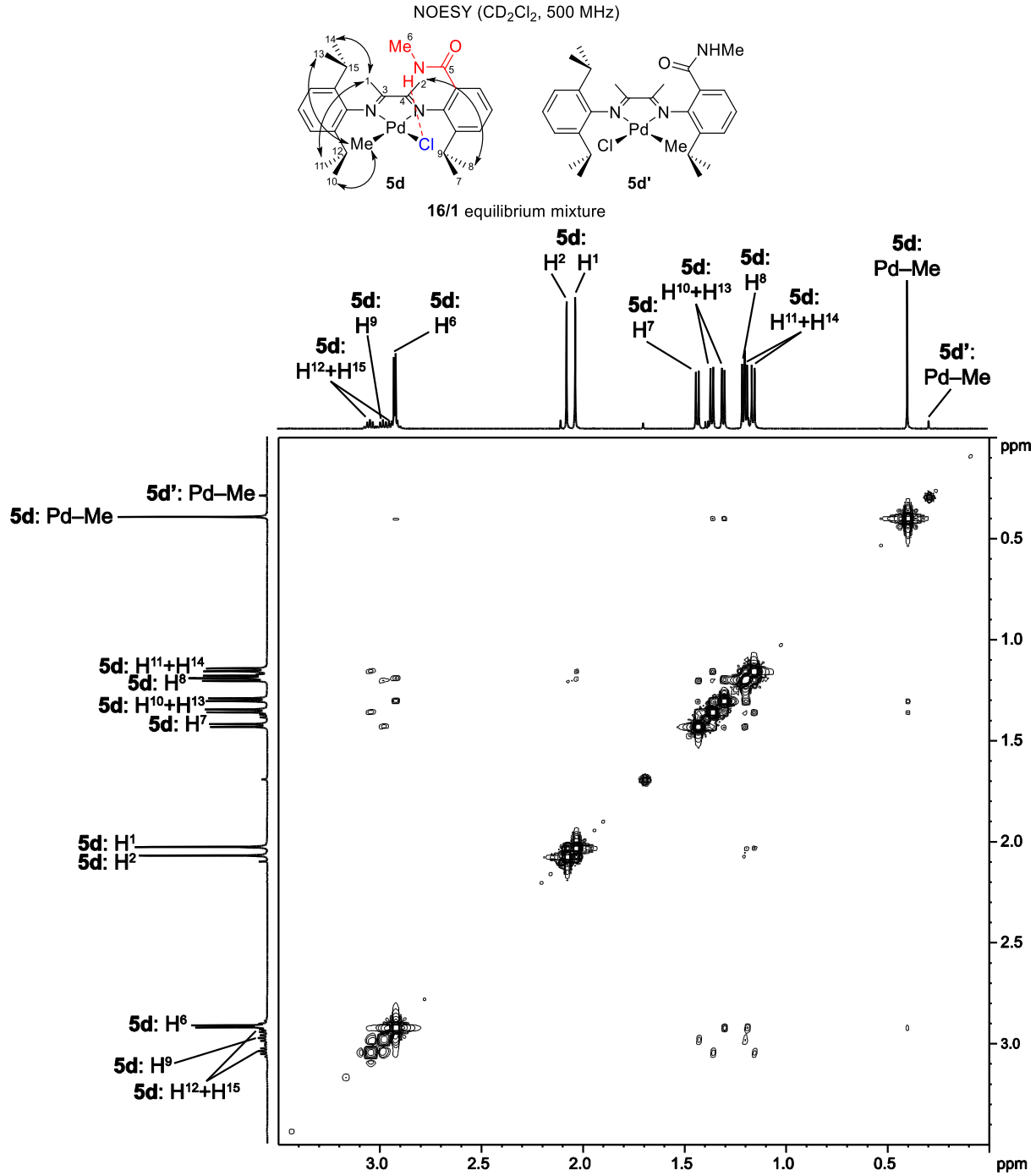

Figure 2.30, continued. NMR spectra of **5d,d'**.

(d)

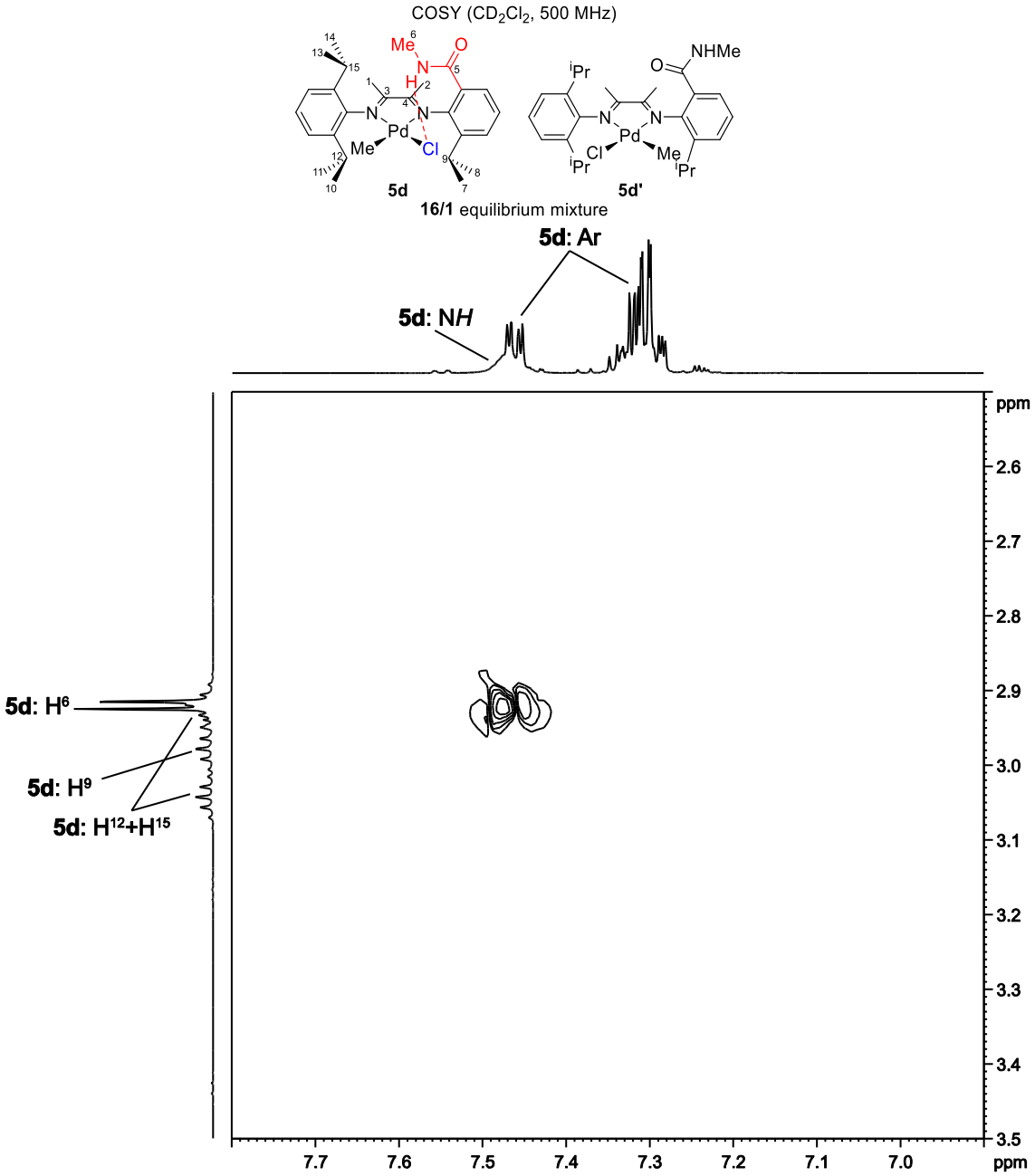

Figure 2.30, continued. NMR spectra of **5d,d'**.

Isomerization Equilibrium of 5d,d'. Pure **5d** was obtained by recrystallization of **5d**,**d'** from CH_2Cl_2/hexanes at –40 °C. **5d** (4 mg) was added to a J. Young NMR tube, and CD_2Cl_2 was transferred in under vacuum at –196 °C. The NMR tube was sealed, and the NMR sample was thawed at –78 °C and transferred to a precooled NMR probe at –40 °C. The isomerization was monitored by gradually warming the sample, collecting ^{1}H NMR spectra at various temperatures (Figure 2.31), and measuring the integral ratio of the Pd–Me resonances. At –20 °C, evolution of the Pd–Me resonance of **5d'** was observed. At 20 °C, the mixture reached equilibrium (**5d**/**5d'** = 16/1) within 15 minutes.

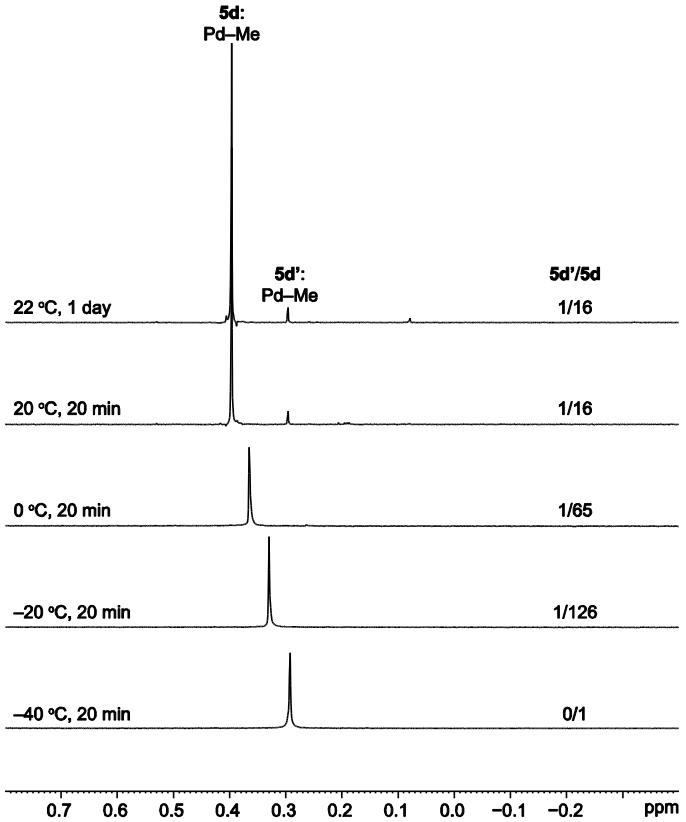

Figure 2.31. Low temperature ^{1}H NMR spectra of **5d,d'** in CD_2Cl_2 (500 MHz). The δ 0.8 to –0.4 region is shown. Temperature and equilibration time are noted for each spectrum.

6c-*anti*. A Schlenk flask was charged with **4c** (463 mg, 1.00 mmol), $(MeCN)_2PdCl_2$ (259 mg, 1.00 mmol), and CH_2Cl_2 (10 mL). The mixture was stirred at room temperature for 3.5 h to give an orange solution. The volatiles were removed under vacuum to yield a yellow powder (603 mg, 94% based on Pd, **6c-*anti*/6c-*syn*** = 1/1.7). A Schlenk flask was charged with the isomer mixture and dry 1,2-dichloroethane (25 mL). The resulting orange solution was refluxed for 2 h. The solvent was removed under vacuum, and the isomer ratio was determined to be **6c-*anti*/6c-*syn*** = 3.6/1 by ^{1}H NMR. This mixture was recrystallized by layering hexanes onto a CH_2Cl_2 solution at –30 °C. Repeating this recrystallization procedure three times yielded orange needles of pure **6c-*anti*** (270 mg, 42% based on Pd). ^{1}H NMR (500 MHz, CD_2Cl_2): δ 7.45 (dd, J = 7.9, 1.2, 2H, Ar), 7.38 (t, J = 7.7, 2H, Ar), 7.15 (dd, J = 7.4, 1.3, 2H, Ar), 3.13 (s, 6H, H^4), 3.13 (septet, J = 6.9, 2H, H^8), 3.10 (s, 6H, H^5), 2.18 (s, 6H, H^1), 1.44 (d, J = 6.8, 6H, H^6), 1.22 (d, J = 6.9, 6H, H^7). ^{13}C{^{1}H} NMR (126 MHz, CD_2Cl_2): δ 182.3 (C^2), 168.2 (C^3), 141.6, 141.3, 128.6, 128.0, 127.3, 124.7 (Ar), 40.6 (C^4), 35.2 (C^5), 29.3 (C^8), 23.9 (C^7), 23.4 (C^6), 22.7 (C^1). IR (cm^{-1}): $\nu_{C=O}$, 1629. Anal. Calcd. for $C_{28}H_{38}Cl_2N_4O_2Pd$, %: C, 52.55; H, 5.99; N, 8.75. Found: C, 52.31; H, 6.22; N, 8.60. ESI-MS (1:1 MeOH:H_2O, positive ion scan, m/z): 603.2 ($[M - Cl]^+$).

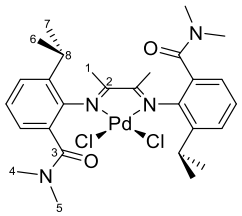

(a)

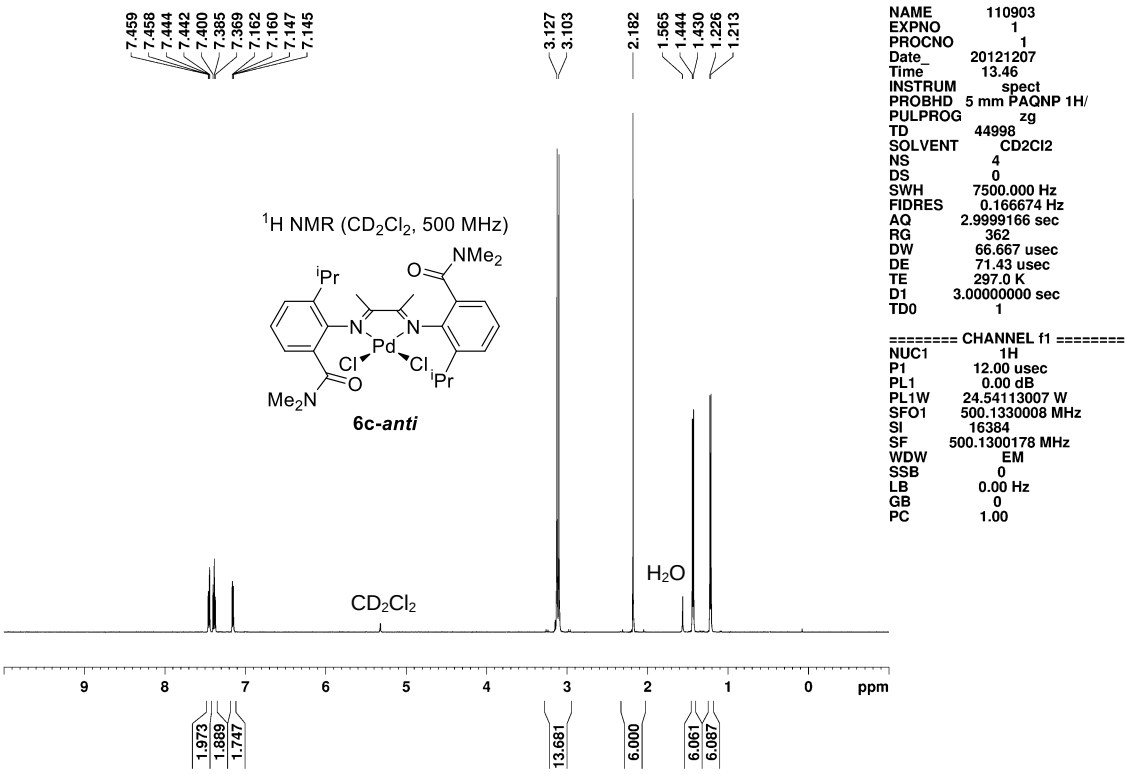

(b)

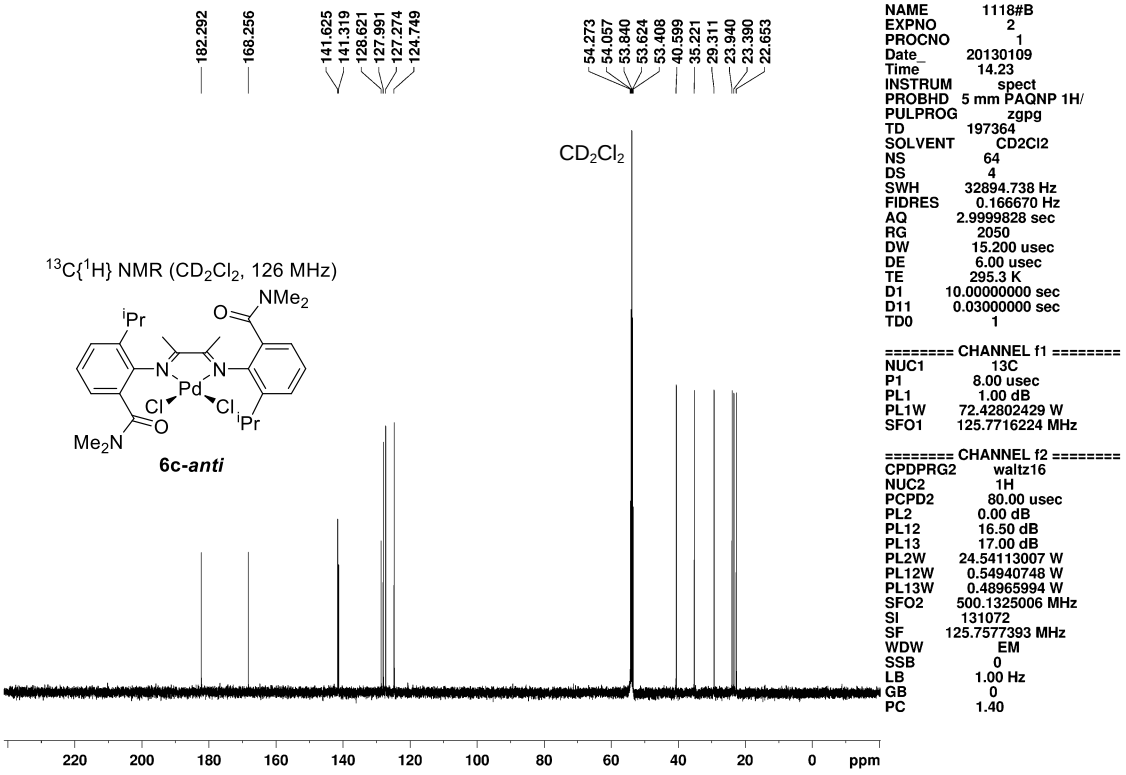

Figure 2.32. NMR spectra of **6c-*anti***.

6c-*syn*. A Schlenk flask was charged with **4c** (935 mg, 2.02 mmol), $(MeCN)_2PdCl_2$ (519 mg, 2.00 mmol), and CH_2Cl_2 (10 mL). The mixture was stirred at room temperature for 2 h to give an orange solution. The volatiles were removed under vacuum to yield a yellow powder (1.22 g, 95% based on Pd, **6c-*anti*/6c-*syn*** = 1/1.8). The mixture was recrystallized by layering hexanes onto a CH_2Cl_2 solution at –30 °C. Repeating the recrystallization procedure four times yielded orange crystals of pure **6c-*syn*** (420 mg, 33% based on Pd). ^{1}H NMR (500 MHz, CD_2Cl_2): δ 7.46 (dd, *J* = 7.9, 1.3, 2H, Ar), 7.40 (t, *J* = 7.7, 2H, Ar), 7.17 (dd, *J* = 7.5, 1.3, 2H, Ar), 3.26 (septet, *J* = 6.9, 2H, H^8), 3.12 (s, 6H, H^4), 3.09 (s, 6H, H^5), 2.18 (s, 6H, H^1), 1.48 (d, *J* = 6.8, 6H, H^6), 1.19 (d, *J* = 6.9, 6H, H^7). ^{13}C{^{1}H} NMR (126 MHz, CD_2Cl_2): δ 181.9 (C^2), 168.1 (C^3), 141.4, 141.0, 128.7, 128.1, 127.3, 125.2 (Ar), 40.6 (C^4), 35.6 (C^5), 29.6 (C^8), 23.8 (C^7), 23.2 (C^6), 22.8 (C^1). IR (cm^{-1}): $\nu_{C=O}$, 1632. Anal. Calcd. for $C_{28}H_{38}Cl_2N_4O_2Pd$, %: C, 52.55; H, 5.99; N, 8.75. Found: C, 52.39; H, 5.75; N, 8.55. ESI-MS (1:1 MeOH:H_2O, positive ion scan, *m*/*z*): 603.2 ($[M - Cl]^+$).

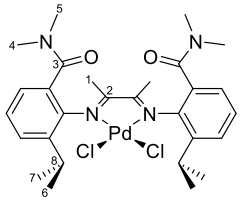

(a)

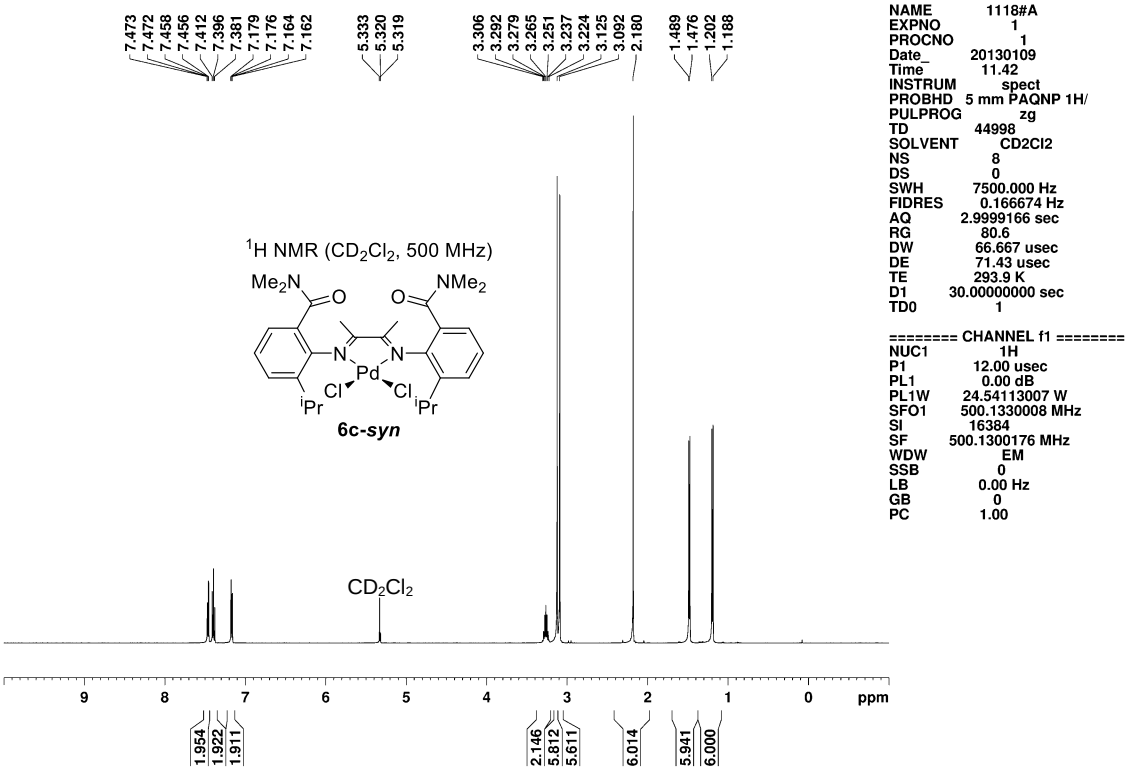

(b)

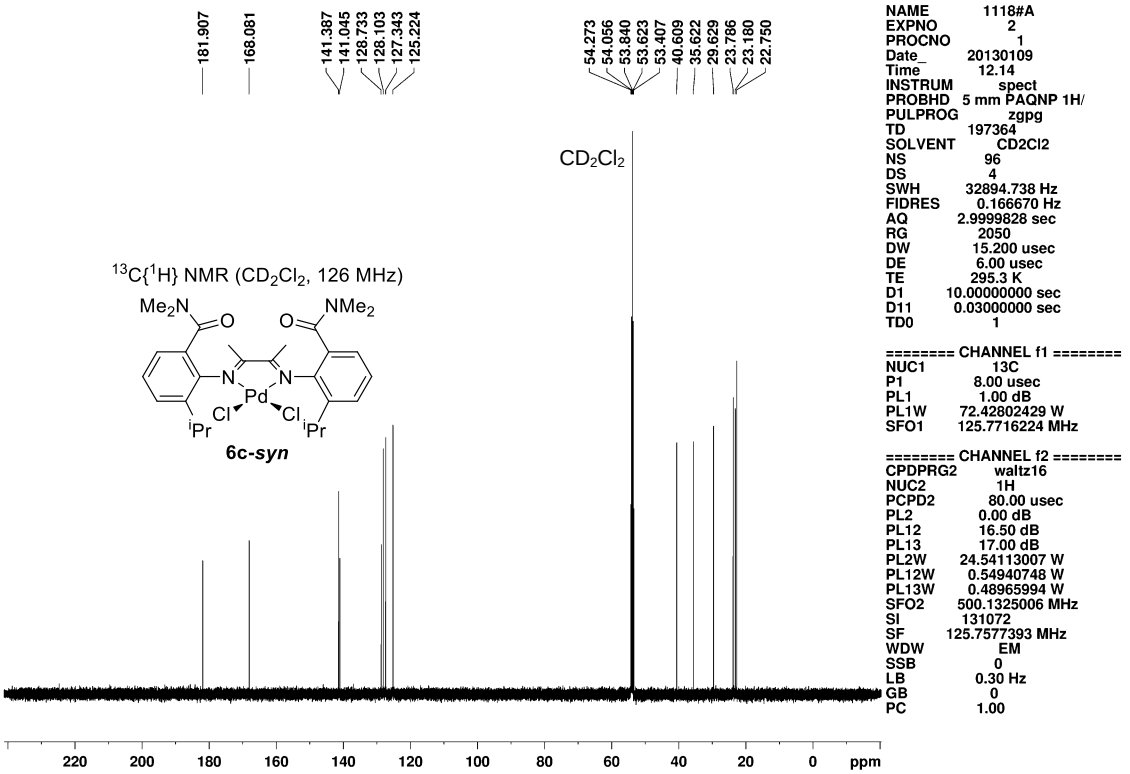

Figure 2.33. NMR spectra of **6c-*syn***.

Isomerization Equilibrium of 6c-*anti,syn*. A J. Young NMR tube was charged with pure **6c-*syn*** (10 mg) and $CDCl_2CDCl_2$ (0.6 mL) under nitrogen to give an orange homogeneous solution. The tube was sealed, and a ^{1}H NMR spectrum was collected at room temperature. The sample was placed in an oil bath at 80(1) °C, and the clock started. The reaction was monitored periodically by "cold-quenching" using running water and subsequent ^{1}H NMR measurements at room temperature (Figure 2.34). The clock was paused when the sample was cooled for monitoring.

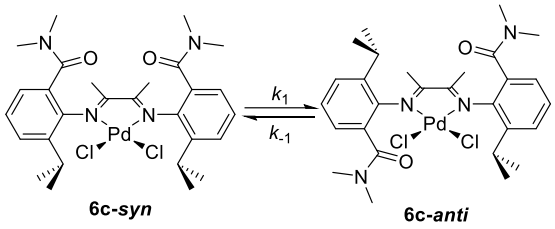

The kinetic data were analyzed by first-order approach to equilibrium kinetics using the following equations:

$$\ln\{([\text{syn}] - [\text{syn}]_e)/([\text{syn}]_0 - [\text{syn}]_e)\} = -k_{obs}t,$$

$$k_{obs} = k_1 + k_{-1},$$

$$k_1/k_{-1} = K_{eq} = [\text{anti}]_e/[\text{syn}]_e$$

where [syn] and $[\text{syn}]_0$ are the mole fractions of **6c-*syn*** at time = t and 0, respectively; $[\text{anti}]_e$ and $[\text{syn}]_e$ are the mole fractions of **6c-*anti*** and **6c-*syn*** at equilibrium; k_{obs} is the observed first-order rate constant for the approach to equilibrium; and k_1 and k_{-1} are the forward (**6c-*syn*** to **6c-*anti***) and reverse (**6c-*anti*** to **6c-*syn***) first-order rate constants. The kinetic profiles are shown in Figures 2.35 and 2.36.

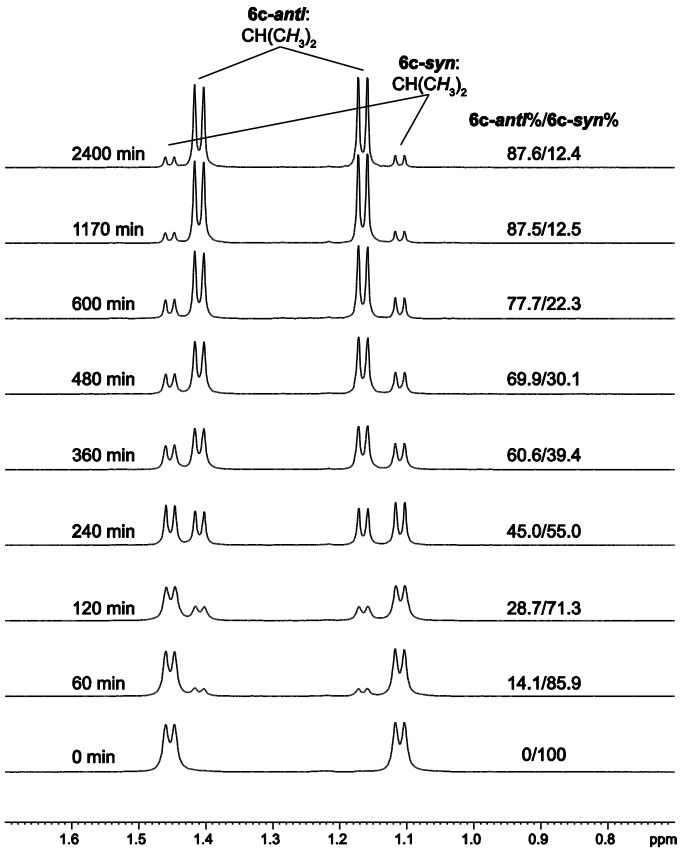

Figure 2.34. Stacked ^{1}H NMR spectra showing the isomerization of **6c-*syn*** to an equilibrium mixture of **6c-*syn*** and **6c-*anti*** in $CDCl_2CDCl_2$ at 80 °C (500 MHz). The ^{i}Pr methyl region (δ 1.7–0.7) is shown.

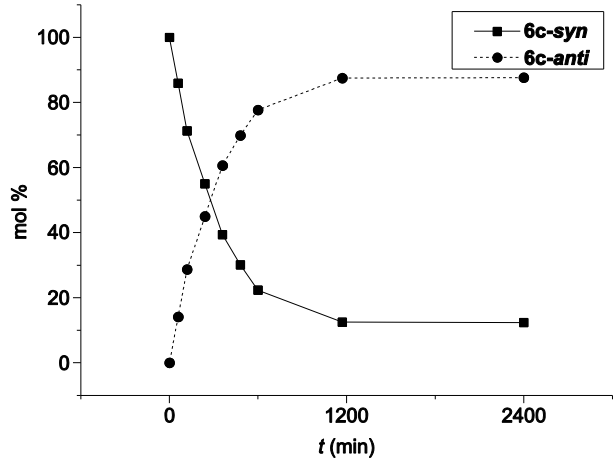

Figure 2.35. Time dependence of molar percentages of **6c-*syn*** (square, solid line) and **6c-*anti*** (circle, dash line) starting from **pure 6c-*syn*** in $CDCl_2CDCl_2$ solution at 80 °C.

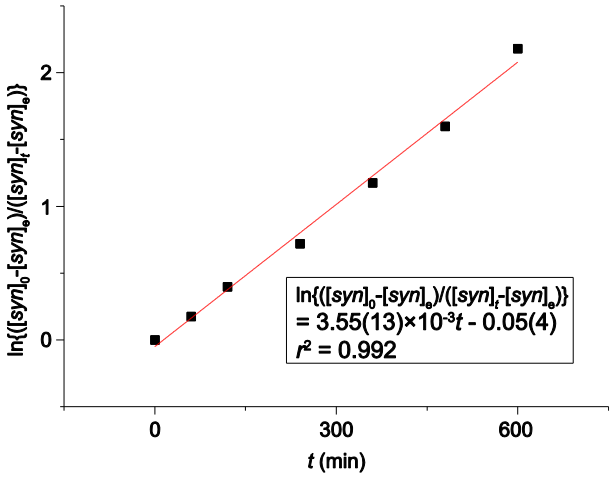

Figure 2.36. Plot of ln{([syn] – [syn]$_e$)/([syn]$_0$ – [syn]$_e$)} versus time. Kinetic parameters are: k_{obs} = 3.55(13) × 10^{-3} min^{-1} = 5.9(2) × 10^{-5} s^{-1}, K_{eq} = 7.04(5), k_1 = 7.3(3) × 10^{-6} s^{-1}, $\Delta G^{\ddagger}_{syn\rightarrow anti,80°C}$ = 29.1(3) kcal mol^{-1}.

6d. A Schlenk flask was charged with **4d'** (419 mg, 1.00 mmol), $(MeCN)_2PdCl_2$ (265 mg, 1.00 mmol, 1.00 equiv), and CH_2Cl_2 (30 mL) under nitrogen. The flask was equipped with a water condenser, and the mixture was stirred at reflux for 20 h to give a red homogeneous solution. The mixture was cooled to room temperature, and the volatiles were removed under vacuum. The red solid residue was dissolved in a minimum volume of CH_2Cl_2 (ca. 5 mL). Et_2O (30 mL) was slowly added, and a red solid precipitated. The solid was collected by vacuum filtration and washed with Et_2O. Yield: 560 mg (94%). ^{1}H NMR (500 MHz, CD_2Cl_2): δ 7.51 (dd, *J* = 7.9, 1.3, 1H, Ar), 7.44 (t, *J* = 7.7, 1H, Ar), 7.39 (t, *J* = 7.8, 1H, Ar), 7.32 (dd, *J* = 7.4, 1.4, 1H, Ar), 7.28–7.26 (m, 1H, Ar), 7.26–7.25 (m, 1H, Ar), 6.75 (br, 1H, amide NH), 3.11 (septet, *J* = 6.8, 1H, ^{i}Pr methine), 3.06 (septet, *J* = 6.9, 1H, ^{i}Pr methine), 3.05 (septet, *J* = 6.9, 1H, ^{i}Pr methine), 3.03 (d, *J* = 4.9, 3H, amide NMe), 2.18 (s, 3H, *Me*C=N), 2.10 (s, 3H, *Me*C=N), 1.48 (d, *J* = 6.8, 3H, ^{i}Pr), 1.46 (d, *J* = 6.8, 3H, ^{i}Pr), 1.41 (d, *J* = 6.8, 3H, ^{i}Pr), 1.24 (d, *J* = 6.9, 3H, ^{i}Pr), 1.23 (d, *J* = 6.9, 3H, ^{i}Pr), 1.20 (d, *J* = 6.9, 3H, ^{i}Pr). ^{13}C{^{1}H} NMR (126 MHz, CD_2Cl_2): δ 180.8, 179.3 (imine C=N), 168.5 (C=O), 141.0, 140.4, 140.3, 139.8, 139.6, 130.6, 129.2, 129.0, 128.0, 125.0, 124.2, 124.0 (Ar), 29.7, 29.4, 29.3 (^{i}Pr methine), 26.7 (amide NMe), 24.0, 23.84, 23.80, 23.6, 23.5, 23.2 (^{i}Pr methyl), 21.6, 21.2 (*Me*C=N).

IR (cm^{-1}): ν_{N-H}, 3330; $\nu_{C=O}$, 1658. Anal. Calcd. for $C_{27}H_{37}Cl_2N_3OPd$, %: C, 54.33; H, 6.25; N, 7.04. Found: C, 54.06; H, 5.97; N, 6.91. ESI-MS (1:1 MeOH:H_2O, positive ion scan, *m*/*z*): 560.0 ([M – Cl]$^+$).

(a)

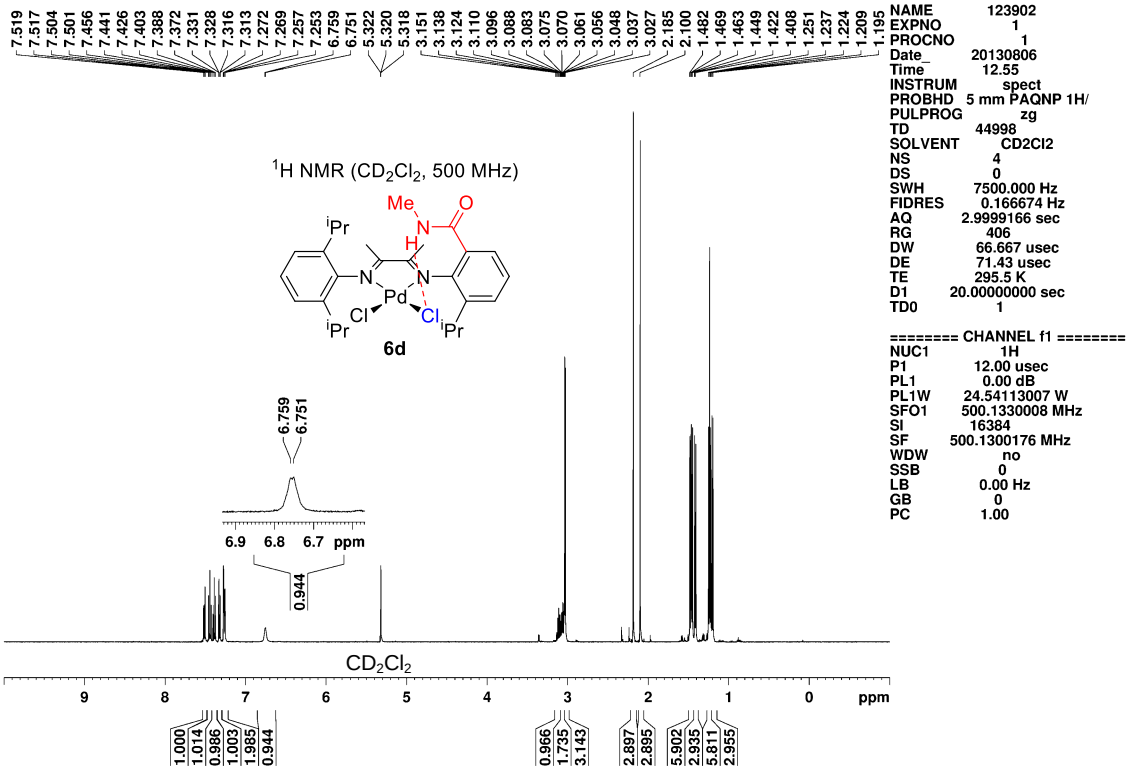

Figure 2.37. NMR spectra of **6d**.

(b)

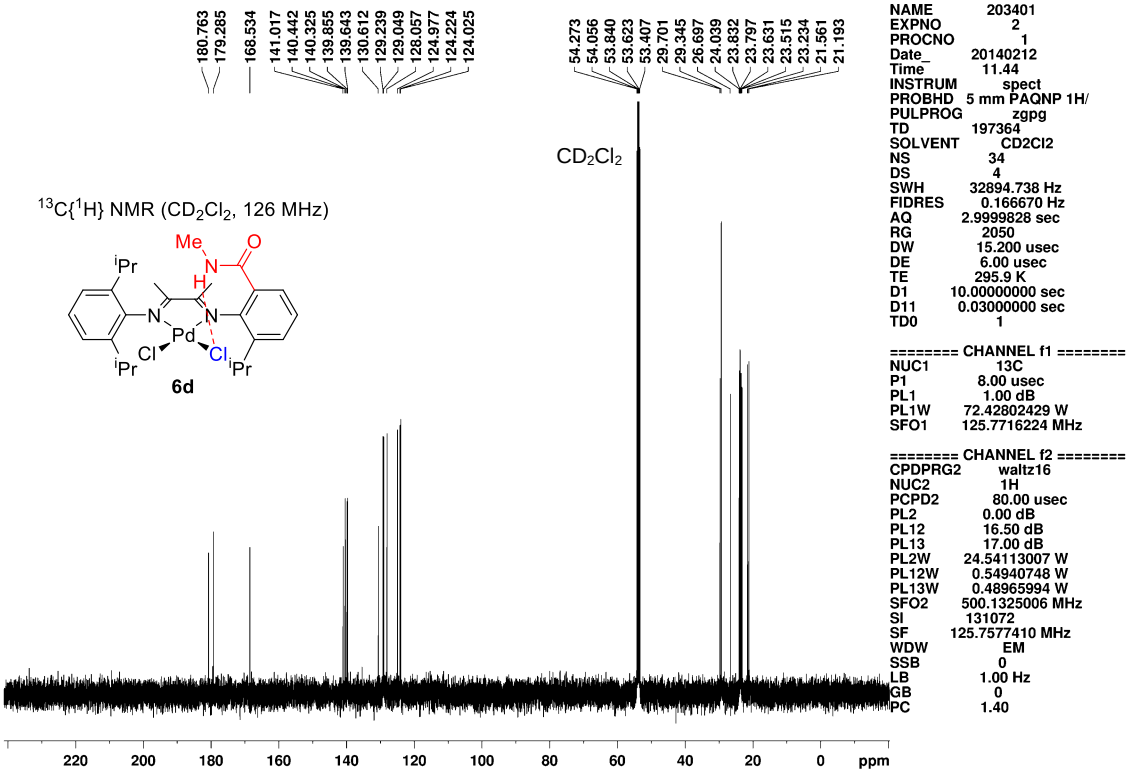

Figure 2.37, continued. NMR spectra of **6d**.

7d. A solution of **5d**,**d'** (81.6 mg, 0.142 mmol) in CH_2Cl_2 (2 mL) was vigorously stirred at room temperature, and AgOAc (26.4 mg, 0.159 mmol, 1.1 equiv) was added in one portion. The mixture was stirred at room temperature for 22 min to give a suspension of an off-white precipitate in a red solution. The suspension was filtered through a pad of Celite, and the filtrate was concentrated to dryness. The red solid residue was dissolved in hexanes/CH_2Cl_2 and kept at –30 °C overnight to give pure product as red granular crystals (59.4 mg, 70%). ^{1}H NMR (500 MHz, CD_2Cl_2): δ 9.43 (br q, *J* = 4.5, 1H, amide NH), 7.43 (dd, *J* = 7.8, 1.1, 1H, Ar), 7.33–7.27 (m, 5H, Ar), 3.58 (septet, *J* = 6.9, 1H, ^{i}Pr methine), 3.09 (septet, *J* = 6.9, 1H, ^{i}Pr methine), 2.90 (d, *J* = 4.6, 3H, amide NMe), 2.90 (septet, *J* = 6.9, 1H, ^{i}Pr methine), 2.12 (s, 3H, *Me*C=N), 1.96 (s, 3H, *Me*C=N), 1.45 (d, *J* = 6.8, 3H, ^{i}Pr), 1.40 (d, *J* = 6.8, 3H, ^{i}Pr), 1.36 (s, 3H, C*H*$_3$CO$_2$), 1.35 (d, *J* = 6.8, 3H, ^{i}Pr), 1.16 (d, *J* = 6.8, 3H, ^{i}Pr), 1.15 (d, *J* = 6.8, 3H, ^{i}Pr), 1.05 (d, *J* = 6.9, 3H, ^{i}Pr), 0.27 (s,

3H, Pd–Me). $^{13}C\{^{1}H\}$ NMR (126 MHz, CD_2Cl_2): δ 177.6 (Me*C*O_2), 175.8, 170.6 (imine C=N), 169.4 (amide C=O), 142.4, 140.6, 139.9, 138.8, 138.6, 131.3, 128.1, 127.7, 126.7, 125.8, 124.3 (2C) (Ar), 29.3, 28.9, 28.6 (^{i}Pr methine), 26.4 (amide NMe), 24.5, 24.2, 23.8, 23.5, 23.2 (^{i}Pr methyl), 22.6 (*Me*CO_2), 22.2 (^{i}Pr methyl), 21.2, 20.1 (*Me*C=N), 3.2 (Pd–Me). Key ^{1}H–^{1}H COSY correlation (CD_2Cl_2): δ/δ 9.43/2.90 (amide NH/NMe). IR (cm^{-1}): ν_{N-H}, 3211; $\nu_{C=O,amide}$, 1653; $\nu_{OCO,asym}$, 1590; $\nu_{OCO,sym}$, 1329. Anal. Calcd. for $C_{30}H_{43}N_3O_3Pd$, %: C, 60.04; H, 7.22; N, 7.00. Found: C, 59.83; H, 6.96; N, 6.93. ESI-MS (1:1 MeOH:H_2O, positive ion scan, *m*/*z*): 540.2 ([M – OAc]$^+$), 524.1 ([M – OAc – CH_4]$^+$), 581.3 ([M – H_2O]$^+$).

(a)

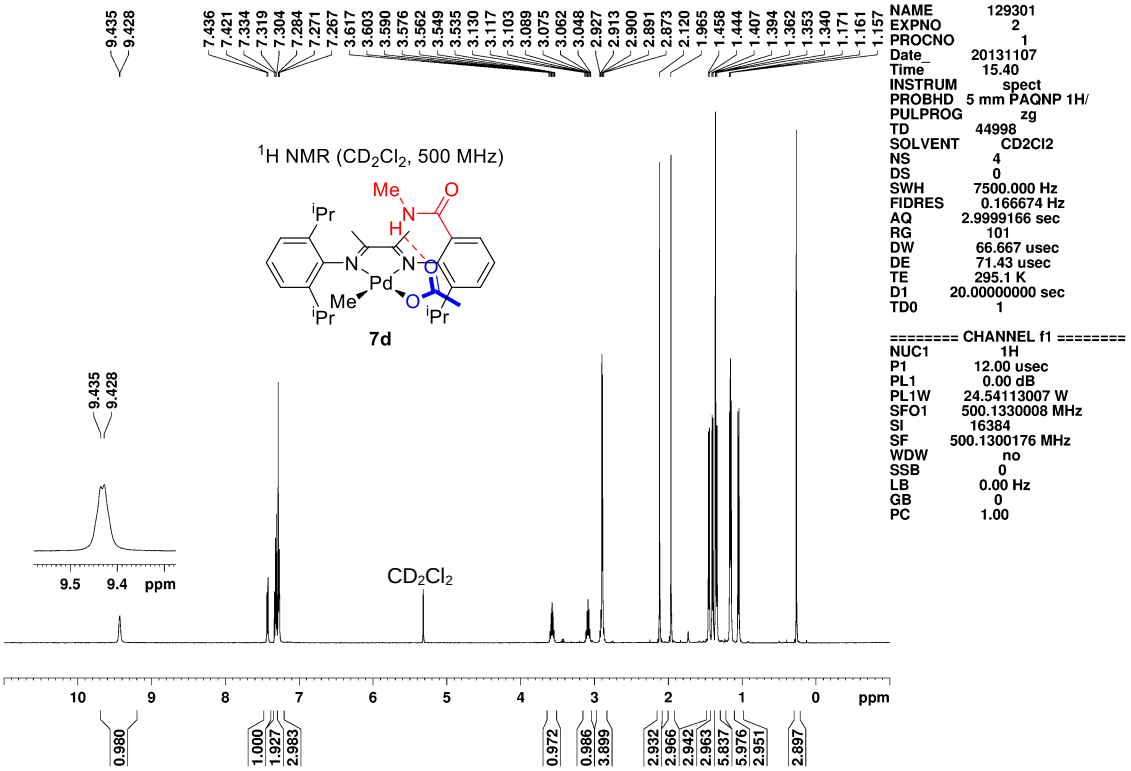

Figure 2.38. NMR spectra of **7d**.

(b)

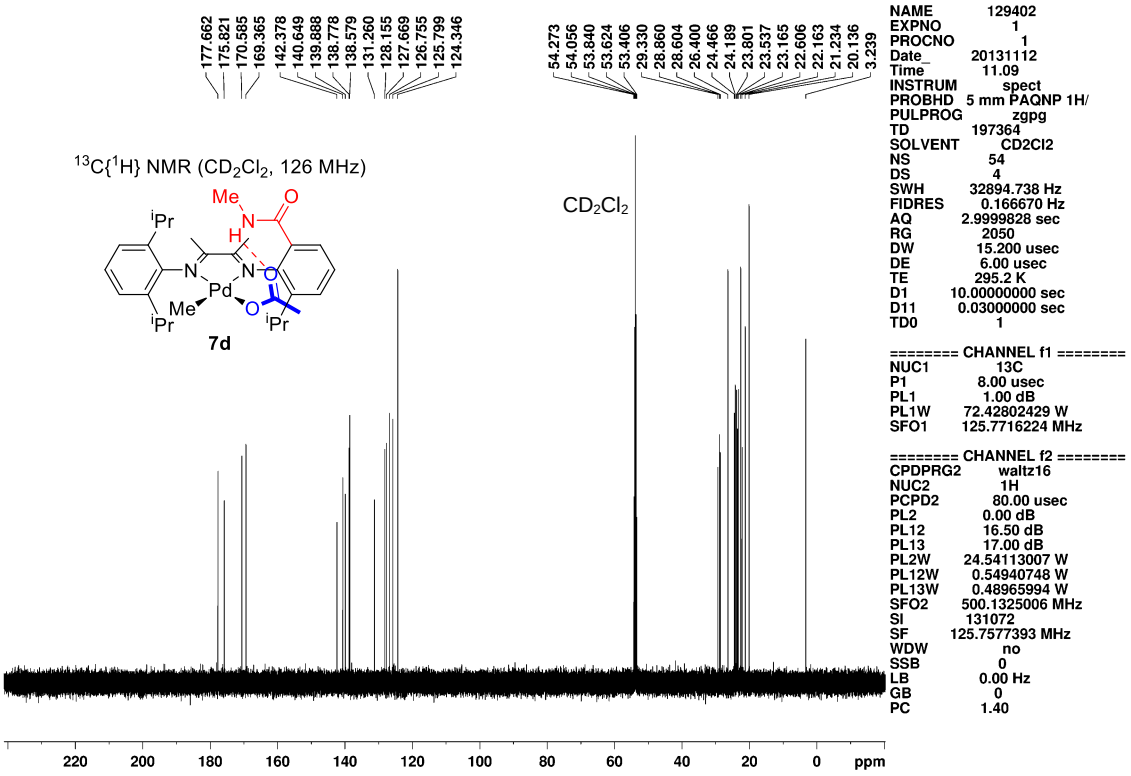

Figure 2.38, continued. NMR spectra of **7d**.

7d-^{13}C$_1$. This compound was prepared by the procedure for **7d** using $AgO_2{}^{13}CCH_3$. Yield: 89%. ^{1}H NMR (500 MHz, CD_2Cl_2): δ 1.36 (d, $^2J_{CH}$ = 6.0, 3H, $^{13}CH_3CO_2$). ^{13}C{^{1}H} NMR (126 MHz, CD_2Cl_2): δ 177.6 (s, Me$^{13}CO_2$), 22.6 (d, $^1J_{CC}$ = 55, *Me*$^{13}CO_2$). IR (cm^{-1}): $\nu_{N–H}$, 3210; $\nu_{C=O,amide}$, 1653; $\nu_{OCO,asym}$, 1557; $\nu_{OCO,sym}$, 1317.

(a)

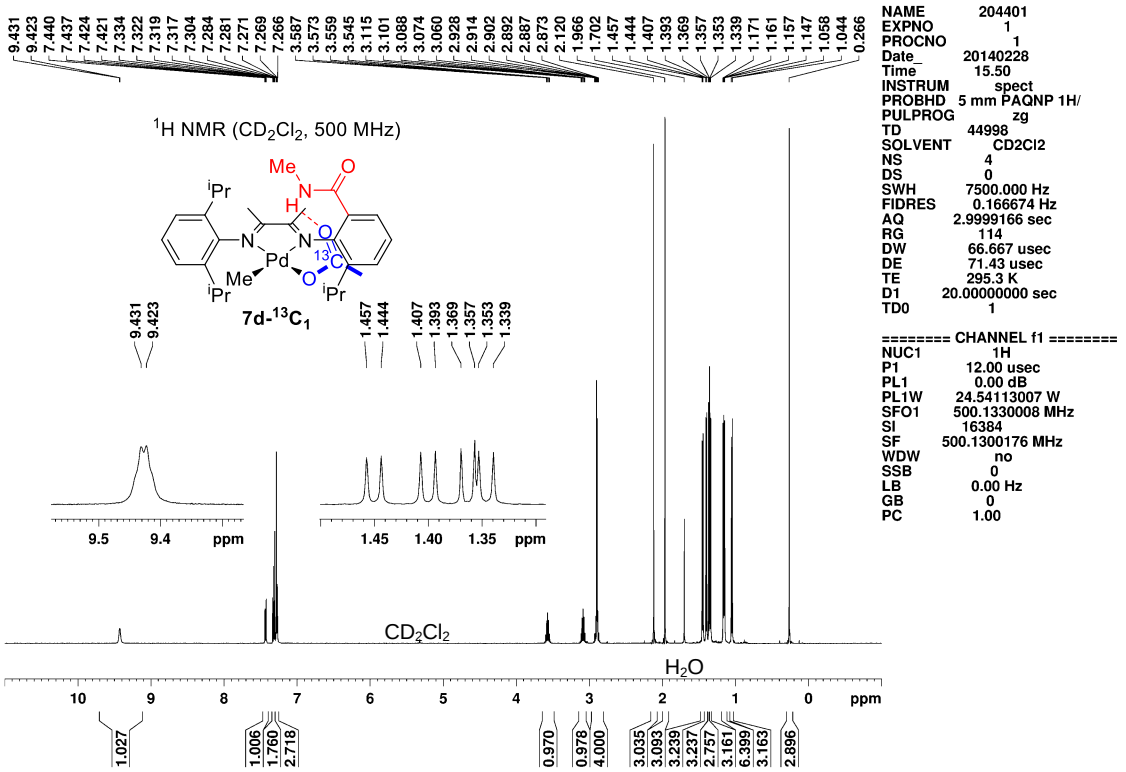

(b)

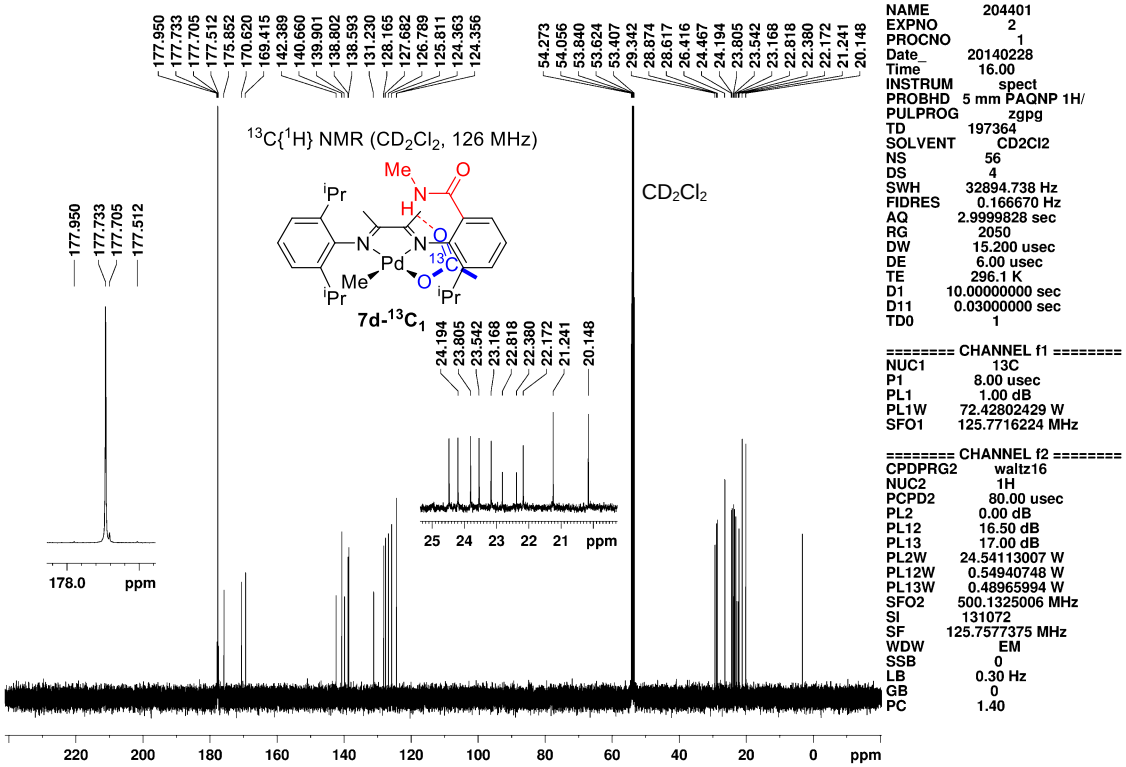

Figure 2.39. NMR spectra of **7d-$^{13}C_1$**.

7e. A solution of **5e** (80.6 mg, 0.143 mmol) in CH_2Cl_2 (3 mL) was vigorously stirred at room temperature, and AgOAc (30.1 mg, 0.180 mmol, 1.26 equiv) was added in one portion. The mixture was stirred at room temperature for 2 h to give a suspension of an off-white precipitate in a brown solution. The suspension was filtered by pipette filtration. Hexanes (12 mL) was added to the filtrate in one portion, and the mixed solution was kept at –40 °C overnight to afford the product as brown needles that contained 0.63 equiv CH_2Cl_2 as determined by ^{1}H NMR integration (79.0 mg, 87%). Recrystallization from CH_2Cl_2/Et_2O at –40 °C yielded brown crystals of **7e**·CH_2Cl_2. ^{1}H NMR (500 MHz, CD_2Cl_2): δ 7.33–7.22 (m, 6H, Ar), 3.11 (septet, J = 6.8, 2H, ^{i}Pr methine), 3.09 (septet, J = 6.8, 2H, ^{i}Pr methine), 2.06 (s, 3H, *Me*C=N), 1.97 (s, 3H, *Me*C=N), 1.41 (d, J = 6.8, 6H, ^{i}Pr), 1.39 (d, J = 6.8, 6H, ^{i}Pr), 1.33 (s, 3H, C*H*$_3$CO$_2$), 1.18 (d, J = 6.9, 6H, ^{i}Pr), 1.15 (d, J = 6.9, 6H, ^{i}Pr), 0.30 (s, 3H, Pd–Me). ^{13}C NMR (126 MHz, CD_2Cl_2): δ 175.2 (Me*C*O$_2$), 174.9, 169.5 (imine C=N), 142.6, 141.7, 138.9, 138.8, 127.9, 127.1, 124.3, 123.6 (Ar), 29.3, 28.8 (^{i}Pr methine), 24.0, 23.9, 23.6, 23.4 (^{i}Pr methyl), 23.1 (*Me*CO$_2$), 21.2, 20.1 (*Me*C=N), 1.6 (Pd–Me). IR (cm^{-1}): ν_{N-H}, 3210; $\nu_{OCO,asym}$, 1615; $\nu_{OCO,sym}$, 1322. Anal. Calcd. for $C_{31}H_{46}N_2O_2Pd{\cdot}CH_2Cl_2$, %: C, 57.36; H, 7.22; N, 4.18. Found: C, 57.33; H, 6.84; N, 3.96. ESI-MS (1:1 MeOH:H_2O, positive ion scan, *m*/*z*): 566.3 ([M – H_2O]$^+$), 509.2 ([M – OAc – CH_4]$^+$).

(a)

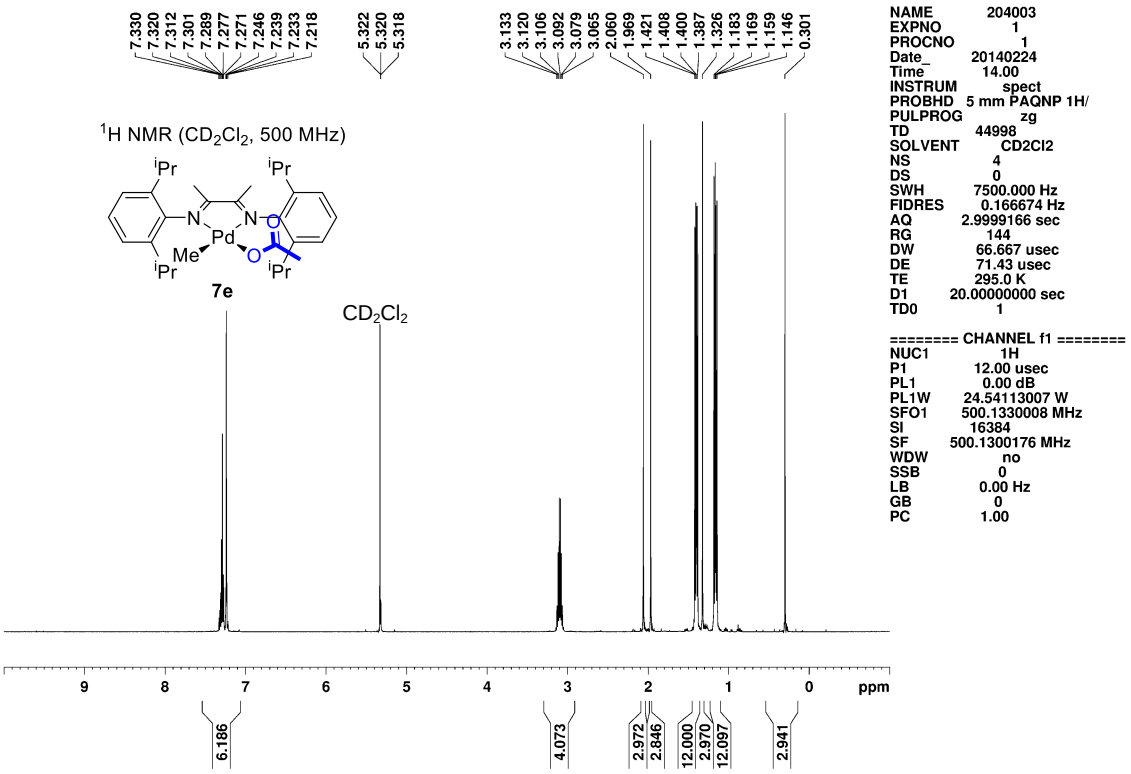

(b)

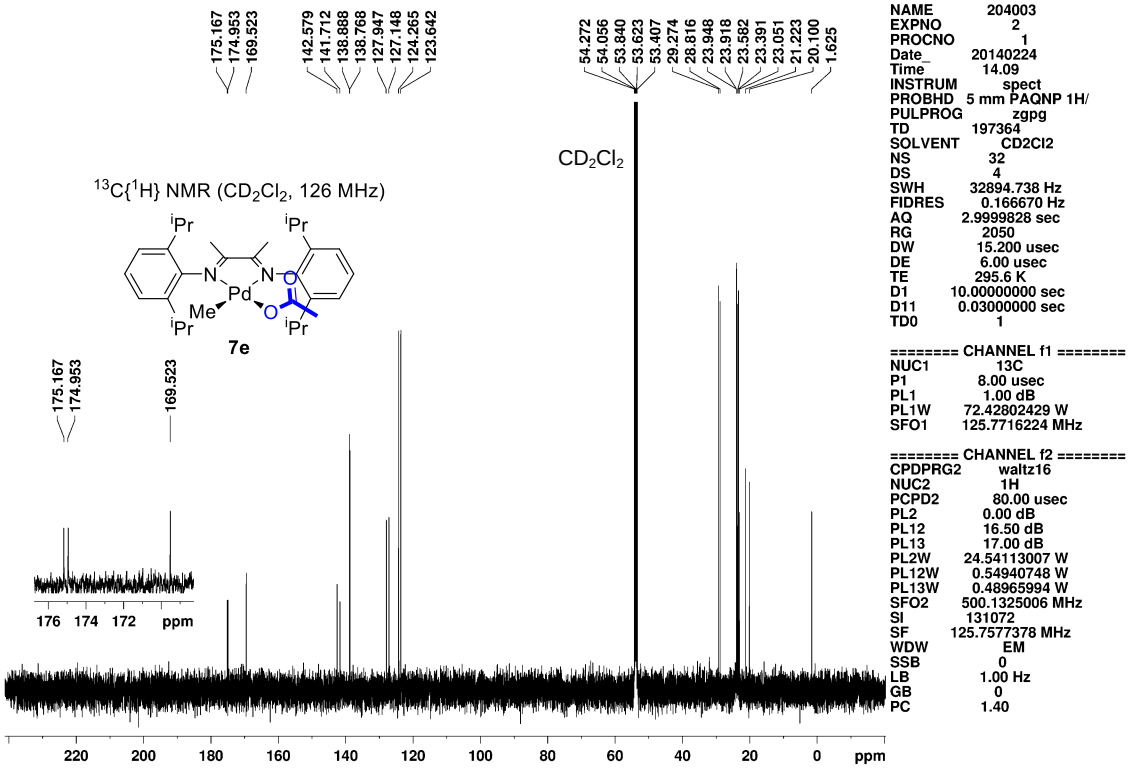

Figure 2.40. NMR spectra of **7e**.

7e-^{13}C$_1$. This compound was prepared by the procedure for **7e** using $AgO_2{}^{13}CCH_3$. Yield: 64%. ^{1}H NMR (500 MHz, CD_2Cl_2): δ 1.33 (d, $^2J_{CH}$ = 6.0, 3H, $^{13}CH_3CO_2$). ^{13}C{^{1}H} NMR (126 MHz, CD_2Cl_2): δ 175.2 (s, Me^{13}CO$_2$), 23.1 (d, $^1J_{CC}$ = 55, *Me*^{13}CO$_2$). IR (cm^{-1}): $\nu_{OCO,asym}$, 1570; $\nu_{OCO,sym}$, 1300.

(a)

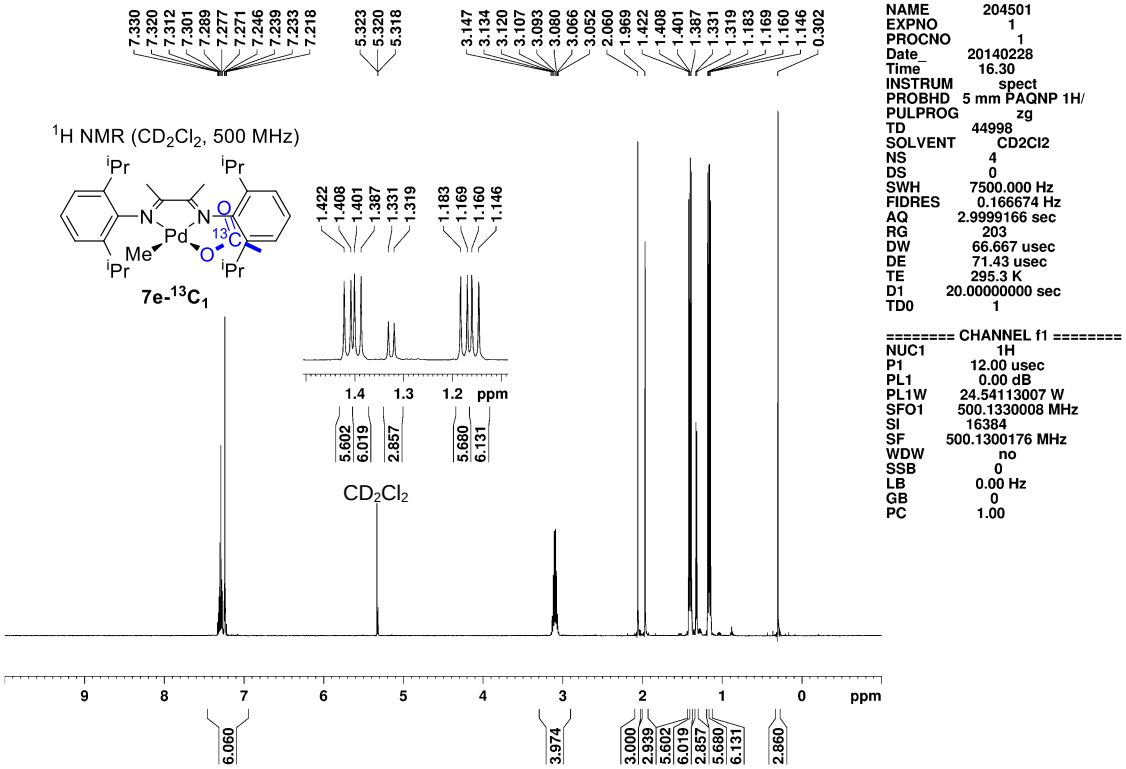

Figure 2.41. NMR spectra of **7e-^{13}C$_1$**.

(b)

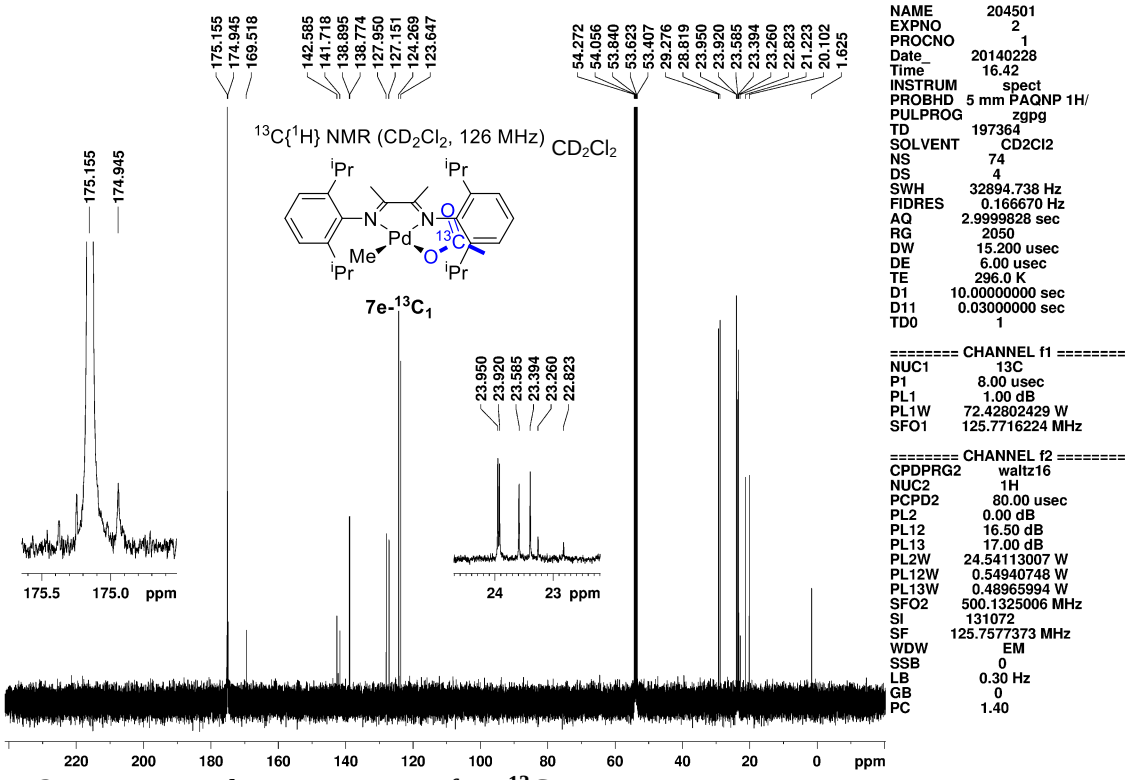

Figure 2.41, continued. NMR spectra of **7e-^{13}C$_1$**.

8a. A glass vial was charged with **5a**,**a'** (54.3 mg, 0.0919 mmol), $AgSbF_6$ (39.1 mg, 1.24 equiv), and pyrazole (6.3 mg, 1.0 equiv). CH_2Cl_2 (2 mL) was added to the reaction mixture, and the vial was agitated for 20 sec to give a suspension of an off-white precipitate in an orange solution. The suspension was filtered by pipette filtration. The filtrate was concentrated to 2 mL, layered with hexanes (8 mL) and kept at –40 °C overnight to give orange needles (73.5 mg, 91%). The solid contained 0.020 equiv CH_2Cl_2 and 0.20 equiv Et_2O as determined by ^{1}H NMR. ^{1}H NMR (500 MHz, CD_2Cl_2): δ 14.38 (br s, 1H, pz NH), 7.38–7.26 (m, 5H, Ar), 7.24–7.23 (m, 1H, pz H^5), 7.21–7.19 (m, 2H, pz H^3 + 1 Ar CH), 6.16 (q, *J* = 2.3, 1H, pz H^4), 3.23 (s, 3H, amide NMe), 3.11 (s, 3H, amide NMe), 3.01 (septet, *J* = 6.8, 1H, ^{i}Pr methine), 2.96 (septet, *J* = 6.9, 1H, ^{i}Pr methine), 2.91 (septet, *J* = 6.9, 1H, ^{i}Pr methine), 2.24 (s, 3H, *Me*C=N), 2.22 (s, 3H, *Me*C=N), 1.40 (d, *J* = 6.8, 3H, ^{i}Pr), 1.36 (d, *J* = 6.8, 3H, ^{i}Pr), 1.23 (d, *J* = 6.9, 3H, ^{i}Pr), 1.22 (d, *J* = 6.9, 3H, ^{i}Pr), 1.16 (d,

J = 6.9, 3H, ^{i}Pr), 1.07 (d, *J* = 6.8, 3H, ^{i}Pr), 0.42 (s, 3H, Pd–Me). ^{1}H NMR (500 MHz, CD_3CN): δ 14.47 (br s, 1H, pz NH), 6.18 (q, *J* = 2.3, 1H, pz H^4), 0.28 (s, 3H, Pd–Me). $^{13}C\{^{1}H\}$ NMR (126 MHz, CD_2Cl_2): δ 178.8, 173.3 (imine C=N), 170.0 (C=O), 141.6 (Ar), 140.7 (pz C^5), 140.3, 140.1, 139.0, 138.5 (Ar), 130.6 (pz C^3), 128.7 (2C), 128.0, 126.8, 125.1, 124.8, 124.5 (Ar), 106.6 (pz C^4), 39.4, 35.2 (amide NMe), 29.2, 29.0 (2C) (^{i}Pr methine), 23.9, 23.8, 23.6, 23.33, 23.25, 23.21 (^{i}Pr methyl), 21.6, 20.4 (*Me*C=N), 7.1 (Pd–Me). ^{19}F NMR (470 MHz, CD_3CN): δ –123.7; overlay of $^{121}SbF_6$ (sextet, J_{SbF} = 1940) and $^{123}SbF_6$ (octet, J_{SbF} = 1050). IR (cm^{-1}): ν_{N-H}, 3134; $\nu_{C=O,}$ 1607. ESI-MS (1:1 MeOH:H_2O, positive ion scan, *m*/*z*): 622.3 ($[M - SbF_6]^+$). ESI-MS (1:1 MeOH:H_2O, negative ion scan, *m*/*z*): 234.9 (SbF_6^-). HRMS (ESI-TOF, positive ion, *m*/*z*): Calc. 622.2737 ($[M - SbF_6]^+$), found 622.2752.

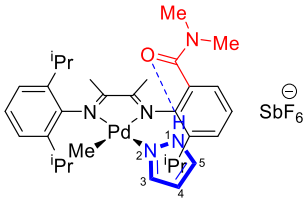

(a)

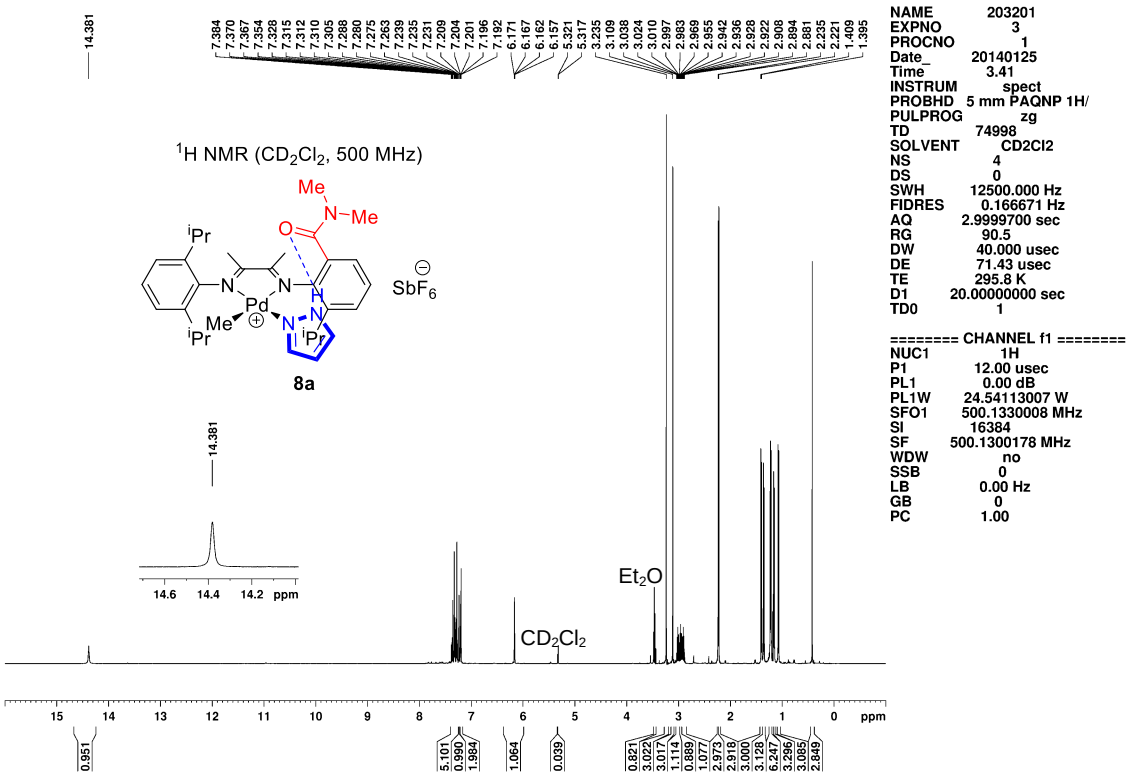

(b)

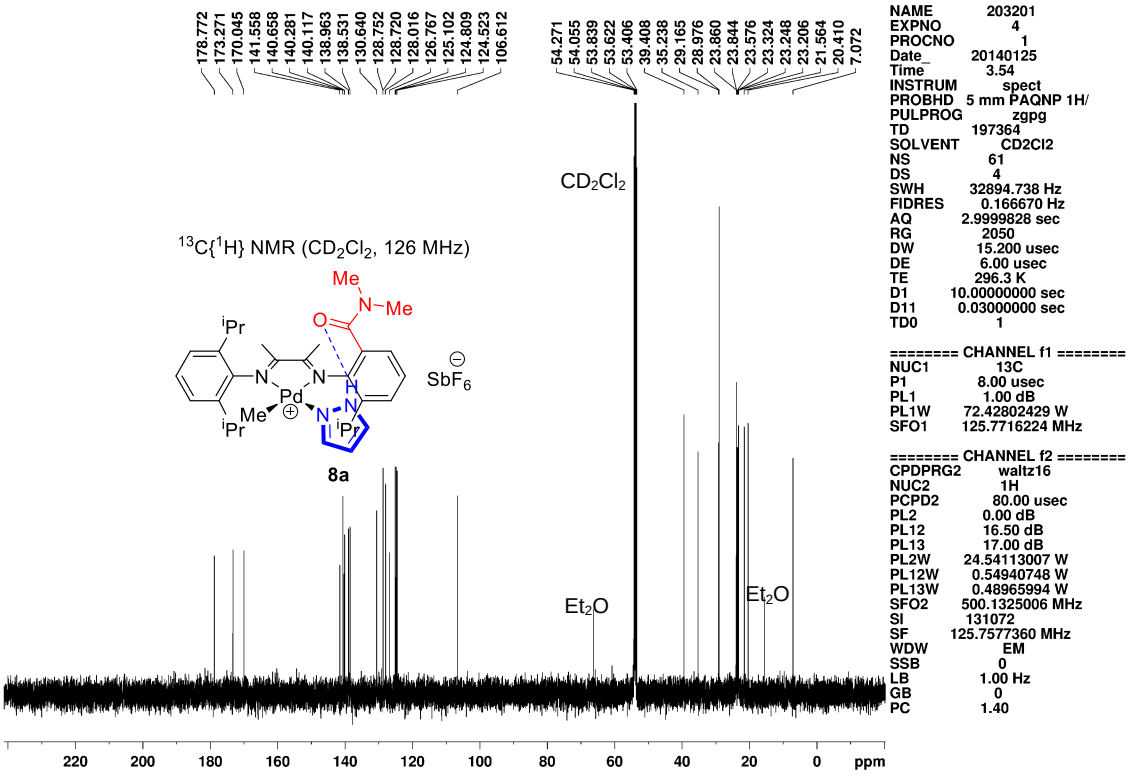

Figure 2.42. NMR spectra of **8a**.

(c)

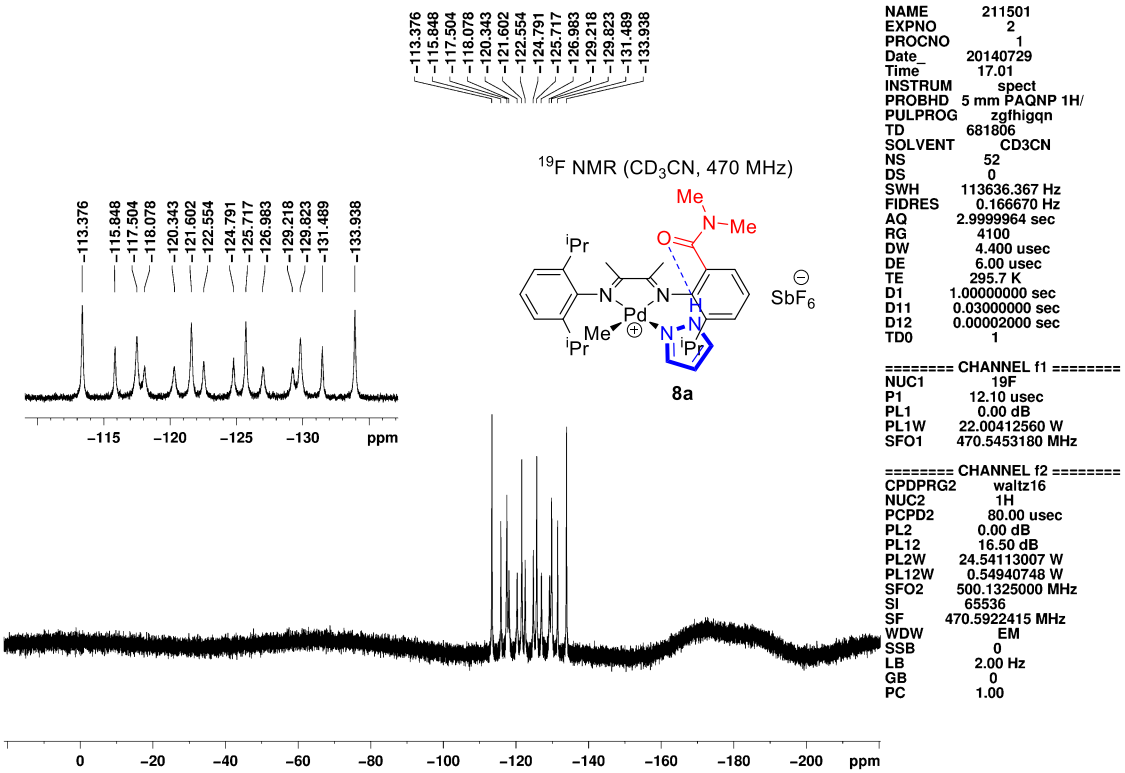

Figure 2.42, continued. NMR spectra of **8a**.

8c-*anti*,*syn*. A glass vial was charged with pure **5c-*anti*** (63.4 mg, 0.102 mmol), $AgSbF_6$ (37.1 mg, 1.06 equiv), and pyrazole (7.0 mg, 1.0 equiv). CH_2Cl_2 (3 mL) was added to the reaction mixture, and the vial was agitated for 10 sec to give a suspension of an off-white precipitate in an orange solution. The suspension was filtered by pipette filtration. The filtrate was layered with hexanes (10 mL) and kept at –40 °C to give yellow crystals (76.0 mg, 84%). This solid is a 6.3/1 mixture of **8c-*anti*** and **8c-*syn***, as determined by ^{1}H NMR at room temperature in ca. 5 min after sample preparation based on the integrals of the Pd–Me resonances. Anti/syn isomerization affords a 1.5/1 equilibrium **8c-*anti*/8c-*syn*** mixture within 5 h at room temperature in CD_2Cl_2 or a 2.0/1 equilibrium **8c-*anti*/8c-*syn*** mixture within 1 h at room temperature in CD_3CN. **8c-*anti***: ^{1}H NMR (500 MHz, CD_2Cl_2): δ 14.42 (br s, 1H, pz NH), 7.53 (dd, J = 7.9, 1.4, 1H, Ar), 7.41 (t, J = 7.7 Hz, 1H, Ar), 7.31–7.22 (m, 3H, Ar), 7.19–7.17 (m, 3H, pz H^3 + pz H^5 + 1 Ar CH), 6.16 (q, J = 2.2, 1H,

pz H^4), 3.23 (s, 3H, amide NMe), 3.110 (s, 3H, amide NMe), 3.108 (s, 3H, amide NMe), 3.05 (s, 3H, amide NMe), 3.05 (septet, J = 6.8, 1H, ^{i}Pr methine), 2.93 (septet, J = 6.8, 1H, ^{i}Pr methine), 2.26 (s, 3H, *Me*C=N), 2.18 (s, 3H, *Me*C=N), 1.35 (d, J = 6.8, 3H, ^{i}Pr), 1.231 (d, J = 6.9, 3H, ^{i}Pr), 1.13 (d, J = 6.9, 3H, ^{i}Pr), 1.04 (d, J = 6.8, 3H, ^{i}Pr), 0.44 (s, 3H, Pd–Me). ^{1}H NMR (500 MHz, CD_3CN): δ 14.49 (br s, 1H, pz NH), 6.18 (q, J = 2.3, 1H, pz H^4), 0.35 (s, 3H, Pd–Me). $^{13}C\{^1H\}$ NMR (126 MHz, CD_2Cl_2): δ 181.8, 173.5 (imine C=N), 170.0, 167.8 (C=O), 142.1, 140.6 (Ar), 140.46 (pz C^5), 140.2, 140.0 (Ar), 130.7 (pz C^3), 128.77, 128.11, 127.95, 127.75, 127.4, 126.6, 125.8, 125.1 (Ar), 106.61 (pz C^4), 39.74, 39.4, 35.4, 35.1 (amide NMe), 28.85, 28.6 (^{i}Pr methine), 23.89, 23.75, 23.15 (^{i}Pr methyl), 23.11 (*Me*C=N), 23.06 (^{i}Pr methyl), 20.3 (*Me*C=N), 5.8 (Pd–Me). **8c-*syn***: ^{1}H NMR (500 MHz, CD_2Cl_2): δ 14.42 (br s, 1H, pz NH), 7.53 (dd, J = 7.9, 1.4, 1H, Ar), 7.41 (t, J = 7.7 Hz, 1H, Ar), 7.31–7.22 (m, 3H, Ar), 7.22–7.21 (m, 1H, pz H^5), 7.19–7.17 (m, 2H, pz H^3 + 1 Ar CH), 6.16 (m, 1H, pz H^4), 3.29 (s, 3H, amide NMe), 3.20 (s, 3H, amide NMe), 3.07 (s, 3H, amide NMe), 2.96 (septet, J = 6.8, 1H, ^{i}Pr methine), 2.94 (septet, J = 6.8, 1H, ^{i}Pr methine), 2.93 (s, 3H, amide NMe), 2.25 (s, 3H, *Me*C=N), 2.17 (s, 3H, *Me*C=N), 1.42 (d, J = 6.8, 3H, ^{i}Pr), 1.234 (d, J = 6.9, 3H, ^{i}Pr), 1.14 (d, J = 6.9, 3H, ^{i}Pr), 1.09 (d, J = 6.8, 3H, ^{i}Pr), 0.46 (s, 3H, Pd–Me). ^{1}H NMR (500 MHz, CD_3CN): δ 14.54 (br s, 1H, pz NH), 6.16 (m, 1H, pz H^4), 0.37 (s, 3H, Pd–Me). $^{13}C\{^1H\}$ NMR (126 MHz, CD_2Cl_2): δ 181.4, 173.2 (imine C=N), 169.9, 167.5 (C=O), 142.0, 140.44, 140.40 (Ar), 140.35 (pz C^5), 140.1 (Ar), 130.8 (pz C^3), 128.74, 128.03, 127.89, 127.82, 127.6, 126.7, 125.9, 125.0 (Ar), 106.57 (pz C^4), 39.72, 39.6, 35.7, 35.5 (amide NMe), 28.92, 28.88 (^{i}Pr methine), 23.87, 23.70 (^{i}Pr methyl), 23.21, 23.15, 23.08 (^{i}Pr methyl + *Me*C=N), 20.5 (*Me*C=N), 6.0 (Pd–Me). ^{19}F NMR (470 MHz, CD_3CN): δ –123.3; overlay of $^{121}SbF_6$ (sextet, J_{SbF} = 1930) and $^{123}SbF_6$ (octet, J_{SbF} = 1050). IR (cm^{-1}): $\nu_{N–H}$, 3131; $\nu_{C=O,}$ 1630, 1606. Anal. Calcd. for $C_{32}H_{45}F_6N_6O_2PdSb$, %: C, 43.29; H, 5.11; N, 9.47. Found: C, 42.73; H, 5.07; N, 9.15. ESI-MS

(1:1 MeOH:H_2O, positive ion scan, *m*/*z*): 651.3 ($[M - SbF_6]^+$). ESI-MS (1:1 MeOH:H_2O, negative ion scan, *m*/*z*): 234.9 (SbF_6^-). HRMS (ESI-TOF, positive ion, *m*/*z*): Calc. 651.2639 ($[M - SbF_6]^+$), found 651.2647.

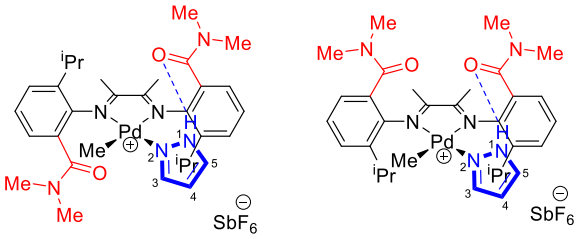

(a)

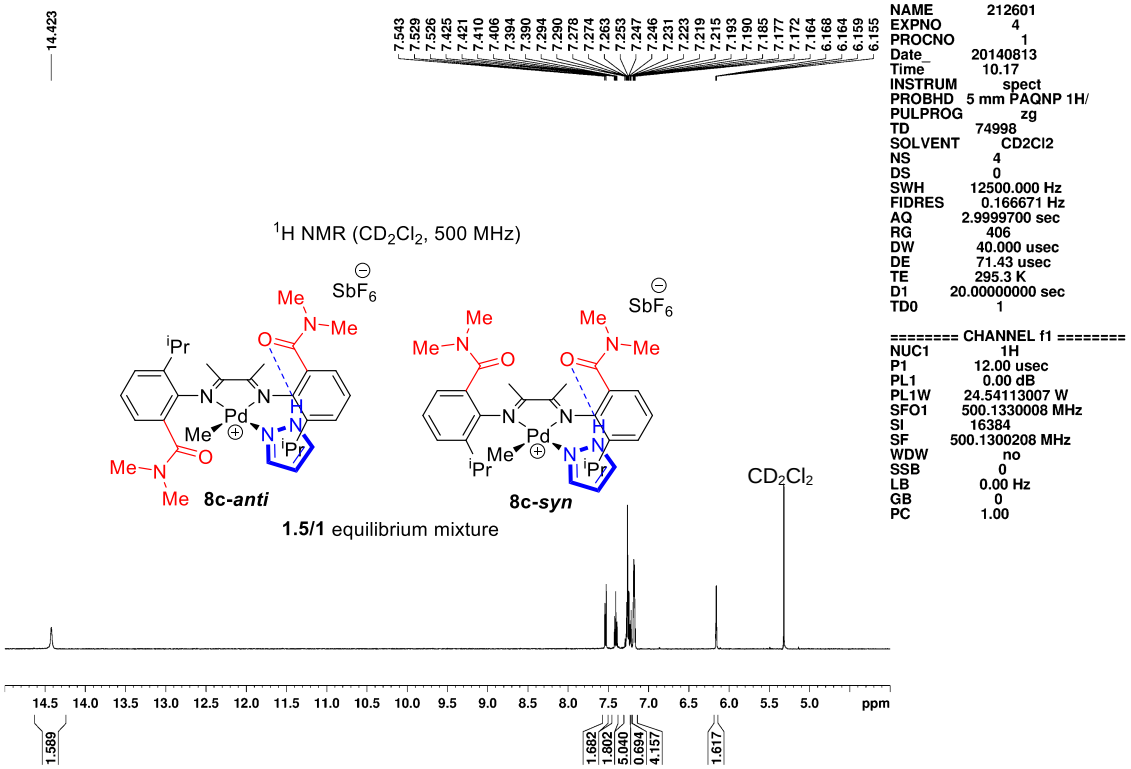

(b)

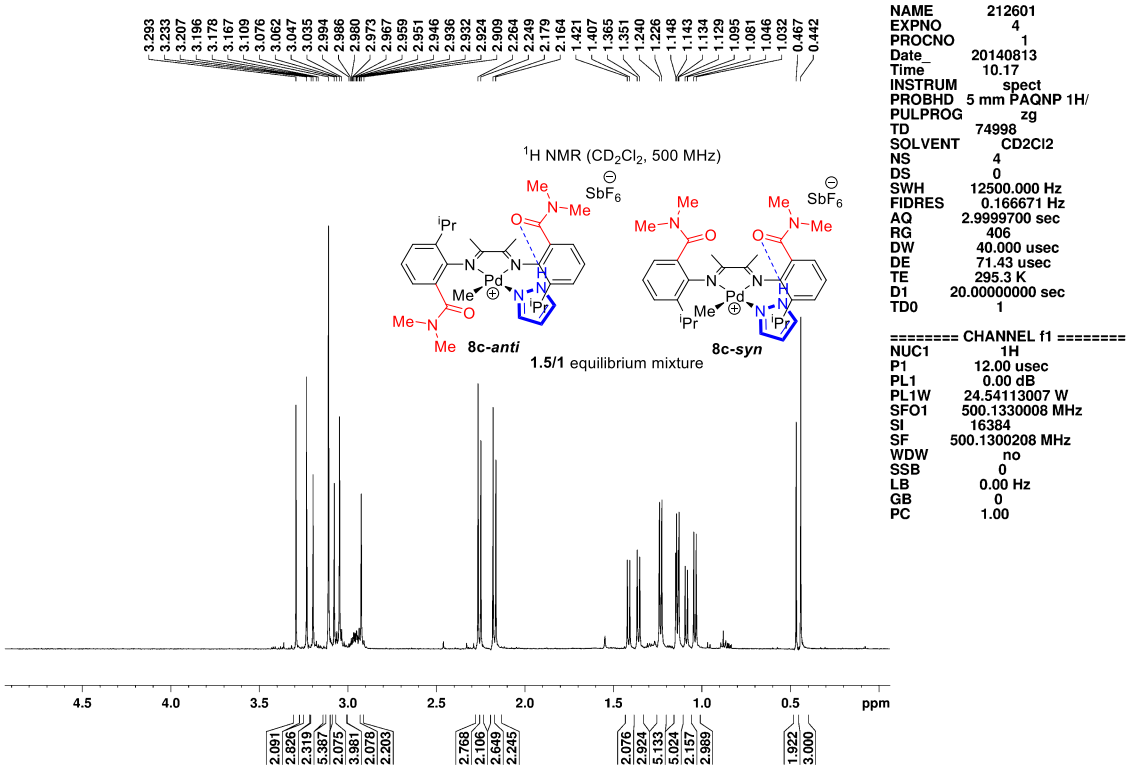

Figure 2.43. NMR spectra of **8c-*anti,syn***.

(c)

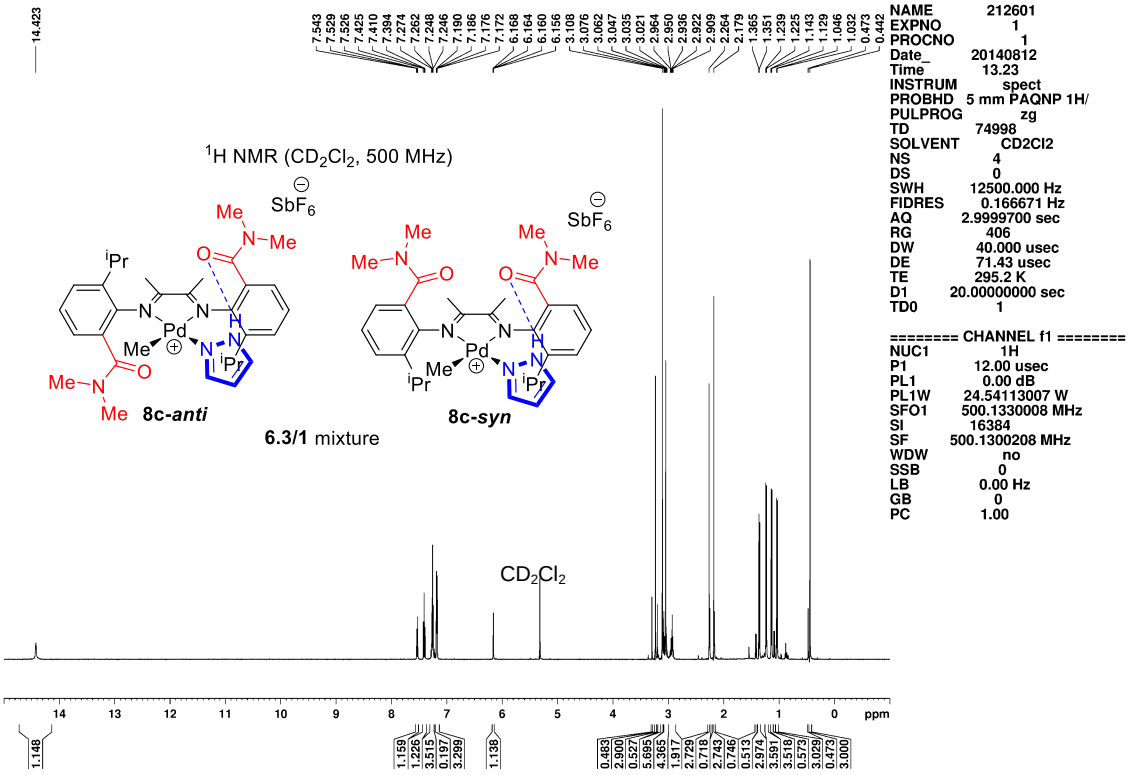

(d)

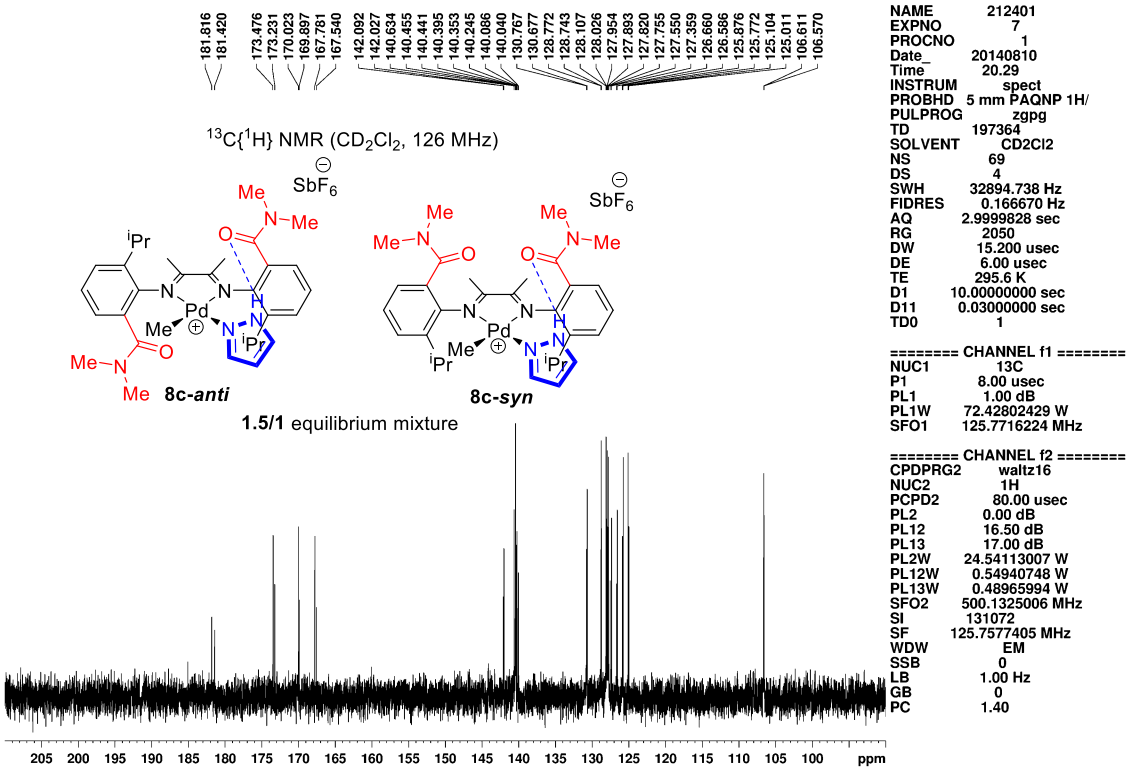

Figure 2.43, continued. NMR spectra of **8c-*anti*,*syn***.

(e)

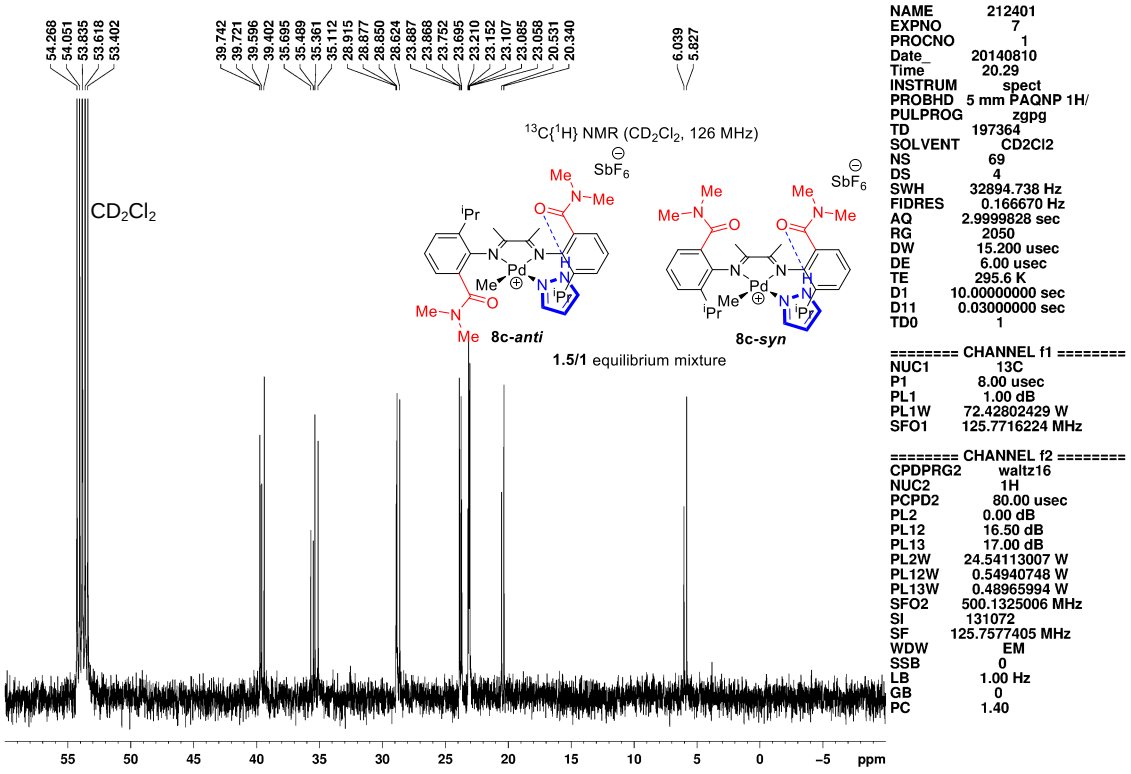


```
NAME          212401
EXPNO              7
PROCNO             1
Date_       20140810
Time           20.29
INSTRUM         spect
PROBHD  5 mm PAQNP 1H/
PULPROG         zgpg
TD            197364
SOLVENT         CD2Cl2
NS                69
DS                 4
SWH           32894.738 Hz
FIDRES        0.166670 Hz
AQ            2.9999828 sec
RG                2050
DW            15.200 usec
DE             6.00 usec
TE             295.6 K
D1          10.00000000 sec
D11          0.03000000 sec
TD0                1

======== CHANNEL f1 ========
NUC1              13C
P1             8.00 usec
PL1            1.00 dB
PL1W       72.42802429 W
SFO1       125.7716224 MHz

======== CHANNEL f2 ========
CPDPRG2        waltz16
NUC2              1H
PCPD2          80.00 usec
PL2            0.00 dB
PL12           16.50 dB
PL13           17.00 dB
PL2W       24.54113007 W
PL12W       0.54940748 W
PL13W       0.48965994 W
SFO2       500.1325006 MHz
SI            131072
SF         125.7577405 MHz
WDW               EM
SSB               0
LB             1.00 Hz
GB                0
PC             1.40
```

(f)

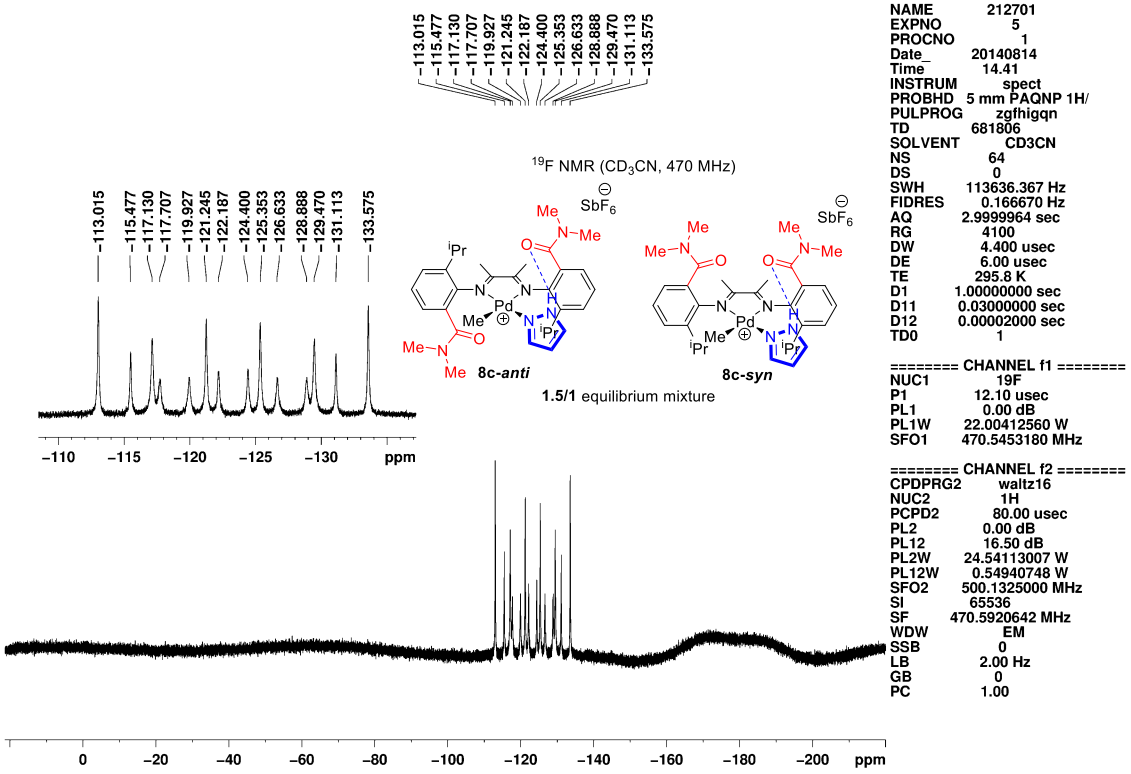


```
NAME          212701
EXPNO              5
PROCNO             1
Date_       20140814
Time           14.41
INSTRUM         spect
PROBHD  5 mm PAQNP 1H/
PULPROG       zgfhigqn
TD            681806
SOLVENT         CD3CN
NS                64
DS                 0
SWH           113636.367 Hz
FIDRES        0.166670 Hz
AQ            2.9999964 sec
RG                4100
DW            4.400 usec
DE             6.00 usec
TE             295.8 K
D1          1.00000000 sec
D11         0.03000000 sec
D12         0.00002000 sec
TD0                1

======== CHANNEL f1 ========
NUC1              19F
P1            12.10 usec
PL1            0.00 dB
PL1W       22.00412560 W
SFO1       470.5453180 MHz

======== CHANNEL f2 ========
CPDPRG2        waltz16
NUC2              1H
PCPD2          80.00 usec
PL2            0.00 dB
PL12           16.50 dB
PL2W       24.54113007 W
PL12W       0.54940748 W
SFO2       500.1325000 MHz
SI             65536
SF         470.5920642 MHz
WDW               EM
SSB               0
LB             2.00 Hz
GB                0
PC             1.00
```

Figure 2.43, continued. NMR spectra of **8c-*anti*,*syn***.

Isomerization Equilibrium of 8c-*anti*,*syn* in CD_2Cl_2. A J. Young NMR tube was charged with pure **5c-*anti*** (18.2 mg, 0.0294 mmol), $AgSbF_6$ (11.4 mg, 0.0331 mmol, 1.13 equiv), and pyrazole (2.0 mg, 0.029 mmol, 1.0 equiv). CD_2Cl_2 (0.5 mL) was transferred in under vacuum at –196 °C. The tube was sealed, and the sample was warmed to room temperature to yield a yellow solution. The sample was then transferred to NMR probe at room temperature, and ^{1}H NMR spectra were collected periodically (Figure 2.44). A 12.6/1 mixture of **8c-*anti*** and **8c-*syn*** formed within 5 min, and equilibrium (1.5/1) was reached within 5 h.

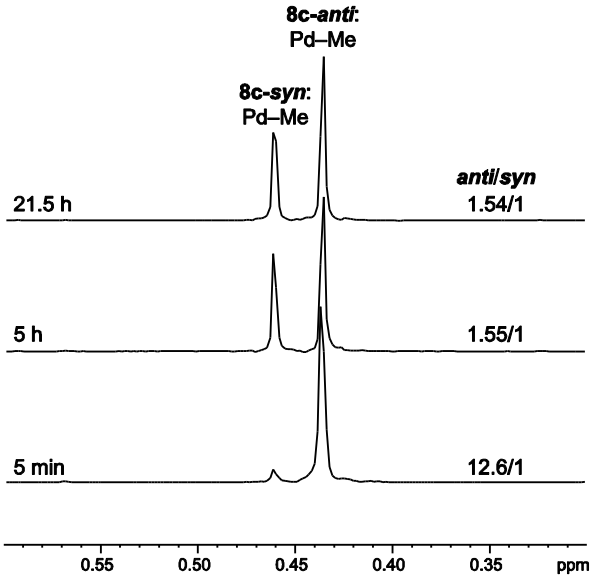

Figure 2.44. Stacked ^{1}H NMR spectra showing the conversion of **8c-*anti*** to **8c-*syn*** in CD_2Cl_2 at room temperature (500 MHz). The Pd–Me region (δ 0.60–0.30) is shown.

Isomerization Equilibrium of 8c-*anti*,*syn* in CD_3CN. A J. Young NMR tube was charged with a 6.3/1 mixture of **8c-*anti*** and **8c-*syn*** (14.5 mg) and CD_3CN (0.448 mL) under nitrogen at room temperature. The tube was sealed, and the anti/syn isomerization was monitored by ^{1}H NMR (Figure 2.45). The mixture reached equilibrium (**8c-*anti*/8c-*syn*** = 2.0/1) within 1 h.

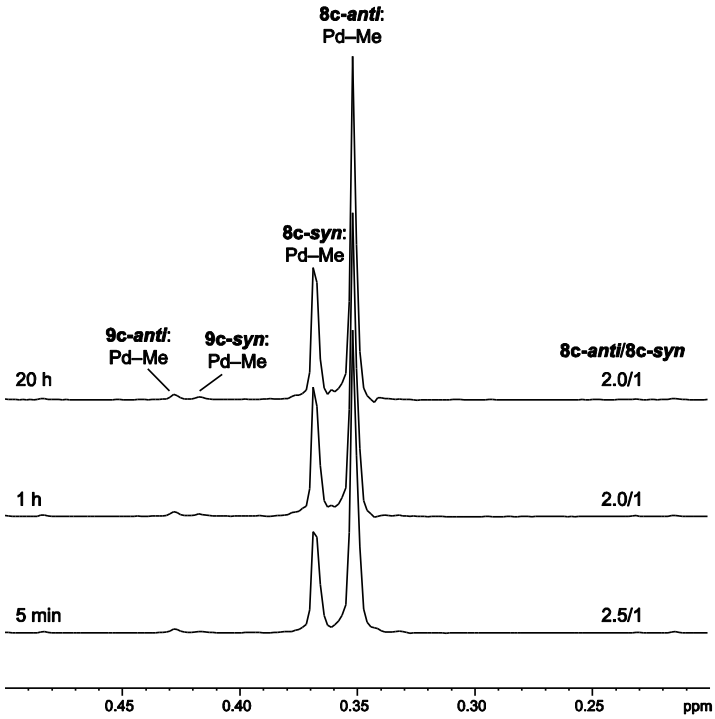

Figure 2.45. Stacked ^{1}H NMR spectra showing the conversion of **8c-*anti*** to **8c-*syn*** in CD_3CN at room temperature (500 MHz). The Pd–Me region (δ 0.50–0.20) is shown.

8d. A glass vial was charged with **5d**,**d'** (52.1 mg, 0.0903 mmol), $AgSbF_6$ (37.3 mg, 1.20 equiv), and pyrazole (6.1 mg, 1.0 equiv). CH_2Cl_2 (2 mL) was added to the reaction mixture, and the vial was agitated for 20 sec to give a suspension of an off-white precipitate in an orange solution. The suspension was filtered by pipette filtration. The filtrate was concentrated to 1 mL, layered with hexanes (8 mL) and kept at –40 °C overnight to give orange needles (70.0 mg, 91%). The solid contained 0.10 equiv CH_2Cl_2 and 0.12 equiv Et_2O as determined by ^{1}H NMR. ^{1}H NMR (500 MHz, CD_2Cl_2): δ 14.09 (br s, 1H, pz NH), 7.38 (m, 1H, Ar), 7.33–7.28 (m, 5H, Ar), 7.26 (m, 2H, pz H^3 + H^5), 6.80 (br q, *J* = 4.5, 1H, amide NH), 6.18 (q, *J* = 2.3, 1H, pz H^4), 3.08 (d, *J* = 4.9, 3H, amide NMe), 3.03 (septet, *J* = 6.8, 1H, ^{i}Pr methine), 2.99 (septet, *J* = 6.9, 1H, ^{i}Pr methine), 2.92 (septet, *J* = 6.9, 1H, ^{i}Pr methine), 2.19 (s, 6H, *Me*C=N), 1.41 (d, *J* = 6.8, 3H, ^{i}Pr), 1.36 (d, *J* = 6.8, 3H, ^{i}Pr), 1.22 (d, *J* = 6.9, 6H, ^{i}Pr), 1.14 (d, *J* = 6.9, 3H, ^{i}Pr), 1.09 (d, *J* = 6.8, 3H, ^{i}Pr), 0.42 (s, 3H, Pd–Me). ^{1}H NMR (500 MHz, CD_3CN): δ 14.00 (br s, 1H, pz NH), 6.18 (q, *J* = 2.3, 1H, pz H^4),

0.28 (s, 3H, Pd–Me). $^{13}C\{^{1}H\}$ NMR (126 MHz, CD_2Cl_2): δ 178.7, 174.0 (imine C=N), 171.1 (C=O), 141.5 (Ar), 140.8 (pz C^5), 140.4, 139.5, 138.9, 138.6 (Ar), 130.9 (pz C^3), 129.3, 128.8, 128.4, 128.3, 125.4, 124.8, 124.5 (Ar), 106.7 (pz C^4), 29.2, 29.0 (2C) (^{i}Pr methine), 27.4 (amide NMe), 24.0, 23.9, 23.45, 23.41, 23.3, 23.2 (^{i}Pr methyl), 21.7, 20.0 (*Me*C=N), 6.9 (Pd–Me). ^{19}F NMR (470 MHz, CD_3CN): δ –124.1; overlay of $^{121}SbF_6$ (sextet, J_{SbF} = 1920) and $^{123}SbF_6$ (octet, J_{SbF} = 1050). IR (cm^{-1}): $\nu_{N–H}$, 3413, 3137; $\nu_{C=O}$, 1626. Anal. Calcd. for $C_{31}H_{44}F_6N_5OPdSb \cdot 0.10CH_2Cl_2 \cdot 0.12C_4H_{10}O$, %: C, 43.99; H, 5.31; N, 8.12. Found: C, 43.45; H, 5.31; N, 8.12. ESI-MS (1:1 MeOH:H_2O, positive ion scan, *m*/*z*): 608.3 ($[M – SbF_6]^+$). ESI-MS (1:1 MeOH:H_2O, negative ion scan, *m*/*z*): 234.9 (SbF_6^-). HRMS (ESI-TOF, positive ion, *m*/*z*): Calc. 608.2581 ($[M – SbF_6]^+$), found 608.2594.

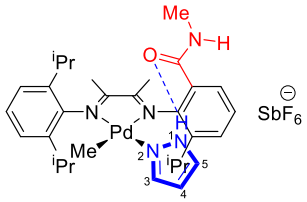

(a)

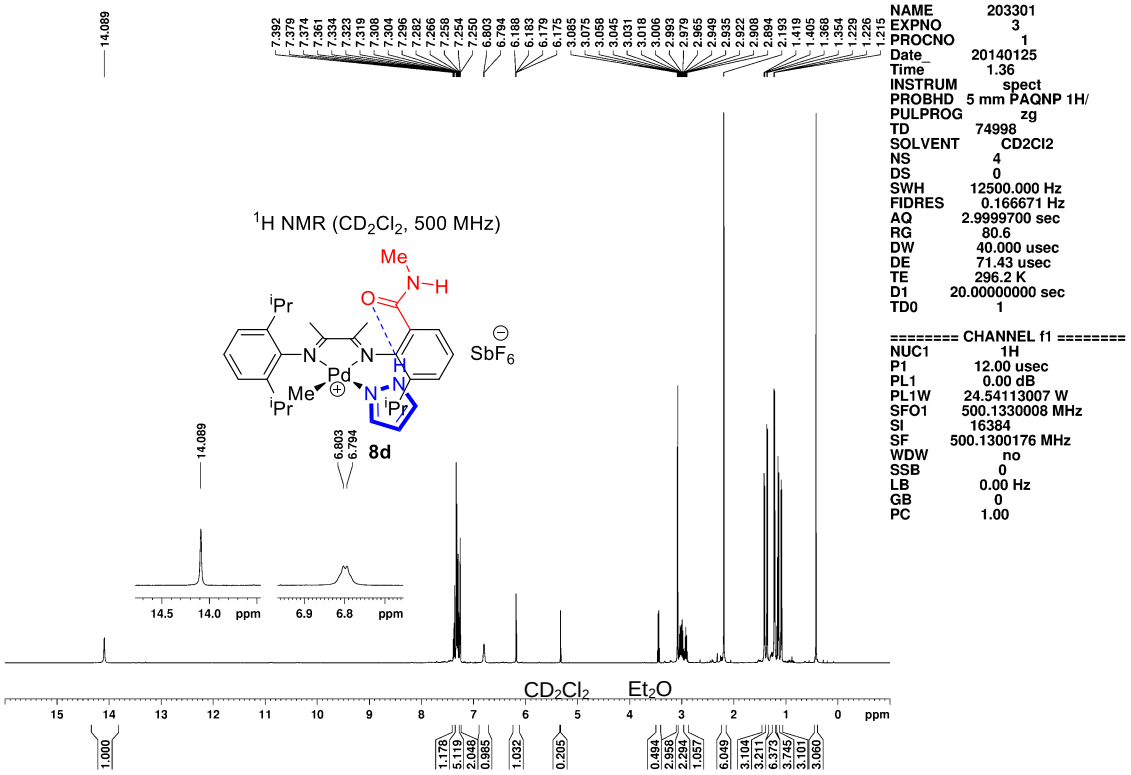

(b)

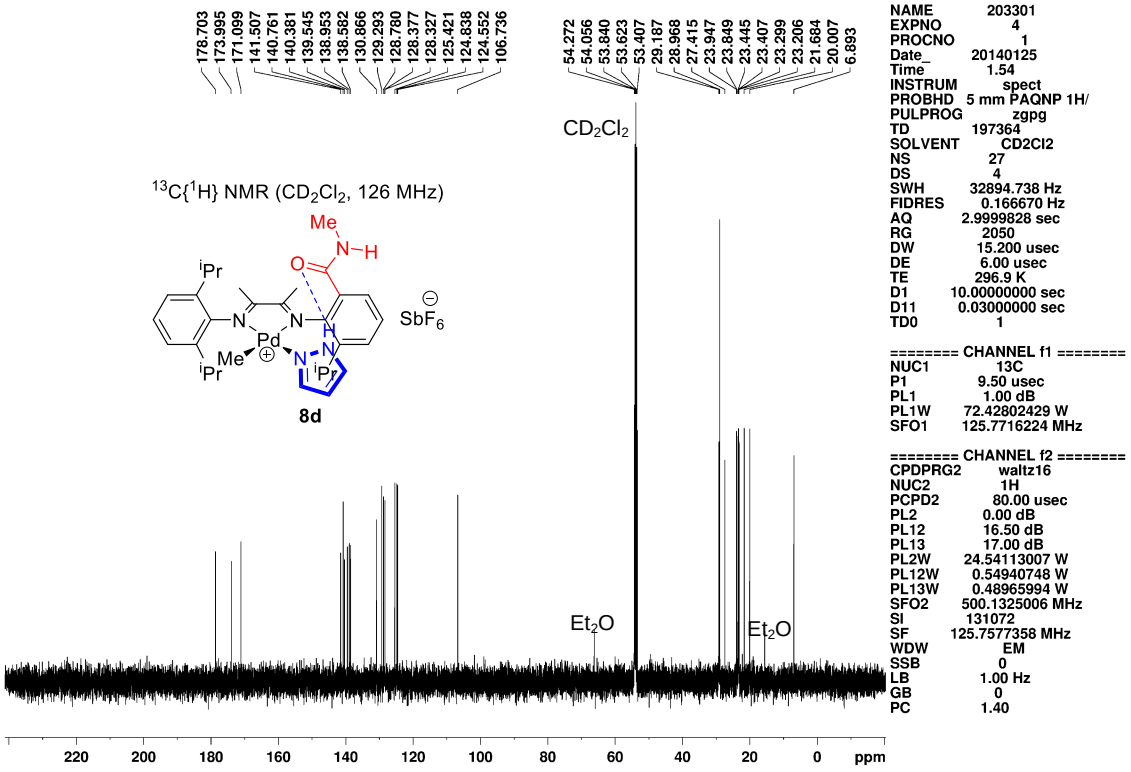

Figure 2.46. NMR spectra of **8d**.

(c)

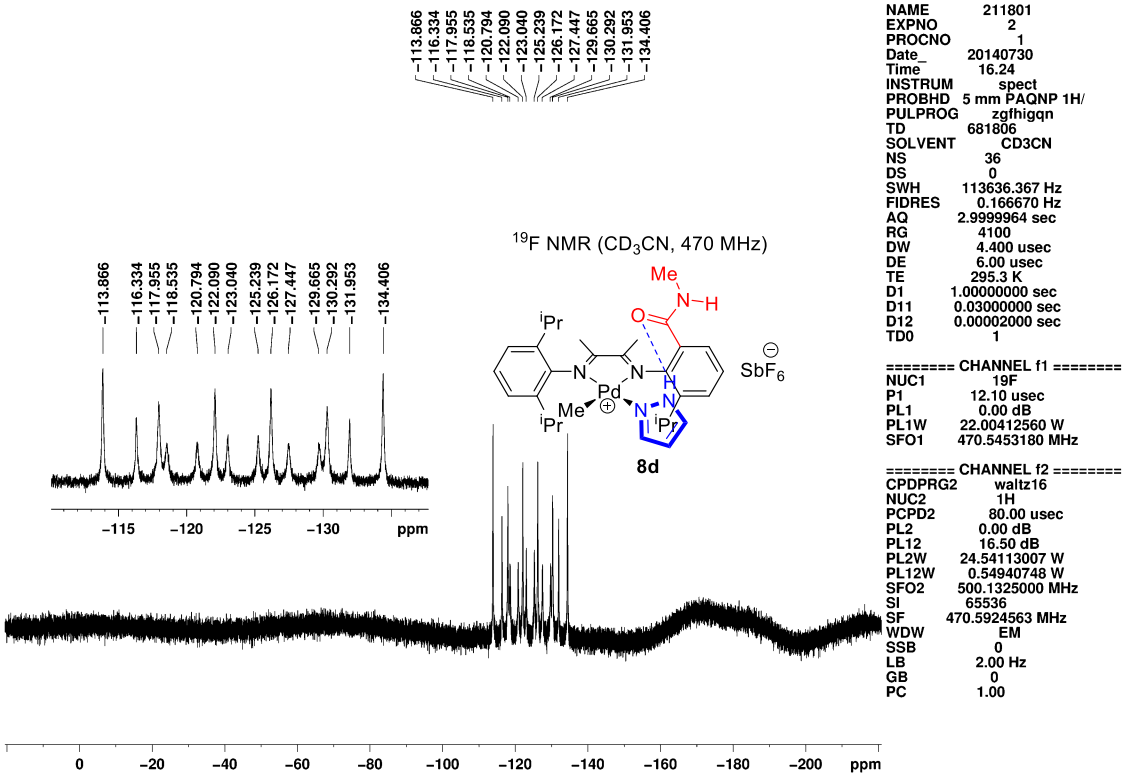

Figure 2.46, continued. NMR spectra of **8d**.

8e. A glass vial was charged with **5e** (51.6 mg, 0.0919 mmol), $AgSbF_6$ (36.5 mg, 1.16 equiv), and pyrazole (6.3 mg, 1.0 equiv). CH_2Cl_2 (2 mL) was added to the reaction mixture, and the vial was agitated for 20 sec to give a suspension of an off-white precipitate in a yellow solution. The suspension was filtered by pipette filtration, and the yellow filtrate was concentrated to 1 mL. Formation of yellow crystals was observed. The mixture was layered with hexanes (8 mL) and kept at –40 °C overnight to give yellow needles (73.3 mg, 96%). The solid contained 0.30 equiv CH_2Cl_2 and 0.022 equiv Et_2O as determined by ^{1}H NMR. ^{1}H NMR (500 MHz, CD_2Cl_2): δ 9.92 (br s, 1H, pz NH), 7.52–7.51 (m, 1H, Ar, pz H^3), 7.42–7.34 (m, 4H, Ar), 7.28 (d, *J* = 7.8, 2H, Ar), 6.63 (td, *J* = 2.2, 0.4, 1H, pz H^5), 6.14 (q, *J* = 2.4, 1H, pz H^4), 2.99 (septet, *J* = 6.8, 2H, ^{i}Pr methine), 2.87 (septet, *J* = 6.8, 2H, ^{i}Pr methine), 2.28 (s, 3H, *Me*C=N), 2.26 (s, 3H, *Me*C=N), 1.38 (d, *J* = 6.8, 6H, ^{i}Pr), 1.23 (d, *J* = 6.9, 6H, ^{i}Pr), 1.23 (d, *J* = 6.9, 6H, ^{i}Pr), 1.14 (d, *J* = 6.8 Hz, 6H, ^{i}Pr), 0.52

(s, 3H, Pd–Me). ^{1}H NMR (500 MHz, CD_3CN): δ 11.29 (br s, 1H, pz NH), 6.49 (t, *J* = 2.1, 1H, pz H^5), 6.07 (q, *J* = 2.3, 1H, pz H^4), 0.28 (s, 3H, Pd–Me). $^{13}C\{^{1}H\}$ NMR (126 MHz, CD_2Cl_2): δ 179.3, 173.3 (imine C=N), 141.5 (pz C^5), 141.38, 141.37, 138.9, 138.2 (Ar), 132.2 (pz C^3), 129.0, 128.8, 125.0, 124.8 (Ar), 107.0 (pz C^4), 29.5, 29.2 (^{i}Pr methine), 24.0, 23.6, 23.3, 23.1 (^{i}Pr methyl), 21.9, 20.6 (*Me*C=N), 8.6 (Pd–Me). ^{19}F NMR (470 MHz, CD_3CN): δ –123.7; overlay of $^{121}SbF_6$ (sextet, J_{SbF} = 1940) and $^{123}SbF_6$ (octet, J_{SbF} = 1050). IR (cm^{-1}): $\nu_{N–H}$, 3364. Anal. Calcd. for $C_{32}H_{47}F_6N_4PdSb \cdot 0.30CH_2Cl_2 \cdot 0.022C_4H_{10}O$, %: C, 45.39; H, 5.62; N, 6.54. Found: C, 45.25; H, 5.56; N, 6.54. ESI-MS (1:1 MeOH:H_2O, positive ion scan, *m*/*z*): 593.3 ($[M – SbF_6]^+$). ESI-MS (1:1 MeOH:H_2O, negative ion scan, *m*/*z*): 234.9 (SbF_6^-).

(a)

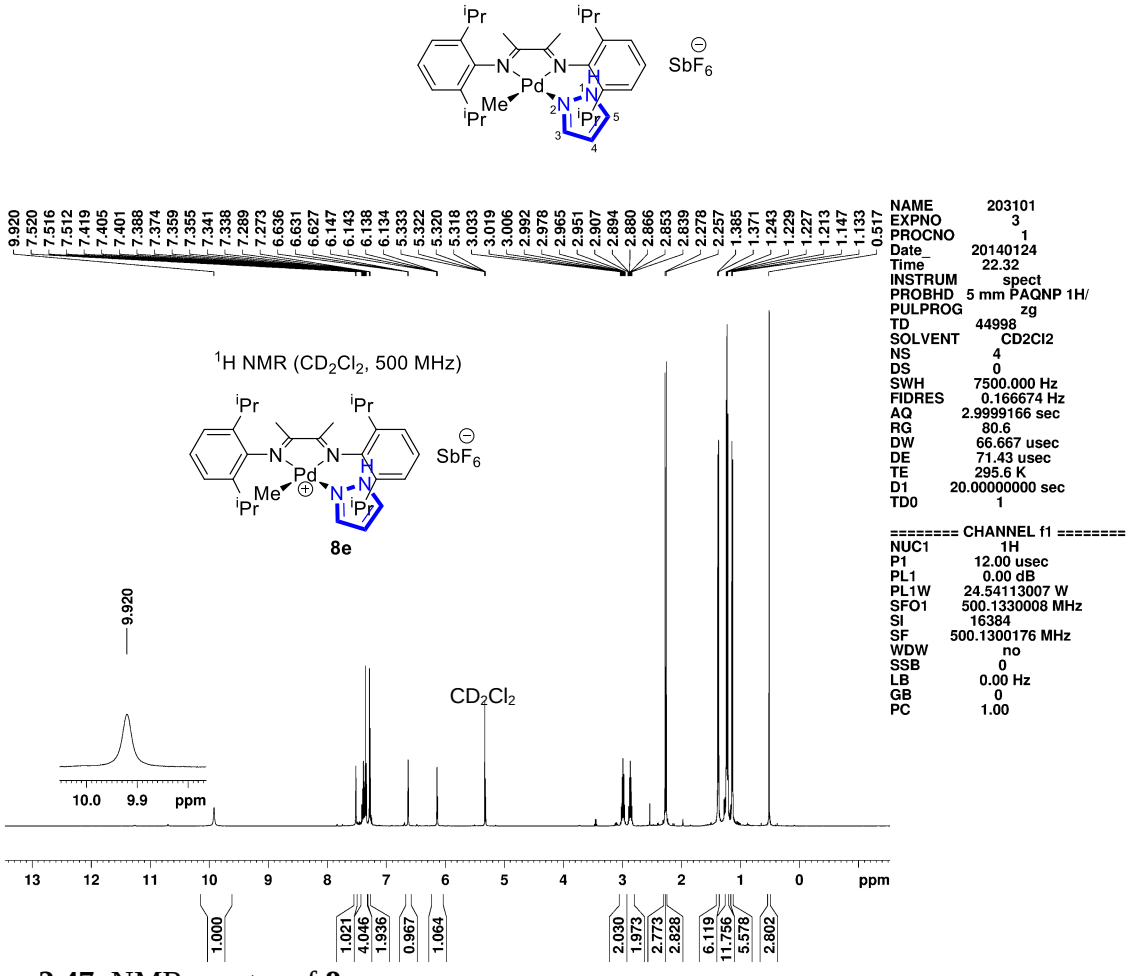

Figure 2.47. NMR spectra of **8e**.

(b)

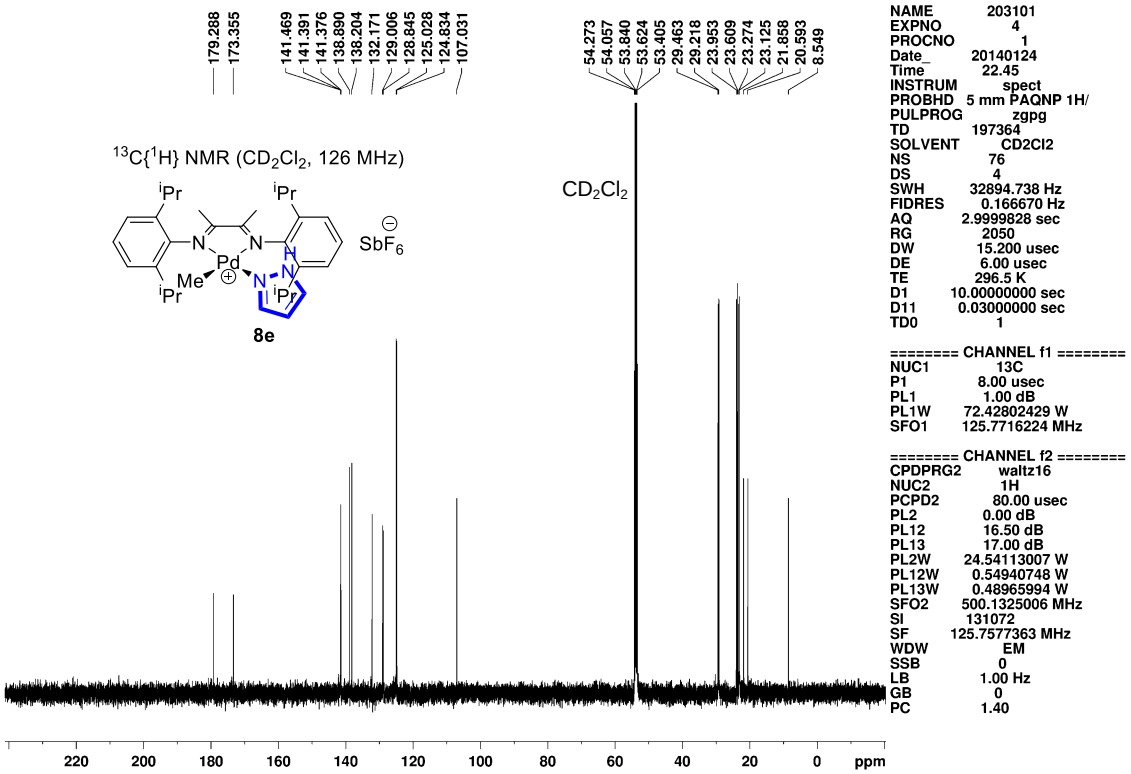

(c)

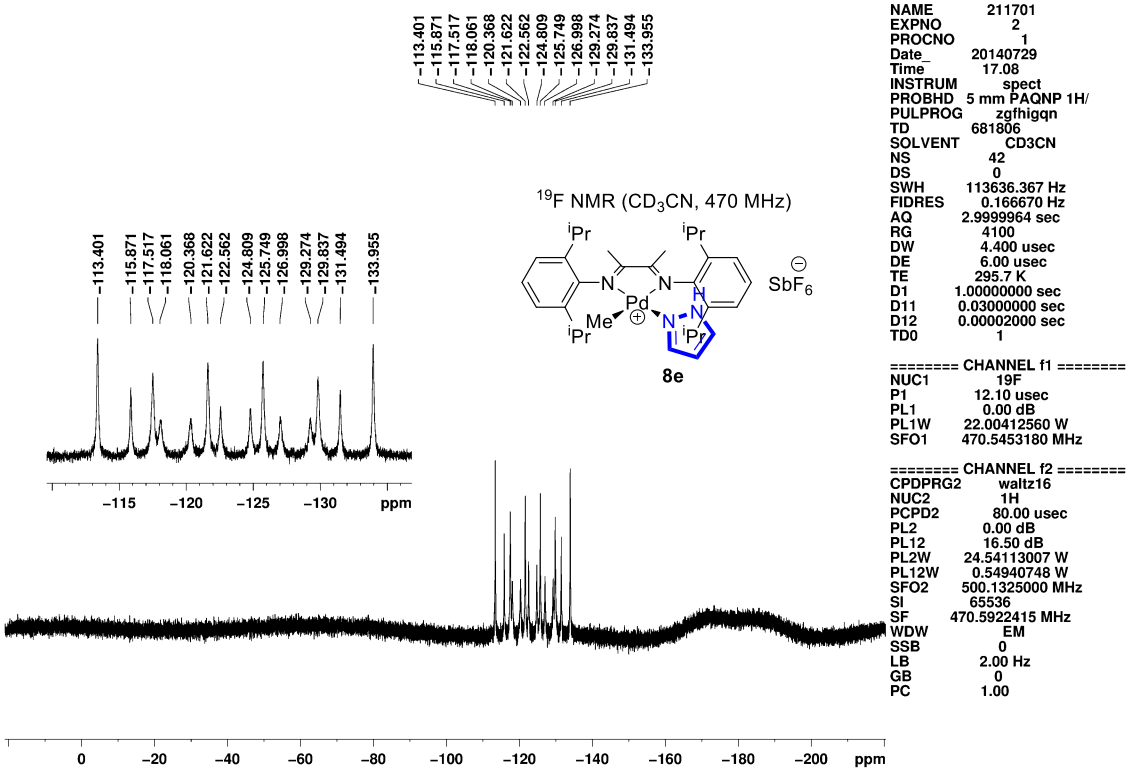

Figure 2.47, continued. NMR spectra of **8e**.

Measurement of Pyrazole Dissociation Constant of (α-Diimine)PdMe(pz)$^+$SbF$_6^-$ in CD$_3$CN. A J. Young NMR tube was charged with (α-diimine)PdMe(pz)$^+$SbF$_6^-$ (10–20 mg) and CD_3CN (0.5–1.5 mL). The tube was sealed, shaken to yield a yellow homogeneous solution, and maintained at room temperature, and NMR spectra were recorded periodically. For **8a**,**d**,**e**, equilibrium was reached after 10 min. For **8c-*anti*,*syn***, equilibrium was reached after 1 h. The dissociation constants, K_{eq} = [(α-diimine)PdMe(CD_3CN)$^+$][pz][(α-diimine)PdMe(pz)$^+$]$^{-1}$ = [pz]^2[(α-diimine)PdMe(pz)$^+$]$^{-1}$ (M), were calculated from ^{1}H NMR integrations.

Generation of 9a,a'. A J. Young NMR tube was charged with **5a**,**a'** (10 mg), $AgSbF_6$ (1.1 equiv), and CD_3CN (ca. 0.5 mL) and maintained at room temperature. A 1.3/1 equilibrium mixture of **9a**/**9a'** was generated in 10 min. **9a**: ^{1}H NMR (500 MHz, CD_3CN): δ 7.577 (dd, *J* = 7.9, 1.1, 1H, Ar), 7.44–7.33 (m, 4H, Ar), 7.30–7.27 (m, 1H, Ar), 3.14 (septet, *J* = 6.8 Hz, 1H, ^{i}Pr methine), 3.07 (s, 3H, amide NMe), 2.98 (s, 3H, amide NMe), 2.94 (septet, *J* = 6.8 Hz, 1H, ^{i}Pr methine), 2.93 (septet, *J* = 6.8 Hz, 1H, ^{i}Pr methine), 2.22 (s, 3H, *Me*C=N), 2.17 (s, 3H, *Me*C=N), 1.37 (d, *J* = 6.8, 3H, ^{i}Pr), 1.30 (d, *J* = 6.8, 3H, ^{i}Pr), 1.28 (d, *J* = 6.8, 3H, ^{i}Pr), 1.26 (d, *J* = 6.9, 3H, ^{i}Pr), 1.22 (d, *J* = 6.8, 3H, ^{i}Pr), 1.15 (d, *J* = 6.9, 3H, ^{i}Pr), 0.34 (s, 3H, Pd–Me). **9a'**: ^{1}H NMR (500 MHz, CD_3CN): δ 7.582 (dd, *J* = 7.9, 1.1, 1H, Ar), 7.44–7.33 (m, 4H, Ar), 7.30–7.27 (m, 1H, Ar), 3.07 (s, 3H, amide NMe), 3.05–2.95 (m, 3H, ^{i}Pr methine), 2.94 (s, 3H, amide NMe), 2.24 (s, 3H, *Me*C=N), 2.17 (s, 3H, *Me*C=N), 1.35 (d, *J* = 6.9, 3H, ^{i}Pr), 1.33 (d, *J* = 6.9, 3H, ^{i}Pr), 1.31 (d, *J* = 6.8, 3H, ^{i}Pr), 1.26 (d, *J* = 6.8, 3H, ^{i}Pr), 1.24 (d, *J* = 6.9, 3H, ^{i}Pr), 1.19 (d, *J* = 6.9, 3H, ^{i}Pr), 0.39 (s, 3H, Pd–Me).

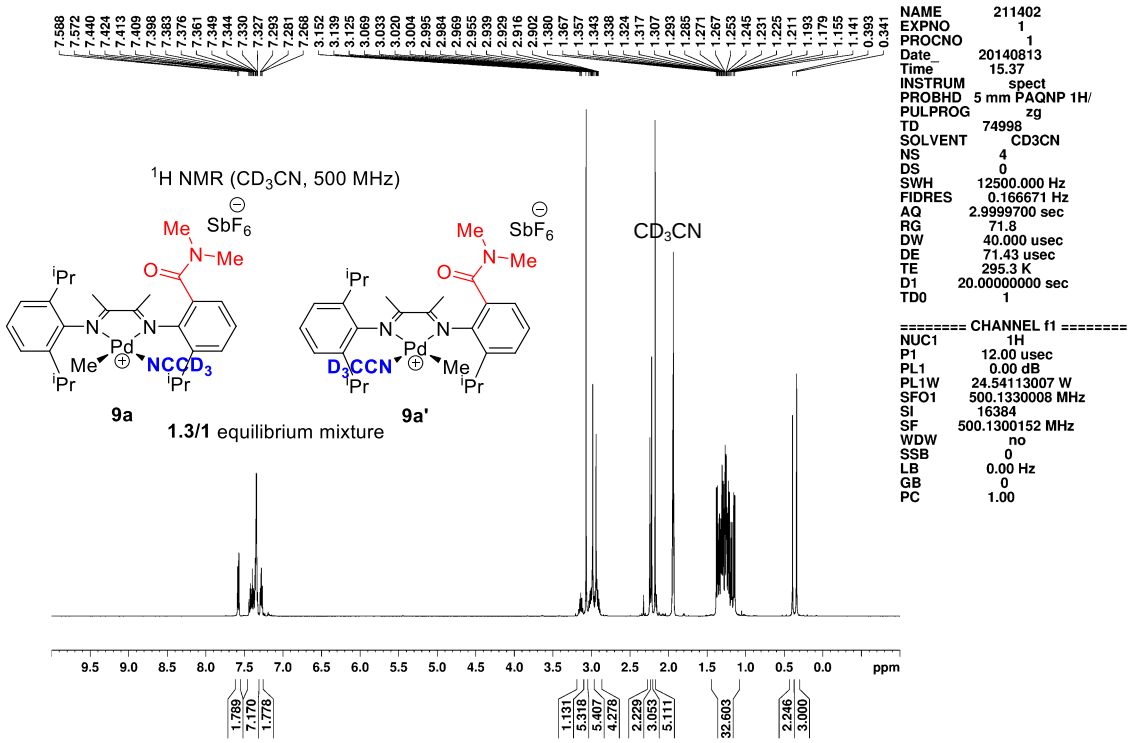

Figure 2.48. ^{1}H NMR spectrum of **9a,a'**.

9c-*anti*,*syn*. The procedure is as above using **5c-*anti***. A 1.6/1 equilibrium mixture of **9c-*anti*/9c-*syn*** was generated in 22 min. **9c-*anti***: ^{1}H NMR (500 MHz, CD_3CN): δ 7.57–7.55 (m, 2H, Ar), 7.44–7.38 (m, 2H, Ar), 7.30–7.24 (m, 2H, Ar), 3.05 (s, 6H, amide NMe), 3.05 (septet, *J* = 6.8 Hz, 1H, ^{i}Pr methine), 2.98 (s, 3H, amide NMe), 2.94 (s, 3H, amide NMe), 2.89 (septet, *J* = 6.9 Hz, 1H, ^{i}Pr methine), 2.21 (s, 3H, *Me*C=N), 2.20 (s, 3H, *Me*C=N), 1.37 (d, *J* = 6.8, 3H, ^{i}Pr), 1.32 (d, *J* = 6.8, 3H, ^{i}Pr), 1.20 (d, *J* = 6.8, 3H, ^{i}Pr), 1.18 (d, *J* = 6.8, 3H, ^{i}Pr), 0.43 (s, 3H, Pd–Me). **9c-*syn***: ^{1}H NMR (500 MHz, CD_3CN): δ 7.57–7.55 (m, 2H, Ar), 7.44–7.38 (m, 2H, Ar), 7.30–7.24 (m, 2H, Ar), 3.26 (septet, *J* = 6.9 Hz, 1H, ^{i}Pr methine), 3.05 (septet, *J* = 6.8 Hz, 1H, ^{i}Pr methine), 3.11 (s, 3H, amide NMe), 3.08 (s, 3H, amide NMe), 2.98 (s, 3H, amide NMe), 2.94 (s, 3H, amide NMe), 2.20 (s, 3H, *Me*C=N), 2.19 (s, 3H, *Me*C=N), 1.40 (d, *J* = 6.8, 3H, ^{i}Pr), 1.33 (d, *J* = 6.8, 3H, ^{i}Pr), 1.21 (d, *J* = 6.8, 3H, ^{i}Pr), 1.20 (d, *J* = 6.8, 3H, ^{i}Pr), 0.42 (s, 3H, Pd–Me).

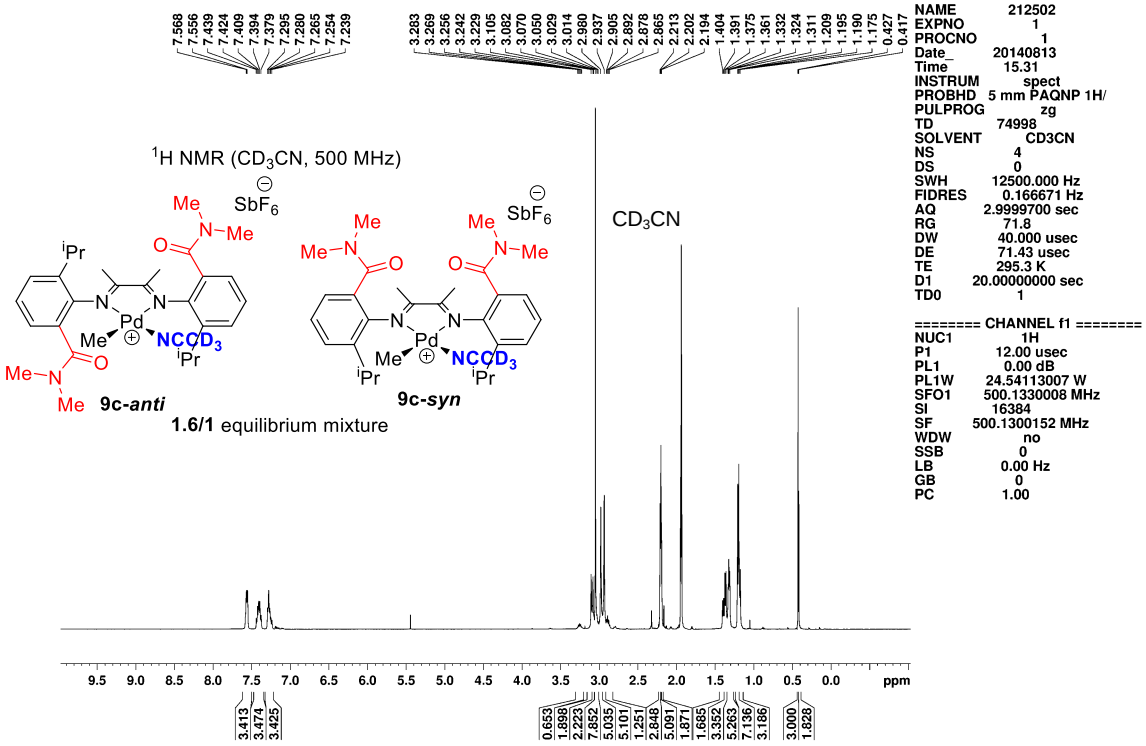

Figure 2.49. ^{1}H NMR spectrum of **9c-*anti,syn***.

Isomerization Equilibrium of 9c-*anti,syn*. A J. Young NMR tube was charged with pure **5c-*anti*** (5.1 mg, 0.0082 mmol), $AgSbF_6$ (5.1 mg, 0.015 mmol, 1.8 equiv), and CD_3CN (0.5 mL) under nitrogen at room temperature. The tube was sealed, and the anti/syn isomerization was monitored by ^{1}H NMR (Figure 2.50). The mixture reached equilibrium (**9c-*anti*/9c-*syn*** = 1.58/1) within 22 min.

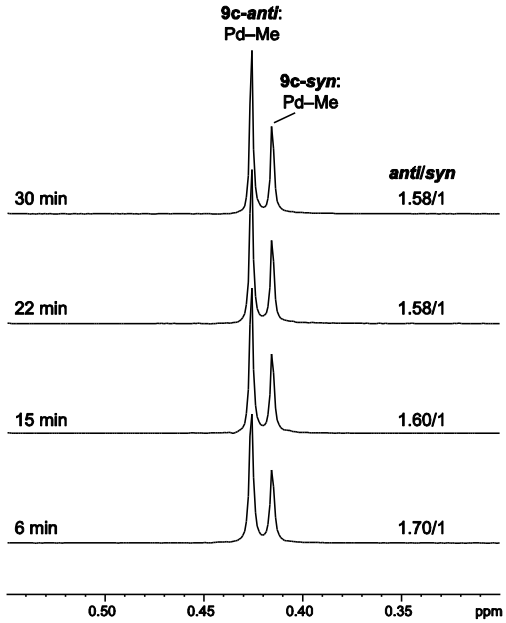

Figure 2.50. Stacked ^{1}H NMR spectra showing the conversion of **9c-*anti*** to **9c-*syn*** in CD_3CN at room temperature (500 MHz). The Pd–Me region (δ 0.55–0.30) is shown.

9d,d'. The procedure is as above using **5d**,**d'**. A 1.1/1 equilibrium mixture of **9d**/**9d'** was generated in 10 min. **9d**: ^{1}H NMR (500 MHz, CD_3CN): δ 7.62–7.60 (m, 1H, Ar), 7.45–7.32 (m, 5H, Ar), 6.85 (br s, 1H, amide NH), 3.16 (septet, *J* = 6.8, 1H, ^{i}Pr methine), 3.042 (septet, *J* = 6.8, 1H, ^{i}Pr methine), 3.038 (septet, *J* = 6.8, 1H, ^{i}Pr methine), 2.86 (d, *J* = 4.7, 3H, amide NMe), 2.24 (s, 3H, *Me*C=N), 2.20 (s, 3H, *Me*C=N), 1.34 (d, *J* = 6.8, 6H, ^{i}Pr), 1.28 (d, *J* = 6.8, 3H, ^{i}Pr), 1.25 (d, *J* = 6.8, 6H, ^{i}Pr), 1.22 (d, *J* = 6.8, 3H, ^{i}Pr), 0.23 (s, 3H, Pd–Me). **9d'**: ^{1}H NMR (500 MHz, CD_3CN): δ 7.62–7.60 (m, 1H, Ar), 7.45–7.32 (m, 5H, Ar), 6.85 (br s, 1H, amide NH), 3.10 (septet, *J* = 6.8, 1H, ^{i}Pr methine), 3.09 (septet, *J* = 6.8, 1H, ^{i}Pr methine), 2.99 (septet, *J* = 6.8, 1H, ^{i}Pr methine), 2.88 (d, *J* = 4.7, 3H, amide NMe), 2.21 (s, 3H, *Me*C=N), 2.19 (s, 3H, *Me*C=N), 1.33 (d, *J* = 6.8, 3H, ^{i}Pr), 1.30 (d, *J* = 6.8, 3H, ^{i}Pr), 1.282 (d, *J* = 6.8, 3H, ^{i}Pr), 1.277 (d, *J* = 6.8, 3H, ^{i}Pr), 1.22 (d, *J* = 6.8, 3H, ^{i}Pr), 1.18 (d, *J* = 6.8, 3H, ^{i}Pr), 0.27 (s, 3H, Pd–Me).

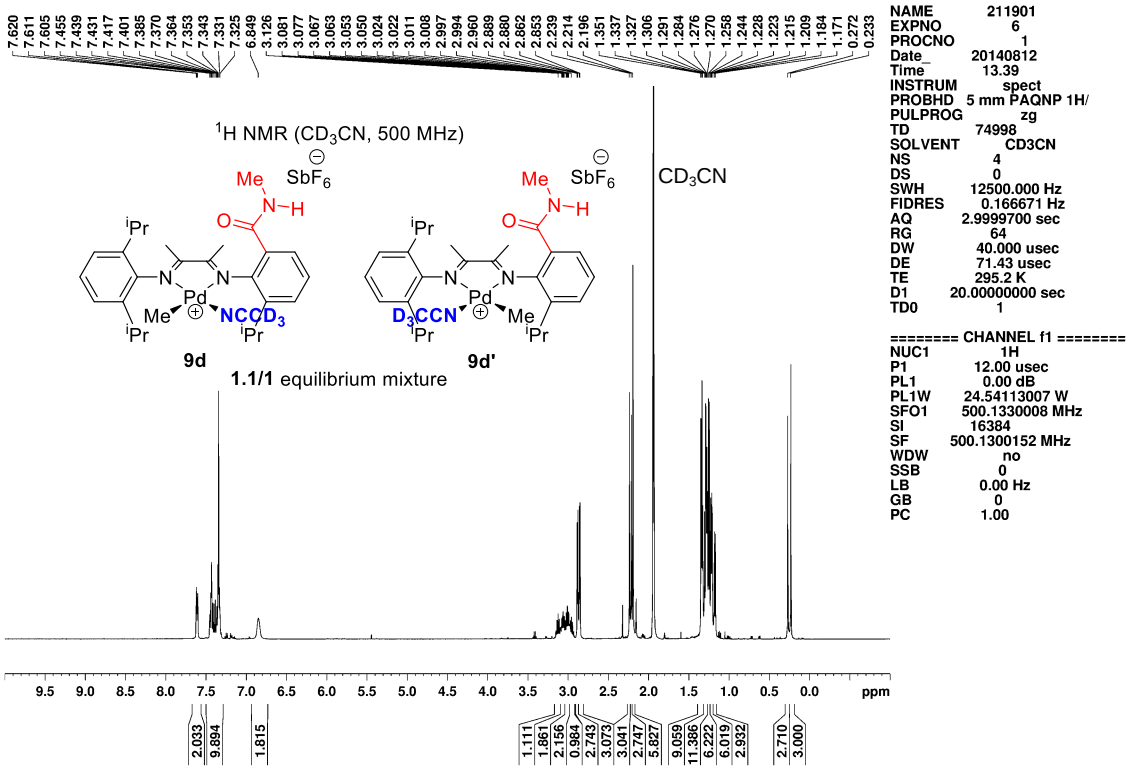

Figure 2.51. ^{1}H NMR spectrum of **9d,d'**.

9e. The procedure is as above using **5e**. **9e** was generated in 10 min. ^{1}H NMR (500 MHz, CD_3CN): δ 7.40–7.33 (m, 6H, Ar), 3.05 (septet, *J* = 6.8, 2H, ^{i}Pr methine), 3.00 (septet, *J* = 6.8, 2H, ^{i}Pr methine), 2.23 (s, 3H, *Me*C=N), 2.22 (s, 3H, *Me*C=N), 1.37 (d, *J* = 6.8, 6H, ^{i}Pr), 1.31 (d, *J* = 6.8, 6H, ^{i}Pr), 1.25 (d, *J* = 6.8, 6H, ^{i}Pr), 1.21 (d, *J* = 6.8, 6H, ^{i}Pr), 0.32 (s, 3H, Pd–Me).

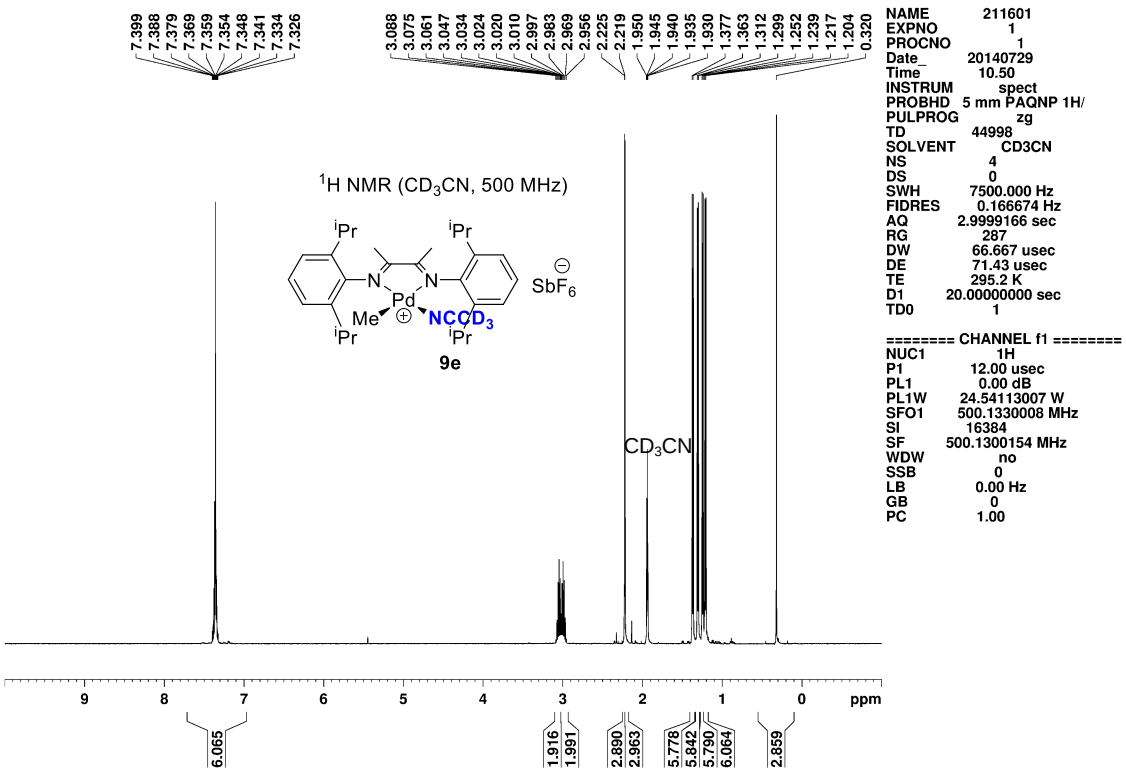

Figure 2.52. ^{1}H NMR spectrum of **9e**.

X-ray Crystallography. Data for **4c-*anti***, **4d'**, **5d**, and **6c-*anti***·3CH_2Cl_2 were collected on a Bruker SMART APEX diffractometer using Mo Kα radiation (0.71073 Å). Data for **5c-*syn***·2CH_2Cl_2, **6d**, **7d**, and **8d** were collected on a Bruker D8 Venture System with CMOS detector and Mo microsource radiation. All data were collected at 100 K except for **6c-*anti***·3CH_2Cl_2, whose data were collected at 200 K. Direct methods were used to locate many atoms from the E-map. Repeated difference Fourier maps allowed recognition of all expected non-hydrogen atoms. Following anisotropic refinement of all non-H atoms, ideal H atom positions were calculated unless otherwise noted. Final refinement was anisotropic for all non-H atoms and isotropic-riding for H atoms. No anomalous bond lengths or thermal parameters were noted unless otherwise indicated. ORTEP diagrams are drawn with 50% probability ellipsoids. Specific comments for each structure follow. **4c-*anti***: Crystals of **4c-*anti*** were obtained by diffusion of hexanes into a CH_2Cl_2 solution of **4c** (1.4/1 anti/syn mixture) at 0 °C. **4d'**: Crystals of **4d'** were obtained by

diffusion of hexanes into a CH_2Cl_2 solution at room temperature. Two independent molecules are present in the asymmetric unit. **5c-*syn***: See the synthetic procedure for single crystal preparation. Two solvent molecules of CH_2Cl_2 are present with one found to be disordered over two positions (0.7 to 0.3 relative occupancy). Identical anisotropic thermal parameters were used for the C-atoms of the disordered CH_2Cl_2 molecule. The coordinates of H31A and H31B were refined and the thermal parameters of these atoms were constrained to be 1.2 times those of C31. **5d**: Crystals of **5d** were obtained by diffusion of hexanes into a CH_2Cl_2 solution at –30 °C. **6c-*anti***: Crystals of **6c-*anti*** were obtained by diffusion of hexanes into a CH_2Cl_2 solution at 0 °C. Initial attempts to collect data at 100 K proved unsuccessful, probably due to a phase transformation. Three CH_2Cl_2 solvent molecules were present with full occupancy. **6d**: Crystals of **6d** were obtained by slow evaporation of a CH_2Cl_2/Et_2O solution at room temperature. **7d**: Crystals of **7d** were obtained by layering hexanes onto a CH_2Cl_2 solution at –30 °C. **8d**: Crystals of **8d** were obtained by layering hexanes onto a CH_2Cl_2 solution at –40 °C. The hydrogen atoms on the nitrogens in **4d'**, **5d**, **6d**, **7d**, and **8d** were located on the difference Fourier maps, and their positions were refined isotropically.

Table 2.2. Crystallographic Data for Compounds 4c-*anti*, 4d', 5c-*syn*·2CH_2Cl_2 and 5d

	4c	**4d'**	**5c-*syn*·2CH_2Cl_2**	**5d**
Empirical formula	$C_{14}H_{19}N_2O$	2[$C_{27}H_{37}N_3O$]	$C_{29}H_{41}ClN_4O_2Pd$ + 2CH_2Cl_2	$C_{28}H_{40}ClN_3OPd$
Formula weight	231.31	839.19	789.36	576.48
Crystal system	Orthorhombic	Monoclinic	Monoclinic	Monoclinic
Space Group	Pbca	$P2_1/c$	$P2_1/c$	$P2_1/c$
a (Å)	15.061(6)	14.480(7)	19.1678(11)	10.792(5)
b (Å)	10.966(4)	20.124(10)	11.6556(7)	15.568(7)
c (Å)	15.944(6)	19.247(7)	16.2196(9)	17.764(7)
β (deg)		121.97(3)	90.122(2)	110.88(2)
V (Å^3)	2633.2(18)	4758(4)	3623.6(4)	2789(2)
Z	8	4	4	4
T (K)	100	100	100	100
Crystal color, habit	clear, fragment	clear, fragment	orange, fragment	clear, fragment
GOF on F^2	0.860	0.839	1.060	1.044
R indices [$I > 2\sigma(I)$]	R1 = 0.0563 wR2 = 0.1093	R1 = 0.0691 wR2 = 0.0813	R1 = 0.0303 wR2 = 0.0669	R1 = 0.0472 wR2 = 0.0826
R indices (all data)	R1 = 0.0996 wR2 = 0.1183	R1 = 0.2228 wR2 = 0.0988	R1 = 0.0401 wR2 = 0.0710	R1 = 0.0806 wR2 = 0.0875

Table 2.3. Crystallographic Data for Compounds 6c-*anti*·3CH_2Cl_2, 6d, 7d and 8d

	6c-*anti*·3CH_2Cl_2	**6d**	**7d**	**8d**
Empirical formula	$C_{28}H_{38}Cl_2N_4O_2Pd$ + 3CH_2Cl_2	$C_{27}H_{37}Cl_2N_3OPd$	$C_{30}H_{43}N_3O_3Pd$	$C_{31}H_{44}N_5OPd$ + SbF_6
Formula weight	894.70	596.90	600.07	844.86
Crystal system	Monoclinic	Monoclinic	Monoclinic	Monoclinic
Space Group	P2/c	$P2_1/c$	$P2_1/c$	$P2_1/c$
a (Å)	20.407(7)	10.6721(7)	13.4747(8)	10.4432(5)
b (Å)	11.594(4)	15.7078(10)	12.2454(7)	13.8723(6)
c (Å)	17.802(6)	17.5157(10)	18.0447(11)	26.0265(9)
β (deg)	110.720(6)	109.248(3)	91.101(2)	110.649(2)
V (Å^3)	3940(2)	2772.1(3)	2976.9(3)	3528.3(3)
Z	4	4	4	4
T (K)	200	100	100	100
Crystal color, habit	orange, fragment	orange, plate	red, brick	yellow, fragment
GOF on F^2	0.991	1.093	1.035	1.067
R indices [$I > 2\sigma(I)$]	R1 = 0.0614 wR2 = 0.1367	R1 = 0.0408 wR2 = 0.0843	R1 = 0.0268 wR2 = 0.0558	R1 = 0.0291 wR2 = 0.0597
R indices (all data)	R1 = 0.0913 wR2 = 0.1460	R1 = 0.0578 wR2 = 0.0837	R1 = 0.0409 wR2 = 0.0608	R1 = 0.0413 wR2 = 0.0642

2.5 References and Notes

(1) Steiner, T. *Angew. Chem., Int. Ed.* **2002**, *41*, 48.

(2) (a) Borovik, A. S. *Acc. Chem. Res.* **2005**, *38*, 54; (b) Lucas, R. L.; Powell, D. R.; Borovik, A. S. *J. Am. Chem. Soc.* **2005**, *127*, 11596; (c) Patel, B. P.; Crabtree, R. H. *J. Am. Chem. Soc.* **1996**, *118*, 13105; (d) Lee, D.-H.; Kwon, H. J.; Patel, B. P.; Liable-Sands, L. M.; Rheingold, A. L.; Crabtree, R. H. *Organometallics* **1999**, *18*, 1615; (e) Kluge, T.; Bette, M.; Rüffer, T.; Bruhn, C.; Wagner, C.; Ströhl, D.; Schmidt, J.; Steinborn, D. *Organometallics* **2013**, *32*, 7090.

(3) Steed, J. W. *Chem. Soc. Rev.* **2009**, *38*, 506.

(4) (a) Raynal, M.; Ballester, P.; Vidal-Ferran, A.; van Leeuwen, P. W. N. M. *Chem. Soc. Rev.* **2014**, *43*, 1660; (b) Crabtree, R. H. *New J. Chem.* **2011**, *35*, 18; (c) Zhao, B.; Han, Z.; Ding, K. *Angew. Chem., Int. Ed.* **2013**, *52*, 4744; (d) Dydio, P.; Reek, J. N. H. *Chem. Sci.* **2014**, *5*, 2135.

(5) Das, S.; Incarvito, C. D.; Crabtree, R. H.; Brudvig, G. W. *Science* **2006**, *312*, 1941.

(6) Höke, T.; Herdtweck, E.; Bach, T. *Chem. Commun.* **2013**, *49*, 8009.

(7) Voss, F.; Herdtweck, E.; Bach, T. *Chem. Commun.* **2011**, *47*, 2137.

(8) (a) Fackler, P.; Berthold, C.; Voss, F.; Bach, T. *J. Am. Chem. Soc.* **2010**, *132*, 15911; (b) Fackler, P.; Huber, S. M.; Bach, T. *J. Am. Chem. Soc.* **2012**, *134*, 12869; (c) Hull, J. F.; Sauer, E. L. O.; Incarvito, C. D.; Faller, J. W.; Brudvig, G. W.; Crabtree, R. H. *Inorg. Chem.* **2009**, *48*, 488.

(9) (a) Dydio, P.; Detz, R. J.; de Bruin, B.; Reek, J. N. H. *J. Am. Chem. Soc.* **2014**, *136*, 8418; (b) Šmejkal, T.; Breit, B. *Angew. Chem., Int. Ed.* **2008**, *47*, 3946; (c) Šmejkal, T.; Breit, B. *Angew. Chem., Int. Ed.* **2008**, *47*, 311.

(10) Du, L.; Cao, P.; Xing, J.; Lou, Y.; Jiang, L.; Li, L.; Liao, J. *Angew. Chem., Int. Ed.* **2013**, *52*, 4207.

(11) (a) Clapham, S. E.; Hadzovic, A.; Morris, R. H. *Coord. Chem. Rev.* **2004**, *248*, 2201; (b) Conley, B. L.; Pennington-Boggio, M. K.; Boz, E.; Williams, T. J. *Chem. Rev.* **2010**, *110*, 2294; (c) Zuo, W.; Lough, A. J.; Li, Y. F.; Morris, R. H. *Science* **2013**, *342*, 1080; (d) Noyori, R.; Ohkuma, T. *Angew. Chem., Int. Ed.* **2001**, *40*, 40; (e) Ikariya, T.; Blacker, A. J. *Acc. Chem. Res.* **2007**, *40*, 1300.

(12) (a) Schmeier, T. J.; Dobereiner, G. E.; Crabtree, R. H.; Hazari, N. *J. Am. Chem. Soc.* **2011**, *133*, 9274; (b) Hull, J. F.; Himeda, Y.; Wang, W.-H.; Hashiguchi, B.; Periana, R.; Szalda, D. J.; Muckerman, J. T.; Fujita, E. *Nat. Chem.* **2012**, *4*, 383; (c) Hou, C.; Jiang, J.; Zhang, S.; Wang, G.; Zhang, Z.; Ke, Z.; Zhao, C. *ACS Catal.* **2014**, *4*, 2990.

(13) (a) DuBois, D. L. *Inorg. Chem.* **2014**, *53*, 3935; (b) Rakowski Dubois, M.; Dubois, D. L. *Acc. Chem. Res.* **2009**, *42*, 1974.

(14) (a) Dogutan, D. K.; Stoian, S. A.; McGuire, R.; Schwalbe, M.; Teets, T. S.; Nocera, D. G. *J.*

Am. Chem. Soc. **2011**, *133*, 131; (b) Shook, R. L.; Peterson, S. M.; Greaves, J.; Moore, C.; Rheingold, A. L.; Borovik, A. S. *J. Am. Chem. Soc.* **2011**, *133*, 5810; (c) Carver, C. T.; Matson, B. D.; Mayer, J. M. *J. Am. Chem. Soc.* **2012**, *134*, 5444.

(15) (a) Costentin, C.; Drouet, S.; Robert, M.; Savéant, J.-M. *Science* **2012**, *338*, 90; (b) Costentin, C.; Passard, G.; Robert, M.; Savéant, J.-M. *J. Am. Chem. Soc.* **2014**, *136*, 11821.

(16) Ittel, S. D.; Johnson, L. K.; Brookhart, M. *Chem. Rev.* **2000**, *100*, 1169.

(17) (a) Johnson, L. K.; Mecking, S.; Brookhart, M. *J. Am. Chem. Soc.* **1996**, *118*, 267; (b) Mecking, S.; Johnson, L. K.; Wang, L.; Brookhart, M. *J. Am. Chem. Soc.* **1998**, *120*, 888; (c) Luo, S.; Jordan, R. F. *J. Am. Chem. Soc.* **2006**, *128*, 12072.

(18) (a) Carfagna, C.; Gatti, G.; Paoli, P.; Binotti, B.; Fini, F.; Passeri, A.; Rossi, P.; Gabriele, B. *Organometallics* **2014**, *33*, 129; (b) Binotti, B.; Carfagna, C.; Zuccaccia, C.; Macchioni, A. *Chem. Commun.* **2005**, 92.

(19) Chen, C.; Luo, S.; Jordan, R. F. *J. Am. Chem. Soc.* **2010**, *132*, 5273.

(20) Chen, C.; Jordan, R. F. *J. Am. Chem. Soc.* **2010**, *132*, 10254.

(21) (a) van Belzen, R.; Hoffmann, H.; Elsevier, C. J. *Angew. Chem., Int. Ed. Engl.* **1997**, *36*, 1743; (b) van Belzen, R.; Klein, R. A.; Kooijman, H.; Veldman, N.; Spek, A. L.; Elsevier, C. J. *Organometallics* **1998**, *17*, 1812; (c) Shirakawa, E.; Yoshida, H.; Nakao, Y.; Hiyama, T. *J. Am. Chem. Soc.* **1999**, *121*, 4290.

(22) van Laren, M. W.; Elsevier, C. J. *Angew. Chem., Int. Ed.* **1999**, *38*, 3715.

(23) (a) van Asselt, R.; Elsevier, C. J. *J. Mol. Catal.* **1991**, *65*, L13; (b) van Asselt, R.; Elsevier, C. J. *Organometallics* **1992**, *11*, 1999.

(24) Fang, X.; Scott, B. L.; Watkin, J. G.; Kubas, G. J. *Organometallics* **2000**, *19*, 4193.

(25) Ackerman, L. J.; Sadighi, J. P.; Kurtz, D. M.; Labinger, J. A.; Bercaw, J. E. *Organometallics* **2003**, *22*, 3884.

(26) Williams, T. J.; Caffyn, A. J. M.; Hazari, N.; Oblad, P. F.; Labinger, J. A.; Bercaw, J. E. *J. Am. Chem. Soc.* **2008**, *130*, 2418.

(27) Golisz, S. R.; Hazari, N.; Labinger, J. A.; Bercaw, J. E. *J. Org. Chem.* **2009**, *74*, 8441.

(28) (a) Fang, X.; Watkin, J. G.; Scott, B. L.; Kubas, G. J. *Organometallics* **2001**, *20*, 3351; see also: (b) Yang, K.; Lachicotte, R. J.; Eisenberg, R. *Organometallics* **1997**, *16*, 5234.

(29) Miyamura, Y.; Kinbara, K.; Yamamoto, Y.; Praveen, V. K.; Kato, K.; Takata, M.; Takano, A.; Matsushita, Y.; Lee, E.; Lee, M.; Aida, T. *J. Am. Chem. Soc.* **2010**, *132*, 3292.

(30) Popeney, C. S.; Rheingold, A. L.; Guan, Z. *Organometallics* **2009**, *28*, 4452.

(31) Leung, D. H.; Ziller, J. W.; Guan, Z. *J. Am. Chem. Soc.* **2008**, *130*, 7538.

(32) Flapper, J.; Reek, J. N. H. *Angew. Chem., Int. Ed.* **2007**, *46*, 8590.

(33) Yamamoto, G.; Koseki, A.; Sugita, J.; Mochida, H.; Minoura, M. *Bull. Chem. Soc. Jpn.* **2006**, *79*, 1585.

(34) Abakumov, G. A.; Cherkasov, V. K.; Druzhkov, N. O.; Kocherova, T. N.; Shavyrin, A. S. *Russ. Chem. Bull., Int. Ed.* **2011**, *60*, 112.

(35) Chauhan, M. S.; McKinnon, D. M. *Can. J. Chem.* **1975**, *53*, 1336.

(36) (a) Gutowsky, H. S.; Holm, C. H. *J. Chem. Phys.* **1956**, *25*, 1228; (b) Hammaker, R. M.; Gugler, B. A. *J. Mol. Spectrosc.* **1965**, *17*, 356.

(37) The labeling scheme in Scheme 2.3 and Figure 2.2 assumes that **4c-*anti*** is the major isomer of **4c**. Attempts to confirm this assumption by low temperature NMR studies of crystalline **4c-*anti*** were thwarted by the poor solubility of this compound at low temperature. However, noting that rotation around the central CMe–CMe bond of **4c** is required to form **6c**, the observation that the kinetic product ratio for **6c** in Scheme 2.5 (**6c-*syn***/**6c-*anti*** = 1.7/1) is close to the isomer ratio for **4c** (1.4/1), suggests that the major isomer of **4c** is **4c-*anti***.

(38) (a) Amoroso, F.; Zangrando, E.; Carfagna, C.; Müller, C.; Vogt, D.; Hagar, M.; Ragaini, F.; Milani, B. *Dalton Trans.* **2013**, *42*, 14583; (b) Scarel, A.; Axet, M. R.; Amoroso, F.; Ragaini, F.; Elsevier, C. J.; Holuigue, A.; Carfagna, C.; Mosca, L.; Milani, B. *Organometallics* **2008**, *27*, 1486; (c) Meduri, A.; Montini, T.; Ragaini, F.; Fornasiero, P.; Zangrando, E.; Milani, B. *ChemCatChem* **2013**, *5*, 1170.

(39) The hydrogen atom positions on all CH_2Cl_2 molecules in **6c-*anti***·$3CH_2Cl_2$ were calculated and refined as riding on the C atom with fixed H–C–H angles and C–H distances, due to the low signal-to-noise ratio and moderate disorder of CH_2Cl_2 molecules. Nevertheless, it is clear that the C–O distances and C–H bond orientations are consistent with C–H···O hydrogen bonds. Estimated distances (Å) and angles (deg): H30a#1···O1 2.11, C30#1···O1 3.063(13), H31b···O2 2.09, C31···O2 3.044(9); O1···H30a#1–C30#1 160, O2···H31b–C31 162.

(40) For **5c-*syn***·$2CH_2Cl_2$, the positions of hydrogen atoms H31a and H31b in one CH_2Cl_2 molecule were refined. The other CH_2Cl_2 molecule was found to be disordered over two positions (C30 or C30X), and the corresponding hydrogen atom positions were calculated. Selected distances (Å) and angles (deg): C31–H31a 0.93(3), H31a···O2 2.24(3), C31···O2 3.154(3); C31–H31a···O2 166(3), H31a···O2–C27 105.7(9).

(41) Yang, K.; Lachicotte, R. J.; Eisenberg, R. *Organometallics* **1998**, *17*, 5102.

(42) An alternative isomerization mechanism for **5c**, in which the arylimine unit trans to the Pd–Me ligand dissociates, undergoes aryl rotation, and re-coordinates to the Pd center, cannot be ruled out.

(43) ^{1}H NMR monitoring of the reaction at 20 °C showed that several intermediate species form

within a few hours and are converted to **6d** in 3 d. The intermediates were not identified.

(44) Aullón, G.; Bellamy, D.; Brammer, L.; Eric, A. B.; Orpen, A. G. *Chem. Commun.* **1998**, 653.

(45) McQuade, D. T.; McKay, S. L.; Powell, D. R.; Gellman, S. H. *J. Am. Chem. Soc.* **1997**, *119*, 8528.

(46) For other examples of Pd complexes that contain intramolecular hydrogen bonding involving carboxylate ligands, see: (a) Ara, I.; Forniés, J.; Lasheras, R.; Martín, A.; Sicilia, V. *Eur. J. Inorg. Chem.* **2006**, 948; (b) Moriya, K.; Yoneda, T.; Saito, S.; Osuka, A. *Chem. Lett.* **2011**, *40*, 455; (c) Kravtsova, S. V.; Romm, I. P.; Stash, A. I.; Belsky, V. K. *Acta Cryst.* **1996**, *C52*, 2201; (d) Chahen, L.; Therrien, B.; Süss-Fink, G. *Eur. J. Inorg. Chem.* **2007**, 5045.

(47) Deacon, G. B.; Phillips, R. J. *Coord. Chem. Rev.* **1980**, *33*, 227.

(48) Rülke, R. E.; Ernsting, J. M.; Spek, A. L.; Elsevier, C. J.; van Leeuwen, P. W. N. M.; Vrieze, K. *Inorg. Chem.* **1993**, *32*, 5769.

(49) Johnson, L. K.; Killian, C. M.; Brookhart, M. *J. Am. Chem. Soc.* **1995**, *117*, 6414.

(50) Darensbourg, D. J.; Wiegreffe, H. P. *Inorg. Chem.* **1990**, *29*, 592.

(51) Jones, R. G.; Wilkins, J. M. *Org. Magn. Reson.* **1978**, *11*, 20.

CHAPTER THREE

Copolymerization of Ethylene with Polar Vinyl Monomers by Amide-Functionalized α-Diimine Pd Catalysts

3.1 Introduction

The synthesis of polar polyethylenes by the direct copolymerization of ethylene and polar vinyl monomers is of significant fundamental and practical interest.[1-3] One class of catalysts that are capable of incorporating polar monomers (PMs) by insertion copolymerization with ethylene are (α-diimine)Pd catalysts, which can incorporate methyl acrylate (MA),[4] acrolein dimethyl acetal,[5] methyl vinyl ketone,[4] *N*-pentenylcarbazole,[6] vinyl silyl ethers,[7] vinyltrialkoxysilanes,[8] and vinyl monomers with remote polar groups.[9] However, the copolymerization of ethylene and PMs by (α-diimine)Pd catalysts has major limitations, including low PM incorporation and retardation of copolymerization by chelate formation following the insertion.[10-11]

Hydrogen bonding (H-bonding) interactions in the second coordination sphere can strongly influence the structures and ligand binding preferences of coordination and organometallic compounds, and their reactivity in transition metal-catalyzed transformations.[12-15] We are interested in how H-bonding interaction may influence the copolymerization of ethylene with PMs. Chapter Two describes the synthesis, structures and coordination chemistry of the first-generation amide-functionalized α-diimine Pd catalysts **1a**,**a'** and **1b**,**b'** (Chart 3.1). **1a**, in which the Cl ligand is *cis* to the amide-functionalized arylimine, exhibits H-bonding interaction between the amide NH group and the Pd-Cl ligand, while the *trans* Cl/amide-functionalized imine isomer **1a'** does not. However, the ethylene polymerization activity of **1a**,**a'** and **1b**,**b'** is poorer compared to the reference catalyst **1c**, which was ascribed to the electron withdrawing effect of the amide

substituents on the N-aryl rings. In order to improve the polymerization performance to the point where ethylene/PM copolymerization studies would be feasible, we designed the second-generation catalysts **1d**,**d'** and **1e**,**e'**. Replacement of two isopropyl groups of **1a**,**a'** and **1b**,**b'** with the more steric demanding benzhydryl (-$CHPh_2$) groups in **1d**,**d'** and **1e**,**e'** was expected to significantly improve ethylene polymerization performance, based on the recent studies of benzhydryl α-diimine Pd catalysts.[16-17] This chapter describes the synthesis of the second-generation catalysts, and the ethylene homopolymerization behavior and the ethylene/PM copolymerization of the first- and second-generation amide-functionalized diimine Pd catalysts. The H-bonding catalyst **1d**,**d'** are capable of incorporating higher level of MA and acrylic acid (AA) in the copolymerization with ethylene than the non-H-bonding catalyst **1f**,**f'**. C-H activation reactions related to the activation of catalysts **1a**,**a'** and **1b**,**b'** to form μ-CH_2 complexes are also discussed.

Chart 3.1. " ' " denotes *cis,trans* isomers.

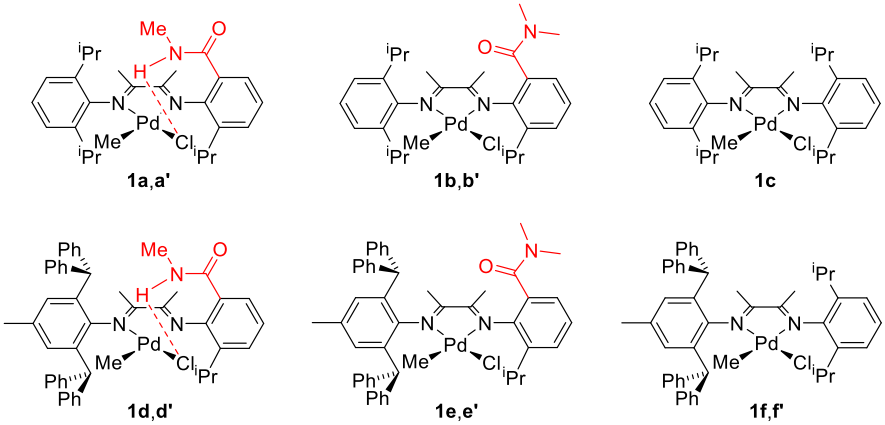

3.2 Results and Discussion

Synthesis of 1d-f,d'-f'. The condensation reaction of α-ketaimine **2** with *o*-aminobenzamide **3** forms the 2,3-dihydroquinazolin-4(1*H*)-one compound **4** (Scheme 3.1). The

^{13}C NMR spectrum of **4** in CD_2Cl_2 exhibit four sets of signals for the phenyl groups and two signals for the isopropyl Me groups, due to the C_1-symmetry of **4** caused by the presence of the quaternary carbon atom (δ 76.8 in CD_2Cl_2).

Scheme 3.1

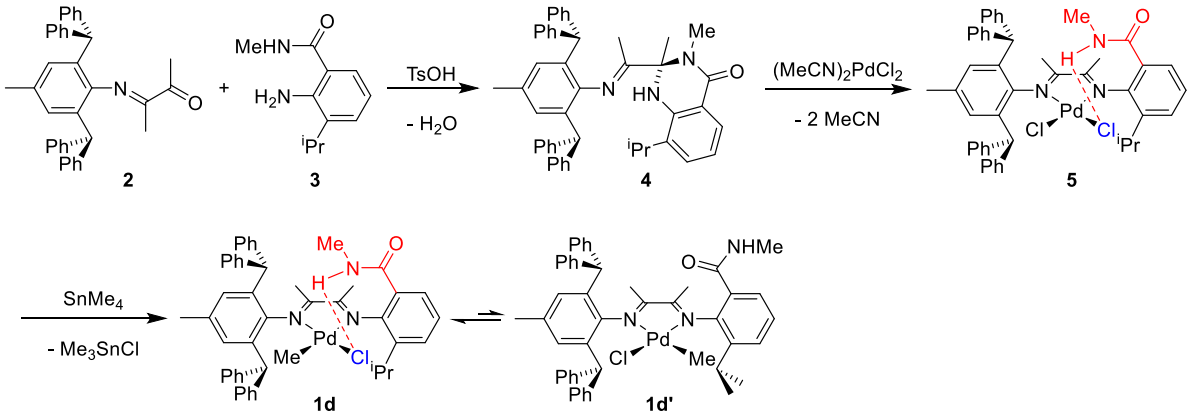

The metalation of **4** with $(MeCN)_2PdCl_2$ at 40 °C leads to opening of the dihydroquinazolinone ring to form the secondary-amide-substituted (α-diimine)$PdCl_2$ complex **5**. The structure of **5** was confirmed by X-ray diffraction (Figure 3.1) and features an intramolecular N-H···Cl H-bonding interaction between the amide NH unit and a Cl ligand with an N···Cl distance of 3.514(9) Å. The ^{1}H NMR spectrum of **5** exhibits an doublet at δ 3.01 for the amide N-Me group, which is coupled to the NH signal (br q, J = 4.9) at δ 6.86. The ^{1}H NMR spectrum also exhibits an upfield resonance at δ -0.34 for the diimine Me group that is adjacent to the benzhydryl units, which is shielded by the two proximal phenyl rings. Similar results were observed for other (α-diimine)PdMeCl complexes bearing *o,o'*-dibenzhydryl-*p*-tolyl unit(s).[16-17]

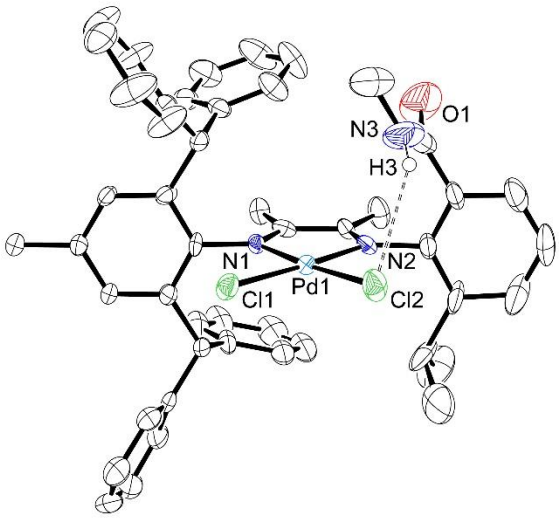

Figure 3.1. Molecular structure of **5** in **5·2(CHCl$_2$CHCl$_2$)**. Solvent molecules are omitted. Hydrogen atoms expect for H3 are omitted. Selected distances (Å): Pd1-Cl1, 2.277(2); Pd1-Cl2, 2.292(2); Pd1-N1, 2.040(6); Pd1-N2, 2.034(6); N3···Cl2, 3.541(9).

The reaction of **5** with $SnMe_4$ yields a 7.7/1 mixture of isomeric (α-diimine)PdMeCl complexes **1d**/**1d'**, which evolves into an equilibrium 5.2/1 mixture of **1d**/**1d'** in a few hours in CD_2Cl_2 at room temperature. The ^{1}H NMR amide NH signal for **1d** in CD_2Cl_2 appears at δ 7.50, which is ca. 1.4 ppm more downfield than that of **1d'** (δ 6.08), consistent with the expected intramolecular H-bonding behavior in **1d** but not **1d'**.

The condensation reaction between compounds **2** and **6** yields α-diimine ligand **7** (Scheme 3.2). **7** reacts with (cod)PdMeCl to form a 1/4.2 mixture of isomeric complexes **1e**/**1e'**, which isomerizes into an equilibrium 1.2/1 mixture within a few hours at room temperature. Ligand **8** and the corresponding (α-diimine)PdMeCl complexes **1f**,**f'** were reported by Chen and coworkers and are synthesized analogously to **1e**,**e'** (Scheme 3.3).[17] **1f**/**1f'** is formed as a 1/1.2 mixture of isomers that evolves to a 1/3.4 equilibrium **1f**/**1f'** mixture over ca. two months at room temperature in CD_2Cl_2. This isomerization is therefore much slower compared to the cases of **1d**,**d'** and **1e**,**e'**.

Scheme 3.2

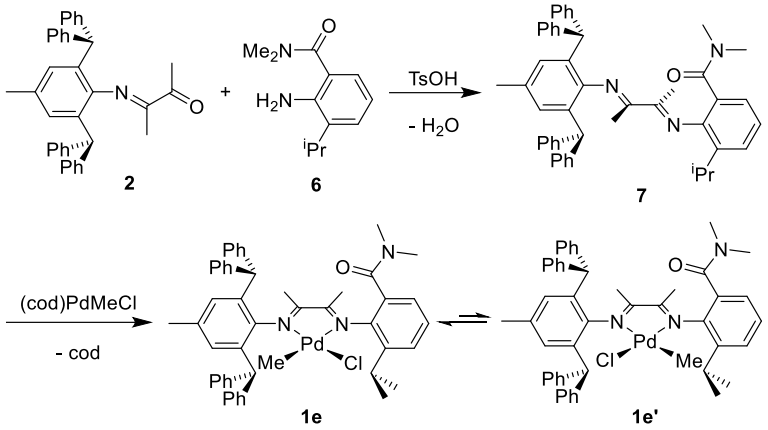

Scheme 3.3

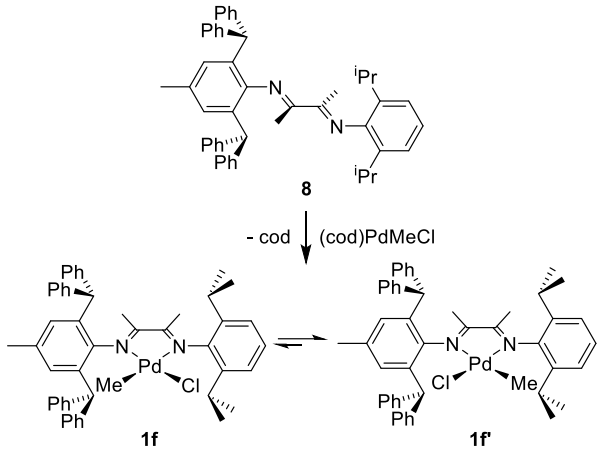

Equilibrium isomer ratios **1a-f**/**1a'-f'** are shown in Table 3.1. The higher values for the **1a**/**1a'** and **1d**/**1d'** ratios compared to the **1b**/**1b'** and **1e**/**1e'** ratios, respectively, is due to the stabilization effect of **1a** and **1d** by intramolecular H-bonding interaction.[18] The equilibrium isomer distribution ratio is influenced by the difference in the donor abilities of the imine ligands. In square planar (α-diimine)PdMeCl complexes that contain two different imine donors, the Me ligand is favored to be *trans* to the more weakly electron-donating of the two imine ligands due to the stronger trans influence of the Me ligand compared to Cl. In the case of **1f**,**f'**, the preference for **1f'** is consistent with the expected weaker donor ability of the 2,6-$(CHPh_2)_2$-4-Me-Ph unit

versus 2,6-$^{i}Pr_2$-Ph (dipp). The same trend was also observed in the change of ratio between **1a**,**a'** and **1d**,**d'**, and between **1b**,**b'** and **1e**,**e'**.

Table 3.1. Equilibrium Isomer Ratios of [ArN=CMeCMe=N-(*o*-R-*o'*-^{i}Pr-Ph)]PdMeCl Complexes

	R = CONHMe	R = $CONMe_2$	R = ^{i}Pr
Ar = dipp	16/1 (**1a**/**1a'**)[a]	4.5/1 (**1b**/**1b'**)[a]	1/1 (**1c**)
Ar = 2,6-$(CHPh_2)_2$-4-Me-Ph	5.2/1 (**1d**/**1d'**)	1.2/1 (**1e**/**1e'**)	1/3.4 (**1f**/**1f'**)

[a]Ref. 18.

Ethylene Homopolymerization. Ethylene polymerization results for the first- and second-generation amide-functionalized (α-diimine)Pd catalysts are provided in Table 3.2. **1a**,**a'** and **1b**,**b'** can be activated by $NaBAr^{F}_4$ (Ar^{F} = 3,5-$(CF_3)_2$-Ph) to generate active single site catalysts for ethylene polymerization that produce highly branched (ca. 91-93 br/1000 C), low MW (M_n 2.4-3.5 kDa) polyethylenes (entries 1-4) at room temperature. Increasing the ethylene pressure from 200 psi to 350 psi does not change the activity or the microstructure of resulting polymer significantly (entry 4), showing that the chain growth and chain transfer are both zero-order on [ethylene], in agreement with the established mechanistic picture for (α-diimine)Pd-catalyzed ethylene polymerization.[19] At 200 psi ethylene pressure, **1b**,**b'** shows ca. 81% lower activity in a 20 h experiment (entry 3) than in a 2 h experiment (entry 2), indicating that decomposition of the catalytically active species is significant. **1a**,**a'** is ca. 74% less active than **1b**,**b'**, and both **1a**,**a'** and **1b**,**b'** exhibit lower activity by an order of magnitude and produce polyethylene with lower MW by two orders of magnitude compared to the benchmark catalyst **1c**. Guan and coworkers studied a series of (α-diimine)Pd catalysts bearing four *ortho*-isopropyl groups and different *para*-substituents on the two N-aryl units and found that electron-withdrawing substituents reduced catalyst activity and polymer MW. The electron-withdrawing effect of the amide groups likely accounts for the low performance of the first-generation catalysts **1a**,**a'** and **1b**,**b'**.

The overall inferior performance of the first-generation catalysts prompted us to study the second-generation catalysts **1d**,**d'** and **1e**,**e'**, in which the detrimental effect of the electron-withdrawing amide groups is counteracted by improved steric properties, resulting from the presence of the benzhydryl groups. In the 2 h experiments at 200 psi (entries 6 and 9), both **1d**,**d'** and **1e**,**e'** exhibit higher activity and higher MW than **1b**,**b'**. The resulting polymers exhibit less branching (77-81 br/1000C) than those produced by the first-generation catalysts. Increasing the reaction time from 2 h to 20 h (entries 7 and 10) results in ca. 77% loss of activity for **1d**,**d'** and ca. 64% loss of activity for **1e**,**e'**, showing that these catalysts also are more thermally stable than **1b**,**b'**. **1d**,**d'** shows no significant improvement in activity or MW in the 350 psi polymerization runs versus 200 psi. The reference catalyst **1f**,**f'** generates a highly active ethylene polymerization catalyst that produces high MW polyethylene (M_n = ca. 300 kDa) with a narrow MW distribution and is ca. 4 times more active than **1d**,**d'** and **1e**,**e'**.

Table 3.2. Ethylene Polymerization[a]

Entry	Cat	C_2H_4 (psi)	Time (h)	Yield (g)	Activity (kg PE mol^{-1} h^{-1})	M_n (10^3)	M_w/M_n	B[b]
1	**1a**,**a'**	200	20	0.20	1.0	2.4	1.85	93
2	**1b**,**b'**	200	2	0.39	20	3.5	1.52	92
3	**1b**,**b'**	200	20	0.76	3.8	3.3	1.61	91
4	**1b**,**b'**	350	20	0.68	3.4	2.9	1.56	92
5[c]	**1c**,**c'**	200	16	8.77	55	138	2.16	98
6	**1d**,**d'**	200	2	0.68	34	26.3	1.81	79
7	**1d**,**d'**	200	20	1.54	7.7	44.0	1.82	79
8	**1d**,**d'**	350	2	0.59	30	24.2	1.75	81
9	**1e**,**e'**	200	2	0.78	39	45.1	1.53	77
10	**1e**,**e'**	200	20	2.75	14	59.7	1.75	79
11	**1f**,**f'**	200	2	2.67	133	292	1.44	73
12	**1f**,**f'**	350	2	3.23	162	327	1.39	74

[a]Conditions: 10 μmol Pd, 20 μmol $NaBAr^F{}_4$, CH_2Cl_2 (40 mL), 25 °C. [b]Branches per 1000C. Determined by ^1H NMR. Corrected for terminal groups of low-MW polymer (M_n < 5000). [c]Ref. 20.

Copolymerization of Ethylene with MA. Catalysts **1d-f**,**d'-f'** were tested for the copolymerization of ethylene with MA. The results are shown in Table 3.3. All the catalysts exhibited significant inhibition in the presence of MA, presumably due to formation of chelate species following MA insertion. However, in contrast to the activity trend of ethylene homopolymerization (**1f**,**f'** > **1e**,**e'** > **1d**,**d'**), the activity trend in the copolymerization of ethylene with MA in CH_2Cl_2 is opposite: **1d**,**d'** > **1e**,**e'** > **1f**,**f'**. Furthermore, The H-bonding catalyst **1d**,**d'** incorporates 1.3 mol% MA , which is ca. twice the level of MA incorporation observed for **1f**,**f'**. For **1d**,**d'** and **1e**,**e'**, changing the solvent from CH_2Cl_2 to a mixture of toluene/CH_2Cl_2 (ca. 4/1) leads to an increase of MA incorporation but a decrease in reaction rate and MW. The ^{1}H NMR spectra of the copolymers exhibit a singlet at δ 3.66 for the Me ester group, a triplet at δ 2.30 for the α-CH_2 of carbonyl and a quintet at δ 1.60 for the β-CH_2 of carbonyl, showing that the MA units are incorporated predominantly in branch ends, which results from chain walking following MA insertion.

Table 3.3. Ethylene/MA Copolymerization[a]

Entry	Cat	Yield (g)	MA TON	C_2H_4 TON	MA incorp. mol%	M_n (10^3)	M_w/M_n	B^b
1	1d,d'	0.31	14	1060	1.3	8.1	2.13	74
2[c]	1d,d'	0.040	3.3	130	2.4	0.98	1.70	82
3	1e,e'	0.22	7.3	760	0.95	4.4	1.76	73
4[c]	1e,e'	0.020	1.0	68	1.4	0.79	1.56	78
5	1f,f'	0.13	2.4	460	0.61	6.9	2.06	77

[a]Conditions: 10 μmol Pd, 20 μmol $NaBAr^F{}_4$, C_2H_4 (14 psi), MA (1.0 M), galvinoxyl (5 μmol), CH_2Cl_2 (total volume 25 mL), 20 h, room temperature (23 °C). [b]Branching density per 1000C. Determined by ^{1}H NMR. Corrected for terminal groups of low-MW polymer (M_n < 5000).
[c]CH_2Cl_2 (5 mL)/toluene (total volume 25 mL) mixture as solvent.

Copolymerization of Ethylene with AA. (*o*-R_2P-C_6H_4-SO_3^-)PdMe and (*o*-R_2P-C_6H_4-$PO(OEt)_2$)$PdMe^+$ catalysts can copolymerize ethylene with AA to yield linear copolymers with in-

chain or chain-end incorporation.[21-22] **1d**,**d'** and **1e**,**e'** produce low-MW ethylene/AA copolymer with 0.88-1.5 mol% AA incorporation. The H-bonding catalyst **1d**,**d'** incorporates AA in ca. 1.7 times as high level as **1e**,**e'** (0.88%) and ca. 3 times as high level as **1f**,**f'** (0.45 mol%). For **1d**,**d'** and **1e**,**e'**, AA is a stronger inhibitor than MA. Interestingly, **1f**,**f'** is quite active and yields high-MW copolymer in ethylene/AA copolymerization, suggesting that AA is a weaker inhibitor than MA for this catalyst. For **1d**,**d'** and **1e**,**e'**, changing solvent from CH_2Cl_2 to toluene/CH_2Cl_2 (4/1) leads to only trace polymer. The ^{1}H NMR spectra of the copolymers exhibit a triplet at δ 2.35 for the α-CH_2 of carbonyl and a quintet at δ 1.62 for the β-CH_2 of carbonyl, showing that the AA units are incorporated predominantly in branch ends, which is similar to the case of MA copolymerization.

Table 3.4. Ethylene/AA Copolymerization[a]

Entry	Cat	Yield (g)	AA TON	C_2H_4 TON	AA incorp. mol%	M_n (10^3)	M_w/M_n	B^b
1	**1d**,**d'**	0.060	3.1	210	1.5	3.0	1.66	73
2[c]	**1d**,**d'**	trace	-	-	-	-	-	-
3	**1e**,**e'**	0.054	1.7	190	0.88	3.2	1.56	74
4[c]	**1e**,**e'**	trace	-	-	-	-	-	-
5	**1f**,**f'**	1.29	21	4600	0.45	65.3	1.63	77

[a]Conditions: 10 μmol Pd, 20 μmol $NaBAr^F_4$, C_2H_4 (14 psi), AA (1.0 M), galvinoxyl (5 μmol), CH_2Cl_2 (total volume 25 mL), 20 h, room temperature (23 °C). [b]Branching density per 1000C. Determined by ^{1}H NMR. Corrected for terminal groups of low-MW polymer (M_n < 5000). [c]CH_2Cl_2 (5 mL)/toluene (total volume 25 mL) mixture as solvent.

Reaction of (α-Diimine)PdMeCl Complexes with Metal Salts. The reaction of **1a**,**a'** and **1b**,**b'** with AgOTf at room temperature in CH_2Cl_2 quantitatively yields 0.5 equiv methane and blue-green μ-CH_2 complexes **9a-OTf** and **9b-OTf** (Scheme 3.4), in which the amide-substituted α-diimine ligands function as bridging ligands to support the Pd_2(μ-CH_2) unit. The solid-state structures of **9a,b-OTf** are shown in Figure 3.2. The dications in both **9a,b-OTf** are C_2-symmetric;

in particular, the solid-state structure of **9a-OTf** contains a crystallographic C_2-axis running through the μ-CH_2 C-atom. **9a-OTf** exhibits a Pd-C-Pd angle of 97.9(4)° and a Pd···Pd distance of 2.9999(10) Å; similarly, **9b-OTf** exhibits a Pd-C-Pd angle of 98.85(18)° and a Pd···Pd distance of 3.0142(4) Å. Both Pd···Pd distances are shorter than the sum of van der Waals radii of Pd atoms (2 x r_{Pd} = 3.26 Å). The μ-CH_2 units in both **9a,b-OTf** are jacketed by the two adjacent aryl rings that are attached to the bridging amide groups (Figures 3.2a, middle; 3.2b, middle). The secondary amide groups of **9a-OTf** are engaged in H-bonding interactions with an adjacent triflate anion (Figure 3.2a, right).

Scheme 3.4

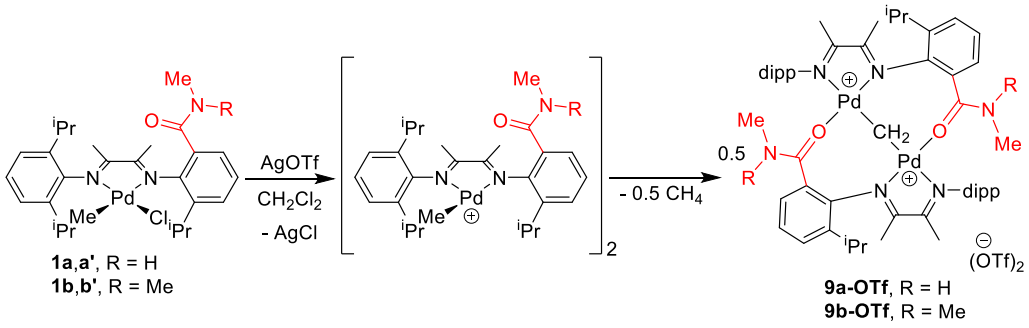

(a)

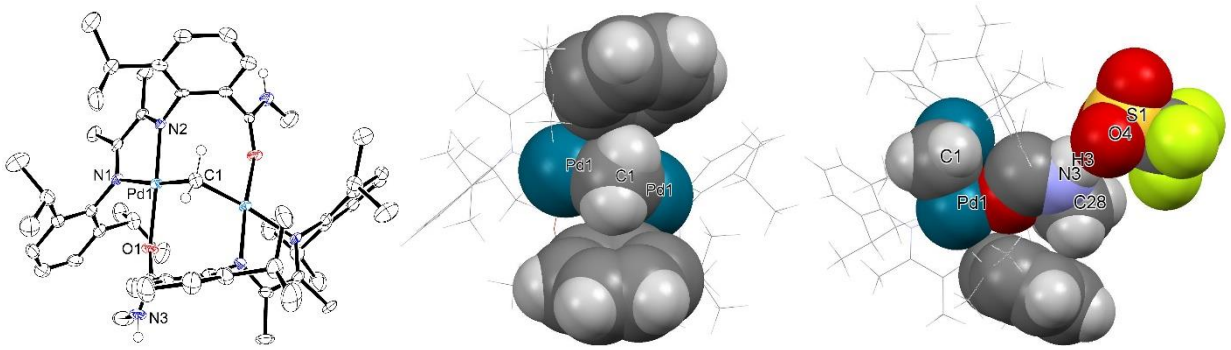

(b)

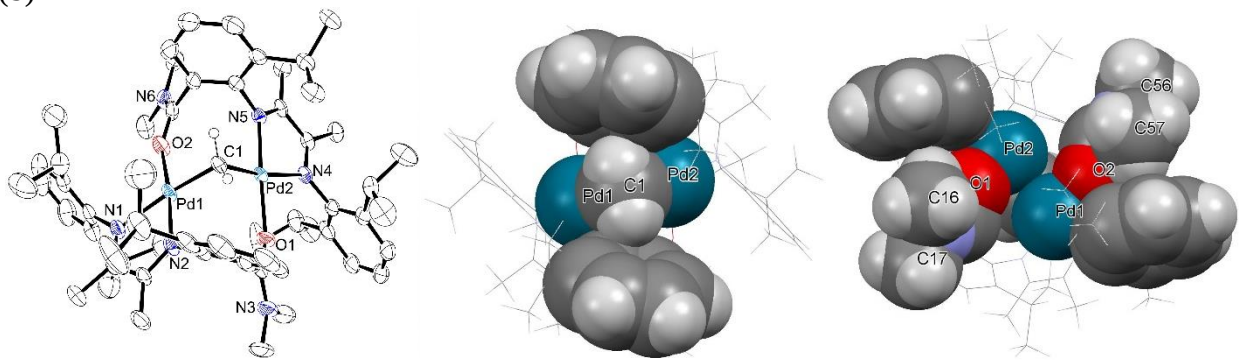

Figure 3.2. (a) Molecular structure of **9a-OTf** in **9a-OTf·4(CH_2Cl_2)**. Solvent molecules, anions and disorder of amide group are omitted. Left: ORTEP graph. Hydrogen atoms except for the H-atoms on C1 and N3 are omitted. Middle: Space-filling model showing the $Pd_2(\mu\text{-}CH_2)$ unit and the two aryl rings in close proximity. Right: Space-filling model showing the environment of an amide group, which is engaged in H-bonding with OTf^-. Selected distances (Å) and angles (°): Pd1-N1, 2.131(6); Pd1-N2, 2.012(5); Pd1-C1, 1.989(7); Pd1-O1, 2.11(3); Pd1···Pd1, 2.9999(10); N3···O4, 2.980(16); H3···O4, 2.11; Pd1-C1-Pd1, 97.9(4); N3-H3···O4, 170. (b) Molecular structure of **9b-OTf** in **9b-OTf·2(CH_2Cl_2)**. Solvent molecules and anions are omitted. Left: ORTEP graph. Hydrogen atoms except for the H-atoms on C1 are omitted. Middle: Space-filling model showing the $Pd_2(\mu\text{-}CH_2)$ unit and the two aryl rings in close proximity. Right: Space-filling model showing the environment of the two amide groups. Selected distances (Å) and angles (°): Pd1-C1, 1.979(4); Pd2-C1, 1.990(4); Pd1-O2, 2.068(3); Pd2-O1, 2.073(3); Pd1-N1, 2.161(3); Pd2-N4, 2.154(3); Pd1-N2, 2.001(3); Pd2-N5, 2.006(3); Pd1···Pd2, 3.0142(4); Pd1-C1-Pd2, 98.85(18).

The ^{1}H NMR and ^{13}C NMR signals of the $\mu\text{-}CH_2$ unit of **9a-OTf** in CD_2Cl_2 appear at δ 2.11 (s) and δ 67.3, respectively. The identity of methylene group was confirmed by HMQC and ^{13}C{gated-^{1}H} NMR experiments. The ^{13}C{gated-^{1}H} NMR spectrum exhibits a triplet (J = 142 Hz) for the $\mu\text{-}CH_2$ C-atom. Similarly, the ^{1}H NMR and ^{13}C NMR signals of the $\mu\text{-}CH_2$ unit of **9b-OTf** in CD_2Cl_2 appear at δ 1.76 (s) and δ 66.6 (t, J = 142 Hz as determined by ^{13}C{gated-^{1}H}

NMR), respectively. The *O-cis* amide N-Me groups in both **9a,b-OTf** are shielded by the dipp aryl rings (Figures 3.2a, right; 3.2b, right), and accordingly, their ^{1}H NMR resonances appear at unusually high field (δ 2.05 for **9a-OTf**; δ 2.23 for **9b-OTf**; c.f. δ 2.94 for **1d**).

Several crystallographically characterized $Pd_2(\mu\text{-}CH_2)$ complexes have been reported previously and listed in Chart 3.2.[23-27] The Pd···Pd distance ranges from 2.70 Å for **11-OTf**, in which the presence of a Pd-Pd bond was suggested, to 3.3 Å for **12**, which a Pd-Pd bond is clearly ruled out. The Pd···Pd distances in **9a,b-OTf** are intermediate within this range and fit well in the statistical range for $\mu\text{-}CH_2$ complexes without a M-M bond (M···M 2.84-3.8 Å).[28]

Chart 3.2. Crystallographically Characterized (μ-CH_2)Pd^{II}_2 Complexes

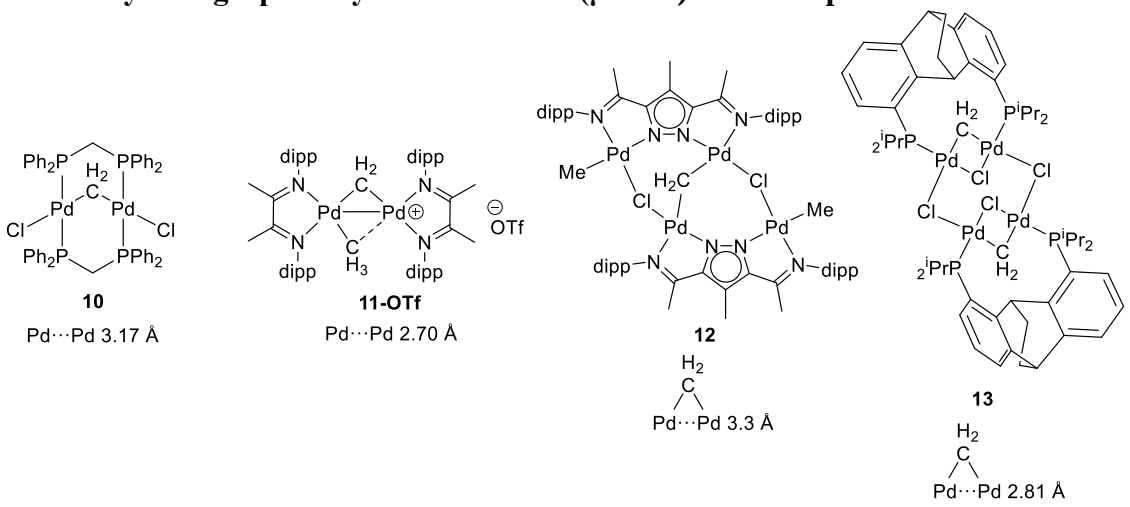

Initial studies showed that **1a**,**a'** and **1b**,**b'** undergo the same type of reaction with 1 equiv $NaBAr^F_4$ to form **9a,b-BAr$^F_4$**, albeit with lower selectivity (NMR yields: 63% for **9a-BAr$^F_4$**; 57% for **9b-BAr$^F_4$**). In contrast, **1a**,**a'** reacts with AgOAc to form the corresponding (α-diimine)PdMe(η^1-OAc) complex. These results suggest that weakly coordinating anions and open coordination sites are crucial for the conversion of (α-diimine)$PdMe^+$ species to (α-diimine)Pd(μ-CH_2)Pd(α-diimine)$^{2+}$ products.

The formation **9a,b-OTf** may proceed through intermolecular Pd-mediated C-H activation of a Pd-Me ligand. Baird and coworkers reported the formation of μ-CH_2 complex **11-OTf** and extrusion of CH_4 in the reaction of (dippN=CMeCMe=Ndipp)$PdMe_2$ and $[Ph_3C]OTf$ in a 2:1 fashion.[25]

9a,b-OTf are inactive in ethylene polymerization (80 psi), likely due to the detrimental effect of triflate anions.[25] In our polymerization conditions, the formation of μ-CH_2 complex would likely be inhibited by ethylene coordination, and should be much slower than ethylene polymerization by **1a**,**a'** and **1b**,**b'**. This reaction is unlikely to dominate the catalyst deactivation but shows how pendent amide group can change reactivity through intermolecular coordination.

3.3 Conclusions

The synthesis of second-generation catalysts **1d**,**d'** and **1e**,**e'** is described. Intramolecular hydrogen bonding influences the equilibrium isomer ratio **1d**/**1d'** due to selective stabilization of the major isomer **1d**. Activation of **1d**,**d'** and **1e**,**e'** by $NaBAr^F_4$ generates active ethylene polymerization catalysts that produce highly branched (77-81 br/1000C) polyethylenes with a moderate MW (M_n ca. 26-60 kDa). The replacement of two isopropyl units in the catalysts **1a**,**a'** and **1b**,**b'** with benzhydryl groups leads to a significant improvement on the overall homopolymerization performance. The H-bonding catalyst **1d**,**d'** is capable of incorporating ca. 2 times as much MA and ca. 3 times as much AA as **1f**,**f'** in the copolymerization with ethylene. The reactions of **1a**,**a'** and **1b**,**b'** with metal salts containing weakly coordinating anions lead to extrusion of CH_4 and the formation of μ-CH_2 complexes, in which the amide carbonyl O-atoms coordinate to Pd centers.

3.4 Experimental Section

General Procedures. All experiments were performed under nitrogen atmosphere using drybox or Schlenk techniques. Nitrogen was purified by passage through activated molecular sieves and Q-5 oxygen scavenger. Hexane, benzene and toluene were purified by passage through activated alumina and BASF R3-11 oxygen scavenger. CH_2Cl_2 and Et_2O were purified by passage through activated alumina. All workup and purification procedures of organic compounds were carried out with reagent grade solvents in air. Acrylic acid and methyl acrylate were dried over $MgSO_4$ and $CaCl_2$, respectively, distilled under reduced pressure, and stored at -40 °C. 3-(2,6-dibenzhydryl-4-methylphenylimino)butan-2-one (**2**),[29] 2-amino-3-isopropyl-*N*-methylbenzamide (**3**), 2-amino-3-isopropyl-*N*,*N*-dimethylbenzamide (**6**), **1a**,**a'**, **1b**,**b'**,[18] **1c**[30] and (cod)PdMeCl[31] were synthesized by literature procedures or modifications thereof.

NMR spectra were recorded on a Bruker DRX-500 spectrometer at room temperature using Teflon-valved tubes. ^1H and ^{13}C chemical shifts are reported relative to $SiMe_4$ and were determined by reference to the residual ^1H and ^{13}C solvent resonances. Coupling constants are given in hertz (Hz). NMR assignments were made with the aid of COSY, NOESY, HMQC, and HMBC experiments. CD_2Cl_2 was distilled from P_2O_5 and stored under vacuum. Elemental analyses were performed by Robertson Microlit Laboratories (Ledgewood, NJ). Mass spectrometry was performed on Agilent 6130 LCMS (low resolution) or Agilent 6224 Tof-MS (high resolution) instruments. The listed *m*/*z* value corresponds to the most intense peak in the isotope pattern.

Ethylene polymerization reactions were performed in a Parr 300 mL stainless steel autoclave equipped with a mechanical stirrer, thermocouple and water cooling loop and controlled by a Parr 4842 controller. Ethylene copolymerization reactions were performed in a 200 mL Fischer-Porter bottle equipped with a magnetic stir bar and a stainless steel pressure head equipped

with inlet and outlet needle valves, a septum-capped ball valve for injections, a check valve for safety, and a pressure gauge. Gel permeation chromatography (GPC) data were obtained on a Polymer Laboratories PLGPC 200 instrument at 150 °C with 1,2,4-trichlorobenzene (stabilized with 125 ppm BHT) as the mobile phase. Three PLgel 10 μm Mixed-B LS columns were used. Molecular weights were calibrated using narrow polystyrene standards (ten-point calibration with M_n from 580 Da to 6035 kDa) and are corrected for linear polyethylene by universal calibration using the following Mark-Houwink parameters: polystyrene, K = 1.75 x 10^{-2} cm^3 g^{-1}, α = 0.67; polyethylene, K = 5.90 x 10^{-2} cm^3 g^{-1}, α = 0.69.[32]

4. A Schlenk flask was charged with **2** (2.50 g, 4.92 mmol), **3** (1.02 g, 4.92 mmol), TsOH · H_2O (ca. 100 mg) and toluene (100 mL). The flask was equipped with a Dean-Stark trap with 3 Å molecular sieves and a condenser. The mixture was refluxed for 23 h. Once the heating was terminated, a white solid precipitated out of the brown solution. The volatiles were removed on a rotovap, and CH_2Cl_2 (ca. 30 mL) was added to dissolve most of the solid. The mixture was filtered, layered with hexane (200 mL), and allowed to sit for 3 d at room temperature to yield pale brown crystals. This crude product was recrystallized from hexane/CH_2Cl_2 to yield pure **4** as white crystals (0.98 g). The mother liquors were combined and taken to dryness. The residue was subjected to flash column chromatography (silica, hexane/EtOAc = 6/1 by volume) to afford additional pure **4** as a white solid (0.13 g). Overall yield: 1.11 g (33%). ^{1}H NMR (CD_2Cl_2): δ 7.76 (dd, J = 7.8, 1.4, 1H), 7.29-7.14 (m, 13H), 6.96 (d, J = 7.2, 2H), 6.90 (d, J = 7.2, 2H), 6.81-6.74 (m, 5H), 6.64 (d, J = 1.4, 1H), 6.61 (d, J = 1.4, 1H), 5.00 (s, 1H, C*H*Ph_2), 4.78 (s, 1H, C*H*Ph_2), 4.63 (br s, 1H, NH), 3.00 (s, 3H, N-Me), 2.68 (septet, J = 6.9, 1H, ^{i}Pr), 2.09 (s, 3H, *p*-Me), 1.62 (s, 3H, C*Me*(N)(N)), 1.18 (d, J = 6.9, 3H, ^{i}Pr), 1.15 (d, J = 6.9, 3H, ^{i}Pr), 0.83 (s, 3H, *Me*C=N). ^{13}C{^{1}H} NMR (CD_2Cl_2): δ 175.2, 163.9, 145.14 (Ar C), 145.12 (Ar C), 144.5 (Ar C), 143.2 (Ar C), 142.92

(Ar C), 142.86 (Ar C), 133.3 (Ar C), 132.2 (Ar C), 131.6 (Ar C), 131.2 (Ar C), 130.2 (Ar CH × 2), 129.97 (Ar CH × 2), 129.92 (Ar CH), 129.84 (Ar CH), 129.76 (Ar CH), 129.70 (Ar CH × 4), 128.7 (Ar CH × 2), 128.52 (Ar CH × 2), 128.48 (Ar CH × 2), 128.3 (Ar CH × 2), 126.75 (Ar CH), 126.67 (Ar CH), 126.6 (Ar CH), 126.5 (Ar CH), 126.4 (Ar CH), 119.8 (Ar CH), 116.9 (Ar C), 76.8 (C), 51.4, 51.3, 31.0, 27.2, 26.0, 22.6, 22.4, 21.2, 17.0. HRMS (ESI-TOF, positive ion, *m*/*z*): Calc. 682.3797 ($[M + H]^+$), found 682.3798.

(a)

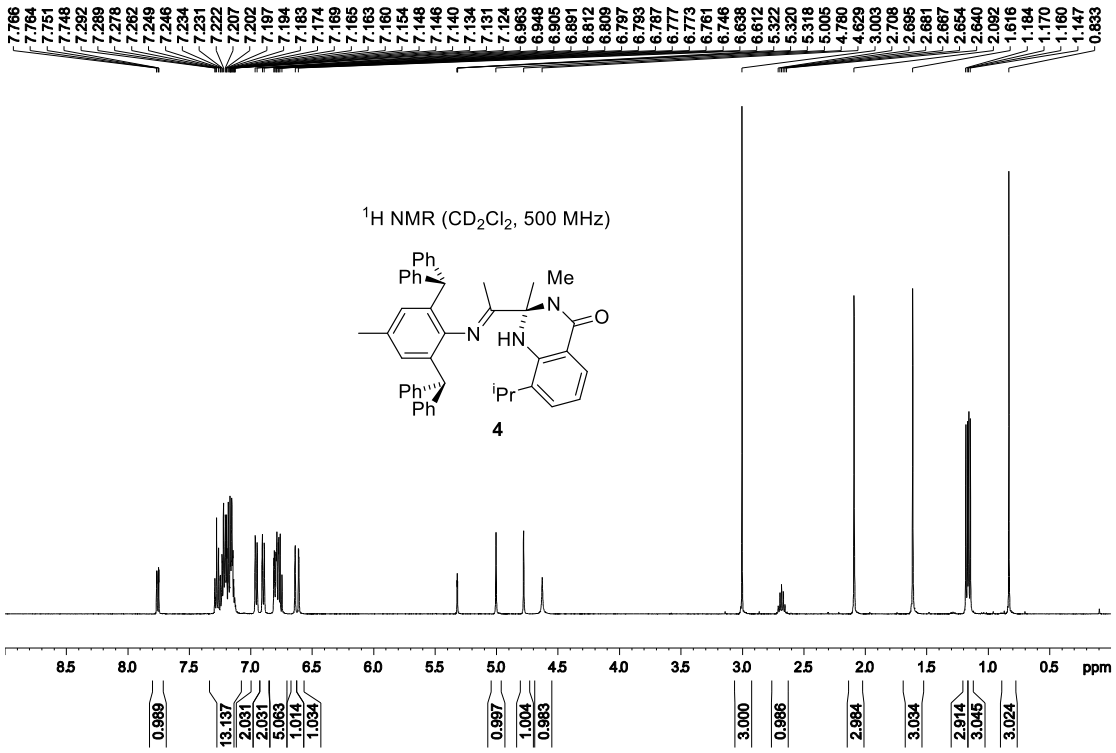

Figure 3.3. NMR spectra of **4**.

(b)

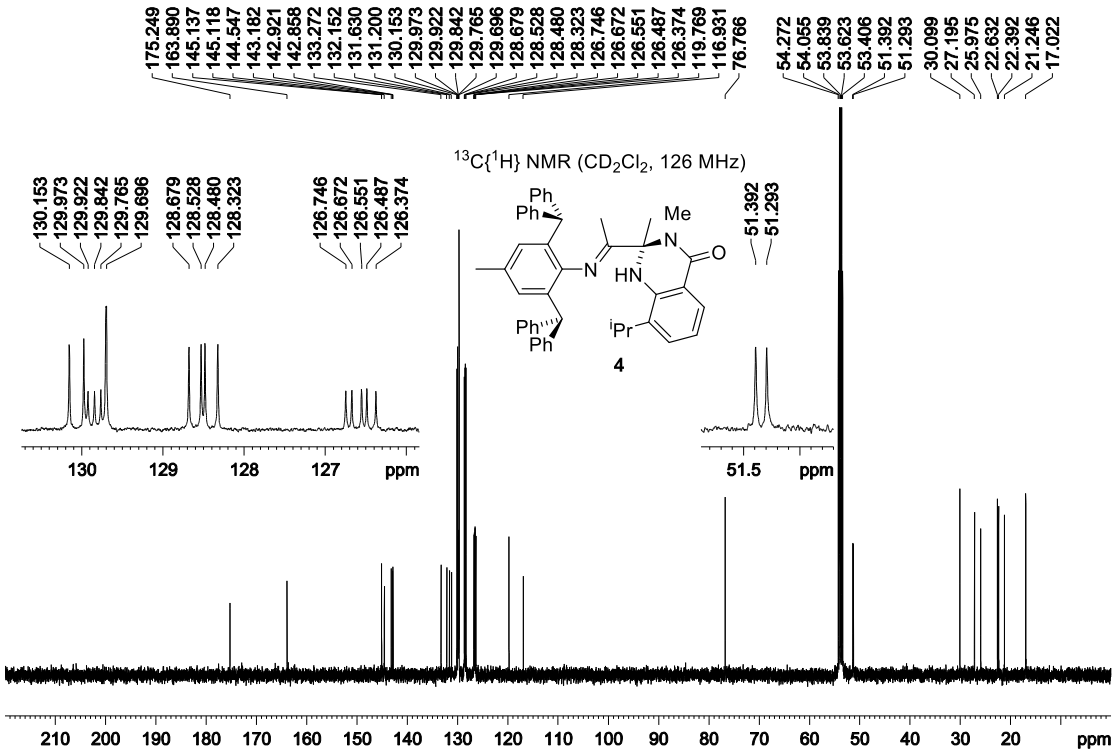

Figure 3.3, continued. NMR spectra of **4**.

5. A Schlenk flask was charged with **4** (869 mg, 1.27 mmol), $(MeCN)_2PdCl_2$ (314 mg, 1.21 mmol) and CH_2Cl_2 (20 mL). The mixture was refluxed for 22 h to yield an orange solution. The mixture was filtered through Celite. The filtrate was concentrated under vacuum to ca. 3 mL, and hexane (100 mL) was added to yield a yellow precipitate. The yellow solid was re-precipitated from hexane/CH_2Cl_2 (100 mL/10 mL) to yield **5** (750 mg, 72%). ^{1}H NMR (CD_2Cl_2): δ 7.52 (dd, *J* = 7.9, 1.0, 1H), 7.47-7.43 (m, 3H), 7.37-7.20 (m, 19H), 6.86 (br q, *J* = 4.9, 1H, N*H*Me), 6.78 (d, *J* = 1.0, 1H), 6.69 (d, *J* = 1.0, 1H), 6.20 (s, 1H, C*H*Ph_2), 5.86 (s, 1H, C*H*Ph_2), 3.15 (septet, *J* = 6.9, 1H, ^{i}Pr), 3.01 (d, *J* = 4.9, 3H, NH*Me*), 2.19 (s, 3H, *p*-Me), 1.60 (s, 3H, *Me*C=N), 1.56 (d, *J* = 6.9, 3H, ^{i}Pr), 1.35 (d, *J* = 6.9, 3H, ^{i}Pr), -0.34 (s, 3H, *Me*C=N). $^{13}C\{^{1}H\}$ NMR (CD_2Cl_2): δ 183.0, 181.4, 168.8, 143.0 (Ar C), 142.7 (Ar C), 141.3 (Ar C), 140.9 (Ar C), 140.4 (Ar C), 140.2 (Ar C), 139.9 (Ar C), 138.3 (Ar C), 136.9 (Ar C), 136.5 (Ar C), 131.4 (Ar C), 131.0 (Ar CH × 2), 130.6 (Ar CH

× 2), 130.0 (Ar CH × 2), 129.8 (Ar CH × 2), 129.7 (Ar CH × 2), 129.4 (Ar CH × 3), 129.3 (Ar CH), 129.2 (Ar CH), 128.63 (Ar CH × 2), 128.57 (Ar CH × 2), 127.8 (Ar CH), 127.6 (Ar CH), 127.5 (Ar CH), 127.0 (Ar CH), 126.9 (Ar CH), 125.0 (Ar CH), 53.2, 52.8, 29.3, 27.0, 23.78, 23.74, 21.7, 20.7, 19.4. ESI-MS (1:1 MeOH:H_2O, positive ion scan, *m*/*z*): 822.4 ($[M - Cl]^+$). Anal. Calcd. for $C_{48}H_{47}Cl_2N_3OPd$, %: C, 67.10; H, 5.51; N, 4.89. Found: C, 66.36; H, 5.10; N, 4.73.

(a)

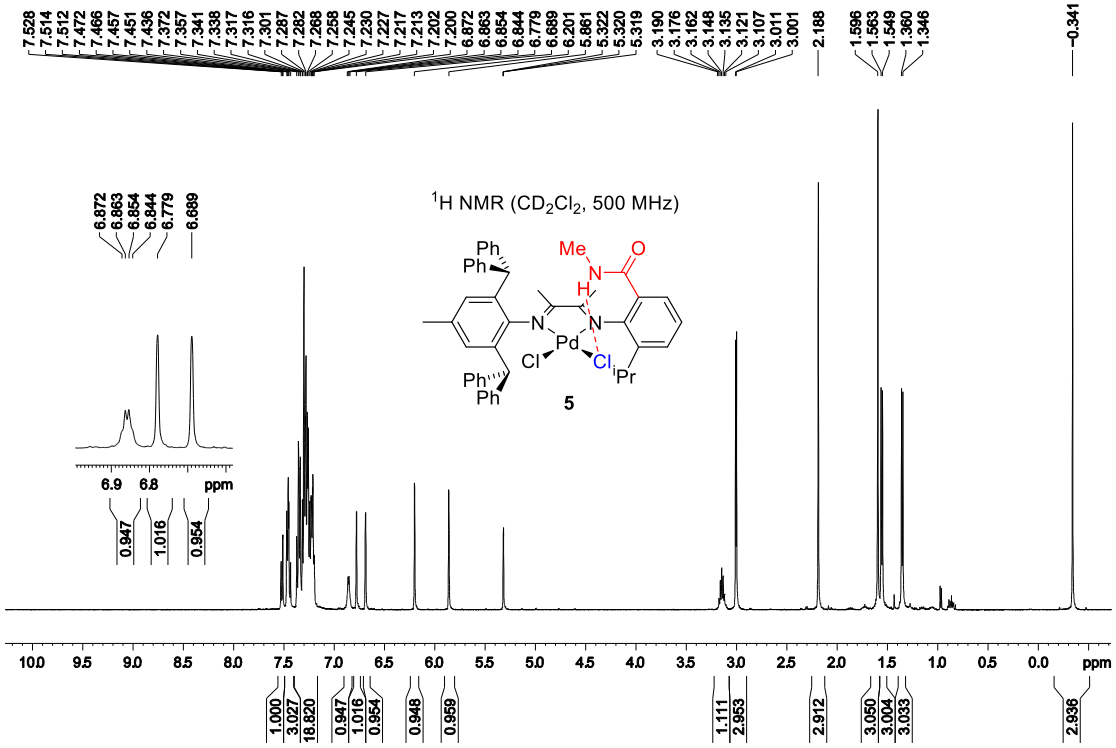

Figure 3.4. NMR spectra of **5**.

(b)

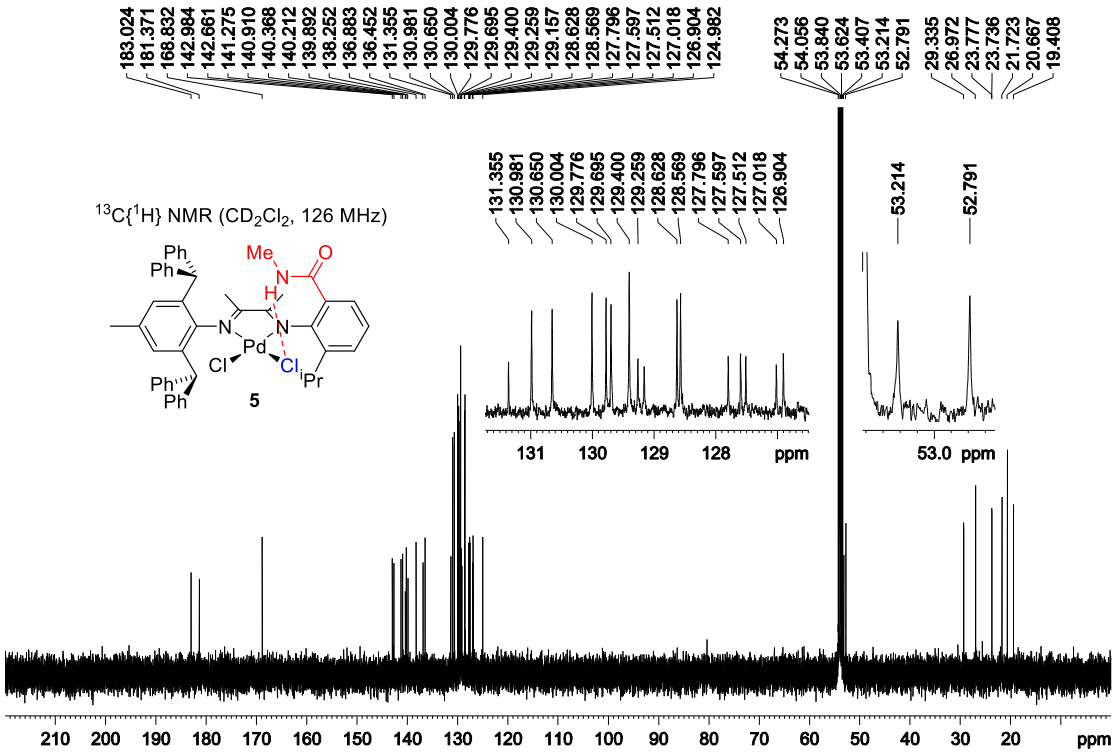

Figure 3.4, continued. NMR spectra of **5**.

7. A Schlenk flask was charged with **2** (900 mg, 1.78 mmol), **6** (350 mg, 1.70 mmol), $TsOH \cdot H_2O$ (ca. 20 mg) and benzene (50 mL). The flask was equipped with a Dean−Stark trap filled with 3 Å molecular sieves and a condenser. The mixture was refluxed for 24 h, cooled to room temperature, and quenched with Et_3N (ca. 5 mL). The volatiles were removed under vacuum to give a brown oil. The oil was subjected to flash column chromatography (silica, hexane/EtOAc= 2/1 by volume) to give a brown oil, which solidified to form a yellow brown solid upon drying under vacuum overnight. Yield: 566 mg (48%). ^{1}H NMR (CD_2Cl_2): δ 7.34-7.18 (m, 13H), 7.13-7.03 (m, 10H), 6.72 (s, 1H), 6.67 (s, 1H), 5.24 (s, 1H, C*H*Ph_2), 5.10 (s, 1H, C*H*Ph_2), 2.88 (br s, 3H, N*Me*Me'), 2.75 (br s, 3H, NMe*Me'*), 2.70 (septet, *J* = 6.9, 1H, ^{i}Pr), 2.16 (s, 3H, *p*-Me), 1.89 (s, 3H, *Me*C=N), 1.23 (d, *J* = 6.9, 3H, ^{i}Pr), 1.19 (d, *J* = 6.9, 3H, ^{i}Pr), 1.07 (s, 3H, *Me*C=N). $^{13}C\{^{1}H\}$ NMR (CD_2Cl_2): δ 170.1 (Me*C*=N), 170.0 (C=O), 169.9 (Me*C*=N, located by HMBC), 145.7 (Ar

C), 145.2 (Ar C), 144.0 (Ar C), 143.6 (Ar C), 143.17 (Ar C), 143.11 (Ar C), 136.6 (Ar C, located by HMBC), 132.3 (Ar C), 132.0 (Ar C), 131.6 (Ar C), 130.1 (Ar CH × 2), 129.91 (Ar CH × 2), 129.88 (Ar CH × 2), 129.80 (Ar CH × 2), 128.94 (Ar CH), 128.92 (Ar CH), 128.8 (Ar CH × 4), 128.6 (Ar CH × 2), 128.5 (Ar CH × 2), 126.66 (Ar CH), 126.60 (Ar CH), 126.58 (Ar CH), 126.54 (Ar CH), 126.46 (Ar C), 126.39 (Ar CH), 124.6 (Ar CH), 124.2 (Ar CH), 52.7, 52.3, 38.2 (br), 34.7, 28.4, 23.2, 23.0, 21.4, 17.4, 16.4. HRMS (APCI-TOF, positive ion, *m*/*z*): Calc. 696.3954 ([M + H]$^+$), found 696.3954.

(a)

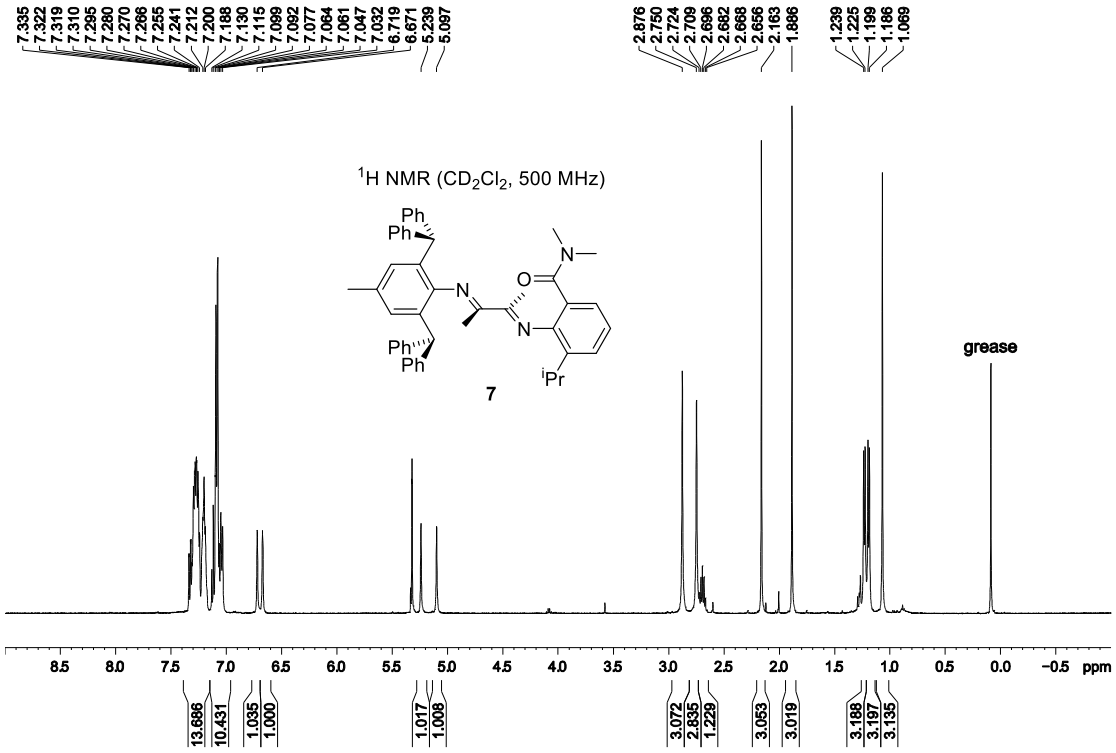

Figure 3.5. NMR spectra of **7**.

(b)

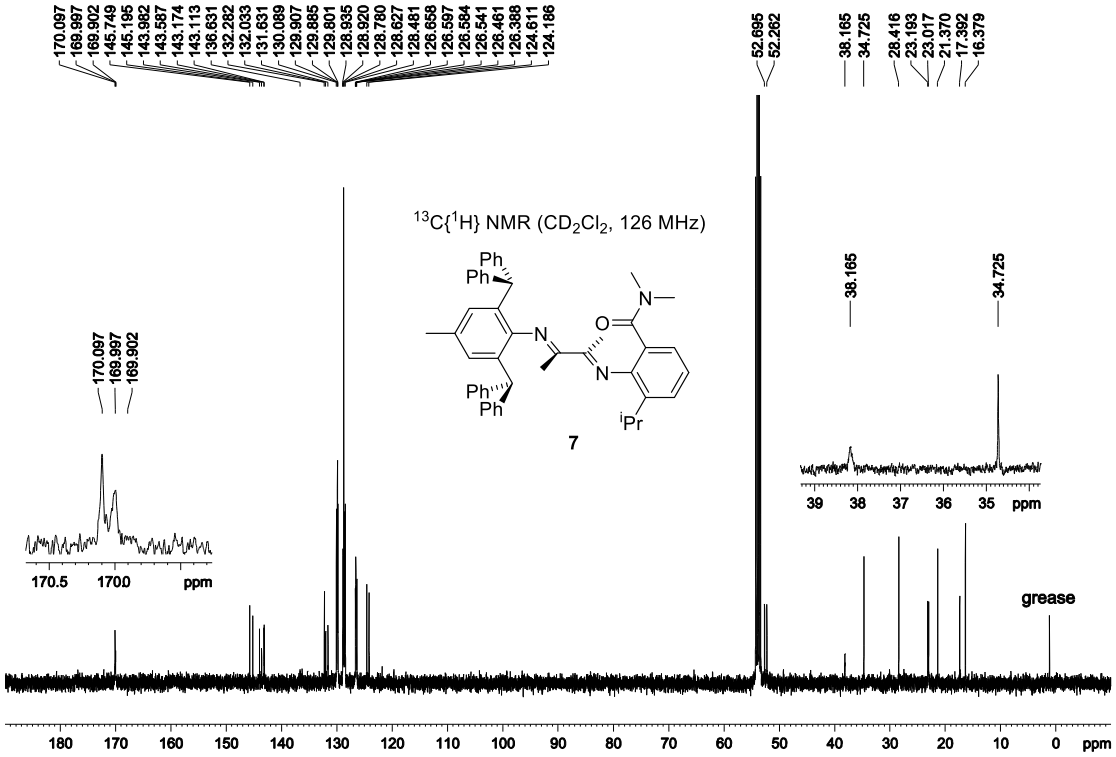

Figure 3.5, continued. NMR spectra of **7**.

8.[17,33] This known compound was synthesized using modified literature procedure and different starting compounds. A Schlenk flask was charged with 3-(2,6-diisopropylphenylimino)butan-2-one[34] (1.38 g, 5.62 mmol), 2,6-dibenzhydryl-4-methylaniline (2.47 g, 5.62 mmol), $TsOH \cdot H_2O$ (ca. 100 mg) and toluene (100 mL). The flask was equipped with a Dean−Stark trap filled with 3 Å molecular sieves and a condenser. The mixture was refluxed for 24 h, cooled to room temperature, and quenched with Et_3N (ca. 5 mL). The volatiles were removed under vacuum to give a yellow oil. The oil was subjected to flash column chromatography (silica, hexane/EtOAc= 50/1 by volume), and the forefront major band was collected and taken to dryness under vacuum to give a pale yellow powder. The powder was taken up in MeOH (100 mL) and refluxed for 30 min. The mixture was cooled to room temperature, and the solid was collected by vacuum filtration and dried under vacuum. Yield: 1.64 g (44%). ^1H NMR ($CDCl_3$): 7.28-7.25 (m,

8H), 7.21-7.17 (m, 4H), 7.16-7.14 (m, 2H), 7.11-7.05 (m, 9H), 6.67 (s, 2H), 5.29 (s, 2H), 2.61 (sept, *J* = 6.8, 2H), 2.18 (s, 3H), 1.88 (s, 3H), 1.22 (d, *J* = 6.8, 6H), 1.17 (d, *J* = 6.8, 6H), 0.88 (s, 3H). $^{13}C\{^{1}H\}$ NMR ($CDCl_3$): δ 170.1 (located by HMBC), 168.0, 146.0, 145.7 (located by HMBC), 143.8, 142.5, 135.1, 132.1, 131.7, 129.9, 129.6, 128.9, 128.6, 128.2, 126.5, 126.3, 124.0, 123.1, 52.4, 28.3, 23.5, 23.3, 21.5, 17.0, 16.2. HRMS (APCI-TOF, positive ion, *m*/*z*): Calc. 667.4052 ([M + H]$^{+}$), found 667.4056.

(a)

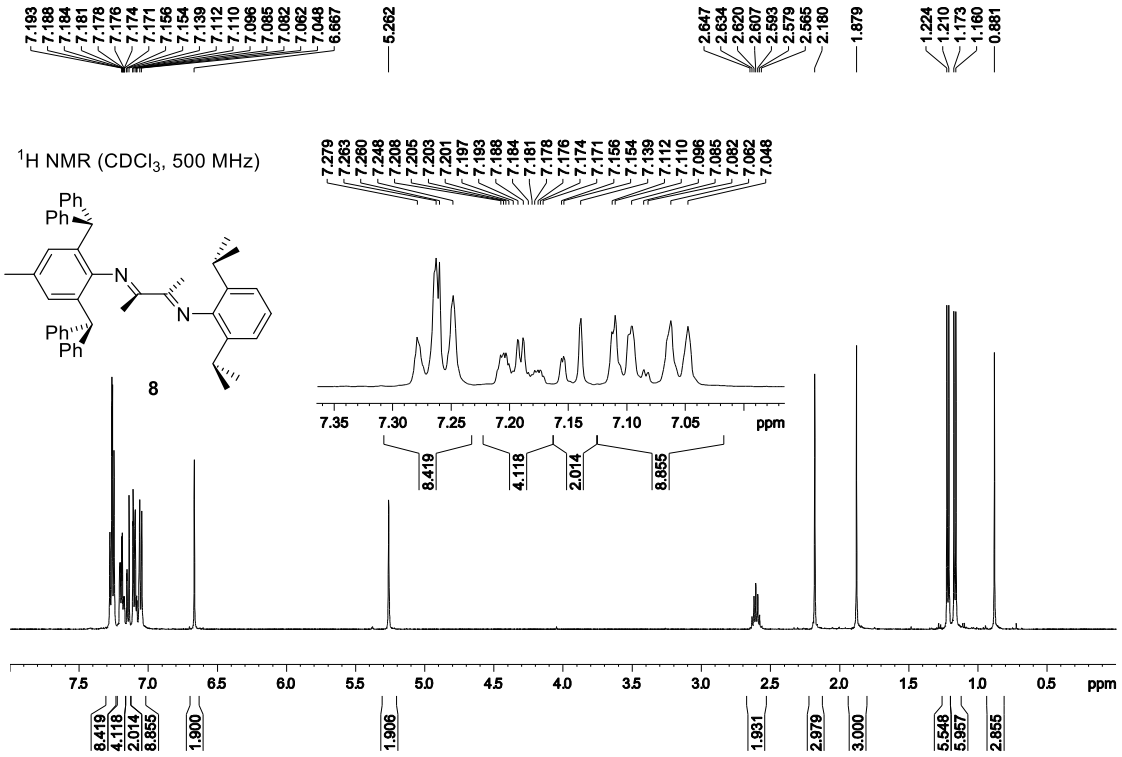

Figure 3.6. NMR spectra of **8**.

(b)

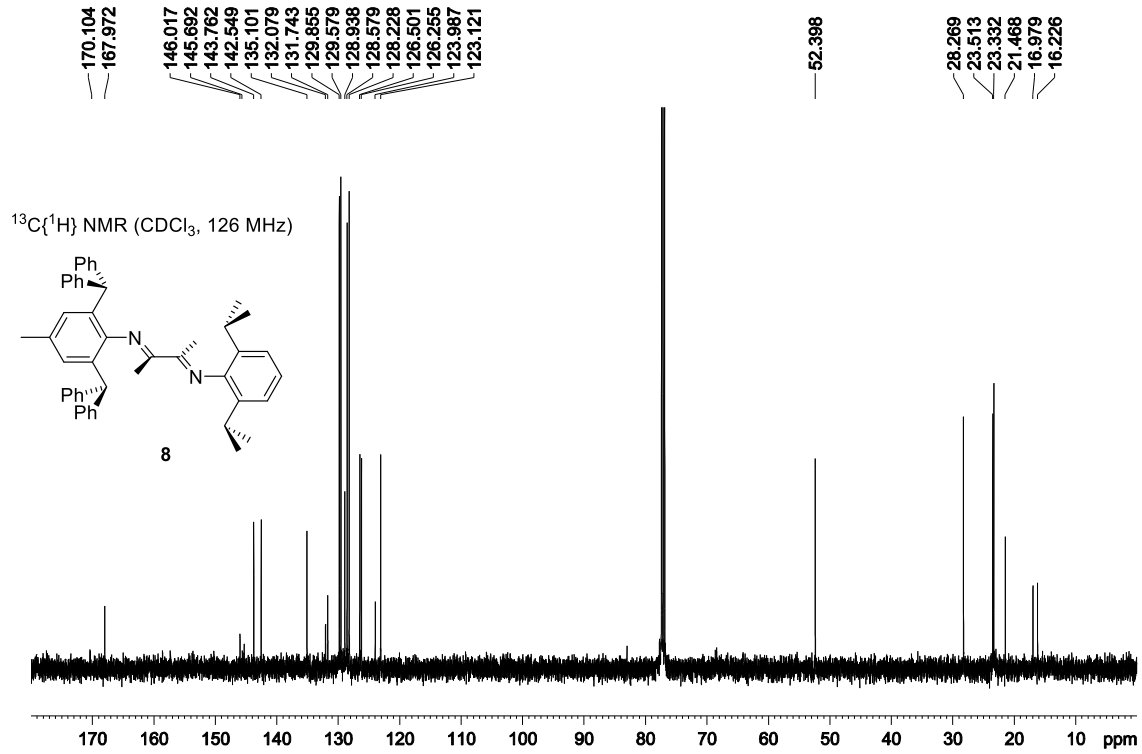

Figure 3.6, continued. NMR spectra of **8**.

1d,d'. A scintillation vial was charged with **5** (699 mg, 0.814 mmol), $SnMe_4$ (436 mg, 2.44 mmol) and CH_2Cl_2 (3 mL). The mixture was stirred at room temperature in the dark for 36 h. The mixture was filtered through Celite. The filtrate was concentrated under vacuum to ca. 2 mL. Et_2O (20 mL) was added, and the mixture was further concentrated under vacuum to yield a yellow precipitate. The yellow solid was collected by vacuum filtration, washed with Et_2O, and dried under vacuum. Yield: 514 mg (75%). The solid is a 7.7/1 mixture of **1d**/**1d'**, as determined by ^{1}H NMR at room temperature based on the integrals of the Pd-Me resonances, and contains 0.06 equiv Et_2O. This mixture isomerized to a 5.2/1 equilibrium **1d**/**1d'** mixture within a few hours at room temperature in CD_2Cl_2. **1d**: ^{1}H NMR (CD_2Cl_2): δ 7.50 (br q, *J* = 4.9, 1H, N*H*Me), 7.48 (dd, *J* = 7.8, 1.2, 1H), 7.38-7.14 (m, 22H), 6.87 (d, *J* = 1.0, 1H), 6.81 (d, *J* = 1.0, 1H), 5.91 (s, 1H, C*H*Ph_2), 5.715 (s, 1H, C*H*Ph_2), 2.98 (septet, *J* = 6.9, 1H, ^{i}Pr), 2.94 (d, *J* = 4.8, 3H, NH*Me*), 2.22 (s, 3H, *p*-

Me), 1.51 (d, *J* = 6.9, 3H, ^{i}Pr), 1.48 (s, 3H, *Me*C=N), 1.33 (d, *J* = 6.9, 3H, ^{i}Pr), 0.88 (s, 3H, Pd-Me), -0.43 (s, 3H, *Me*C=N). $^{13}C\{^{1}H\}$ NMR (CD_2Cl_2): δ 179.7, 172.9, 169.3, 142.8 (Ar C), 142.6 (Ar C), 141.5 (Ar C), 141.3 (Ar C), 141.0 (Ar C), 140.7 (Ar C), 138.7 (Ar C), 137.0 (Ar C), 135.7 (Ar C), 135.5 (Ar C), 130.77 (Ar CH × 2), 130.75 (Ar C), 130.5 (Ar CH × 2), 129.8 (Ar CH × 2), 129.7 (Ar CH × 2), 129.52 (Ar CH × 2), 129.46 (Ar CH), 129.37 (Ar CH), 129.2 (Ar CH × 2), 128.74 (Ar CH × 2), 128.70 (Ar CH × 2), 127.43 (Ar CH), 127.40 (Ar CH), 127.2 (Ar CH), 127.06 (Ar CH), 127.04 (Ar CH), 126.9 (Ar CH), 125.1 (Ar CH), 52.7, 52.49, 28.8, 26.5, 24.22, 23.2, 21.56, 19.7, 19.4, 4.0. **1d'**: ^{1}H NMR (CD_2Cl_2): δ 7.58-7.54 (m, 1H), 7.49-7.46 (m, 2H), 7.38-7.14 (m, 20H), 6.74 (d, *J* = 1.0, 1H), 6.64 (d, *J* = 1.0, 1H), 6.10 (s, 1H, C*H*Ph$_2$), 6.08 (br q, *J* = 4.9, 1H, N*H*Me), 5.708 (s, 1H, C*H*Ph$_2$), 3.21 (septet, *J* = 6.9, 1H, ^{i}Pr), 2.91 (d, *J* = 5.0, 3H, NH*Me*), 2.19 (s, 3H, *p*-Me), 1.59 (s, 3H, *Me*C=N), 1.46 (d, *J* = 6.9, 3H, ^{i}Pr), 1.30 (d, *J* = 6.9, 3H, ^{i}Pr), 0.45 (s, 3H, Pd-Me), -0.28 (s, 3H, *Me*C=N). $^{13}C\{^{1}H\}$ NMR (CD_2Cl_2): δ 52.8, 52.48, 28.6, 27.1, 24.20, 23.3, 21.54, 21.4, 18.4, 4.0. The ^{13}C resonances of **1d'** within δ 180-120 overlap with those of **1d** and are not listed. ESI-MS (1:1 MeOH:H_2O, positive ion scan, *m*/*z*): 802.5 ($[M - Cl]^+$). Anal. Calcd. for $C_{49}H_{50}ClN_3OPd \cdot 0.06(C_4H_{10}O)$, %: C, 70.13; H, 6.05; N, 4.98. Found: C, 69.68; H, 5.71; N, 4.91.

(a)

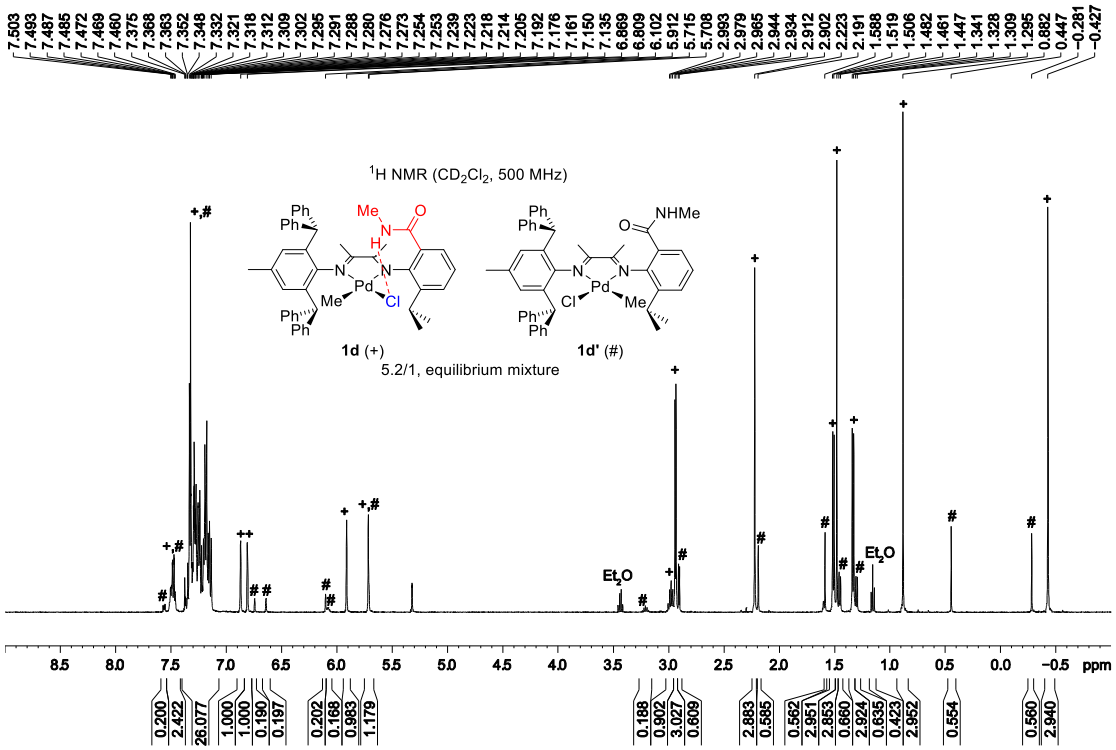

(b)

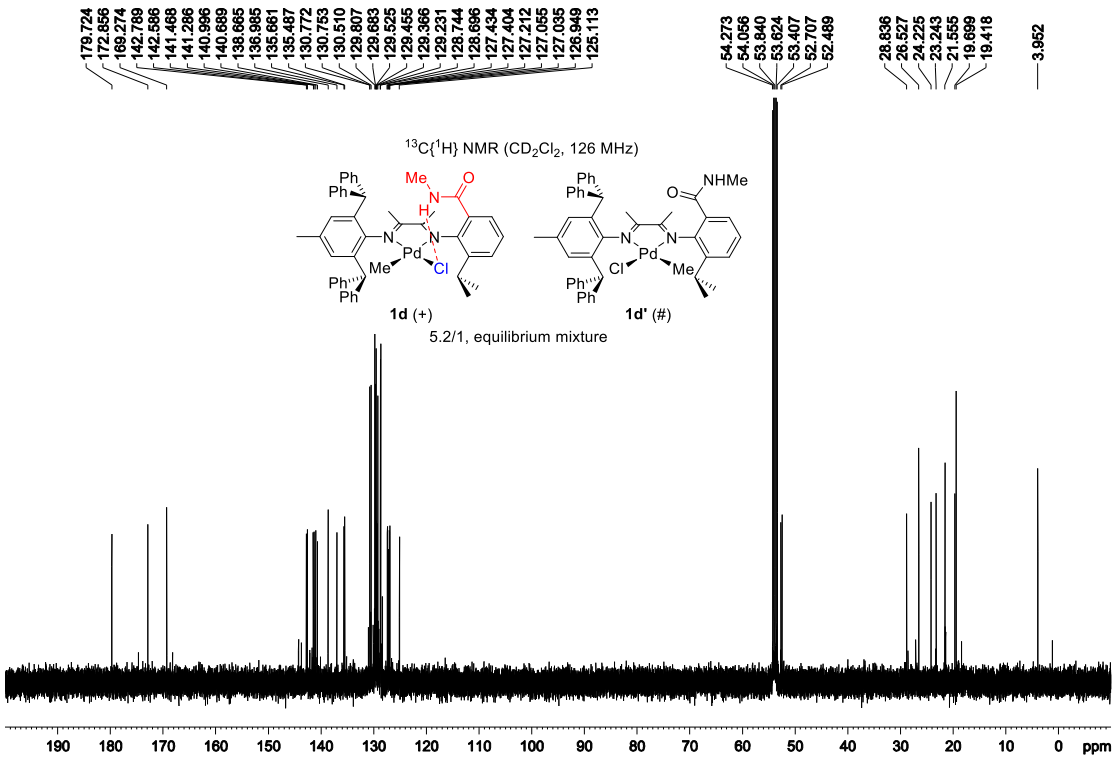

Figure 3.7. NMR spectra of **1d,d'**.

(c)

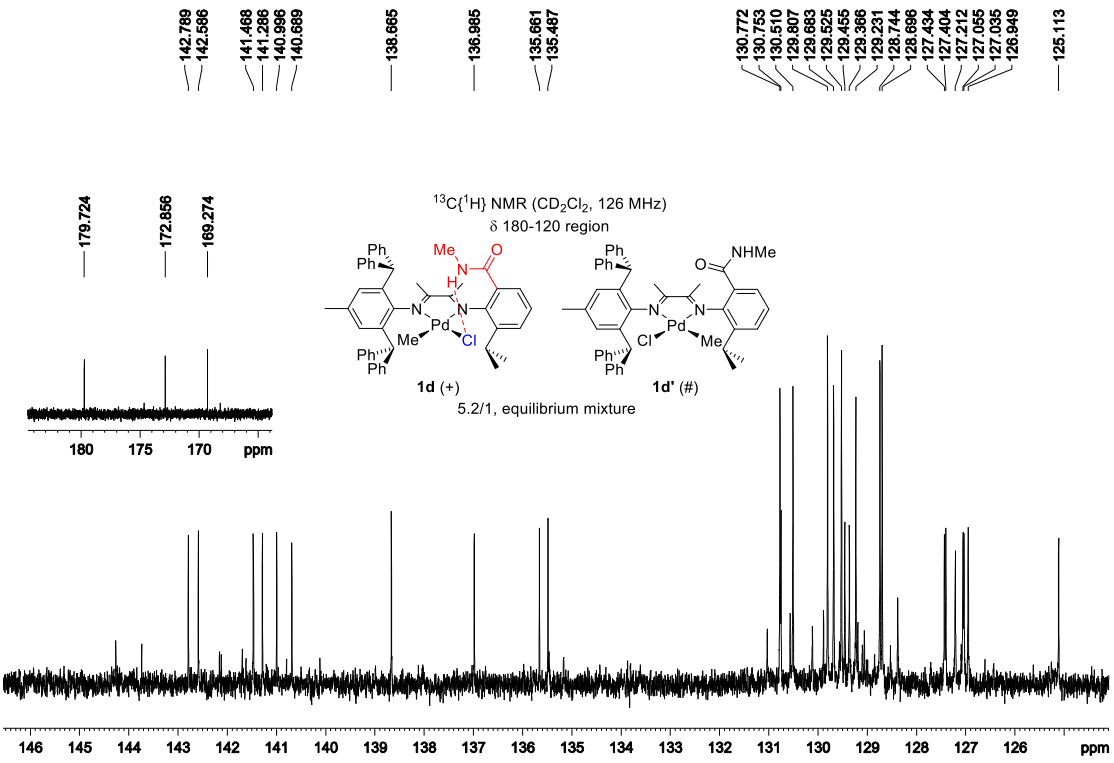

(d)

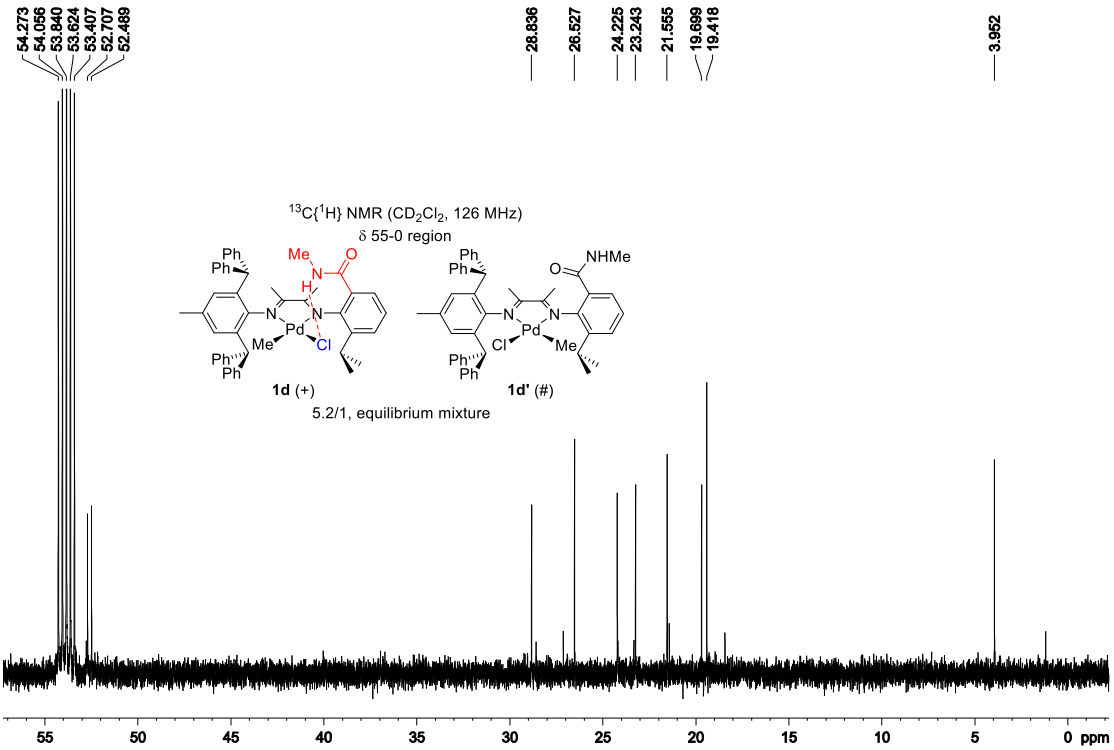

Figure 3.7, continued. NMR spectra of **1d,d'**.

1e,e'. A Schlenk flask was charged with **7** (1.50 g, 2.15 mmol), (cod)PdMeCl (0.518 g, 1.95 mmol) and Et_2O (20 mL). The mixture was stirred at room temperature for 2 d to yield an orange suspension. The orange solid was collected by vacuum filtration, washed with Et_2O, and dried under vacuum. Yield: 1.61 g (97%). The solid is a 1/4.2 mixture of **1e**/**1e'**, as determined by ^{1}H NMR at -20 °C based on the integrals of the Pd-Me resonances, and contains 0.19 equiv Et_2O. This mixture isomerized to a 1.2/1 equilibrium **1e**/**1e'** mixture within a few hours at room temperature in CD_2Cl_2. **1e**: ^{1}H NMR (CD_2Cl_2): δ 7.49 (dd, *J* = 8.0, 1.0, 1H), 7.44-7.13 (m, 22H), 6.92 (d, *J* = 1.0, 1H), 6.82 (d, *J* = 1.0, 1H), 6.01 (s, 1H, C*H*Ph_2), 5.65 (s, 1H, C*H*Ph_2), 3.316 (septet, *J* = 6.9, 1H, ^{i}Pr), 3.17 (s, 3H, N*Me*Me'), 3.07 (s, 3H, NMe*Me'*), 2.24 (s, 3H, *p*-Me), 1.606 (s, 3H, *Me*C=N), 1.55 (d, *J* = 6.9, 3H, ^{i}Pr), 1.30 (d, *J* = 6.9, 3H, ^{i}Pr), 0.80 (s, 3H, Pd-Me), -0.35 (s, 3H, *Me*C=N). ^{13}C{^{1}H} NMR (CD_2Cl_2, -20 °C): δ 179.6, 173.2, 168.5, 52.0, 51.8, 40.2, 34.8, 28.9, 24.2, 23.12, 21.25, 20.8, 18.9, 3.4. The aromatic ^{13}C resonances of **1e** overlap with those of **1e'** and are not listed. **1e'**: ^{1}H NMR (CD_2Cl_2): δ 7.54 (dd, *J* = 8.0, 1.0, 1H), 7.44-7.13 (m, 22H), 6.76 (d, *J* = 1.0, 1H), 6.65 (d, *J* = 1.0, 1H), 6.18 (s, 1H, C*H*Ph_2), 5.64 (s, 1H, C*H*Ph_2), 3.322 (septet, *J* = 6.9, 1H, ^{i}Pr), 3.05 (s, 3H, N*Me*Me'), 3.03 (s, 3H, NMe*Me'*), 2.20 (s, 3H, *p*-Me), 1.614 (s, 3H, *Me*C=N), 1.47 (d, *J* = 6.9, 3H, ^{i}Pr), 1.31 (d, *J* = 6.9, 3H, ^{i}Pr), 0.59 (s, 3H, Pd-Me), -0.29 (s, 3H, *Me*C=N). ^{13}C{^{1}H} NMR (CD_2Cl_2, -20 °C): δ 178.9, 174.7, 167.5, 143.6 (Ar C), 143.2 (Ar C), 141.7 (Ar C), 141.3 (Ar C), 141.0 (Ar C), 140.7 (Ar C), 140.3 (Ar C), 135.1 (Ar C), 134.96 (Ar C), 134.94 (Ar C), 130.6 (Ar CH × 2), 130.1 (Ar CH × 2), 129.6 (Ar CH × 2), 129.4 (Ar CH × 2), 129.0 (Ar CH × 2), 128.8 (Ar CH × 2), 128.38 (Ar CH), 128.33 (Ar CH), 128.1 (Ar CH × 4), 127.5 (Ar C), 127.3 (Ar CH), 126.82 (Ar CH), 126.80 (Ar CH), 126.6 (Ar CH), 126.2 (Ar CH), 126.1 (Ar CH), 125.1 (Ar CH), 52.1, 51.7, 39.5, 34.7, 28.5, 24.3, 23.07, 22.2, 21.23, 17.7, 1.8. ESI-MS (1:1 MeOH:H_2O, positive ion scan, *m*/*z*): 816.5 ([M – Cl]$^+$). Anal. Calcd. for $C_{50}H_{52}ClN_3OPd$·0.19($C_4H_{10}O$), %: C,

70.33; H, 6.27; N, 4.85. Found: C, 70.20; H, 6.07; N, 4.83.

(a)

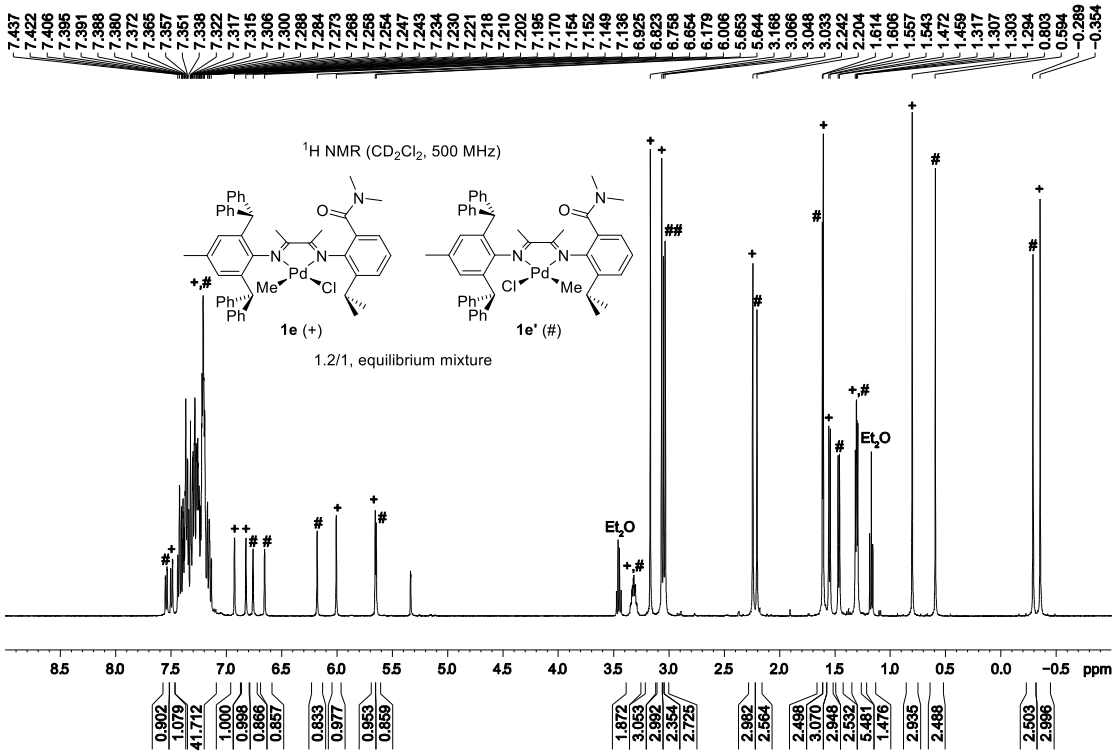

Figure 3.8. NMR spectra of **1e,e'**.

(b)

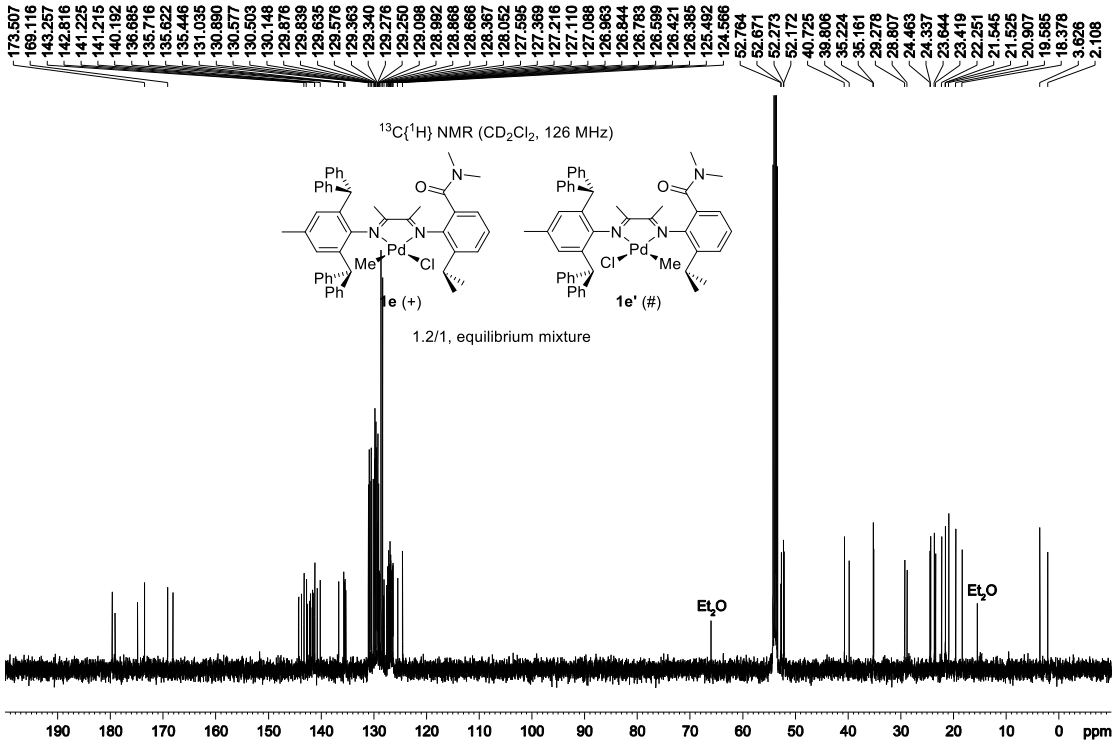

(c)

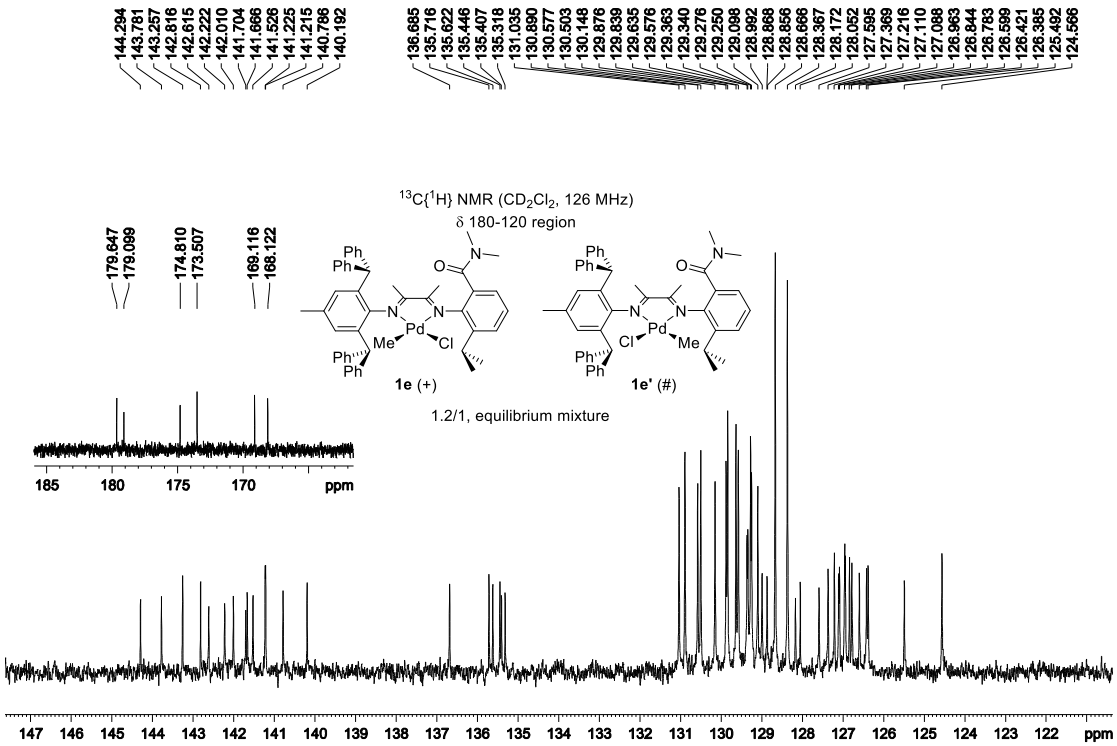

Figure 3.8, continued. NMR spectra of **1e,e'**.

(d)

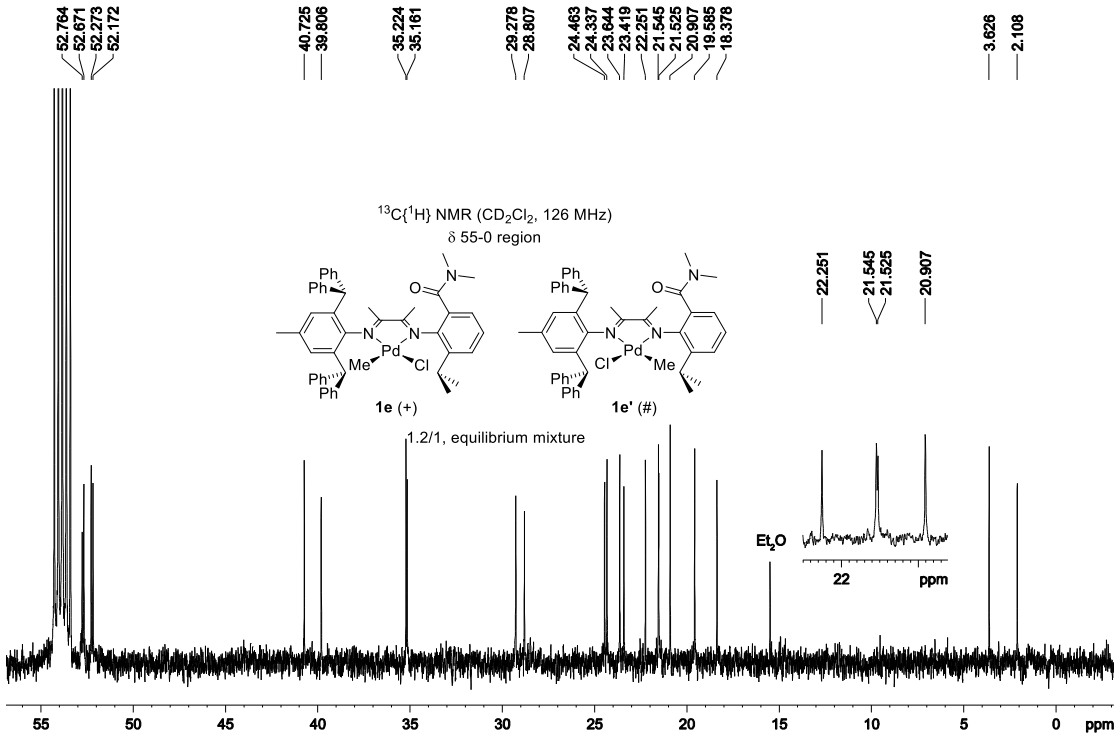

Figure 3.8, continued. NMR spectra of **1e,e'**.

1f,f'.[17] A Schlenk flask was charged with **8** (830 mg, 1.24 mmol), (cod)PdMeCl (300 mg, 1.13 mmol) and Et_2O (20 mL). The mixture was stirred at room temperature for 20 h to yield an orange suspension. The orange solid was collected by vacuum filtration, washed with Et_2O, and dried under vacuum. Yield: 885 mg (95%). The solid is a 1/1.2 mixture of **1f**/**1f'**, as determined by ^{1}H NMR at room temperature based on the integrals of the Pd-Me resonances, and contains 0.05 equiv Et_2O. This mixture isomerized to a 1/3.4 equilibrium **1f**/**1f'** mixture within ca. two months at room temperature in CD_2Cl_2. **1f**: ^{1}H NMR (CD_2Cl_2): δ 7.39-7.15 (m, 23H), 6.86 (s, 2H), 5.91 (s, 2H, C*H*Ph_2), 3.15 (septet, *J* = 6.9, 2H, ^{i}Pr), 2.24 (s, 3H, *p*-Me), 1.52 (d, *J* = 6.9, 6H, ^{i}Pr), 1.41 (s, 3H, *Me*C=N), 1.290 (d, *J* = 6.9, 6H, ^{i}Pr), 0.89 (s, 3H, Pd-Me), -0.33 (s, 3H, *Me*C=N). ^{13}C{^{1}H} NMR (CD_2Cl_2): δ 179.0, 170.8, 142.9 (Ar C × 2), 141.9 (Ar C), 141.6 (Ar C × 2), 141.2 (Ar C), 138.6 (Ar C × 2), 136.8 (Ar C), 135.58 (Ar C × 2), 130.44 (Ar CH × 4), 129.8 (Ar CH × 4), 129.6

(Ar CH × 2), 129.3 (Ar CH × 4), 128.7 (Ar CH × 4), 127.4 (Ar CH × 2), 127.3 (Ar CH), 127.0 (Ar CH × 2), 123.7 (Ar CH × 2), 52.6 (CH × 2), 29.4 (CH × 2), 24.1 (CH_3 × 2), 24.0 (CH_3 × 2), 21.54 (CH_3), 20.0 (CH_3), 19.1 (CH_3), 3.5 (CH_3). **1f'**: ^{1}H NMR (CD_2Cl_2): δ 7.39-7.15 (m, 23H), 6.70 (s, 2H), 5.97 (s, 2H, C*H*Ph_2), 3.20 (septet, *J* = 6.9, 2H, ^{i}Pr), 2.20 (s, 3H, *p*-Me), 1.45 (d, *J* = 6.9, 6H, ^{i}Pr), 1.42 (s, 3H, *Me*C=N), 1.288 (d, *J* = 6.9, 6H, ^{i}Pr), 0.58 (s, 3H, Pd-Me), -0.28 (s, 3H, *Me*C=N). ^{13}C{^{1}H} NMR (CD_2Cl_2): δ 175.8, 174.2, 143.8 (Ar C × 2), 142.1 (Ar C × 2), 141.8 (Ar C), 141.7 (Ar C), 139.0 (Ar C × 2), 135.60 (Ar C), 135.2 (Ar C × 2), 130.46 (Ar CH × 4), 130.1 (Ar CH × 4), 129.1 (Ar CH × 6), 128.4 (Ar CH × 4), 128.2 (Ar CH), 127.2 (Ar CH × 2), 126.6 (Ar CH × 2), 124.4 (Ar CH × 2), 52.7 (CH × 2), 29.0 (CH × 2), 24.5 (CH_3 × 2), 23.6 (CH_3 × 2), 21.51 (CH_3), 20.6 (CH_3), 18.7 (CH_3), 3.0 (CH_3). ESI-MS (1:1 MeOH:H_2O, positive ion scan, *m*/*z*): 787.5 ([M – Cl]$^+$). Anal. Calcd. for $C_{50}H_{53}ClN_2Pd$, %: C, 72.89; H, 6.48; N, 3.40. Found: C, 72.99; H, 6.21; N, 3.27.

(a)

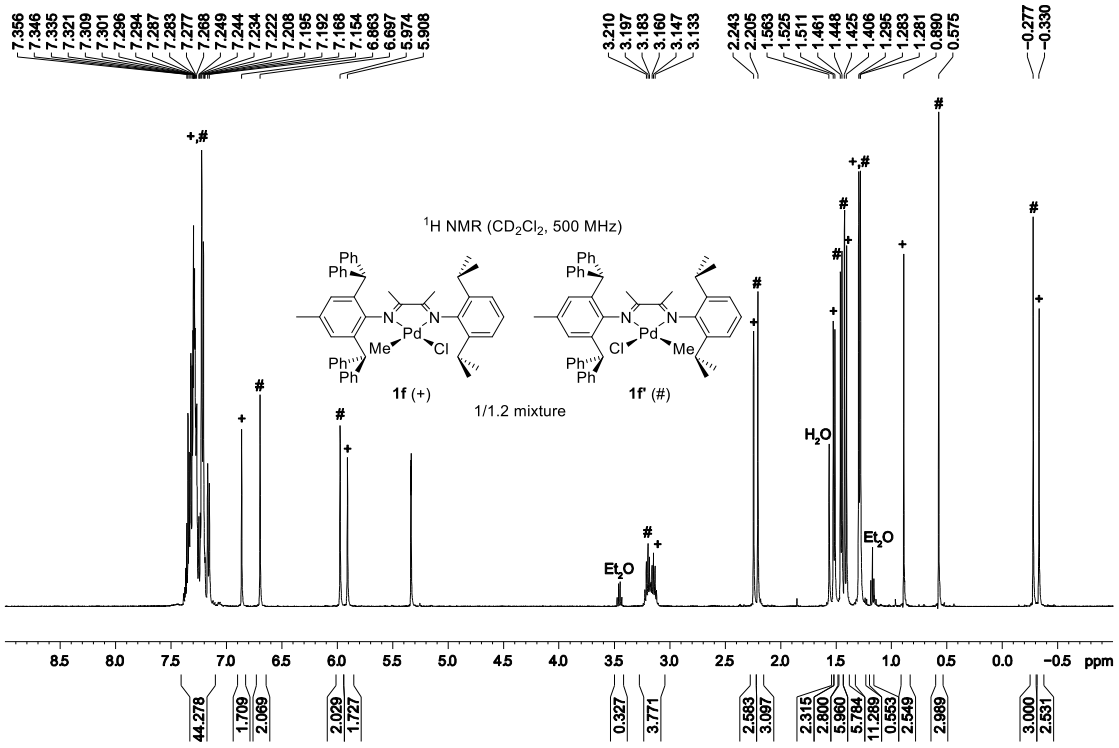

Figure 3.9. NMR spectra of **1f,f'**.

(b)

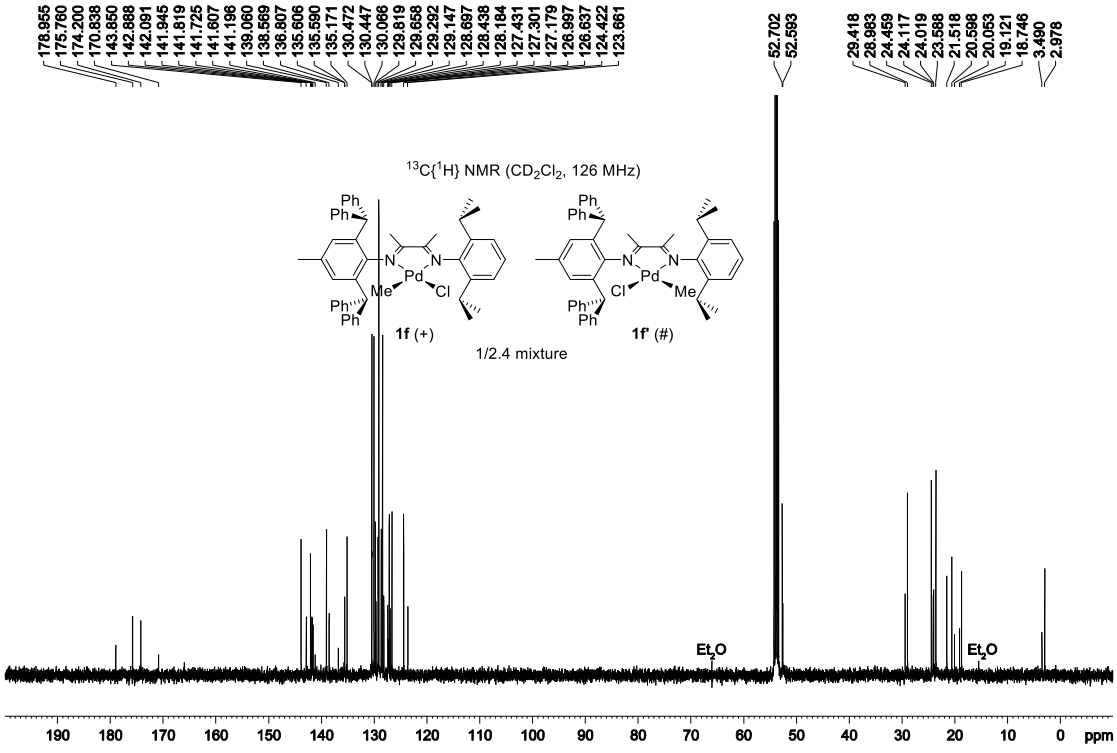

(c)

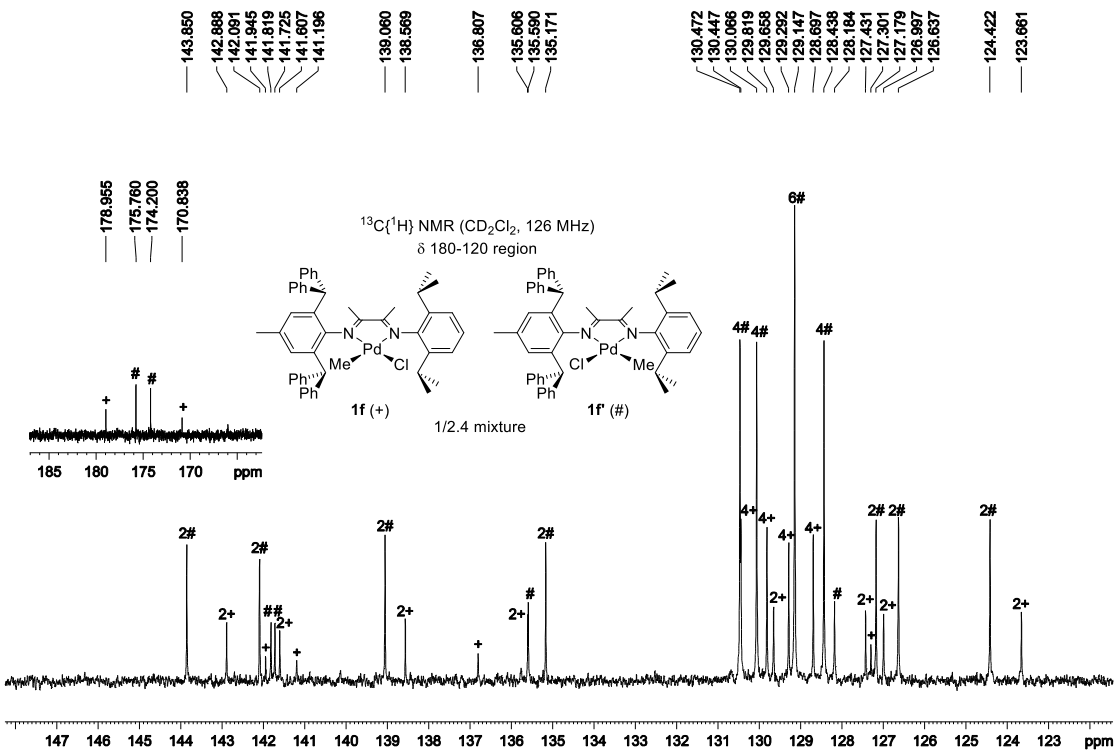

Figure 3.9, continued. NMR spectra of **1f,f'**.

(d)

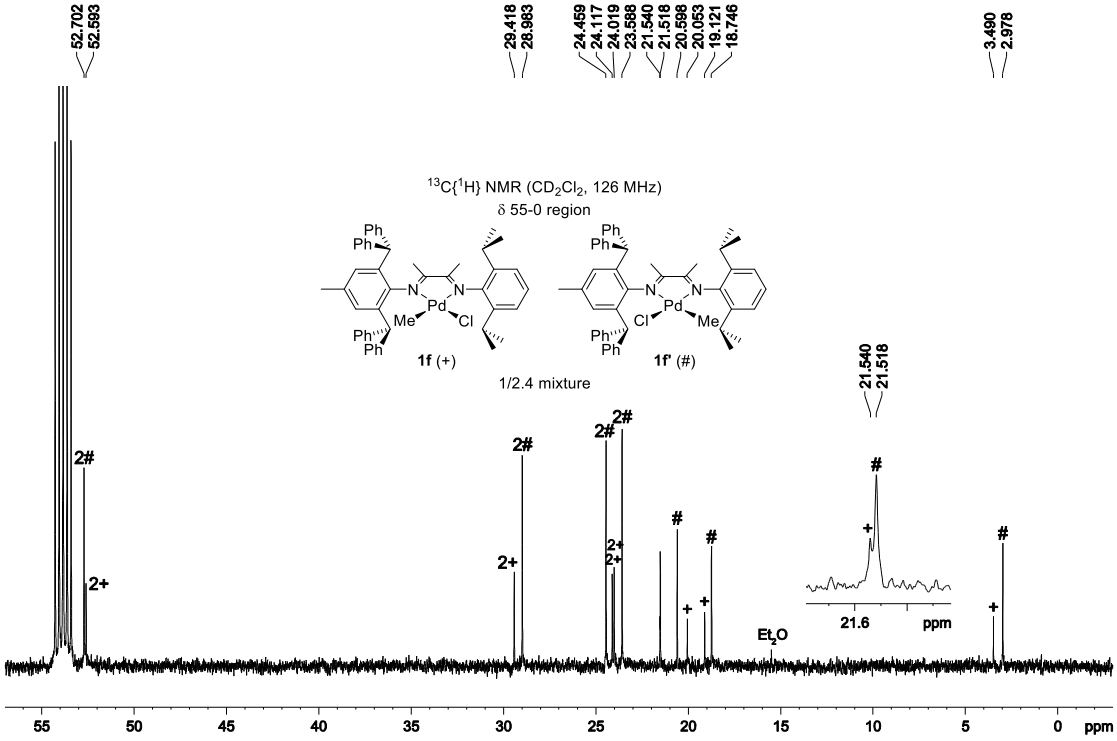

Figure 3.9, continued. NMR spectra of **1f,f'**.

9a-OTf. A mixture of **1a**,**a'** (102 mg, 0.177 mmol) was dissolved in CH_2Cl_2 (3 mL). The mixture was vigorously stirred, and AgOTf (52.0 mg, 0.202 mmol, 1.14 equiv) was added in one portion. The mixture was stirred at room temperature for 17 h to give a dark green solution and an off-white precipitate. The mixture was filtered through Celite. The filtrate was layered with Et_2O and maintained at –30 °C for 3 d to afford **9a-OTf** as dark blue microcrystals (83.5 mg, 68 %). ^{1}H NMR (CD_2Cl_2): δ 8.71 (br q, *J* = 4.6, 2H, amide N*H*), 7.48 (dd, *J* = 7.9, 1.0, 2H, Ar), 7.39 (t, *J* = 7.7, 2H, Ar), 7.33–7.29 (m, 6H, Ar), 7.11 (dd, *J* = 7.6, 1.2, 2H, Ar), 3.44 (septet, *J* = 6.9, 2H, ^{i}Pr methine), 2.70 (septet, *J* = 6.8, 2H, ^{i}Pr methine), 2.38 (septet, *J* = 6.9, 2H, ^{i}Pr methine), 2.14 (s, 6H, *Me*C=N), 2.12 (s, 6H, *Me*C=N), 2.11 (s, 2H, μ-C*H*$_2$), 2.05 (d, *J* = 4.8, 6H, amide N*Me*), 1.40 (d, *J* = 6.8, 6H, ^{i}Pr), 1.34 (d, *J* = 7.0, 6H, ^{i}Pr), 1.32 (d, *J* = 6.9, 6H, ^{i}Pr), 1.23 (d, *J* = 6.9, 6H, ^{i}Pr), 1.10 (d, *J* = 6.9, 6H, ^{i}Pr), 1.09 (d, *J* = 6.9, 6H, ^{i}Pr). ^{13}C{^{1}H} NMR (CD_2Cl_2): δ 180.5, 173.2 (C=O),

171.1, 141.3, 140.3, 139.1, 138.7, 137.9, 129.6, 129.1, 128.2, 126.5 (2C), 124.6, 124.50 (Ar), 120.9 (q, $^{1}J_{CF}$ = 320, *C*$F_3SO_3^-$), 67.3 (μ-*C*H_2), 29.7, 28.9, 28.5 (^{i}Pr methine), 27.0 (amide NMe), 25.5, 24.1, 23.6, 22.7, 22.6, 21.90 (^{i}Pr), 21.88 (*Me*C=N), 20.2 (*Me*C=N). ^{19}F NMR (CD_2Cl_2): δ –78.9. Anal. Calcd. for $C_{57}H_{76}F_6N_6O_8Pd_2S_2$: C, 50.18; H, 5.62; N, 6.16. Found C, 49.92; H, 5.70; N, 6.01. ESI-MS (MeOH:H_2O = 1:1 by volume, positive ion scan, *m*/*z*): 533.2 ([M – 2 OTf]$^{2+}$), 1065.6 ([M – 2 OTf – H]$^{+}$).

(a)

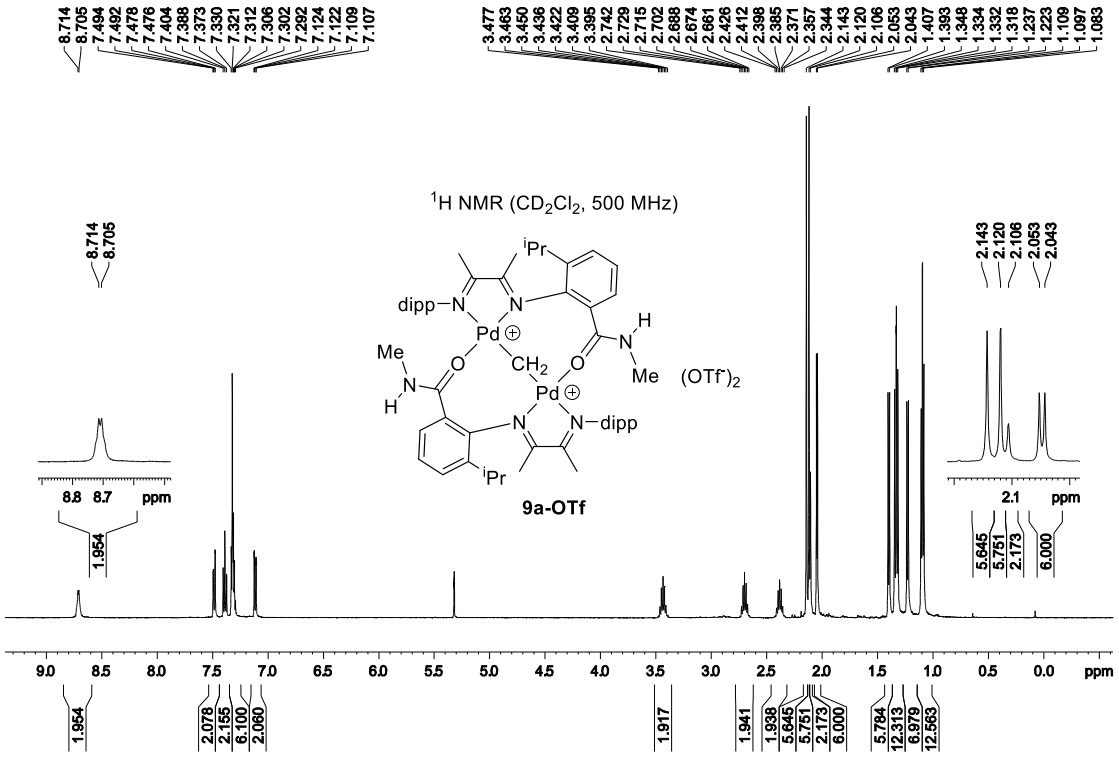

Figure 3.10. NMR spectra of **9a-OTf**.

(b)

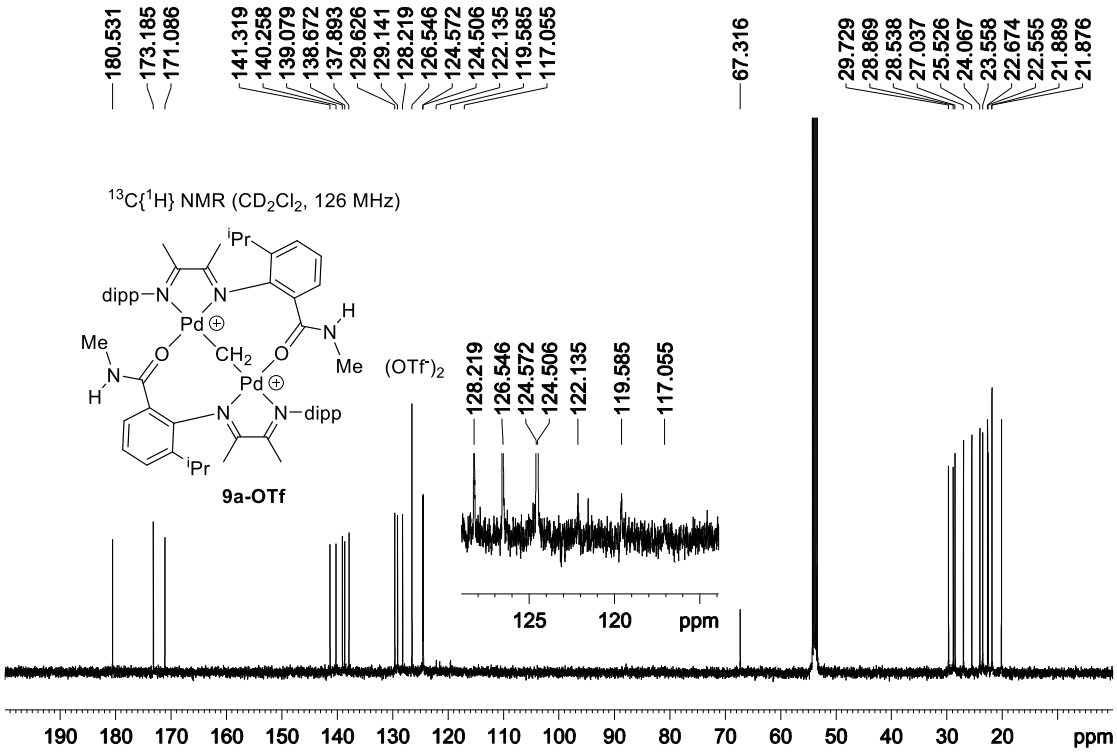

(c) $^{13}C\{gated\text{-}^{1}H\}$ NMR (expansion of δ 72-62 region)

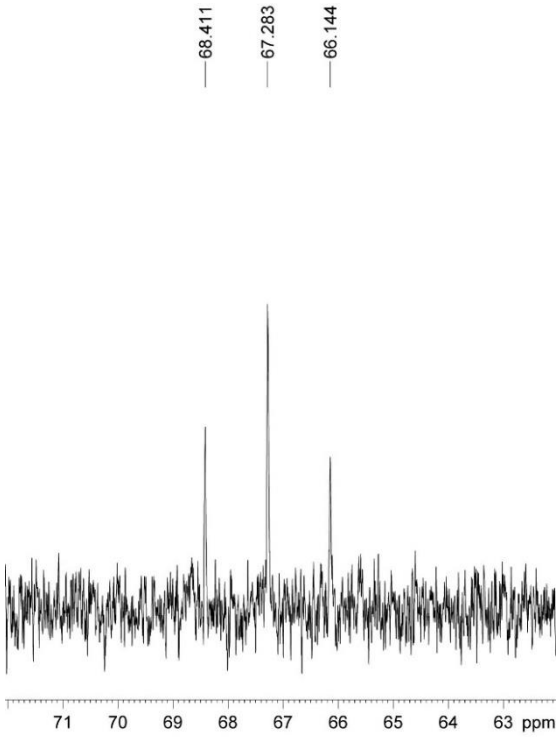

Figure 3.10, continued. NMR spectra of **9a-OTf**.

(d)

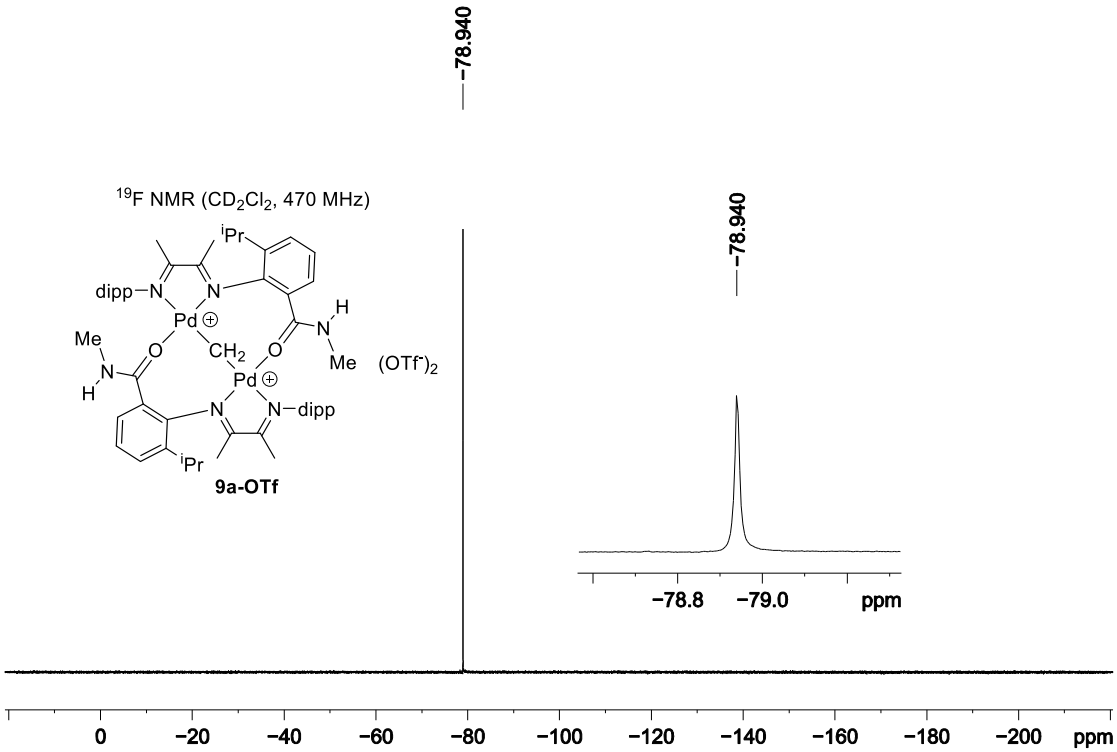

9a-OTf

(e) HMQC (CD_2Cl_2, expansion of δ 3.8-0.7/75-15 region)

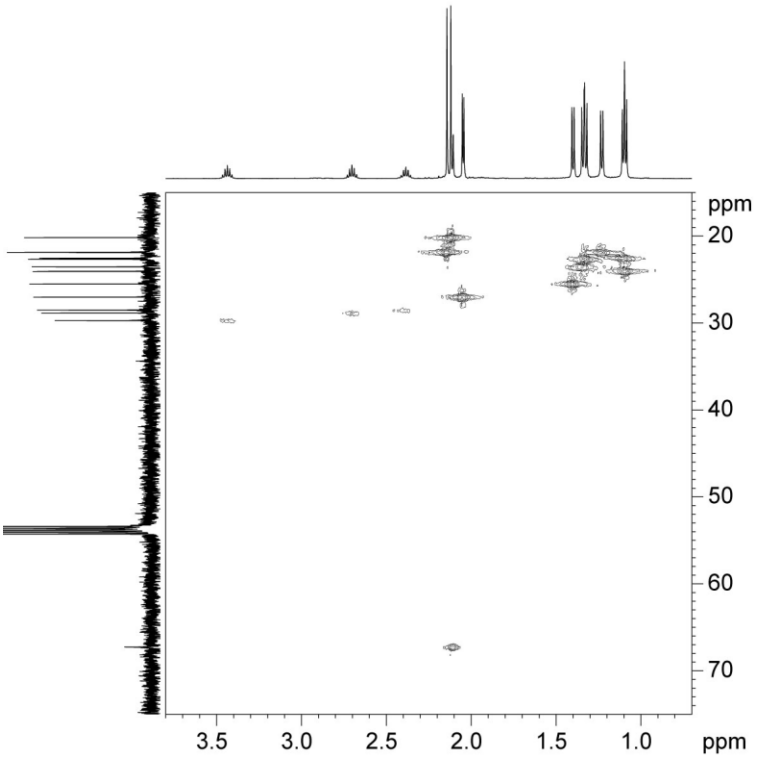

Figure 3.10, continued. NMR spectra of **9a-OTf**.

9b-OTf. A mixture of **1b**,**b'** (102 mg, 0.173 mmol) was dissolved in CH_2Cl_2 (3 mL). The mixture was vigorously stirred, and AgOTf (51.0 mg, 0.198 mmol, 1.14 equiv) was added in one portion. The mixture was stirred at room temperature for 17 h to give a black solution and off-white precipitate. The mixture was filtered through Celite, and the filtrate was taken to dryness under vacuum. The black residue was recrystallized twice by layering Et_2O onto a CH_2Cl_2 solution at –30 °C to afford **9b-OTf** as black needles (82.5 mg, 69 %). This material contains 0.65 equiv hexane, as determined by ^{1}H NMR. ^{1}H NMR (CD_2Cl_2): δ 7.48 (dd, *J* = 8.0, 1.2, 2H, Ar), 7.38 (t, *J* = 7.7, 2H, Ar), 7.32 (dd, *J* = 7.5, 1.9, 2H, Ar), 7.29 (t, *J* = 7.4, 2H, Ar), 7.26 (dd, *J* = 7.4, 1.9, 2H, Ar), 6.88 (dd, *J* = 7.6, 1.3, 2H, Ar), 3.56 (septet, *J* = 6.8, 2H, ^{i}Pr methine), 2.81 (s, 6H, amide NMe *trans* to O), 2.80 (septet, *J* = 6.8, 2H, ^{i}Pr methine), 2.36 (septet, *J* = 6.8, 2H, ^{i}Pr methine), 2.27 (s, 6H, *Me*C=N), 2.23 (s, 6H, amide NMe *cis* to O), 2.21 (s, 6H, *Me*C=N), 1.75 (s, 2H, μ-*C*H_2), 1.41 (d, *J* = 6.9, 6H, ^{i}Pr), 1.33 (d, *J* = 6.8, 6H, ^{i}Pr), 1.31 (d, *J* = 6.8, 6H, ^{i}Pr), 1.26 (d, *J* = 6.9, 6H, ^{i}Pr), 1.08 (d, *J* = 6.9, 6H, ^{i}Pr), 1.06 (d, *J* = 6.9, 6H, ^{i}Pr). ^{13}C{^{1}H} NMR (CD_2Cl_2): δ 180.7, 171.6 (C=O), 171.1, 141.6, 140.6, 139.8, 139.0, 138.7, 129.3, 129.1, 127.8, 125.4, 125.1, 124.6, 124.0 (Ar), 121.0 (q, $^1J_{CF}$ = 321, *C*$F_3SO_3^-$), 66.6 (μ-*C*H_2), 40.2, 35.6 (amide NMe), 29.7, 28.6, 28.4 (^{i}Pr methine), 25.6, 24.2, 23.5, 22.24 (2C) (^{i}Pr), 22.20 (*Me*C=N), 21.7 (^{i}Pr), 20.1 (*Me*C=N). ^{13}C{^{1}H–gated} NMR (CD_2Cl_2): δ 66.6 (t, $^1J_{CH}$ = 142, μ-*C*H_2). ^{19}F NMR (CD_2Cl_2): δ –78.6. Anal. Calcd. for $C_{59}H_{80}F_6N_6O_8Pd_2S_2 \cdot 0.65C_6H_{14}$: C, 52.16; H, 6.20; N, 5.80. Found C, 51.94; H, 6.32; N, 5.66. ESI-MS (MeOH:H_2O = 1:1 by volume, positive ion scan, *m*/*z*): 547.4 ([M – 2 OTf]$^{2+}$), 1131.6 ([M – 2 OTf – 2 H + K]$^+$).

(a)

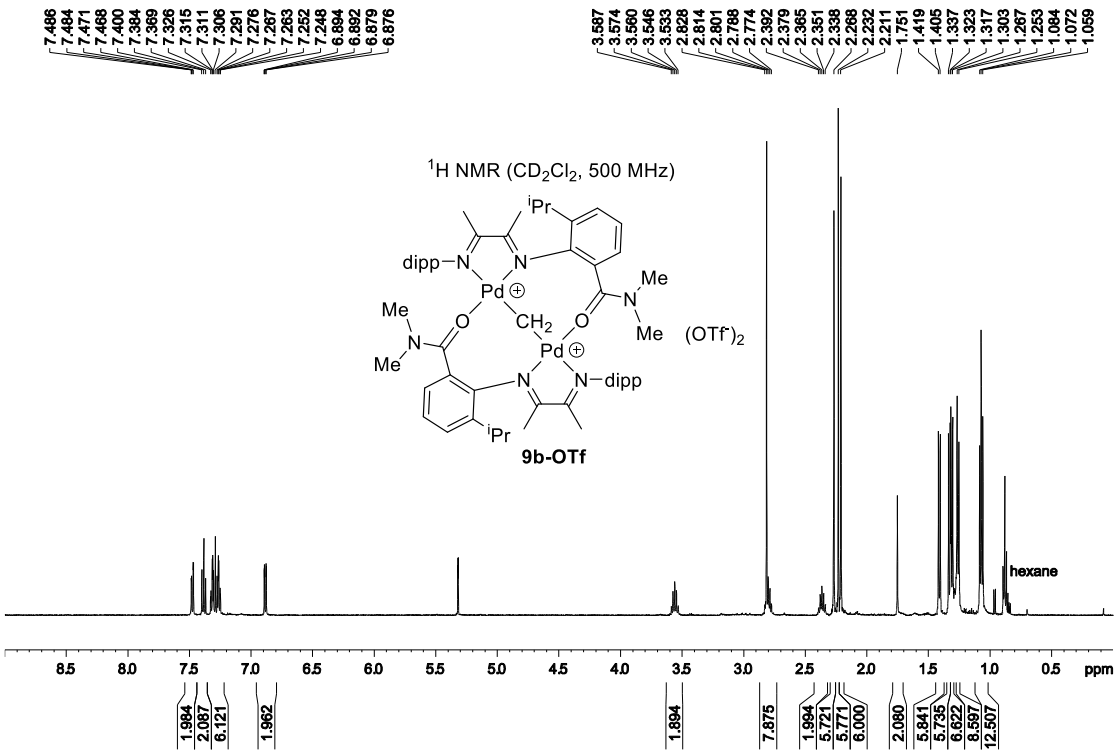

(b)

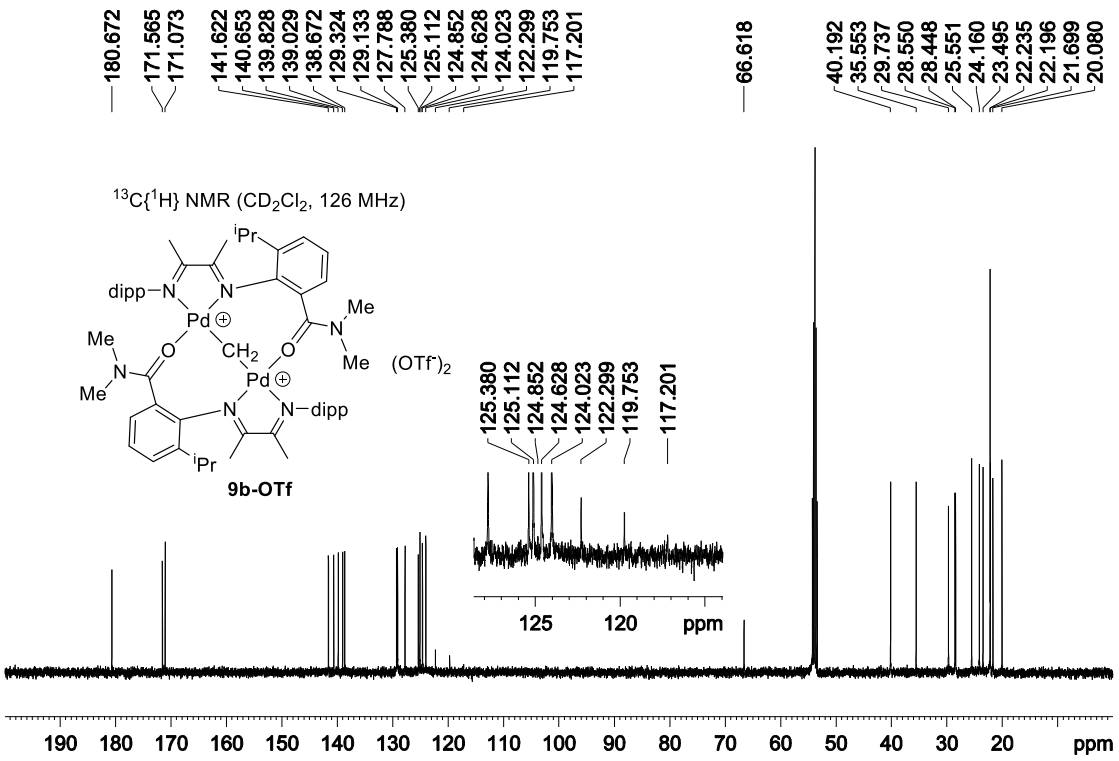

Figure 3.11. NMR spectra of **9b-OTf**.

(c) DEPT-135 NMR (CH_3 and CH positive; CH_2 negative)

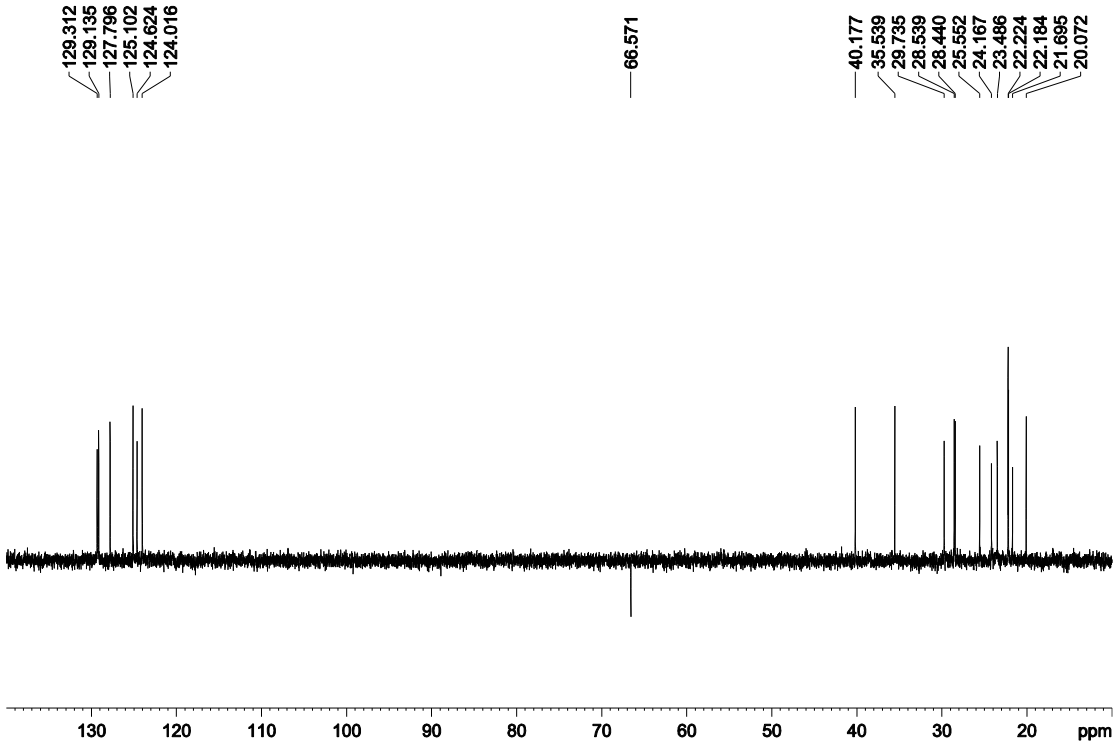

(d) $^{13}C\{gated\text{-}^{1}H\}$ NMR (expansion of δ 71-62 region)

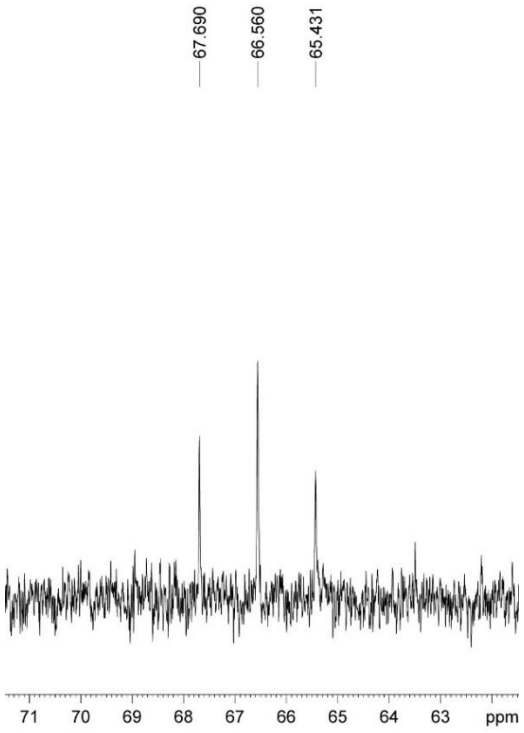

Figure 3.11, continued. NMR spectra of **9b-OTf**.

(e)

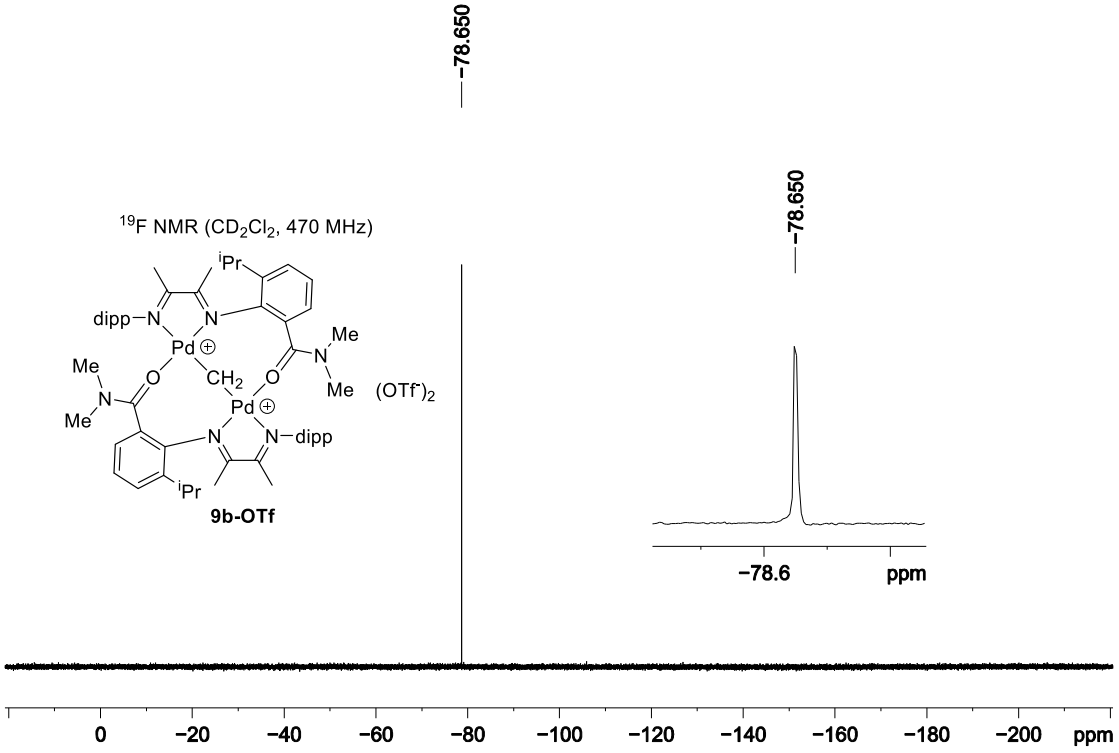

(f) HMQC (CD_2Cl_2, expansion of δ 1.90-1.60/70-60 region)

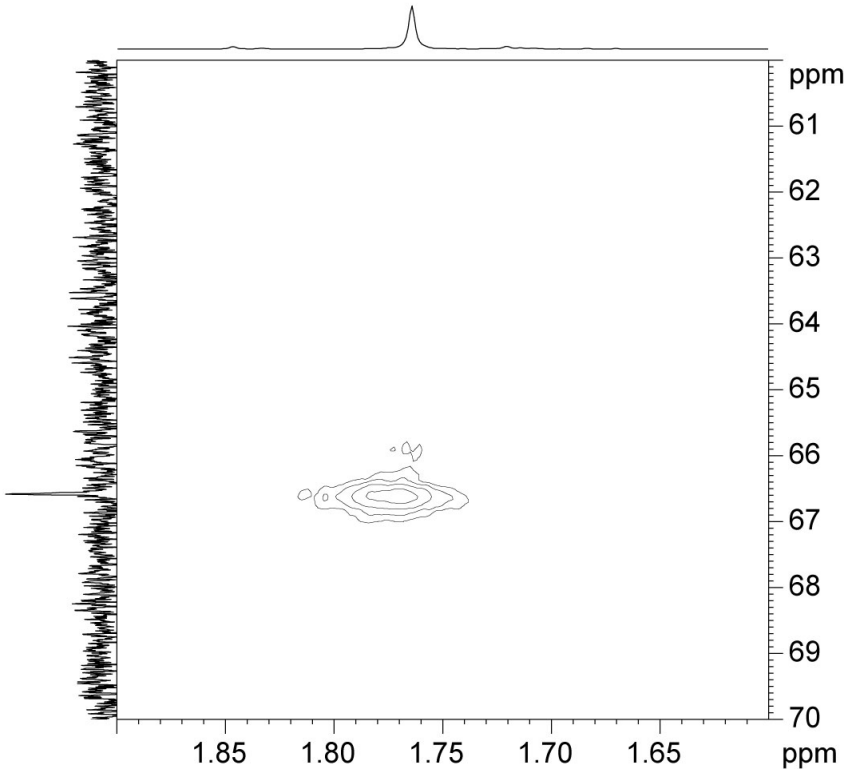

Figure 3.11, continued. NMR spectra of **9b-OTf**.

Ethylene Polymerization. In a glovebox, Na[B{3,5-$(CF_3)_2C_6H_3$}$_4$] (17.6 mg, 20 μmol) and CH_2Cl_2 (35 mL) were placed in a stainless steel autoclave. The catalyst (10 μmol) was dissolved in CH_2Cl_2 (5 mL), and the solution was transferred to a stainless steel injection tube with valves on both ends of the tube. One end of the tube was connected to the autoclave, and the other to a high-pressure nitrogen line. For 200 psi experiments: The autoclave was maintained at 25 °C and pressurized with ethylene to 150 psi. The ethylene line was closed, and the contents of the injection tube were injected into the autoclave, increasing the autoclave pressure to 200 psi. The injector was sealed from the autoclave, and ethylene was added to increase the autoclave pressure to 250 psi. For 350 psi experiments: The autoclave was maintained at 25 °C and pressurized with ethylene to 250 psi. The ethylene line was closed, and the contents of the injection tube were injected into the autoclave, increasing the autoclave pressure to 300 psi. The injector was sealed from the autoclave, and ethylene was added to increase the autoclave pressure to 400 psi. After the specified reaction time, the autoclave was vented. The volatiles were removed on a rotovap to yield the polymer, which was dried overnight in a vacuum oven.

Ethylene Copolymerizations with Methyl Acrylate or Acrylic Acid. In a glovebox, a Fischer-Porter bottle was charged with $NaBAr^F{}_4$ (17.6 mg, 20 μmol), galvinoxyl (2.1 mg, 5 μmol), comonomer (25 mmol, 1.0 M; 1.7 mL for acrylic acid or 2.3 mL for methyl acrylate) and the specified solvent (total volume 25 mL). The catalyst (10 μmol) was added, and the bottle was sealed. The bottle was removed from the glovebox and attached to a stainless steel double manifold (vacuum/ethylene) line. The bottle was charged with ethylene to 14 psi, and the mixture was stirred in water bath at room temperature. After 20 h, the bottle was vented. The volatiles were removed on a rotovap. Acetone (10 mL) was added to precipitate the oily polymer and remove the acetone-soluble impurities. After all droplets of polymer precipitated, the acetone phase was decanted off.

The residue was rinsed again with acetone (10 mL). The polymer was dissolved in a minimal volume of hexane, transferred into a tared scintillation vial, taken to dryness under vacuum, and dried overnight in a vacuum oven.

X-ray Crystallography. Data were measured on a Bruker D8 VENTURE with a PHOTON 100 CMOS detector system equipped with a Mo-target X-ray tube (λ = 0.71073 Å). All atoms were refined with anisotropic thermal parameters. Hydrogen atoms were included in idealized positions for structure factor calculations. All structures are drawn with thermal ellipsoids at 50% probability. Specific details of each compound follow: **5·2(CHCl$_2$CHCl$_2$)**: Crystals were grown by diffusion of hexane into a $CHCl_2CHCl_2$ solution of **5** at room temperature. Crystallographic data and details of the data collection and structure refinement are listed in Table 3.5. Enhanced rigid body restraints and geometric restraints were utilized for disorder modeling of 2 independent $CHCl_2CHCl_2$ solvent molecules. **9a-OTf·4(CH$_2$Cl$_2$)**: Crystals were grown by layering hexane onto a CH_2Cl_2 solution of **9a-OTf** and storing at -40 °C under N_2. Crystallographic data and details of the data collection and structure refinement are listed in Table 3.6. The *N*-methyl amide group was found to be disordered and refined over two positions with a ratio of ca. 70:30. The thermal parameters were constrained to be the same for the two positions. Enhanced rigid body restraints were also utilized for some atoms. **9b-OTf·2(CH$_2$Cl$_2$)**: Crystals were grown by layering hexane onto a CH_2Cl_2 solution of **9b-OTf** and storing at -40 °C under N_2. Crystallographic data and details of the data collection and structure refinement are listed in Table 3.7. Both $CF_3SO_3^-$ counter anions and one of the CH_2Cl_2 solvent molecules were found to be disordered. All disorders were independently modelled over two positions using restraints/constraints. The crystal contained many disordered solvent molecules located in large solvent accessible voids. The diffuse contribution to scattering was treated by application of the program SQUEEZE[35-36] as

implemented in Platon[37] using the "fab" file construct. SQUEEZE algorithm located voids, centered at (0, 0, 0.5) and (0.5, 0.5, 1) with a volume of 501 $Å^3$ and an electron counts of 164 each.

Table 3.5. X-ray Crystallographic Parameters of 5·2($CHCl_2CHCl_2$).

Empirical formula	$C_{52}H_{51}Cl_{10}N_3OPd$
Formula weight	1194.86
Temperature/K	100(2)
Crystal system	monoclinic
Space group	$P2_1/c$
a/Å	21.5758(18)
b/Å	14.2713(12)
c/Å	18.9212(15)
α/°	90
β/°	115.547(2)
γ/°	90
Volume/$Å^3$	5256.5(8)
Z	4
ρ_{calc}/g cm^{-3}	1.510
μ/mm^{-1}	0.903
F(000)	2432.0
Crystal size/mm^3	0.2 × 0.12 × 0.08
Radiation	MoKα (λ = 0.71073)
2Θ range for data collection/°	4.746 to 52.904
Index ranges	$-26 \leq h \leq 27$, $-17 \leq k \leq 17$, $-23 \leq l \leq 23$
Reflections collected	106577
Independent reflections	10817 [R_{int} = 0.0584, R_{sigma} = 0.0401]
Data/restraints/parameters	10817/173/702
Goodness-of-fit on F^2	1.070
Final R indexes [I>=2σ (I)]	R_1 = 0.0953, wR_2 = 0.2030
Final R indexes [all data]	R_1 = 0.1150, wR_2 = 0.2123
Largest diff. peak/hole / e $Å^{-3}$	1.92/-1.13

Table 3.6. X-ray Crystallographic Parameters of 9a-OTf·4(CH_2Cl_2).

Empirical formula	$C_{61}H_{84}Cl_8F_6N_6O_8Pd_2S_2$
Formula weight	1703.86
Temperature/K	100(2)
Crystal system	monoclinic
Space group	C2/c
a/Å	22.325(3)
b/Å	14.681(3)
c/Å	24.274(4)
α/°	90
β/°	107.794(5)
γ/°	90
Volume/Å^3	7575(2)
Z	4
ρ_{calc}/g cm^{-3}	1.494
μ/mm^{-1}	0.879
F(000)	3480.0
Crystal size/mm^3	0.20 × 0.14 × 0.02
Radiation	MoKα (λ = 0.71073)
2Θ range for data collection/°	4.434 to 49.99
Index ranges	$-26 \leq h \leq 26$, $-17 \leq k \leq 17$, $-28 \leq l \leq 28$
Reflections collected	67681
Independent reflections	6646 [R_{int} = 0.0775, R_{sigma} = 0.0441]
Data/restraints/parameters	6646/90/443
Goodness-of-fit on F^2	1.070
Final R indexes [I>=2σ (I)]	R_1 = 0.0677, wR_2 = 0.1680
Final R indexes [all data]	R_1 = 0.0998, wR_2 = 0.1870
Largest diff. peak/hole / e Å^{-3}	1.46/-1.16

Table 3.7. X-ray Crystallographic Parameters of 9b-OTf·2(CH_2Cl_2).

Empirical formula	$C_{61}H_{84}Cl_4F_6N_6O_8Pd_2S_2$
Formula weight	1562.06
Temperature/K	100(2)
Crystal system	monoclinic
Space group	$P2_1/n$
a/Å	15.5396(8)
b/Å	20.2487(10)
c/Å	25.5041(13)
α/°	90
β/°	101.408(2)
γ/°	90
Volume/Å^3	7866.5(7)
Z	4
ρ_{calc}/g cm^{-3}	1.319
μ/mm^{-1}	0.709
F(000)	3208.0
Crystal size/mm^3	0.26 × 0.16 × 0.14
Radiation	MoKα (λ = 0.71073)
2Θ range for data collection/°	4.34 to 52.87
Index ranges	$-17 \leq h \leq 19$, $-25 \leq k \leq 25$, $-31 \leq l \leq 27$
Reflections collected	84906
Independent reflections	15907 [R_{int} = 0.0742, R_{sigma} = 0.0755]
Data/restraints/parameters	15907/48/870
Goodness-of-fit on F^2	1.026
Final R indexes [I>=2σ (I)]	R_1 = 0.0512, wR_2 = 0.1011
Final R indexes [all data]	R_1 = 0.1056, wR_2 = 0.1175
Largest diff. peak/hole / e Å^{-3}	0.98/-0.85

3.5 References

(1) Ito, S.; Nozaki, K. *Chem. Rec.* **2010**, *10*, 315.

(2) Nakamura, A.; Ito, S.; Nozaki, K. *Chem. Rev.* **2009**, *109*, 5215.

(3) Franssen, N. M. G.; Reek, J. N. H.; de Bruin, B. *Chem. Soc. Rev.* **2013**, *42*, 5809.

(4) Johnson, L. K.; Mecking, S.; Brookhart, M. S. *J. Am. Chem. Soc.* **1996**, *118*, 267.

(5) Li, W.; Zhang, X.; Meetsma, A.; Hessen, B. *J. Am. Chem. Soc.* **2004**, *126*, 12246.

(6) Li, W.; Zhang, X.; Meetsma, A.; Hessen, B. *Organometallics* **2008**, *27*, 2052.

(7) Luo, S.; Jordan, R. F. *J. Am. Chem. Soc.* **2006**, *128*, 12072.

(8) Chen, Z.; Liu, W.; Daugulis, O.; Brookhart, M. *J. Am. Chem. Soc.* **2016**, *138*, 16120.

(9) Chen, G.; Ma, X. S.; Guan, Z. *J. Am. Chem. Soc.* **2003**, *125*, 6697.

(10) Mecking, S.; Johnson, L. K.; Wang, L.; Brookhart, M. S. *J. Am. Chem. Soc.* **1998**, *120*, 888.

(11) Williams, B. S.; Leatherman, M. D.; White, P. S.; Brookhart, M. S. *J. Am. Chem. Soc.* **2005**, *127*, 5132.

(12) Davis, H.; Phipps, R. J. *Chem. Sci.* **2017**, doi: 10.1039/C6SC04157D.

(13) Raynal, M.; Ballester, P.; Vidal-Ferran, A.; van Leeuwen, P. W. N. M. *Chem. Soc. Rev.* **2014**, *43*, 1660.

(14) Dydio, P.; Reek, J. N. H. *Chem. Sci.* **2014**, *5*, 2135.

(15) Crabtree, R. H. *New J. Chem.* **2011**, *35*, 18.

(16) Dai, S.; Sui, X.; Chen, C. *Angew. Chem., Int. Ed.* **2015**, *54*, 9948.

(17) Dai, S.; Zhou, S.; Zhang, W.; Chen, C. *Macromolecules* **2016**, *49*, 8855.

(18) Zhai, F.; Jordan, R. F. *Organometallics* **2014**, *33*, 7176.

(19) Tempel, D. J.; Johnson, L. K.; Huff, R. L.; White, P. S.; Brookhart, M. S. *J. Am. Chem. Soc.* **2000**, *122*, 6686.

(20) Allen, K. E.; Campos, J.; Daugulis, O.; Brookhart, M. *ACS Catal.* **2015**, *5*, 456.

(21) Rünzi, T.; Fröhlich, D.; Mecking, S. *J. Am. Chem. Soc.* **2010**, *132*, 17690.

(22) Contrella, N. D.; Sampson, J. R.; Jordan, R. F. *Organometallics* **2014**, *33*, 3546.

(23) Balch, A. L.; Hunt, C. T.; Lee, C.-l.; Olmstead, M. M.; Farr, J. P. *J. Am. Chem. Soc.* **1981**, *103*, 3764.

(24) Klopfenstein, S. R.; Kluwe, C.; Kirschbaum, K.; Davies, J. A. *Can. J. Chem.* **1996**, *74*, 2331.

(25) Brownie, J. H.; Baird, M. C.; Zakharov, L. N.; Rheingold, A. L. *Organometallics* **2003**, *22*, 33.

(26) Sachse, A.; John, M.; Meyer, F. *Angew. Chem., Int. Ed.* **2010**, *49*, 1986.

(27) Schnetz, T.; Rominger, F.; Hofmann, P. *Acta Cryst.* **2010**, *E66*, m453.

(28) Puddephatt, R. J. *Polyhedron* **1988**, *7*, 767.

(29) Luo, B.-T.; Liu, H.; Lin, Z.-J.; Jiang, J.; Shen, D.-S.; Liu, R.-Z.; Ke, Z.; Liu, F.-S. *Organometallics* **2015**, *34*, 4881.

(30) Johnson, L. K.; Killian, C. M.; Brookhart, M. S. *J. Am. Chem. Soc.* **1995**, *117*, 6414.

(31) Rulke, R. E.; Ernsting, J. M.; Spek, A. L.; Elsevier, C. J.; van Leeuwen, P. W. N. M.; Vrieze, K. *Inorg. Chem.* **1993**, *32*, 5769.

(32) Grinshpun, V.; Rudin, A. *Makromol. Chem., Rapid Commun.* **1985**, *6*, 219.

(33) Mao, J.; Zhu, B.; Zhang, W.; Yi, J.; Zhang, M.; Li, H.; Li, R.; Jia, D.; Wang, Y.; Tan, K.; Sun, T.; Sun, W. CN Patent 104250270.

(34) Abakumov, G. A.; Cherkasov, V. K.; Druzhkov, N. O.; Kocherova, T. N.; Shavyrin, A. S. *Russ. Chem. Bull.* **2011**, *60*, 112.

(35) van der Sluis, P.; Spek, A. L. *Acta Cryst.* **1990**, *A46*, 194.

(36) Spek, A. L. *Acta Cryst.* **2015**, *C71*, 9.

(37) Spek, A. L. *Acta Cryst.* **2009**, *D65*, 148.

CHAPTER FOUR

Amide-Functionalized α-Diimine Ni Complexes

4.1 Introduction

α-Diimine nickel(II) complexes are active catalysts for ethylene polymerization and can be adapted to produce polyethylenes with a wide range of physical properties by tailoring the α-diimine ligand structure and varying the reaction conditions.[1-5] Compared to α-diimine Pd catalysts, which can incorporate a variety of polar monomers (PMs) into polyethylene, α-diimine Ni catalysts are typically more active in ethylene homopolymerization but are unable to copolymerize ethylene with polar monomers, due to the hard character and electrophilic nature of the Ni^{II} center in the active (α-diimine)NiR^+ species. Protection of the PMs with capping reagents, such as AlR_3 (R = Me, ^{i}Bu, etc.) and $B(C_6F_5)_3$, is required for copolymerization with ethylene by α-diimine Ni catalysts.[6-10] α-Diimine Ni catalysts that are capable of incorporating unprotected PMs would be of great interest.

Chapter Two describes the synthesis, structures and coordination chemistry of a series of amide-functionalized α-diimine Pd(II) complexes, which exhibit hydrogen bonding interactions involving the amide groups.[11] The (α-diimine)PdMeCl complexes are activated by $Na[BAr^F_4]$ (Ar^F = 3,5-$(CF_3)_2C_6H_3$) to form active catalysts for ethylene homopolymerization and the copolymerization of ethylene with acrylic acid and methyl acrylate.[12] We are interested in how amide functionalities can influence the properties of analogous (α-diimine)NiX_2 complexes. This chapter describes the synthesis of amide-functionalized (α-diimine)Ni complexes **1-3** and initial studies of the ethylene polymerization behavior of **1**.

4.2 Results and Discussion

Synthesis of Five-Coordinate (α-Diimine)NiBr$_2$ Complexes. The reaction of **L1** with (dme)NiBr$_2$ (dme = 1,2-dimethoxyethane) yields the five-coordinate complex (**L1**)NiBr$_2$ (**1**, Scheme 4.1). In the solid-state structure of **1**, the **L1** ligand coordinates to Ni in a κ^3-*O,N,N* fashion through the carbonyl oxygen atom and the two imine nitrogen donor atoms (Figure 4.1a). Similarly, **L2** reacts with (dme)NiBr$_2$ to yield the five-coordinate complex (**L2**)NiBr$_2$ (**2**). While **2** contains two carbonyl groups, only one oxygen atom coordinates to Ni (Figure 4.1b). The τ values[13] of the two independent molecules of **1** in the solid-state structure are τ_5 = 0.46 and 0.41, and the τ value of **2** is τ_5 = 0.62, showing that these structures are intermediate between trigonal bipyramidal and square pyramidal geometries. Complexes **1** and **2** are both paramagnetic and exhibit broad ^{1}H NMR resonances.

Scheme 4.1

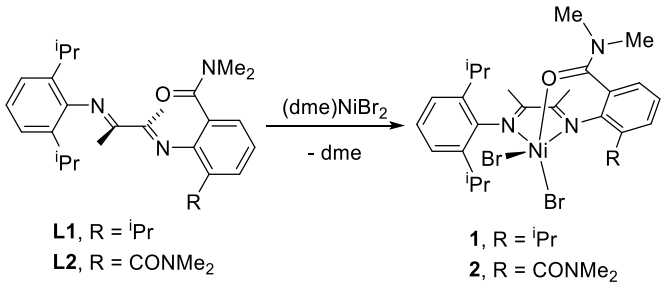

(a) (b)

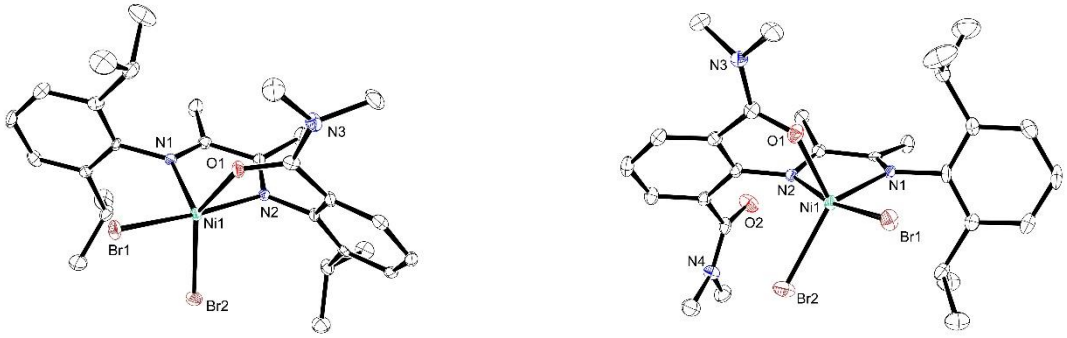

Figure 4.1. (a) Molecular structure of one independent molecule of **1** in **1·2CH$_2$Cl$_2$**. The structure of the other independent molecule is similar. Hydrogen atoms are omitted. Selected bond lengths (Å): Ni1-O1, 2.073(3); Ni1-N1, 2.028(3); Ni1-N2, 2.038(3); Ni1-Br1, 2.4267(7); Ni1-Br2, 2.4430(7). (b) Molecular structure of **2** in **2·0.25H$_2$O**. Hydrogen atoms and the H_2O molecule are omitted. Selected bond lengths (Å): Ni1-O1, 2.0080(18); Ni1-N1, 2.062(2); Ni1-N2, 2.090(2); Ni1-Br1, 2.4469(5); Ni1-Br2, 2.4075(5).

Synthesis of Complex 3. The reaction of **L1** and (py)$_2$NiMe$_2$ yields the diamagnetic, air-sensitive complex (**L1**)NiMe$_2$ (**3**, Scheme 4.2). **3** is stable at -40 °C in the solid state but decomposes at room temperature within a few days in C_6D_6 solution. **3** was characterized by ^{1}H NMR, ^{13}C NMR and 2D-NMR methods. The NMR spectroscopic data for **3** are consistent with the proposed square planar structure. The NOESY spectrum of **3** shows that the *O-trans* N-Me group of the amide unit is in close proximity to a Ni-*Me* group but not to the diimine backbone methyl groups, which establishes that the carbonyl oxygen of the –CONMe$_2$ group points away from the Ni center and rules out *O*-coordination. The presence of the two strong-field alkyl ligands disfavors *O*-coordination and favors the square planar configuration.

Scheme 4.2

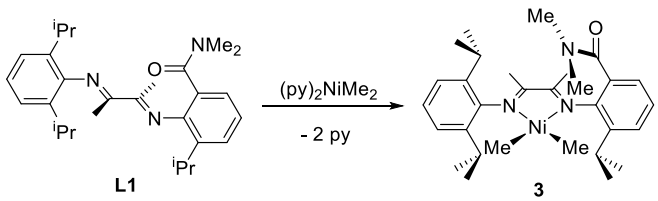

Ethylene Polymerization. Preliminary experiments show that activation of **1** by Et_2AlCl generates an active catalyst for ethylene polymerization (Table 4.1). The activity of **1** is on the order of 10^4-10^5 g/(mol Ni·h) and exhibits a strong dependence on the loading of the Et_2AlCl cocatalyst. The activity of **1** decreased by a factor of 2.6 when the Al loading was increased from 100 to 1000 equiv vs **1**. **1** forms semicrystalline polyethylene with a broad, bimodal molecular-weight distribution (MWD, M_w/M_n = 6.63-7.13). As shown in Figure 4.2, the MWD is not strongly sensitive to the Al loading, which suggests that the deviation from the expected Schulz-Flory MWD is due to the presence of multiple catalytically active species rather than to chain transfer to Al. The MWD plots at two different Al loading levels (Figure 4.2) exhibit a major low-MW fraction each that are similar in MW (entry 1, M_p = 28422; entry 2, M_p = 28194), which are likely to be formed by the same active species.

Table 4.1. Ethylene Polymerization[a]

entry	cat.	Al/Ni	Yield (g)	act.[b]	M_n (10^3)	M_w/M_n	T_m (°C)
1	**1**	100	0.21	140	24.4	7.13	109.2
2	**1**	1000	0.079	53	12.8	6.63	111.9

[a]Condition: 3.0 μmol Ni, Et_2AlCl, ethylene (80 psi), toluene (50 mL), 23 °C, 30 min. [b]Activity (kg/(mol Ni·h)).

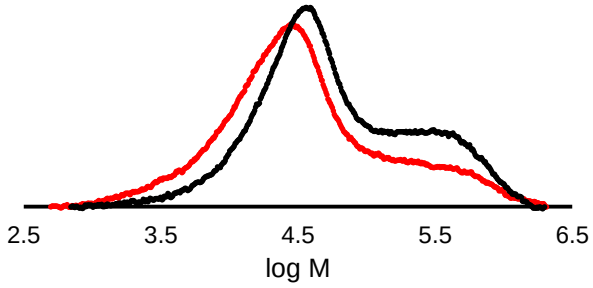

Figure 4.2. MWD plots of polyethylene samples produced by catalyst 1. Black: Table 4.1, entry 1; red: Table 4.1, entry 2.

4.3 Conclusions

The amide-functionalized α-diimine ligands **L1** and **L2** coordinate in a κ^3-*O,N,N* fashion in five-coordinate (**L1**)$NiBr_2$ and (**L2**)$NiBr_2$, respectively, while **L1** coordinates in a κ^2-*N,N* fashion in square planar (**L1**)$NiMe_2$. **1** reacts with Et_2AlCl to generate an active ethylene polymerization catalyst that produces semicrystalline polyethylene with a broad molecular-weight distribution.

4.4 Experimental Section

General Procedures. All experiments were performed under nitrogen using drybox or Schlenk techniques. Nitrogen was purified by passage through activated molecular sieves and Q-5 oxygen scavenger. Hexane and toluene were purified by passage through activated alumina and BASF R3-11 oxygen scavenger, and CH_2Cl_2 and Et_2O were purified by passage through activated alumina. **L1**, **L2**,[11] and $(py)_2NiMe_2$[14] were synthesized by literature procedures.

NMR spectra were recorded on a Bruker DRX-500 spectrometer at room temperature using Teflon-valved tubes. ^1H and ^{13}C NMR chemical shifts are reported relative to $SiMe_4$ and were determined by reference to the residual ^1H and ^{13}C solvent resonances. Coupling constants are given in hertz (Hz). NMR assignments were made with the aid of COSY, NOESY and HMQC experiments. C_6D_6 was distilled from Na/benzophenone and stored under vacuum. Elemental analyses were performed by Robertson Microlit Laboratories (Ledgewood, NJ).

Ethylene polymerization reactions were performed in a 200 mL Fischer-Porter bottle equipped with a magnetic stir bar and a stainless steel pressure head equipped with inlet and outlet needle valves, a septum-capped ball valve for injections, a check valve for safety, and a pressure gauge. Gel permeation chromatography (GPC) data were obtained on a Polymer Laboratories

PLGPC 200 instrument at 150 °C with 1,2,4-trichlorobenzene (stabilized with 125 ppm BHT) as the mobile phase. Three PLgel 10 μm Mixed-B LS columns were used. Molecular weights were calibrated using narrow polystyrene standards (ten-point calibration with M_n from 580 Da to 6035 kDa) and are corrected for linear polyethylene by universal calibration using the following Mark-Houwink parameters: polystyrene, $K = 1.75 \times 10^{-2}$ cm^3 g^{-1}, $\alpha = 0.67$; polyethylene, $K = 5.90 \times 10^{-2}$ cm^3 g^{-1}, $\alpha = 0.69$.[15] DSC measurements were performed on a TA Instruments DSC 2920 instrument. Samples (ca. 5 mg) were annealed by heating to 170 °C at 20 °C/min, cooled to 30 °C at 20 °C/min, and then analyzed while being heated to 170 °C at 20 °C/min.

κ^3-*O,N,N*-(L1)NiBr$_2$ (1). A Schlenk flask was charged with **L1** (351 mg, 0.810 mmol), (dme)NiBr$_2$ (250 mg, 0.810 mmol) and CH_2Cl_2 (100 mL). The mixture was stirred at room temperature for 19 h to afford a brown suspension containing a yellow powder. The mixture was filtered by cannula, and the filtrate was layered with hexane (100 mL) and maintained at room temperature for 1 d to yield brown needles of **1·2CH$_2$Cl$_2$** (443 mg, 67%). The crystals of **1·2CH$_2$Cl$_2$** were pulverized and dried under vacuum before elemental analysis. Anal. Calcd. for $C_{28}H_{39}Br_2N_3NiO$, %: C, 51.57; H, 6.03; N, 6.44. Found: C, 51.16; H, 6.07; N, 6.22.

κ^3-*O,N,N*-(L2)NiBr$_2$ (2). A Schlenk flask was charged with **L2** (395 mg, 0.854 mmol), (dme)NiBr$_2$ (278 mg, 0.900 mmol) and CH_2Cl_2 (10 mL). The mixture was stirred at room temperature for 22.5 h to give a brown suspension containing a yellow powder. The solid was removed by vacuum filtration, and the filtrate was concentrated under vacuum to ca. 5 mL. Et_2O (30 mL) was added in one portion, and the resulting brown solid was collected by vacuum filtration. Recrystallization of this material by layering hexane (30 mL) on a CH_2Cl_2 solution (5 mL) at room temperature for 5 d yielded brown crystals of **2** (277 mg, 48%). Anal. Calcd. for $C_{28}H_{38}Br_2N_4NiO_2$, %: C, 49.37; H, 5.62; N, 8.23. Found: C, 49.09; H, 5.64; N, 7.98.

κ^2-*N*,*N*-(L1)NiMe$_2$ (3). A vial was charged with **L1** (171 mg, 0.394 mmol) and toluene (8 mL). The solution was maintained at -40 °C for 1 h. $(py)_2NiMe_2$ (97 mg, 0.39 mmol) was added to the pre-cooled solution of **L1**, and the mixture turned dark green instantly. The mixture was maintained at -40 °C for 20 min and then stirred at room temperature for 2 h. The dark blue mixture was filtered through Celite and taken to dryness under vacuum. The residue was dissolved in a mixture of toluene (3 mL) and hexane (50 mL) and maintained at -40 °C for 3 d. A small amount of unreacted **L1** crystallized from solution and was separated by decantation. The mother liquor was taken to dryness under vacuum to yield a blue powder. Yield: 112 mg (54%). ^{1}H NMR (C_6D_6): δ 7.35 (d, *J* = 7.8, 1H), 7.30-7.25 (m, 3H), 7.13 (t, *J* = 7.5, 1H), 7.02 (d, *J* = 7.5, 1H), 3.65 (septet, *J* = 6.8, 1H, H^7), 3.25 (septet, *J* = 6.8, 1H, H^{10}), 3.04 (septet, *J* = 6.8, 1H, H^{13}), 2.73 (s, 3H, H^5), 2.70 (s, 3H, H^6), 1.44 (d, *J* = 6.8, 3H, H^{14}), 1.42 (d, *J* = 6.8, 3H, H^8), 1.40 (d, *J* = 6.8, 3H, H^{11}), 1.12 (d, *J* = 6.8, 3H, H^{15}), 0.99 (d, *J* = 6.8, 3H, H^{12}), 0.97 (d, *J* = 6.8, 3H, H^9), 0.88 (s, 3H, H^1), 0.71 (s, 3H, H^2), 0.59 (s, 3H, H^4), 0.18 (s, 3H, H^3). ^{13}C{^{1}H NMR (C_6D_6): δ 168.8, 166.8, 164.1, 147.1, 146.8, 141.6, 139.9, 139.4, 129.9, 126.7, 126.5, 125.7, 124.4, 123.79, 123.72, 39.2 (C^5), 34.1 (C^6), 28.9 (C^{10}), 28.7 (C^7), 28.3 (C^{13}), 24.2 (^{i}Pr), 24.06 (^{i}Pr), 24.00 (^{i}Pr), 23.85 (^{i}Pr), 23.82 (^{i}Pr), 23.3 (^{i}Pr), 22.9 (C^4), 21.0 (C^3), -2.9 (C^1), -4.0 (C^2). Elemental analysis was precluded by the low thermal stability of **3**.

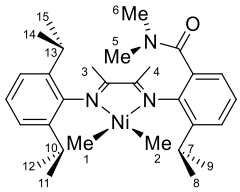

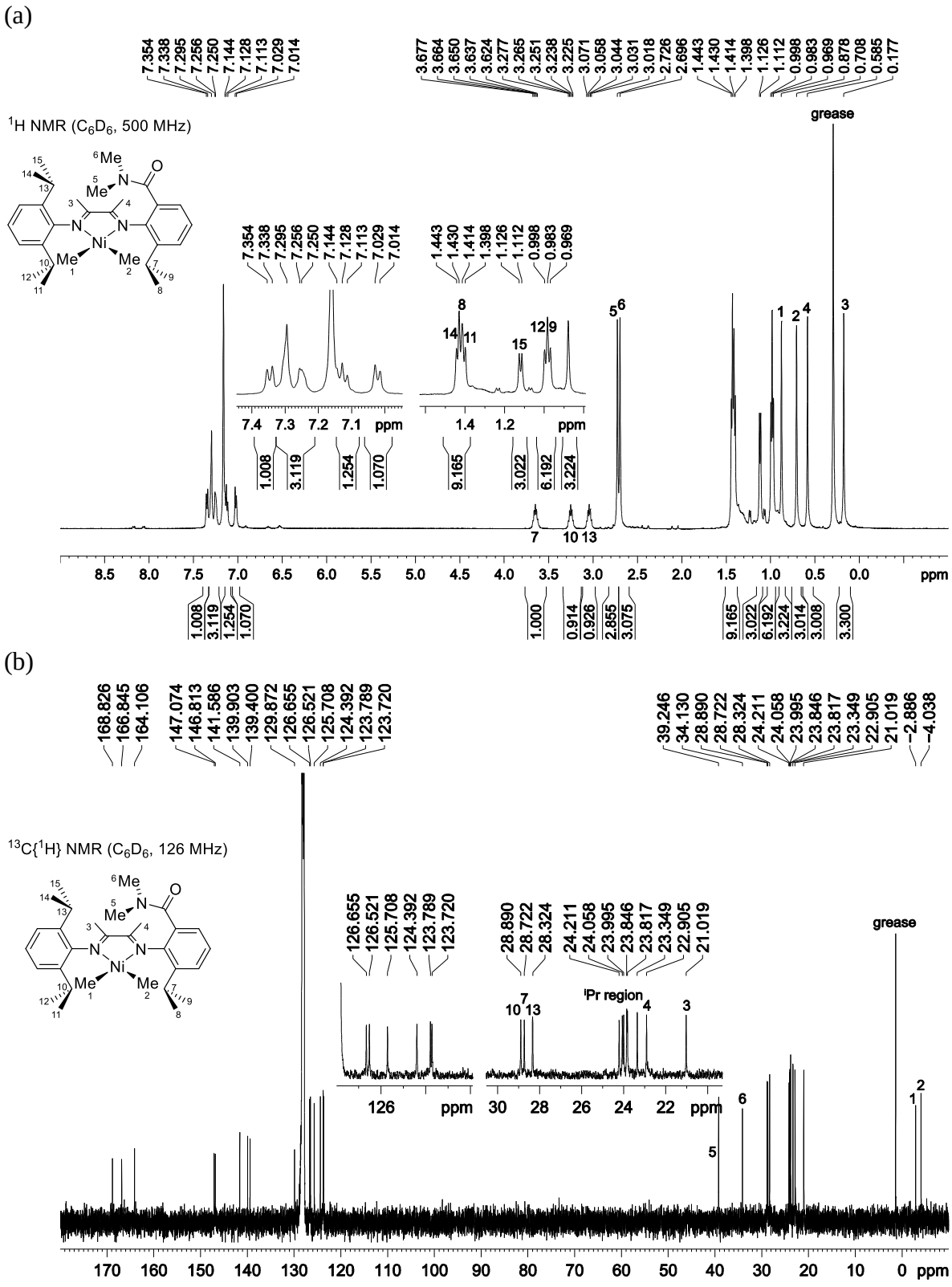

Figure 4.3. NMR spectra of **3**.

(c) HMQC (C_6D_6, expansion of δ 4.1 to -0.3/50 to -10 region)

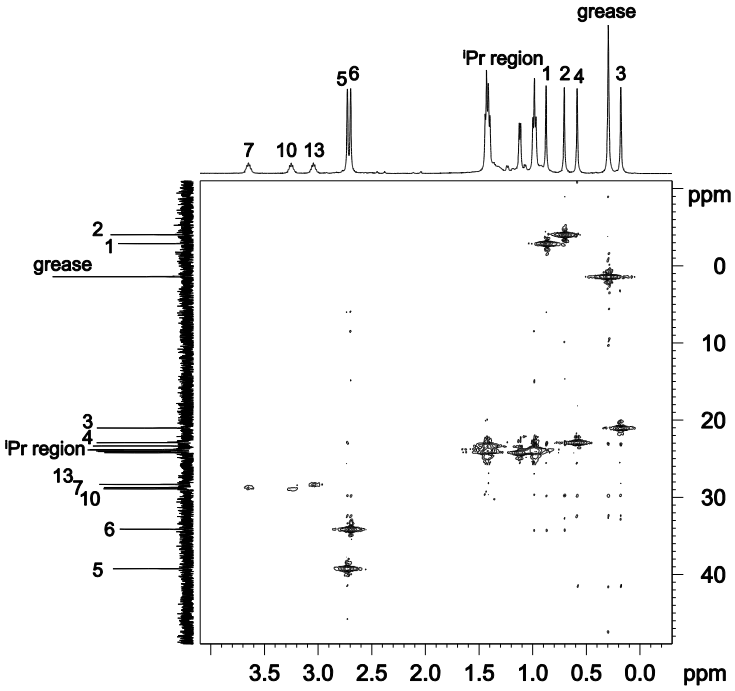

(d) NOESY (C_6D_6, expansion of δ 4.1 to -0.3/4.1 to -0.3 region)

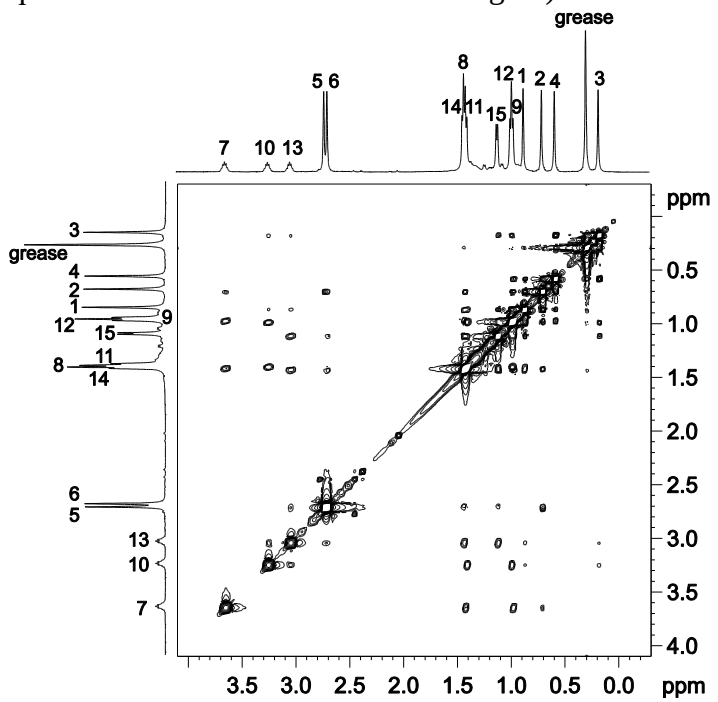

Figure 4.3, continued. NMR spectra of **3**.

Ethylene Polymerization. In a glovebox, a Fischer-Porter bottle was charged with the catalyst (3.0 μmol) and toluene (50 mL), and the bottle was sealed. The bottle was removed from

the glovebox and attached to a stainless steel double manifold (vacuum/ethylene) line. The bottle was charged with ethylene (14 psi), and Et_2AlCl (100 or 1000 equiv vs catalyst) was injected against pressure through the ball valve. The ethylene pressure was increased to 80 psi, and the mixture was stirred at room temperature. After 30 min, the bottle was vented. A 5% solution of HCl in MeOH (100 mL) was added, and the mixture was stirred for 10 min to precipitate the polymer. The polymer was collected by vacuum filtration, washed with acetone and dried overnight in a vacuum oven.

X-ray Crystallography. Data were measured on a Bruker D8 VENTURE with a PHOTON 100 CMOS detector system equipped with a Mo-target X-ray tube ($\lambda = 0.71073$ Å). All atoms were refined with anisotropic thermal parameters. Hydrogen atoms were included in idealized positions for structure factor calculations. All structures are drawn with thermal ellipsoids at 50% probability. Specific details for each compound follow: **1·2CH$_2$Cl$_2$**: Crystals were grown by bilayer diffusion of hexane into a CH_2Cl_2 solution of **1** at room temperature under N_2. Crystallographic data and details of the data collection and structure refinement are listed in Table 4.2. The asymmetric unit comprises two molecules of **1** and four CH_2Cl_2 molecules. **2·0.25H$_2$O**: Crystals were grown by bilayer diffusion of hexane into a CH_2Cl_2 solution of **2** at room temperature under N_2. Crystallographic data and details of the data collection and structure refinement are listed in Table 4.3. Large residual peak was identified on final refinement cycles and was assigned to ¼ occupied O-atom, which was refined with anisotropic thermal parameters. The H atoms attached to it were also identified in the difference Fourier map and allowed to be refined at 0.84 Å within a default 0.02 Å standard deviation with their thermal parameters constrained to be 1.5 times of the U_{eq} value of the O atom.

Table 4.2. Crystal Data and Structure Refinement for 1·2CH_2Cl_2.

Empirical formula	$C_{60}H_{86}Br_4Cl_8N_6Ni_2O_2$
Formula weight	1644.00
Temperature/K	100(2)
Crystal system	monoclinic
Space group	*C*2/*c*
a/Å	70.192(11)
b/Å	9.5989(15)
c/Å	20.982(3)
α/°	90
β/°	96.294(8)
γ/°	90
Volume/$Å^3$	14051(4)
Z	8
$\rho_{calc}g/cm^3$	1.554
μ/mm^{-1}	3.159
F(000)	6688.0
Crystal size/mm^3	0.25 × 0.15 × 0.03
Radiation	MoKα (λ = 0.71073)
2Θ range for data collection/°	4.284 to 52.858
Index ranges	$-87 \leq h \leq 87$, $-11 \leq k \leq 11$, $-26 \leq l \leq 26$
Reflections collected	122809
Independent reflections	14340 [R_{int} = 0.0623]
Data/restraints/parameters	14340/0/759
Goodness-of-fit on F^2	1.037
Final R indexes [I>=2σ (I)]	R_1 = 0.0450, wR_2 = 0.1074
Final R indexes [all data]	R_1 = 0.0685, wR_2 = 0.1170
Largest diff. peak/hole / e $Å^{-3}$	1.33/-1.57

Table 4.3. Crystal Data and Structure Refinement for 2·0.25H_2O.

Empirical formula	$C_{28}H_{38.5}Br_2N_4NiO_{2.25}$
Formula weight	685.66
Temperature/K	100(2)
Crystal system	orthorhombic
Space group	*Pbca*
a/Å	17.3488(13)
b/Å	17.6218(11)
c/Å	19.4844(13)
α/°	90
β/°	90
γ/°	90
Volume/$Å^3$	5956.7(7)
Z	8
$\rho_{calc}g/cm^3$	1.529
μ/mm^{-1}	3.367
F(000)	2804.0
Crystal size/mm^3	0.28 × 0.17 × 0.14
Radiation	MoKα (λ = 0.71073)
2Θ range for data collection/°	4.624 to 52.83
Index ranges	$-21 \leq h \leq 14$, $-22 \leq k \leq 22$, $-22 \leq l \leq 24$
Reflections collected	26660
Independent reflections	6056 [R_{int} = 0.0528]
Data/restraints/parameters	6056/2/359
Goodness-of-fit on F^2	1.007
Final R indexes [I>=2σ (I)]	R_1 = 0.0347, wR_2 = 0.0609
Final R indexes [all data]	R_1 = 0.0659, wR_2 = 0.0685
Largest diff. peak/hole / e $Å^{-3}$	0.55/-0.45

4.5 References

(1) Johnson, L. K.; Killian, C. M.; Brookhart, M. S. *J. Am. Chem. Soc.* **1995**, *117*, 6414.

(2) Ittel, S. D.; Johnson, L. K.; Brookhart, M. S. *Chem. Rev.* **2000**, *100*, 1169.

(3) Gates, D. P.; Svejda, S. A.; Oñate, E.; Killian, C. M.; Johnson, L. K.; White, P. S.; Brookhart, M. *Macromolecules* **2000**, *33*, 2320.

(4) Guan, Z.; Popeney, C. S. *Top. Organomet. Chem.* **2009**, *26*, 179.

(5) Guo, L.; Dai, S.; Sui, X.; Chen, C. *ACS Catal.* **2016**, *6*, 428.

(6) Correia, S. G.; Marques, M. M.; Ascenso, J. R.; Ribeiro, A. F. G.; Gomes, P. T.; Dias, A. R.;

Blais, M.; Rausch, M. D.; Chien, J. C. W. *J. Polym. Sci. A Polym. Chem.* **1999**, *37*, 2471.

(7) Marques, M. M.; Fernandes, S. N.; Correia, S. G.; Caroço, S.; Gomes, P. T.; Dias, A. R.; Mano, J.; Rausch, M. D.; Chien, J. C. W. *Polym. Int.* **2001**, *50*, 579.

(8) McLain, S. J.; Sweetman, K. J.; Johnson, L. K.; McCord, E. F. *Polym. Mater. Sci. Eng.* **2002**, *86*, 320.

(9) Johnson, L. K.; Bennett, A. M. A.; Dobbs, K.; Ionkin, A. S.; Ittel, S. D.; McCord, E. F.; Radzewich, C. E.; Yin, Z.; Wang, L.; Brookhart, M. S. *Polym. Mater. Sci. Eng.* **2002**, *86*, 319.

(10) Long, B. K.; Eagan, J. M.; Mulzer, M.; Coates, G. W. *Angew. Chem., Int. Ed.* **2016**, *55*, 7106.

(11) Zhai, F.; Jordan, R. F. *Organometallics* **2014**, *33*, 7176.

(12) Zhai, F.; Jordan, R. F. unpublished results.

(13) Addison, A. W.; Rao, T. N.; Reedijk, J.; van Rijn, J.; Verschoor, G. C. *J. Chem. Soc., Dalton Trans.* **1984**, 1349.

(14) Cámpora, J.; del Mar Conejo, M. a.; Mereiter, K.; Palma, P.; Pérez, C.; Reyes, M. L.; Ruiz, C. *J. Organomet. Chem.* **2003**, *683*, 220.

(15) Grinshpun, V.; Rudin, A. *Makromol. Chem., Rapid Commun.* **1985**, *6*, 219.

CHAPTER FIVE

Facile Ring Expansion and Formation of Peracid Triggered by Autoxidation of Heterocyclic Aminals

5.1 Introduction

Aminyl radicals are generated through the decomposition of R_2N-X compounds (X = N, O, S, halogen, pyridine-2-thioneoxycarbonyl, etc.),[1-3] addition of carbon radicals to imines,[4] and H-atom abstraction from secondary amines via free-radical or single-electron-oxidation/proton-transfer mechanisms.[5] Aminyl radicals undergo a variety of synthetically useful reactions, including H-atom abstraction, addition to alkenes,[6] and β-cleavage (Scheme 5.1).[7-8] One example of the latter process is oxidation of 2,2-disubstituted 2,3-dihydroquinazolin-4(1*H*)-ones to form 2-substituted quinazolin-4(3*H*)-ones, which are of interest for their potential biomedical applications (Scheme 5.2).[9-11] Wang and Tang and coworkers investigated the Cu-catalyzed aerobic oxidation of 2,2-disubstituted dihydroquinazolinones (**A**) at 130 °C and exploited this reaction in the tandem construction of quinazolinones.[12-13] A mechanism for this process involving Cu-mediated single-electron oxidation at N^1 followed by deprotonation to yield an aminyl radical and subsequent β-C-C cleavage was proposed. The β-cleavage is selective and occurs in the order: H > alkyl > Me > Ph > substituted aryls. Similarly, Moore and coworkers showed that $KMnO_4$ oxidation of 2-benzoyl-2-phenyl dihydroquinazolinone **C** led to elimination of the benzoyl group with formation of 2-phenyl-quinazolinone **D**.[14]

Scheme 5.1

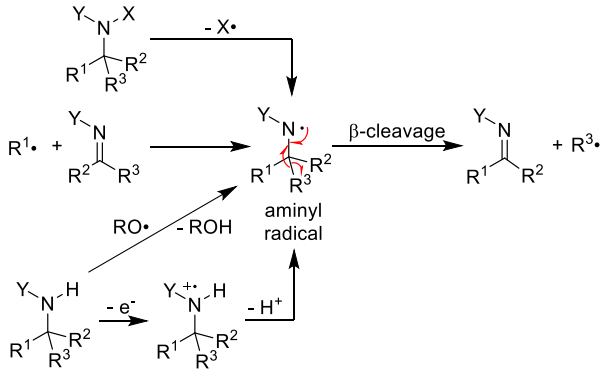

Scheme 5.2. Examples of Oxidative C-C Bond Cleavage of 2,2-Disubstituted 2,3-Dihydroquinazolin-4(1*H*)-ones

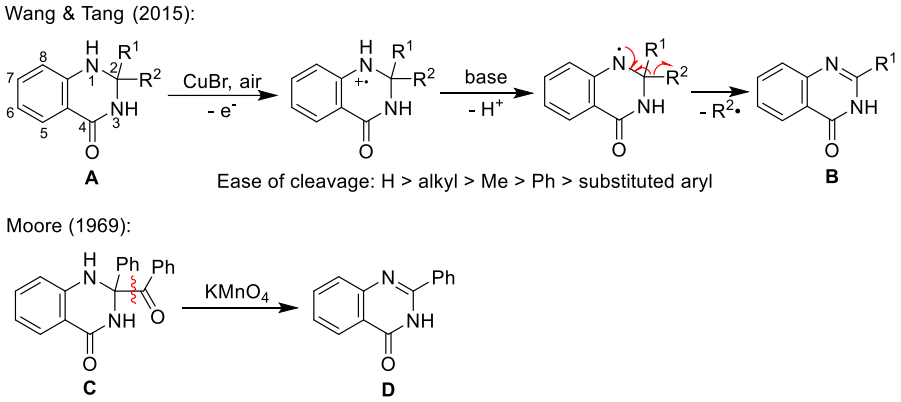

Here we report unusually facile autoxidation reactions of 2-acyl-2,3-dihydroquinazolin-4(1*H*)-ones **4a** and **5a** and 2,2'-bis(dihydroquinazolinone) **6a** (Scheme 5.3) under O_2 or air in solution at room temperature. These reactions generate aminyl radicals that undergo β-C-C cleavage, and subsequent trapping of the resulting C-based radicals by O_2 leads to diverse products with good selectivity, depending on the structure of substrate. The room-temperature and metal-free reaction conditions minimize decomposition and enable convenient isolation of the organic hydroperoxide products in some cases.

Scheme 5.3

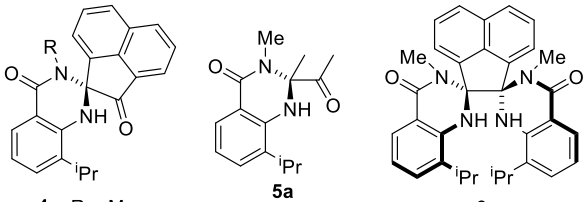

4a, R = Me
4b, R = H

5a

6a

5.2 Results and Discussion

Synthesis of 4a,b and 5a. As part of a project related to amide-functionalized α-diimine ligands,[15] we prepared 2-acyl 2,3-dihydroquinazolin-4(1*H*)-ones **4a,b** and **5a**. *o*-Aminobenzamides **1a,b** undergo TsOH-catalyzed condensation with acenaphthenequinone (**2**) in a 1:1 fashion to yield spiro(dihydroquinazolinone)s **4a,b** in 88-94% yield (Scheme 5.4). Similar Brønsted acid[16-17] or Lewis acid[18]-catalyzed syntheses of spiro(dihydroquinazolinone)s have been reported. We also extended the scope of TsOH-catalyzed condensation to butanedione (**3**), yielding **5a** (Scheme 5.4).

Scheme 5.4

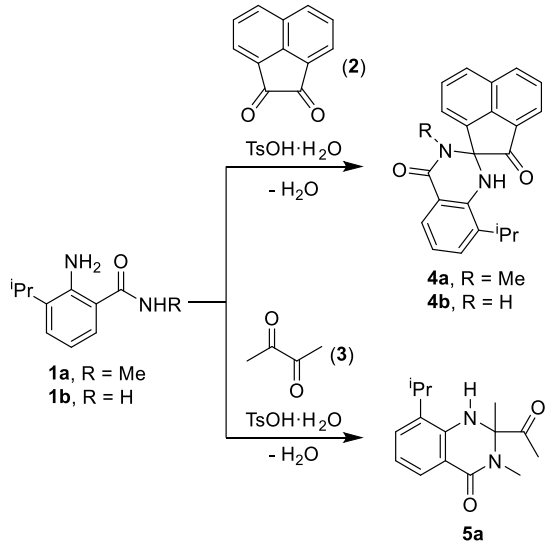

The structure of **4a** was confirmed by X-ray diffraction (Figure 5.1). The C1-C12 bond

(length 1.576(5) Å) is significantly longer than the typical sp^3-C-C(=O) single bond (1.511 Å)[19] due to ring strain in the acenaphthene 5-membered ring. The ^{1}H NMR spectra of **4a,b** and **5a** exhibited two doublets and a septet for the desymmetrized isopropyl groups due to the presence of the stereogenic carbon center. The ^{13}C NMR resonance for the spiro carbon for all the three compounds appear at δ ca. 75.

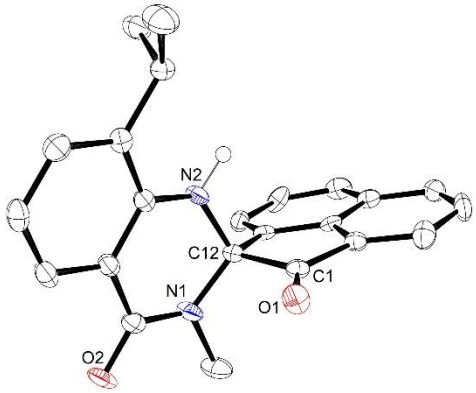

Figure 5.1. Molecular structure of **4a**. Hydrogen atoms are omitted except for the H atom on N2.

Observation of 1:2 Condensation. The 1:2 condensation between **2** and **1a** is disfavored due to the steric congestion around the ketone unit in **4a**. However, the $Sc(OTf)_3$-catalyzed condensation of **2** with 2.0 equiv of **1a** in ^{t}BuOH at 120 °C affords a small amount (6%) of bicondensation product **6a**, along with 94% of **4a** (Scheme 5.5).

Scheme 5.5

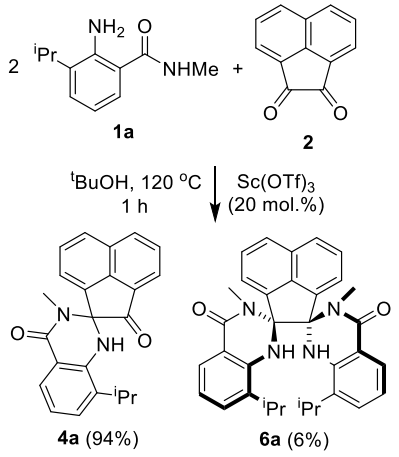

6a was isolated in 1% yield by fractional recrystallization under N_2 due to its air sensitivity (vide infra) and difficulty in separation by silica chromatography. X-ray diffraction analysis of **6a** revealed the *RR*/*SS* configuration of the two spiro chiral centers (Figure 5.2). **6a** contains approximately a C_2-symmetry with the C_2 axis running along the central C-C bond of the naphthalene unit. The length of the very long C-C bond between the two spiro carbon atoms (C12-C23, 1.681(2) Å) is comparable to those in other 1,1,2,2-tetrasubstituted acenaphthenes[20-22] and results from strong steric crowding between the two dihydroquinazolinone units. The aryl rings of two heterocyclic units stack intramolecularly in a displaced face-to-face fashion with a centroid-centroid distance of 3.74 Å. The NMR spectrum of **6a** is consistent with the 2-fold symmetry observed in the solid-state structure. The ^{13}C NMR resonance of the spiro carbons appears at δ 89.9, ca. 15 ppm downfield from that of **4a**. The elongated C12-C23 single bond causes planarization of these carbon atoms, which may account for this unusual downfield shift.

We observed no other organic products in this reaction. The absence of the meso (*RS*/*SR*) diastereomer is likely due to steric repulsion between the two isopropyl groups or the two N-Me groups.

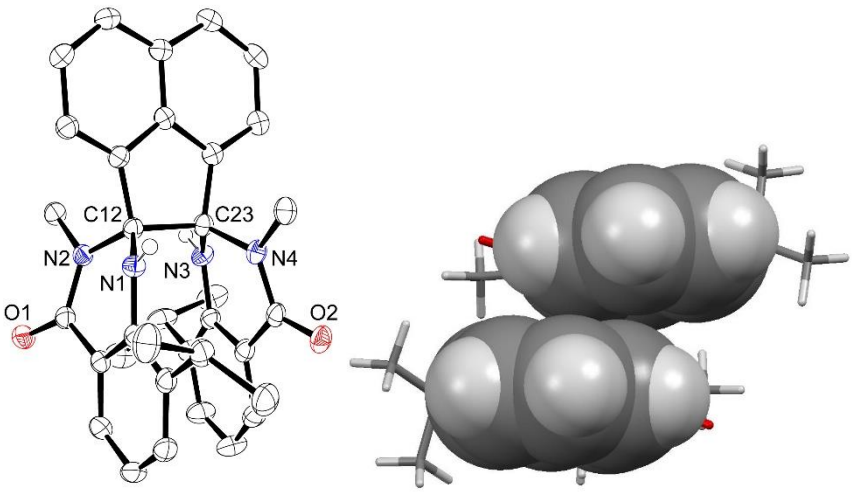

Figure 5.2. Molecular structure of **6a**. Hydrogen atoms are omitted except for the H atoms on N1 and N3. Left: ORTEP plot. Right: Space filling model showing the packing between two aryl rings.

Autoxidation of 4a. 4a undergoes oxidation to **8a** under air over days in $CDCl_3$ at room temperature (Scheme 5.6), from which single crystals of **8a** were isolated. The structure of **8a** was revealed by X-ray diffraction to be an *N*-aryl 1,8-naphthalimide (Figure 5.3b). The ^1H NMR spectrum of **8a** is characteristic of two-fold symmetry and a characteristic doublet for the N-Me unit in secondary amide, both in accord with the solid-state structure.

To gain more insight in the reaction mechanism, we studied the oxidation of **4a** under O_2. **4a** reacts with 1 atm O_2 via ring expansion to form hydroperoxide compound **7a** (Scheme 5.6) in halogenated solvents (CH_2Cl_2, $CHCl_3$, CCl_4, C_6H_5F) with net incorporation of two oxygen atoms as evidenced by ESI-MS. Under optimized condition, pure **7a** was isolated as precipitate in 85% yield from CCl_4 at 65 °C.

Scheme 5.6

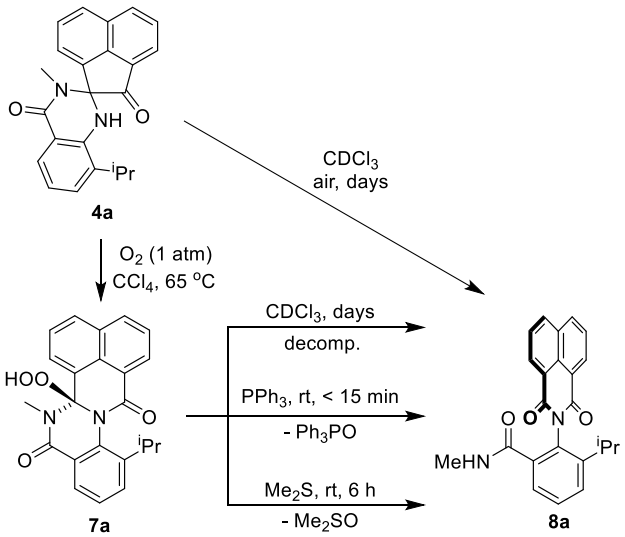

The structure of hydroperoxide **7a** was revealed by single crystal X-ray diffraction (Figure 5.3a). **7a** contains a fused ring structure; the pyrimidone ring (A) remains intact from **4a** and the 6-membered lactam ring (B) results from ring expansion of the 5-membered acenaphthene ring of **4a** via acyl migration from the spiro carbon to the adjacent amine nitrogen. The O1-O2 bond length

(1.4695(19) Å) and the C1-O1-O2 angle (106.66(13)°) are both close to the data for other hydroperoxylamidine[23] and alkyl peroxides.[24]

7a was characterized by ^{1}H NMR, ^{13}C NMR, and multiple 2D NMR experiments. The hydroperoxy proton resonance appears at δ 8.1 in dry $CDCl_3$ but is shifted downfield by 1.8 ppm in CD_3CN (δ 9.9) and 3.2 ppm in THF-d_8 (δ 11.3) due to hydrogen bonding with solvents. The hydroperoxy proton resonance exhibits a NOESY correlation with only one of the isopropyl methyl doublets (Figure 5.4), in agreement with the proximal relationship observed in the crystal structure. The ^{13}C NMR resonance of the hydroperoxy-bound carbon atom appears at δ 103.0, and this assignment was confirmed by observation of the long-range ^{3}J coupling between this carbon and the N-Me hydrogen atoms in HMBC spectrum (Figure 5.4).

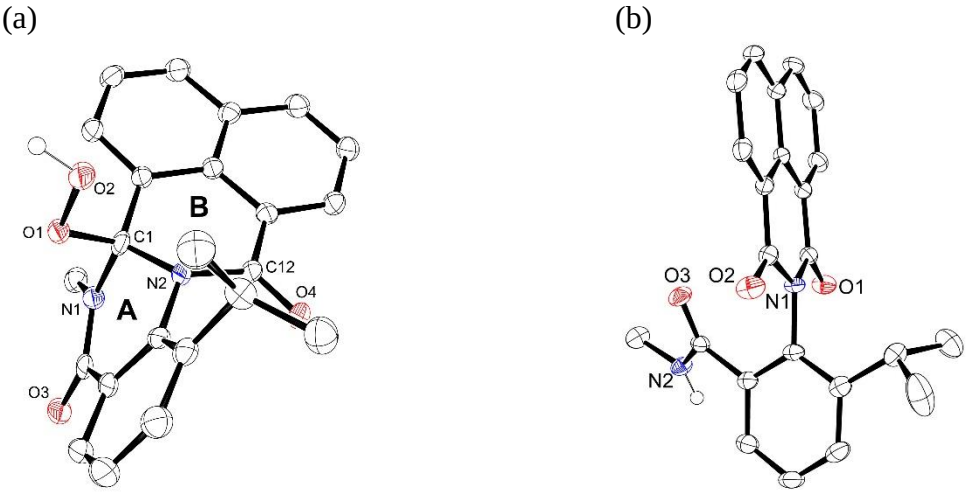

Figure 5.3. (a) Molecular structure of **7a**. Hydrogen atoms are omitted except for the H atom on O2. (b) Molecular structure of **8a**. Hydrogen atoms are omitted except for the H atom on N2.

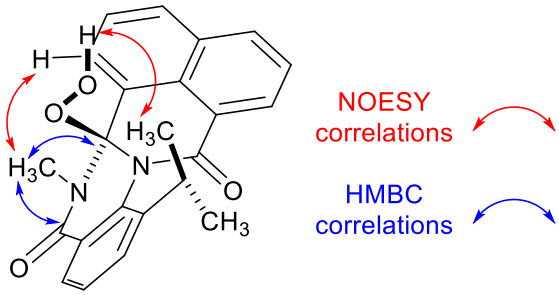

Figure 5.4. Important NOESY and HMBC correlations for **7a**.

7a undergoes facile stoichiometric oxygen atom transfer to PPh_3 or Me_2S at room temperature to form imide **8a** (Scheme 5.6). **7a** also slowly degrades in $CDCl_3$ solution to yield **8a**. In this case the identity of the oxygen acceptor is unknown. These results show that **7a** is an intermediate in the oxidative transformation of **4a** to **8a**. The conversion of **7a** to **8a** proceeds via oxygen atom transfer to form intermediate hydroxylamidine **10a** followed by formal N-H elimination (Scheme 5.7). **8a** can be conveniently synthesized in a one-pot two-step procedure by aerobic oxidation of **4a** followed by reduction of **7a** using Me_2S, in 92% isolated yield.

Scheme 5.7

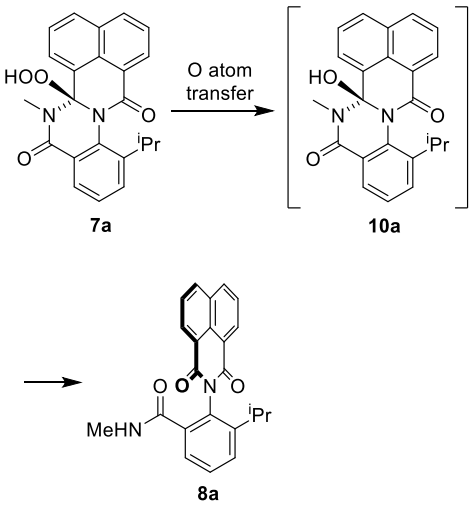

Mechanism of Conversion of 4a to 7a. Available evidence suggests that autoxidation of **4a** to **7a** proceeds through a radical chain mechanism. When **4a** was heated under 1 atm O_2 in CCl_4

at 60 °C for 1 h, 100% conversion to **7a** (95%) and **8a** (5%) was observed; however, only 5% conversion occurred in the presence of 1.6 equiv of the radicacl inhibitor BHT. The reaction proceeds in the dark, precluding mechanisms involving singlet O_2 ($^1O_2$). A proposed mechanism is shown in Scheme 5.8. The aminyl radical **E**, generated from **4a** through H-atom abstraction or one-electron oxidation and loss of H^+, undergoes ring expansion through a β-acyl 1,2-migration (intramolecular β-C-C cleavage) to yield a C-based radical (**F**). Trapping of **F** by O_2 and subsequent H-atom abstraction from **4a** forms **7a** and regenerates **E**. The conversion of **4a** to **7a** does not require external radical initiator. The reaction may be initiated by trace peroxy radicals or a SET/proton transfer mechanism.

Scheme 5.8

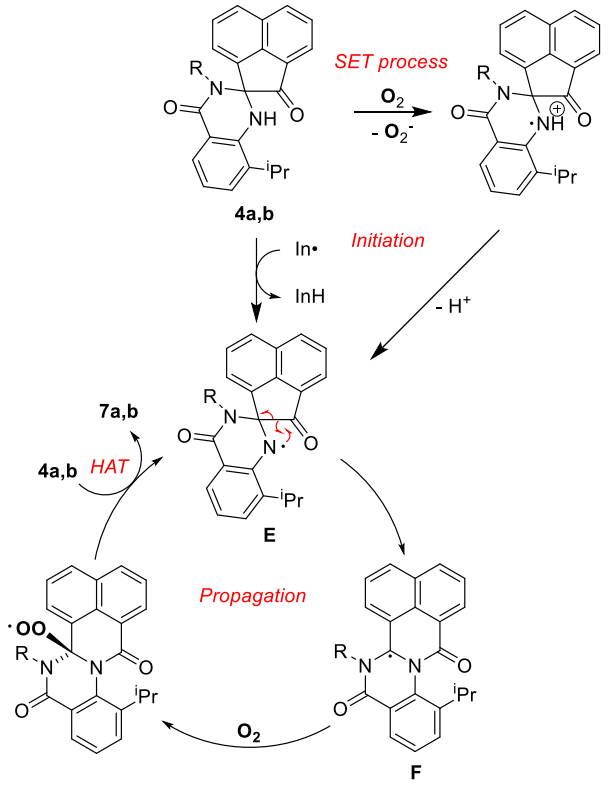

Autoxidation of 4b. Compound **4b** lacks a methyl group on the amide nitrogen and therefore is less electron-rich than **4a**. **4b** does not react with O_2 in CD_2Cl_2 and CCl_4, likely due to

higher amine N-H bond dissociation energy relative to **4a**.[25] However, **4b** undergoes aerobic oxidation in CD_2Cl_2/TFA (100:1) to form imide **8b** (77%) and compound **9** (18%) within 6 d at room temperature (Scheme 5.9).[26] The identities of **8b** and **9** were confirmed through independent synthesis in combination with ^{1}H NMR and X-ray crystallography (Figure 5.5a).

Scheme 5.9

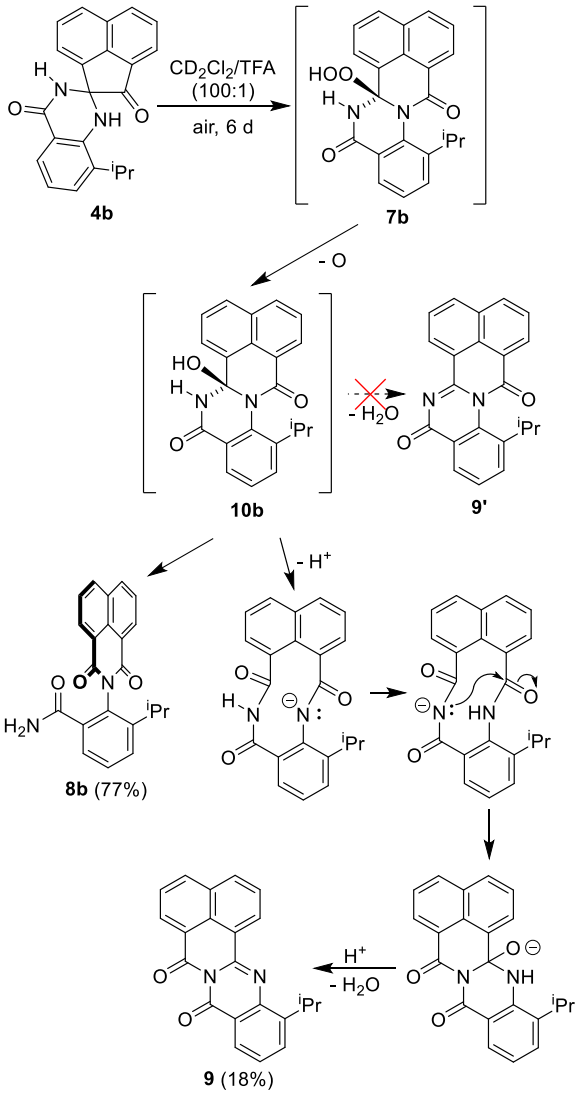

The formation of **8b** and **9** may proceed through the mechanism shown in Scheme 5.9. First, the autoxidation of **4b** likely proceeds via a similar radical mechanism as observed for **4a**

(Scheme 5.8) to form hydroperoxide **7b**. This intermediate undergoes oxygen atom transfer to afford hydroxylamidine **10b**. **10b** may transform via two pathways: formal N-H elimination to yield isomer **8b**, or double ring opening through transannular C-N bond cleavage followed by rearrangement and dehydration to yield **9**. The direct dehydration product of **10b**, **9'**, was not observed as a major product. Our studies of the attempted synthesis of **9**' suggested that **9'** is highly energetic and isomerizes to **9**, in agreement with previous report by Lindeman et al.[27-28]

Oxidative C-C Bond Cleavage of 5a. 5a is structurally similar to **4a,b** except that the 2-acyl group is not incorporated in a cyclic unit. **5a** undergoes facile C-C bond cleavage to yield quinazolinone **11** and peracetic acid in several solvents (CD_2Cl_2, $CDCl_3$, C_6D_6) in the presence of O_2 (Scheme 5.10). Under 1 atm O_2, the oxidation of **5a** is complete within a few hours at room temperature. Peracetic acid was identified through analysis of volatiles of NMR-scale oxidation reactions by NMR techniques and by its reaction with PPh_3 to generate $O{=}PPh_3$.[29] The autoxidation reaction of **5a** likely proceeds through a radical chain mechanism, involving β-cleavage of aminyl radical **G** to generate **11** and acetyl radical, followed by trapping of the latter species with O_2 and H-atom abstraction (Scheme 5.10). BHT inhibits the autoxidation of **5a**.

Scheme 5.10

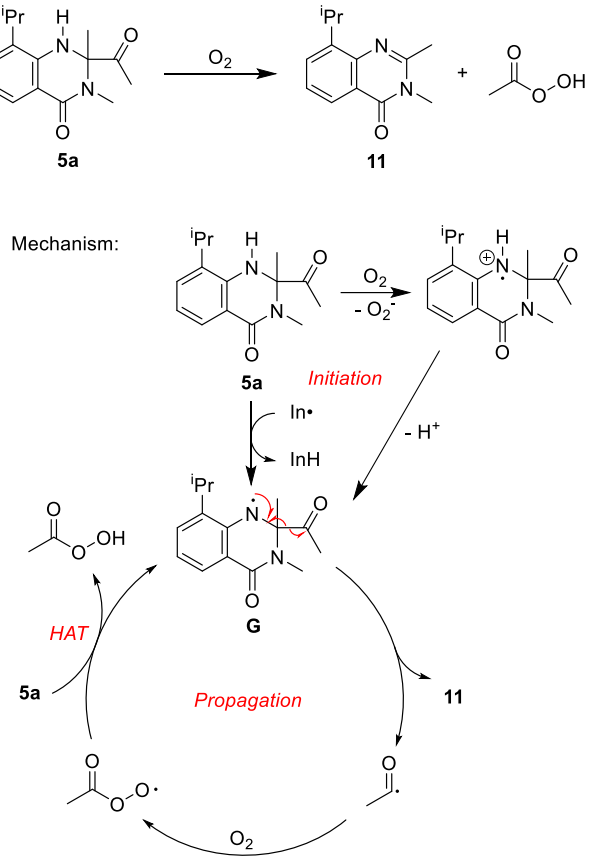

Autoxidation of 6a. The bicondensation product **6a** is air-sensitive in several solvents (CD_2Cl_2, $CDCl_3$, CD_3CN) and forms **12** by formal dehydrogenation and cleavage of the strained acenaphthene C-C bond. The structure of **12** was confirmed by X-ray diffraction (Figure 5.5b). We were unable to study the autoxidation mechanism of **6a** in detail due to the limited availability of this compound. We propose that the reaction proceeds by a radical chain process, involving β-cleavage of an initially formed aminyl radical to generate a C-based radical **H**. Subsequent H-atom abstraction by O_2 yields **12** and the hydroperoxy radical, which abstracts an H-atom from **6** to complete the cycle (Scheme 5.11). The byproduct H_2O_2 was detected in the reaction in CD_3CN. A similar aerobic oxidative C-C cleavage reaction in tetrasubstituted acenaphthene system has been reported.[30]

Scheme 5.11

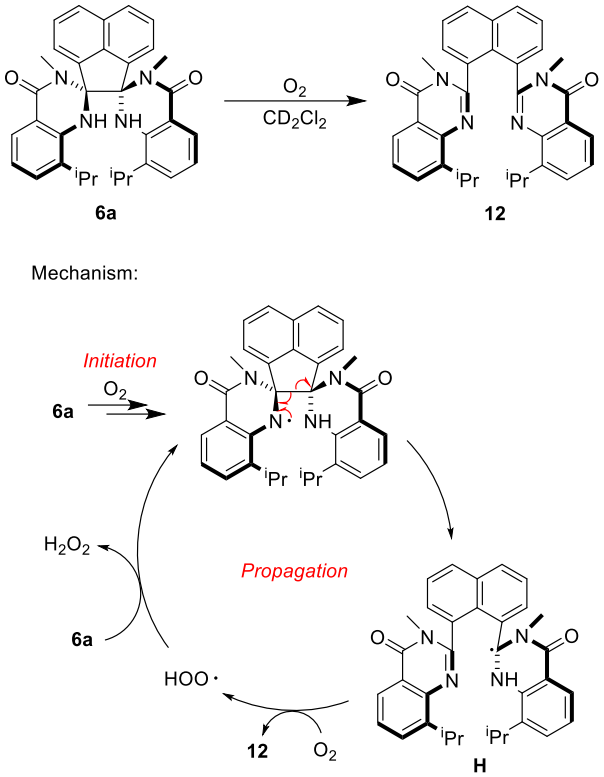

(a) (b)

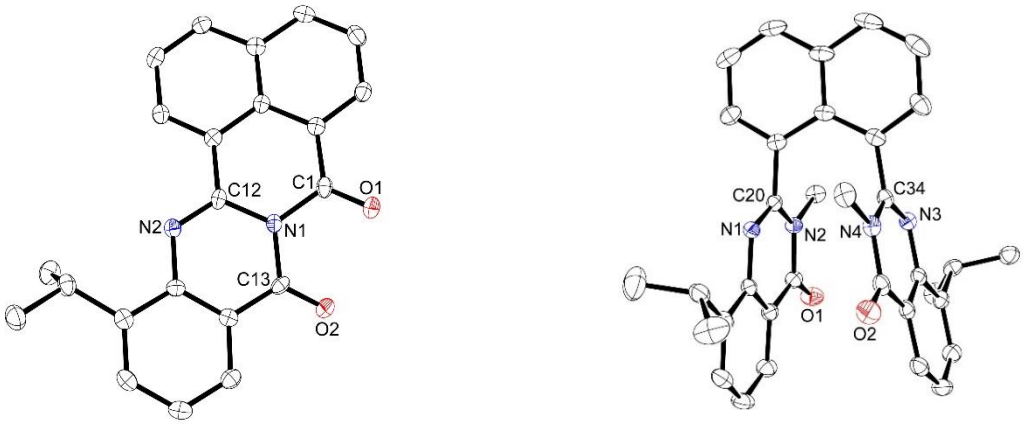

Figure 5.5. Molecular structures of (a) **9** and (b) **12**. Hydrogen atoms are omitted.

5.3 Conclusions

2-Acyl-2,3-dihydroquinazolin-4(1*H*)-one compounds **4a** and **5a** undergo facile C-C cleavage reactions with O_2 by a radical mechanism. The reaction pathway is dependent on the structure of substrate. The strained spirocyclic **4a** undergoes ring expansion by 1,2-acyl migration to form C-based radical followed by trapping with O_2. Compound **5a**, in which the 2-acetyl is not part of a cyclic structure, undergoes fragmentation to generate acetyl radical, which is trapped by O_2 to form peracetic acid. Bis(dihydroquinazolinone) **6a** undergoes C-C cleavage and formal dehydrogenation by O_2.

5.4 Experimental Section

General Procedures. Experiments were conducted under air with reagent grade solvents unless indicated otherwise. Nitrogen was purified by passage through activated molecular sieves and Q–5 oxygen scavenger. Solvents for manipulations under N_2 were purified as follows: hexane was purified by passage through activated alumina and BASF R3–11 oxygen scavenger, and THF and CH_2Cl_2 were purified by passage through activated alumina.

^{t}BuOH (anhydrous, ≥99.5%, Sigma-Aldrich), CCl_4 (anhydrous, ≥99.5%, Sigma-Aldrich), acenaphthenequinone (**2**, >90.0%, Sigma-Aldrich), $Sc(OTf)_3$ (>98.0%, TCI), and silica gel (60 M, particle size 0.04-0.063 mm, Macherey-Nagel) were used as purchased. 2-Amino-3-isopropylbenzoic acid and 2-amino-3-isopropyl-*N*-methylbenzamide (**1a**) were synthesized by literature procedures.[15]

NMR spectra were recorded on a Bruker DRX-500 spectrometer at room temperature. NMR samples under N_2 or O_2 atmosphere were prepared using Teflon-valved tubes. ^{1}H and ^{13}C chemical shifts are reported relative to $SiMe_4$ and were determined by reference to the residual ^{1}H

and ^{13}C solvent resonances. Coupling constants are given in hertz (Hz). NMR assignments were made with the aid of COSY, NOESY, HMQC, and HMBC experiments. $CDCl_3$ and CD_2Cl_2 were distilled from P_2O_5 and stored under vacuum. C_6D_6 and THF-d_8 were distilled from Na/benzophenone. DMSO-d_6 and CD_3CN were used as received.

Infrared spectra were recorded on thin-film samples on NaCl plates using a Nicolet NEXUS 470 FT-IR spectrometer. Mass spectrometry was performed on Agilent 6130 LCMS (low resolution) or Agilent 6224 Tof-MS (high resolution) instruments. The listed *m*/*z* value corresponds to the most intense peak in the isotope pattern.

2-Amino-3-isopropylbenzamide (1b). A flask was charged with 3-isopropylanthranilic acid (2.00 g, 11.2 mmol), benzene (30 mL) and thionyl chloride (4 mL). The yellow suspension was heated to reflux for 2.5 h to give an orange solution. The volatiles were removed on a rotovap to yield the crude acyl chloride as a red oil. The oil was dissolved in dry THF (20 mL) and added dropwise to an aqueous NH_3 solution (20 mL, 30 wt %) at 0 °C. The mixture was stirred at 0 °C for 30 min and quenched with water (ca. 100 mL). The THF was removed on a rotovap. The aqueous residue was extracted with Et_2O (3 × 30 mL). The organic phase was washed with brine, dried with anhydrous $MgSO_4$, filtered, and taken to dryness under vacuum to give a yellow solid residue. The residue was subjected to flash column chromatography (silica, hexane/EtOAc = 50/50 by volume) to yield **1b** as an off-white solid (1.34 g, 67%). ^1H NMR (DMSO-d_6): δ 7.73 (br s, 1H, C(O)N*H*H'), 7.40 (d, *J* = 7.8, 1H), 7.13 (d, *J* = 7.4, 1H), 7.09 (br s, 1H, C(O)NH*H'*), 6.53-6.49 (m, 3H, ArNH_2 + 1 ArH), 2.98 (septet, *J* = 6.8, 1H), 1.14 (d, *J* = 6.8, 6H). $^{13}C\{^1H\}$ NMR (DMSO-d_6): δ 172.1, 147.0, 132.9, 127.8, 126.4, 114.5, 114.2, 26.1, 22.3. IR (cm^{-1}): 3390, 3186, 1641, 1609. HRMS (ESI-TOF, positive ion, *m*/*z*): Calc. 357.2291 ($[2M + H]^+$), found 357.2288.

8'-Isopropyl-3'-methylspiro[acenaphthylene-1(2*H*),2'(3'*H*)-quinazoline]-2,4'(1'*H*)-dione (4a). A Schlenk flask was charged with acenaphthenequinone (**2**, 182 mg, 1.00 mmol), **1a** (202 mg, 1.05 mmol, 1.05 equiv) and $TsOH \cdot H_2O$ (95 mg, 0.50 mmol, 0.50 equiv). Dry ^{t}BuOH (6 mL) was added via syringe, and the mixture was heated at 80 °C under N_2 for 30 min, yielding an orange suspension. Water (20 mL) was added to precipitate the product. The resulting orange powder was collected by vacuum filtration, washed with water (10 mL) and MeOH (2 mL), and dried in a vacuum desiccator. Yield: 315 mg (88%). ^{1}H NMR ($CDCl_3$): δ 8.23 (d, *J* = 8.2, 1H), 8.06-8.02 (m, 2H), 7.96 (dd, *J* = 7.8, 1.0, 1H), 7.84 (t, *J* = 7.7, 1H), 7.76-7.72 (m, 2H), 7.28 (dd, *J* = 7.8, 0.9, 1H), 6.97 (t, *J* = 7.7, 1H), 4.35 (br s, 1H, NH), 2.69 (s, 3H), 2.63 (sept, *J* = 6.8, 1H), 1.10 (d, *J* = 6.8, 3H), 1.06 (d, *J* = 6.8, 3H). ^{13}C{^{1}H} NMR ($CDCl_3$): δ 199.2, 164.6, 141.4, 140.9, 136.6, 133.1, 132.7, 130.8, 129.6, 129.3, 129.17, 129.14, 127.1, 126.3, 123.5, 121.7, 120.4, 117.1, 78.5 (spiro C), 29.7, 26.8, 22.33, 22.29. IR (cm^{-1}): 3317, 1729, 1641. HRMS (ESI-TOF, positive ion, *m*/*z*): Calc. 357.1603 ($[M + H]^+$), found 357.1600. Note: **4a** is stable in air in solid state but undergoes slow oxidation under air in solution. Hence, quick handling is needed.

8'-Isopropylspiro[acenaphthylene-1(2*H*),2'(3'*H*)-quinazoline]-2,4'(1'*H*)-dione (4b). A Schlenk flask was charged with **2** (182 mg, 1.00 mmol), **1b** (202 mg, 1.05 mmol, 1.05 equiv) and $TsOH \cdot H_2O$ (95 mg, 0.50 mmol, 0.50 equiv). Dry ^{t}BuOH (5 mL) was added via syringe, and the mixture was heated at 80 °C under N_2 for 50 min, yielding an orange suspension. Water (20 mL) was added to precipitate the product. The resulting orange powder was collected by vacuum filtration, washed with water (10 mL) and MeOH (2 mL), and dried in a vacuum desiccator. Yield: 320 mg (94%). ^{1}H NMR ($CDCl_3$): δ 8.21 (d, *J* = 8.2, 1H), 8.05 (d, *J* = 8.4, 1H), 8.02 (d, *J* = 7.0, 1H), 7.91-7.89 (m, 2H), 7.83 (t, *J* = 7.6, 1H), 7.79 (t, *J* = 7.7, 1H), 7.32 (d, *J* = 7.9, 1H), 6.95 (t, *J* = 7.8, 1H), 5.95 (br s, 1H, NH), 4.47 (br s, 1H, NH), 2.65 (sept, *J* = 6.8, 1H), 1.142 (d, *J* = 6.8,

3H), 1.136 (d, J = 6.8, 3H). $^{13}C\{^{1}H\}$ NMR (DMSO-d_6): δ 200.4, 163.6, 143.6, 141.0, 138.8, 132.2, 131.8, 129.9, 129.4, 129.17, 129.09, 128.8, 126.0, 124.8, 122.2, 121.2, 117.4, 114.7, 74.0 (spiro C), 25.5, 22.6, 22.2. IR (cm^{-1}): 3382, 1730, 1664. HRMS (ESI-TOF, positive ion, m/z): Calc. 343.1447 ($[M + H]^+$), found 343.1446.

2-Acetyl-2,3-dihydro-8-isopropyl-2,3-dimethylquinazolin-4(1*H*)-one (5a). A Schlenk flask was charged with butanedione (**3**, 1.36 mL, 15.6 mmol), **1a** (7.08 g, 36.8 mmol, 2.36 equiv), $TsOH·H_2O$ (200 mg) and benzene (50 mL) under N_2. The flask was equipped with a Dean-Stark trap filled with 4 Å molecular sieves and a condenser. The mixture was refluxed for 3.5 d, cooled to room temperature, and quenched with Et_3N (ca. 5 mL). The volatiles were removed under vacuum. The residue was subjected to flash column chromatography (silica, hexane/EtOAc/Et_3N = 15/5/1 by volume) to afforded **5a** as white crystals (2.54 g, 63% based on **3**), while unreacted **1a** (2.94 g, 15.3 mmol) was recovered. ^{1}H NMR (CD_2Cl_2, N_2): δ 7.71 (dd, J = 7.7, 1.3, 1H), 7.28 (dd, J = 7.8, 1.2, 1H), 6.87 (t, J = 7.7, 1H), 4.58 (br s, 1H, NH), 3.10 (s, 3H), 2.91 (sept, J = 6.8, 1H), 2.15 (s, 3H), 1.73 (s, 3H), 1.28 (d, J = 6.8, 3H), 1.22 (d, J = 6.8, 3H). $^{13}C\{^{1}H\}$ NMR (CD_2Cl_2, N_2): δ 208.0, 164.1, 141.7, 133.7, 129.9, 126.5, 120.3, 117.0, 77.8, 29.4, 27.2, 25.3, 22.9, 22.60, 22.58. HRMS (APCI-TOF, positive ion, m/z): Calc. 261.1603 ($[M + H]^+$), found 201.1617. Note: **5a** is stable in air in solid state but undergoes oxidation under air in solution. Hence, quick handling is needed.

***rac*-8,8”-Diisopropyl-3,3”-dimethyldispiro[quinazoline-2(3*H*),1’(2’*H*)-acenaphthylene-2’,2”(3”*H*)-quinazoline]-4(1*H*), 4”(1”*H*)-dione (6a).** A Teflon-valved Schlenk flask was charged with **2** (182 mg, 1.00 mmol), **1a** (384 mg, 2.00 mmol, 2.0 equiv) and $Sc(OTf)_3$ (98 mg, 0.20 mmol, 0.20 equiv). Dry ^{t}BuOH (5 mL) was added via syringe. The flask was sealed, and the mixture was heated at 120 °C under N_2 for 1 h and then cooled to room temperature to

yield an orange suspension. The ^{1}H NMR spectrum of an aliquot revealed that a 94:94:6 mixture of **1a**:**4a**:**6a** was present. The volatiles were removed under vacuum. The residue was dissolved in EtOAc (50 mL). The EtOAc phase was washed with water and brine, dried with anhydrous $MgSO_4$, filtered, and taken to dryness under vacuum to give an orange solid residue. The residue was subjected to two consecutive recrystallizations from hexane/EtOAc (2/1 by volume), from which pure **4a** (160 mg, 45%) was collected in total. The mother liquor was taken to dryness under vacuum, and the residue was recrystallized from hexane/CH_2Cl_2 at -40 °C under N_2 to yield a solid mixture of **1a** and **4a**. The mother liquor, which was enriched in **6a**, was taken to dryness under vacuum. Subsequent diffusion of pentane into an EtOAc solution of this material at room temperature under N_2 yielded red crystals of **4a** and colorless crystals of **6a**. The crystals of **6a** were separated from the mixture and recrystallized twice by diffusion of hexane into a CH_2Cl_2 solution at room temperature under N_2 to afford colorless rod-shaped crystals of **6a** that contained 0.34 equiv CH_2Cl_2 and 0.35 equiv hexane, as determined by ^{1}H NMR integration (5.5 mg, 1%). ^{1}H NMR ($CDCl_3$, N_2): δ 8.04-8.01 (m, 2H), 7.81-7.77 (m, 4H), 7.14 (dd, *J* = 7.7, 1.3, 2H), 6.95 (dd, *J* = 7.8, 1.3, 2H), 6.62 (t, *J* = 7.6, 2H), 4.69 (br s, 2H, NH), 2.66 (sept, *J* = 6.8, 2H), 2.40 (s, 6H), 1.38 (d, *J* = 6.8, 6H), 1.10 (d, *J* = 6.8, 6H). ^{13}C{^{1}H} NMR ($CDCl_3$, N_2): δ 162.3, 140.04, 140.02, 136.5, 131.9, 130.7, 129.4, 129.0, 127.6, 125.6, 122.9, 119.1, 115.7, 89.9 (spiro C), 30.7, 27.0, 23.6, 21.5. HRMS (ESI-TOF, positive ion, *m*/*z*): Calc. 1061.5442 ($[2M + H]^+$), found 1061.5438. Note: **6a** undergoes slow oxidation under air in solution and in solid state. Hence, quick handling is needed.

6,6a-Dihydro-6a-hydroperoxy-1-isopropyl-6-methyl-5*H*,13*H*-benz[4,5]isoquino[2,1-*a*]quinazoline-5,13-dione (7a). A Teflon-valved Schlenk tube was charged with **4a** (100 mg, 0.28 mmol) and dry CCl_4 (15 mL). The flask was sealed under O_2 (1 atm), and the orange suspension

was heated at 65 °C for 4.5 h until the orange color faded completely and a white suspension formed. The mixture was cooled to room temperature, and hexane (15 mL) was added. The white powder was collected by vacuum filtration, washed with hexane, and dried in a vacuum desiccator. Yield: 93 mg (85%). ^{1}H NMR ($CDCl_3$): δ 8.56 (d, *J* = 7.1, 1H, H^{12}), 8.22 (d, *J* = 8.1, 1H, H^{10}), 8.16 (d, *J* = 8.2, 1H, H^{9}), 8.09 (s, 1H, OO*H*), 8.07 (d, *J* = 7.1, 1H, H^{7}), 7.97 (d, *J* = 8.2, 1H, H^{4}), 7.79 (t, *J* = 7.8, 1H, H^{8}), 7.76 (t, *J* = 7.7, 1H, H^{11}), 7.65 (d, *J* = 7.7, 1H, H^{2}), 7.49 (t, *J* = 7.7, 1H, H^{3}), 3.06 (sept, *J* = 6.8, 1H, C*H*MeMe'), 2.71 (s, 3H, NCH_3), 1.42 (d, *J* = 6.8, 3H, CH*Me*Me'), 1.14 (d, *J* = 6.9, 3H, CHMe*Me'*). ^{13}C{^{1}H} NMR ($CDCl_3$): δ 164.0 (C^{5}), 163.4 (C^{13}), 146.2 (C^{1}), 133.6 (C^{10}), 132.9 (C^{14a}), 132.5 (C^{9a}), 131.1 (C^{2}), 130.8 (C^{9}), 129.5 (C^{12}), 128.2 (C^{7}), 127.9 (C^{3}), 127.5 (C^{12b}), 127.1 (C^{11}), 126.1 (C^{8}), 125.8 (C^{4}), 125.0 (C^{4a}), 124.7 (C^{6b}), 122.9 (C^{12a}), 103.0 (C^{6a}), 30.4 (N*C*H_3), 28.6 (*C*HMeMe'), 25.5 (CHMe*Me'*), 22.6 (CH*Me*Me'). Key ^{1}H-^{13}C HMBC correlations ($CDCl_3$): δ/δ 2.71/103.0 (NCH_3/C^{6a}), 2.71/164.0 (NCH_3/C^{5}). Key ^{1}H-^{1}H NOESY correlations ($CDCl_3$): δ/δ 8.09/1.14 (OO*H*/CHMe*Me'*), 8.09/3.06 (OO*H*/C*H*MeMe'). IR (cm^{-1}): 3275, 1666, 1652. HRMS (ESI-TOF, positive ion, *m*/*z*): Calc. 388.1423 (M^{+}), found 388.1403.

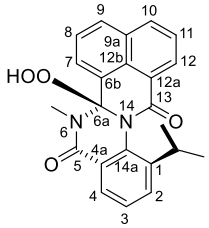

7a

2-{1,3-dioxo-1*H*-benz[*de*]isoquinolin-2(3*H*)-yl}-3-isopropyl-*N*-methylbenzamide (8a). A flask was charged with **4a** (100 mg, 0.281 mmol) and CH_2Cl_2 (20 mL). The mixture was stirred vigorously at room temperature for 48 h until the characteristic yellow color of **3a** faded completely and a white suspension formed. ^{1}H NMR analysis of an aliquot showed that a 96:4 mixture of **7a**:**8a** was present. Me_2S (30 μL, 0.408 mmol, 1.45 equiv) was added via microliter syringe. The mixture was stirred at room temperature to yield a pale-brownish solution within 5

min and then a white suspension after 18 h. The mixture was diluted with CH_2Cl_2 (30 mL), washed with water (2 × 15 mL) and brine (20 mL), dried over anhydrous Na_2SO_4, filtered, and taken to dryness under vacuum to give an off-white powder. The crude product was purified by flash column chromatography (silica, EtOAc) to yield **8a** (96 mg, 92%) as an off-white powder. ^{1}H NMR (DMSO-d_6): δ 8.53 (dd, J = 8.2, 1.2, 2H), 8.51 (dd, J = 7.3, 1.3, 2H), 8.29 (br q, J = 4.6, 1H, NH), 7.91 (dd, J = 8.2, 7.3, 2H), 7.67-7.63 (m, 1H), 7.57-7.53 (m, 2H), 2.86 (sept, J = 6.8, 1H), 2.47 (d, J = 4.6, 3H), 1.10 (d, J = 6.8, 6H). ^{13}C{^{1}H} NMR (DMSO-d_6): δ 166.7, 163.7, 147.4, 134.6, 133.2, 131.9, 131.6, 130.9, 128.7, 128.2, 128.0, 127.3, 126.0, 122.3, 27.8, 26.0, 23.4. IR (cm^{-1}): 3375, 1707, 1663. HRMS (ESI-TOF, positive ion, m/z): Calc. 767.2846 ([2M + Na]$^+$), found 767.2863.

Aerobic Oxidation of 4a in $CDCl_3$. An NMR tube was charged with **4a** (2.8 mg, 7.8 μmol). $CDCl_3$ (1.0 mL) was added to yield a yellow solution. The tube was loosely capped and maintained in the dark at room temperature. The oxidation was monitored by collecting ^{1}H NMR spectra periodically. A mixture of **8a** (87%) and unreacted **4a** (13%) formed after 5 d.

Reaction of 7a with PPh_3. A Teflon-valved NMR tube was charged with **7a** (6.0 mg, 0.015 mmol) and PPh_3 (4.6 mg, 0.018 mmol, 1.2 equiv), and CD_2Cl_2 (0.5 mL) was added by vacuum transfer at -196 °C. The tube was sealed and warmed to room temperature to yield a white suspension, which turned to a colorless solution after gentle agitation for 1 min. ^{1}H and ^{31}P{^{1}H} NMR spectra showed that quantitative generation of **8a** and Ph_3PO (1.0 equiv) had occurred within 15 min.

Reaction of 7a with Me_2S. An NMR tube was charged with **7a** (3.1 mg, 8.7 μmol), and CD_2Cl_2 (0.5 mL) was added to yield a white suspension. Me_2S (2.0 μL, 0.027 mmol, 3.5 equiv) was added via syringe. The tube was capped and agitated briefly to yield a colorless solution within

1 min. The tube was maintained at room temperature, and the reaction was monitored by collecting ^{1}H NMR spectra periodically. Quantitative generation of **8a** and DMSO (1.0 equiv) occurred within 6 h.

Scheme 5.12. Synthesis of 8b and 9

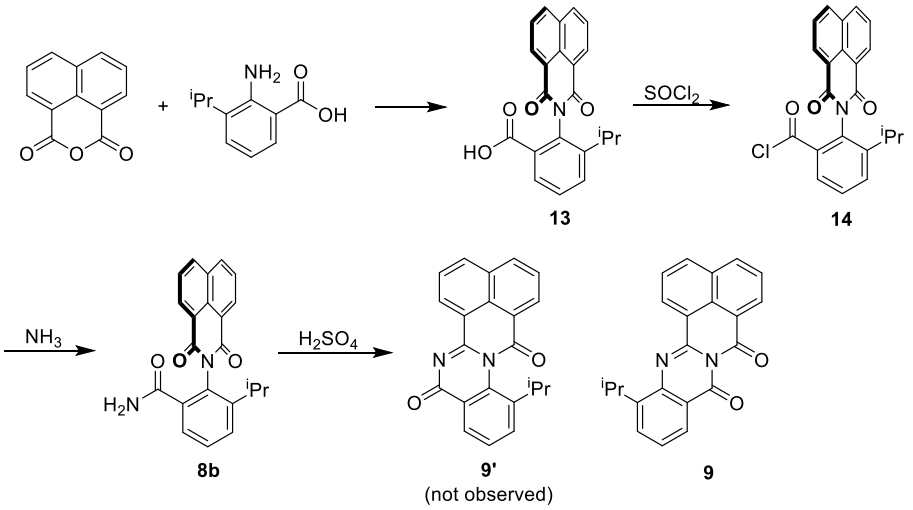

2-{1,3-Dioxo-1*H*-benz[*de*]isoquinolin-2(3*H*)-yl}-3-isopropylbenzoic acid (13). A flask was charged with 1,8-naphthalic anhydride (990 mg, 5.00 mmol), 2-amino-3-isopropylbenzoic acid (896 mg, 5.00 mmol), DMF (15 mL) and Et_3N (0.70 mL, 5.0 mmol). The mixture was heated at 140 °C under air for 16 h. The volatiles were distilled off under vacuum to yield a light yellow powder. The powder was suspended in CH_2Cl_2 (30 mL), and aqueous HCl (2 M, 30 mL) was added. A yellow solid precipitated and was collected by vacuum filtration. The solid was recrystallized from hot MeOH, and the resulting yellow microcrystals were dried in a vacuum oven at 70 °C for 2 d to give pure **13** as a pale yellow powder. Yield: 968 mg (54%). ^{1}H NMR (500 MHz, DMSO-d_6): δ 12.77 (s, 1H), 8.56-8.53 (m, 4H), 7.96 (dd, J = 7.7, 1.2, 1H), 7.92 (t, J = 7.7, 2H), 7.78 (dd, J = 7.8, 1.0, 1H), 7.60 (t, J = 7.8, 1H), 2.90 (septet, J = 6.8, 1H), 1.10 (d, J = 6.9, 6H). ^{13}C{^{1}H} NMR (126 MHz, DMSO-d_6): δ 166.1, 163.9, 147.5, 134.8, 133.5, 131.6, 131.0, 130.7, 129.2, 129.0,

128.4, 128.0, 127.4, 122.2, 27.8, 23.4. IR (cm^{-1}): 3207, 1710, 1667. HRMS (ESI-TOF, positive ion, *m*/*z*): Calc. 360.1236 ($[M + H]^+$), found 360.1240.

2-{1,3-Dioxo-1*H*-benz[*de*]isoquinolin-2(3*H*)-yl}-3-isopropylbenzoyl chloride (14). A flask was charged with **13** (539 mg, 1.50 mmol), benzene (20 mL) and $SOCl_2$ (3.0 mL, 4.5 mmol, 3.0 equiv). The mixture was heated to reflux for 4 h to afford a precipitate. 2/3 of the liquid was removed by distillation, and the remaining mixture was cooled to room temperature. Hexane (ca. 50 mL) was added to precipitate the acid chloride. The resulting pale yellow powder was collected by vacuum filtration, washed with hexane, and dried under vacuum. Yield: 523 mg (92%). ^{1}H NMR (500 MHz, acetone-d_6): 8.61 (dd, *J* = 7.3, 1.0, 2H), 8.55 (dd, *J* = 8.2, 1.0, 2H), 8.34 (dd, *J* = 8.0, 1.2, 1H), 8.03 (dd, *J* = 8.0, 1.0, 1H), 7.95 (t, *J* = 7.8, 2H), 7.81 (t, *J* = 7.9, 1H), 3.07 (septet, *J* = 6.8, 1H), 1.18 (d, *J* = 6.9, 6H).

2-{1,3-Dioxo-1*H*-benz[*de*]isoquinolin-2(3*H*)-yl}-3-isopropylbenzamide (8b). A flask was charged with **14** (400 mg, 1.06 mmol) and PhCl (10 mL). The suspension was heated to 90 °C to yield a colorless solution. NH_3 gas was bubbled through the mixture at 90 °C for 50 min, and a white precipitate formed. Hexane (10 mL) was added, and the white precipitate was collected by vacuum filtration. The white solid was mixed with MeOH (15 mL), stirred for 10 min, collected by vacuum filtration, washed with cold MeOH and dried under vacuum. ^{1}H NMR ($CDCl_3$): δ 8.64 (d, *J* = 7.2, 2H), 8.27 (d, *J* = 7.8, 2H), 7.79 (t, *J* = 7.7, 2H), 7.64-7.61 (m, 1H), 7.55-7.52 (m, 2H), 5.89 (br s, 1H, CON*H*H'), 5.27 (br s, 1H, CONH*H'*), 2.91 (septet, *J* = 6.8, 1H), 1.19 (d, *J* = 6.8, 6H). ^{13}C{^{1}H} NMR (DMSO-d_6): δ 168.3, 163.7, 147.4, 134.6, 133.2, 131.9, 131.5, 130.9, 128.6, 128.2, 128.0, 127.3, 126.2, 122.3, 27.8, 23.4. IR (cm^{-1}): 3378, 3206, 1671, 1616. HRMS (ESI-TOF, positive ion, *m*/*z*): Calc. 359.1396 ($[M + H]^+$), found 359.1395.

13-Isopropylbenz[4,5]isoquino[1,2-*b*]quinazoline-7,9-dione (9). A flask was charged with **8b** (200 mg, 0.558 mmol) and H_2SO_4 (98 wt %, 5 mL). The mixture was heated at 140 °C for 30 min to yield a clear red solution. The mixture was poured over ice (100 g), and the resulting yellow precipitate was collected by vacuum filtration, washed with water and dried under vacuum. The crude product was purified by flash column chromatography (silica, hexane/EtOAc = 2/1 by volume) and reprecipitated from hexane/EtOAc to yield a yellow powder. Yield: 127 mg (67%). ^{1}H NMR ($CDCl_3$): δ 8.99 (d, *J* = 7.4, 1H), 8.64 (d, *J* = 7.2, 1H), 8.24 (d, *J* = 7.4, 1H), 8.22 (d, *J* = 8.0, 1H), 8.12 (d, *J* = 8.0, 1H), 7.78 (t, *J* = 8.0, 1H), 7.76 (t, *J* = 7.8, 1H), 7.71 (d, *J* = 7.5, 1H), 7.47 (t, *J* = 7.7, 1H), 4.16 (septet, *J* = 6.9, 1H), 1.42 (d, *J* = 6.9, 6H). ^{13}C{^{1}H} NMR ($CDCl_3$): δ 162.0, 161.5, 146.4, 146.0, 142.7, 134.7, 132.0, 131.86, 131.83, 131.5, 129.0, 127.76, 127.73, 127.5, 127.1, 125.6, 124.1, 123.3, 122.4, 27.9, 23.6. IR (cm^{-1}): 1746. HRMS (ESI-TOF, positive ion, *m*/*z*): Calc. 341.1290 ($[M + H]^+$), found 341.1288.

8-Isopropyl-2,3-dimethylquinazolin-4(3*H*)-one (11). ^{1}H NMR (CD_2Cl_2): δ 8.04 (dd, *J* = 8.0, 1.6, 1H), 7.62 (dd, *J* = 7.5, 1.4, 1H), 7.37 (t, *J* = 7.7, 1H), 4.02 (sept, *J* = 6.8, 1H), 3.57 (s, 3H), 2.60 (s, 3H), 1.28 (d, *J* = 6.8, 6H). ^{13}C{^{1}H} NMR (CD_2Cl_2): δ 162.9, 153.5, 145.9, 145.2, 130.4, 126.3, 124.2, 120.7, 31.1, 27.2, 24.1, 23.5. HRMS (ESI-TOF, positive ion, *m*/*z*): Calc. 203.1184 ($[M + H]^+$), found 203.1182.

Peracetic acid. ^{1}H NMR (CD_2Cl_2): δ 11.25 (s, 1H), 2.17 (s, 3H). ^{13}C{^{1}H} NMR (CD_2Cl_2): δ 172.2, 17.2.

***rac*-8,8'-Diisopropyl-3,3'-dimethyl-2,2'-(naphthalene-1",8"-diyl)bisquinazoline-4(3*H*), 4'(3'*H*)-dione (12).** A Teflon-valved NMR tube was charged with **6a** (1.2 mg). Dry CD_2Cl_2 was added by vacuum transfer, and O_2 (1 atm) was added. The tube was sealed and agitated at room temperature in the dark for 21.5 h. The ^{1}H NMR spectrum showed that quantitative formation

of **12** had occurred. ^{1}H NMR ($CDCl_3$): δ 8.14 (dd, *J* = 8.4, 1.3, 2H), 7.70 (dd, *J* = 8.3, 6.9, 2H), 7.55-7.52 (m, 4H), 7.43 (dd, *J* = 7.8, 1.4, 2H), 7.17 (t, *J* = 7.8, 2H), 3.94 (sept, *J* = 6.8, 2H), 3.14 (s, 6H), 1.44 (d, *J* = 6.8, 6H), 1.08 (d, *J* = 6.8, 6H). ^{13}C{^{1}H} NMR ($CDCl_3$): δ 161.5, 153.5, 146.1, 143.8, 134.3, 132.8, 131.0, 130.1, 129.3, 126.99, 126.92, 126.3, 123.6, 120.5, 32.9, 26.6, 25.5, 21.6. IR (cm^{-1}): 1676, 1596, 1569. HRMS (ESI-TOF, positive ion, *m*/*z*): Calc. 529.2604 ([M + H]$^{+}$), found 529.2602.

X-ray Crystallography. Data were measured on a Bruker D8 VENTURE with a PHOTON 100 CMOS detector system equipped with a Mo-target X-ray tube (λ = 0.71073 Å). All atoms were refined with anisotropic thermal parameters. All structures are drawn with thermal ellipsoids at 50% probability. Specific details for each compound follow: **4a.** Crystals were obtained by diffusion of hexane into a CH_2Cl_2 solution of **4a** under N_2 at room temperature. Crystallographic data and details of the data collection and structure refinement are listed in Table 5.1. All atoms including disordered oxygen and carbon atoms were refined anisotropically. Hydrogen atoms were included in idealized positions for structure factor calculations except for the one bound to N2, which was located on the difference Fourier map and allowed to be freely refined. The acenaphthene group is disordered over two orientations in 85:15 ratio, and was modeled using geometric restraints and constraints on thermal parameters of carbon atoms. **6a.** Crystals were obtained by diffusion of hexane into a CH_2Cl_2 solution of **6a** under N_2 at room temperature. Crystallographic data and details of the data collection and structure refinement are listed in Table 5.2. All the elements were refined with anisotropic thermal parameters. One ^{i}Pr group is disordered over two orientations in 83:17 ratio, and was modeled with the application of soft geometric (SADI) restraints utilizing the non-disordered ^{i}Pr group. RIGU and EADP constraints were also used for the disordered atoms. Hydrogen atoms were included in idealized

positions for structure factor calculations except for those attached to N atoms, which were located on the difference Fourier map and allowed to be fully refined. The crystal contained many disordered solvent molecules located in large solvent-accessible voids. The diffuse contribution to scattering was treated by application of the program SQUEEZE[31-32] as implemented in Platon[33] using the "fab" file construct. The SQUEEZE algorithm located 3 voids, centered at (0, 0, 0), (1/3, 2/3, 2/3), and (2/3, 1/3, 1/3), with the same volume and the electron count (1187 $Å^3$ / 186). **7a.** Crystals were obtained by diffusion of pentane into a THF solution of **7a** under N_2 at room temperature. Crystallographic data and details of the data collection and structure refinement are listed in Table 5.3. All atoms were refined with anisotropic thermal parameters. Hydrogen atoms were included in idealized positions for structure factor calculations except the H2 atom attached to the peroxy group, which was located in the difference Fourier map and allowed to be freely refined to give O-H bond length of 0.93(3) Å. The crystal contained many disordered solvent molecules located in large solvent-accessible voids. The diffuse contribution to scattering was treated by application of the program SQUEEZE[31-32] as implemented in Platon[33] using the "fab" file construct. The SQUEEZE algorithm located 3 voids, centered at (0, 0, -0.025), (0.333, 0.667, 0.141), and (0.667, 0.333, 0.808) with a volume of 1349 $Å^3$ and the electron count of 216. **8a.** Crystals were obtained by slow evaporation/oxidation of a $CDCl_3$ solution of **4a** under air at room temperature for 5 d. Crystallographic data and details of the data collection and structure refinement are listed in Table 5.4. All elements were refined anisotropically. Hydrogen atoms were included in idealized positions for structure factor calculations except the H atom on N2, which was located on the difference Fourier map and refined with no restrains. **9.** Crystals were obtained by diffusion of hexane into a $CHCl_3$ solution of **9** at room temperature. Crystallographic data and details of the data collection and structure refinement are listed in Table 5.5. All atoms were refined

with anisotropic thermal parameters. Hydrogen atoms were included in idealized positions for structure factor calculations. **12.** Crystals were obtained by slow evaporation of a hexane/CH_2Cl_2 solution of **12** at room temperature. Crystallographic data and details of the data collection and structure refinement are listed in Table 5.6. All atoms were refined anisotropically. Hydrogen atoms were included in idealized positions for structure factor calculations.

(a)

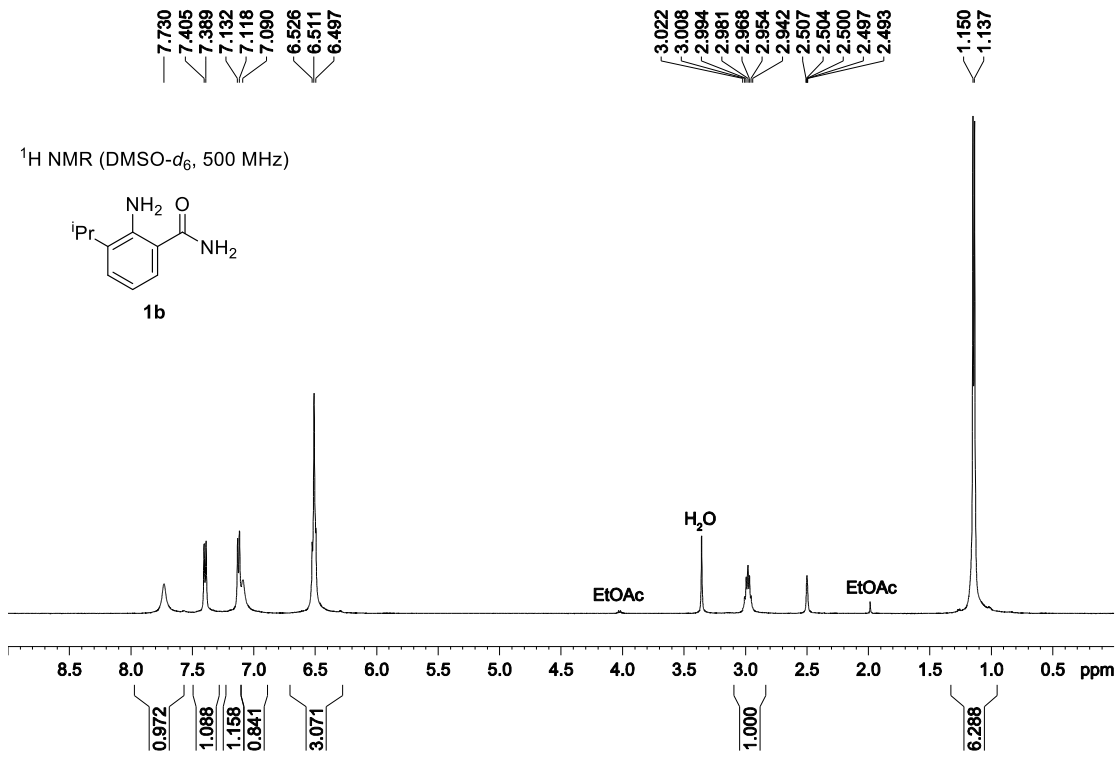

(b)

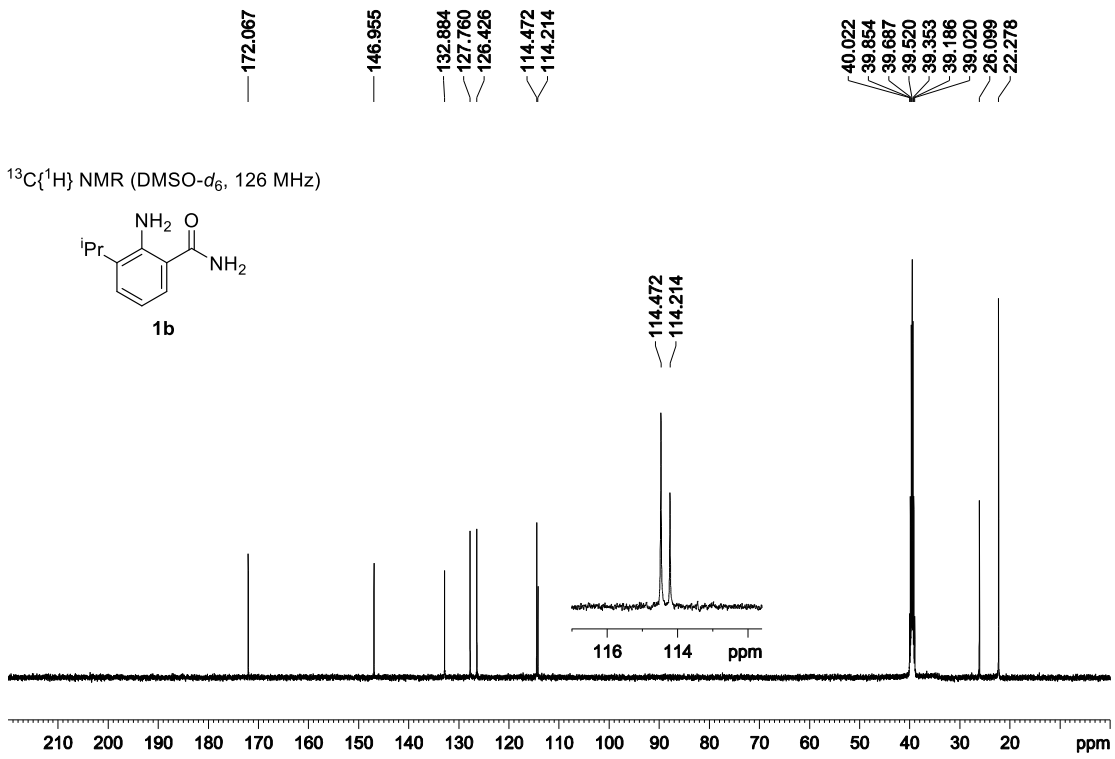

Figure 5.6. NMR spectra of **1b**.

(a)

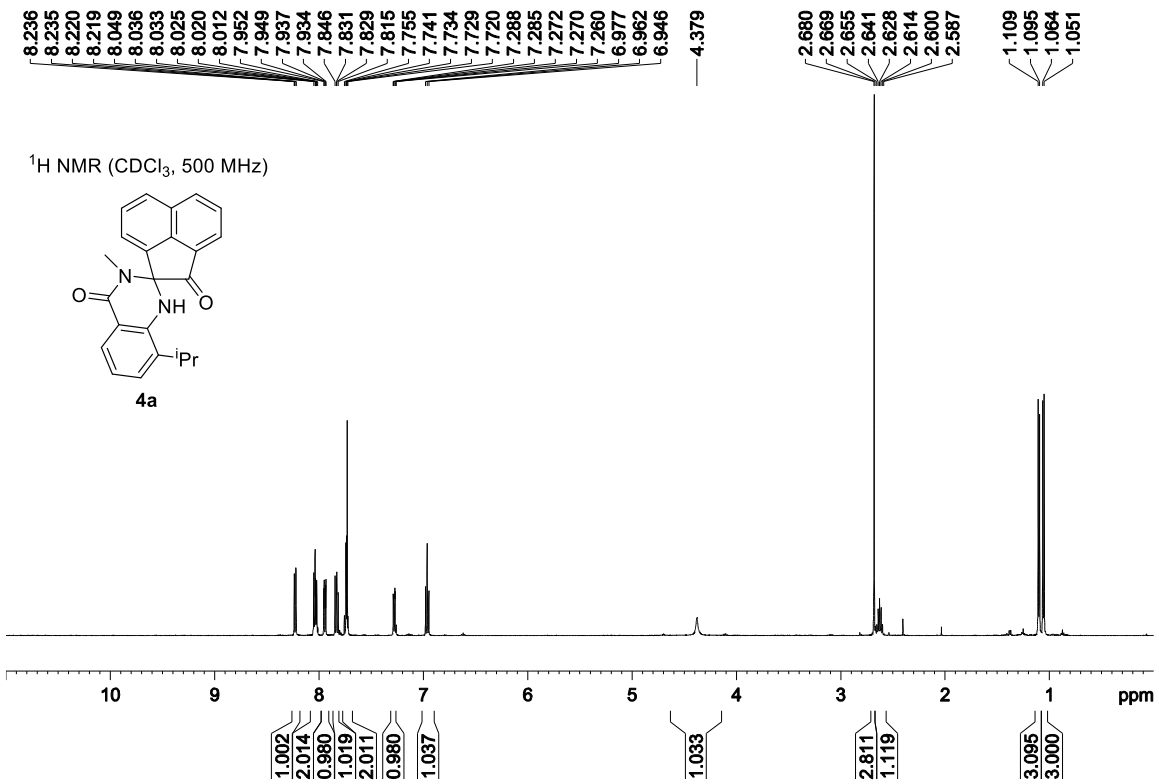

(b)

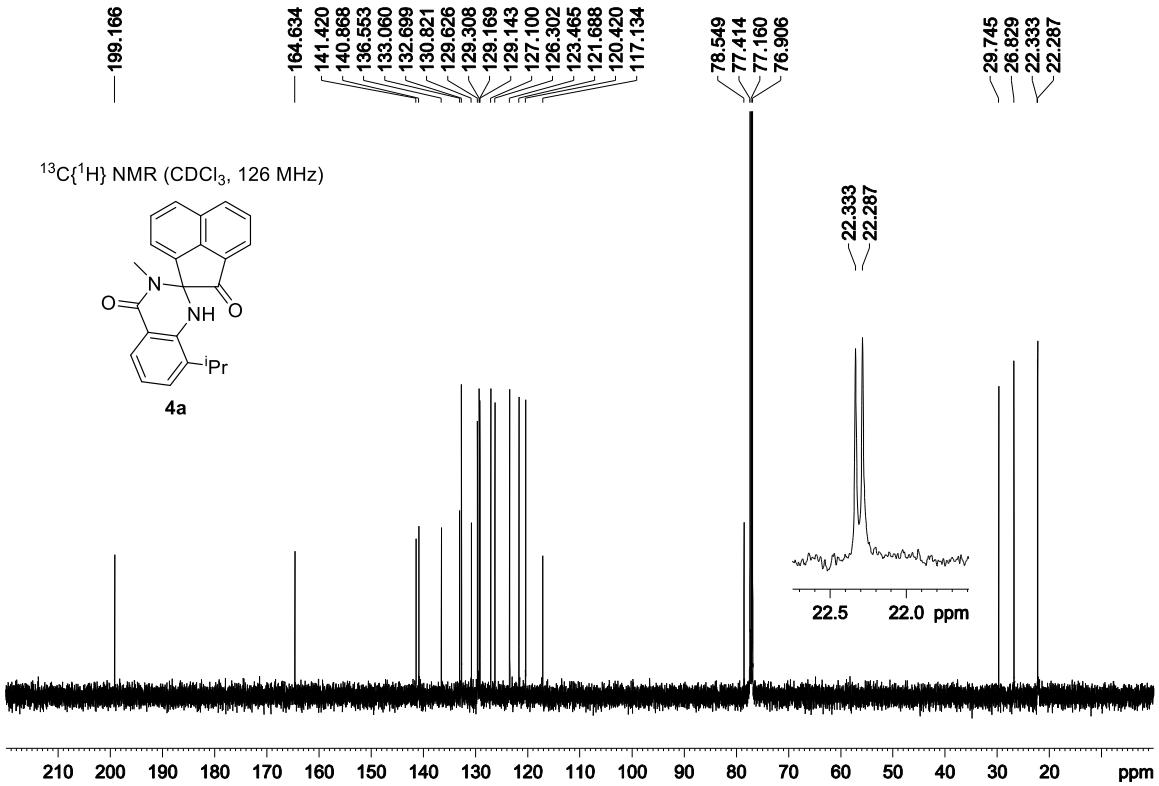

Figure 5.7. NMR spectra of **4a**.

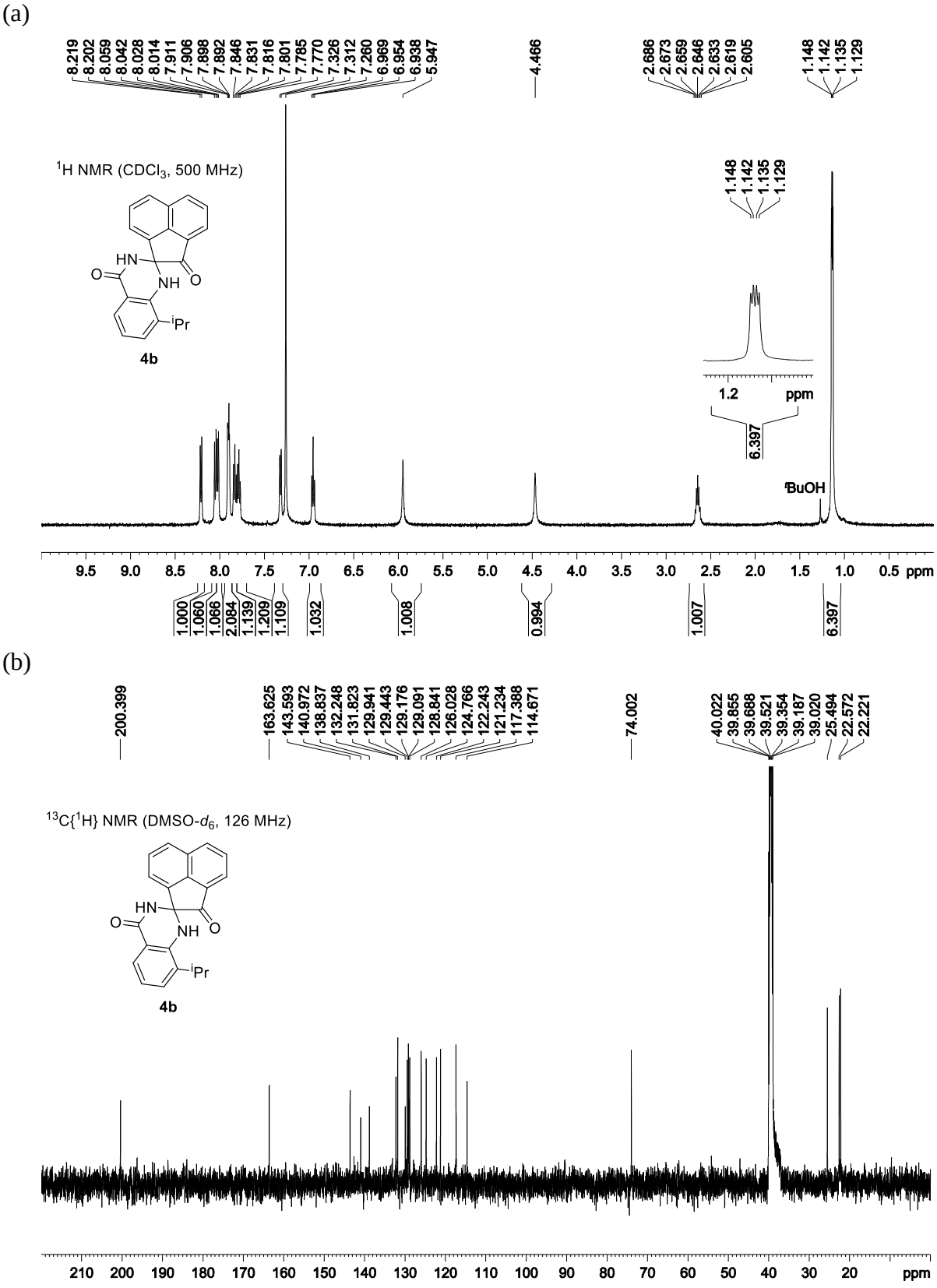

Figure 5.8. NMR spectra of **4b**.

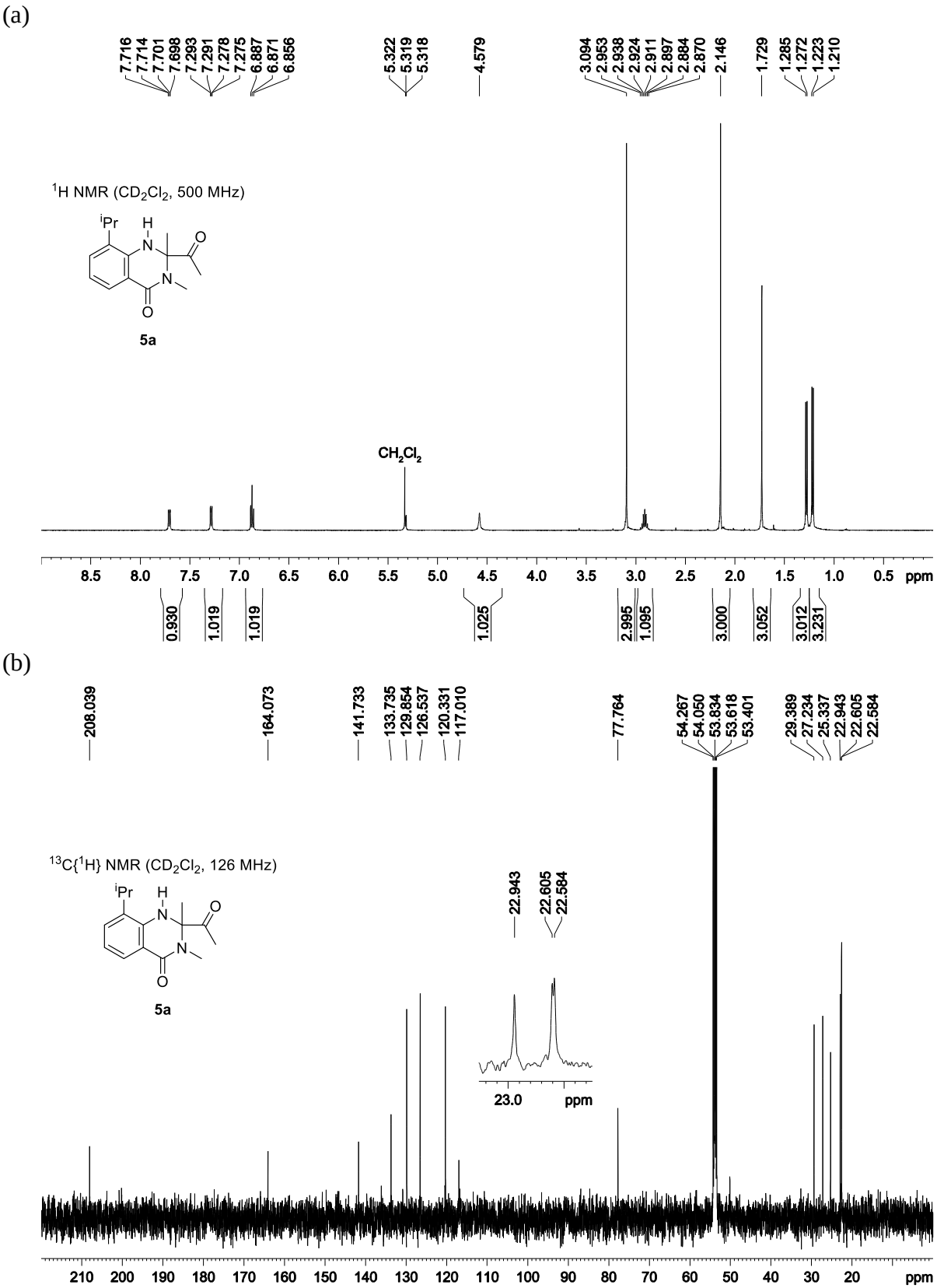

Figure 5.9. NMR spectra of **5a**.

(a)

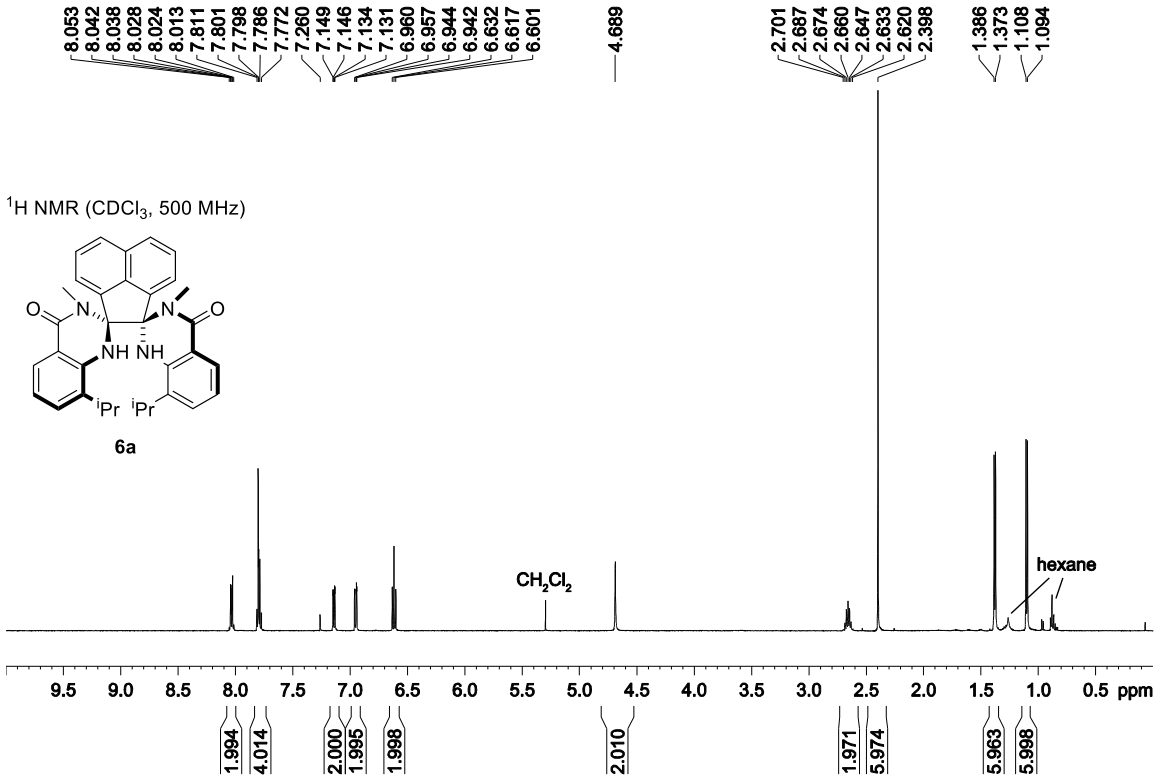

(b)

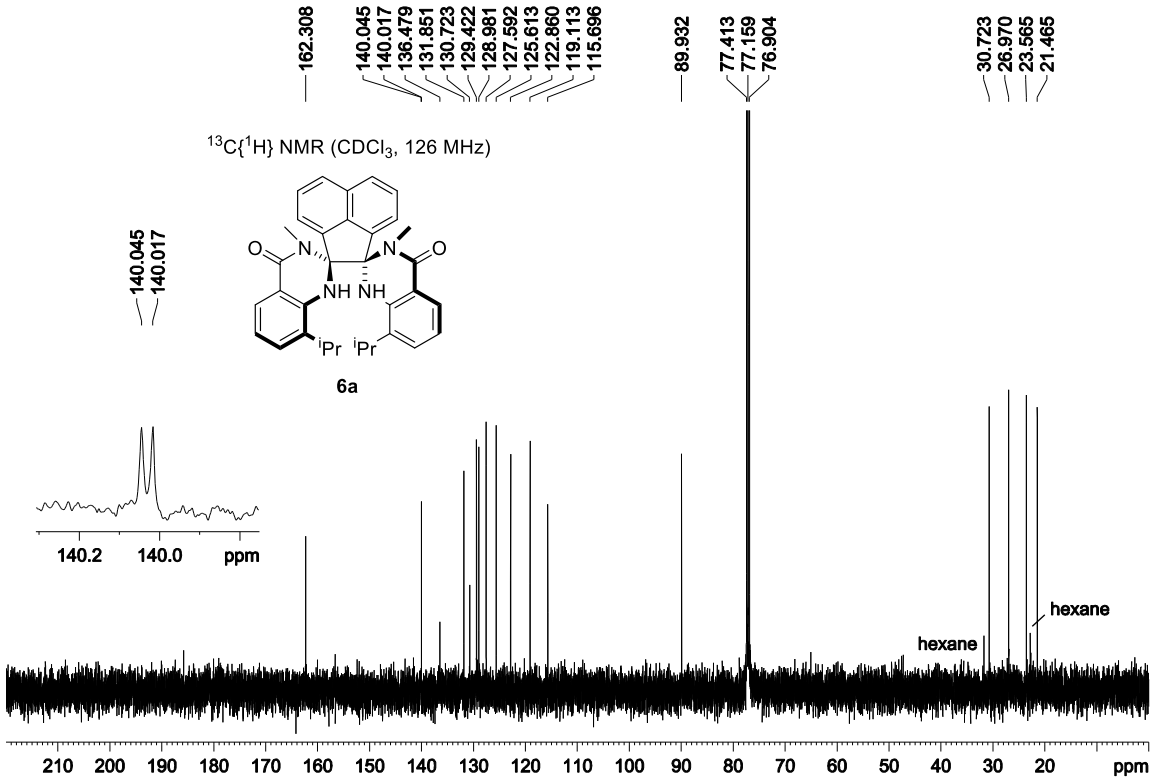

Figure 5.10. NMR spectra of **6a**.

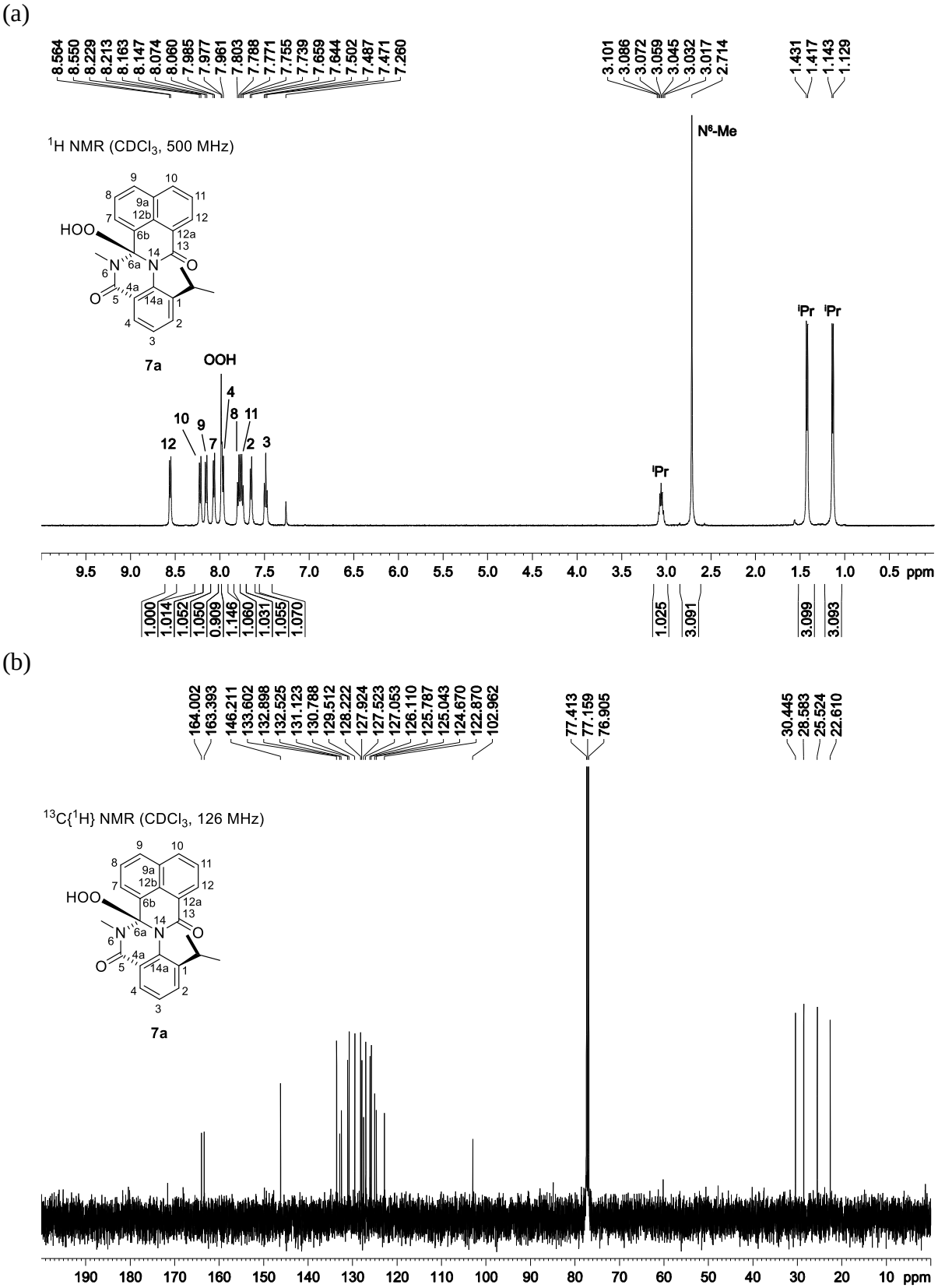

Figure 5.11. NMR spectra of **7a**.

(c)

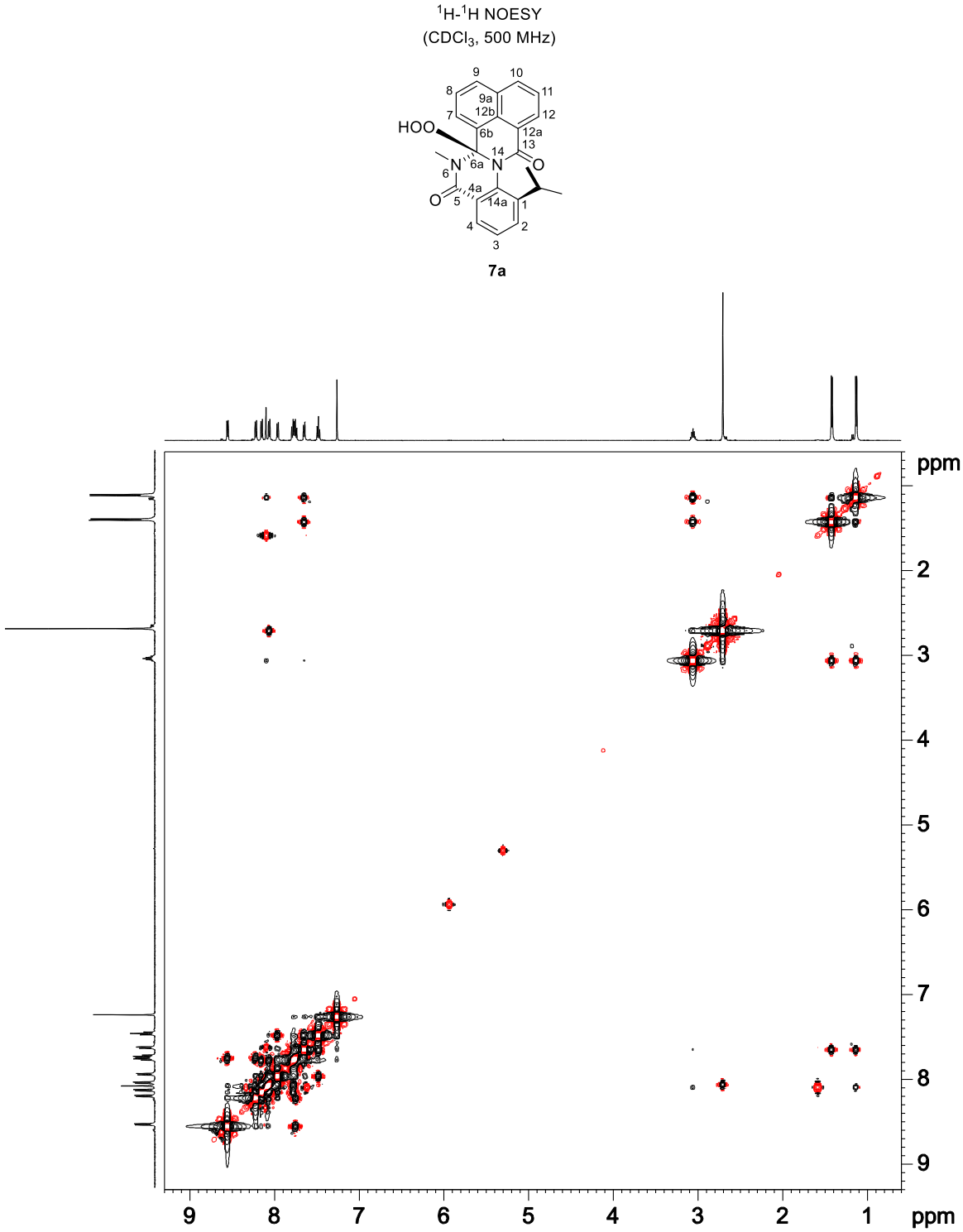

Figure 5.11, continued. NMR spectra of **7a**.

(d)

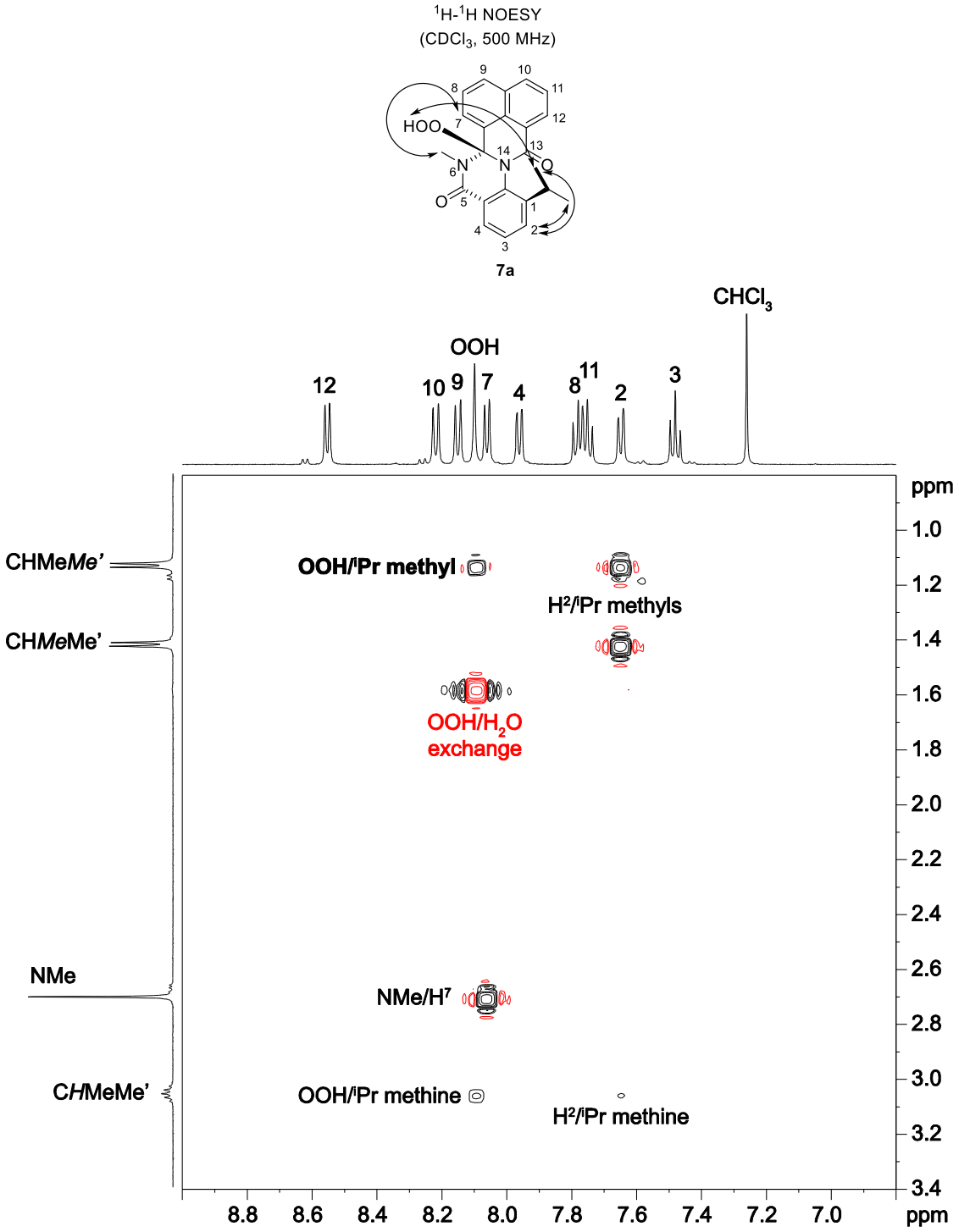

Figure 5.11, continued. NMR spectra of **7a**.

(e)

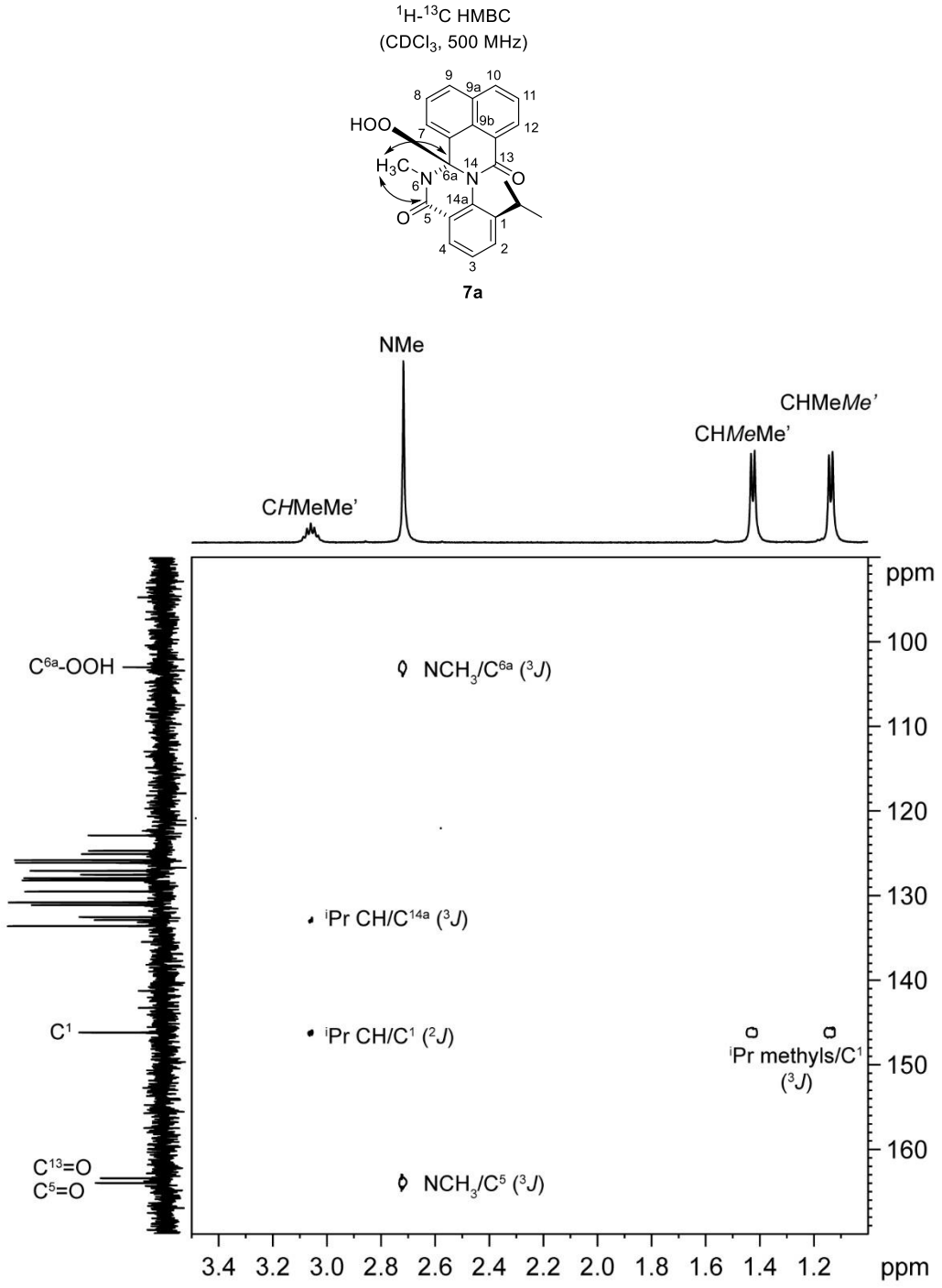

Figure 5.11, continued. NMR spectra of **7a**.

(a)

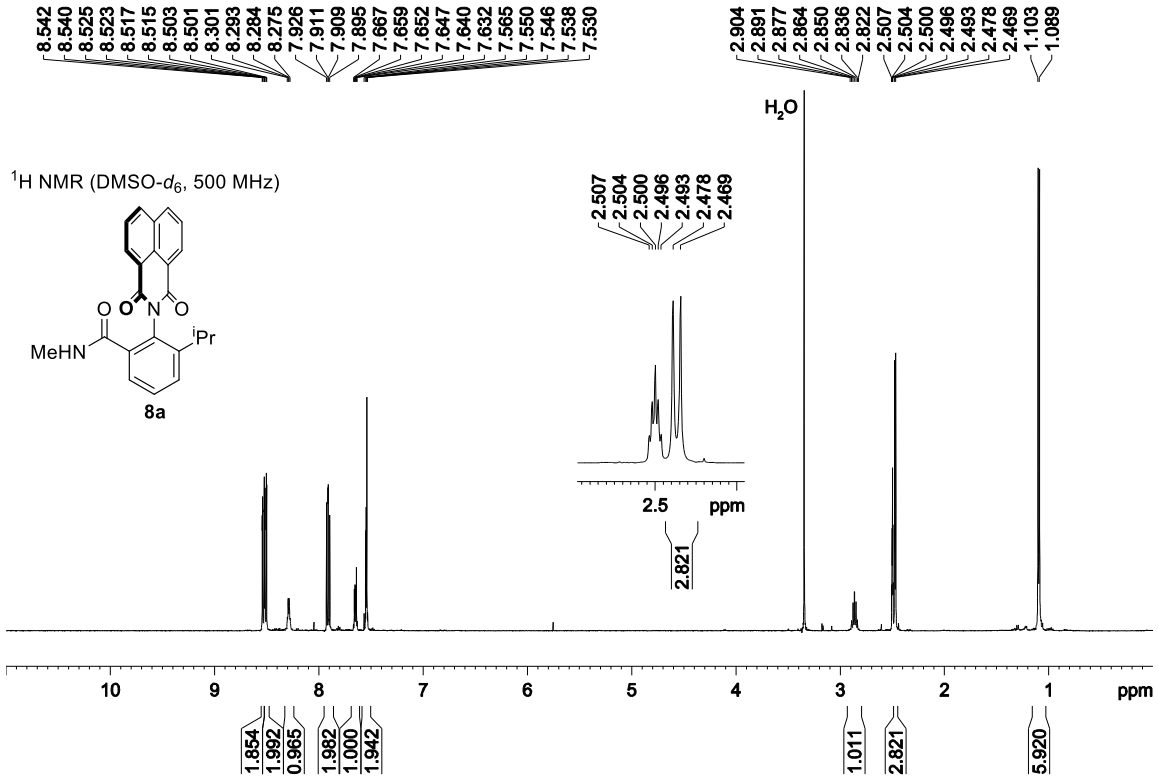

(b)

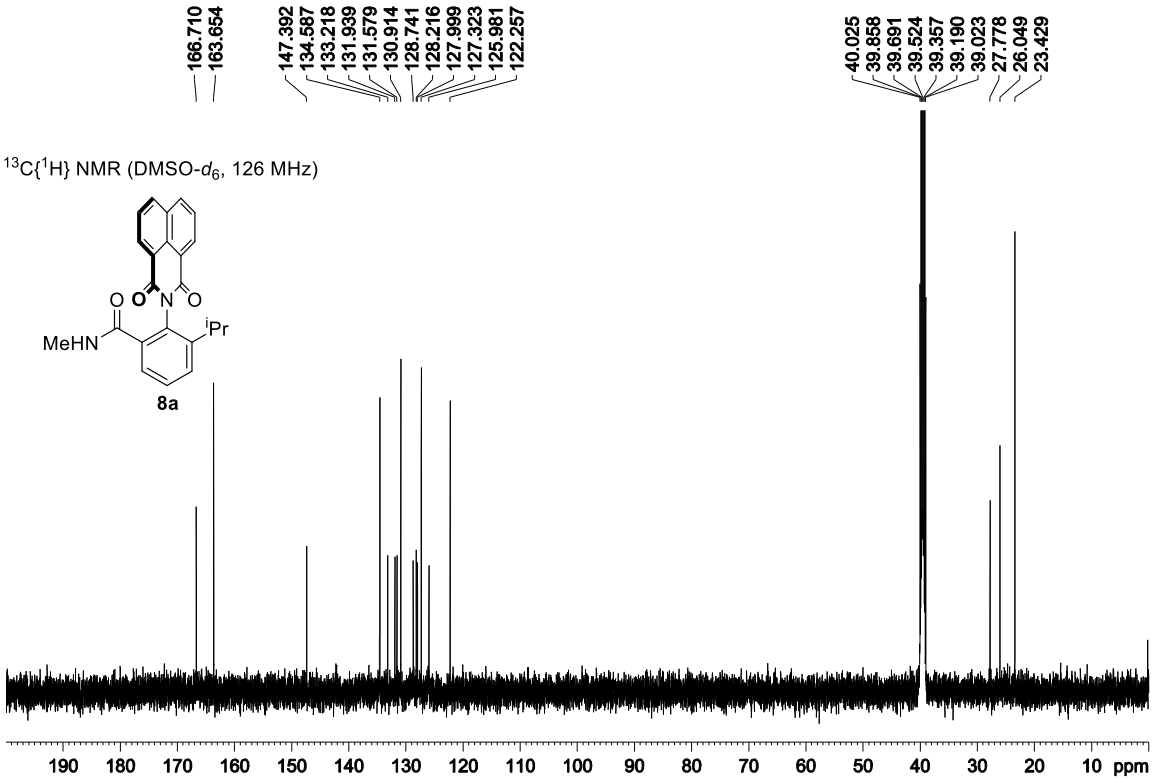

Figure 5.12. NMR spectra of **8a**.

(a)

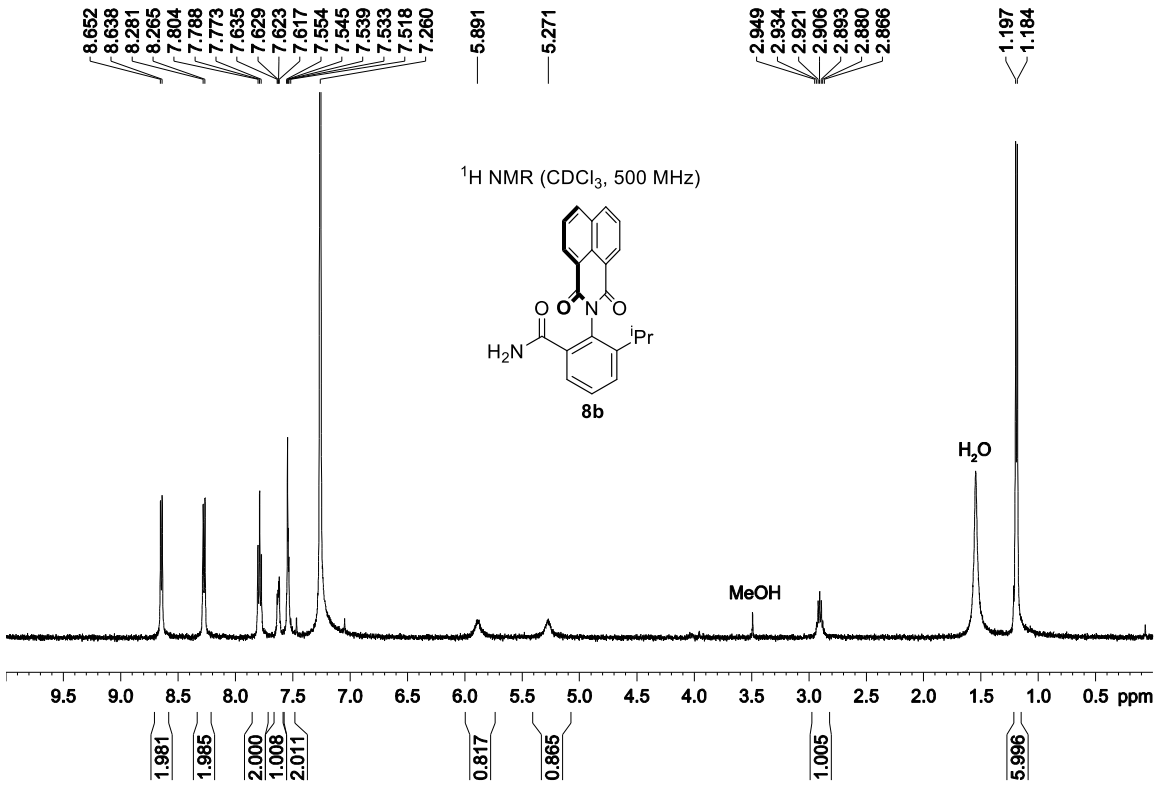

(b)

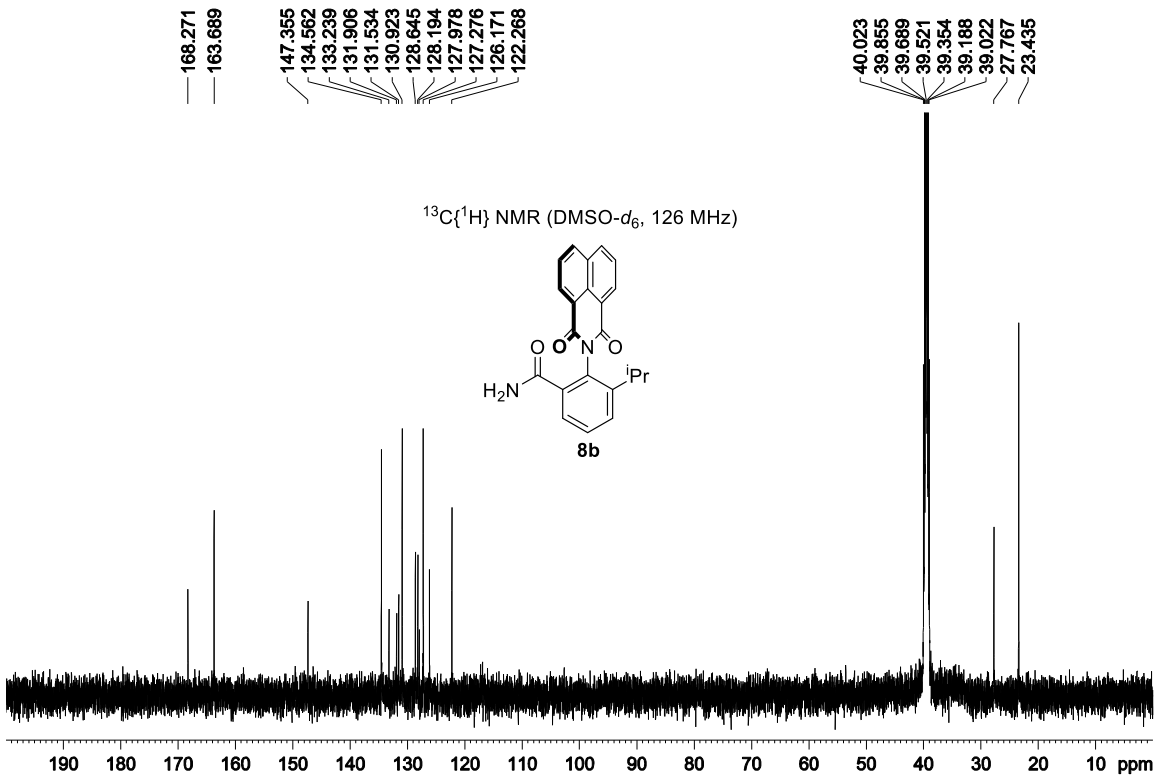

Figure 5.13. NMR spectra of **8b**.

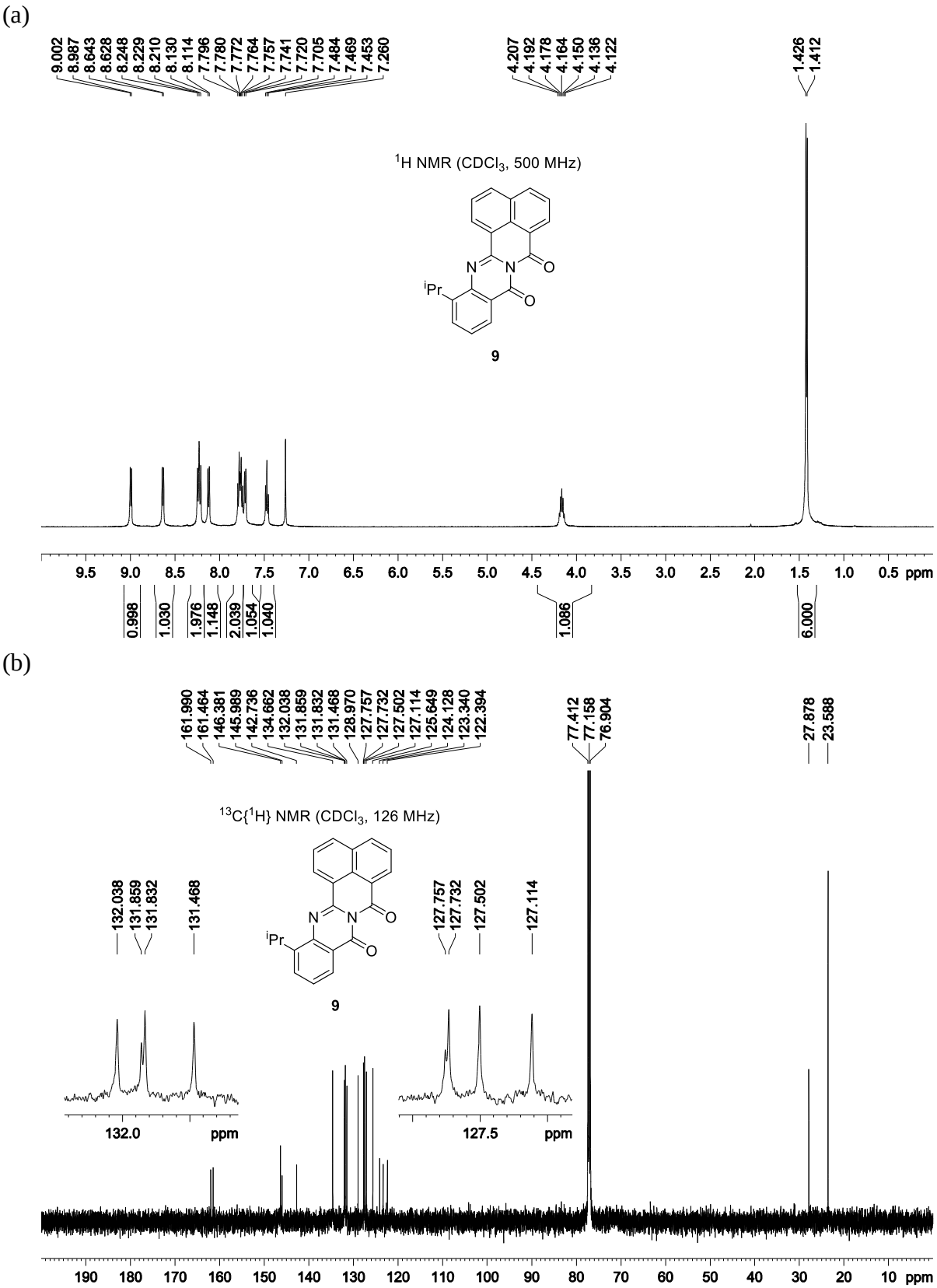

Figure 5.14. NMR spectra of **9**.

(a)

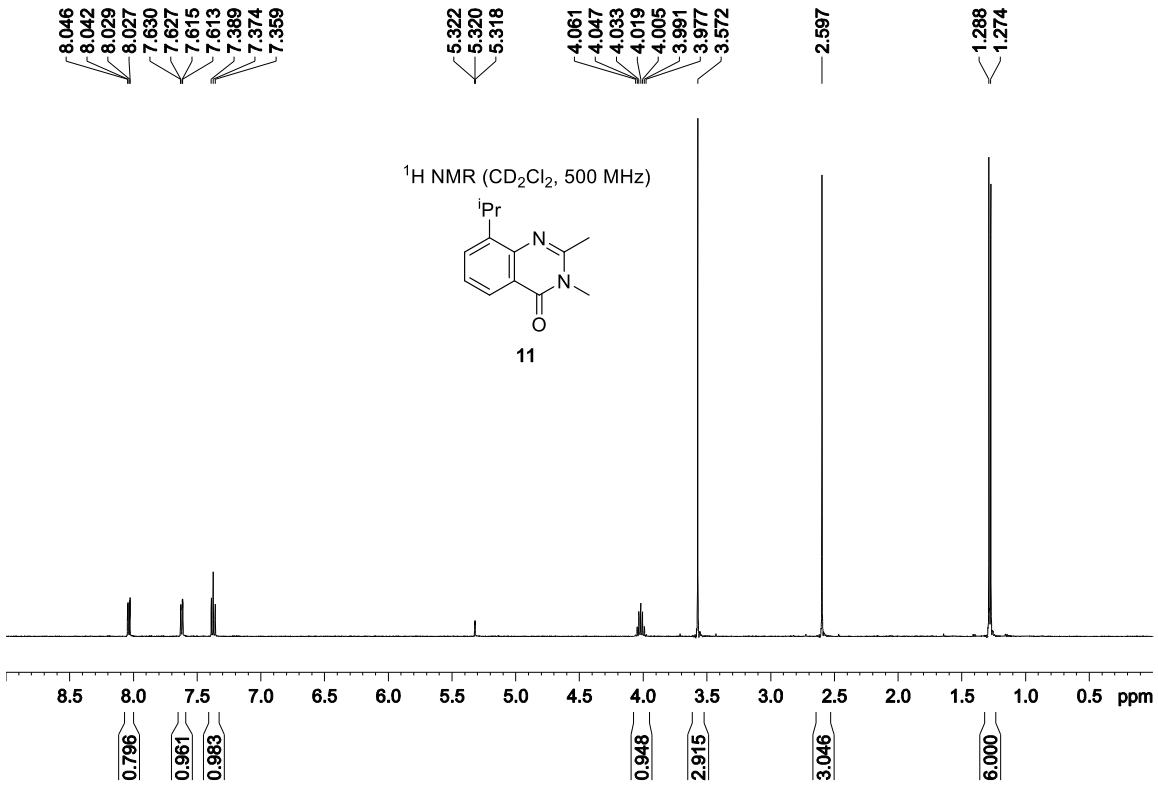

(b)

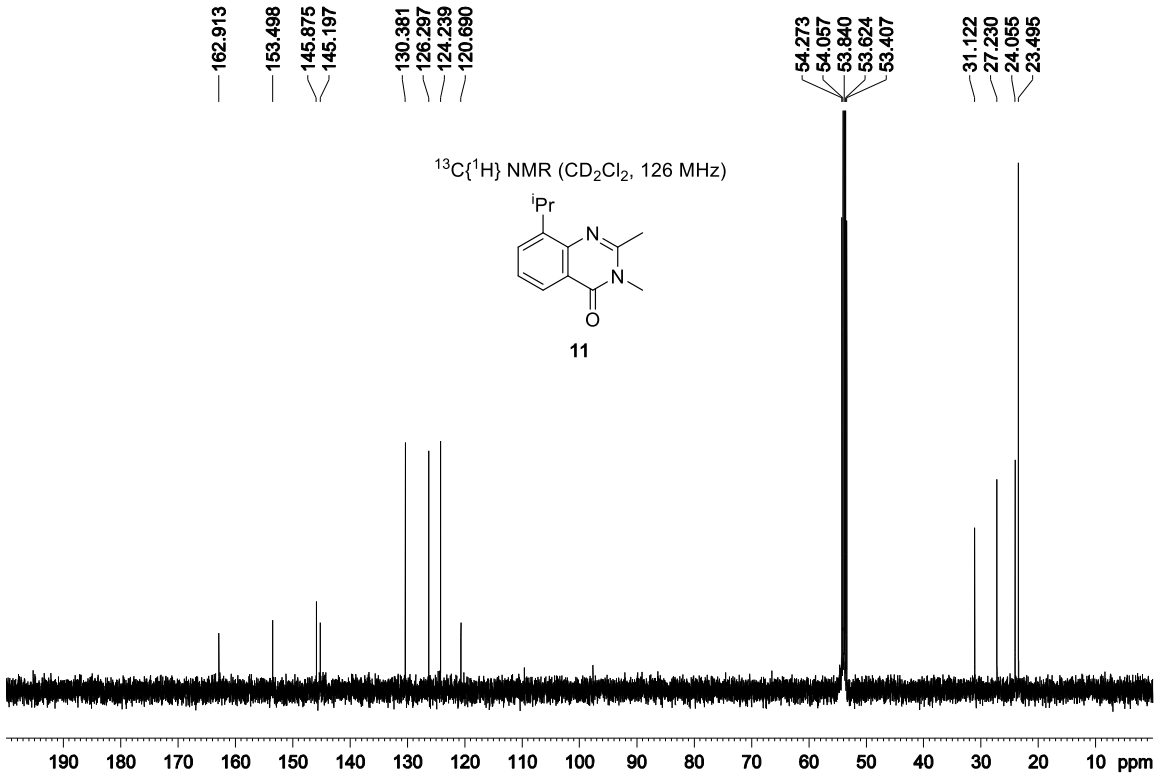

Figure 5.15. NMR spectra of **11**.

(a)

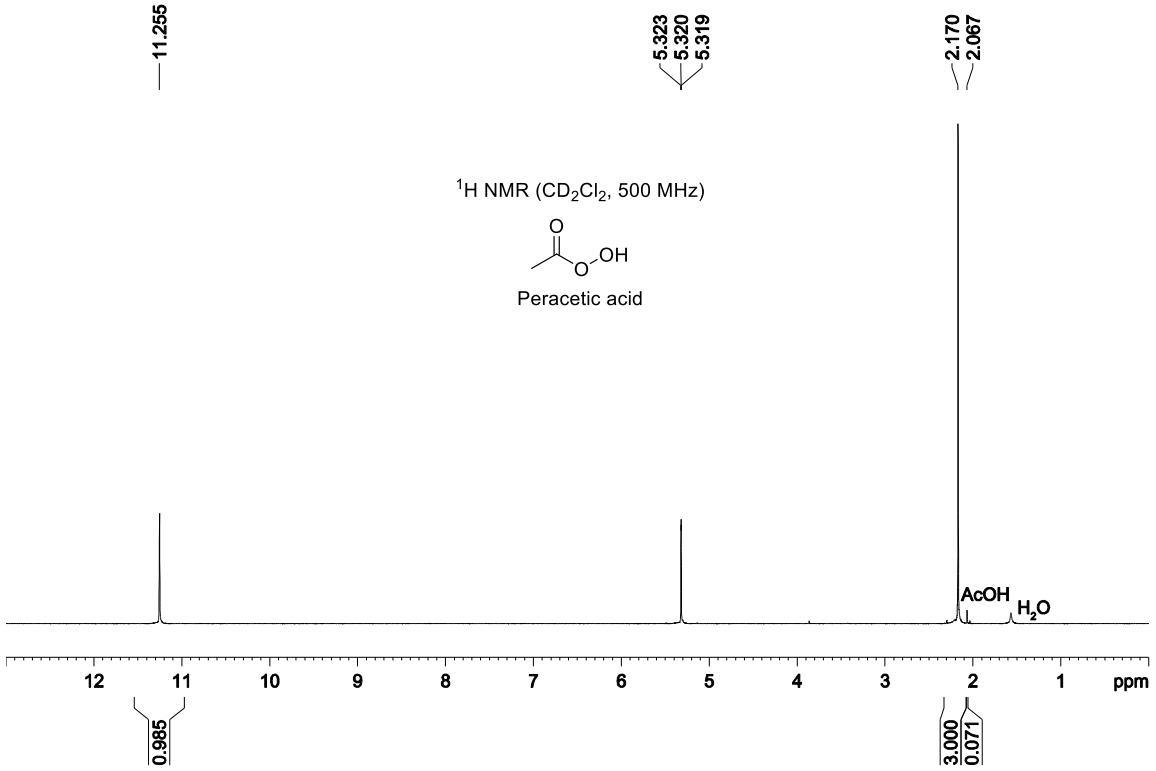

(b)

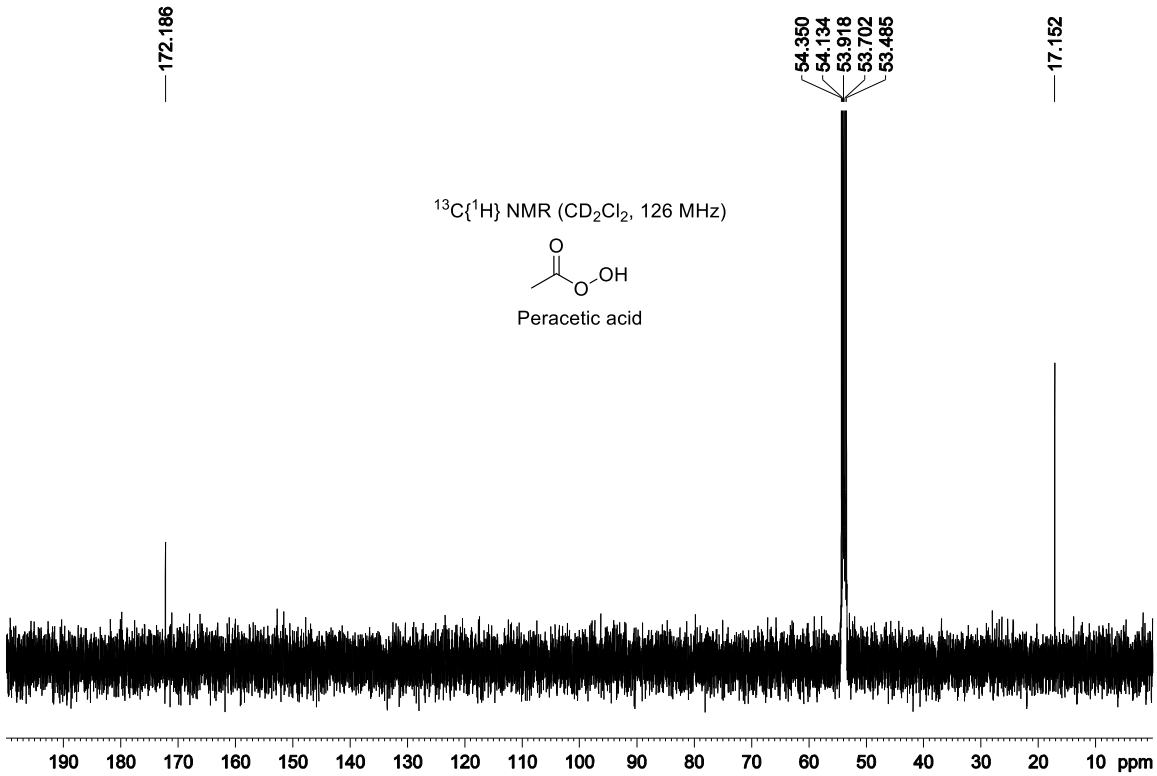

Figure 5.16. NMR spectra of peracetic acid.

(a)

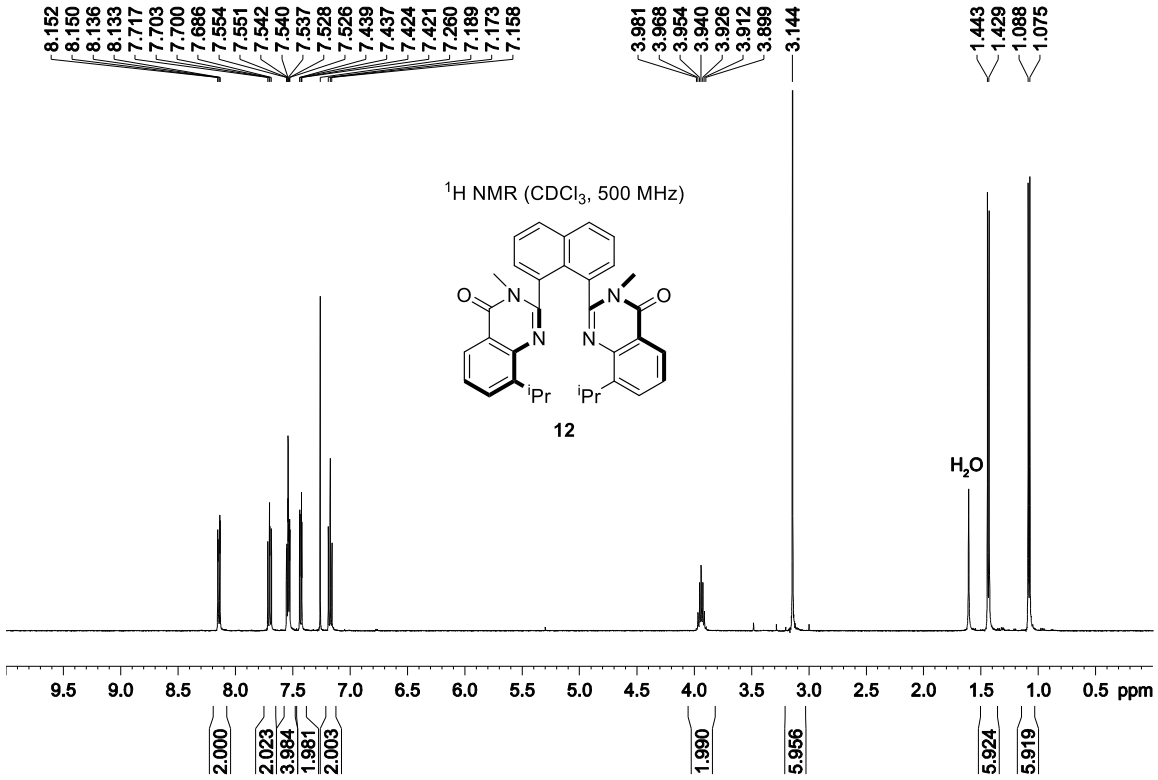

(b)

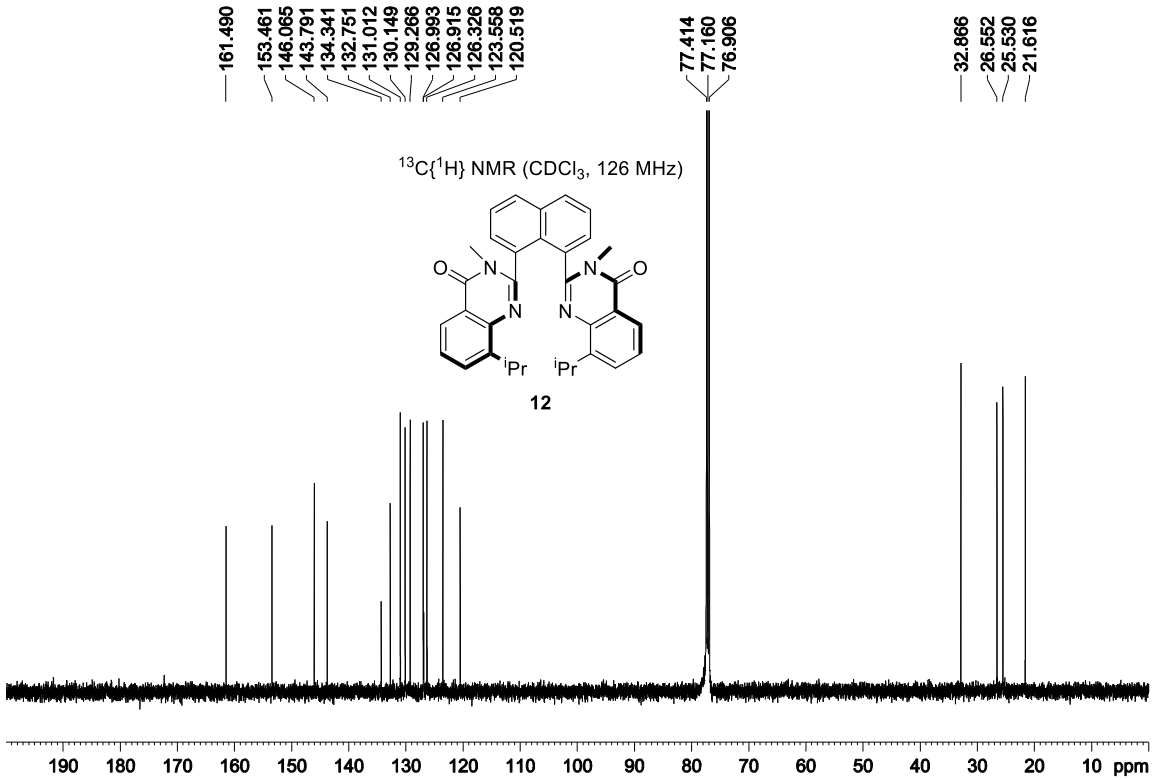

Figure 5.17. NMR spectra of **12**.

(a)

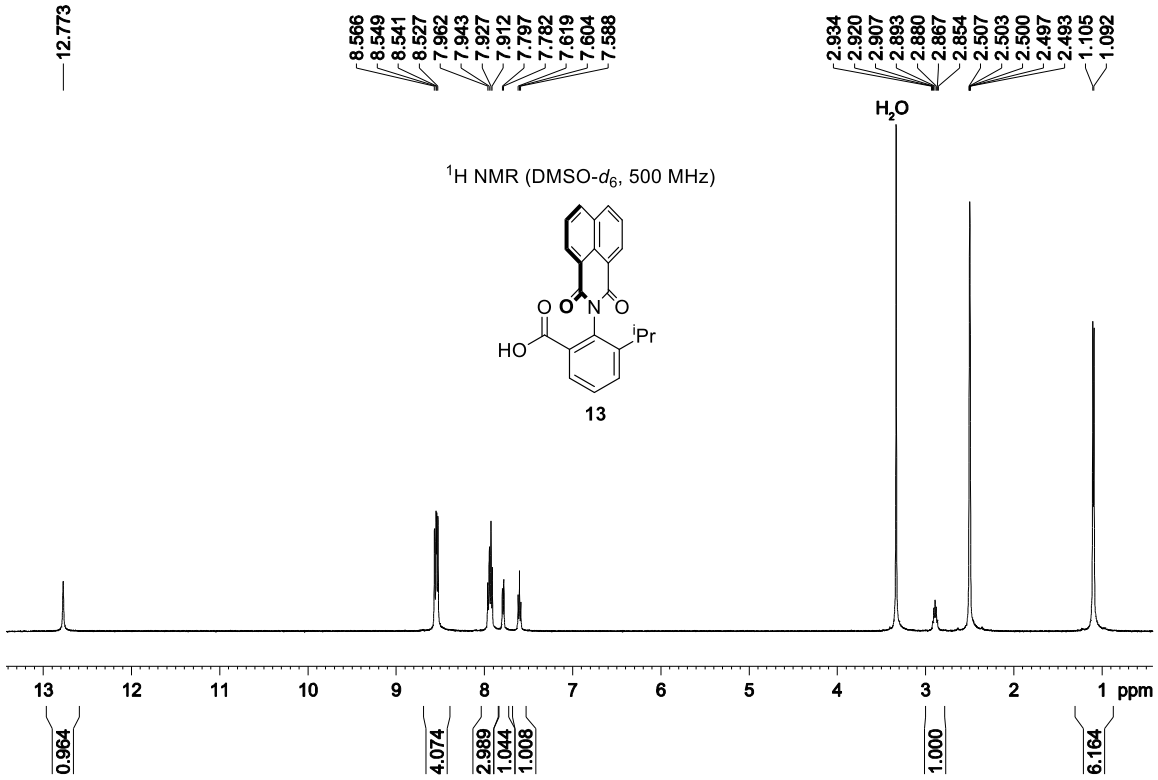

(b)

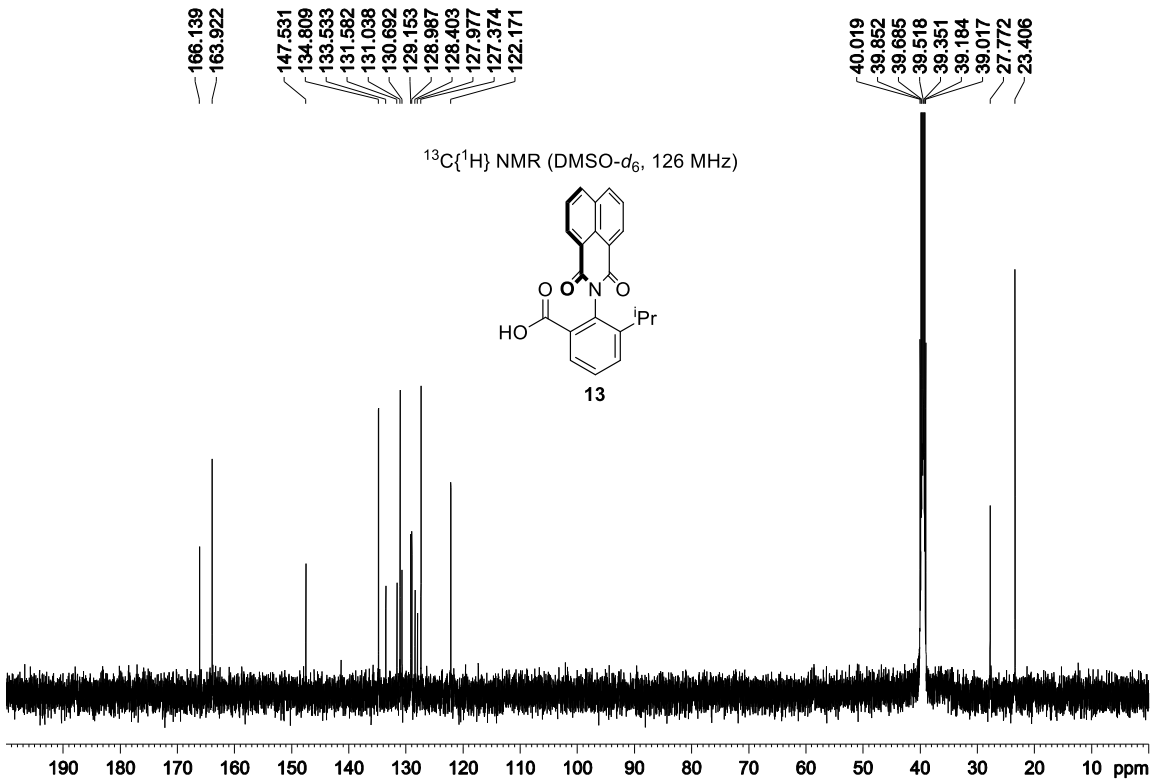

Figure 5.18. NMR spectra of **13**.

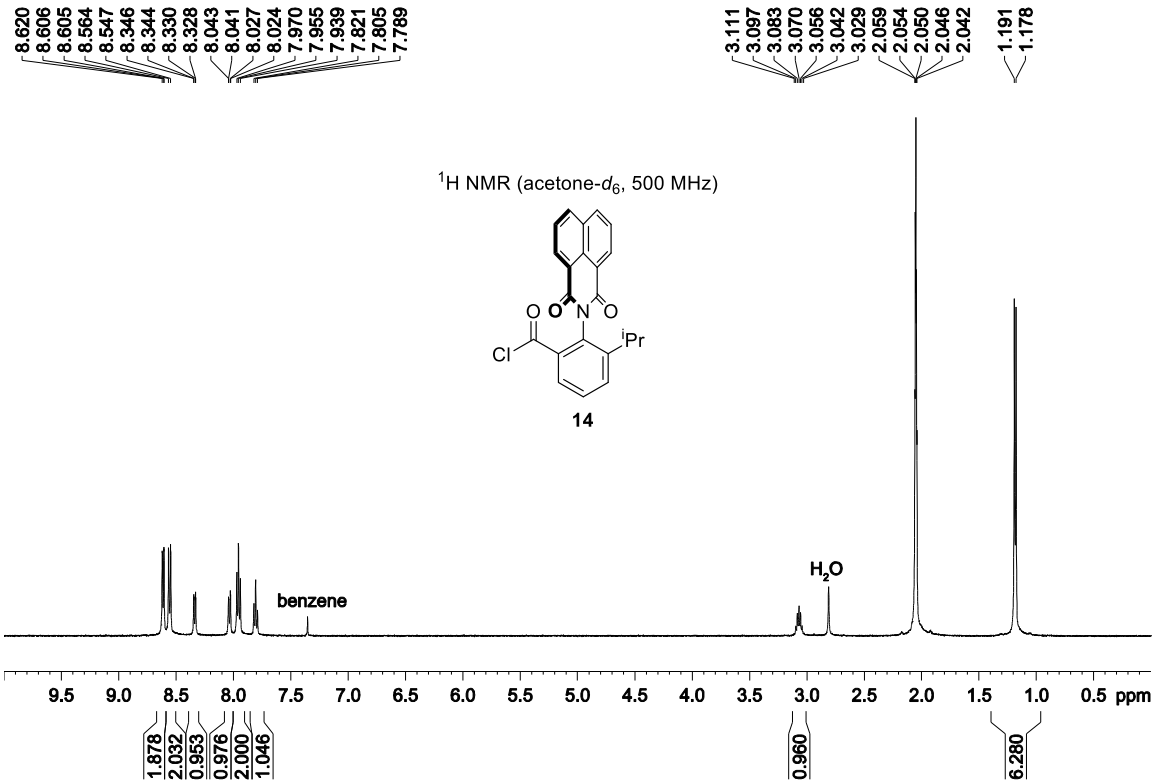

Figure 5.19. ^{1}H NMR spectrum of **14**.

Table 5.1. X-ray Crystallographic Parameters of 4a.

Empirical formula	$C_{23}H_{20}N_2O_2$	
Formula weight	356.41	
Temperature	100(2) K	
Wavelength	0.71073 Å	
Crystal system	Monoclinic	
Space group	$P2_1/c$	
Unit cell dimensions	a = 9.2660(11) Å	α = 90°.
	b = 15.0394(17) Å	β = 104.785(3)°.
	c = 13.5414(16) Å	γ = 90°.
Volume	1824.6(4) $Å^3$	
Z	4	
Density (calculated)	1.297 Mg/m^3	
Absorption coefficient	0.084 mm^{-1}	
F(000)	752	
Crystal size	0.270 x 0.150 x 0.060 mm^3	
Theta range for data collection	2.273 to 25.068°.	
Index ranges	-11<=h<=11, -17<=k<=17, -16<=l<=16	
Reflections collected	21427	
Independent reflections	3218 [R(int) = 0.0706]	
Completeness to theta = 25.068°	99.9 %	
Refinement method	Full-matrix least-squares on F^2	
Data / restraints / parameters	3218 / 37 / 290	
Goodness-of-fit on F^2	1.052	
Final R indices [I>2sigma(I)]	R1 = 0.0591, wR2 = 0.1177	
R indices (all data)	R1 = 0.1043, wR2 = 0.1356	
Extinction coefficient	n/a	
Largest diff. peak and hole	0.193 and -0.370 $e \cdot Å^{-3}$	

Table 5.2. X-ray Crystallographic Parameters of 6a.

Empirical formula	$C_{34}H_{34}N_4O_2$
Formula weight	530.65
Temperature/K	100(2)
Crystal system	trigonal
Space group	R-3
a/Å	33.259(3)
b/Å	33.259(3)
c/Å	15.5227(18)
α/°	90
β/°	90
γ/°	120
Volume/Å^3	14870(3)
Z	18
ρ_{calc}/g cm^{-3}	1.067
μ/mm^{-1}	0.067
F(000)	5076.0
Crystal size/mm^3	0.38 × 0.19 × 0.13
Radiation	MoKα (λ = 0.71073)
2Θ range for data collection/°	4.242 to 52.89
Index ranges	-41 ≤ h ≤ 41, -41 ≤ k ≤ 41, -19 ≤ l ≤ 19
Reflections collected	113664
Independent reflections	6786 [R_{int} = 0.0496, R_{sigma} = 0.0256]
Data/restraints/parameters	6786/33/384
Goodness-of-fit on F^2	1.055
Final R indexes [I>=2σ (I)]	R_1 = 0.0529, wR_2 = 0.1308
Final R indexes [all data]	R_1 = 0.0729, wR_2 = 0.1406
Largest diff. peak/hole / e Å^{-3}	0.52/-0.44

Table 5.3. X-ray Crystallographic Parameters of 7a

Empirical formula	$C_{23}H_{20}N_2O_4$
Formula weight	388.41
Temperature/K	100.0
Crystal system	trigonal
Space group	R-3
a/Å	42.788(3)
b/Å	42.788(3)
c/Å	7.4202(6)
α/°	90
β/°	90
γ/°	120
Volume/Å^3	11765(2)
Z	18
ρ_{calc}/g cm^{-3}	0.987
μ/mm^{-1}	0.068
F(000)	3672.0
Crystal size/mm^3	0.28 × 0.16 × 0.14
Radiation	MoKα (λ = 0.71073)
2Θ range for data collection/°	5.038 to 50.096
Index ranges	$-40 \leq h \leq 50$, $-50 \leq k \leq 49$, $-8 \leq l \leq 8$
Reflections collected	17818
Independent reflections	4528 [R_{int} = 0.0503]
Data/restraints/parameters	4528/0/269
Goodness-of-fit on F^2	1.058
Final R indexes [I>=2σ (I)]	R_1 = 0.0504, wR_2 = 0.1260
Final R indexes [all data]	R_1 = 0.0890, wR_2 = 0.1400
Largest diff. peak/hole / e Å^{-3}	0.33/-0.29

Table 5.4. X-ray Crystallographic Parameters of 8a.

Empirical formula	$C_{23}H_{20}N_2O_3$	
Formula weight	372.41	
Temperature	100(2) K	
Wavelength	0.71073 Å	
Crystal system	Triclinic	
Space group	P-1	
Unit cell dimensions	a = 7.4731(6) Å	α = 93.623(2)°.
	b = 9.4040(8) Å	β = 100.659(2)°.
	c = 14.3670(12) Å	γ = 111.227(2)°.
Volume	915.54(13) $Å^3$	
Z	2	
Density (calculated)	1.351 Mg/m^3	
Absorption coefficient	0.090 mm^{-1}	
F(000)	392	
Crystal size	0.250 x 0.190 x 0.110 mm^3	
Theta range for data collection	2.347 to 27.149°.	
Index ranges	-9<=h<=9, -12<=k<=12, -18<=l<=18	
Reflections collected	12673	
Independent reflections	4026 [R(int) = 0.0248]	
Completeness to theta = 25.242°	99.8 %	
Refinement method	Full-matrix least-squares on F^2	
Data / restraints / parameters	4026 / 0 / 260	
Goodness-of-fit on F^2	1.024	
Final R indices [I>2sigma(I)]	R1 = 0.0443, wR2 = 0.1062	
R indices (all data)	R1 = 0.0639, wR2 = 0.1161	
Extinction coefficient	n/a	
Largest diff. peak and hole	0.475 and -0.303 $e.Å^{-3}$	

Table 5.5. X-ray Crystallographic Parameters of 9.

Empirical formula	$C_{22}H_{16}N_2O_2$
Formula weight	340.37
Temperature/K	100.01
Crystal system	orthorhombic
Space group	$Pca2_1$
a/Å	22.720(3)
b/Å	8.2209(9)
c/Å	17.0117(19)
α/°	90
β/°	90
γ/°	90
Volume/Å^3	3177.5(6)
Z	8
ρ_{calc}/g cm^{-3}	1.423
μ/mm^{-1}	0.092
F(000)	1424.0
Crystal size/mm^3	0.28 × 0.06 × 0.02
Radiation	MoKα (λ = 0.71073)
2Θ range for data collection/°	4.312 to 54.908
Index ranges	$-29 \leq h \leq 26$, $-10 \leq k \leq 10$, $-16 \leq l \leq 21$
Reflections collected	23365
Independent reflections	5866 [R_{int} = 0.0532, R_{sigma} = 0.0601]
Data/restraints/parameters	5866/1/473
Goodness-of-fit on F^2	1.038
Final R indexes [I>=2σ (I)]	R_1 = 0.0439, wR_2 = 0.0834
Final R indexes [all data]	R_1 = 0.0731, wR_2 = 0.0936
Largest diff. peak/hole / e Å^{-3}	0.24/-0.22

Table 5.6. X-ray Crystallographic Parameters of 12.

Empirical formula	$C_{34}H_{32}N_4O_2$
Formula weight	528.63
Temperature	100(2) K
Wavelength	0.71073 Å
Crystal system	Monoclinic
Space group	*C*2/*c*
Unit cell dimensions	a = 18.3177(14) Å α = 90°. b = 11.2752(9) Å β = 100.871(3)°. c = 26.814(2) Å γ = 90°.
Volume	5438.8(7) $Å^3$
Z	8
Density (calculated)	1.291 Mg/m^3
Absorption coefficient	0.082 mm^{-1}
F(000)	2240
Crystal size	0.440 x 0.260 x 0.250 mm^3
Theta range for data collection	2.264 to 27.189°.
Index ranges	-23<=h<=23, -14<=k<=14, -33<=l<=33
Reflections collected	43993
Independent reflections	6023 [R(int) = 0.0480]
Completeness to theta = 25.242°	99.9 %
Refinement method	Full-matrix least-squares on F^2
Data / restraints / parameters	6023 / 0 / 367
Goodness-of-fit on F^2	1.038
Final R indices [I>2sigma(I)]	R1 = 0.0427, wR2 = 0.1036
R indices (all data)	R1 = 0.0593, wR2 = 0.1128
Extinction coefficient	n/a
Largest diff. peak and hole	0.314 and -0.259 e.$Å^{-3}$

5.5 References and Notes

(1) Danen, W. C.; Neugebauer, F. A. *Angew. Chem., Int. Ed. Engl.* **1975**, *14*, 783.

(2) Newcomb, M.; Deeb, T. M.; Marquardt, D. J. *Tetrahedron* **1990**, *46*, 2317.

(3) Bowman, W. R.; Clark, D. N.; Marmon, R. J. *Tetrahedron Lett.* **1991**, *32*, 6441.

(4) Bowman, W. R.; Stephenson, P. T.; Young, A. R. *Tetrahedron Lett.* **1995**, *36*, 5623.

(5) Lewis, F. D.; Correa, P. E. *J. Am. Chem. Soc.* **1981**, *103*, 7347.

(6) Musa, O. M.; Horner, J. H.; Shahin, H.; Newcomb, M. *J. Am. Chem. Soc.* **1996**, *118*, 3862.

(7) Maeda, Y.; Ingold, K. U. *J. Am. Chem. Soc.* **1980**, *102*, 328.

(8) Friestad, G. K. *Tetrahedron* **2001**, *57*, 5461.

(9) Horton, D. A.; Bourne, G. T.; Smythe, M. L. *Chem. Rev.* **2003**, *103*, 893.

(10) Mhaske, S. B.; Argade, N. P. *Tetrahedron* **2006**, *62*, 9787.

(11) For related chemistry, see: (a) Bergman, J.; Arewång, C.-J.; Svensson, P. H. *J. Org. Chem.* **2014**, *79*, 9065; (b) Cabrera-Rivera, F. A.; Ortz-Nava, C.; Escalante, J.; Hernández-Pérez, J. M.; Hô, M. *Synlett* **2012**, *23*, 1057; (c) Bergman, J.; Bergman, S. *J. Org. Chem.* **1985**, *50*, 1246.

(12) Wang, L.-X.; Xiang, J.-F.; Tang, Y.-L. *Eur. J. Org. Chem.* **2014**, 2682.

(13) Hu, B.-Q.; Wang, L.-X.; Yang, L.; Xiang, J.-F.; Tang, Y.-L. *Eur. J. Org. Chem.* **2015**, 4504.

(14) Moore, J. A.; Sutherland, G. J.; Sowerby, R.; Kelly, E. G.; Palermo, S.; Webster, W. *J. Org. Chem.* **1969**, *34*, 887.

(15) Zhai, F.; Jordan, R. F. *Organometallics* **2014**, *33*, 7176.

(16) Revathy, K.; Lalitha, A. *J. Iran. Chem. Soc.* **2015**, *12*, 2045.

(17) Mane, M. M.; Pore, D. M. *J. Chem. Sci.* **2016**, *128*, 657.

(18) Hu, Y.; Wang, M. M.; Chen, H.; Shi, D. Q. *Tetrahedron* **2011**, *67*, 9342.

(19) Allen, F. H.; Kennard, O.; Watson, D. G.; Brammer, L.; Orpen, A. G.; Taylor, R. *J. Chem. Soc., Perkin Trans. 2* **1987**, S1.

(20) Parvez, M.; Simion, D. V.; Sorensen, T. S. *Acta Cryst.* **2001**, *E57*, o366.

(21) Caram, J. A.; Mirífico, M. V.; Aimone, S. L.; Piro, O. E.; Castellano, E. E.; Vasini, E. J. *J. Phys. Org. Chem.* **2004**, *17*, 1091.

(22) Kawai, H.; Takeda, T.; Fujiwara, K.; Suzuki, T. *Tetrahedron Lett.* **2004**, *45*, 8289.

(23) Dorninger, R.; Klepp, K.; Rametsteiner, R.; Schiffer, R.; Schmidt, H.; Schwarzinger, C. *Monatsh. Chem.* **2006**, *137*, 185.

(24) Hartung, J.; Svoboda, I. In *The Chemistry of Peroxides*; Rappoport, Z., Ed.; John Wiley & Sons: Chichester, UK, 2006; Vol. 2, pp 93-144.

(25) Pratt, D. A.; DiLabio, G. A.; Mulder, P.; Ingold, K. U. *Acc. Chem. Res.* **2004**, *37*, 334.

(26) **4b** undergoes slow aerobic oxidation at room temperature in CD_2Cl_2/TFA (100:1) and in $CDCl_3$ that was not freshly distilled, while the same reaction does not occur in CD_2Cl_2/CD_3CO_2D (9:1). These results show that strong acid or trace strongly acidic impurity may promote this autoxidation. We speculate that strong acid may facilitate the rate-determining H-atom transfer step from **7b** to peroxyl radical via an acid-catalysis mechanism proposed by Pratt et al. See: Valgimigli, L.; Amorati, R.; Petrucci, S.; Pedulli, G. F.; Hu, D.; Hanthorn, J. J.; Pratt, D. A. *Angew.*

Chem., Int. Ed. **2009**, *48*, 8348.

(27) Ponomarev, I. I.; Skuratova, N. A.; Lindeman, S. V.; Sinichkin, M. K.; Vinogradova, S. V.; Rusanov, A. L. *Vysokomol. Soedin.* **1994**, *36*, 730.

(28) Lindeman, S. V.; Ponomarev, I. I.; Rusanov, A. L. *Acta Cryst.* **1995**, *C51*, 2157.

(29) Trace AcOH (ca. 5%) was observed in the reaction, likely due to decomposition of peracetic acid, reaction with unreacted **5a**, or involvement of trace reductive impurity.

(30) Kawai, H.; Takeda, T.; Fujiwara, K.; Wakeshima, M.; Hinatsu, Y.; Suzuki, T. *Chem. Eur. J.* **2008**, *14*, 5780.

(31) van der Sluis, P.; Spek, A. L. *Acta Cryst.* **1990**, *A46*, 194.

(32) Spek, A. L. *Acta Cryst.* **2015**, *C71*, 9.

(33) Spek, A. L. *Acta Cryst.* **2009**, *D65*, 148.

CHAPTER SIX

6-Iminoyl Dihydroindolo[3,2-*c*]quinoline as an α-Aminoimine-Type Bidentate Ligand

6.1 Introduction

α-Aminoimine compounds may serve as bidentate N,N ligands in metal complexes, and their unsymmetrical structures lead to interesting isomerism phenomena in square planar (N^N)PdMeCl complexes.[1-2] Pd complexes that contain sterically bulky α-aminoimine ligands have been exploited as catalysts for Suzuki-Miyaura coupling reactions of aryl bromides and chlorides,[3] living polymerization of ethylene, and the copolymerization of methyl acrylate (MA) and ethylene to form copolymers with in-chain MA units.[4] Several (α-aminoimine)Pd complexes have been characterized crystallographically (Chart 6.1),[3-4] but the structural diversity of this class of compounds has not been elaborated.

Chart 6.1. Crystallographically Characterized Square Planar (α-Aminoimine)Pd Complexes

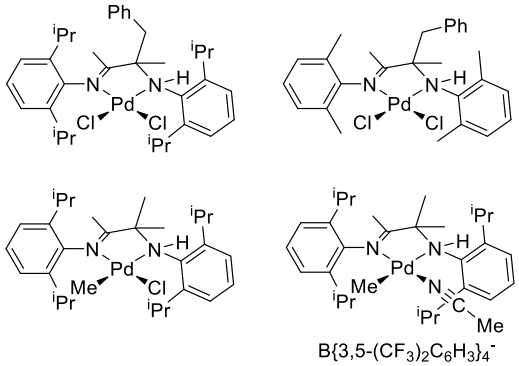

Chapter Two describes the reaction of 2-iminoyl-dihydroquinazolinone **A** and $(MeCN)_2PdCl_2$, which yields the amide-functionalized (α-diimine)$PdCl_2$ complex **B** through metalation-triggered C-N bond cleavage and ring opening (Scheme 6.1).[5] In an attempt to synthesize the indolyl-substituted (α-diimine)$PdCl_2$ complex **C** by a similar ring opening reaction

of 6-iminoyl-dihydroindolo[3,2-*c*]quinoline compound **6**, **(6)PdCl$_2$**, which contains the intact non-ring-opened ligand **6**, was formed. This chapter describes the synthesis of **6** and **(6)PdCl$_2$** and the single crystal structure of the latter compound.

Scheme 6.1

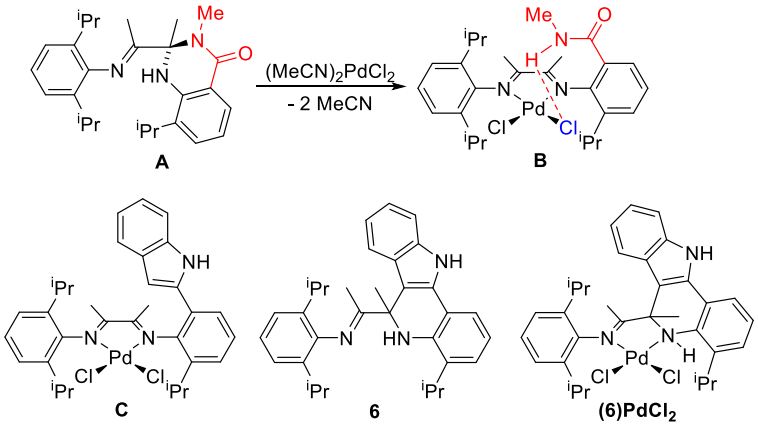

6.2 Results and Discussion

Indolylaniline compound **4** was prepared through a typical Fischer indole synthesis, as shown in Scheme 6.2. The reaction of anthranilic acid **1** with 3.0 equiv of MeLi yielded *o*-aminoacetophenone **2**.[6,7] Condensation of **2** with phenylhydrazine afforded the corresponding phenylhydrazone as a mixture of E,Z isomers (**3-*E*,*Z***), which was converted to indole **4** under acidic conditions.

Scheme 6.2

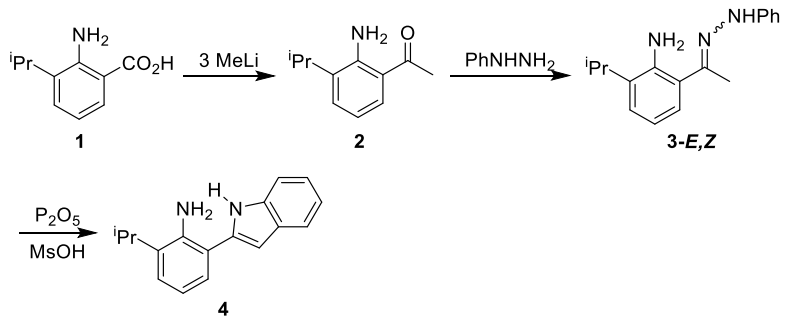

While **3-*E*** and **3-*Z*** were not separated, samples enriched in either isomer were obtained during crystallization experiments and enabled NMR assignments. Intramolecular H-bonding between the amino group and the hydrazone N-atom is possible for **3-*E***, whereas this interaction is strongly disfavored in **3-*Z*** due to steric repulsion (Scheme 6.3). Similar E,Z isomeris, of *ortho*-amino (or amido) phenyl ketone hydrazones has been observed in the solid state.[8,9]

The ^{1}H NMR chemical shifts of the amino groups in **3-*E*** (δ 6.00) and **3-*Z*** (δ 3.78) in $CDCl_3$ differ by 2.22 ppm due to the presence of intramolecular H-bonding in **3-*E***. Interestingly, the room-temperature ^{1}H and ^{13}C NMR spectra of **3-*E*** each contain a single sharp resonance for the isopropyl Me groups, whereas the NMR spectra of **3-*Z*** contain two broad resonances for the two isopropyl Me groups (a and b, Scheme 6.3). These results show that the isopropyl Me groups in **3-*E*** are equivalent as expected for the H-bonded planar structure, while those in **3-*Z*** are inequivalent, consistent with a sterically-induced non-planar conformation.

Scheme 6.3

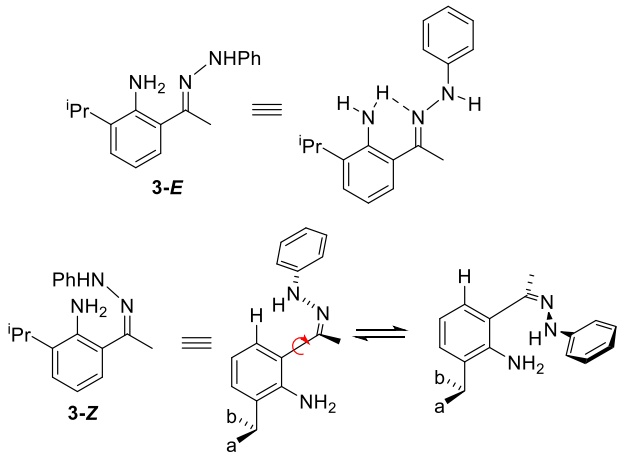

The condensation reaction between α-ketaimine **5** and indolylaniline **4** forms the dihydroindolo[3,2-*c*]quinoline product **6** by initial generation of the expected diimine product followed by nucleophilic attack of indole-C^3 (not N^1) on the adjacent imine carbon and a 1,3-H^+

shift (Scheme 6.4). Nucleophilic attack of the indole nitrogen N^1 on the imine carbon, analogous to the cyclization reaction that generates **A**, would generate **6'**, which was not observed. Product **6** was isolated in low (9%) yield. The ^{1}H NMR spectrum of **6** exhibits a broad signal at δ 8.42 for the indole N-*H* unit, consistent with the assignment of structure **6**.

Scheme 6.4

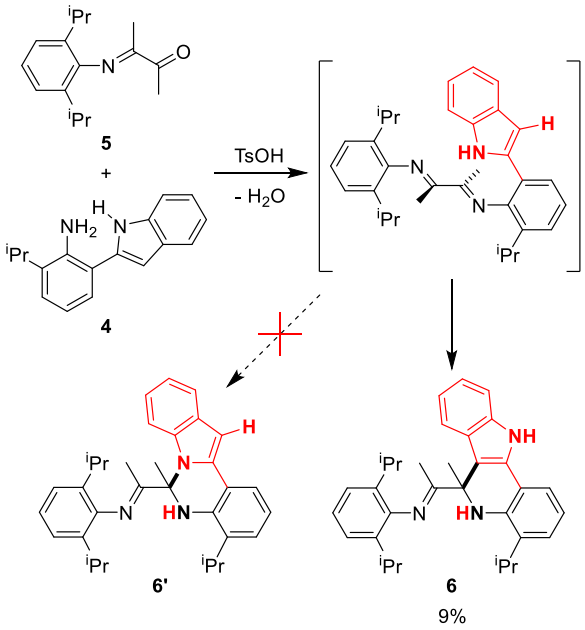

The reaction of **6** with $(MeCN)_2PdCl_2$ yields the square planar complex **(6)PdCl$_2$** through κ^2-C=*N*,*N*H coordination (Scheme 6.5). The solid-state structure of **(6)PdCl$_2$** is shown in Figure 6.1a. The imine N-atom (N3) is a stronger donor than the amine N-atom (N2), and accordingly the Pd-N3 bond is ca. 0.07 Å shorter than the Pd-N2 bond. The 5-membered chelate ring is puckered due to the presence of the sp^3-carbon atom C19, and the indole unit and the C18 methyl group occupy axial and equatorial positions, respectively. In the crystal, **(6)PdCl$_2$** molecules are arranged in pairs that are liked by intermolecular hydrogen bonds between the indole NH unit on one molecule and a Cl ligand of the other molecule (Figure 6.1b).

Scheme 6.5

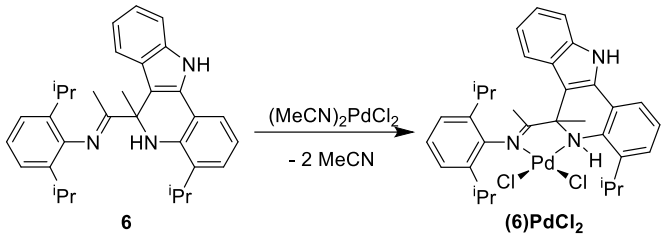

(a) (b)

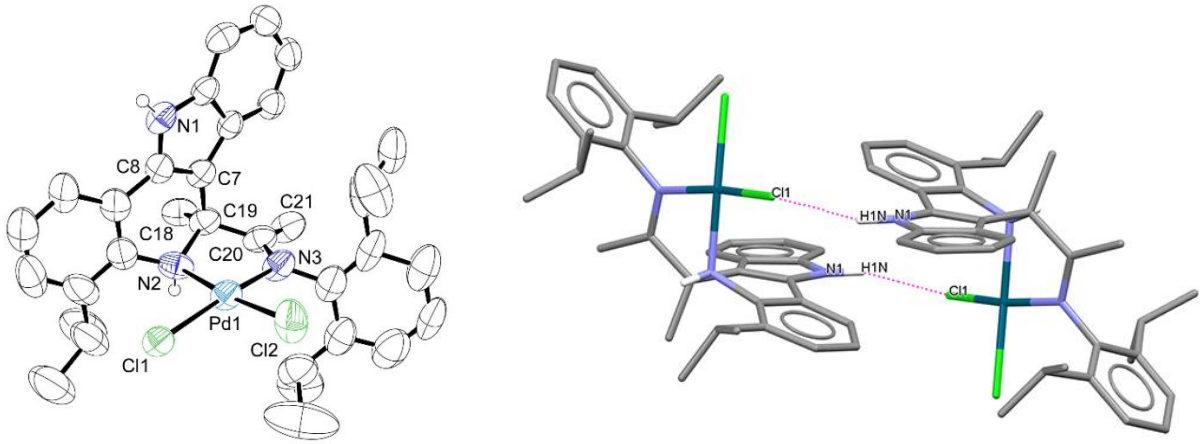

Figure 6.1. (a) Molecular structure of **(6)PdCl₂**. Hydrogen atoms are omitted except for the H-atoms on N1 and N2. Selected bond lengths (Å): Pd1-N2, 2.084(7); Pd1-N3, 2.008(6); C20-N3, 1.281(10); C19-N2, 1.533(9); C19-C20, 1.510(11); C7-C19, 1.509(10). (b) Intermolecular H-bonding of **(6)PdCl₂** in the solid state. Selected distances (Å) and angles (°): N1···Cl1, 3.183(6); N1-H1N···Cl1, 158(7).

In Scheme 6.1, the ring opening of **A** is triggered by coordination of the amine N (and perhaps the imine N) to Pd, which significantly decreases the pK_a of the amine NH and drives the elimination of the amide unit. In contrast, **(6)PdCl₂** is stable for at least 20 h at 90 °C in CD_2Cl_2/CD_3CO_2D (10/1 by volume) under N_2. The anti arrangement of the N-*H* and indolyl groups in **(6)PdCl₂** may disfavor elimination of the indole and formation of the diimine product.

6.3 Experimental Section

General Procedures. All experiments were performed under nitrogen using drybox or Schlenk techniques unless otherwise noted. Nitrogen was purified by passage through activated molecular sieves and Q-5 oxygen scavenger. Solvents for manipulations under N_2 were purified as follows: benzene was purified by passage through activated alumina and BASF R3-11 oxygen scavenger, and CH_2Cl_2 was purified by passage through activated alumina. 1,2-Dimethoxyethane (anhydrous, Aldrich) was used as received. All workup and purification procedures of organic compounds were carried out with reagent grade solvents in air. 2-Amino-3-isopropylbenzoic acid (**1**)[10] and 3-(2,6-diisopropylphenylimino)butan-2-one (**5**)[11] were synthesized by reported procedures.

NMR spectra were recorded on a Bruker DRX-500 spectrometer at ambient temperature unless otherwise indicated. ^1H and ^{13}C NMR chemical shifts are reported relative to $SiMe_4$ and were determined by reference to the residual ^1H and ^{13}C solvent resonances. Coupling constants are given in hertz (Hz).

Elemental analysis was performed by Robertson Microlit Laboratories (Ledgewood, NJ). Infrared spectra were recorded on thin-film samples on NaCl plates using a Nicolet NEXUS 470 FT-IR spectrometer. Mass spectrometry was performed on Agilent 6130 LCMS (low resolution) or Agilent 6224 Tof-MS (high resolution) instruments. The listed *m*/*z* value corresponds to the most intense peak in the isotope pattern.

2'-Amino-3'-isopropylacetophenone (2). A Schlenk flask was charged with **1** (2.00 g, 11.2 mmol) and anhydrous 1,2-dimethoxyethane (100 mL). The mixture was cooled to 0 °C, and MeLi (1.6 M in Et_2O, 23.0 mL, 36.8 mmol, 3.3 equiv) was added dropwise via syringe at 0 °C to yield an orange solution. The mixture was stirred at 0 °C for 2 h and quenched with aqueous

saturated NH_4Cl. The 1,2-dimethoxyethane was removed on a rotovap. The remaining aqueous phase was extracted with CH_2Cl_2 (3 x 30 mL). The combined organic layer was washed with brine, dried with Na_2SO_4, filtered, and taken to dryness under vacuum to give a yellow oil. The residue was purified by flash column chromatography (silica, hexane/EtOAc = 4/1 by volume) and dried under vacuum to yield a yellow oil. Yield: 1.35 g (68%). ^{1}H NMR ($CDCl_3$): δ 7.64 (dd, J = 8.1, 1.5, 1H), 7.29 (dd, J = 7.4, 1.5, 1H), 6.67 (t, J = 7.8, 1H), 6.62 (br s, 2H), 2.89 (septet, J = 6.8, 1H), 2.60 (s, 3H), 1.27 (d, J = 6.8, 6H). ^{13}C{^{1}H} NMR ($CDCl_3$): δ 201.4, 147.9, 133.4, 130.4, 130.0, 118.0, 115.4, 28.5, 27.0, 22.1. IR (cm^{-1}): ν_{N-H} 3483, 3323; $\nu_{C=O}$ 1645. HRMS (ESI-TOF, positive ion, m/z): Calc. 178.1232 ([M + H]$^+$), found 178.1238.

(a)

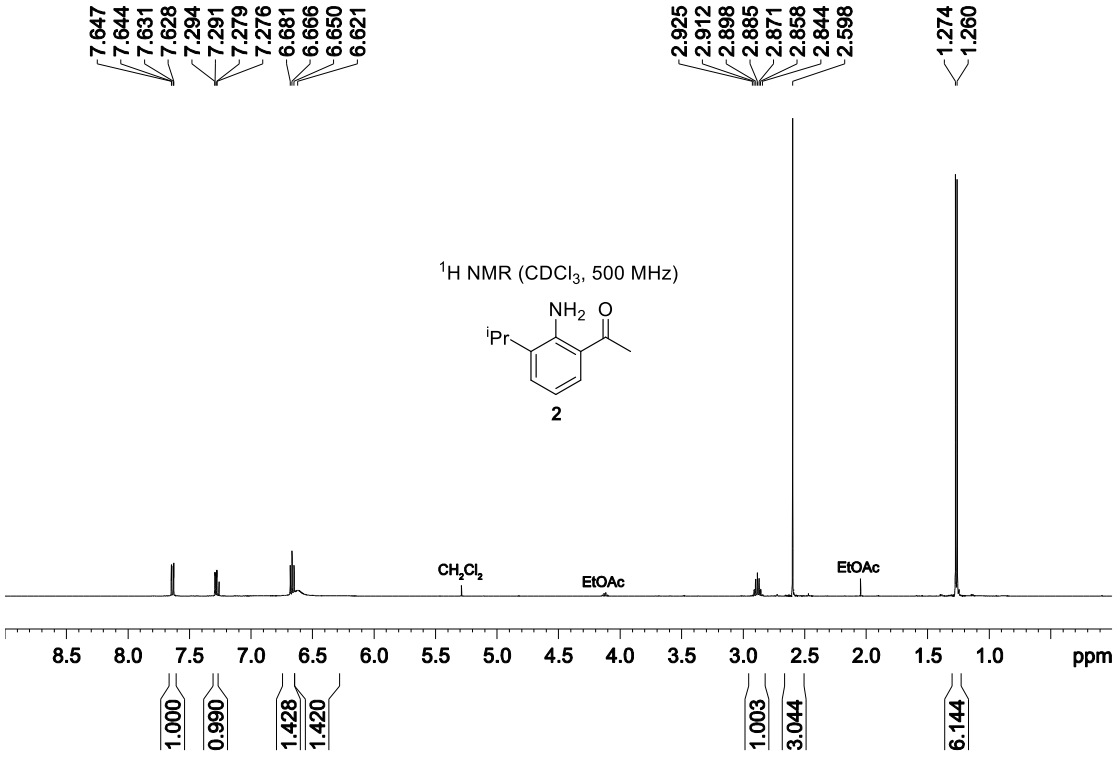

Figure 6.2. NMR spectra of **2**.

(b)

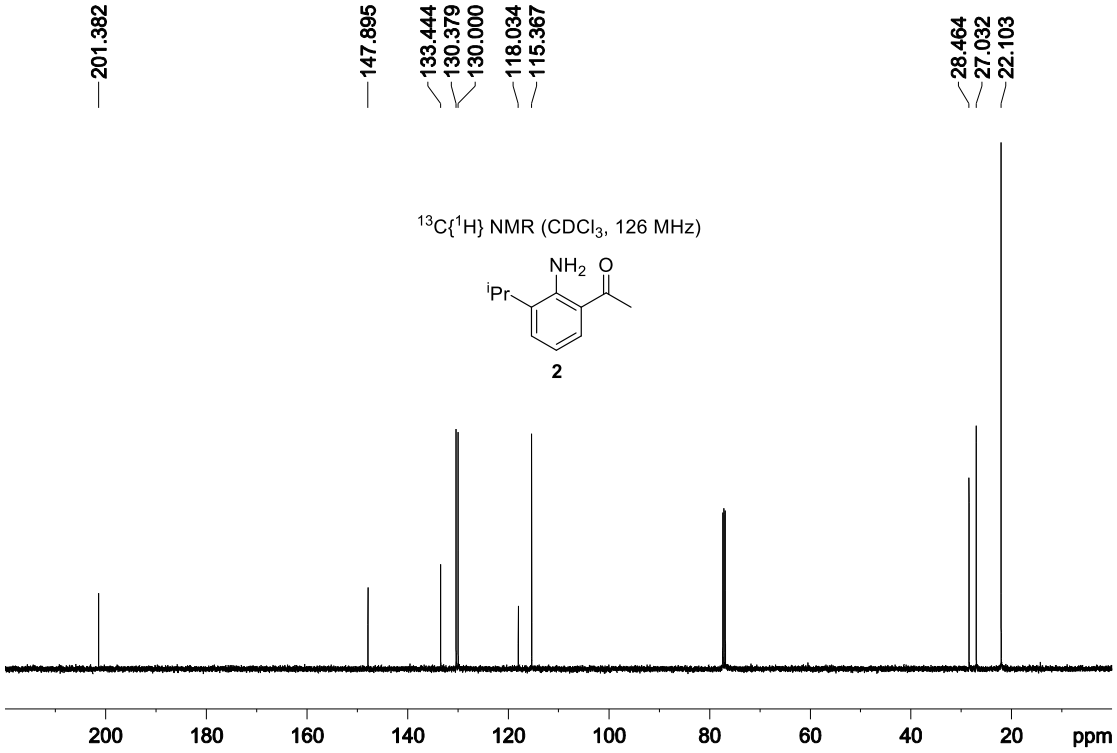

Figure 6.2, continued. NMR spectra of **2**.

2'-Amino-3'-isopropylacetophenone phenylhydrazone (3). A flask was charged with **2** (1.35 g, 7.62 mmol), phenylhydrazine (1.2 mL, 12 mmol, 1.6 equiv), anhydrous EtOH (10 mL) and AcOH (0.5 mL). The mixture was refluxed for 24 h under air and cooled to room temperature. The mixture was maintained at -30 °C for 3 d, resulting in the formation of yellow crystals. The crystals were collected by vacuum filtration, rinsed with EtOH, and dried under vacuum. Yield: 1.69 g (83%, sum of 4 crops). The isolated product comprised a mixture of **3-*E*** and **3-*Z***. The isomers was not separated, however, samples enriched in either **3-*E*** and **3-*Z*** were obtained during crystallization experiments and enabled NMR assignments. Data for **3-*E***: ^{1}H NMR ($CDCl_3$): δ 7.32-7.28 (m, 2H), 7.26 (dd, *J* = 7.8, 1.5, 1H), 7.23 (br s, 1H, NH), 7.14 (dd, *J* = 7.8, 1.4, 1H), 7.10-7.07 (m, 2H), 6.90 (tt, *J* = 7.3, 1.0, 1H), 6.77 (t, *J* = 7.8, 1H), 6.00 (br s, 2H, NH_2), 3.00 (septet, *J* = 6.8, 1H), 2.34 (s, 3H), 1.32 (d, *J* = 6.8, 6H, ^{i}Pr). ^{13}C{^{1}H} NMR ($CDCl_3$): δ 145.9, 145.2, 142.8,

133.1, 129.5, 126.3, 125.1, 121.3, 120.3, 116.7, 113.1, 27.7, 22.4, 14.3 (^{i}Pr). Data for **3-*Z***: ^{1}H NMR ($CDCl_3$): δ 7.24-7.20 (m, 4H, 3 ArH + NH), 7.01-6.98 (m, 2H), 6.94 (dd, *J* = 7.6, 1.6, 1H), 6.87 (t, *J* = 7.5, 1H), 6.82 (tt, *J* = 7.3, 1.0, 1H), 3.78 (br s, 2H, NH_2), 2.93 (septet, *J* = 6.8, 1H), 2.30 (s, 3H), 1.33 (br d, *J* = 6.8, 3H, ^{i}Pr), 1.30 (br d, *J* = 6.8, 3H, ^{i}Pr). ^{13}C{^{1}H} NMR ($CDCl_3$): δ 145.5, 144.1, 139.4, 133.3, 129.3, 126.2, 125.7, 120.7, 119.8, 119.0, 112.9, 28.0, 24.4, 22.4 (br, ^{i}Pr), 22.3 (br, ^{i}Pr). IR (cm^{-1}, isomer mixture): 3452, 3328, 3266, 1602. HRMS (ESI-TOF, positive ion, *m*/*z*): Calc. 268.1814 ($[M + H]^+$), found 268.1823.

(a)

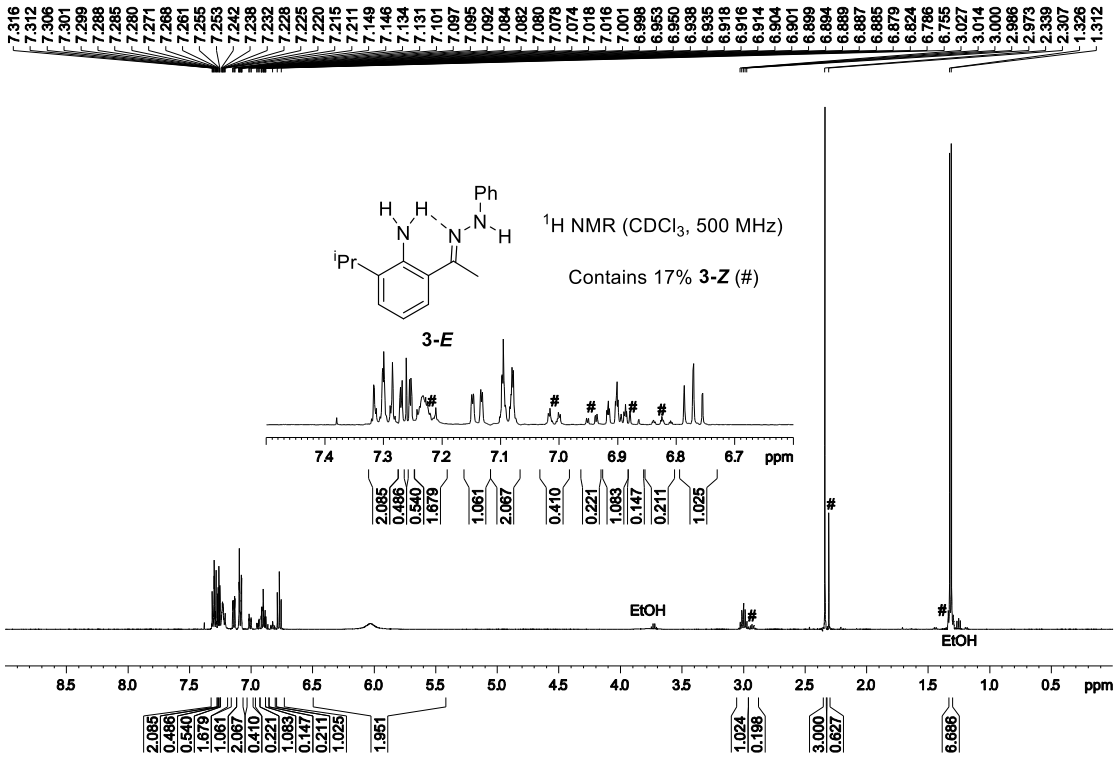

(b)

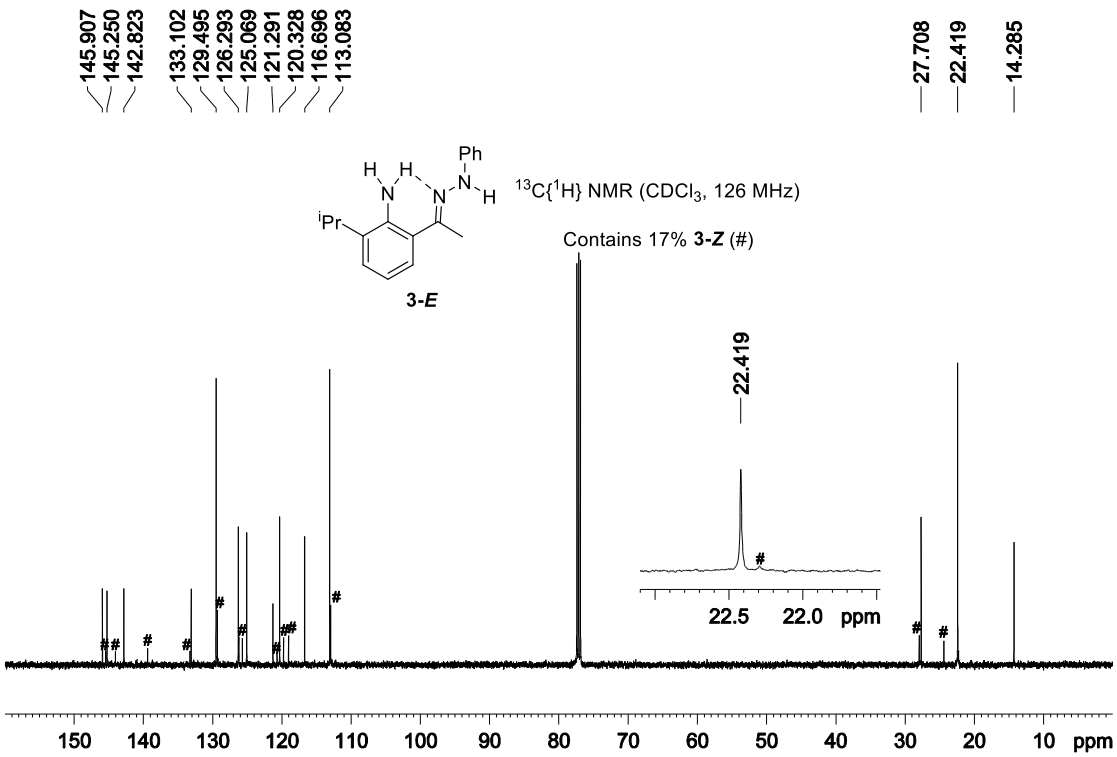

Figure 6.3. NMR spectra of **3-*E***.

(a)

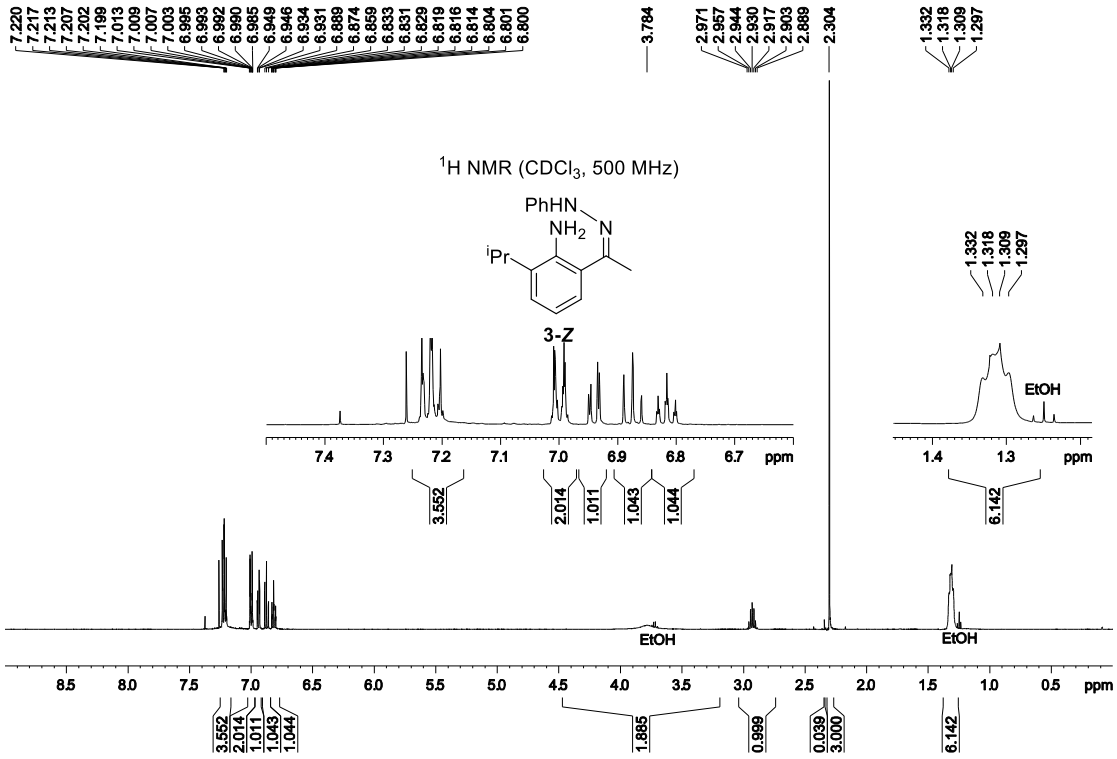

(b)

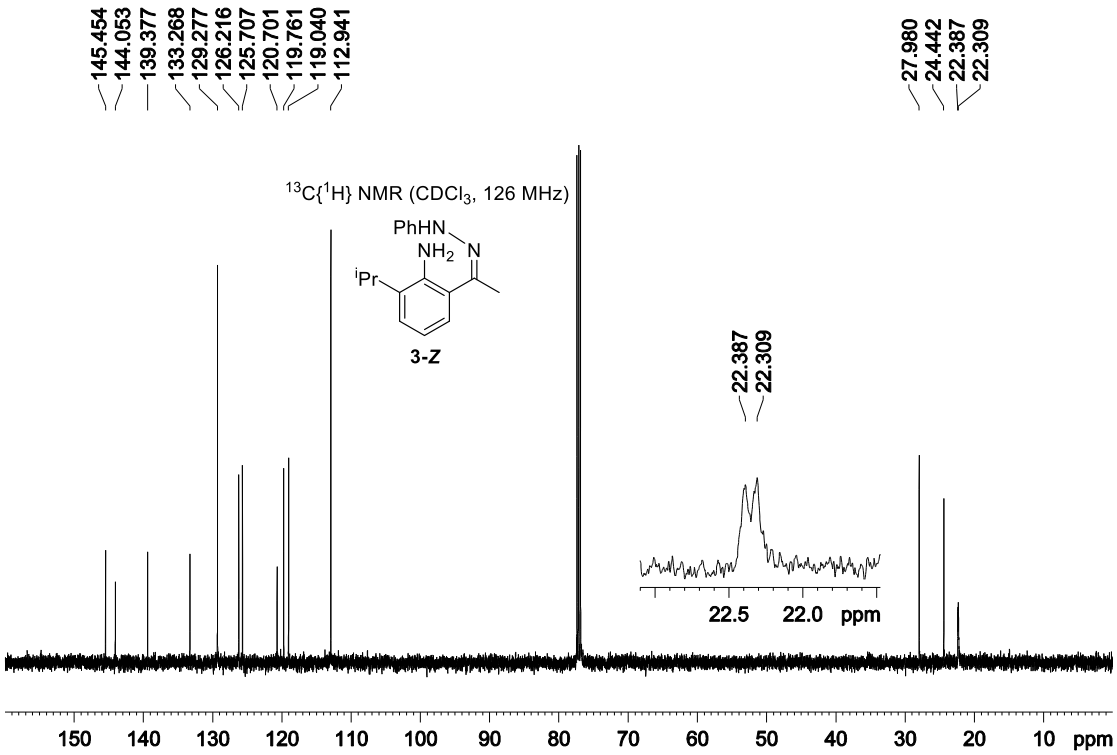

Figure 6.4. NMR spectra of **3-*Z***.

2-(2-Indolyl)-6-isopropylaniline (4). $MeSO_3H$ (12 mL) was added to a flask and heated to 80 °C. P_2O_5 (1.65 g) was added in one portion, and the mixture was stirred at 80 °C under air for 15 min until all of the solid dissolved. Hydrazone **3** (E,Z isomer mixture, 1.36 g, 5.09 mmol) was added in one portion. The mixture was stirred at 80 °C for 30 min and poured over a mixture of ice and NaOH (8 g) to precipitate a white solid. The solid was collected by vacuum filtration, washed with water, and dissolved in CH_2Cl_2 (20 mL). The solution was washed with brine in a separatory funnel, dried with $MgSO_4$, filtered, and taken to dryness under vacuum to yield a red oil, which slowly solidified at -30 °C to form a white solid. Yield: 0.990 g (78%). Prolonged exposure to air leads to a color change to brown, and thus quick manipulation is required. The product should be stored under N_2 to minimize oxidation. ^{1}H NMR ($CDCl_3$): δ 8.37 (br s, 1H, NH), 7.65 (dd, *J* = 7.8, 1.0, 1H), 7.42-7.40 (m, 1H), 7.24 (dd, *J* = 7.6, 1.6, 1H), 7.23-7.20 (m, 2H), 7.16-7.13 (m, 1H), 6.89 (t, *J* = 7.6, 1H), 6.72 (dd, *J* = 2.2, 0.8, 1H), 4.38 (br s, 2H, NH_2), 2.98 (septet, *J* = 6.8, 1H), 1.33 (d, *J* = 6.8, 6H). $^{13}C\{^1H\}$ NMR ($CDCl_3$): δ 141.4, 136.4, 136.3, 133.4, 129.0, 127.3, 125.6, 122.2, 120.5, 120.2, 119.2, 118.8, 110.9, 102.1, 28.1, 22.5. IR (cm^{-1}): ν_{N-H}, 3397, 3232. HRMS (ESI-TOF, positive ion, *m*/*z*): Calc. 251.1548 ($[M + H]^+$), found 251.1551.

(a)

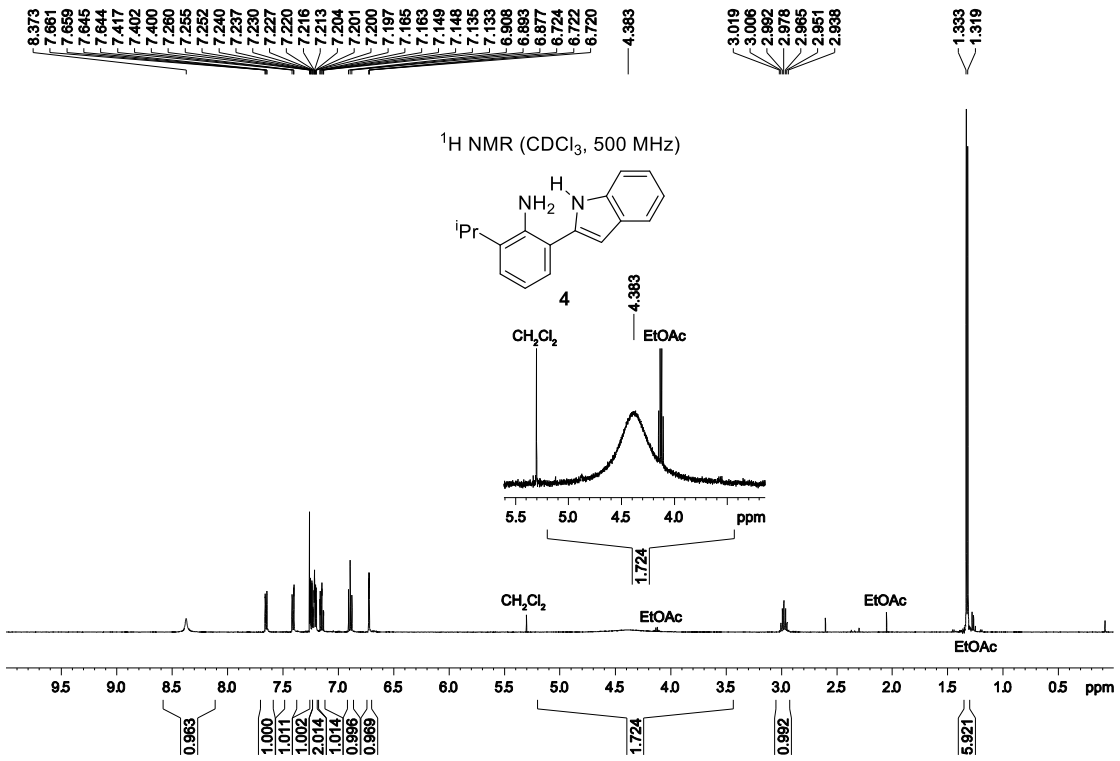

(b)

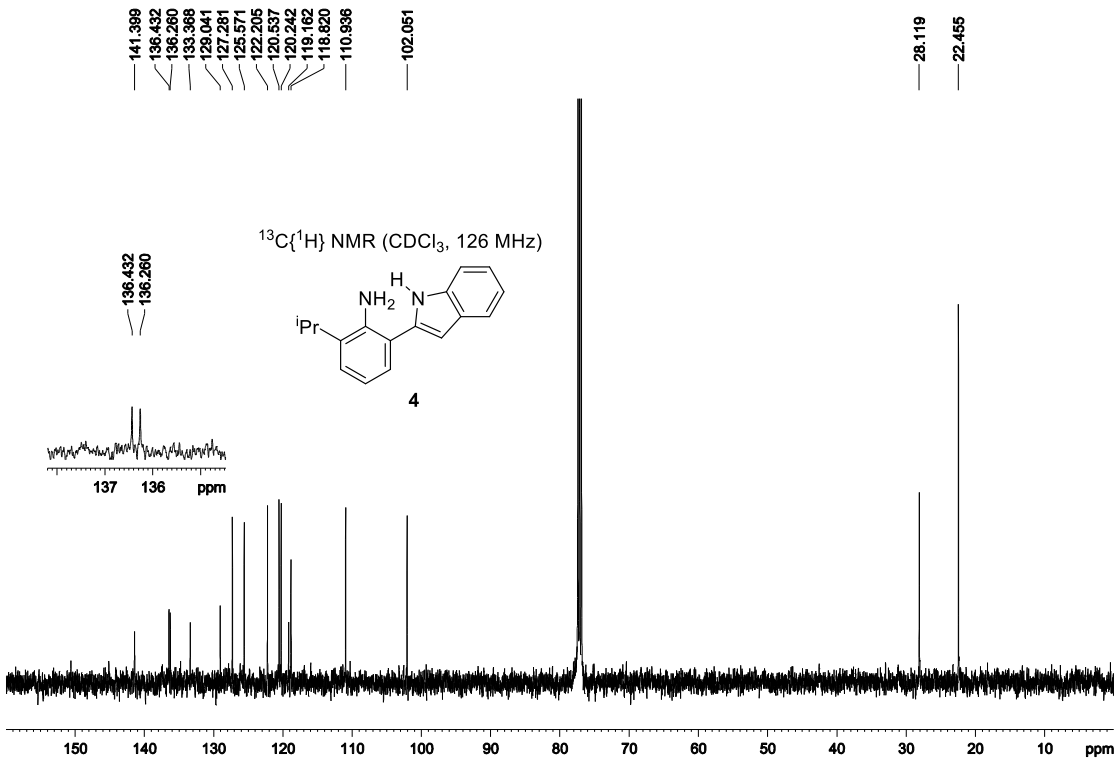

Figure 6.5. NMR spectra of **4**.

6-[1-(2,6-Diisopropylphenylimino)ethyl]-6,11-dihydro-4-isopropyl-6-methyl-5*H*-indolo[3,2-*c*]quinoline (6). A Schlenk flask was charged with **5** (246 mg, 1.00 mmol), **4** (250 mg, 1.00 mmol), $TsOH \cdot H_2O$ (20 mg) and benzene (50 mL). The flask was equipped with a Dean-Stark trap containing 4 Å molecular sieves and a water condenser. The mixture was refluxed under nitrogen for 2 d. The mixture was cooled to room temperature and quenched with Et_3N (1 mL). The volatiles were removed under vacuum to give a yellow oil. The oil was purified by flash column chromatography (silica, hexane/EtOAc/Et_3N = 80/10/1 by volume) and taken to dryness under vacuum to yield a white solid. This material was recrystallized by diffusion of pentane into a CH_2Cl_2 solution at room temperature, yielding analytically pure **6** as white needles (42 mg, 9%). ^{1}H NMR (CD_2Cl_2): δ 8.42 (br s, 1H, indole NH), 7.71 (d, *J* = 7.9, 1H), 7.43 (d, *J* = 7.9, 1H), 7.20-7.06 (m, 5H), 6.99-6.93 (m, 2H), 6.78 (t, *J* = 7.6, 1H), 4.94 (br s, 1H, amine NH), 3.04 (septet, *J* = 6.8, 1H), 2.76 (septet, *J* = 6.8, 1H), 2.20 (septet, *J* = 6.8, 1H), 2.17 (s, 3H), 1.57 (s, 3H), 1.30 (d, *J* = 6.8, 3H), 1.29 (d, *J* = 6.8, 3H), 1.18 (d, *J* = 6.8, 3H), 1.12 (d, *J* = 6.8, 3H), 0.83 (d, *J* = 6.8, 3H), 0.75 (d, *J* = 6.8, 3H). ^{13}C{^{1}H} NMR (CD_2Cl_2): δ 174.5, 146.3, 141.4, 137.8, 136.6, 136.2, 132.7, 132.4, 126.7, 125.6, 123.4, 123.1, 123.0, 122.2, 120.6, 119.8, 118.4, 118.1, 114.2, 111.6, 110.3, 63.0, 28.3, 28.0, 27.8, 26.9, 23.5, 23.1, 23.0, 22.8, 22.5, 22.3, 16.8. HRMS (ESI-TOF, positive ion, *m*/*z*): Calc. 478.3222 ($[M + H]^+$), found 478.3219.

(a)

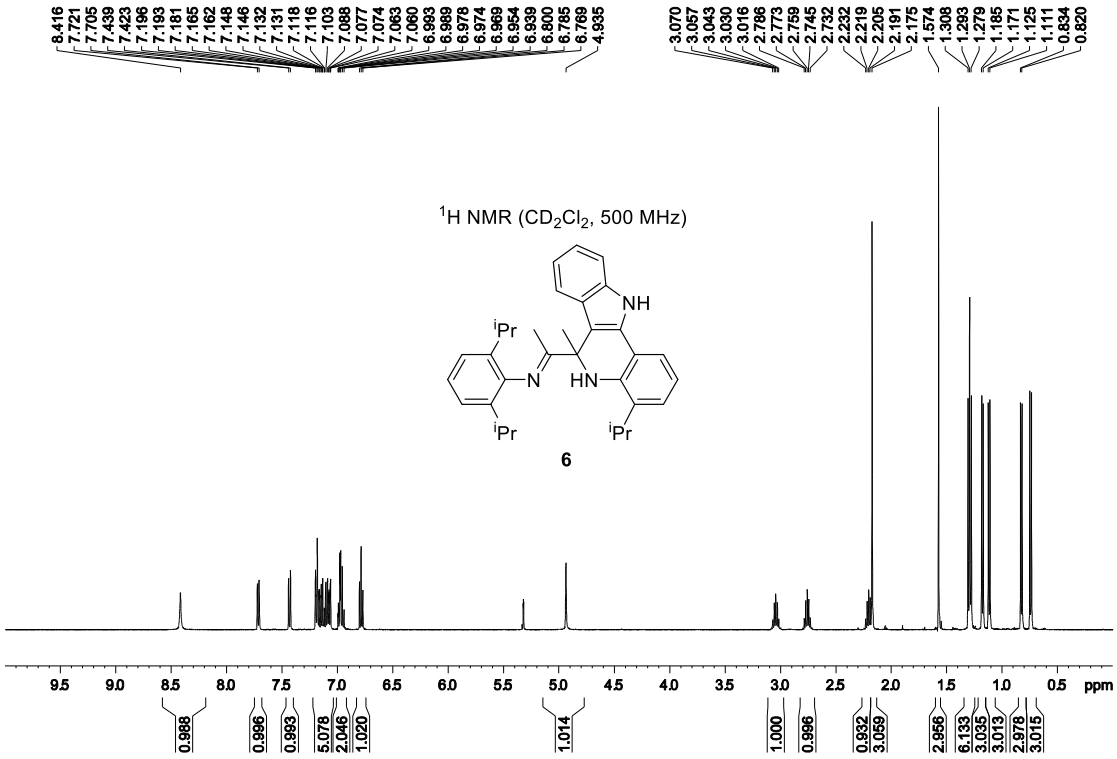

(b)

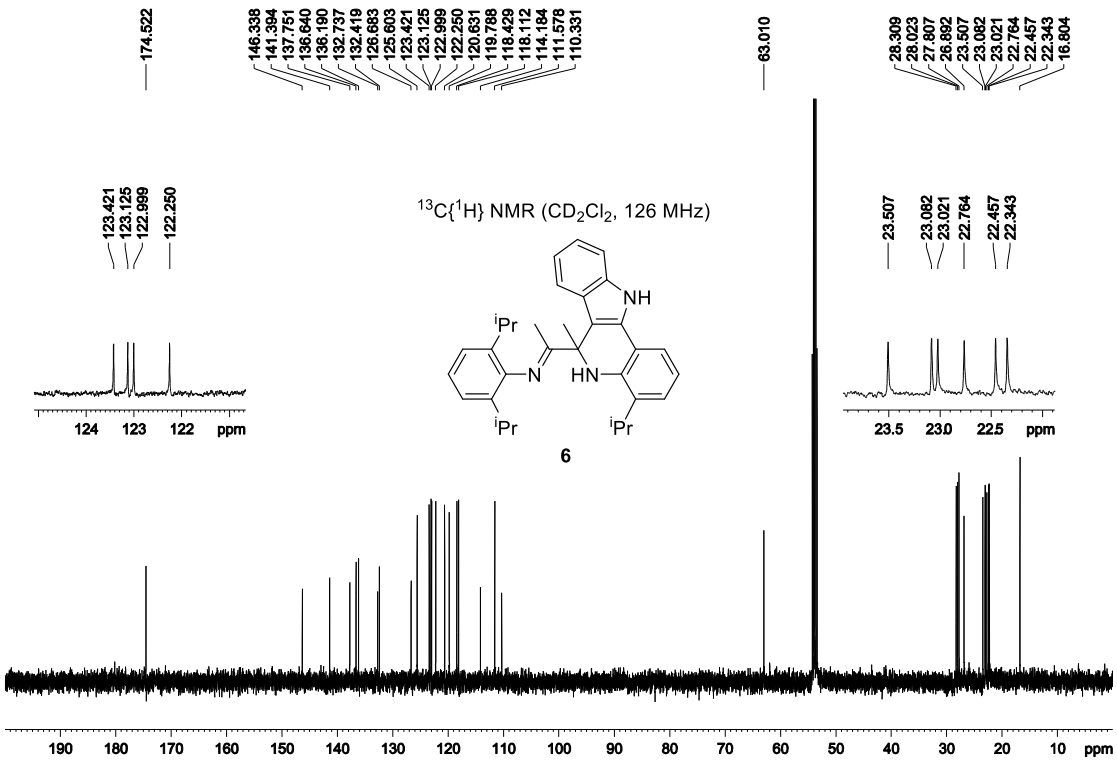

Figure 6.6. NMR spectra of **6**.

(6)PdCl$_2$. A Schlenk flask was charged with **6** (179 mg, 0.375 mmol), (MeCN)$_2$PdCl$_2$ (96 mg, 0.37 mmol) and CH_2Cl_2 (35 mL). The mixture was refluxed for 22 h and cooled to room temperature. The mixture was concentrated under vacuum to ca. 10 mL, and the yellow precipitate was collected by vacuum filtration. The solid was dissolved in CH_2Cl_2 (160 mL) upon gentle heating. The solution was filtered through Celite to remove trace solid particles, and the filtrate was taken to dryness to yield **(6)PdCl$_2$** as a yellow powder (168 mg, 69%). The solid contains 0.16 equiv CH_2Cl_2 and 0.10 equiv hexane as determined by ^{1}H NMR. ^{1}H NMR (CD_2Cl_2): δ 9.30 (br s, 1H, indole NH), 7.57 (d, *J* = 8.2, 1H), 7.49 (d, *J* = 7.8, 1H), 7.40 (t, *J* = 7.6, 1H), 7.34-7.19 (m, 6H), 7.15 (t, *J* = 7.5, 1H), 5.77 (br s, 1H, amine NH), 3.61 (septet, *J* = 6.8, 1H), 3.28 (septet, *J* = 6.8, 1H), 2.70 (septet, *J* = 6.8, 1H), 2.44 (s, 3H), 1.89 (d, *J* = 6.8, 3H), 1.68 (s, 3H), 1.63 (d, *J* = 6.8, 3H), 1.43 (d, *J* = 6.8, 3H), 1.42 (d, *J* = 6.8, 3H), 1.31 (d, *J* = 6.8, 3H), 1.18 (d, *J* = 6.8, 3H). ^{13}C NMR analysis was precluded by the low solubility of **(6)PdCl$_2$** in common NMR solvents. ESI-MS (1:1 MeOH:H_2O, positive ion scan, *m*/*z*): 582.3 ([M – Cl – HCl]$^+$). Anal. Calcd. for $C_{33}H_{39}Cl_2N_3Pd \cdot 0.16(CH_2Cl_2) \cdot 0.10(C_6H_{14})$, %: C, 59.88; H, 6.06; N, 6.20. Found: C, 59.65; H, 5.75; N, 6.30.

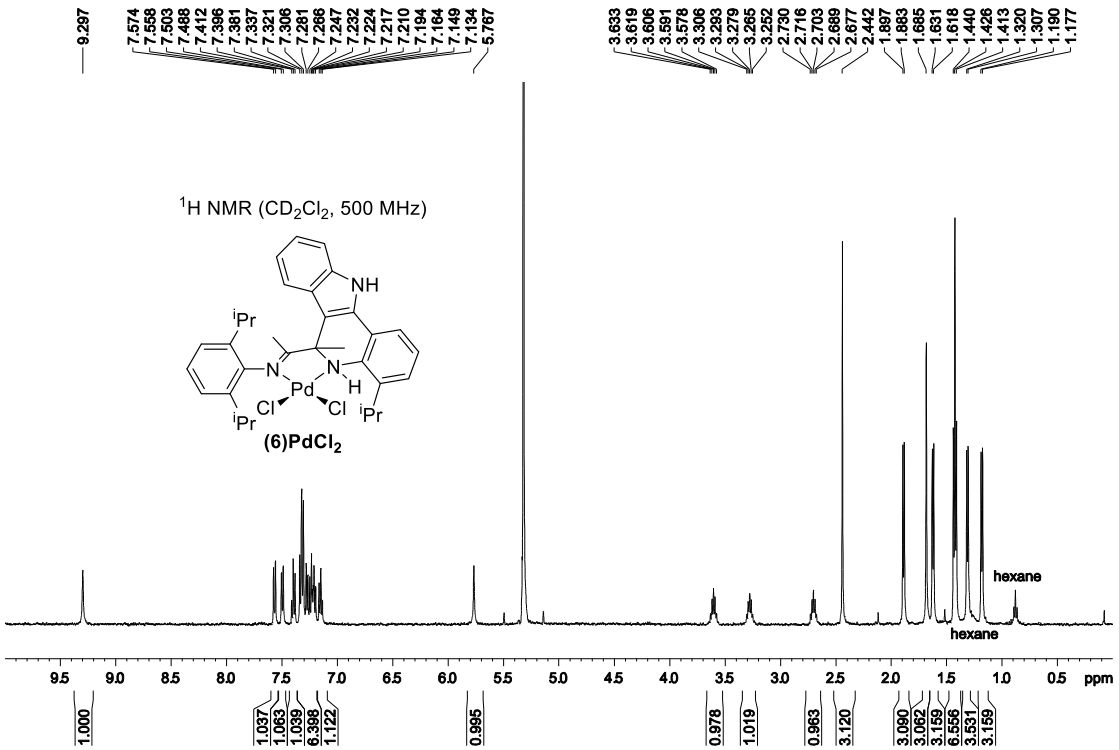

Figure 6.7. ^{1}H NMR spectrum of **(6)PdCl$_2$**.

X-ray Crystallographic Analysis of (6)PdCl$_2$. Crystals were grown by diffusion of hexane into a CH_2Cl_2 solution of **(6)PdCl$_2$** at 0 °C. Data were measured on a Bruker D8 VENTURE with a PHOTON 100 CMOS detector system equipped with a Mo-target X-ray tube (λ = 0.71073 Å). Crystallographic data and details of the data collection and structure refinement are listed in Table 6.1. All atoms were refined with anisotropic thermal parameters. Hydrogen atoms were included in idealized positions for structure factor calculations except those bound to nitrogen atoms N1 and N2. These hydrogen atoms (H1N and H2N) were located on the difference Fourier map and allowed to be refined at 0.88 Å within a default 0.02 Å standard deviation with their thermal parameters being constrained to be 1.2 times of the U_{eq} value of the N atoms. **(6)PdCl$_2$** was crystallized in a large unit cell with a volume of 16484(2) Å^3. Disordered solvent molecules were treated by application of the program SQUEEZE[12-13] as implemented in Platon[14] using the "fab" file construct and ABIN command in XL. SQUEEZE algorithm located a void,

centered at (0, 0, 0), with a large volume of 3916 $Å^3$ (ca. 22% of the unit cell volume) and an electron count of 537.

Table 6.1. X-ray Crystallographic Parameters of (6)$PdCl_2$.

Empirical formula	$C_{33}H_{39}N_3PdCl_2$
Formula weight	654.97
Temperature/K	120(2)
Crystal system	Trigonal
Space group	R-3
a/Å	28.4722(19)
b/Å	28.4722(19)
c/Å	23.4797(16)
α/°	90
β/°	90
γ/°	120
Volume/$Å^3$	16484(2)
Z	18
ρ_{calc}/g cm^{-3}	1.188
μ/mm^{-1}	0.675
F(000)	6084
Crystal size/mm^3	0.140 × 0.130 × 0.080
Radiation	MoKα (λ = 0.71073)
2Θ range for data collection/°	2.351 to 25.167
Index ranges	$-33 \leq h \leq 33$, $-33 \leq k \leq 33$, $-28 \leq l \leq 28$
Reflections collected	84533
Independent reflections	6532 [R(int) = 0.0480]
Data/restraints/parameters	6532/2/366
Goodness-of-fit on F^2	1.033
Final R indexes [I>=2σ (I)]	R1 = 0.0812, wR2 = 0.2020
Final R indexes [all data]	R1 = 0.1121, wR2 = 0.2278
Largest diff. peak/hole / e $Å^{-3}$	3.161/-2.133

6.4 References

(1) Yang, F.-Z.; Wang, Y.-H.; Chang, M.-C.; Yu, K.-H.; Huang, S.-L.; Liu, Y.-H.; Wang, Y.; Liu, S.-T.; Chen, J.-T. *Inorg. Chem.* **2009**, *48*, 7639.

(2) Lee, J.-J.; Yang, F.-Z.; Lin, Y.-F.; Chang, Y.-C.; Yu, K.-H.; Chang, M.-C.; Lee, G.-H.; Liu, Y.-H.; Wang, Y.; Liu, S.-T.; Chen, J.-T. *Dalton Trans.* **2008**, 5945.

(3) Cao, G.; Yang, H.-Q.; Luo, B.-T.; Liu, F.-S. *J. Organomet. Chem.* **2013**, *745–746*, 158.

(4) Hu, H.; Chen, D.; Gao, H.; Zhong, L.; Wu, Q. *Polym. Chem.* **2016**, *7*, 529.

(5) Zhai, F.; Jordan, R. F. *Organometallics* **2014**, *33*, 7176.

(6) Lee, J. I.; Youn, J. S. *Bull. Korean Chem. Soc.* **2008**, *29*, 1853.

(7) Mangas-Sánchez, J.; Busto, E.; Gotor-Fernández, V.; Gotor, V. *Org. Lett.* **2012**, *14*, 1444.

(8) Yavorskii, A. S.; Pavlovskii, V. I.; Andronati, S. A.; Dvorkin, A. A.; Gifeisman, T. Sh.; Simonov, Yu. A. *Zh. Obshch. Khim.* **1990**, *60*, 354.

(9) Richter, P. H.; Schleuder, M.; Reck, G.; Hagen, A. *Pharmazie* **1992**, *47*, 828.

(10) Yamamoto, G.; Koseki, A.; Sugita, J.; Mochida, H.; Minoura, M. *Bull. Chem. Soc. Jpn.* **2006**, *79*, 1585.

(11) Abakumov, G. A.; Cherkasov, V. K.; Druzhkov, N. O.; Kocherova, T. N.; Shavyrin, A. S. *Russ. Chem. Bull.* **2011**, *60*, 112.

(12) Spek, A. L. *Acta Cryst.* **2015**, *C71*, 9.

(13) van der Sluis, P.; Spek, A. L. *Acta Cryst.* **1990**, *A46*, 194.

(14) Spek, A. L. *Acta Cryst.* **2009**, *D65*, 148.

CHAPTER SEVEN

Chiral (α-Diimine)Ni Catalysts Based on Menthyl Substituents

7.1 Introduction

(α-Diimine)Pd catalysts produce highly branched polyethylene and can copolymerize ethylene with polar monomers.[1-4] The steric properties of the α-diimine ancillary ligand strongly influence the activity and microstructure of the resulting polymer. Besides the benchmark Brookhart-type ^{i}Pr-substituted α-diimine ligand, a few other designs of α-diimine ligands were reported to exhibit distinct reactivity.[5-9] For example, Chen and coworkers reported that benzhydryl-substituted α-diimine Pd catalysts are highly active and thermally stable and produce polyethylene with a low branching density (ca. 25-30 br/1000C).[7] The benzhydryl groups are more sterically demanding but more weakly electron-donating compared to ^{i}Pr. Guan and coworkers showed that electron-withdrawing groups on the N-aryl rings may lead to low MW and activity.[10] Thus, the alkyl groups that exhibit similar electronic-donating ability to ^{i}Pr but are more sterically bulky may provide a means of improving the performance of (α-diimine)Pd catalysts in ethylene polymerization.

The (*1R,2S,5R*)-menthyl group is a widely used chiral auxiliary group in the design of asymmetric catalysts.[11-15] The menthyl C_6 ring is locked in a stable chair conformation due to the presence of three equatorial substituents. Also, enantiopure menthyl groups are readily available. Nozaki and coworkers showed that the replacement of the *P*-^{i}Pr groups in the (*o*-$^{i}Pr_2P$-C_6H_4-SO_3^-)PdMe ethylene polymerization catalyst with menthyl groups lead to an increase in the polyethylene MW by two orders of magnitude, which was ascribed to the distinct steric profile of the menthyl group.[16] This result inspired us to study the coordination chemistry of menthyl-

substituted α-diimine ligands and understand how the menthyl groups may influence the ethylene polymerization behavior of the corresponding (α-diimine)Ni catalysts. This chapter describes the synthesis, coordination chemistry and conformational isomerism and dynamics of the menthyl α-diimine ligands **L1** and **L2**. The steric effects in (α-diimine)Ni-catalyzed ethylene polymerization and 1-hexene polymerization are discussed.

7.2 Results and Discussion

Synthesis of Menthyl-Substituted Anilines. The synthesis of *o*-menthylaniline **3** and **4** is shown in Scheme 7.1. Transmetalation of the Grignard reagent formed from (*1R,2S,5R*)-menthyl chloride with $ZnCl_2$ yields a ca. 1:1 mixture of menthylzinc and neomenthylzinc reagents.[17-18] Subsequent Pd-catalyzed Negishi coupling of *o*-iodoanilines **1** and **2** with this mixture of zinc reagents in THF/*N*-ethylpyrrolidone (NEP) at room temperature yields **3** and **4** in high diastereoselectivity (>20:1).[18]

Scheme 7.1

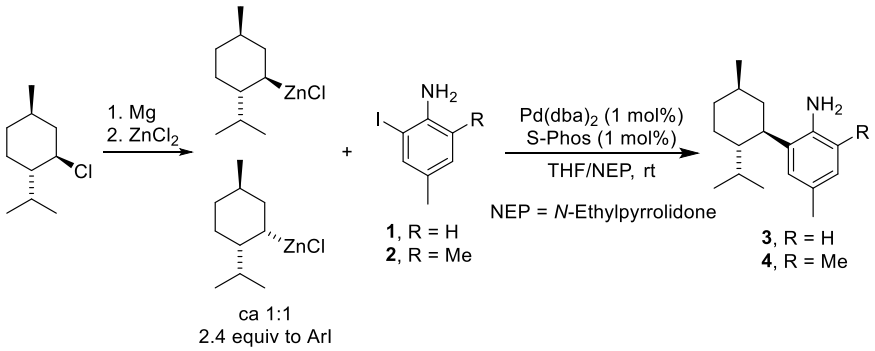

Anilines **3** and **4** both exhibit hindered rotation of the menthyl group. **3** exists as a 12/1 equilibrium mixture of the anticlinal isomer **3-*ac*** and the synclinal isomer **3-*sc*** in C_6D_6 at room temperature (Scheme 7.2). The room-temperature NOESY/EXSY spectrum of **3** exhibits exchange correlations between the two isomers and several NOE correlations of the major isomer **3-*ac***,

enabling the assignment of **3-*ac***. In the variable-temperature ^{1}H NMR spectra of **3** in C_6D_6, coalescence of aromatic resonances is observed at ca. 40 °C and coalescence of *p*-Me resonances at ca. 35 °C (Figure 7.1). The rotational barrier of menthyl group was determined to be $\Delta G^{\ddagger}_{ac\rightarrow sc}$ = 16.2(6) kcal mol^{-1}. **4** also exists as a 12/1 mixture of rotamers **4-*ac*** and **4-*sc*** at room temperature. Hindered rotation of menthyl group was observed in the complex *N*,*O*-[2-(menthyloxy)phenyl]amido dimethylaluminum.[19]

The synclinal isomers are disfavored in the cases of **3** and **4** due to the steric repulsion between the *ortho*-amino group and two axial H-atoms, H_I and H_B. The isomer equilibrium is sensitive to the steric bulk of the *ortho*-substituent(s) of the menthyl group. For example, the room-temperature ^{1}H NMR spectrum of **3·HCl** exhibits only one set of signals, consistent with the sole presence of the anticlinal isomer, due to the larger size of NH_3^+ versus NH_2.

Scheme 7.2

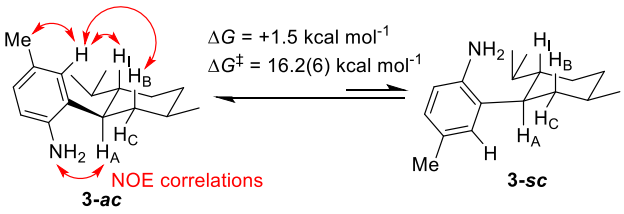

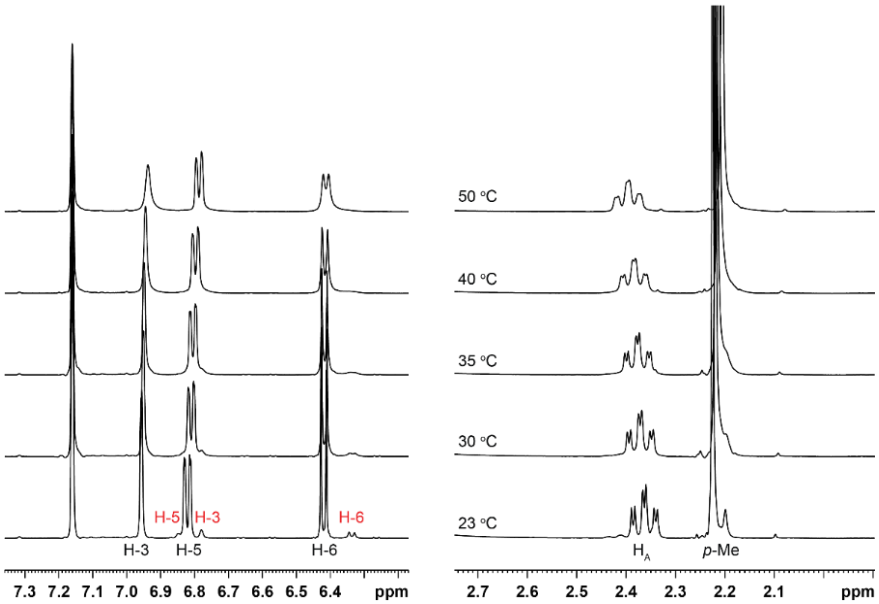

Figure 7.1. Variable temperature ^{1}H NMR spectra of **3** in C_6D_6 (23 to 50 °C, 500 MHz). The δ 7.3-6.2 and δ 2.7-2.0 regions are shown.

Synthesis of Ligands L1 and L2. Ligands **L1** and **L2** were prepared by $ZnCl_2$-templated synthesis followed by demetalation (Scheme 7.3). The reactions of acenaphthenequinone with 2.2 equiv of aniline **3** and **4** in the presence of excess $ZnCl_2$ in AcOH yield the diamagnetic, tetrahedral complexes **(L1)ZnCl$_2$** and **(L2)ZnCl$_2$-*anti***, respectively. The Zn complexes were readily isolated by filtration and demetalated with aqueous $K_2C_2O_4$ in CH_2Cl_2 to form the free ligands **L1** and **L2**.

The Zn complexes and the free ligands exhibit isomerism in solution as discussed below.

Scheme 7.3

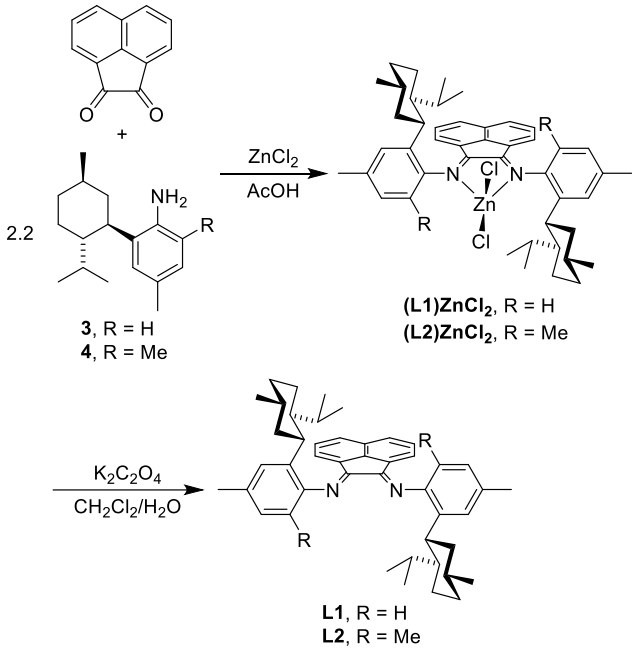

Terminology for Isomers. Multiple dynamic processes occur in solution for **L1**, **L2** and their metal complexes, including imine *Z,E* isomerization, hindered rotation of the N-aryl groups, and hindered rotation of the menthyl groups.

The imine C=N bonds in bis(imino)acenaphthene (BIAN) compounds may exhibit *Z* or *E* configurations. In general, the *E,E* and *Z,E* isomers of free BIANs are often observed, and the *E,E* isomer is favored versus *Z,E*. The interconversion of these isomers is usually fast on the lab time scale at room temperature.[20]

For *N,N'*-diaryl-BIAN ligands, the *ortho*-substituents on the N-aryl units are located above and below the N=C-C=N plane. For **L1** and **L2**, the relative position of two menthyl groups are defined as *syn* if they are on the same side of the N=C-C=N plane or *anti* if they are on the opposite sides (applicable to both *Z,E* and *E,E* conformers).

In the *E,E* isomer, the two anticlinal (*ac*) menthyl groups may adopt two orientations. The orientation in which the menthyl ^{i}Pr group points to the acenaphthene backbone is termed as *endo*,

and the orientation in which the menthyl ^{i}Pr group points away from the acenaphthene backbone is termed as *exo*.

The menthyl groups in **L1**, **L2** and complexes of these ligands can adopt synclinal and anticlinal rotational conformers. The synclinal (*sc*) isomer will be destabilized by the steric bulk on the adjacent N atom in both free ligands and metal complexes. Thus, the *ac* conformation should be favored.

Isomerism of L1 and L2. L1 exists as an equilibrium mixture of C_2-symmetric **L1-*E,E*** (85%), C_1-symmetric **L1-*Z,E*** (13%) and trace amounts of other conformers (2%) in CD_2Cl_2 solution at room temperature (Scheme 7.4). The isomer assignments are supported by the ^{1}H NMR chemical shifts of *ortho*-acenaphthene (*o*-An) resonances. The *anti,syn* exchange process (i.e. N-aryl rotation) of **L1** was observed by ^{1}H NMR spectroscopy in the temperature range -60 to 23 °C. Upon cooling to -60 °C, all of the ^{1}H resonances of **L1-*E,E*** at room temperature resolved into pairs of resonances (Figure 7.2), which show that the C_1-symmetric *syn* conformer, **L1-*E,E-syn***, is predominant (ca. 70%) at -60 °C.[21] The *anti,syn* exchange process of **L1** is shown in Scheme 7.5, in which the *anti* conformer exchanges with two degenerate states for the *syn* conformer. The same process also permutes the *endo* and the *exo* menthyl groups in the *syn* conformer. At room temperature, the permutation of menthyl groups is fast enough to show only one set of signals in the ^{1}H and ^{13}C NMR spectra. Note that the ^{1}H NMR spectrum for **L1-*E,E-syn*** at -60 °C exhibited a highfield (δ ca. -0.1) doublet for one isopropyl Me unit of the *endo* menthyl group due to ring current effect of the acenaphthene backbone. Therefore, a doublet signal in the range δ 0 to -0.4 is characteristic for an *endo* menthyl group.

Scheme 7.4

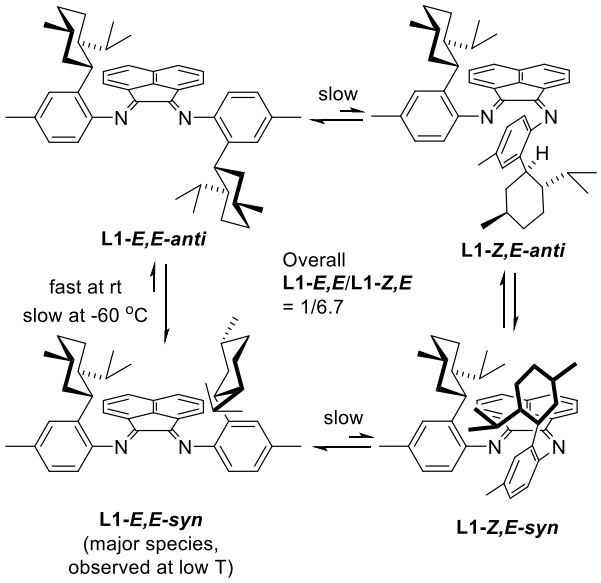

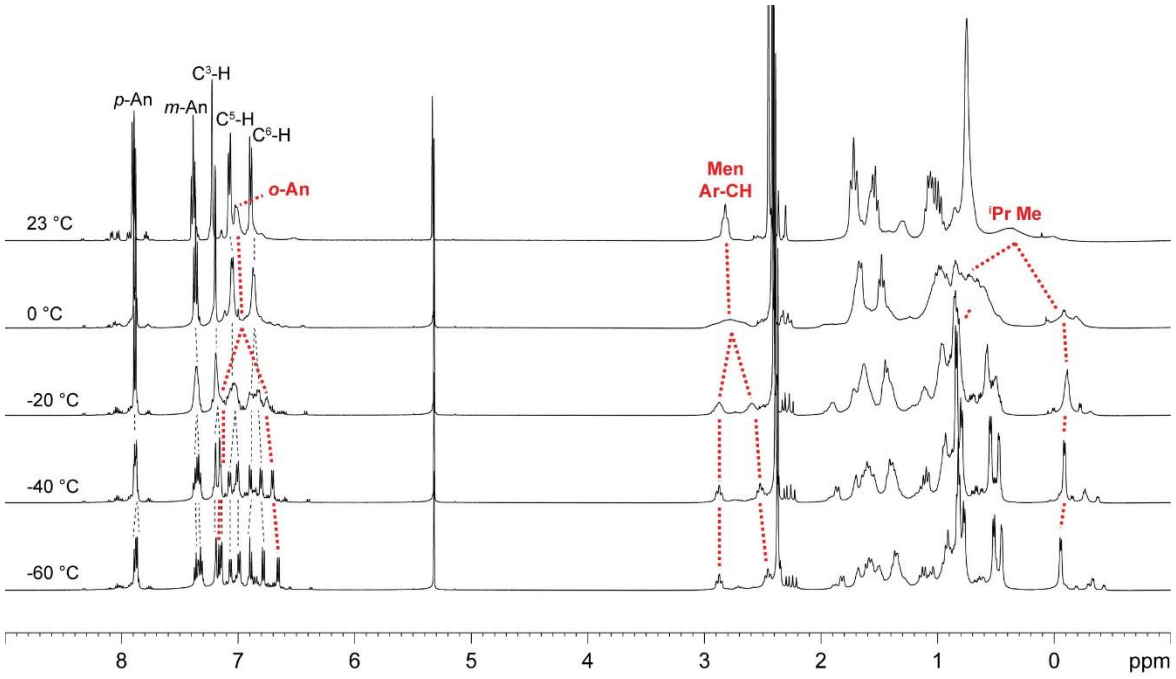

Figure 7.2. Variable temperature ^{1}H NMR spectra of **L1** in CD_2Cl_2 (-60 to 23 °C, 500 MHz). The δ 9 to -1 region is shown. The most prominent exchanging pairs of resonances are labeled in bold dashed lines.

Scheme 7.5

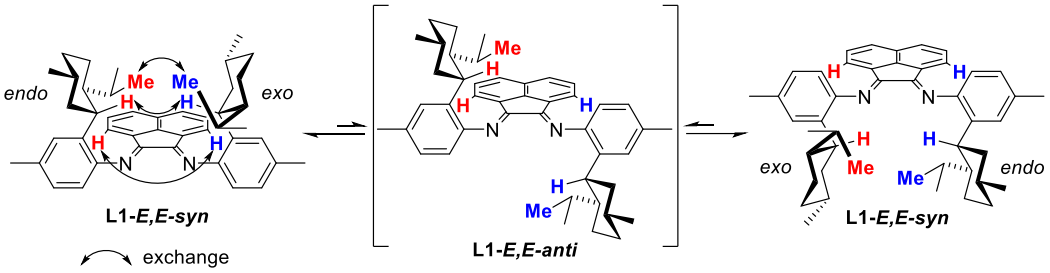

L2 contains more *ortho*-substituents than **L1**, and accordingly, the N-aryl rotation is slower in **L2** than in **L1**, which enables analysis of the *anti*,*syn* exchange process at room temperature. The as-synthesized **L2** contains a high content of **L2-*anti*** (3.1:1 mixture of **L2-*E,E-anti*/*Z,E-anti*** in fast *Z,E* equilibrium) due to the *anti* conformation of **(L2)ZnCl$_2$-*anti*** (vide infra). The conversion of **L2-*anti*** to **L2-*syn*** (30:1 mixture of **L2-*E,E-syn*/*Z,E-syn*** in fast *Z,E* equilibrium) reaches a final *anti*,*syn* equilibrium mixture that is dominated by **L2-*E,E-syn*** (12/4/81/3 mixture of **L2- *E,E-anti*/*Z,E-anti*/*E,E-syn*/*Z,E-syn***, overall *anti*/*syn* = 1/5.2) within 5 d in CH_2Cl_2 at room temperature (Scheme 7.6). The compositions were quantified based on the ^{1}H NMR integrals of δ 0 to -0.4 ^{i}Pr doublets of the *endo* menthyl groups; the C_2-symmetric conformer **L2-*E,E-anti*** exhibits a doublet corresponding to 6 H-atoms from two *endo* menthyl groups, while all the other conformers exhibit a doublet corresponding to 3 H-atoms from one *endo* menthyl group. **L2-*syn*** can be enriched by flash column chromatography due to the slow *anti*,*syn* isomerization kinetics at room temperature.

Scheme 7.6. Equilibrium Isomer Distribution at Room Temperature

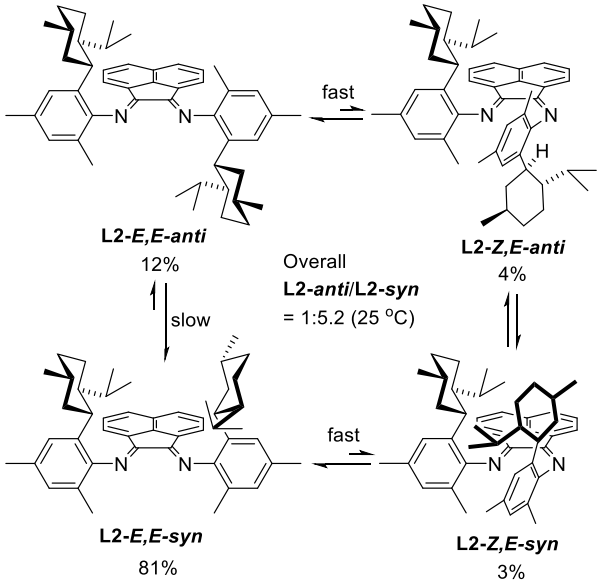

Tetrahedral (L1,2)$ZnCl_2$ Complexes. (L1)$ZnCl_2$ exists as a 10/1 equilibrium mixture of **(L1)$ZnCl_2$-*anti*** and **(L1)$ZnCl_2$-*syn*** in CD_2Cl_2 at room temperature (Scheme 7.7). The major isomer **(L1)$ZnCl_2$-*anti*** exhibits C_2-symmetry and contains two *endo* menthyl groups based on the ^1H and ^{13}C NMR spectra. **(L2)$ZnCl_2$-*anti*** isomerizes to an 11/1 equilibrium mixture of **(L2)$ZnCl_2$-*anti*** and **(L2)$ZnCl_2$-*syn*** in $CDCl_2CDCl_2$ at 105 °C within 2 d, which is similar in equilibrium isomer distribution compared to **(L1)$ZnCl_2$**.

Scheme 7.7

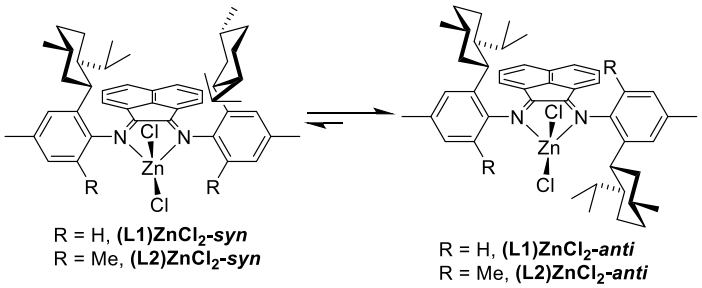

Tetrahedral (L1,2)$NiBr_2$ Complexes. The reaction between **L1** and (dme)$NiBr_2$ at room temperature yields the paramagnetic, tetrahedral complex **(L1)$NiBr_2$-*anti*** (Scheme 7.8). The

solid-state structure of **(L1)NiBr$_2$-*anti*** was revealed by X-ray diffraction to contain two *endo* menthyl units (Figure 7.3). The paramagnetic ^{1}H NMR spectrum of **(L1)NiBr$_2$-*anti*** in CD_2Cl_2 shows only one set of peaks that corresponds to a two-fold symmetric species, suggesting that **(L1)NiBr$_2$-*anti*** also adopts *anti* conformation in solution. The reaction between **L2** (mixture of isomers) and (dme)$NiBr_2$ at 80 °C yields **(L2)NiBr$_2$-*anti***. The *anti* conformation of **(L2)NiBr$_2$-*anti*** is supported by its C_2-symmetric ^{1}H NMR spectrum.

Scheme 7.8

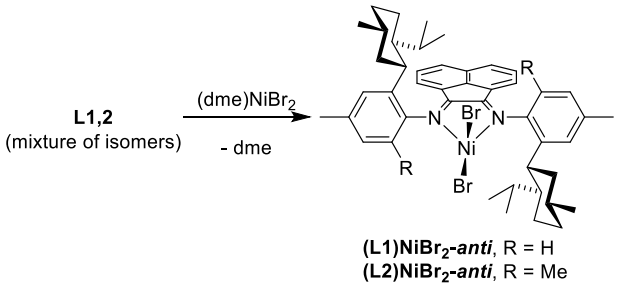

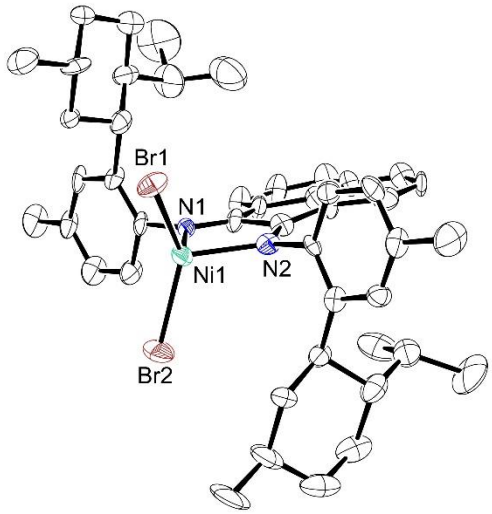

Figure 7.3. Molecular structure of **(L1)NiBr$_2$-*anti***. Hydrogen atoms are omitted.

Isomerism of Square Planar (L1)PdCl$_2$ Complexes. The reaction of **L1** and $(MeCN)_2PdCl_2$ in CH_2Cl_2 yields an 16:1 equilibrium mixture of **(L1)PdCl$_2$-*syn*** and **(L1)PdCl$_2$-**

anti (Scheme 7.9). The major conformer **(L1)PdCl$_2$-*syn*** can be purified by recrystallization. Pure **(L1)PdCl$_2$-*syn*** reaches isomerization equilibrium in 3 d at room temperature, showing that coordination to the Pd center dramatically hinders the rotation of N-aryls compared to the case of free ligand **L1**. The ^{1}H NMR resonances for the two inequivalent menthyl groups of **(L1)PdCl$_2$-*syn*** were completely assigned based on COSY and HMQC spectra. The NOESY correlations between the two menthyl groups (in red, Figure 7.4) support the assignment of the *syn* conformation. The NMR spectra of **(L1)PdCl$_2$-*anti*** confirm the C_2-symmetry, and the ^{i}Pr doublet at δ -0.27 indicates that the two menthyl groups are both *endo*.

Scheme 7.9

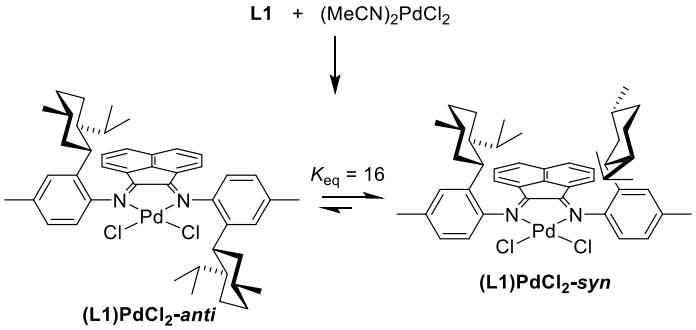

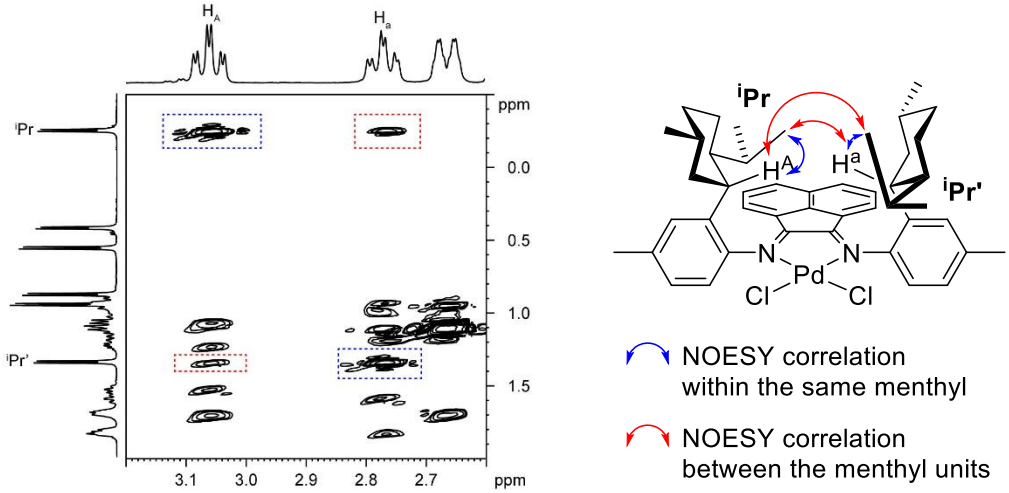

Figure 7.4. NOESY spectrum of **(L1)PdCl$_2$-*syn*** (CD_2Cl_2, expansion of δ 3.2-2.6/δ 2.0 to -0.5 region).

The structures of **(L1)PdCl$_2$-*syn*** and **(L1)PdCl$_2$-*anti*** were confirmed by X-ray diffraction (Figure 7.5). **(L1)PdCl$_2$-*syn*** contains one *endo* menthyl and one *exo* menthyl group that face each other and thus completely block one axial face of the square planar Pd center (Figure 7.5b). The isopropyl units in both menthyl groups are in close proximity to the other menthyl group, as shown in Figure 7.5c. For instance, the *endo* menthyl ^{i}Pr unit exhibits short C-H···H-C distances with the axial H-atoms H_d (2.463 Å) and H_a (2.853 Å) of the *exo* menthyl group. These short distances in the solid-state structure are consistent with the observed NOESY correlations for **(L1)PdCl$_2$-*syn***. For all four independent molecules in the solid-state structure of **(L1)PdCl$_2$-*syn***, the corresponding ^{i}Pr'···H_D and ^{i}Pr···H_d distances vary in the range 2.26-2.73 Å due to the slight differences in the relative displacements between the side-by-side menthyl groups rendered mainly by rotation of the N-aryl units. Significant bowing of the N-aryl units to the less hindered side of the chelate plane was not observed and is thus not required for maintaining the menthyl units in the *syn* conformation. **(L1)PdCl$_2$-*anti*** exhibits two *endo* menthyl groups, which is consistent to the NMR spectra. The menthyl groups do not have short contacts with either the $PdCl_2$ unit or the acenaphthene backbone in these structures.

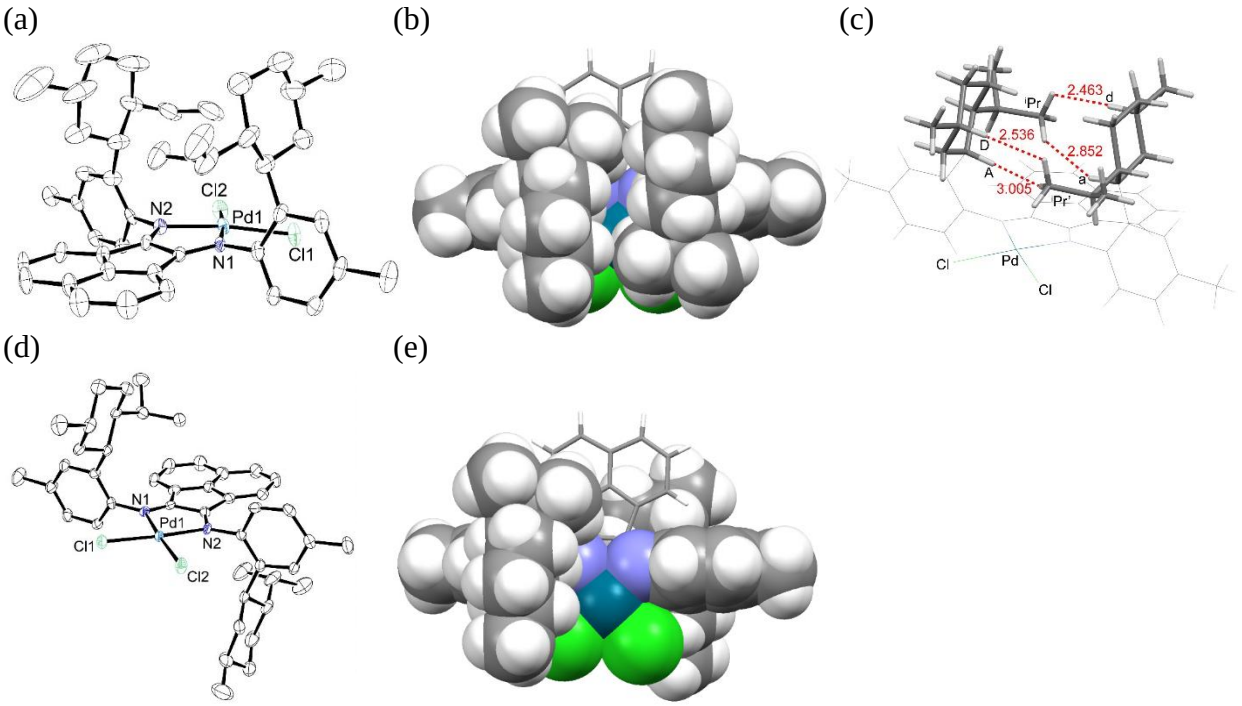

Figure 7.5. (a) Molecular structure of one independent molecule of **(L1)PdCl$_2$-*syn*** in **4[(L1)PdCl$_2$-*syn*]·3.4(CH$_2$Cl$_2$)**. The structure of the other independent molecules are similar but disordered. Hydrogen atoms and solvent molecules are omitted. (b) Top view of space filling model of **(L1)PdCl$_2$-*syn***. (c) Short C-H···H-C distances (Å) between the menthyl units in **(L1)PdCl$_2$-*syn***. (d) Molecular structure of **(L1)PdCl$_2$-*anti*** in **(L1)PdCl$_2$-*anti*·2.5(CH$_2$Cl$_2$)**. Hydrogen atoms and solvent molecules are omitted. (e) Top view of space filling model of **(L1)PdCl$_2$-*anti***.

Square Planar (L1,2)Ni(acac)$^+$B(C$_6$F$_5$)$_4^-$ Complexes. Square planar (α-diimine)Ni(acac)$^+$ complexes with non-coordinating anions are useful olefin polymerization precatalysts, which can be activated by aluminum alkyls.[22-24] The reaction of **L1** with Ni(acac)$_2$ and Ph$_3$C$^+$B(C$_6$F$_5$)$_4^-$ at room temperature yields air-stable **(L1)Ni(acac)** as a 50/1 equilibrium mixture of **(L1)Ni(acac)-*syn*** and **(L1)Ni(acac)-*anti*** (Scheme 7.10). The assignment of **(L1)Ni(acac)-*syn*** is based on the symmetry implied by ^{1}H and ^{13}C NMR spectra. The ^{1}H NMR signal for the two acac Me groups appears as a broad singlet at δ 1.61 in CD$_2$Cl$_2$ at room temperature, suggesting the presence of a fast permutation process between the two Me groups. The salt metathesis reaction of **(L1)NiBr$_2$-*anti***, Ag(acac) and LiB(C$_6$F$_5$)$_4$ etherate generates the

kinetic isomer **(L1)Ni(acac)-*anti***. The *anti*,*syn* isomerization of **(L1)Ni(acac)-*anti*** was monitored by ^{1}H NMR spectroscopy at room temperature (Figure 7.6a). The approach to equilibrium displays first-order kinetics with a lifetime of 2.6 h (Figure 7.6b).

Scheme 7.10

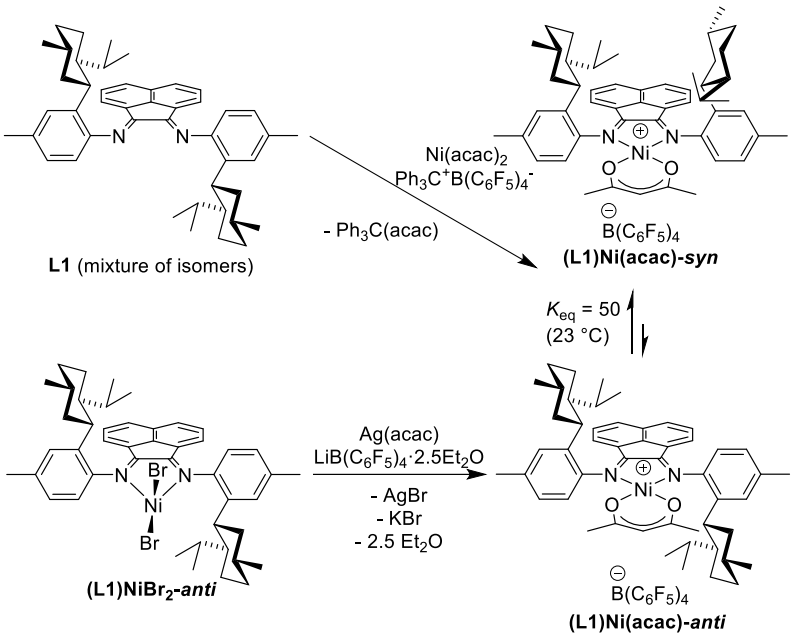

(a) (b)

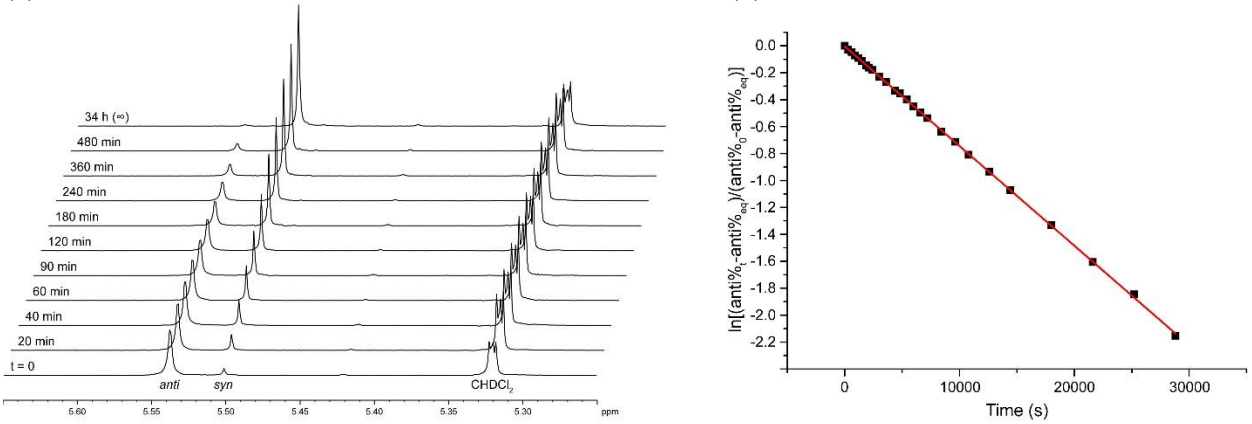

Figure 7.6. (a) Stacked ^{1}H NMR spectra showing conversion of **(L1)Ni(acac)-*anti*** to **(L1)Ni(acac)-*syn***. (b) First-order kinetic plot for approach to equilibrium.

The isomerization time scale of **(L1)Ni(acac)** at room temperature is comparable to the typical time scale for a polymerization run (a few minutes to hours), and therefore the *anti*,*syn* interconversion may complicate the interpretation of polymerization results. Accordingly, we investigated the more sterically hindered complexes **(L2)Ni(acac)-*syn*** and **(L2)Ni(acac)-*anti***, in which more highly substituted N-aryls are expected to slow the *anti*,*syn* exchange.

The metalation of **L2-*syn*** (enriched mixture containing 95% *syn* and 5% *anti*) with $Ni(acac)_2$ and $Ph_3C^+B(C_6F_5)_4^-$ yields a 91/9 mixture of **(L2)Ni(acac)-*syn*/*anti*** (Scheme 7.11). The two isomers could not be separated by silica chromatography or crystallization, and the mixture was used for further study. The reaction of **(L2)NiBr$_2$-*anti*** with Ag(acac) and $KB(C_6F_5)_4$ yields *syn*-free **(L2)Ni(acac)-*anti*** quantitatively, confirming both the retention of *anti* configuration and the conformational purity of **(L2)NiBr$_2$-*anti***. **(L2)Ni(acac)-*anti*** is conformationally stable at room temperature but isomerizes slowly (2 d) in $CDCl_2CDCl_2$ solution at 100 °C to an 89/11 equilibrium mixture of **(L2)Ni(acac)-*syn*/*anti***.

Scheme 7.11

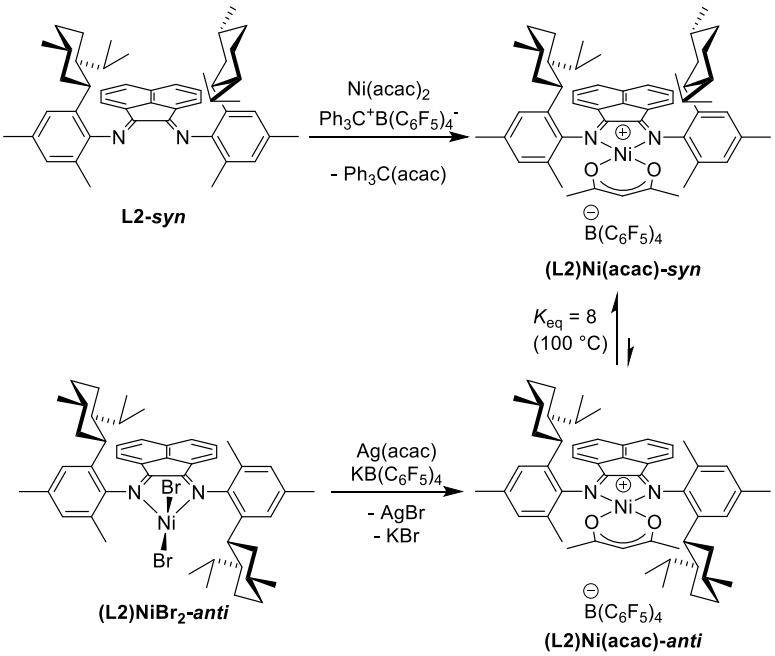

Summary of Conformational Behavior of L1, L2 and their Metal Complexes. Tetrahedral complexes (**L1,2**)MX_2 (MX_2 = $ZnCl_2$, $NiBr_2$) favor C_2-symmetric *anti* (*endo,endo*) conformations. The *exo* orientation of menthyl group is disfavored due to the expected steric repulsion between X ligands and the *exo* menthyl ^{i}Pr group (Figure 7.7).

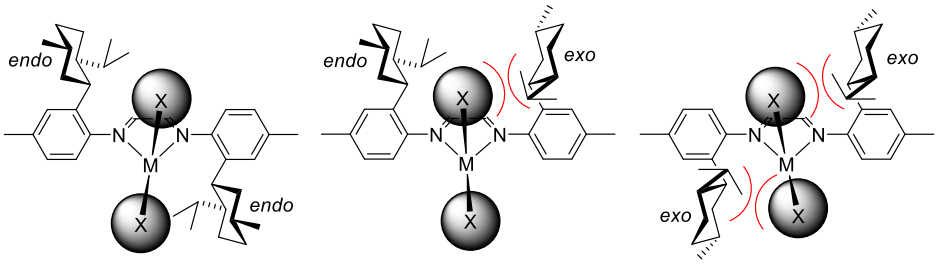

Figure 7.7. Steric repulsion between the X ligands and the *exo* menthyl ^{i}Pr groups.

In contrast, preference for the *syn* over the *anti* conformations was observed in the square planar complexes **(L1)PdCl$_2$** and **(L1,2)Ni(acac)**. This preference does not appear to be a consequence of significant steric repulsions and thus may originate from the preference for the *syn* isomer in the free ligands **L1** and **L2**. We hypothesize that the *syn* conformation may be stabilized over the *anti* conformation by attractive dispersive interactions between the menthyl units in close proximity, as suggested by the presence of multiple short C-H···H-C distances in the solid-state structure of **(L1)PdCl$_2$-*syn***.[25] Attractive dispersion interactions between large alkyl groups provide important stabilization for a variety of organic and coordination compounds[26-29] and also influence the assembly of alkyl groups in solution and in the solid state.[30-31] It should be noted that solvophobic effects may also contribute to the preference for the *syn* conformation.[30]

The preference for the *syn* conformation is weakened in the presence of two *o*-Me groups, as in the case of **(L2)Ni(acac)** versus **(L1)Ni(acac)**. A plausible explanation for this trend is that the *syn* conformation that maximizes the attractive dispersion interaction between the menthyl

groups may cause distortions of the other parts of the molecule, and such distortions are better tolerated in the less rigid **(L1)Ni(acac)**.

Ethylene Polymerization. The ethylene polymerization behavior of (**L2**)Ni complexes was studied at room temperature in order to minimize *anti*,*syn* isomerization. **(L2)NiBr$_2$-*anti***, **(L2)Ni(acac)-*anti*** and **(L2)Ni(acac)-*syn*/*anti*** (91/9) all generate very active catalysts for ethylene polymerization at 15 psi ethylene pressure upon activation by Et_2AlCl (200 or 2000 equiv) (Table 7.1). The activities are on the order of 10^6 g/(mol Ni h). The Al loading has only a minor effect on the overall performance. The labile ligands (Br vs acac) have only a minor effect on the microstructure of polyethylene but strongly influence the activity (entries 2 and 4). Interestingly, the catalyst mixture **(L2)Ni(acac)-*syn*/*anti*** (91/9) exhibits ca. 2 times higher MW and ca. 3 times more branching than **(L2)Ni(acac)-*anti*** (entries 4 and 6). This comparison shows that the difference between the steric profiles of **(L2)Ni(acac)-*anti*** and **(L2)Ni(acac)-*syn*** originating from the different steric bulk of *endo* and *exo* menthyl groups, strongly influences the activity and microstructure of resulting polyethylene.

Table 7.1. Ethylene Polymerization[a]

entry	cat.	Al/Ni	A^b	M_n (10^3)	M_w/M_n	B^c	T_m (°C)
1	**(L2)NiBr$_2$-*anti***	200	3.2	109.0	2.27	n.d.	111.2
2	**(L2)NiBr$_2$-*anti***	2000	4.1	101.0	2.16	16	112.9
3	**(L2)Ni(acac)-*anti***	200	6.4	98.7	2.33	n.d.	111.0
4	**(L2)Ni(acac)-*anti***	2000	6.6	105.8	2.40	19	113.4
5	**(L2)Ni(acac)-*syn*/*anti*** (91/9)	200	2.5	218.1	1.91	n.d.	111.5
6	**(L2)Ni(acac)-*syn*/*anti*** (91/9)	2000	2.7	196.0	2.13	53	110.5

[a]Conditions: 0.50 μmol Ni, 22 °C, Et_2AlCl, 15 psi C_2H_4, toluene/PhCl (49 mL/1 mL). [b]Activity (10^6 g/(mol Ni h)). [c]Branching density per 1000 C = $[CH_3]/([CH_3]+[CH_2]+[CH])\times1000$. Determined by ^1H NMR.

Zhu and coworkers reported the *anti* and *syn* isomers of [*N,N'*-(2,4-^{t}Bu$_2$-6-Me-Ph)$_2$-BIAN]NiBr$_2$ and studied their ethylene polymerization behavior upon activation by MAO. The *syn* isomer produced polyethylene with lower MW and much higher branching compared to the *anti* isomer.[32] In contrast, **(L2)Ni(acac)-*syn*** produces higher MW polyethylene than **(L2)Ni(acac)-*anti***, suggesting that chain transfer is inhibited in the *syn* conformation, in which the two menthyl groups totally block on axial face of the catalyst.

1-Hexene Polymerization. Sterically bulky (α-diimine)Ni catalysts exhibit chain-straightening reactivity for α-olefin polymerization.[33-38] As shown in Scheme 7.12, consecutive 1,2-insertions of 1-hexene generate butyl branches. The catalyst may also undergo 1,2-insertion followed by chain walking to the chain-end C6 carbon and subsequent chain growth to form a methyl branch. Finally, 2,1-insertions, subsequent chain walking to the chain-end C6 carbon and further chain growth will result in 6,1-enchainment, which does not create new branches. As a result, the resulting polyhexenes produced by (α-diimine)Ni catalysts are usually less branched than expected. The steric profile of α-diimine ligand influences the regioselectivity of 1-hexene insertion and has a major effect on the microstructure of the resulting polyhexene.

Scheme 7.12

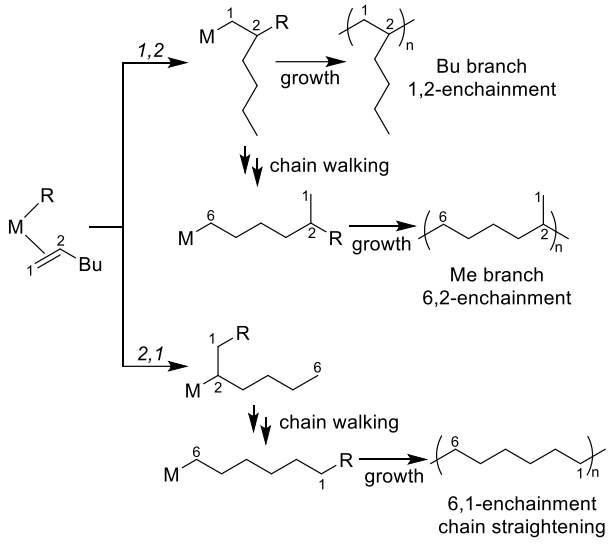

Activation of the (**L2**)Ni precatalysts **(L2)NiBr$_2$-*anti***, **(L2)Ni(acac)-*anti*** and **(L2)Ni(acac)-*syn*/*anti*** (91/9) with Et_2AlCl generates 1-hexene polymerization catalysts that produce polyhexenes with relatively narrow MW distributions (Table 7.2). **(L2)NiBr$_2$-*anti*** and **(L2)Ni(acac)-*anti*** produce polyhexenes with very similar branching levels. However, **(L2)Ni(acac)-*anti*** produces polyhexene with higher M_n and sharper MW distribution compared to that produced by **(L2)NiBr$_2$-*anti***. These results show that the labile ligands (Br or acac) have only a minor effect on the microstructure of polymer but influence chain transfer.

(L2)Ni(acac)-*syn*/*anti* (91/9) produces polyhexene with a bimodal MW distribution, in which the high-MW, minor distribution is produced by the *anti* component (Figure 7.8a) and the low-MW, major distribution is produced by the *syn* component. The difference between the MWs of the polymers produced by **(L2)Ni(acac)-*syn*** and **(L2)Ni(acac)-*anti*** is due to the rate of chain growth in these polymerizations with limited chain transfer, consistent with the observed turnover frequencies. The presence of two separate distributions strongly indicates that *anti*,*syn* isomerization of the active species or chain shuttling between the *anti*,*syn* isomers are minimal,

consistent with the isomerization behavior of **(L2)Ni(acac)-*syn*/*anti***.

^{13}C NMR analysis (Figure 7.8b) showed that 1,2-enchainment is the predominant enchainment mode in the polyhexene produced by **(L2)Ni(acac)-*anti***. In sharp contrast, the polyhexene produced by **(L2)Ni(acac)-*syn*/*anti*** (91/9) exhibits less branching and higher crystallinity, and ^{13}C NMR analysis showed a major 6,1-enchainment and a significant decrease in 1,2-enchainment as a result of increased steric bulk in the *syn* isomer.

Table 7.2. 1-Hexene Polymerization[a]

entry	cat.	TOF (h^{-1})	M_n (10^3)	M_w/M_n	B^c	$x_{6,1}{}^d$	$x_{6,2}{}^d$	$x_{1,2}{}^d$	T_m (°C)
1	**(L2)NiBr$_2$-*anti***	1430	45.4	1.60	95	n.d.	n.d.	n.d.	-[e]
2	**(L2)Ni(acac)-*anti***	3020	64.2	1.48	98	0.41	0.06	0.53	-[e]
3	**(L2)Ni(acac)-*syn*/*anti* (91/9)**	970	29.3	1.62[b]	84	0.50	0.24	0.26	49.9

[a]Conditions: [1-hexene] = 3.2 M, Ni (5.0 μmol), PhCl (1 mL), toluene (total volume 25 mL), [Et_2AlCl]/[Ni] = 200, 22 °C, 30 min. [b]Bimodal distribution (see Figure 7.8a). [c]Branching density per 1000 C = [CH_3]/([CH_3]+[CH_2]+[CH])×1000. Determined by ^{1}H NMR. [d]Fractions of 6,1-, 6,2-, and 1,2-enchainment. Determined by ^{13}C{^{1}H} NMR. [e]Amorphous polymers.

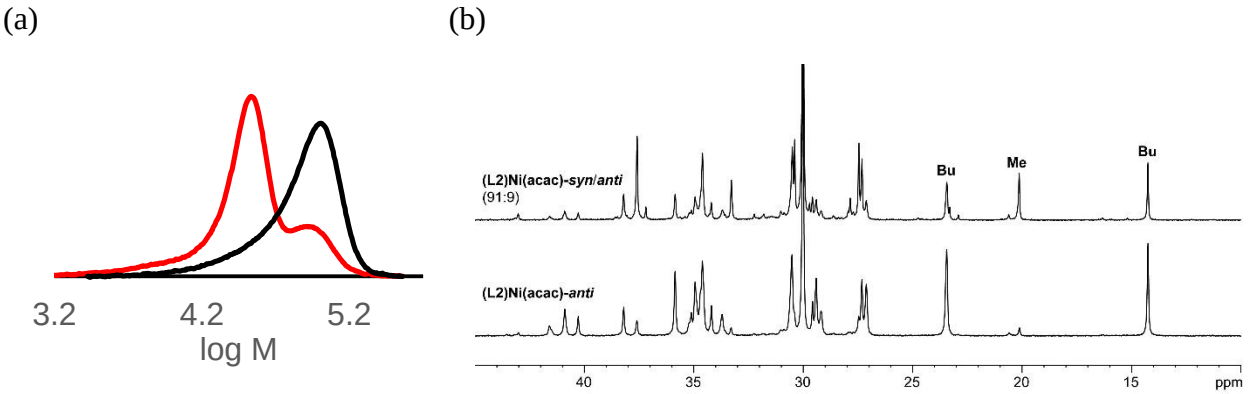

Figure 7.8. (a) MW distribution of polyhexenes. Black: Table 7.2, entry 2. Red: Table 7.2, entry 3. (b) ^{13}C{^{1}H} NMR spectra of polyhexenes at 120 °C in $CDCl_2CDCl_2$ (δ 45-10). Upper: Table 7.2, entry 3. Lower: Table 7.2, entry 2.

7.3 Conclusions

The synthesis, isomerization behavior and coordination chemistry of (*1R,2S,5R*)-menthyl substituted α-diimine ligands **L1** and **L2** are described. The *syn* conformation, in which the two menthyl groups face each other on the same side of N=C-C=N plane, is favored for **L1**, **L2** and square planar complexes of these ligands, possibly due to attractive dispersion interactions between the two menthyl groups. In contrast, the *anti* conformation, in which both menthyl groups adopt the *endo* orientation, is favored for tetrahedral complexes of **L1** and **L2**. The *anti*,*syn* isomerization of square planar complexes **(L1)Ni(acac)-*anti*,*syn*** is facile at room temperature. Square planar complexes **(L2)Ni(acac)-*anti*,*syn*** are kinetically stable at room temperature, and the *syn* isomer produces polyethylene with higher MW and branching level than the *anti* isomer. The *syn* isomer also produces polyhexene with less branches and a higher degree of chain straightening compared to the *anti* isomer. These differences in polymerization behavior are attributed to the significantly different steric profiles of the two isomers.

7.4 Experimental Section

General Procedures. All manipulations of organometallic compounds were performed under nitrogen or vacuum using Schlenk or high-vacuum techniques or in a nitrogen-filled drybox unless otherwise indicated. Nitrogen was purified by passage through activated molecular sieves and Q–5 oxygen scavenger. Hexane and pentane were purified by passage through activated alumina and BASF R3–11 oxygen scavenger. THF, CH_2Cl_2 and Et_2O were purified by passage through activated alumina. *N*-Ethylpyrrolidone (NEP) was distilled from CaH_2 under vacuum and stored under N_2. All workup and purification procedures for organic compounds were carried out with reagent-grade solvents in air. $LiB(C_6F_5)_4 \cdot x(Et_2O)$ was obtained from Boulder Scientific. The

Et_2O content in $LiB(C_6F_5)_4 \cdot x(Et_2O)$ was determined by ^1H NMR with C_6Me_6 as internal standard (x = 2.7). (*1R,2S,5R*)-(-)-Menthyl chloride,[39] 2-iodo-4-methylaniline (**1**)[40] and $KB(C_6F_5)_4$ [41] were synthesized by literature procedures.

NMR spectra were recorded on a Bruker DRX-500 or DRX-400 spectrometer in Teflon-valved tubes at ambient temperature unless otherwise indicated. ^1H and ^{13}C chemical shifts are reported relative to $SiMe_4$ and were determined by reference to the residual ^1H and ^{13}C solvent resonances. ^{19}F NMR chemical shifts are reported relative to $CFCl_3$ and were determined by reference to external $BF_3 \cdot Et_2O$ (δ -153). Coupling constants are given in hertz (Hz). NMR assignments were made with the aid of COSY, NOESY, HMQC and HMBC experiments. C_6D_6 was distilled from Na/benzophenone and stored under vacuum. CD_2Cl_2 was distilled from P_2O_5 and stored under vacuum. $CDCl_2CDCl_2$ was distilled from P_2O_5 and stored under N_2. Elemental analyses were performed by Robertson Microlit Laboratories (Ledgewood, NJ). Mass spectrometry was performed on Agilent 6130 LC-MS (low resolution) or Agilent 6224 Tof-MS (high resolution) instruments. The listed *m*/*z* value corresponds to the most intense peak in the isotope pattern.

NMR spectra for polymers were obtained as follows. ^1H NMR: A mixture of polymer (30–40 mg) and $CDCl_2CDCl_2$ (0.6 g) in an NMR tube was heated to 120 °C, affording a homogeneous solution. The tube was inserted into a preheated NMR probe at 120 °C, and NMR spectra were obtained after a 5 min temperature equilibration period. Parameters: 400 MHz, pulse width 90°, acquisition time 3.7 s, pulse delay 42 s, >10 scans. $^{13}C\{^1H\}$ NMR: A mixture of polymer (90-100 mg) and $CDCl_2CDCl_2$ (0.6 g, containing 0.025 M $Cr(acac)_3$) in an NMR tube was heated to 100 °C, affording a homogeneous solution. The tube was inserted into a preheated NMR probe at 100 °C, and NMR spectra were obtained after a 5 min temperature equilibration period. Parameters: 100

MHz, pulse width 90°, acquisition time 2.0 s; pulse delay 8.0 s, >3500 scans.

Gel permeation chromatography (GPC) data were obtained on a Polymer Laboratories PLGPC 200 instrument at 150 °C with 1,2,4-trichlorobenzene (stabilized with 125 ppm BHT) as the mobile phase. Three PLgel 10 μm Mixed-B LS columns were used. Molecular weights were calibrated using narrow polystyrene standards (ten-point calibration with M_n from 580 Da to 6035 kDa) and are corrected for linear polyethylene by universal calibration using the following Mark-Houwink parameters: polystyrene, $K = 1.75 \times 10^{-2}$ cm^3 g^{-1}, $\alpha = 0.67$; polyethylene, $K = 5.90 \times 10^{-2}$ cm^3 g^{-1}, $\alpha = 0.69$.[42] DSC measurements were performed on a TA Instruments DSC 2920 instrument. Samples (ca. 5 mg) were annealed by heating to 170 °C at 20 °C/min, cooled to 30 °C at 20 °C/min, and then analyzed while being heated to 170 °C at 20 °C/min.

Data for $B(C_6F_5)_4^-$. $^{13}C\{^1H\}$ NMR (CD_2Cl_2): 148.5 (d, J = 242), 138.7 (d, J = 247), 136.7 (d, J = 244), 124.5 (br, C_{ipso}). ^{19}F NMR (CD_2Cl_2): -133.6 (br s, 8F, F_{ortho}), -164.2 (t, J = 20, 4F, F_{para}), -168.0 (t, J = 18, 8F, F_{meta}).

MenMgCl/NeomMgCl. A 3-neck flask was charged with Mg turnings (1.74 g, 71.6 mmol, 1.2 equiv) under N_2, and equipped with a Schlenk adapter on one side arm, a septum on the other side arm, and a water condenser on the central arm. A second adapter was installed atop the condenser and connected to a N_2 bubbler. THF (30 mL) was added via syringe. 1,2-Dibromoethane (0.3 mL) was added via syringe. The mixture was stirred at room temperature for 5 min and heated to ca. 60 °C, and a solution of (-)-menthyl chloride (9.94 g, 56.9 mmol) in THF (10 mL) was added dropwise via syringe. The mixture was refluxed for 1 h and cooled to room temperature. The gray solution (ca. 47 mL) was transferred via cannula to a separate Schlenk flask for storage. The concentration of Grignard reagent was determined by titration with I_2 to be 0.79 M. Yield: 65%. This synthesis can be implemented on 30-gram scale with similar yield. The Grignard solution can

be stored under N_2 at 0 °C for at least 7 months with little change in concentration or reactivity.

2-[(1*R*,2*S*,5*R*)-Menthyl]-4-methylaniline (3). A Schlenk flask was charged with anhydrous $ZnCl_2$ (4.08 g, 30 mmol), THF (30 mL) and NEP (5 mL) under N_2, and the mixture was stirred vigorously until dissolution of the $ZnCl_2$ was complete (ca. 10 min). A solution of MenMgCl/NeomMgCl in THF (26 mmol in 40 mL) was added via syringe, and the mixture was stirred at room temperature. A second Schlenk flask was charged with 2-iodo-4-methylaniline (**1**, 2.52 g, 10.8 mmol), $Pd(dba)_2$ (58 mg, 0.10 mmol), 2-dicyclohexylphosphino-2',6'-dimethoxybiphenyl (S-Phos, 41 mg, 0.10 mmol) and THF (10 mL) under N_2, and the mixture was stirred at room temperature for 5 min. The Zn reagent solution was transferred into the second flask via cannula, and the mixture was stirred at room temperature for 21 h and quenched with saturated aqueous NH_4Cl solution (50 mL). The THF was removed on a rotovap. The remaining aqueous phase was extracted with Et_2O (3 x 50 mL). The combined organic phase was washed with water (2 x 20 mL) and brine (20 mL), dried with $MgSO_4$, filtered, and taken to dryness under vacuum to yield a yellow oil. The oil was subjected to flash column chromatography (silica, hexane/Et_2O = 10/1 by volume) to yield a yellow oil as a crude product. Further purification as follows removes trace colored impurities. The oil was dissolved in hexane (70 mL), and HCl solution (2 M in Et_2O, 5 mL, 10 mmol) was added slowly while the mixture was stirred. The mixture was kept at 0 °C for 20 min to allow full precipitation of the HCl salt, **3·HCl**. The white powder was collected by vacuum filtration, washed with hexane, and dried under vacuum. Yield: 2.21 g (73% based on iodoarene). The salt was suspended in Et_2O (70 mL) in a separatory funnel, washed with saturated aqueous $NaHCO_3$ solution (3 x 50 mL), dried with $MgSO_4$, filtered, and taken to dryness under vacuum to yield a colorless oil. Yield: 1.76 g (66% based on iodoarene). The equilibrium **3-*ac*/*sc*** ratio is 12/1 in C_6D_6 at room temperature. HRMS (ESI-TOF, positive ion,

m/*z*): Calc. 246.2222 ([M + H]$^+$), found 246.2226. Data for **3-*ac***: ^{1}H NMR (C_6D_6): δ 6.96 (d, *J* = 1.6, 1H, C^3-H), 6.82 (dd, *J* = 8.0, 1.5, 1H, C^5-H), 6.42 (d, *J* = 8.0, 1H, C^6-H), 2.93 (br s, 2H, NH_2), 2.36 (td, *J* = 11.4, 3.4, 1H, H_A), 2.22 (s, 3H, C^4-C*H*$_3$), 1.81 (septet d, *J* = 7.0, 2.7, 1H, ^{i}Pr methine), 1.79-1.71 (m, 3H, H_C + H_F + H_G), 1.56 (tt, *J* = 11.4, 2.8, 1H, H_I), 1.39-1.29 (m, 1H, H_D), 1.10 (qd, *J* = 12.4, 3.3, 1H, H_H), 1.03 (q, *J* = 12.4, 1H, H_B), 0.98 (qd, *J* = 12.3, 3.4, 1H, H_E), 0.89 (d, *J* = 6.5, 3H, $C^{5'}$-C*H*$_3$), 0.82 (d, *J* = 7.0, 3H, ^{i}Pr), 0.71 (d, *J* = 6.9, 3H, ^{i}Pr). ^{13}C{^{1}H} NMR (C_6D_6): δ 141.9 (C^1), 130.6 (C^2), 128.0 (C^4), 127.4 (C^3), 127.1 (C^5), 116.7 (C^6), 46.9 ($C^{2'}$), 44.7 ($C^{6'}$), 40.2 ($C^{1'}$), 35.7 ($C^{4'}$), 33.8 ($C^{5'}$), 27.6 (^{i}Pr methine), 25.2 ($C^{3'}$), 22.8 ($C^{5'}$-*C*H$_3$), 21.9 (^{i}Pr), 21.0 (C^4-*C*H$_3$), 16.3 (^{i}Pr). Key ^{1}H-^{1}H NOESY correlations (C_6D_6): 6.96/1.56 (C^3-H/H_I), 6.96/1.03 (C^3-H/H_B), 2.82/2.36 (NH_2/H_A). Key ^{1}H NMR resonances of **3-*sc***: ^{1}H NMR (C_6D_6): δ 6.84 (d, *J* = 8.0, 1H, C^5-H), 6.78 (s, 1H, C^3-H), 6.34 (d, *J* = 7.9, 1H, C^6-H), 2.41 (td, *J* = 11.4, 3.4, 1H, H_A), 2.20 (s, 3H, C^4-C*H*$_3$), 1.69 (septet d, *J* = 7.0, 2.7, 1H, ^{i}Pr methine), 1.50 (q, *J* = 12.4, 1H, H_B), 1.39-1.29 (m, 1H, H_D), 0.92 (d, *J* = 6.5, 3H, $C^{5'}$-C*H*$_3$), 0.88 (d, *J* = 7.0, 3H, ^{i}Pr), 0.73 (d, *J* = 7.0, 3H, ^{i}Pr). Key ^{1}H-^{1}H COSY correlations (C_6D_6): 6.84/6.34 (C^5-H/C^6-H), 1.69/0.88, 1.69/0.73 (^{i}Pr C*H*/C*H*$_3$), 1.34/0.92 ($C^{5'}$-C*H*$_3$/H_D).

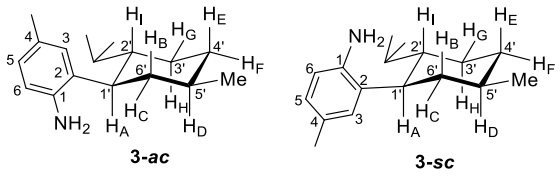

(a)

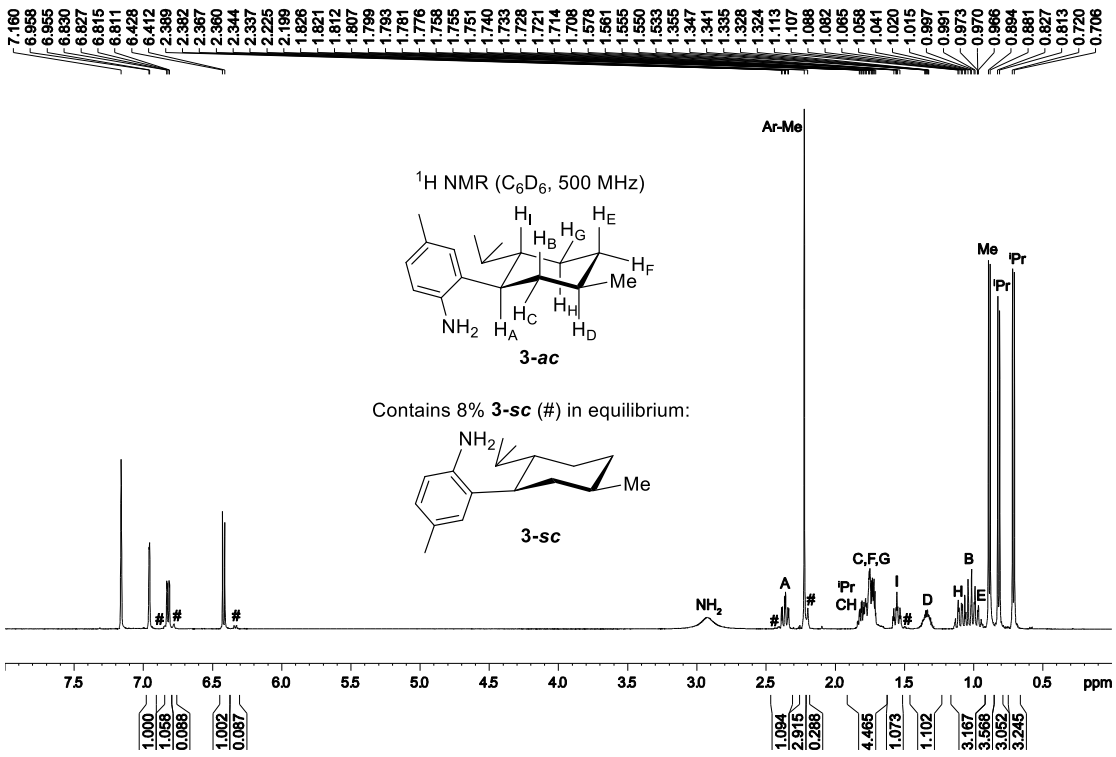

(b)

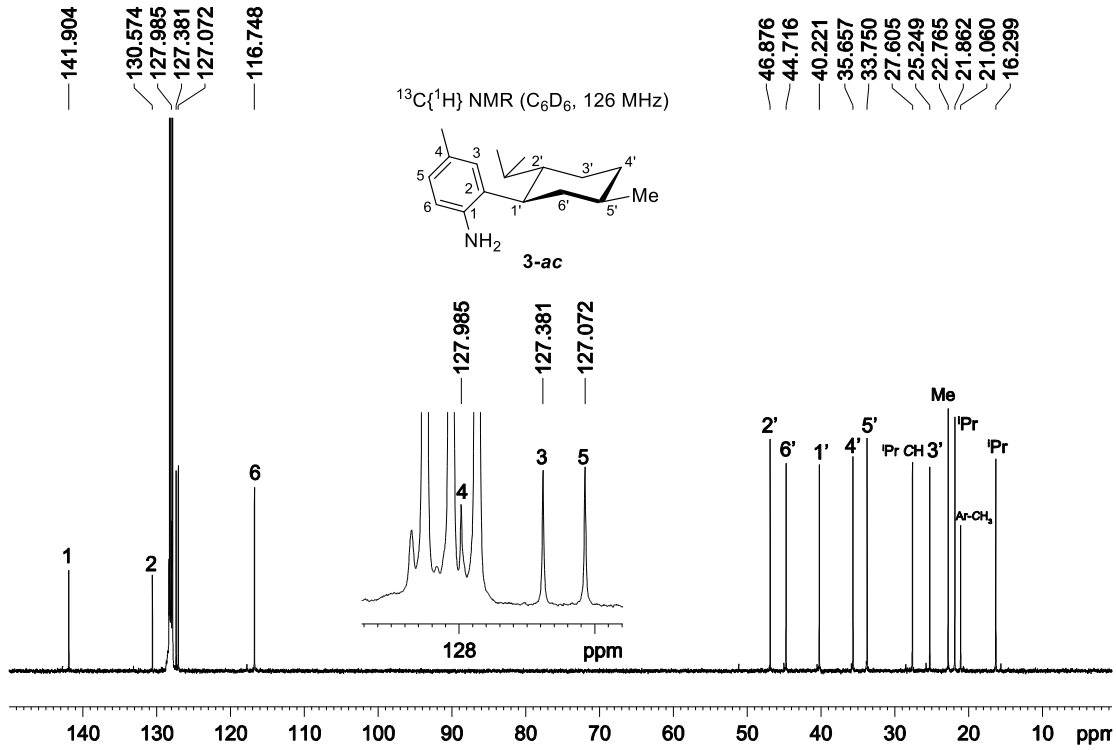

Figure 7.9. NMR spectra of **3**.

(c) COSY (C_6D_6, expansion of δ 3.3-0.0/3.3-0.0 region)

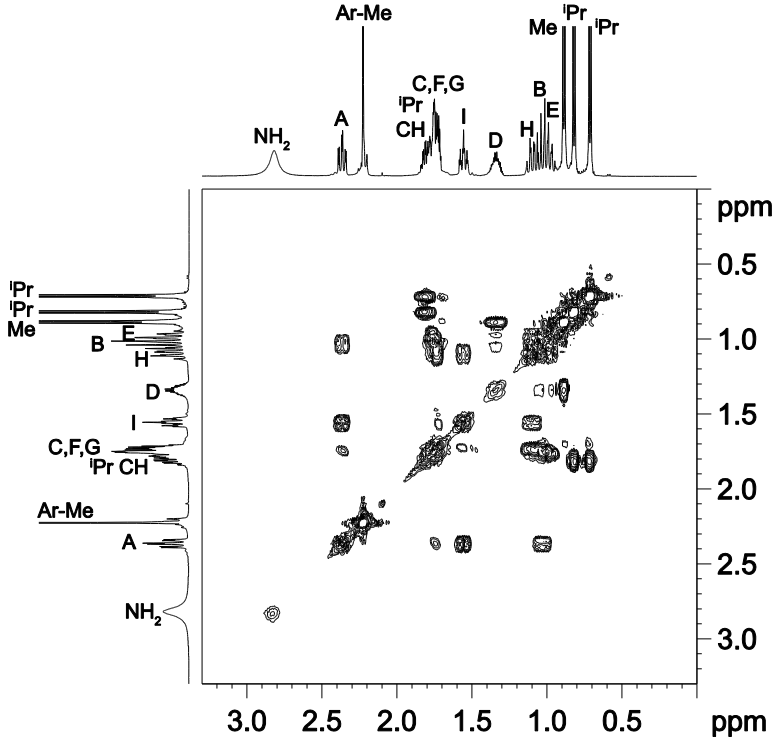

(d) HMQC (C_6D_6, expansion of δ 2.7-0.4/55-10 region)

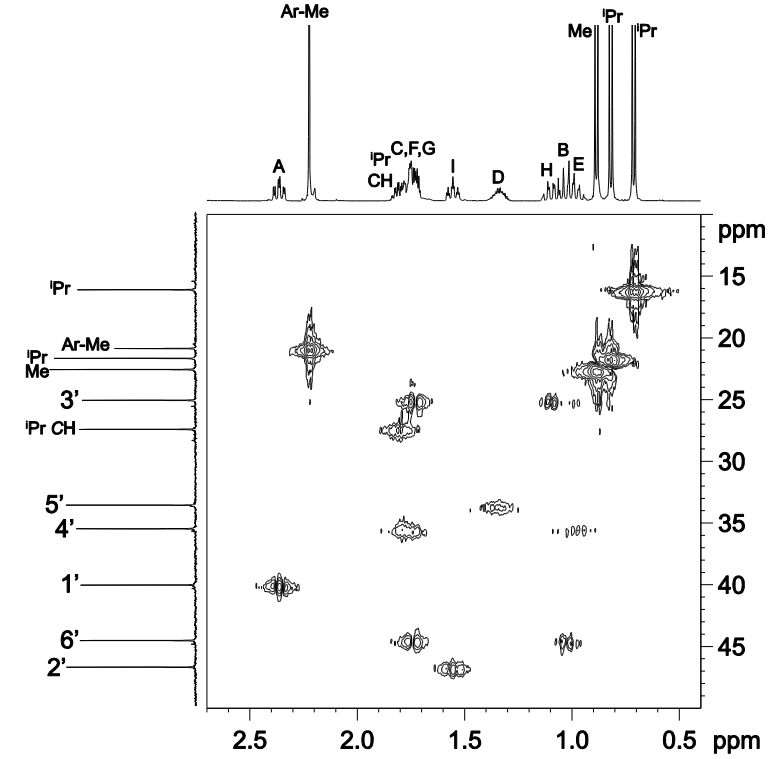

Figure 7.9, continued. NMR spectra of **3**.

(e) NOESY/EXSY (C_6D_6, expansion of δ 7.3-6.2/7.3-6.2 region). Black labels: **3-*ac***; red labels: **3-*sc***.

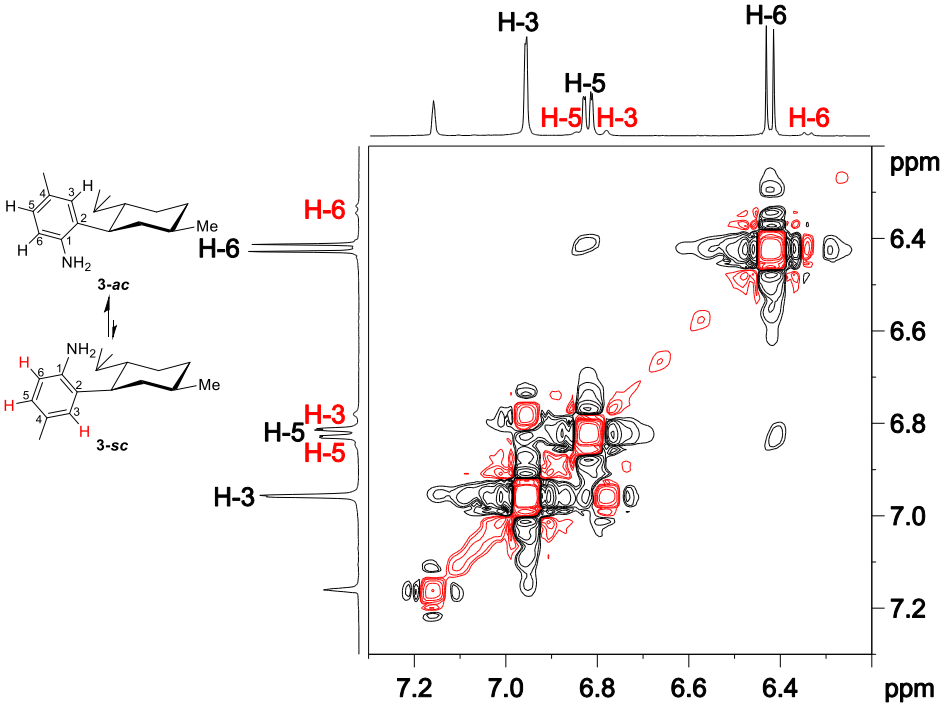

(f) NOESY/EXSY (C_6D_6, expansion of δ 7.3-2.5/3.0-0.6 region)

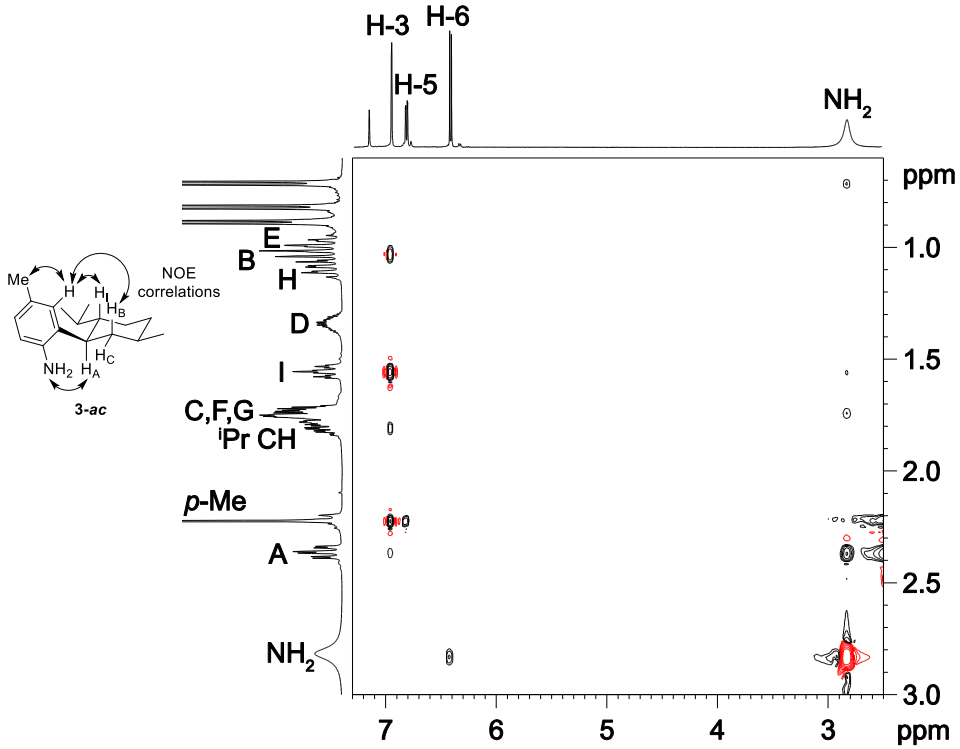

Figure 7.9, continued. NMR spectra of **3**.

Data for **3·HCl**: ^{1}H NMR (DMSO-d_6): δ 10.17 (br s, 3H, Ar-NH_3^+), 7.29 (d, J = 8.0, 1H, C^6-H), 7.15 (d, J = 1.1, 1H, C^3-H), 7.06 (dd, J = 8.1, 1.3, 1H, C^5-H), 2.76 (td, J = 11.3, 2.7, 1H, H_A), 2.28 (s, 3H, C^4-CH_3), 1.82-1.69 (m, 3H, H_C + H_F + H_G), 1.64 (tt, J = 11.3, 2.4, 1H, H_I), 1.58-1.50 (m, 1H, H_D), 1.39 (septet d, J = 6.9, 2.1, 1H, ^{i}Pr methine), 1.12 (qd, J = 12.5, 2.3, 1H, H_H), 0.98 (qd, J = 12.5, 2.6, 1H, H_E), 0.86 (q, J = 12.1, 1H, H_B), 0.82 (d, J = 6.5, 3H, $C^{5'}$-CH_3), 0.79 (d, J = 7.0, 3H, ^{i}Pr), 0.64 (d, J = 6.9, 3H, ^{i}Pr). ^{13}C{^{1}H} NMR (DMSO-d_6): δ 139.1, 137.6, 127.9, 127.3, 127.2, 123.8, 45.0 ($C^{2'}$ + $C^{6'}$), 39.6 ($C^{1'}$), 34.6 ($C^{4'}$), 32.2 ($C^{5'}$), 27.0 (^{i}Pr methine), 24.2 ($C^{3'}$), 22.2 ($C^{5'}$-CH$_3$), 21.7 (^{i}Pr), 20.8 (C^4-CH$_3$), 16.1 (^{i}Pr).

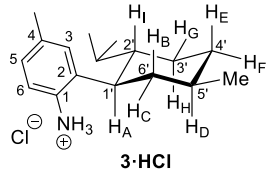

(a)

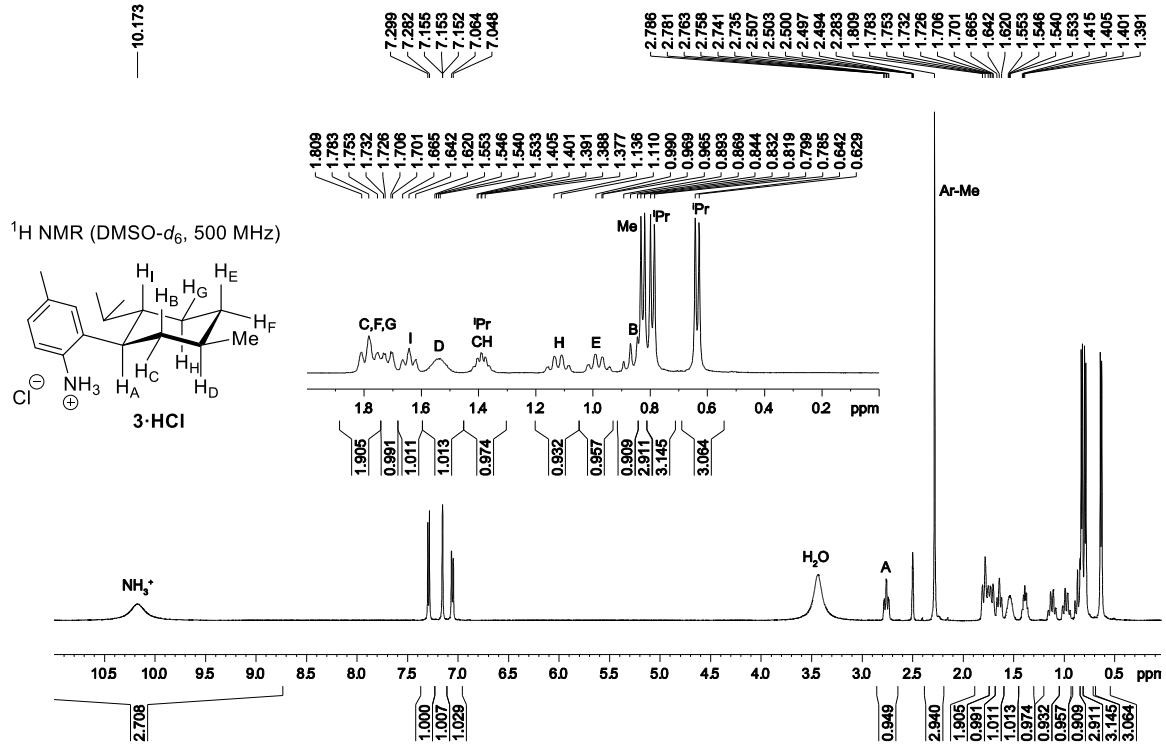

Figure 7.10. NMR spectra of **3·HCl**.

(b)

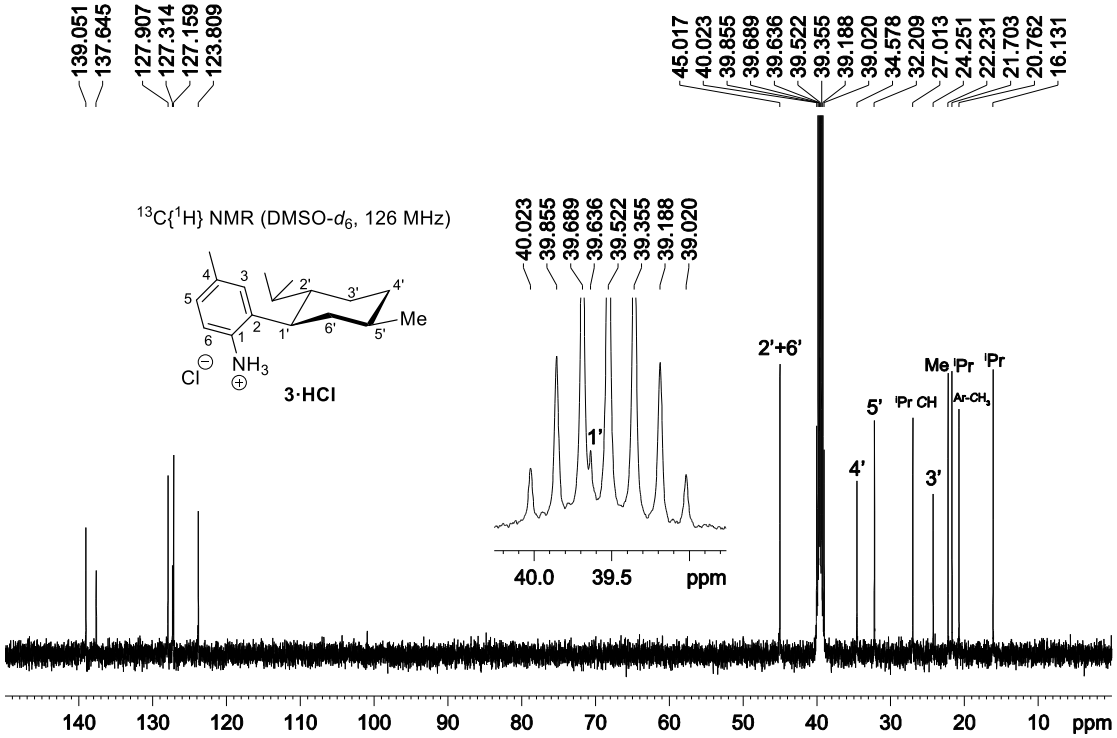

(c) HMQC (DMSO-d_6, expansion of δ 3.8-0.5/55-10 region)

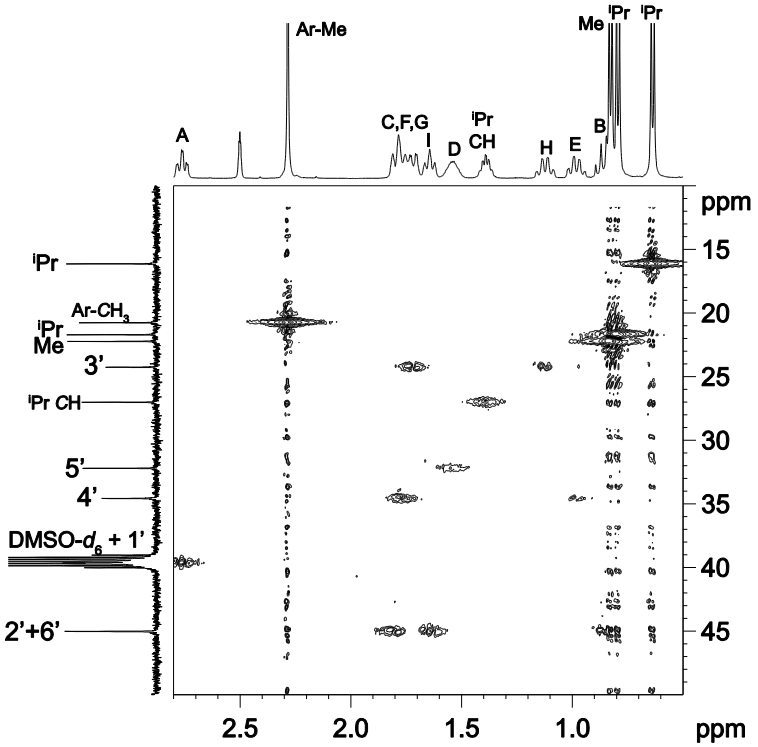

Figure 7.10, continued. NMR spectra of **3·HCl**.

2-[(1*R*,2*S*,5*R*)-Menthyl]-4,6-dimethylaniline (**4**). A Schlenk flask was charged with anhydrous $ZnCl_2$ (6.83 g, 50 mmol), THF (50 mL) and NEP (10 mL) under N_2, and the mixture was stirred vigorously until dissolution of the $ZnCl_2$ was complete (ca. 10 min). A solution of MenMgCl/NeomMgCl in THF (40 mmol in 80 mL) was added via syringe, and the mixture was stirred at room temperature. A second Schlenk flask was charged with 2-iodo-4,6-dimethylaniline (**2**, 4.10 g, 16.6 mmol), $Pd(dba)_2$ (98 mg, 0.17 mmol), S-Phos (70 mg, 0.17 mmol) and THF (30 mL) under N_2, and the mixture was stirred at room temperature for 10 min. The Zn reagent solution was then transferred into the second flask via cannula. The mixture was stirred at room temperature for 18 h and quenched with saturated aqueous NH_4Cl solution (50 mL). The THF was removed on a rotovap. The remaining aqueous phase was extracted with Et_2O (3 x 50 mL). The combined extract was washed with water (2 x 20 mL) and brine (20 mL), dried with $MgSO_4$, filtered, and taken to dryness under vacuum to yield a brown oil. The residue was subjected to flash column chromatography (silica, hexane/Et_2O = 10/1 by volume) to yield a yellow oil as crude product. Distillation (95-110 °C, 10^{-3} mmHg) yielded **4** as a yellow thick oil. Yield: 2.74 g (64%). The equilibrium **4-*ac*/*sc*** ratio is 12/1 in C_6D_6 at room temperature. HRMS (APCI-TOF, positive ion, *m*/*z*): Calc. 260.2378 ($[M + H]^+$), found 260.2389. Data for **4-*ac***: ^{1}H NMR (C_6D_6): δ 6.90 (s, 1H), 6.72 (s, 1H), 3.07 (br s, 2H, NH_2), 2.31 (td, *J* = 11.4, 3.3, 1H, H_A), 2.25 (s, 3H, C^4-C*H*$_3$), 1.95 (s, 3H, C^6-C*H*$_3$), 1.86 (septet d, *J* = 6.9, 2.6, 1H, ^{i}Pr methine), 1.82-1.71 (m, 3H, $H_C + H_F + H_G$), 1.60 (tt, *J* = 11.2, 2.7, 1H, H_I), 1.42-1.32 (m, 1H, H_D), 1.16-0.96 (m, 3H, $H_B + H_E + H_H$), 0.90 (d, *J* = 6.5, 3H, $C^{5'}$-C*H*$_3$), 0.84 (d, *J* = 7.0, 3H, ^{i}Pr), 0.73 (d, *J* = 6.9, 3H, ^{i}Pr). ^{13}C{^{1}H}NMR (C_6D_6): δ 139.9, 129.8, 128.7, 127.2, 125.2, 122.7, 46.9, 44.8, 40.5, 35.7, 33.8, 27.6, 25.3, 22.8, 21.9, 21.1, 18,3, 16.3. Key ^{1}H NMR resonances of **4-*sc***: ^{1}H NMR (C_6D_6): δ 6.74 (s, 1H, Ar), 6.72 (s, 1H, Ar), 3.19 (br s, 2H, NH_2), 2.48 (td, *J* = 12.2, 2.2, 1H, H_A), 2.22 (s, 3H, C^4-C*H*$_3$), 1.92 (s, 3H, C^6-C*H*$_3$).

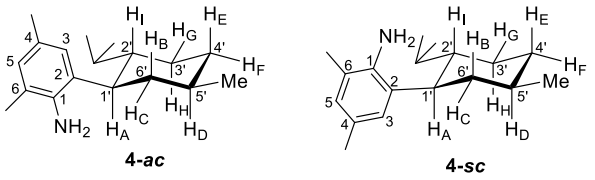

(a)

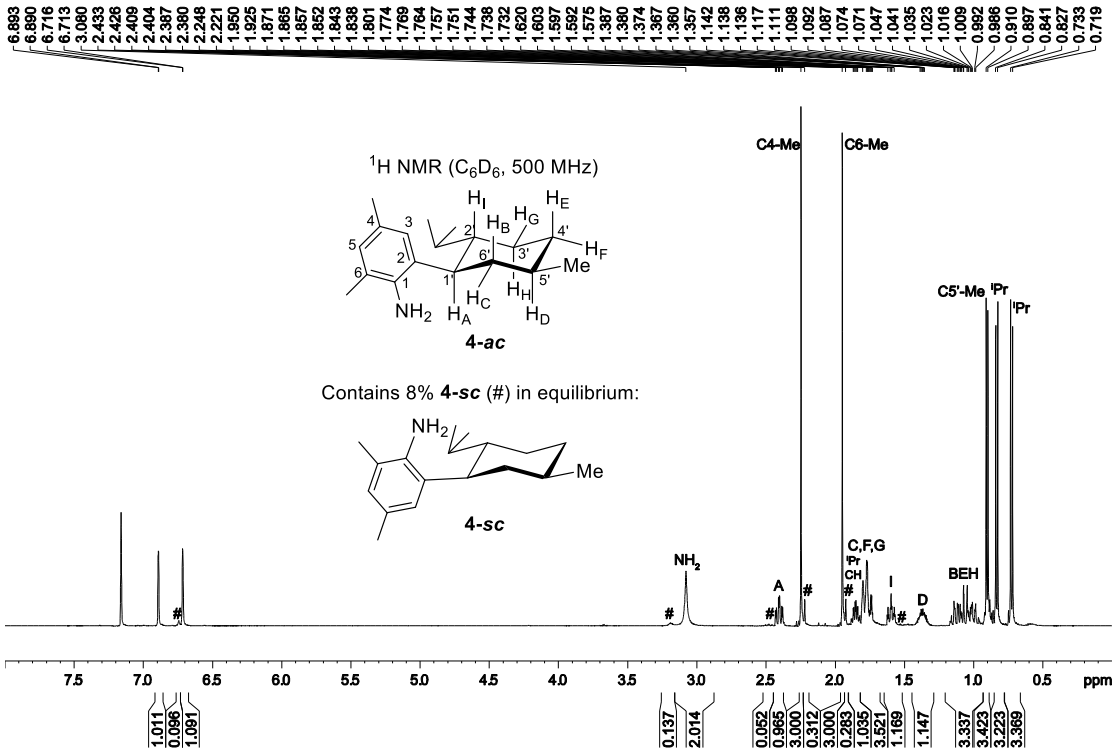

Figure 7.11. NMR spectra of **4**.

(b)

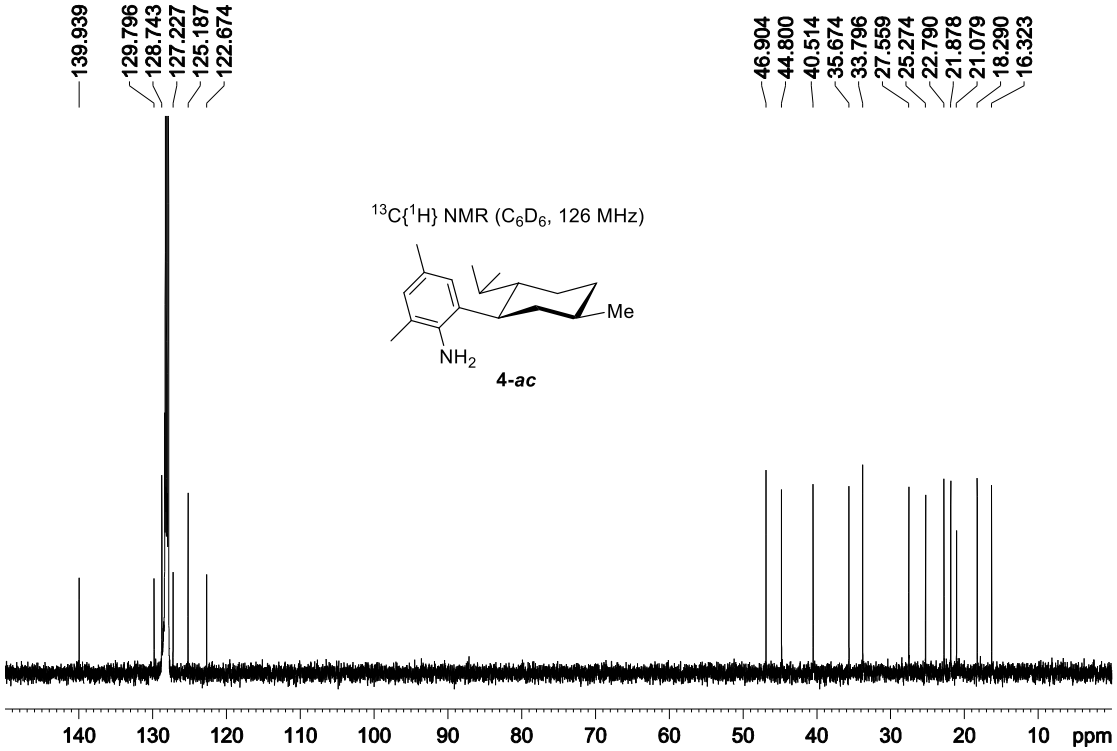

Figure 7.11, continued. NMR spectra of **4**.

(L1)ZnCl$_2$. A Schlenk flask was charged with acenaphthenequinone (206 mg, 1.13 mmol), **3** (611 mg, 2.49 mmol, 2.2 equiv) and anhydrous $ZnCl_2$ (386 mg, 2.83 mmol, 2.5 equiv) under N_2. N_2-sparged AcOH (4 mL) was added via syringe. The mixture was refluxed for 1 h and cooled to room temperature, yielding an orange precipitate and a dark red solution. The orange powder was collected by vacuum filtration, washed with AcOH (10 mL) and then ^{i}PrOH (2 mL), and dried under vacuum. Yield: 761 mg (87%). The equilibrium **(L1)ZnCl$_2$-*anti*/*syn*** ratio is ca. 10/1 in CD_2Cl_2 at room temperature based on ^{1}H NMR integration of the most high-field ^{i}Pr doublets. Anal. Calcd. for $C_{46}H_{56}Cl_2N_2Zn$, %: C, 71.45; H, 7.30; N, 3.62. Found: C, 71.19; H, 6.99; N, 3.54. Data for **(L1)ZnCl$_2$-*anti***: ^{1}H NMR (CD_2Cl_2): δ 8.16 (d, J = 8.1, 2H), 7.58 (dd, J = 8.2, 7.5, 2H), 7.36 (d, J = 1.2, 2H), 7.27 (d, J = 7.3, 2H), 7.18 (dd, J = 8.0, 1.2, 2H), 7.10 (d, J = 8.0, 2H), 3.00 (td, J = 11.4, 3.6, 2H, H_A), 2.49 (s, 6H, *p*-CH_3), 2.10 (dq, J = 12.5, 2.8, 2H, H_C), 1.80-1.72 (m, 4H,

H_D + H_F), 1.65-1.61 (m, 2H, H_G), 1.53 (tt, *J* = 11.1, 2.3, 2H, H_I), 1.34 (septet d, *J* = 6.9, 1.7, 2H, ^{i}Pr methine), 1.13 (q, *J* = 12.1, 2H, H_B), 1.06 (qd, *J* = 12.4, 2.3, 2H, H_H), 0.99 (qd, *J* = 12.6, 2.4, 2H, H_E), 0.89 (d, *J* = 6.3, 6H, C^5-C*H*$_3$), 0.63 (d, *J* = 6.9, 6H, ^{i}Pr), -0.13 (d, *J* = 6.8, 6H, ^{i}Pr). $^{13}C\{^1H\}$ NMR (CD_2Cl_2): δ 164.2 (C=N), 145.2, 141.1, 140.3, 139.8, 132.8, 131.2, 129.3, 128.8, 127.9, 126.8, 125.9, 122.4, 48.0 (C^2), 45.3 (C^6), 41.7 (C^1), 35.4 (C^4), 32.3 (C^5), 28.2 (^{i}Pr methine), 24.7 (C^3), 22.5 (C^5-*C*H$_3$), 21.7 (^{i}Pr), 21.6 (*p*-*C*H$_3$), 16.1 (^{i}Pr). Key ^{1}H NMR resonances of **(L1)ZnCl$_2$-*syn***: ^{1}H NMR (CD_2Cl_2): δ 8.15 (d, *J* = 8.2, 1H), 8.14 (d, *J* = 8.2, 1H), 7.557 (t, *J* = 8.0, 1H), 7.550 (t, *J* = 8.0, 1H), 7.32 (s, 1H), 7.05 (d, *J* = 7.3, 1H), 6.70 (br d, *J* = 7.2, 1H), 0.58 (d, *J* = 6.8, 3H), 0.40 (br d, *J* = 6.8, 3H), -0.25 (br d, *J* = 6.8, 3H).

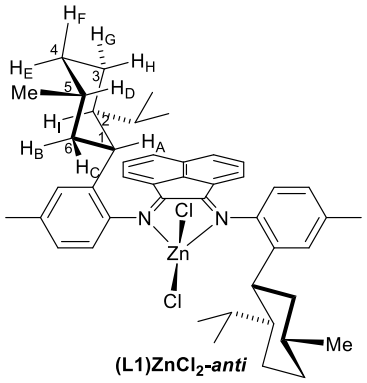

(L1)ZnCl$_2$-*anti*

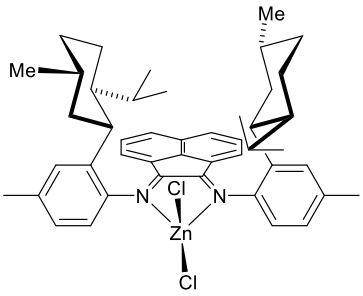

(L1)ZnCl$_2$-*syn*

(a)

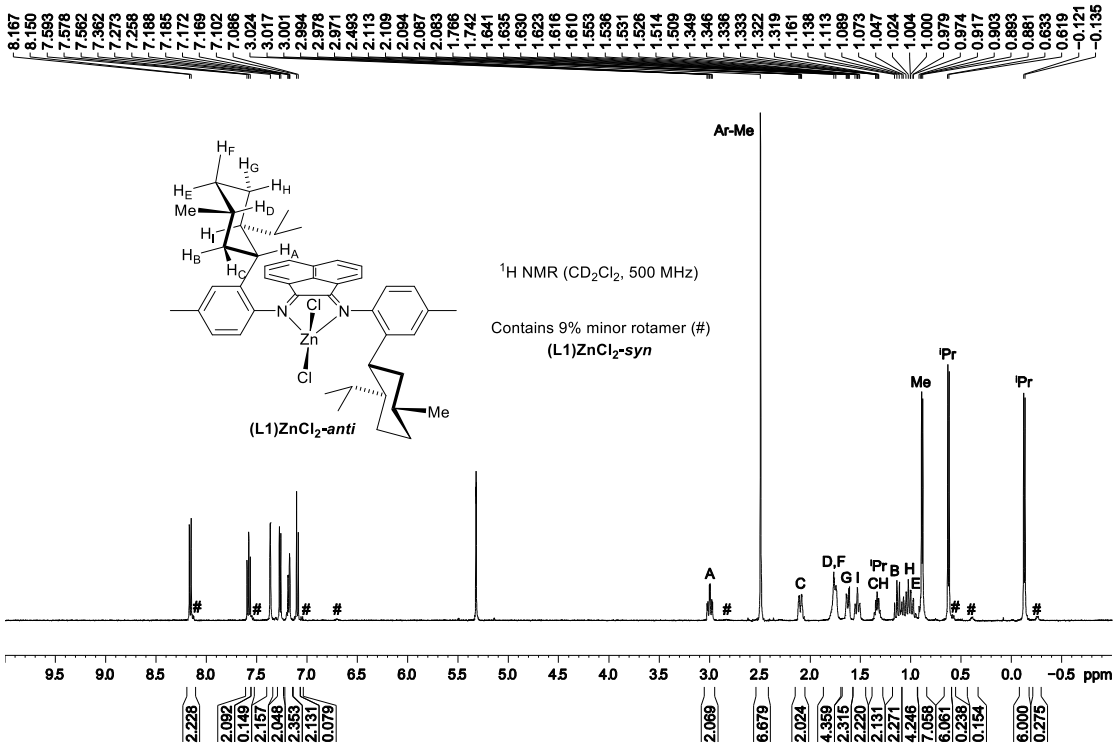

(b)

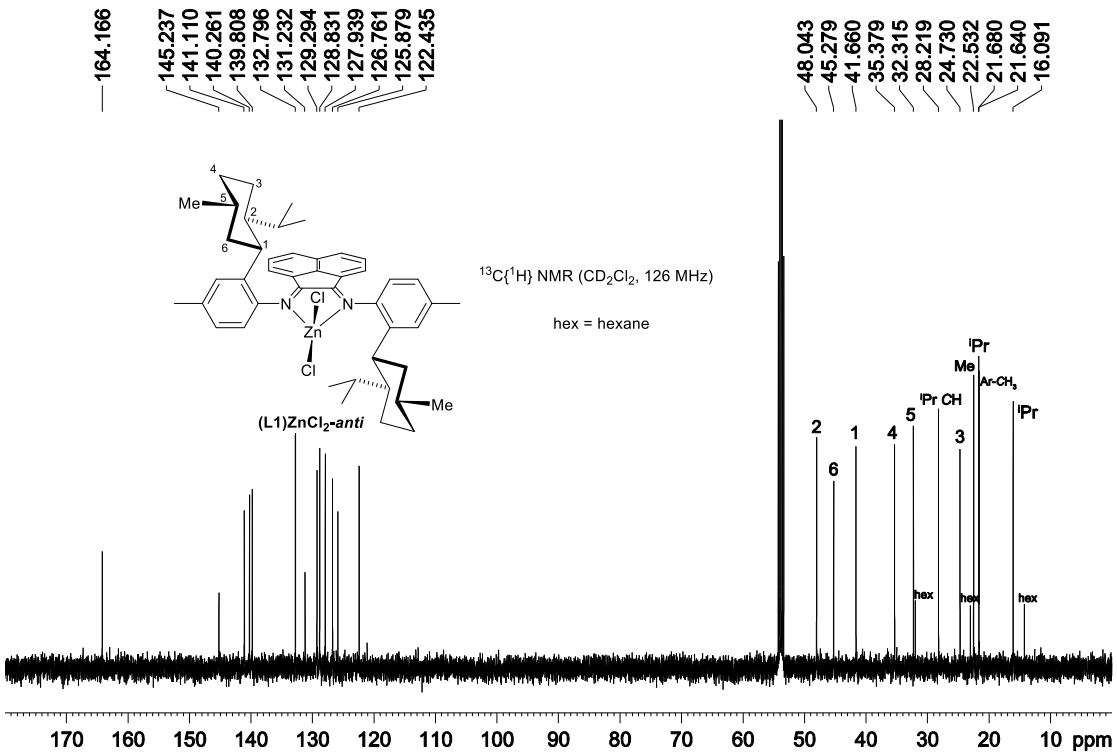

Figure 7.12. NMR spectra of **(L1)ZnCl2**.

(c) COSY (CD_2Cl_2, expansion of δ 3.4 to -0.4/3.4 to -0.4 region)

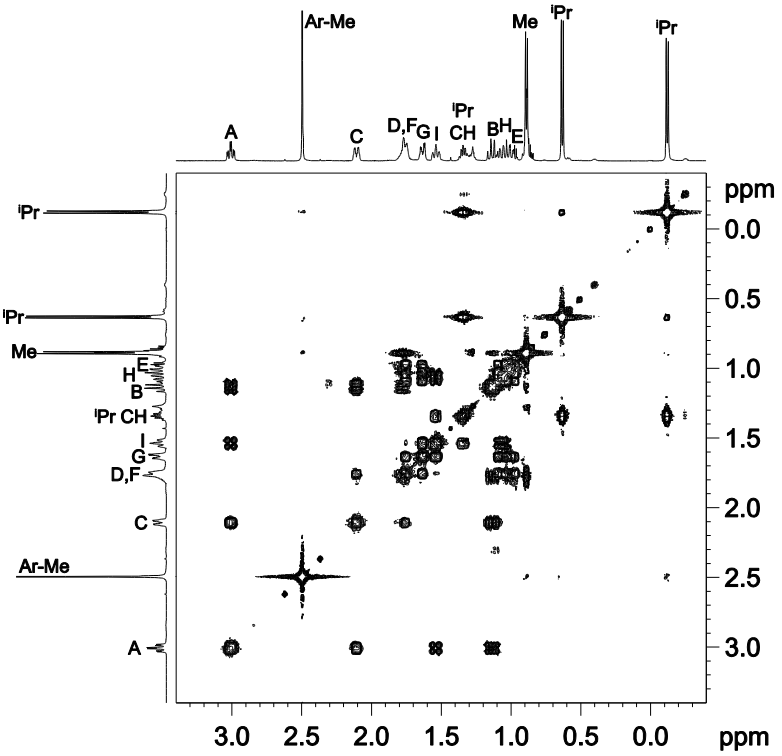

(d) HMQC (CD_2Cl_2, expansion of δ 3.4 to -0.4/55-10 region)

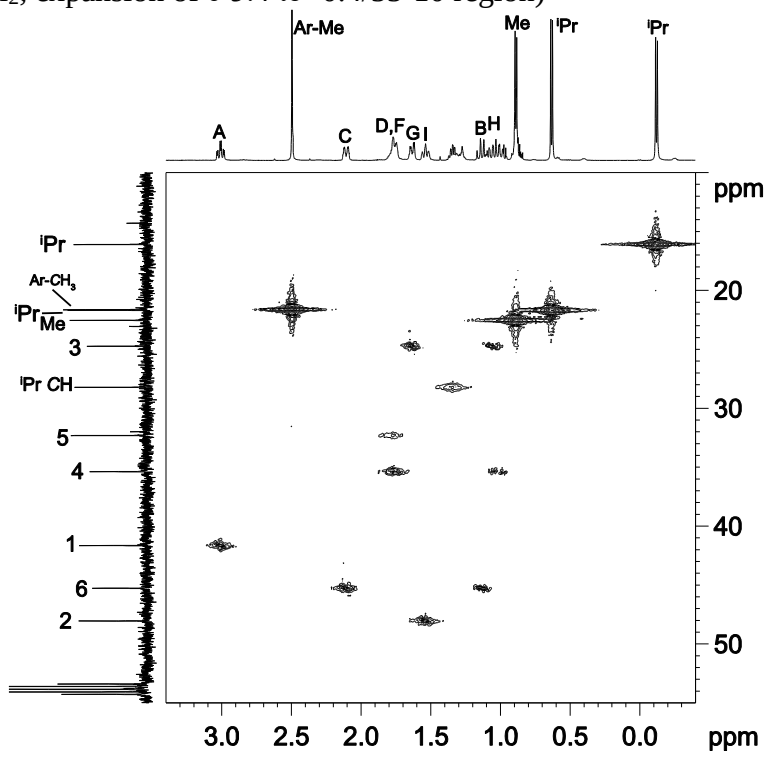

Figure 7.12, continued. NMR spectra of **(L1)ZnCl$_2$**.

(L2)ZnCl$_2$. A Schlenk flask was charged with acenaphthenequinone (366 mg, 2.01 mmol), **4** (1.20 g, 4.63 mmol, 2.3 equiv) and anhydrous $ZnCl_2$ (740 mg, 5.43 mmol, 2.7 equiv) under N_2. N_2-sparged AcOH (8 mL) was added via syringe. The mixture was refluxed for 1 h and cooled to room temperature, yielding a brown precipitate and a dark red solution. The solid was collected by vacuum filtration, washed with AcOH (10 mL) and then Et_2O (4 mL), and dried under vacuum to yield **(L2)ZnCl$_2$-*anti*** as a yellow powder. Yield: 761 mg (87%). Heating a solution of **(L2)ZnCl$_2$-*anti*** in $CDCl_2CDCl_2$ (ca. 9 mg in 0.5 mL) at 105 °C for 2 d yielded an 11/1 equilibrium mixture of **(L2)ZnCl$_2$-*anti*/*syn***. Anal. Calcd. for $C_{48}H_{60}Cl_2N_2Zn$, %: C, 71.95; H, 7.55; N, 3.50. Found: C, 71.97; H, 7.31; N, 3.35. Data for **(L2)ZnCl$_2$-*anti***: ^{1}H NMR (CD_2Cl_2): δ 8.18 (d, *J* = 8.2, 2H), 7.58 (dd, *J* = 8.3, 7.3, 2H), 7.19 (s, 2H), 7.07 (s, 2H), 7.05 (d, *J* = 7.3, 2H), 2.91 (td, *J* = 11.3, 3.7, 2H, H_A), 2.45 (s, 6H, *p*-C*H*$_3$), 2.21 (s, 6H, *o*-C*H*$_3$), 2.06 (dq, *J* = 12.7, 2.9, 2H, H_C), 1.83-1.68 (m, 4H, H_D + H_F), 1.61-1.55 (m, 2H, H_G), 1.49 (tt, *J* = 9.9, 2.5, 2H, H_I), 1.22 (septet d, *J* = 6.8, 1.3, 2H, ^{i}Pr methine), 1.07 (q, *J* = 11.9, 2H, H_B), 1.01-0.92 (m, 4H, H_E + H_H), 0.87 (d, *J* = 6.5, 6H, C^5-C*H*$_3$), 0.54 (d, *J* = 6.9, 6H, ^{i}Pr), -0.35 (d, *J* = 6.9, 6H, ^{i}Pr). ^{13}C{^{1}H} NMR (CD_2Cl_2): δ 165.0 (C=N), 144.7, 139.97, 139.95, 138.5, 133.0, 131.0, 130.3, 129.2, 129.0, 126.9, 126.6, 126.1, 47.9 (C^2), 45.9 (C^6), 42.1 (C^1), 35.2 (C^4), 32.3 (C^5), 28.2 (^{i}Pr methine), 24.8 (C^3), 22.5 (C^5-*C*H$_3$), 21.6 (^{i}Pr), 21.5 (*p*-*C*H$_3$), 18.9 (*o*-*C*H$_3$), 16.0 (^{i}Pr). Key ^{1}H NMR resonances of **(L2)ZnCl$_2$-*syn***: ^{1}H NMR ($CDCl_2CDCl_2$): δ 6.85 (d, *J* = 7.4, 1H), 6.41 (d, *J* = 7.4, 1H), 3.25 (t, *J* = 11.5, 1H), 2.81 (t, *J* = 11.5, 1H), 0.34 (d, *J* = 6.3, 3H), -0.49 (d, *J* = 6.8, 3H).

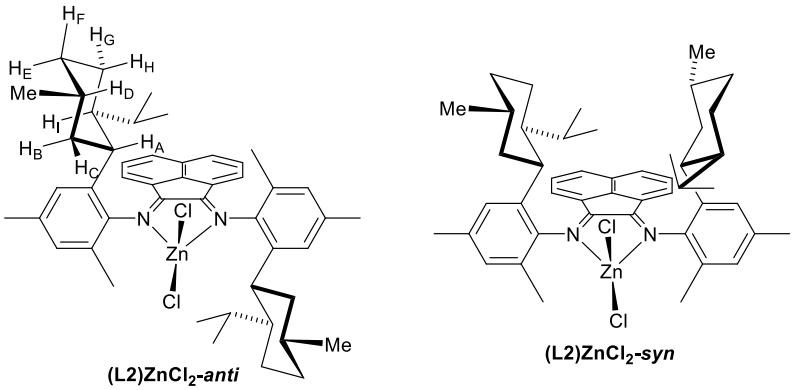

(a)

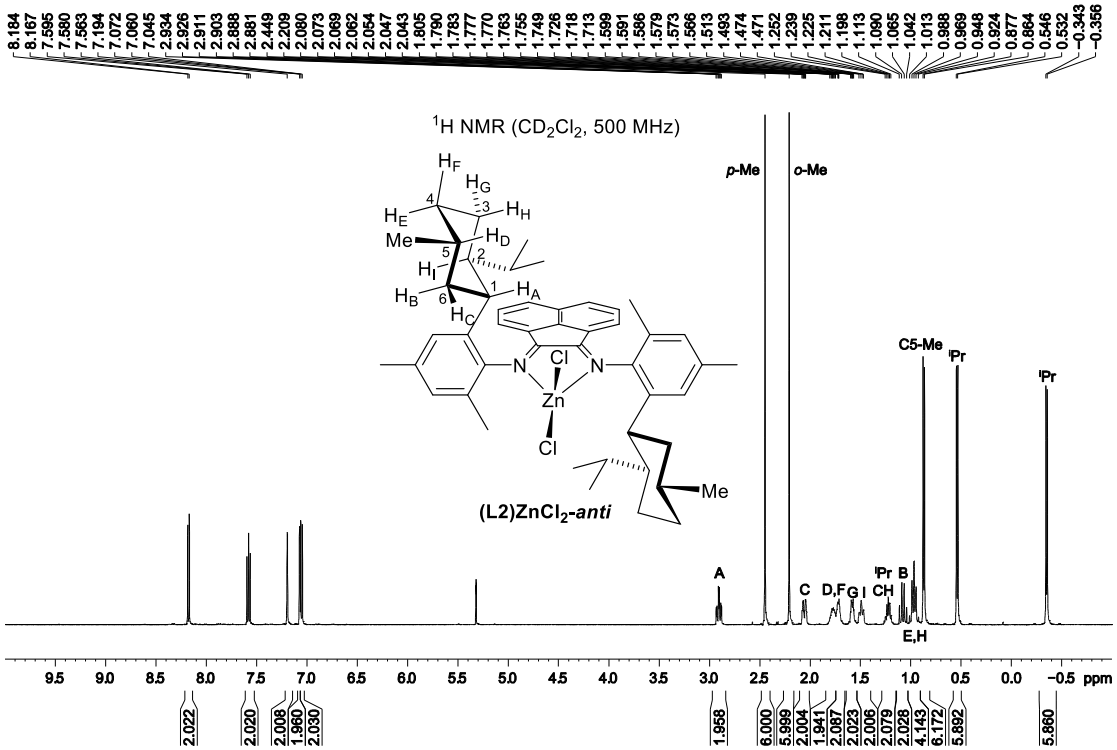

Figure 7.13. NMR spectra of **(L2)ZnCl2-*anti***.

(b)

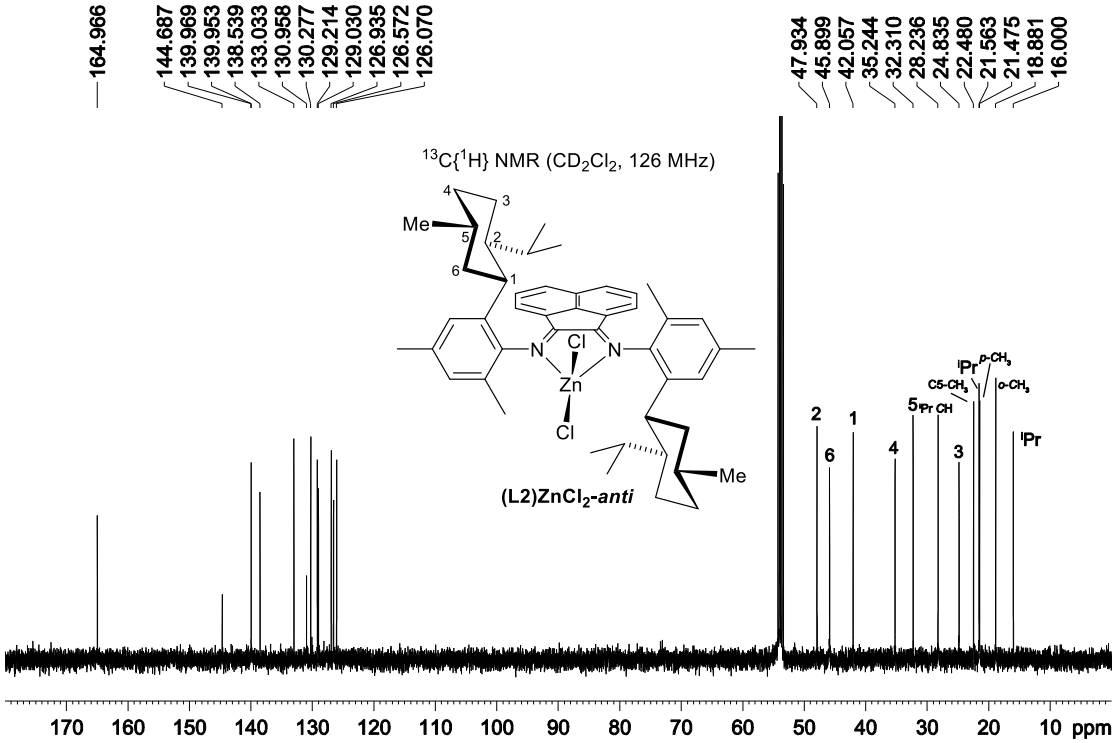

(c) COSY (CD_2Cl_2, expansion of δ 8.5 to -0.5/8.5 to -0.5 region)

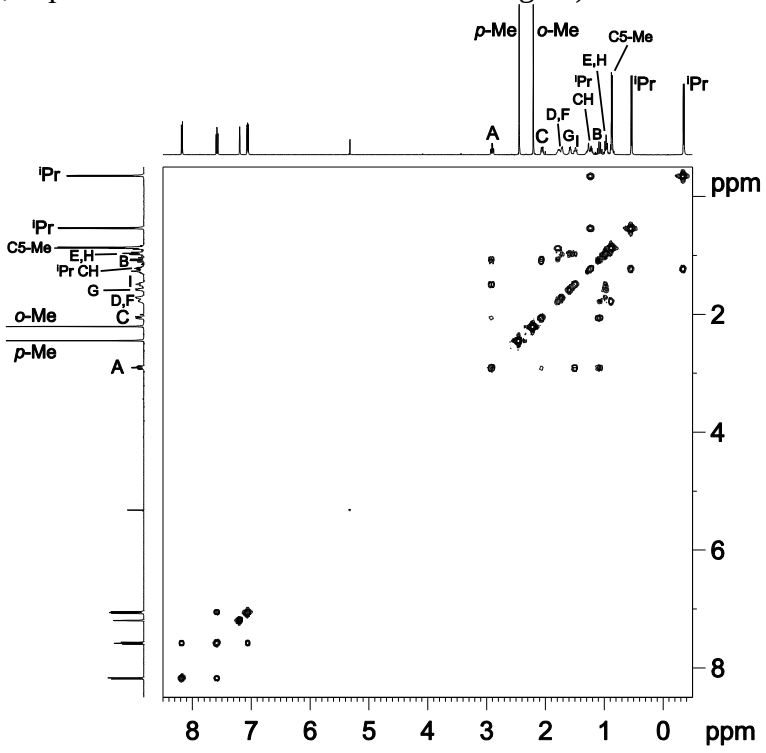

Figure 7.13, continued. NMR spectra of **(L2)ZnCl$_2$-*anti***.

(d) HMQC (CD_2Cl_2, expansion of δ 8.5 to -0.5/150-10 region)

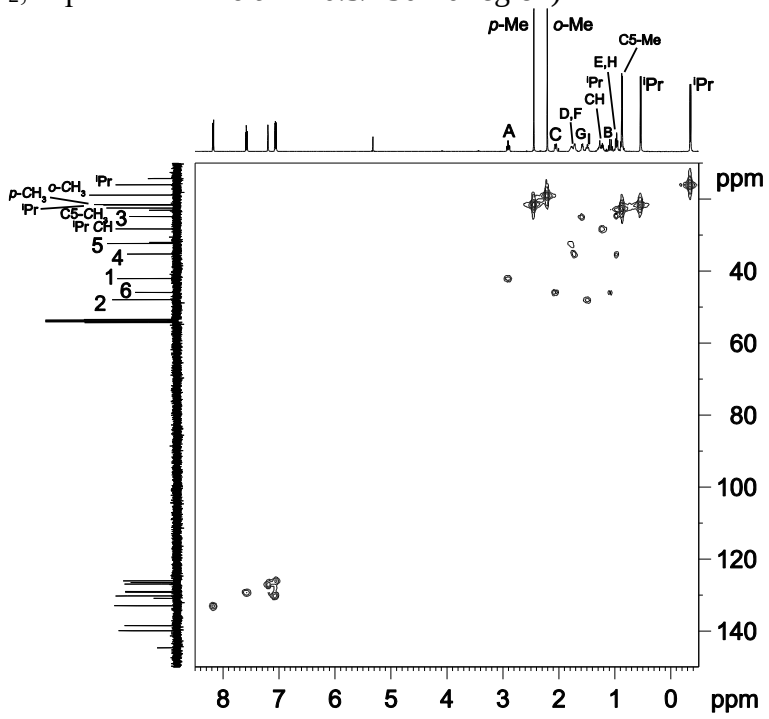

Figure 7.13, continued. NMR spectra of **(L2)ZnCl$_2$-*anti***.

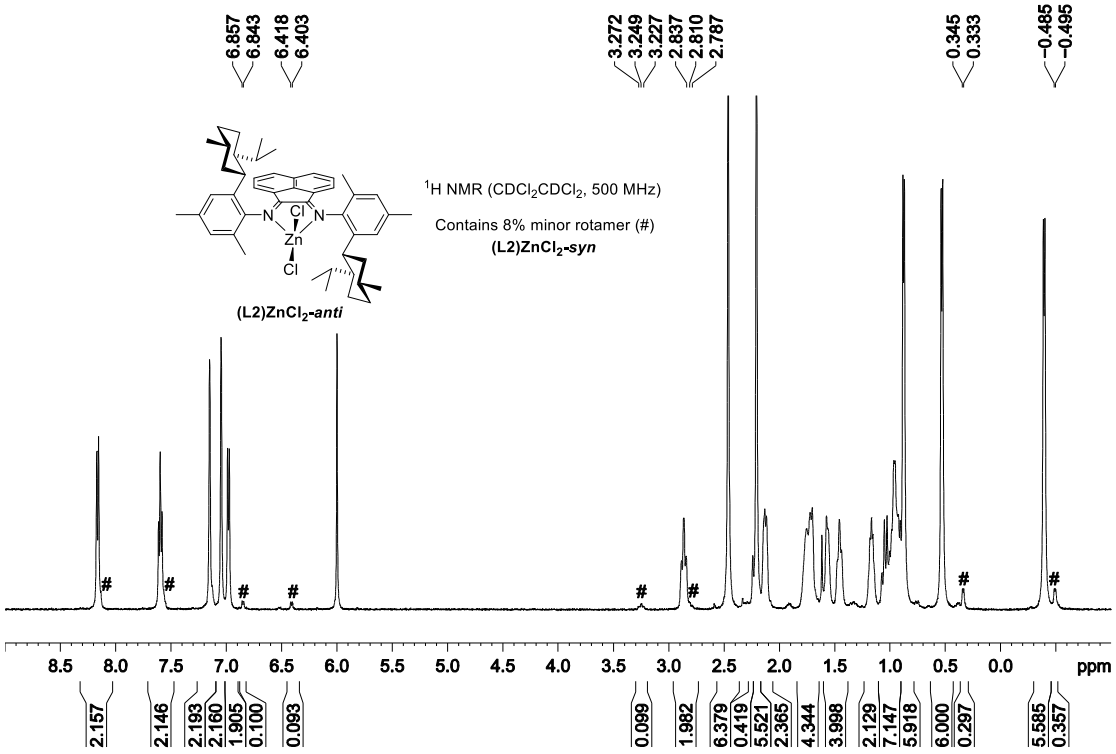

Figure 7.14. ^{1}H NMR spectrum of a 11/1 mixture of **(L2)ZnCl$_2$-*anti*/*syn***.

L1. A separatory funnel was charged with **(L1)ZnCl$_2$** (760 mg, 0.98 mmol) and CH_2Cl_2 (20 mL). $K_2C_2O_4 \cdot H_2O$ aqueous solution (553 mg, 3.00 mmol in 20 mL) was added, and the funnel was capped and shaken vigorously for 5 min. The cloudy aqueous layer was removed. The red organic layer was washed with water (2 x 10 mL) and brine (10 mL), dried with Na_2SO_4, filtered, and taken to dryness under vacuum to yield a yellow solid. Yield: 572 mg (91%). The *Z,E* equilibrium **L1-*E,E*/*Z,E*** ratio is 6.7/1 in CD_2Cl_2 at room temperature based on ^{1}H NMR integration of the aromatic resonances. HRMS (ESI-TOF, positive ion, *m*/*z*): Calc. 637.4522 ([M + H]$^+$), found 637.4524. Data for **L1-*E,E***: ^{1}H NMR (CD_2Cl_2): δ 7.89 (d, *J* = 8.2, 2H), 7.37 (t, *J* = 7.8, 2H), 7.21 (s, 2H), 7.06 (d, *J* = 8.3, 2H), 7.00 (br, 2H), 6.88 (d, *J* = 7.9, 2H), 2.81 (br t, *J* = 9.9, 2H), 2.44 (s, 6H), 1.75-1.48 (m, 10H), 1.29 (br, 2H), 1.11-0.93 (m, 6H), 0.74-0.37 (br, 18H). ^{13}C{^{1}H} NMR (CD_2Cl_2): δ 160.6, 147.8, 141.9, 136.3, 134.7, 131.5, 129.6, 128.9, 128.1, 127.7, 127.2, 123.8, 117.7, 47.8, 45.1, 41.3, 35.6, 33.5, 28.1, 25.0, 22.6, 21.9, 21.4, 16.3. Key ^{1}H NMR resonances of **L1-*Z,E***: ^{1}H NMR (CD_2Cl_2): δ 8.09 (d, *J* = 7.1, 1H), 8.03 (d, *J* = 8.2, 1H), 7.94 (d, *J* = 8.2, 1H), 7.79 (t, *J* = 7.7, 1H). NMR experiments at -60 °C resolved the resonances of **L1-*E,E*-*syn***, which is the major species (ca. 70%) in the mixture. Data for **L1-*E,E*-*syn***: ^{1}H NMR (CD_2Cl_2, -60 °C): δ 7.88 (d, *J* = 8.2, 1H, *p*-An), 7.87 (d, *J* = 8.2, 1H, *p*-An), 7.36 (t, *J* = 7.7, 1H, *m*-An), 7.32 (t, *J* = 7.7, 1H, *m*-An), 7.19 (s, 1H, C^3-H or C$^{3'}$-H), 7.16 (d, *J* = 7.2, 1H, *o*-An), 7.14 (s, 1H, C^3-H or C$^{3'}$-H), 7.07 (d, *J* = 7.7, 1H, C^5-H or C$^{5'}$-H), 6.99 (d, *J* = 8.0, 1H, C^5-H or C$^{5'}$-H), 6.89 (d, *J* = 7.8, 1H, C^6-H or C$^{6'}$-H), 6.78 (d, *J* = 7.8, 1H, C^6-H or C$^{6'}$-H), 6.66 (d, *J* = 7.2, 1H, *o*-An), 2.87 (td, *J* = 11.5, 3.4, 1H), 2.46 (td, *J* = 11.5, 3.4, 1H), 2.37 (s, 6H), 1.83-1.30 (m, 10H), 1.16-0.75 (m, 17H), 0.52 (d, *J* = 6.9, 3H), 0.45 (d, *J* = 6.4, 3H), -0.06 (d, *J* = 6.9, 3H). ^{13}C{^{1}H} NMR (CD_2Cl_2, -60 °C): δ 160.6, 159.4, 147.6, 145.8, 140.8, 137.1, 134.6, 133.4, 133.3, 130.5, 128.4, 128.34, 128.28, 128.20, 127.4 (2C), 127.12, 127.07, 126.8, 126.3, 123.2, 122.9, 117.1, 116.3, 47.5, 47.0,

43.9, 43.4, 39.8 (2C), 34.5 (2C), 32.4, 32.3, 27.6, 27.1, 24.1, 23.8, 22.2, 22.0, 21.4, 21.1, 20.9, 20.8, 16.0, 15.7.

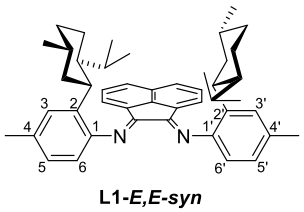

(a)

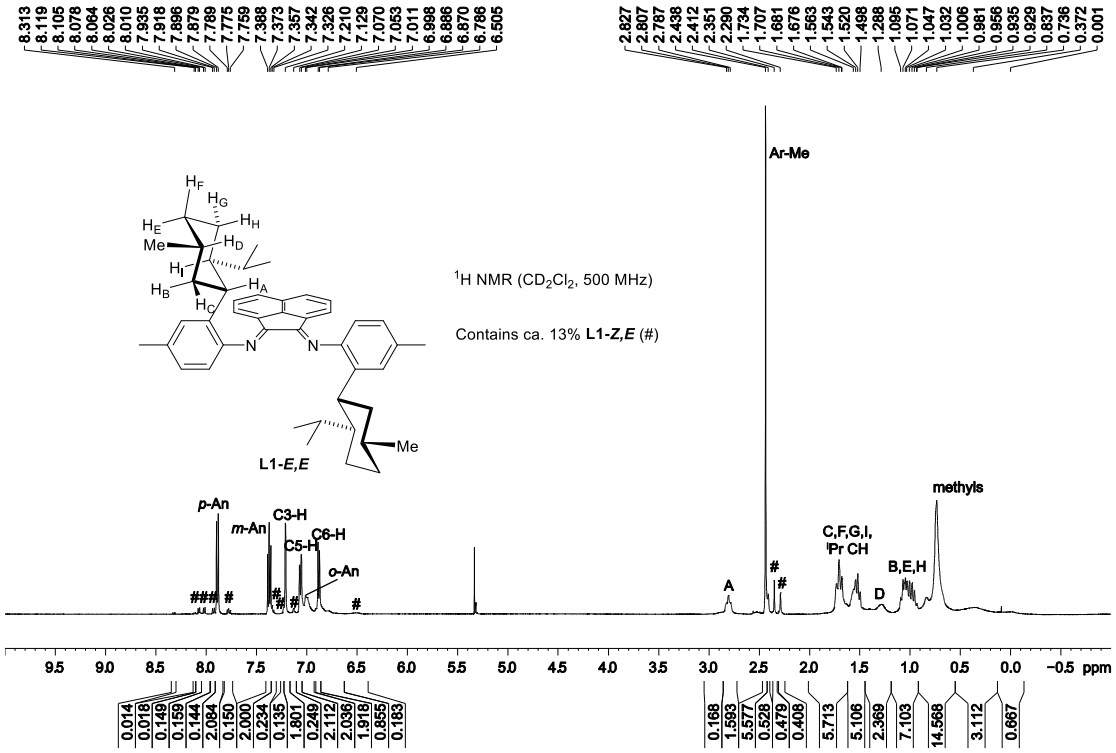

Figure 7.15. Room-temperature NMR spectra of **L1**.

(b)

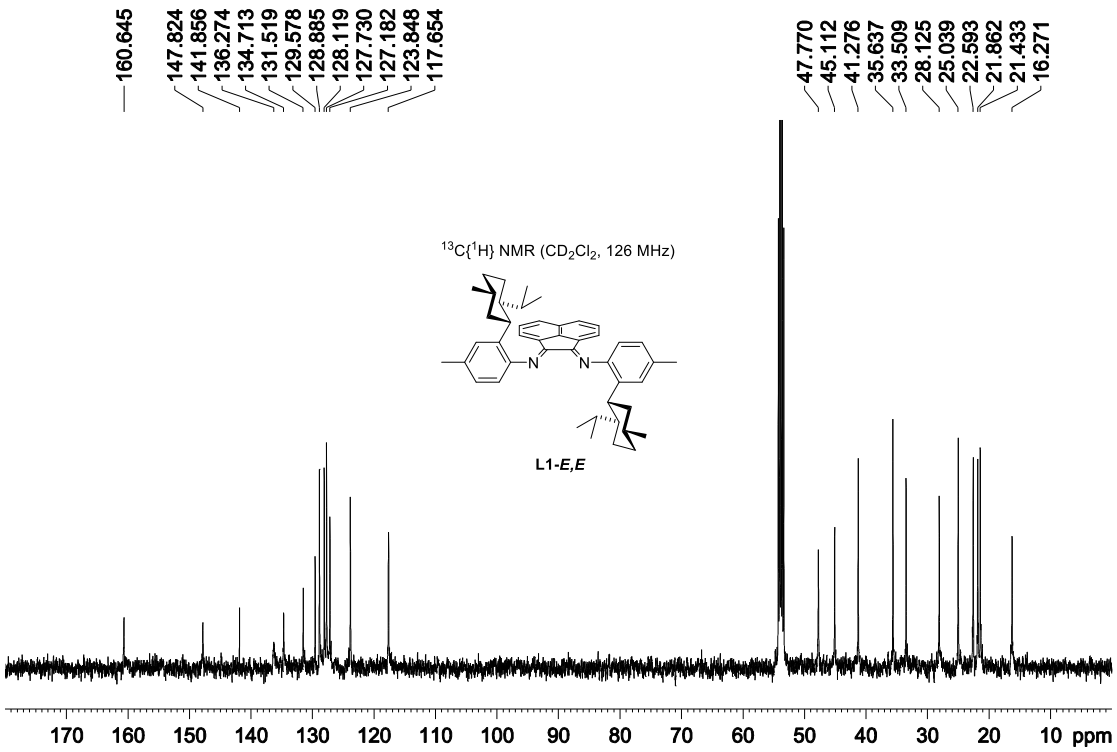

(c) COSY (CD_2Cl_2, expansion of δ 3.4 to -0.8/3.4 to -0.8 region)

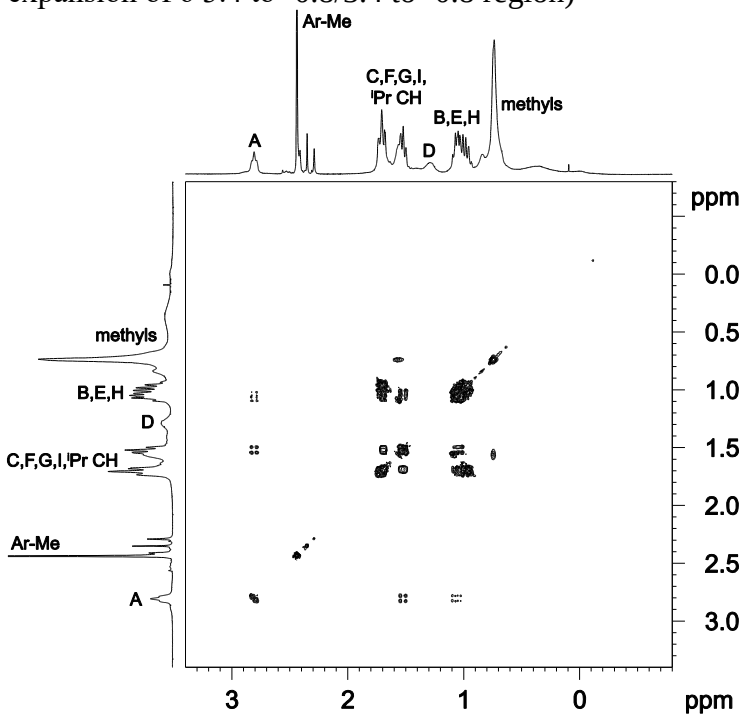

Figure 7.15, continued. Room-temperature NMR spectra of **L1**.

(d) HMQC (CD_2Cl_2, expansion of δ 9-0/150-0 region)

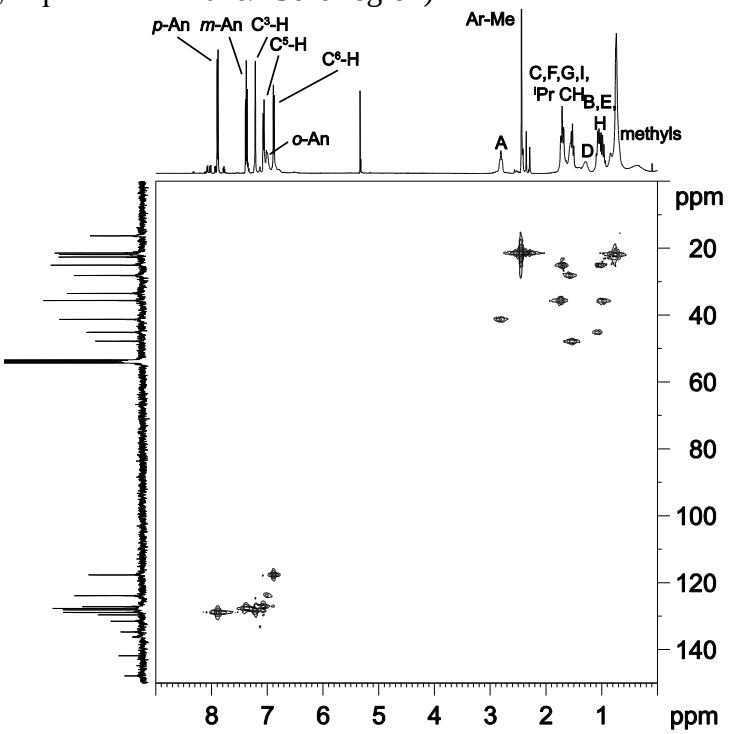

Figure 7.15, continued. Room-temperature NMR spectra of **L1**.

(a)

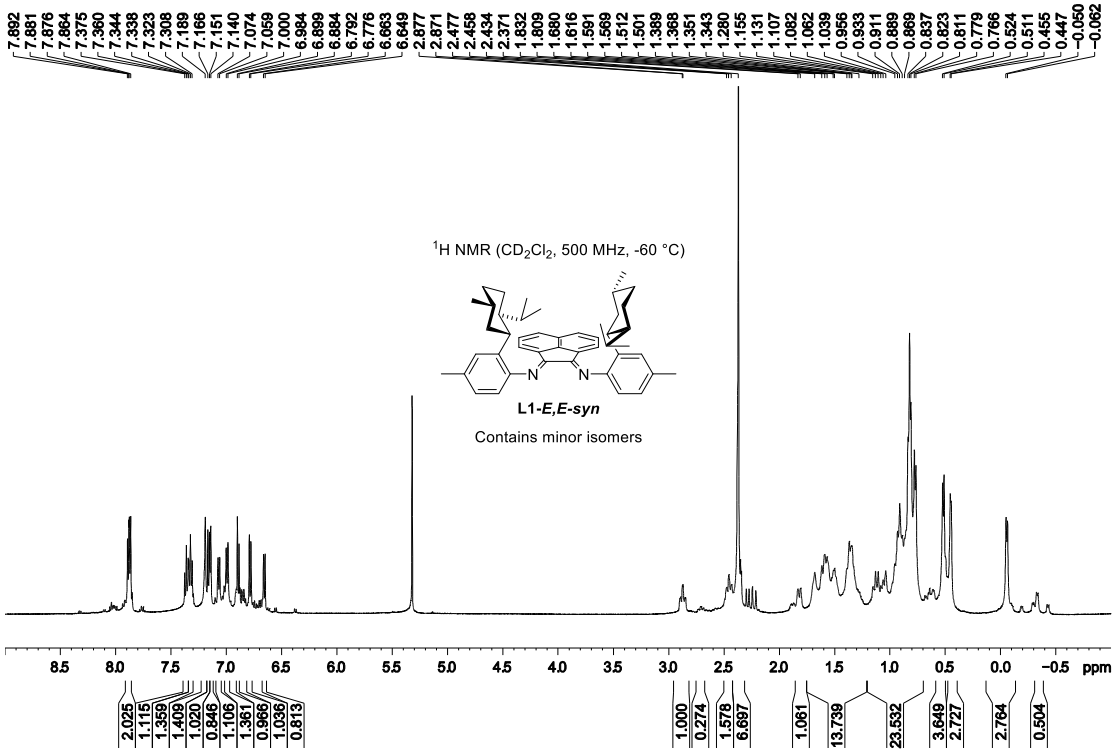

Figure 7.16. NMR spectra of **L1** at -60 °C.

(b)

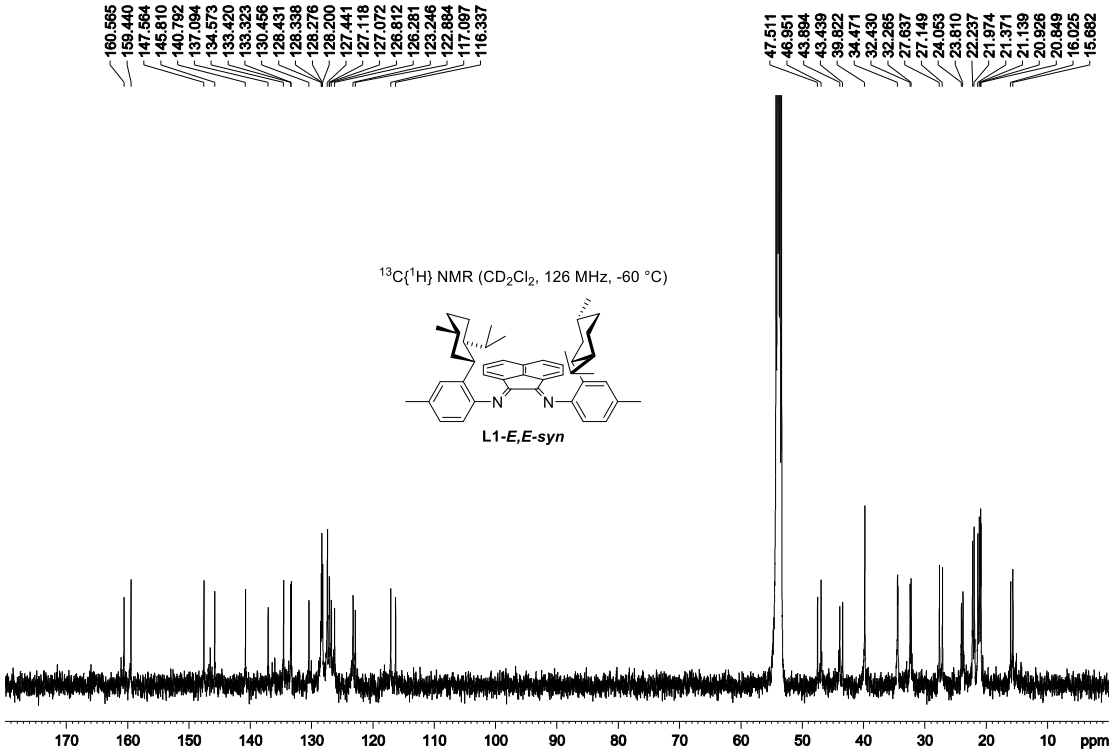

(c) NOESY/EXSY (CD_2Cl_2, -60 °C, expansion of δ 8.2-6.2/8.2-6.2 region)

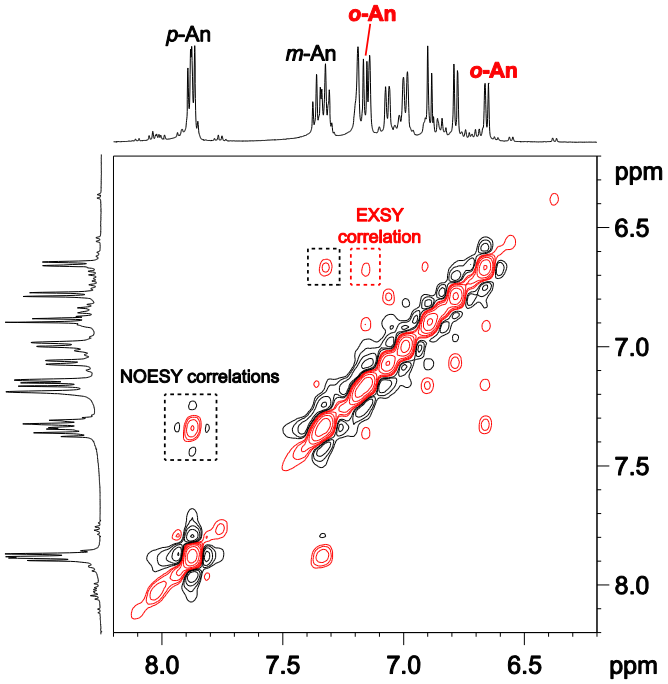

Figure 7.16, continued. NMR spectra of **L1** at -60 °C.

(d) NOESY/EXSY (CD_2Cl_2, -60 °C, expansion of δ 3.5 to -0.5/3.5 to -0.5 region)

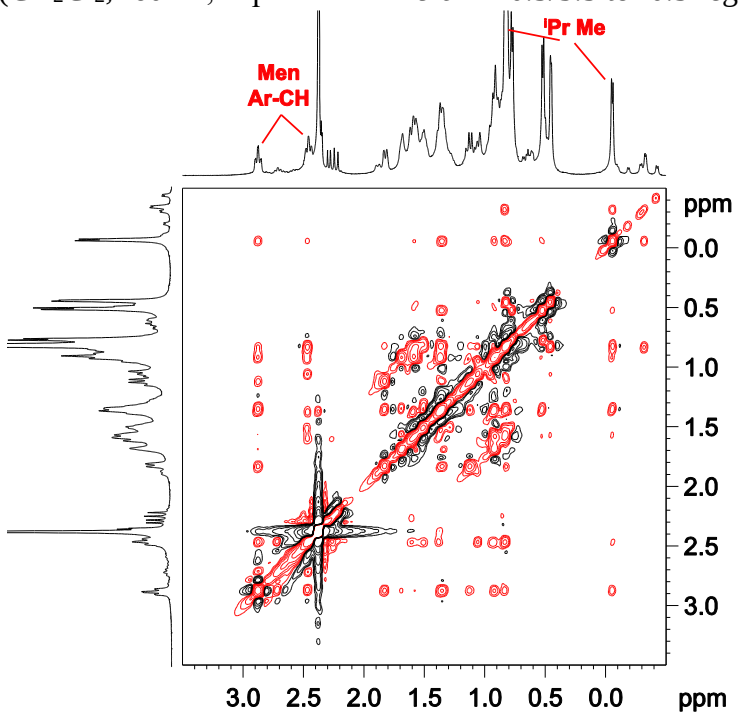

(e) HMQC (CD_2Cl_2, -60 °C, expansion of δ 9 to -1/150-10 region)

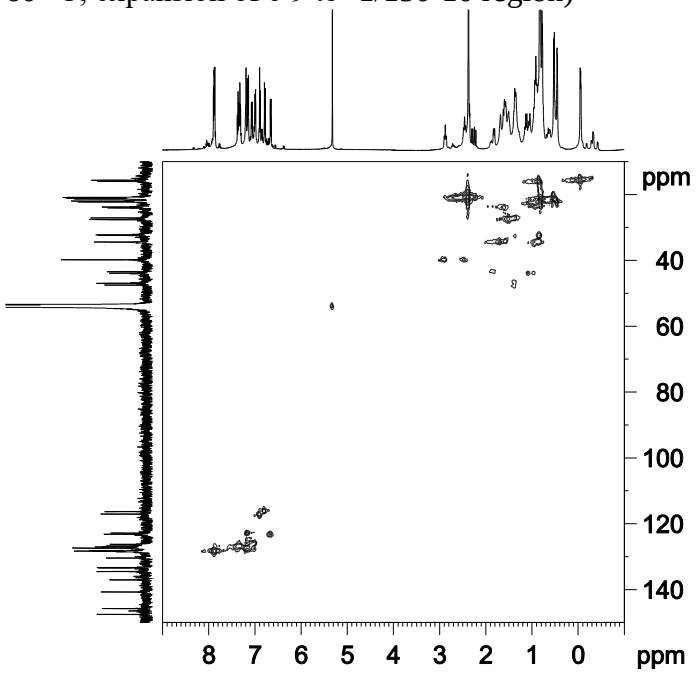

Figure 7.16, continued. NMR spectra of **L1** at -60 °C.

L2-*anti*. A separatory funnel was charged with **(L2)ZnCl$_2$** (850 mg, 1.06 mmol) and CH_2Cl_2 (20 mL). $K_2C_2O_4 \cdot H_2O$ aqueous solution (586 mg, 3.20 mmol in 20 mL) was added, and the funnel was capped and shaken vigorously for 4 min. The cloudy aqueous layer was removed. The red organic layer was washed with water (2 x 10 mL) and brine (10 mL), dried with Na_2SO_4, filtered, and taken to dryness under vacuum to yield a red foam. Yield: 641 mg (91%). This material is a 67/22/11 mixture of **L2-*E,E-anti*/*Z,E-anti*/*E,E-syn*** (overall *anti*/*syn* = 89/11) based on ^{1}H NMR integration of the ^{i}Pr doublets. Elongation of workup may increase the fraction of **L2-*E,E-syn***. The equilibrium **L2-*E,E-anti*/L2-*Z,E-anti*** ratio is ca. 3.1/1 in CD_2Cl_2 at room temperature. HRMS (ESI-TOF, positive ion, *m*/*z*): Calc. 665.4835 ($[M + H]^+$), found 665.4837. Anal. Calcd. for $C_{48}H_{60}N_2$, %: C, 86.69; H, 9.09; N, 4.21. Found: C, 86.44; H, 8.96; N, 4.01. Data for **L2-*E,E-anti***: ^{1}H NMR (CD_2Cl_2): δ 7.882 (d, *J* = 8.2, 2H), 7.356 (t, *J* = 7.8, 2H), 7.036 (s, 2H), 6.96 (s, 2H), 6.83 (d, *J* = 7.2, 2H), 2.64 (td, *J* = 11.3, 3.0, 2H), 2.41 (s, 6H), 2.04 (s, 6H), 2.03-1.97 (m, 2H), 1.72-1.32 (m, 10H), 1.02-0.82 (m, 12H), 0.62 (d, *J* = 6.9, 6H), -0.35 (d, *J* = 6.9, 6H). Key ^{1}H NMR resonances of **L2-*Z,E-anti***: ^{1}H NMR (CD_2Cl_2): δ 8.122 (d, *J* = 7.3, 1H), 8.035 (d, *J* = 8.2, 1H), 7.954 (d, *J* = 8.2, 1H), 7.789 (t, *J* = 7.8, 1H), 7.362 (t, *J* = 7.7, 1H), 6.91 (s, 1H), 6.88 (s, 1H), 6.83 (d, *J* = 7.3, 1H, overlapped), 6.79 (s, 2H), 2.30 (s, 3H), 2.27 (s, 3H), 2.12 (s, 3H), 1.76 (s, 3H), -0.16 (d, *J* = 6.9, 3H).

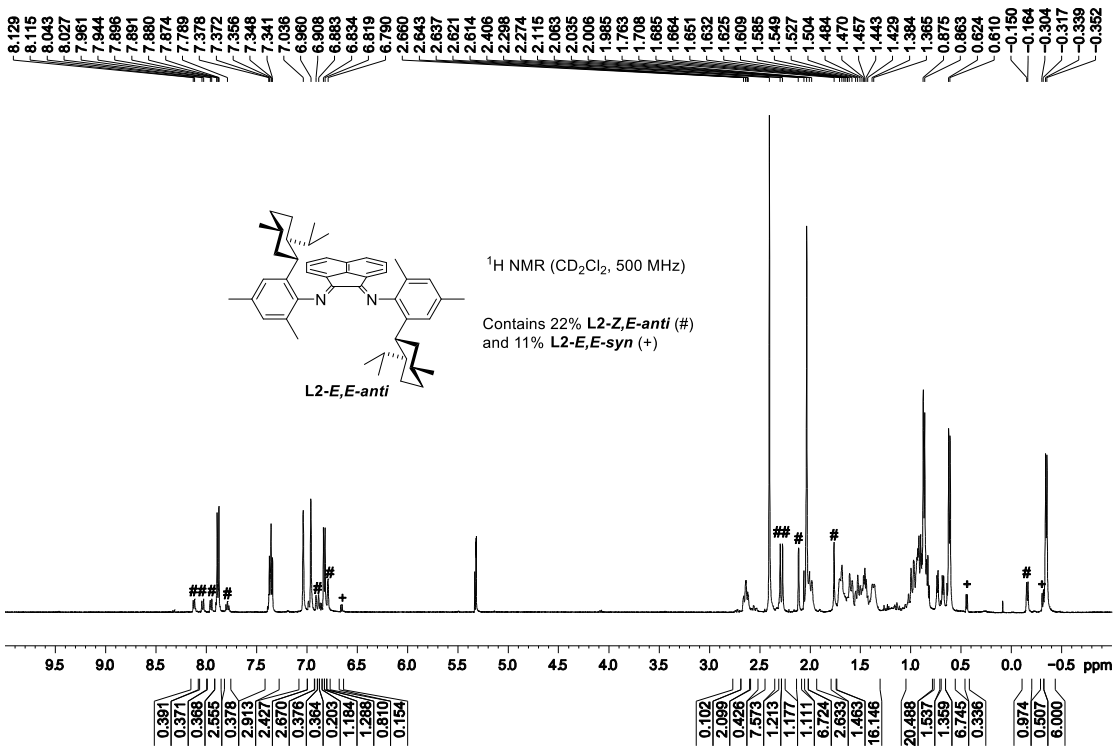

Figure 7.17. ^{1}H NMR spectrum of a 67/22/11 mixture of **L2-*E,E-anti*/*Z,E-anti*/*E,E-syn***.

L2-*syn*. A mixture of **L2** isomers (221 mg, 0.332 mmol) was dissolved in CH_2Cl_2 (5 mL) and stirred at room temperature for 5 d to reach final isomerization equilibrium with *anti*,*syn* and *Z,E* equilibria (a 12:4:81:3 mixture of **L2-*E,E-anti*/*Z,E-anti*/*E,E-syn*/*Z,E-syn***, overall *anti*/*syn* = 16:84). The volatiles were removed under vacuum, and the residue was subjected to flash column chromatography (silica, hexane/CH_2Cl_2 = 1/1 to 1/2 by volume) to yield enriched **L2-*syn*** as an orange powder (a 5/92/3 mixture of **L2-*E,E-anti*/*E,E-syn*/*Z,E-syn*** in *Z,E* but not *anti*,*syn* equilibrium, overall *anti*/*syn* = 5/95). Recovery: 183 mg (83%). The *Z,E* equilibrium **L2-*E,E-syn*/*Z,E-syn*** ratio is ca. 30/1 in CD_2Cl_2 at room temperature. Data for **L2-*E,E-syn***: ^{1}H NMR (CD_2Cl_2): δ 7.894 (d, *J* = 8.2, 1H), 7.889 (d, *J* = 8.2, 1H), 7.374 (t, *J* = 7.7, 1H), 7.364 (t, *J* = 7.7, 1H), 7.04 (s, 2H), 6.98 (s, 1H), 6.95 (s, 1H), 6.86 (d, *J* = 7.2, 1H), 6.66 (d, *J* = 7.2, 1H), 2.72 (td, *J* = 11.5, 3.4, 1H), 2.62 (td, *J* = 11.5, 3.4, 1H), 2.40 (s, 6H), 2.06 (s, 3H), 2.04 (s, 3H), 1.99-1.95 (m, 1H), 1.75-1.44 (m, 10H), 1.16-1.12 (m, 1H), 1.10-0.89 (m, 6H), 0.87 (d, *J* = 6.9, 3H), 0.85 (d, *J* =

6.4, 3H), 0.82 (d, *J* = 6.9, 3H), 0.63 (d, *J* = 6.9, 3H), 0.44 (d, *J* = 6.4, 3H), -0.31 (d, *J* = 6.9, 3H). $^{13}C\{^{1}H\}$ NMR (CD_2Cl_2): δ 161.7, 161.4, 147.3, 146.6, 141.0, 135.5, 133.81, 133.79, 133.5, 131.3, 130.6, 130.1, 129.09, 129.07, 129.05, 128.98, 128.17, 128.15, 125.6, 125.4, 124.7, 124.6, 123.4, 123.1, 47.9, 46.6, 45.5, 45.4, 41.73, 41.67, 35.58, 35.56, 33.8, 33.5, 28.2, 27.9, 25.0 (2C), 22.6, 22.4, 21.9, 21.8, 21.36, 21.32, 18.2, 18.0, 16.6, 15.8. Key ^{1}H NMR resonances of **L2-*Z,E-syn***: ^{1}H NMR (CD_2Cl_2): δ -0.24 (d, *J* = 6.9, 3H).

(a)

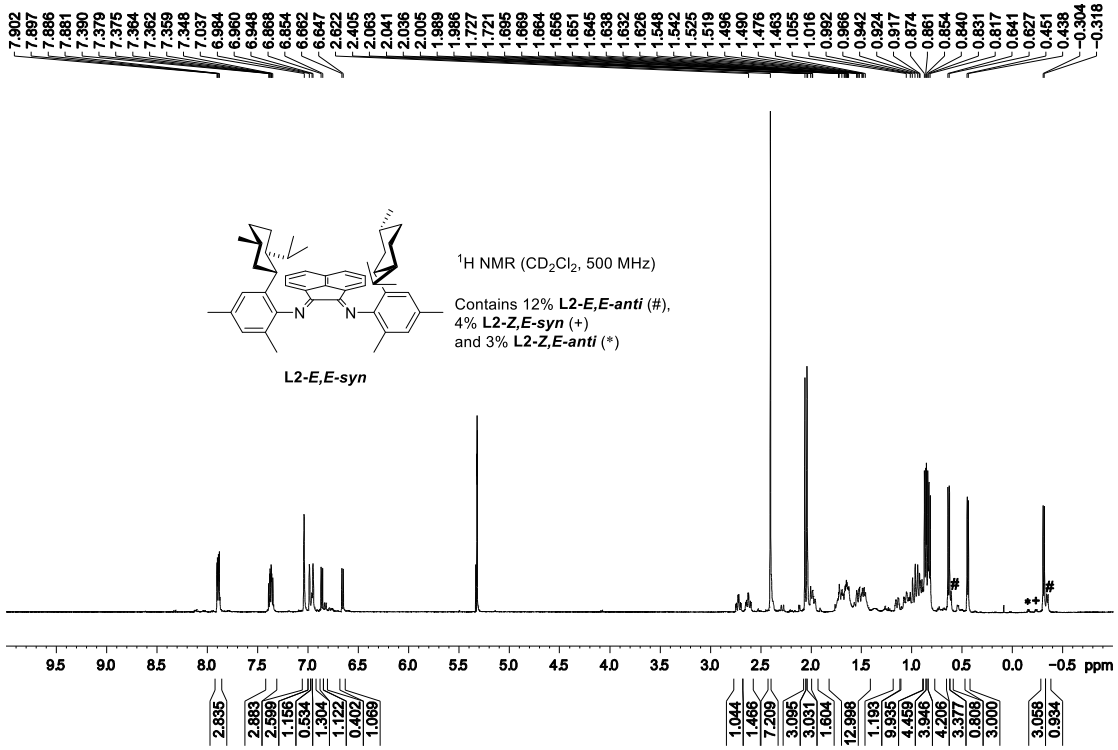

Figure 7.18. NMR spectra of an isomer mixture of **L2** in *Z,E* and *anti,syn* equilibria.

(b)

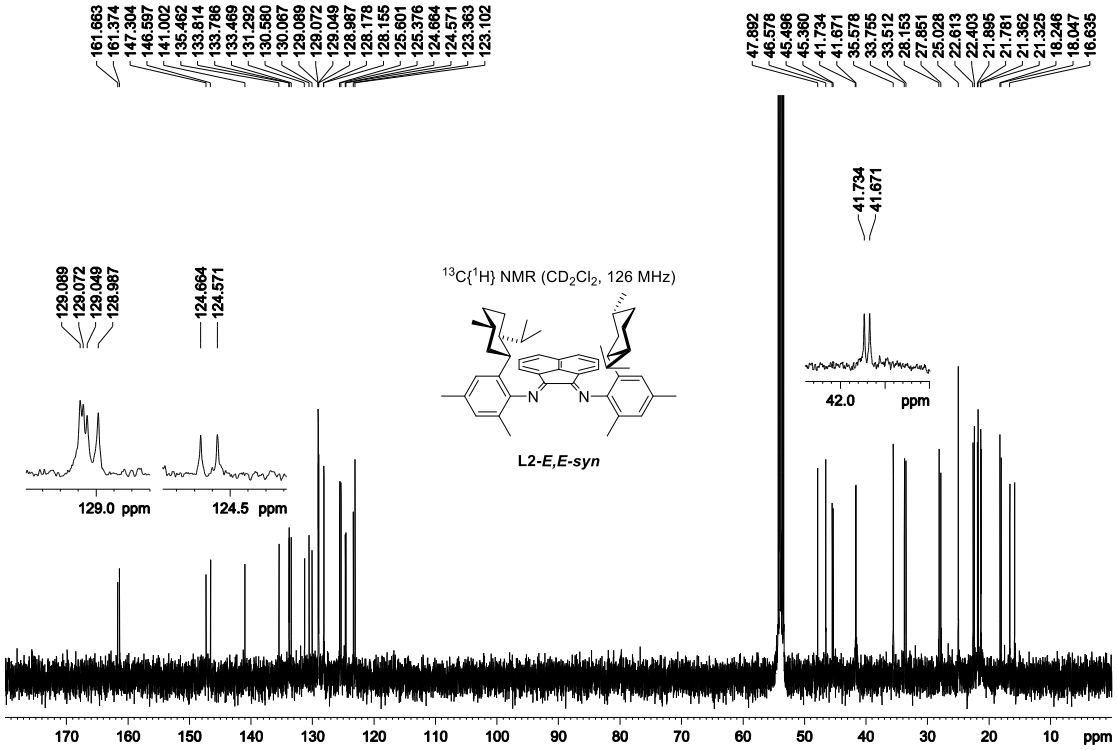

Figure 7.18, continued. NMR spectra of an isomer mixture of **L2** in *Z,E* and *anti,syn* equilibria.

(L1)NiBr$_2$-*anti*. A scintillation vial was charged with **L1** (186 mg, 0.29 mmol), (dme)NiBr$_2$ (90 mg, 0.29 mmol), and CH_2Cl_2 (5 mL) under N_2. The mixture was stirred at room temperature for 24 h to yield a dark red mixture. The mixture was filtered through Celite. The filtrate was concentrated under vacuum to ca. 2 mL, and hexane (10 mL) was added to afford a brownish orange precipitate. The solid was collected by vacuum filtration, washed with hexane, and dried under vacuum. Yield: 158 mg (63%). ^{1}H NMR (CD_2Cl_2, paramagnetic): δ 25.98 (s, $\Delta\nu_{1/2}$ = 12, 6H), 24.41 (s, $\Delta\nu_{1/2}$ = 260, 2H), 24.24 (s, $\Delta\nu_{1/2}$ = 18, 2H), 21.87 (s, $\Delta\nu_{1/2}$ = 28, 2H), 18.59 (s, $\Delta\nu_{1/2}$ = 19, 2H), 15.27 (d, J = 7, $\Delta\nu_{1/2}$ = 8, 2H), 13.26 (s, $\Delta\nu_{1/2}$ = 155, 2H), 6.73 (d, J = 6, $\Delta\nu_{1/2}$ = 11, 2H), 5.09 (s, $\Delta\nu_{1/2}$ = 25, 2H), 5.05 (s, $\Delta\nu_{1/2}$ = 36, 2H), 4.10 (s, $\Delta\nu_{1/2}$ = 35, 2H), 3.89 (s, $\Delta\nu_{1/2}$ = 23, 2H), 2.79 (s, $\Delta\nu_{1/2}$ = 30, 2H), 2.58 (s, $\Delta\nu_{1/2}$ = 65, 2H), 2.08 (s, $\Delta\nu_{1/2}$ = 15, 6H), 1.61 (d, J = 8, $\Delta\nu_{1/2}$ = 12, 2H), 1.38 (s, $\Delta\nu_{1/2}$ = 11, 6H), 0.30 (s, $\Delta\nu_{1/2}$ = 42, 2H), -0.59 (s, $\Delta\nu_{1/2}$ = 38, 6H), -16.84

(d, $\Delta\nu_{1/2}$ = 97, 2H). Anal. Calcd. for $C_{46}H_{56}Br_2N_2Ni$, %: C, 64.59; H, 6.60; N, 3.27. Found: C, 64.80; H, 6.31; N, 3.00.

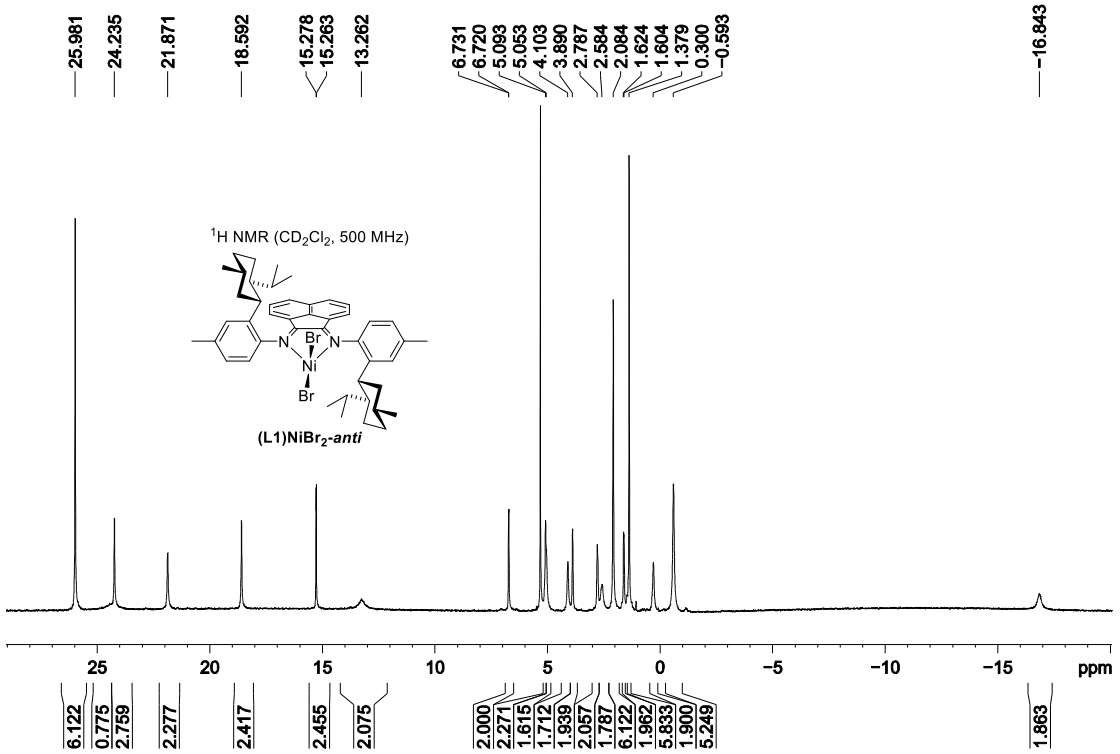

Figure 7.19. ^{1}H NMR spectrum of **(L1)NiBr$_2$-*anti***.

(L2)NiBr$_2$-*anti*. A Schlenk flask was charged with **L2** (150 mg, 0.23 mmol), (dme)$NiBr_2$ (70 mg, 0.23 mmol), and CH_2ClCH_2Cl (5 mL) under N_2. The mixture was stirred at 80 °C for 17 h to yield a dark red mixture. The volatiles were removed under vacuum, and the solid residue was dissolved in CH_2Cl_2 (10 mL). The mixture was filtered through Celite. The filtrate was concentrated under vacuum to ca. 1 mL, and pentane (10 mL) was added to afford a brown precipitate. The solid was collected by vacuum filtration, washed with pentane, and dried under vacuum. Yield: 159 mg (80%). ^{1}H NMR (CD_2Cl_2, paramagnetic): δ 26.30 (s, $\Delta\nu_{1/2}$ = 6, 6H), 25.34 (s, $\Delta\nu_{1/2}$ = 270, 2H), 25.17 (s, $\Delta\nu_{1/2}$ = 10, 2H), 21.96 (s, $\Delta\nu_{1/2}$ = 20, 2H), 19.25 (s, $\Delta\nu_{1/2}$ = 10, 2H), 16.05 (s, $\Delta\nu_{1/2}$ = 58, 6H), 15.79 (d, J = 8, $\Delta\nu_{1/2}$ = 3, 2H), 15.57 (s, $\Delta\nu_{1/2}$ = 132, 2H), 6.61 (d, J = 7,

$\Delta\nu_{1/2}$ = 8, 2H), 6.33 (s, $\Delta\nu_{1/2}$ = 23, 2H), 5.78 (s, $\Delta\nu_{1/2}$ = 19, 2H), 4.87 (s, $\Delta\nu_{1/2}$ = 28, 2H), 3.36-3.24 (m, 4H), 2.15 (s, $\Delta\nu_{1/2}$ = 9, 6H), 1.36 (s, $\Delta\nu_{1/2}$ = 8, 6H), 0.85 (s, $\Delta\nu_{1/2}$ = 9, 2H), 0.38 (s, $\Delta\nu_{1/2}$ = 48, 2H), -1.46 (s, $\Delta\nu_{1/2}$ = 37, 2H), -1.70 (s, $\Delta\nu_{1/2}$ = 27, 2H). Anal. Calcd. for $C_{48}H_{60}Br_2N_2Ni$, %: C, 65.25; H, 6.85; N, 3.17. Found: C, 67.78; H, 7.08; N, 3.21.

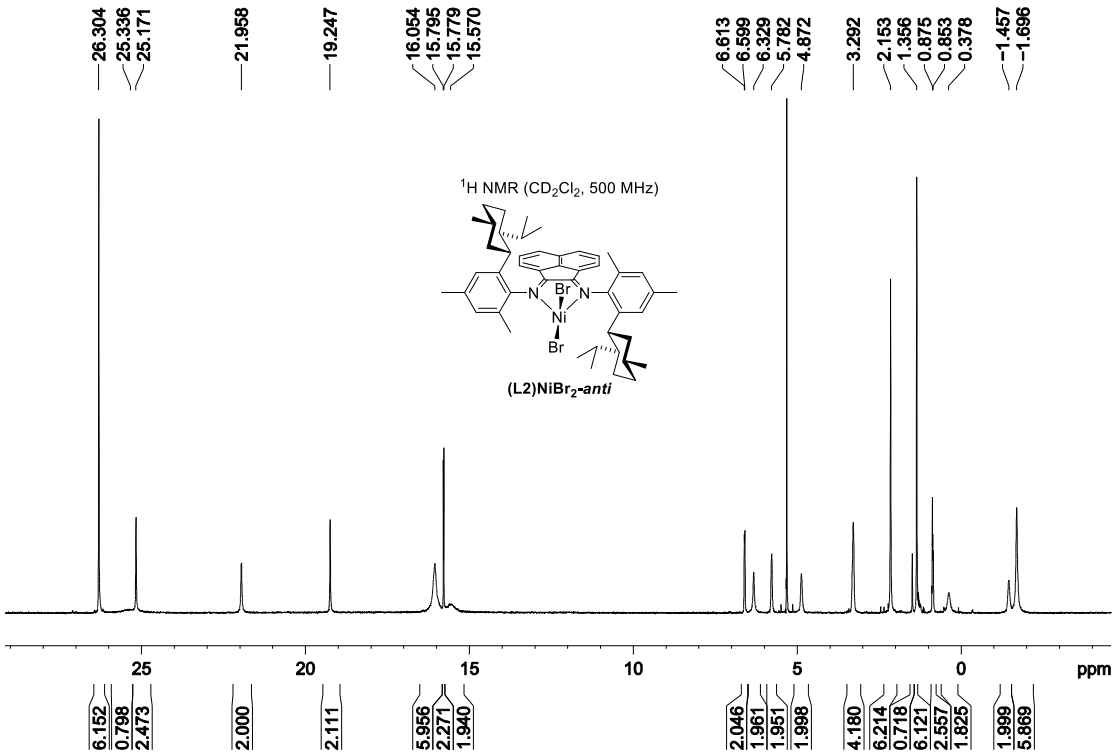

Figure 7.20. ^{1}H NMR spectrum of **(L2)NiBr$_2$-*anti***.

(L1)PdCl$_2$-*syn*/*anti*. A Schlenk flask was charged with **L1** (58 mg, 0.091 mmol), $(MeCN)_2PdCl_2$ (22 mg, 0.087 mmol), and CH_2Cl_2 (2.5 mL) under N_2. The mixture was stirred at room temperature for 30 min to afford an orange solution. The mixture was filtered through a pipette filter to remove trace solid particles. The filtrate was concentrated to ca. 2 mL, and hexane (15 mL) was added to form a yellow precipitate. The yellow powder was collected by vacuum filtration and dried under vacuum. Yield: 54 mg (76%). This material is a 16/1 mixture of **(L1)PdCl$_2$-*syn*/*anti*** based on ^{1}H NMR integration. Diffusion of hexane into a CH_2Cl_2 solution at

0 °C yielded pure **(L1)PdCl$_2$-*syn*** as yellow needles (50 mg, 70%). *Syn*/*anti* isomerization afforded an equilibrium 16/1 mixture of **(L1)PdCl$_2$-*syn*/*anti*** within 3 d in CD_2Cl_2 at room temperature. ESI-MS (1:1 MeOH:H_2O, positive ion scan, *m*/*z*): 741.3 ([M – HCl – Cl]$^+$). Anal. Calcd. for $C_{46}H_{56}Cl_2N_2Pd$, %: C, 67.85; H, 6.93; N, 3.44. Found: C, 67.58; H, 6.74; N, 3.45. Data for **(L1)PdCl$_2$-*syn***: ^{1}H NMR (CD_2Cl_2): δ 8.147 (d, *J* = 8.2, 1H), 8.143 (d, *J* = 8.3, 1H), 7.510 (dd, *J* = 8.3, 7.4, 1H), 7.506 (dd, *J* = 8.3, 7.4, 1H), 7.31 (s, 1H), 7.29 (s, 1H), 7.24 (dd, *J* = 8.0, 1.2, 1H), 7.195 (dd, *J* = 8.0, 1.2, 1H), 7.186 (d, *J* = 8.0, 1H), 7.16 (d, *J* = 8.0, 1H), 6.90 (d, *J* = 7.3, 1H), 6.67 (d, *J* = 7.3, 1H), 3.05 (td, *J* = 11.3, 3.6, 1H, H_A), 2.76 (td, *J* = 11.1, 3.6, 1H, H_a), 2.65 (dq, *J* = 13.1, 2.7, 1H, H_C), 2.47 (s, 6H, Ar-C*H*$_3$), 1.86-1.80 (m, 3H, H_F + H_g + C$^{7'}$-*H*), 1.72-1.67 (m, 3H, H_D + H_G + H_f), 1.59 (t, *J* = 11.4, 1H, H_i), 1.53 (t, *J* = 11.1, 1H, H_I), 1.34 (d, *J* = 6.7, C$^{7'}$-C*H*$_3$), 1.23 (septet d, *J* = 7.0, 1.6, C^7-H), 1.17 (qd, *J* = 12.7, 2.7, H_h), 1.14-1.00 (m, 4H, H_B + H_E + H_H + H_c), 0.97-0.90 (m, 6H, H_b + H_d + H_e + C^5-C*H*$_3$), 0.89 (d, *J* = 7.0, 3H, C$^{7'}$-C*H*$_3$), 0.56 (d, *J* = 6.9, 3H, C^7-C*H*$_3$), 0.42 (d, *J* = 5.9, 3H, C$^{5'}$-C*H*$_3$), -0.25 (d, *J* = 6.8, 3H, C^7-C*H*$_3$). ^{13}C{^{1}H} NMR (CD_2Cl_2): δ 176.0 (C=N), 175.5 (C=N), 147.4, 142.32, 142.28, 140.3, 140.0, 139.3, 138.6, 133.0 (Ar CH), 132.9 (Ar CH), 129.0, 129.0 (2C, Ar CH), 128.9 (Ar CH), 128.5 (Ar CH), 127.5 (Ar CH), 127.4 (Ar CH), 127.2 (Ar CH), 126.8 (Ar CH), 125.4, 124.8, 123.1 (Ar CH), 122.3 (Ar CH), 48.1 (C^2), 48.0 (C$^{2'}$), 45.6 (C$^{6'}$), 44.0 (C^6), 42.5 (C^1), 41.9 (C$^{1'}$), 35.6 (C^4), 35.1 (C$^{4'}$), 33.4 (C^5), 33.2 (C$^{5'}$), 28.0 (C^7), 27.5 (C$^{7'}$), 25.4 (C$^{3'}$), 25.3 (C^3), 22.7 (C^5-*C*H$_3$), 22.3 (C$^{5'}$-*C*H$_3$), 22.2 (C$^{7'}$-*C*H$_3$), 21.8 (2C, *p*-*C*H$_3$), 21.6 (C^7-*C*H$_3$), 20.2 (C$^{7'}$-*C*H$_3$), 16.7 (C^7-*C*H$_3$). Key ^{1}H NMR resonances of **(L1)PdCl$_2$-*anti***: ^{1}H NMR (CD_2Cl_2): δ 8.13 (d, *J* = 8.2, 2H), 7.47 (t, *J* = 7.7, 2H), 3.11 (td, *J* = 11.2, 3.5, 2H), 1.12 (2H, ^{i}Pr CH, located by COSY), 0.46 (d, *J* = 6.9, 6H), -0.27 (d, *J* = 6.9, 6H).

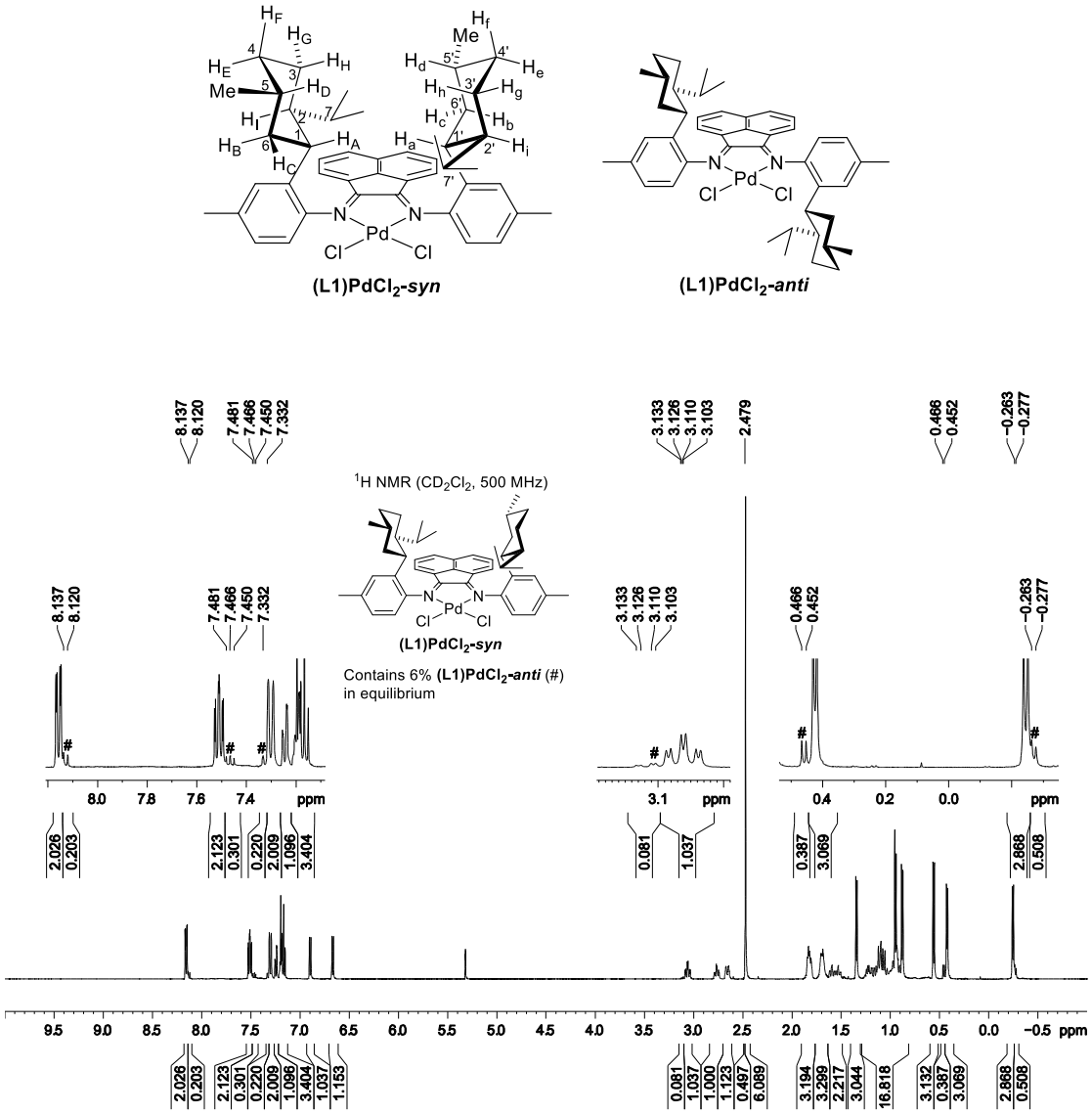

Figure 7.21. ^{1}H NMR spectrum of an equilibrium 16/1 mixture of **(L1)PdCl$_2$-*syn*/*anti***.

(a)

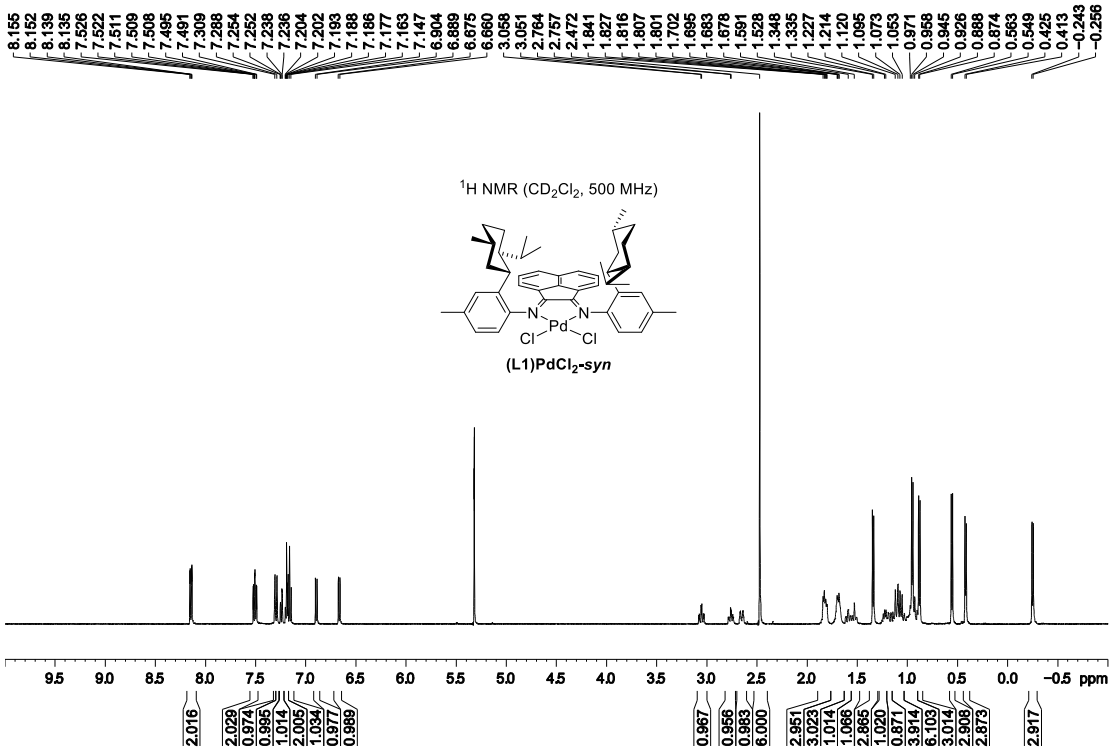

(b)

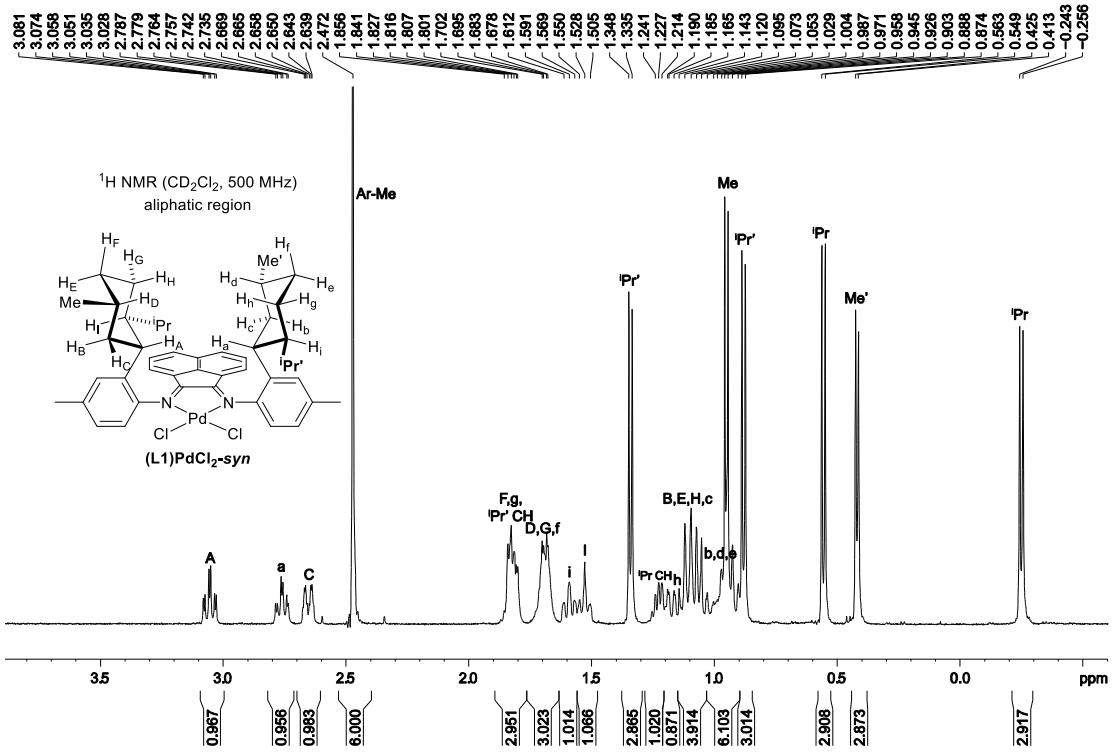

Figure 7.22. NMR spectra of **(L1)PdCl$_2$-*syn***.

(c)

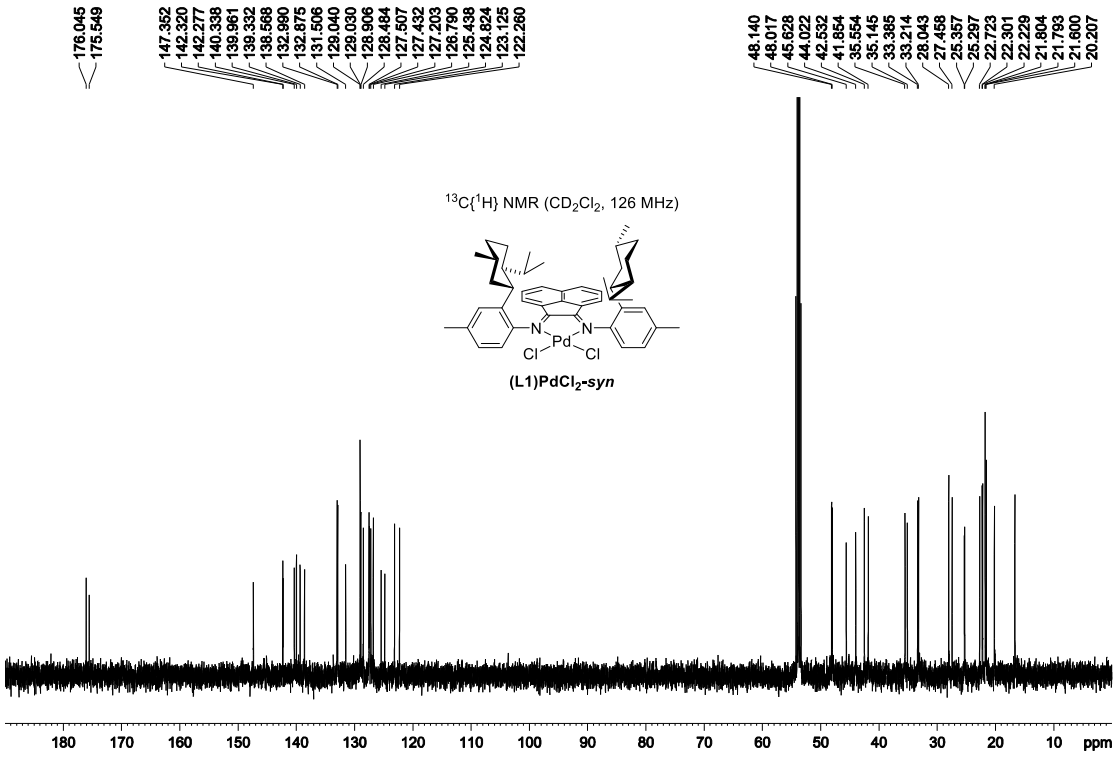

(d)

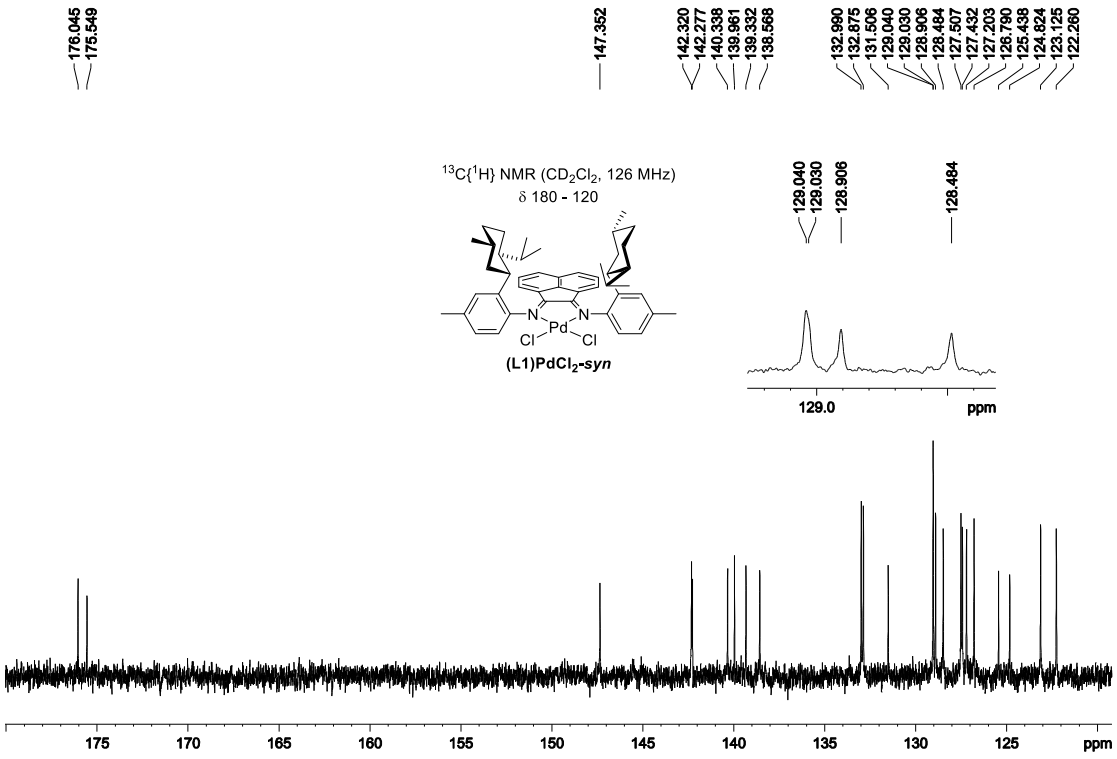

Figure 7.22, continued. NMR spectra of **(L1)$PdCl_2$-*syn***.

(e)

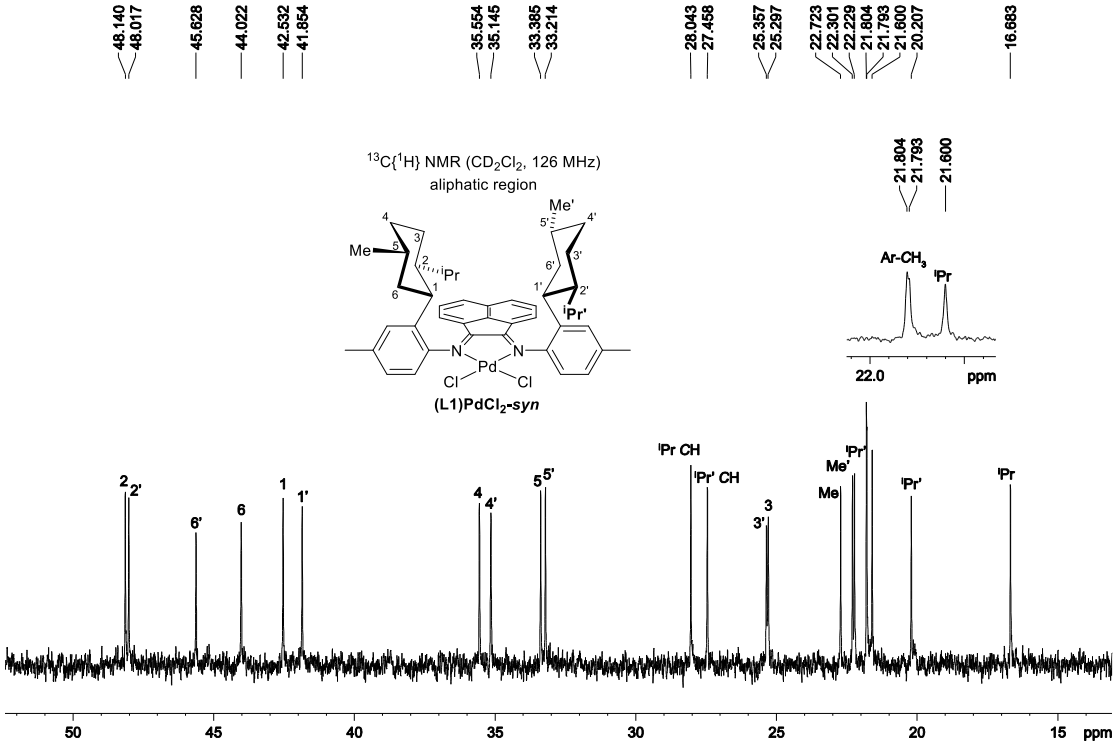

(f) COSY (CD_2Cl_2, expansion of δ 3.4 to -0.4/3.4 to -0.4 region)

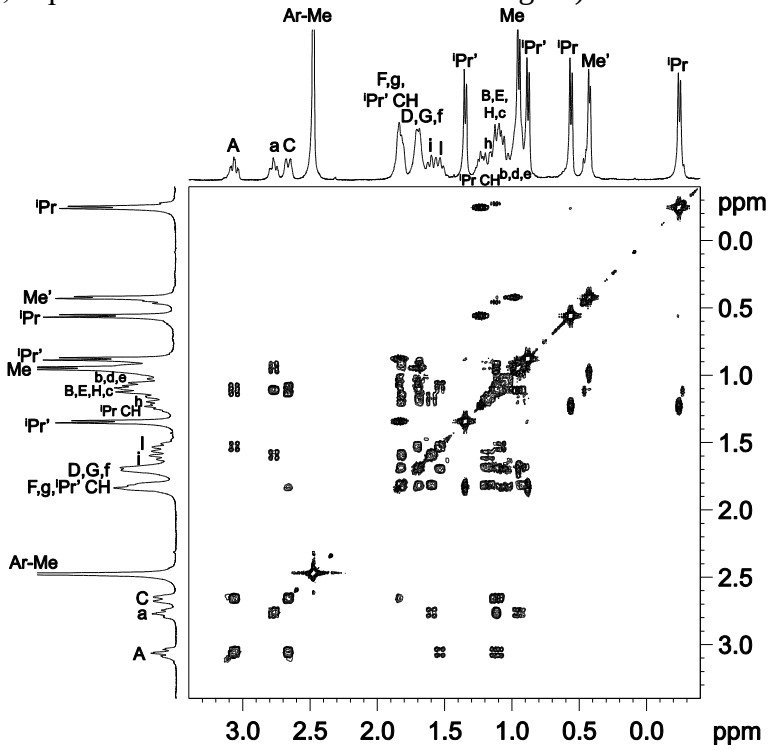

Figure 7.22, continued. NMR spectra of **(L1)PdCl$_2$-*syn***.

(g) HMQC (CD_2Cl_2, expansion of δ 3.4 to -0.4/55-10 region)

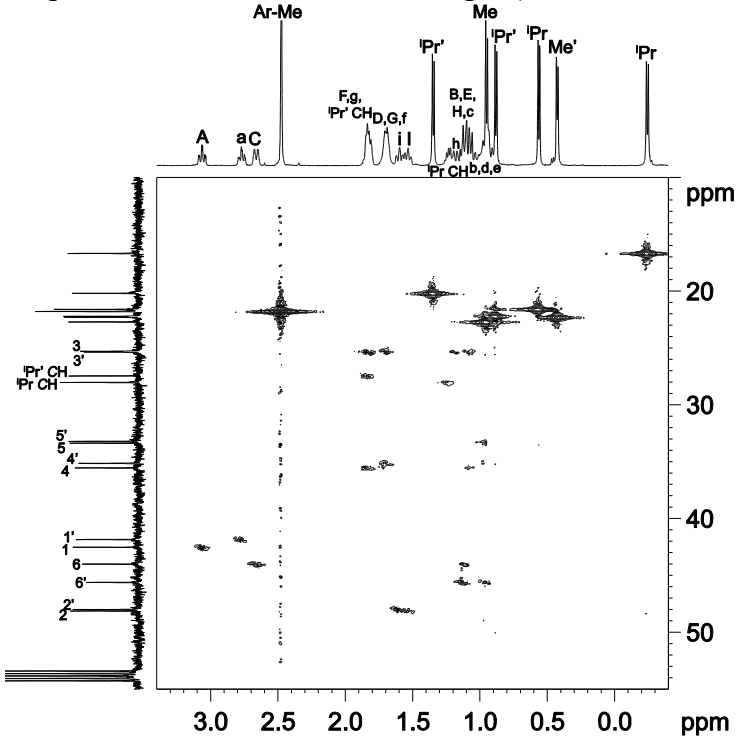

Figure 7.22, continued. NMR spectra of **(L1)PdCl$_2$-*syn***.

(h) NOESY (CD_2Cl_2, expansion of δ 3.5 to -0.5/3.5 to -0.5 region)

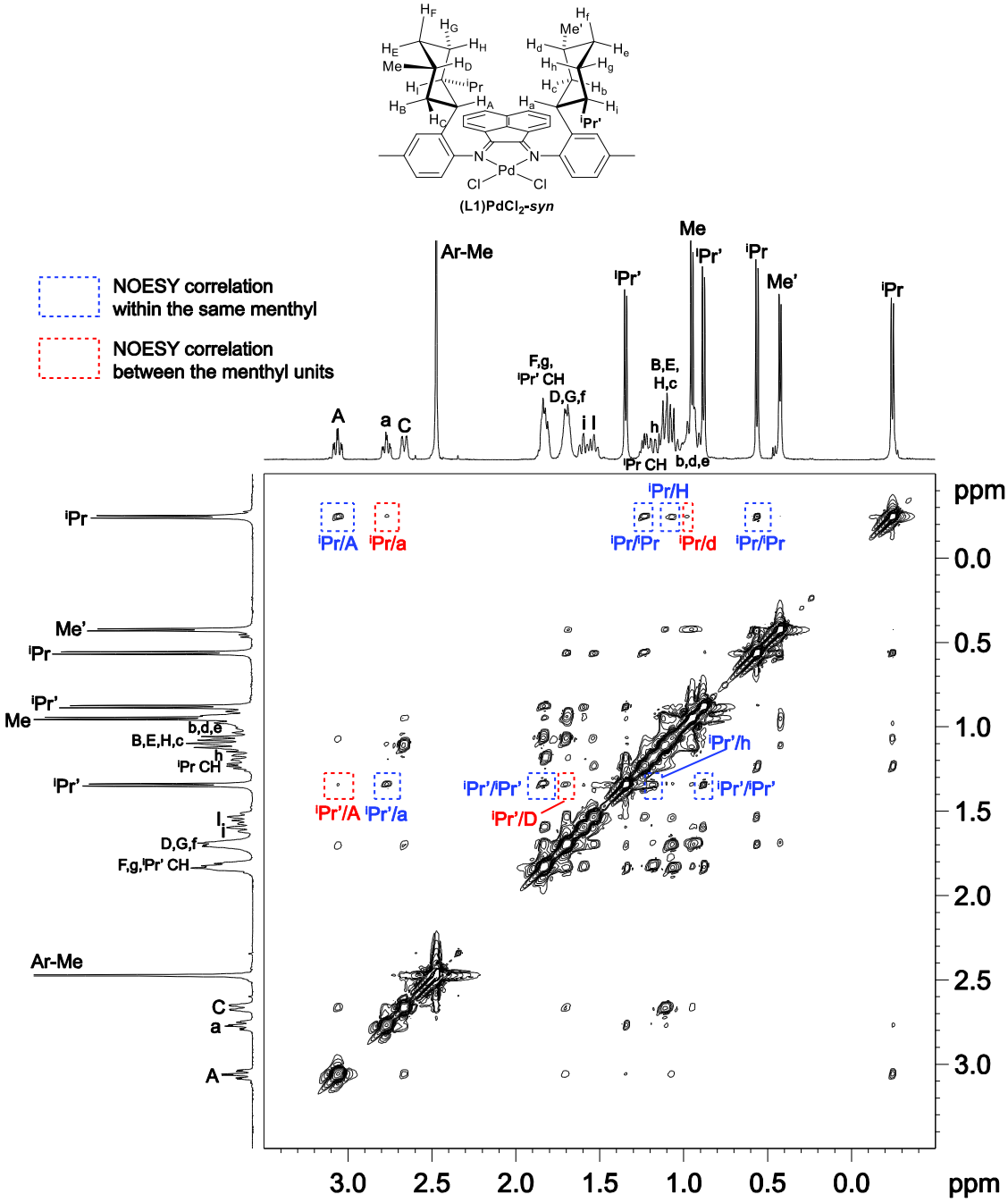

Figure 7.22, continued. NMR spectra of **(L1)PdCl₂-*syn***.

(L1)Ni(acac)-*syn*. A Schlenk flask was charged with **L1** (200 mg, 0.31 mmol), $Ni(acac)_2$ (81 mg, 0.31 mmol), $Ph_3C^+B(C_6F_5)_4^-$ (290 mg, 0.31 mmol) and CH_2Cl_2 (50 mL) under N_2. The mixture was stirred at room temperature for 2 h to form a dark red solution. The volatiles were removed under vacuum. The solid residue was subjected to flash column chromatography (silica, CH_2Cl_2) and taken to dryness under vacuum to yield a red brittle foam. Yield: 315 mg (76%). This material is a 98/2 mixture of **(L1)Ni(acac)-*syn*/*anti*** based on ^{1}H NMR integration of the acac methane singlets. Anal. Calcd. for $C_{75}H_{63}BF_{20}N_2NiO_2$, %: C, 61.12; H, 4.31; N, 1.90. Found: C, 60.92; H, 4.05; N, 1.95. ESI-MS (1:1 MeOH:H_2O, positive ion scan, *m*/*z*): 793.6 ($[M - B(C_6F_5)_4]^+$). ESI-MS (1:1 MeOH:H_2O, negative ion scan, *m*/*z*): 679.2 ($[B(C_6F_5)_4]^-$). ^{1}H NMR (CD_2Cl_2): δ 8.185 (d, *J* = 8.2, 1H), 8.182 (d, *J* = 8.3, 1H), 7.567 (dd, *J* = 8.2, 7.5, 1H), 7.561 (dd, *J* = 8.3, 7.4, 1H), 7.30 (s, 2H), 7.21-7.14 (m, 4H), 7.06 (d, *J* = 7.3, 1H), 6.84 (d, *J* = 7.3, 1H), 5.50 (s, 1H, acac CH), 3.57 (td, *J* = 11.4, 3.3, 1H, H_A), 3.23 (td, *J* = 11.4, 3.5, 1H, H_a), 2.42 (s, 6H, *p*-C*H*$_3$), 1.95-1.91 (m, 3H, $H_C + H_F + H_g$), 1.88-1.77 (m, 3H, $H_D + H_G + H_f$), 1.72 (t, *J* = 10.4, 1H, H_i), 1.61 (s, 6H, acac CH_3), 1.56-1.51 (m, 2H, H_I + $C^{7'}$-*H*), 1.46 (d, *J* = 6.6, 3H, $C^{7'}$-C*H*$_3$), 1.36 (qd, *J* = 12.8, 3.2, 1H, H_h), 1.28 (q, *J* = 12.2, 1H, H_B), 1.23 (qd, *J* = 12.5, 2.5, 1H, H_H), 1.17-1.13 (m, 3H, $H_c + H_d$ + C^7-*H*), 1.12 (qd, *J* = 12.7, 3.0, 1H, H_E), 1.02 (q, *J* = 12.0, 1H, H_b), 1.00 (qd, *J* = 12.0, 3.5, 1H, H_e), 0.93 (d, *J* = 6.5, 3H, C^5-C*H*$_3$), 0.90 (d, *J* = 6.9, 3H, $C^{7'}$-C*H*$_3$), 0.57 (d, *J* = 6.9, 3H, C^7-C*H*$_3$), 0.49 (d, *J* = 6.2, 3H, $C^{5'}$-C*H*$_3$), -0.15 (d, *J* = 6.8, 3H, C^7-C*H*$_3$). ^{13}C{^{1}H} NMR (CD_2Cl_2): δ 187.7 (2C, acac C=O), 173.2 (C=N), 172.6 (C=N), 148.9, 141.6, 141.0, 140.4, 139.9, 138.6, 138.4, 133.8 (Ar CH), 133.7 (Ar CH), 131.7, 129.42 (Ar CH), 129.37 (Ar CH), 129.2 (Ar CH), 128.7 (Ar CH), 128.2 (Ar CH), 128.1 (Ar CH), 127.5 (Ar CH), 127.0 (Ar CH), 124.5, 123.8, 122.9 (Ar CH), 122.5 (Ar CH), 102.5 (acac CH), 48.5 (C^2), 47.5 ($C^{2'}$), 45.8 ($C^{6'}$), 44.4 (C^6), 43.4 (C^1), 42.9 ($C^{1'}$), 35.2 (C^4), 35.0 ($C^{4'}$), 33.8 (C^5), 33.6 ($C^{5'}$), 28.1 (C^7), 28.0 ($C^{7'}$), 25.51 ($C^{3'}$), 25.45 (C^3), 24.7 (br, 2C,

acac CH_3), 22.6 (C^5-CH_3), 22.1 ($C^{5'}$-CH_3), 22.0 ($C^{7'}$-CH_3), 21.8 (2C, *p*-CH_3), 21.5 (C^7-CH_3), 18.3 ($C^{7'}$-CH_3), 16.6 (C^7-CH_3).

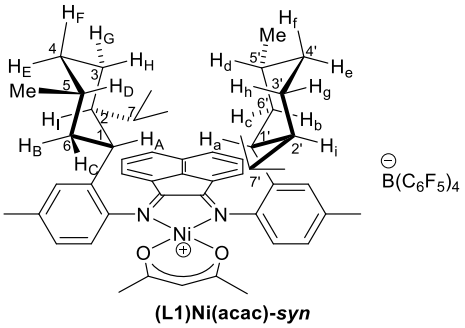

(a)

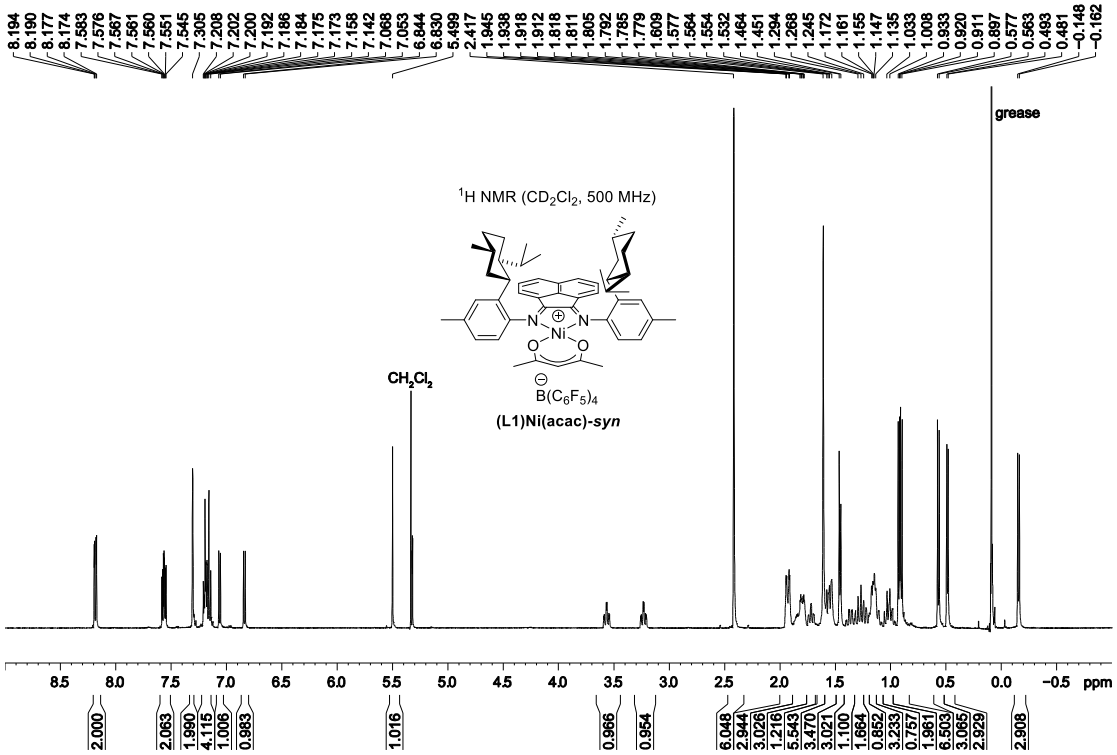

Figure 7.23. NMR spectra of **(L1)Ni(acac)-*syn***.

(b)

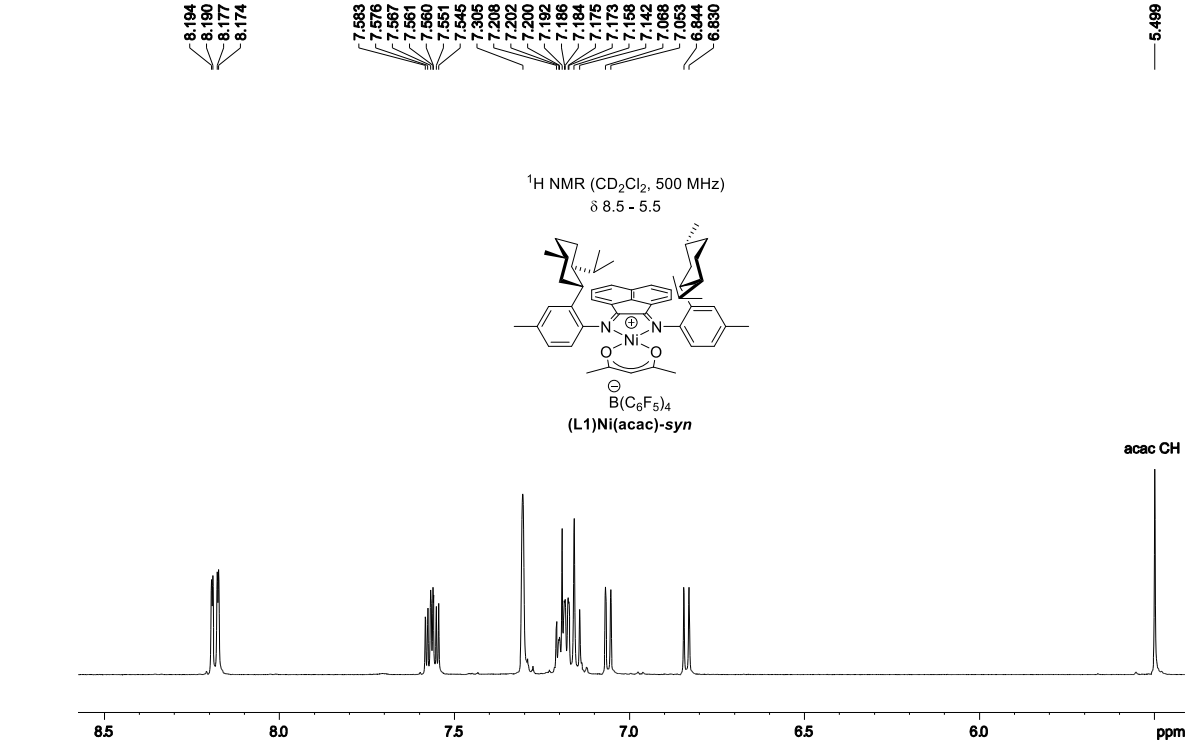

(c)

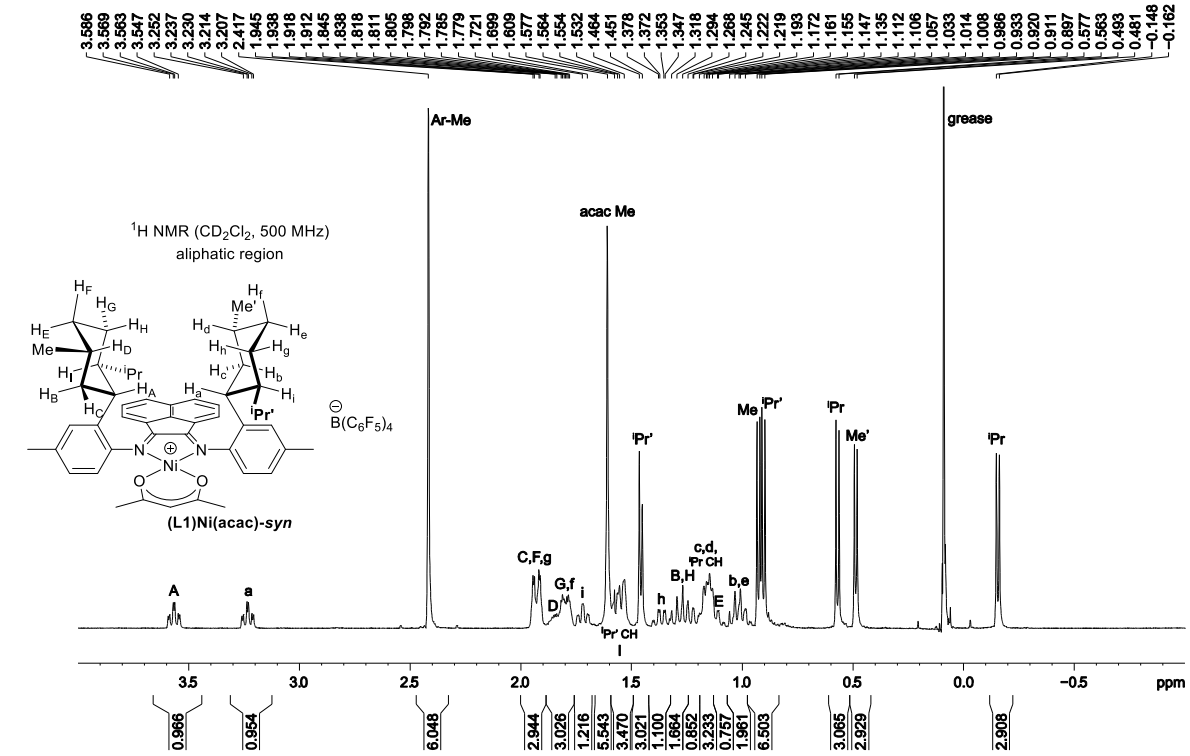

Figure 7.23, continued. NMR spectra of **(L1)Ni(acac)-*syn***.

(d)

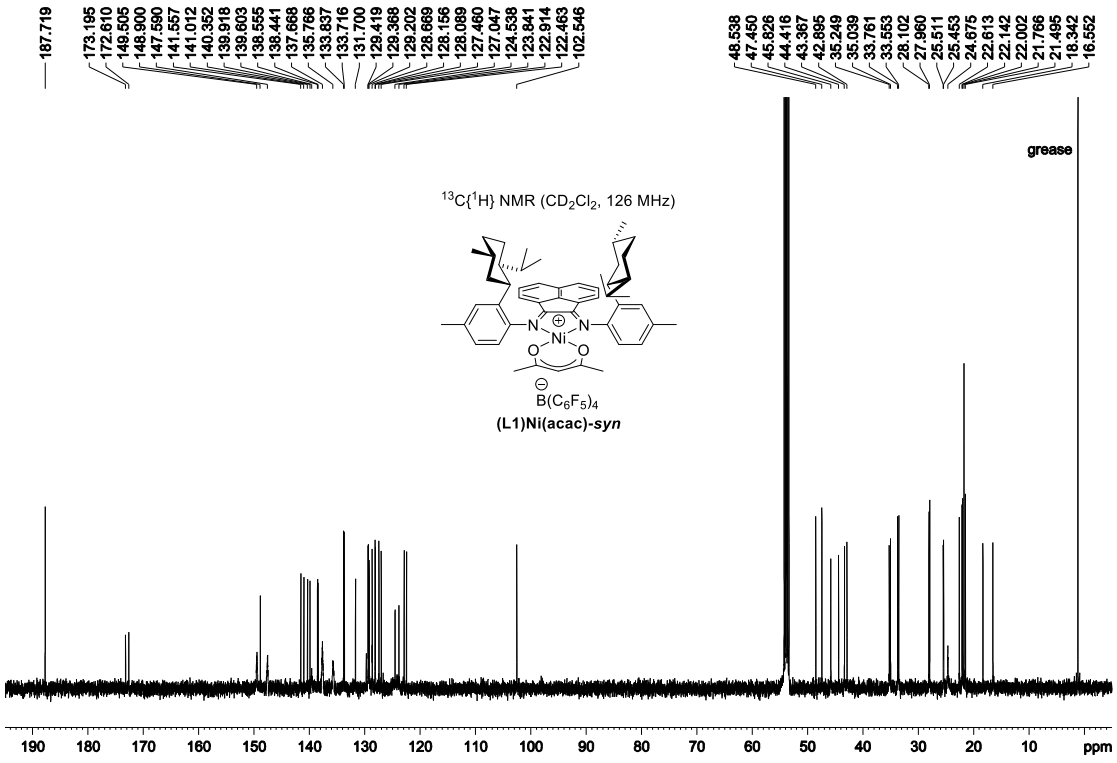

(e)

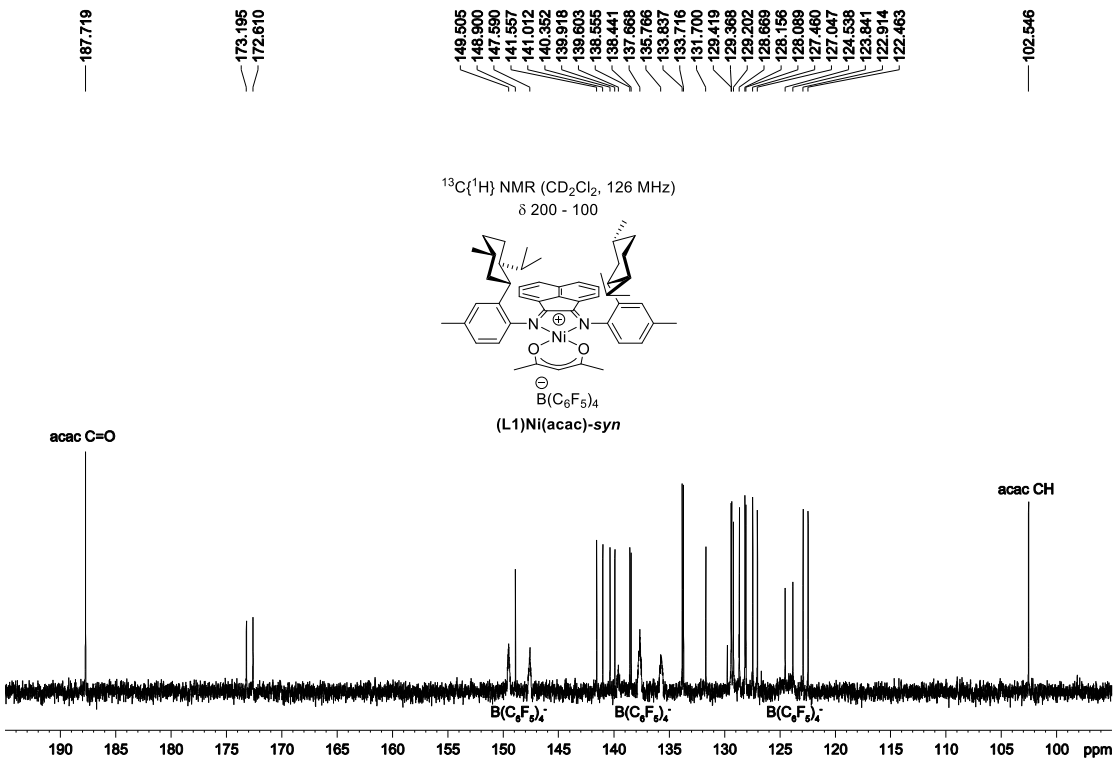

Figure 7.23, continued. NMR spectra of **(L1)Ni(acac)-*syn***.

(f)

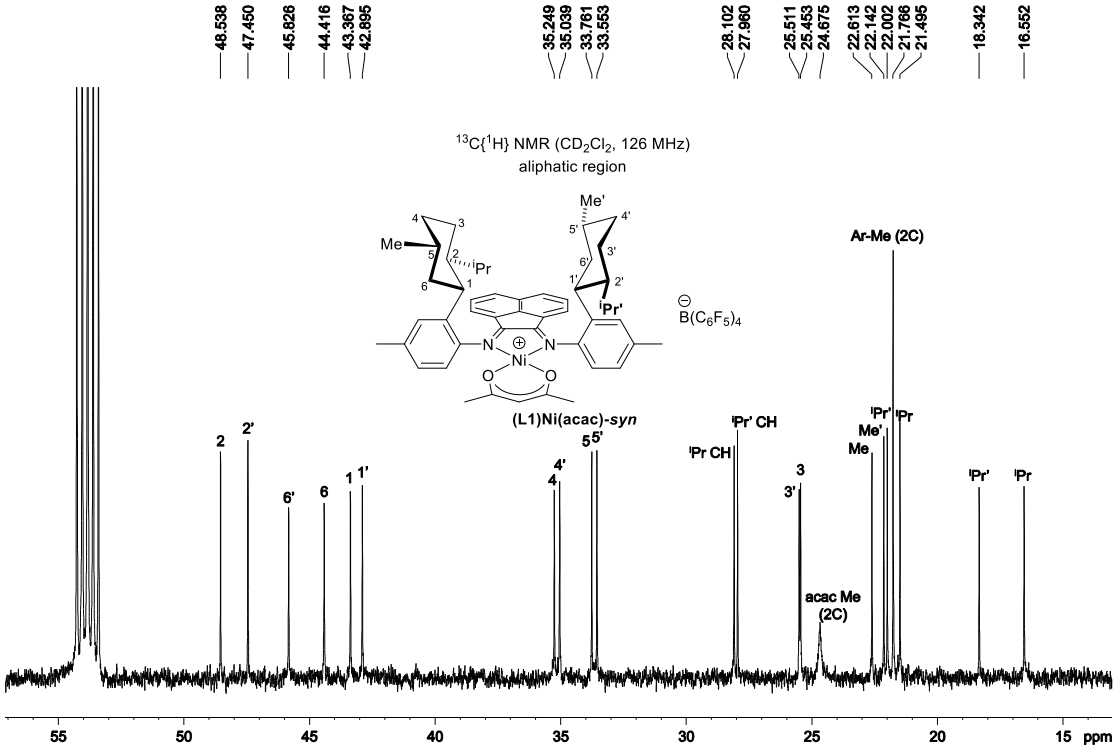

(g) COSY (CD_2Cl_2, expansion of δ 4.0 to -0.4/4.0 to -0.4 region)

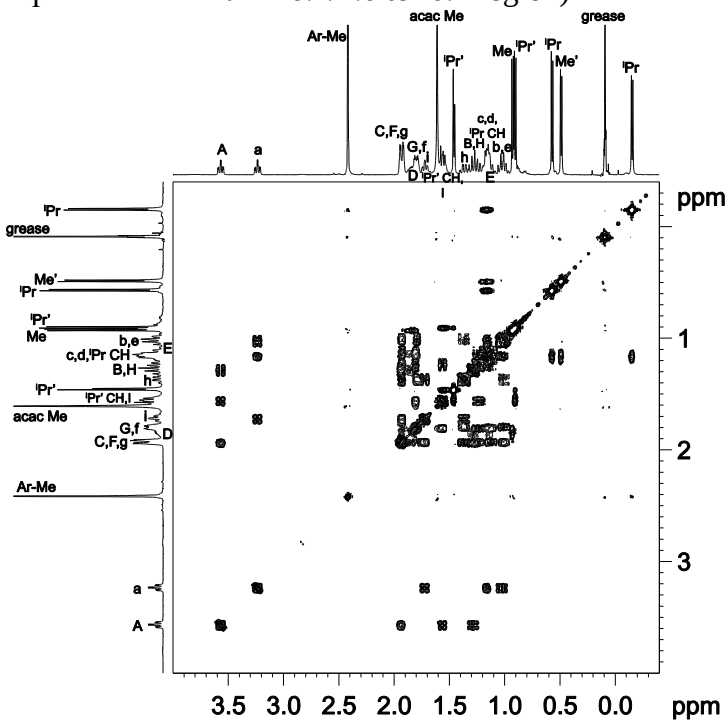

Figure 7.23, continued. NMR spectra of **(L1)Ni(acac)-*syn***.

(h) HMQC (CD_2Cl_2, expansion of δ 6.0 to -0.3/110-10 region)

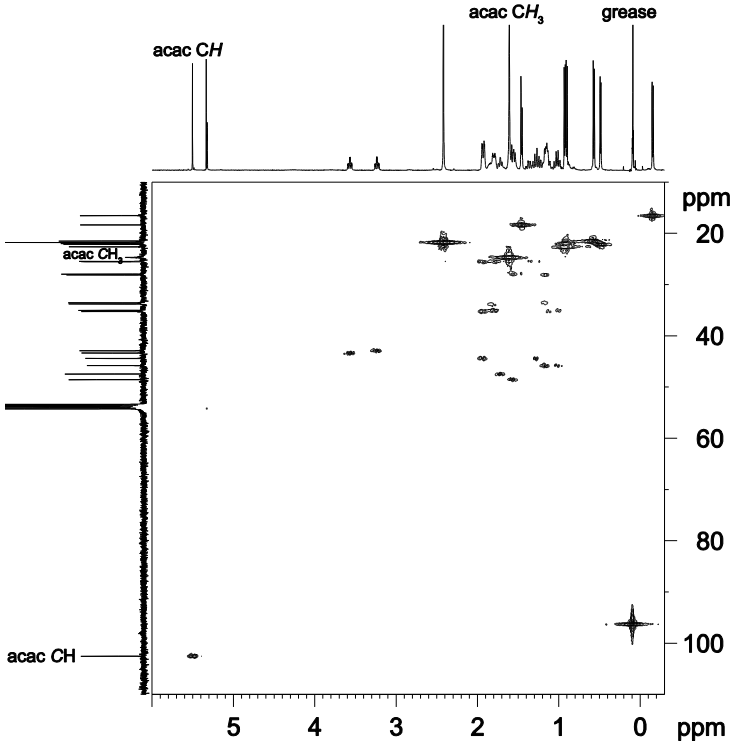

Figure 7.23, continued. NMR spectra of **(L1)Ni(acac)-*syn***.

(L1)Ni(acac)-*anti*. An NMR tube was charged with **(L1)NiBr$_2$-*anti*** (15.4 mg, 18 μmol), Ag(acac) (4.0 mg, 19 mmol) and $LiB(C_6F_5)_4 \cdot 2.7(Et_2O)$ (18.0 mg, 20 mmol) under N_2. CD_2Cl_2 was transferred in under vacuum at -196 °C. The mixture was warmed to room temperature and briefly agitated to yield a red solution of **(L1)Ni(acac)-*anti*** and a white precipitate. The initial solution contained a 9/91 mixture of **(L1)Ni(acac)-*syn*/*anti***, which isomerized into an equilibrium 98/2 mixture of **(L1)Ni(acac)-*syn*/*anti*** in 34 h at room temperature. ^{1}H NMR (CD_2Cl_2): δ 8.168 (d, *J* = 8.3, 2H), 7.534 (t, *J* = 7.7, 2H), 7.29 (s, 2H), 7.18 (d, *J* = 8.2, 2H), 7.15 (d, *J* = 8.2, 2H), 6.92 (d, *J* = 7.3, 2H), 5.54 (s, 1H, acac CH), 3.75 (td, *J* = 11.2, 2.9, 2H), 2.42 (s, 6H), 1.90-1.72 (m, 8H), 1.69 (s, 6H, acac CH_3), 1.60-1.56 (m, 2H), 1.35-1.06 (m, 8H), 0.87 (d, *J* = 6.4, 6H), 0.58 (d, *J* = 6.9, 6H), -0.10 (d, *J* = 6.9, 6H).

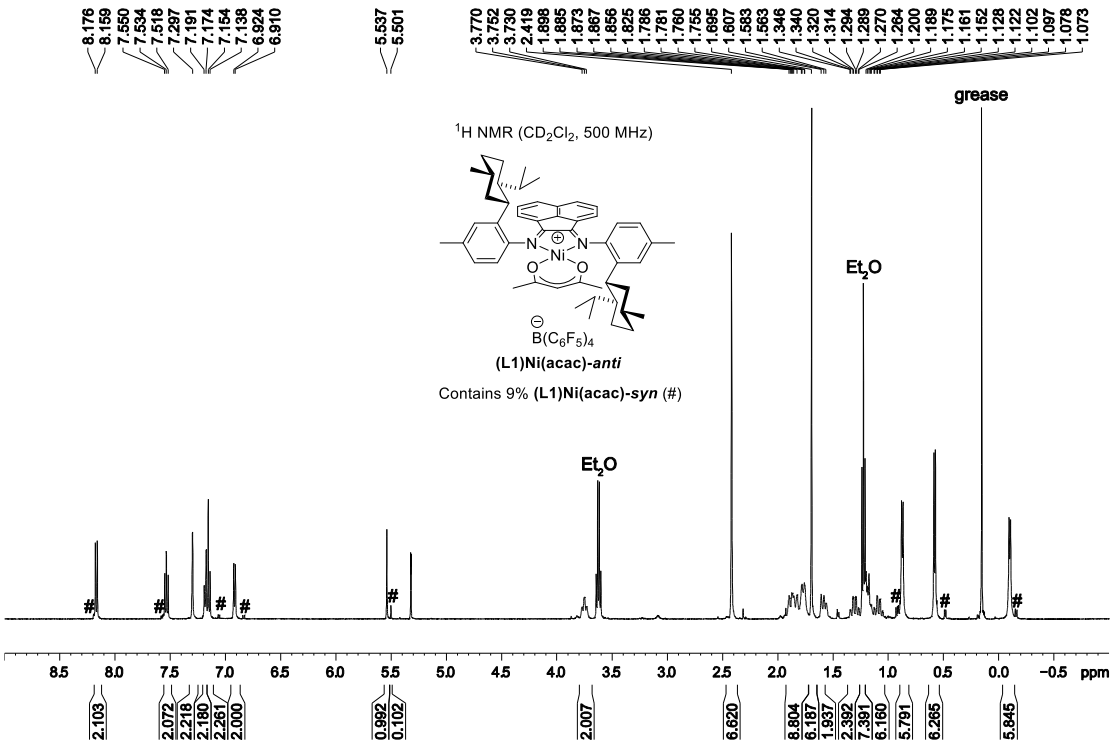

Figure 7.24. ^{1}H NMR spectrum of a 9/91 mixture of **(L1)Ni(acac)-*syn*/*anti***.

(L2)Ni(acac)-*syn*. A scintillation vial was charged with enriched **L2-*syn*** (80 mg, 0.12 mmol, overall *anti*/*syn* = 5/95), $Ni(acac)_2$ (31 mg, 0.12 mmol), $Ph_3C^+B(C_6F_5)_4^-$ (111 mg, 0.12 mmol) and CH_2Cl_2 (5 mL) under N_2. The mixture was stirred at room temperature for 1.5 h. The volatiles were removed under vacuum, and the residue was subjected to flash column chromatography (silica, hexane/CH_2Cl_2 = 1/1 to 1/2 by volume) and taken to dryness under vacuum to yield **(L2)Ni(acac)-*syn*** as an magenta brittle foam. Yield: Recovery: 162 mg (90%). This material is a 91/9 mixture of **(L2)Ni(acac)-*syn*/*anti*** based on ^{1}H NMR integration of the ^{i}Pr methyl doublets. ESI-MS (1:1 MeOH:H_2O, positive ion scan, *m*/*z*): 821.6 ($[M - B(C_6F_5)_4]^+$). ESI-MS (1:1 MeOH:H_2O, negative ion scan, *m*/*z*): 679.2 ($[B(C_6F_5)_4]^-$). Anal. Calcd. for $C_{77}H_{67}BF_{20}NNiO_2$, %: C, 61.58; H, 4.50; N, 1.87. Found: C, 61.64; H, 4.18; N, 1.75. ^{1}H NMR (CD_2Cl_2): δ 8.21-8.18 (m, 2H), 7.59-7.55 (m, 2H), 7.16 (s, 1H), 7.13 (s, 1H), 7.06 (s, 1H), 7.04 (s, 1H), 6.88 (d, *J* = 7.2, 1H), 6.78 (d, *J* = 7.2, 1H), 5.52 (s, 1H, acac CH), 3.29-3.23 (m, 2H), 2.47 (s, 3H), 2.46 (s, 3H), 2.37 (s,

6H), 2.02-1.98 (m, 1H), 1.94-1.85 (m, 3H), 1.82-1.76 (m, 2H), 1.72 (t, *J* = 11.5, 1H), 1.65-1.57 (m, 7H, acac Me + 1 aliphatic H), 1.54 (septet, *J* = 6.8, 1H), 1.43-1.35 (m, 4H), 1.30-0.97 (m, 8H), 0.91 (d, *J* = 6.4, 3H), 0.89 (d, *J* = 6.9, 3H), 0.60 (d, *J* = 6.9, 3H), 0.47 (d, *J* = 6.4, 3H), -0.33 (d, *J* = 6.9, 3H). $^{13}C\{^{1}H\}$ NMR (CD_2Cl_2): δ 188.0 (2C, acac C=O), 173.53 (C=N), 173.48 (C=N), 149.0, 140.9, 140.1, 139.9, 139.7, 137.5, 137.2, 133.98 (Ar CH), 133.94 (Ar CH), 131.7, 130.3, 129.9, 129.81 (2C, Ar CH), 129.76 (Ar CH), 129.72 (Ar CH), 127.0 (Ar CH), 126.6 (Ar CH), 126.40 (Ar CH), 126.34 (Ar CH), 124.6, 123.9, 102.5 (acac CH), 47.53, 47.49, 46.1, 45.2, 43.5, 43.3, 35.2, 35.0, 34.0, 33.7, 28.2, 27.9, 25.5, 25.4, 24.7 (br, 2C, acac CH_3), 22.6, 22.1, 22.0, 21.69, 21.67, 21.5, 18.71, 18.66, 17.9, 16.4.

(a)

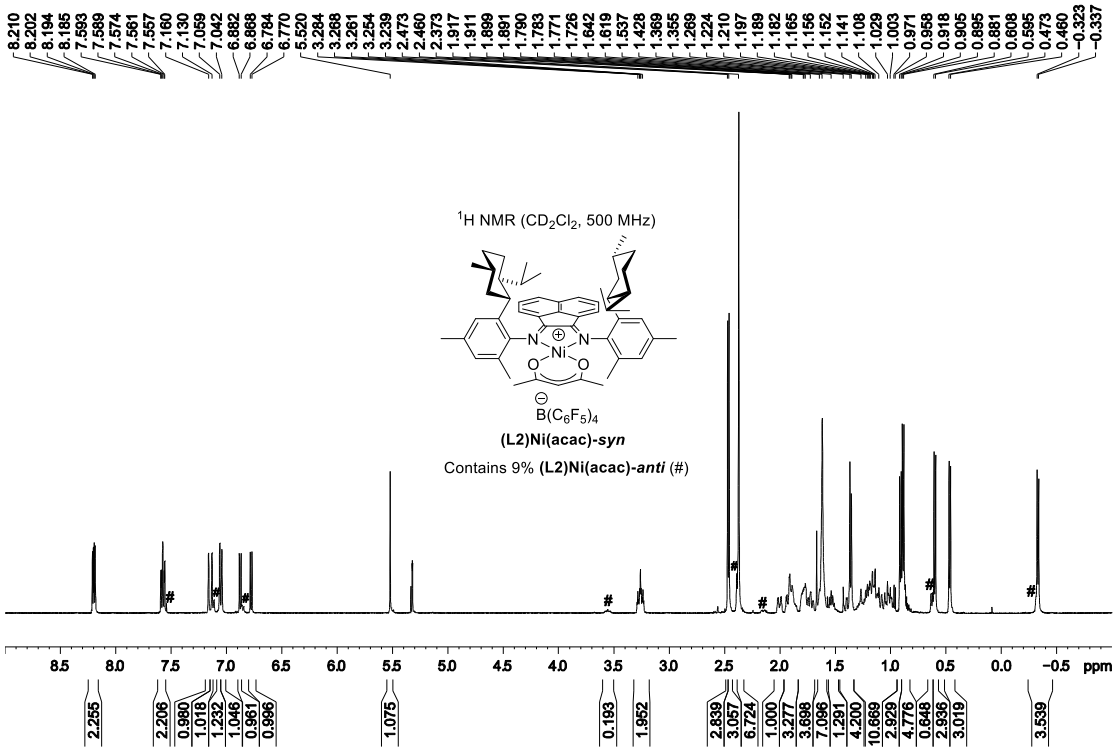

Figure 7.25. NMR spectra of a 91/9 mixture of **(L2)Ni(acac)-*syn*/*anti***.

(b)

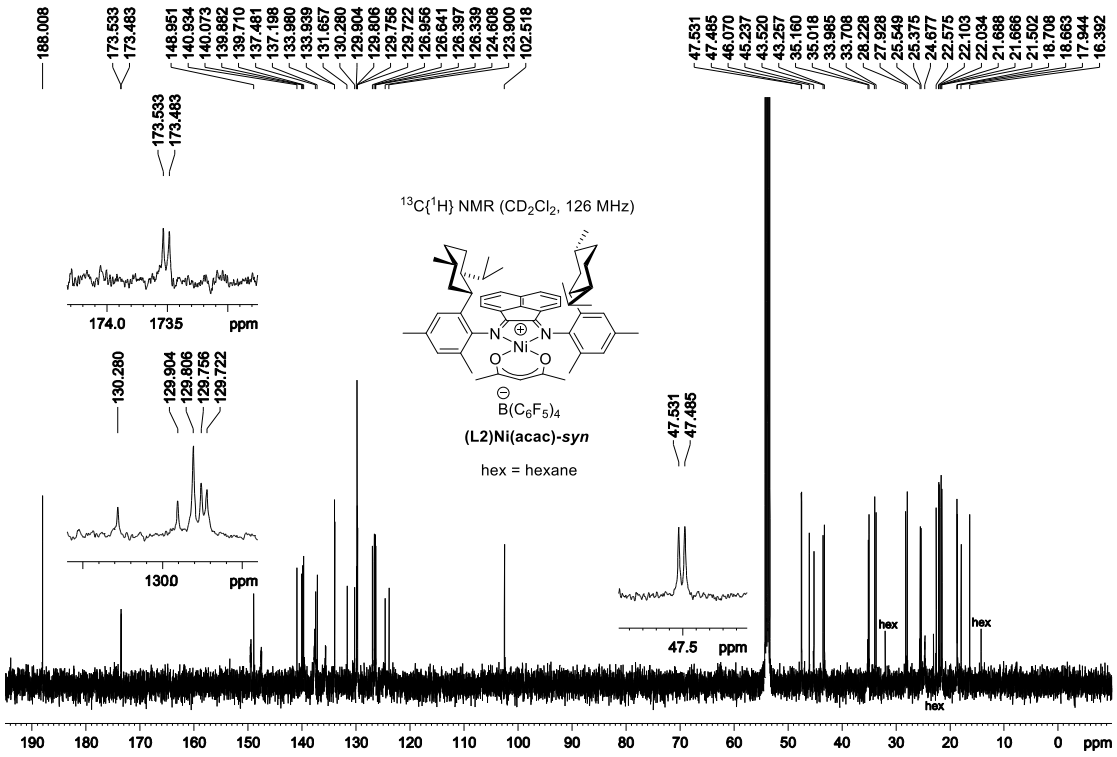

(c) HMQC (CD_2Cl_2, expansion of δ 9 to -1/150-10 region)

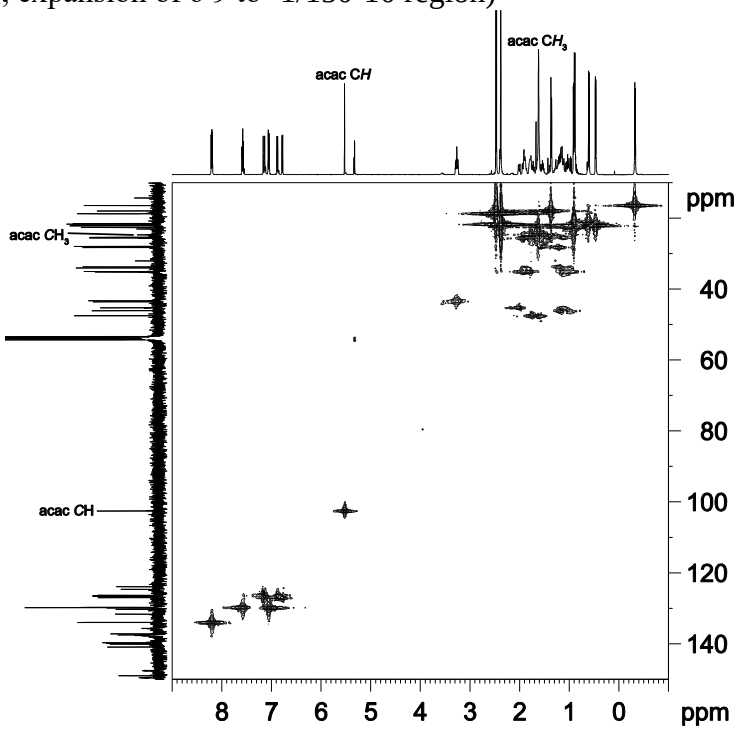

Figure 7.25, continued. NMR spectra of a 91/9 mixture of **(L2)Ni(acac)-*syn*/*anti***.

(L2)Ni(acac)-*anti*. A scintillation vial was charged with **(L2)NiBr$_2$-*anti*** (100 mg, 0.113 mmol), Ag(acac) (24.6 mg, 0.118 mmol), KB(C_6F_5)$_4$ (82.0 mg, 0.114 mmol), and CH_2Cl_2 (5 mL) under N_2. The mixture was stirred at room temperature for 3 h to yield a red solution and a white precipitate. The mixture was filtered through a pad of Celite. The filtrate was taken to dryness under vacuum to afford a red brittle foam. Yield: 167 mg (98%). This material was free from the *syn* isomer as measured by ^{1}H NMR. Heating a solution of **(L2)Ni(acac)-*anti*** in $CDCl_2CDCl_2$ (ca. 16 mg in 0.5 mL) at 100 °C for 3 d yielded an equilibrium 89/11 mixture of **(L2)Ni(acac)-*syn*/*anti***. ESI-MS (1:1 MeOH:H_2O, positive ion scan, *m*/*z*): 821.6 ([M – B(C_6F_5)$_4$]$^+$). ESI-MS (1:1 MeOH:H_2O, negative ion scan, *m*/*z*): 679.2 ([B(C_6F_5)$_4$]$^-$). Anal. Calcd. for $C_{77}H_{67}BF_{20}NNiO_2$, %: C, 61.58; H, 4.50; N, 1.87. Found: C, 61.25; H, 4.56; N, 1.90. ^{1}H NMR (CD_2Cl_2): δ 8.19 (d, *J* = 8.3, 2H), 7.56 (dd, *J* = 8.0, 7.3, 2H), 7.11 (s, 2H), 7.06 (s, 2H), 6.85 (d, *J* = 7.3, 2H), 5.53 (s, 1H, acac CH), 3.56 (td, *J* = 11.2, 2.9, 2H, H_A), 2.39 (s, 6H, *o*-CH_3), 2.37 (s, 6H, *p*-CH_3), 2.19-2.12 (m, 2H, H_C), 1.90-1.84 (m, 2H, H_F), 1.83-1.74 (m, 4H, H_D + H_G), 1.67 (s, 6H, acac CH_3), 1.66-1.61 (m, 2H, H_I), 1.27 (septet, *J* = 6.7, 2H, ^{i}Pr methine), 1.20-1.02 (m, 6H, H_B + H_E + H_H), 0.88 (d, *J* = 6.4, 6H, C^5-CH_3), 0.63 (d, *J* = 6.9, 6H, ^{i}Pr), -0.32 (d, *J* = 6.9, 6H, ^{i}Pr). ^{13}C{^{1}H} NMR (CD_2Cl_2): δ 188.3 (acac C=O), 173.6 (C=N), 148.8, 140.0, 139.9, 137.3, 134.0, 131.5, 130.4 (Ar CH), 129.8 (Ar CH), 129.7 (Ar CH), 126.63 (Ar CH), 126.56 (Ar CH), 124.3, 102.4 (acac CH), 46.9 (C^2), 45.3 (C^6), 44.0 (C^1), 35.3 (C^4), 34.3 (C^5), 28.1 (^{i}Pr methine), 25.4 (C^3), 24.9 (acac CH_3), 22.6 (C^5-*C*H_3), 21.7 (*p*-*C*H_3), 21.6 (^{i}Pr), 18.6 (*o*-*C*H_3), 16.6 (^{i}Pr).

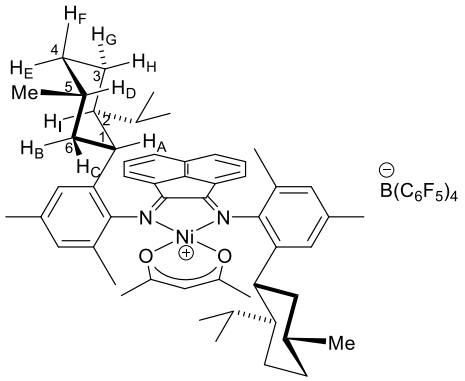

(a)

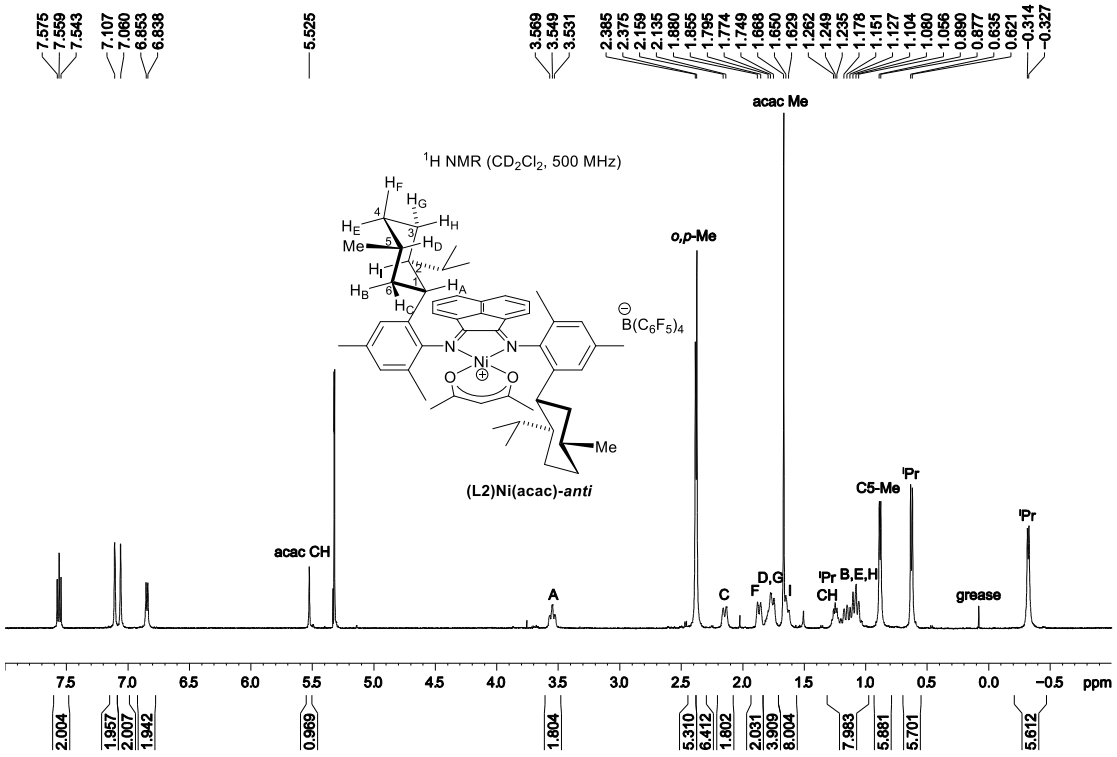

Figure 7.26. NMR spectra of **(L2)Ni(acac)-*anti***.

(b)

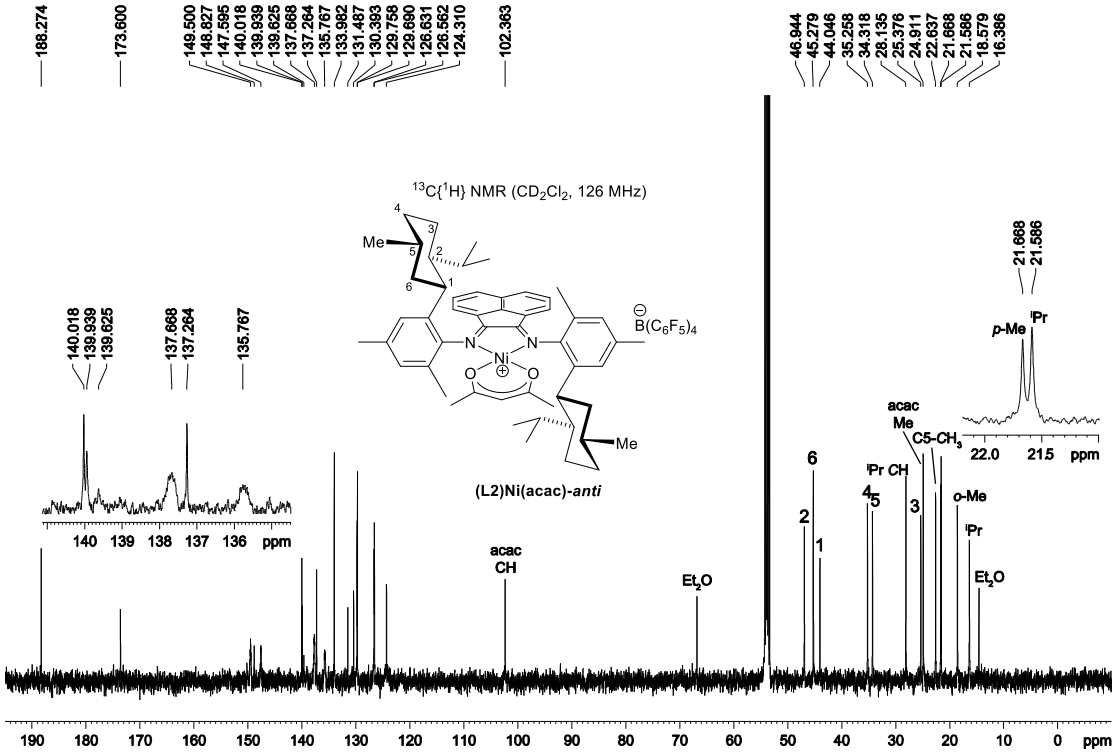

(c) HMQC (CD_2Cl_2, expansion of δ 4.0 to -0.5/55-10 region)

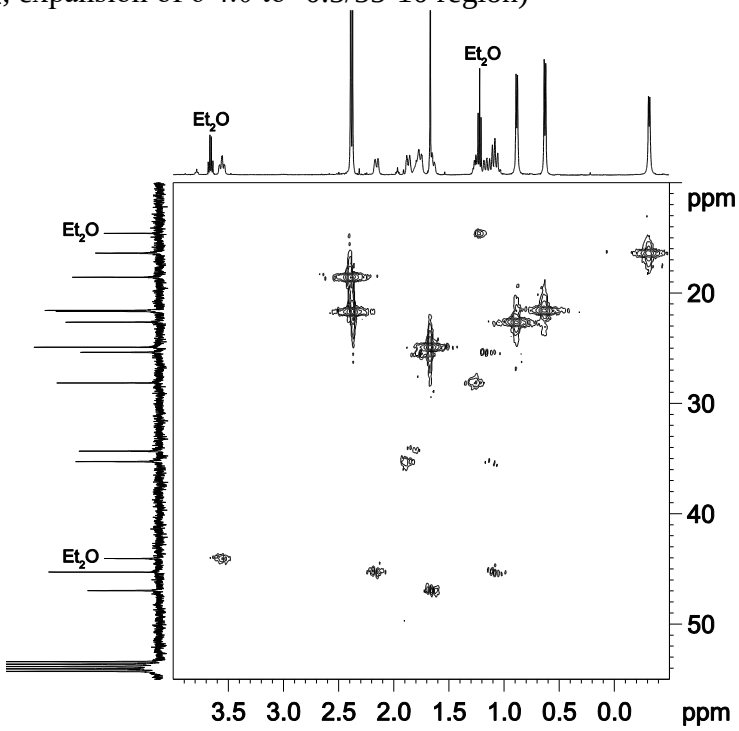

Figure 7.26, continued. NMR spectra of **(L2)Ni(acac)-*anti***.

Ethylene Polymerization. In a glovebox, a 200 mL Fischer-Porter bottle equipped with a magnetic stir bar and a stainless steel pressure head equipped with inlet and outlet needle valves, a septum-capped ball valve for injections, a check valve for safety, and a pressure gauge, was charged with Et_2AlCl (1.0 mmol, 2000 equiv vs catalyst) and toluene (49 mL). The bottle was sealed, removed from the glovebox and attached to a stainless steel double manifold (vacuum/ethylene) line. The bottle was charged with ethylene to the specified pressure, and the mixture was stirred in a water bath at room temperature. After equilibration for 20 min, the bottle was vented to 14 psi, and catalyst solution (0.50 μmol in 1 mL PhCl) was injected from the ball valve. The bottle was quickly charged with ethylene back to the specified pressure. After 15 min, the bottle was vented. A 5% solution of HCl in MeOH (100 mL) was added, and the mixture was stirred for 10 min to precipitate the polymer. The polymer was collected by vacuum filtration, washed with acetone and dried overnight in vacuum oven.

1-Hexene Polymerization. In a glovebox, a Schlenk flask was charged with catalyst (5.0 μmol) and PhCl (1 mL). The flask was capped with septum, removed from the glovebox and attached to a Schlenk line. 1-Hexene (10 mL) and toluene (14 mL, total volume 25 mL) were syringed in. Et_2AlCl (1.0 mmol, 200 equiv to Ni) was injected, and the mixture was stirred at room temperature. After 30 min, A 5% solution of HCl in MeOH (50 mL) and then acetone (100 mL) were added under air. The polymer was collected by vacuum filtration, washed with acetone and dried overnight in vacuum oven.

X-ray Crystallography. Data were measured on a Bruker D8 VENTURE with a PHOTON 100 CMOS detector system equipped with a Mo-target X-ray tube ($\lambda = 0.71073$ Å). All atoms were refined with anisotropic thermal parameters. Hydrogen atoms were included in idealized positions for structure factor calculations. All structures are drawn with thermal

ellipsoids at 50% probability. Specific details for each compound follow: **(L1)NiBr$_2$-*anti***: Crystals were grown by diffusion of hexane into a CH_2Cl_2 solution of **(L1)NiBr$_2$-*anti*** at 0 °C. Crystallographic data and details of the data collection and structure refinement are listed in Table 7.5. Some restraints on anisotropic thermal parameters (RIGU, ISOR) were imposed on benzene rings. The crystal contained many disordered solvent molecules located in large solvent accessible voids. The diffuse contribution to scattering was treated by application of the solvent mask as incorporated in OLEX2. The mask algorithm located a large void, centered at (-0.8, -0.5, 0) with a volume of 670.8 Å^3 and an electron count of 176. **(L1)PdCl$_2$-*anti*·2.5(CH$_2$Cl$_2$)**: Crystals were grown by diffusion of hexane into a CH_2Cl_2 solution containing a 20:1 mixture of **(L1)PdCl$_2$-*syn*/*anti*** at 0 °C. **(L1)PdCl$_2$-*anti*** crystallized as yellow blocks, while the major component **(L1)PdCl$_2$-*syn*** formed thin plates and was not crystalline. Crystallographic data and details of the data collection and structure refinement are listed in Table 7.3. The compound crystallized in the non-enantiogenic Sohncke space group $P2_12_12$ with a Flack parameter of -0.033(10). All elements (including those of a disordered CH_2Cl_2 molecule) were refined with anisotropic thermal parameters. Disorder refinement was carried out with the help of constraints on thermal parameters for a minor part. RIGU/SIMU were also used for the refinement of other CH_2Cl_2 solvent molecules. The crystal also contained disordered solvent molecules located in solvent accessible voids. The diffuse contribution to scattering was treated by application of the program SQUEEZE[43-44] as implemented in Platon[45] using the "fab" file construct. SQUEEZE algorithm located two voids, centered at (0, 0.5, -0.035) and (0.5, 0, 0.035), with a volume of 295 Å^3 and an electron count of 30 each. **4[(L1)PdCl$_2$-*syn*]·3.4(CH$_2$Cl$_2$)**: Crystals were grown by diffusion of hexane into a CH_2Cl_2 solution containing containing a 20:1 mixture of **(L1)PdCl$_2$-*syn*/*anti*** at 0 °C. **(L1)PdCl$_2$-*syn*** crystallized as thin yellow plates. Most crystals showed no or weak diffraction.

Crystallographic data and details of the data collection and structure refinement are listed in Table 7.4. The compound crystallized in the non-enantiogenic Sohncke space group P1 with a Flack parameter of -0.033(8). The crystal has 4 independent chiral molecules in the unit cell, 3 of which exhibited disorder of menthyl moiety. Each was independently modelled. All elements (including those of disordered parts) were refined with anisotropic thermal parameters. Three fully occupied and well-defined CH_2Cl_2 molecules were found in the unit cell. A 40% occupied CH_2Cl_2 molecule was also observed. Disorder refinement was carried out with the help of constraints on thermal parameters (RIGU; ISOR for several atoms). The crystal also contained disordered solvent molecules located in solvent accessible voids. The diffuse contribution to scattering was treated by application of the program SQUEEZE[43-44] as implemented in Platon[45] using the "fab" file construct. The total solvent accessible volume is 389.5 $Å^3$ with 62 electrons in it.

Table 7.3. X-ray Crystallographic Parameters of (L1)$NiBr_2$-*anti*.

Empirical formula	$C_{46}H_{56}Br_2N_2Ni$
Formula weight	855.45
Temperature/K	100(2)
Crystal system	monoclinic
Space group	$P2_1$
a/Å	10.135(2)
b/Å	18.051(4)
c/Å	14.624(4)
α/°	90
β/°	109.375(5)
γ/°	90
Volume/$Å^3$	2523.8(10)
Z	2
ρ_{calc}/g cm^{-3}	1.126
μ/mm^{-1}	1.995
F(000)	888.0
Crystal size/mm^3	0.24 × 0.02 × 0.02
Radiation	MoKα (λ = 0.71073)
2Θ range for data collection/°	4.26 to 50.304
Index ranges	$-11 \leq h \leq 12$, $-21 \leq k \leq 21$, $-17 \leq l \leq 17$
Reflections collected	28815
Independent reflections	8589 [R_{int} = 0.0799, R_{sigma} = 0.1309]
Data/restraints/parameters	8589/145/468
Goodness-of-fit on F^2	1.032
Final R indexes [I>=2σ (I)]	R_1 = 0.0600, wR_2 = 0.1109
Final R indexes [all data]	R_1 = 0.0995, wR_2 = 0.1183
Largest diff. peak/hole / e $Å^{-3}$	0.64/-0.54
Flack parameter	0.061(8)

Table 7.4. X-ray Crystallographic Parameters of (L1)$PdCl_2$-*anti*·2.5(CH_2Cl_2).

Empirical formula	$C_{48.50}H_{61}Cl_7N_2Pd$	
Formula weight	1026.54	
Temperature	100(2) K	
Wavelength	0.71073 Å	
Crystal system	Orthorhombic	
Space group	$P2_12_12$	
Unit cell dimensions	a = 16.1282(7) Å	α = 90°.
	b = 23.3147(11) Å	β = 90°.
	c = 14.2866(6) Å	γ = 90°.
Volume	5372.1(4) $Å^3$	
Z	4	
Density (calculated)	1.269 Mg/m^3	
Absorption coefficient	0.725 mm^{-1}	
F(000)	2124	
Crystal size	0.300 x 0.280 x 0.140 mm^3	
Theta range for data collection	2.255 to 26.393°.	
Index ranges	-20<=h<=19, -29<=k<=18, -13<=l<=17	
Reflections collected	20124	
Independent reflections	10626 [R(int) = 0.0240]	
Completeness to theta = 25.242°	99.3 %	
Refinement method	Full-matrix least-squares on F^2	
Data / restraints / parameters	10626 / 24 / 545	
Goodness-of-fit on F^2	1.064	
Final R indices [I>2sigma(I)]	R1 = 0.0419, wR2 = 0.0999	
R indices (all data)	R1 = 0.0485, wR2 = 0.1041	
Absolute structure parameter	-0.033(10)	
Extinction coefficient	n/a	
Largest diff. peak and hole	1.563 and -0.795 e.$Å^{-3}$	

Table 7.5. X-ray Crystallographic Parameters of 4[(L1)$PdCl_2$-*syn*]·3.4(CH_2Cl_2).

Empirical formula	$C_{187.40}H_{230.80}Cl_{14.80}N_8Pd_4$	
Formula weight	3545.65	
Temperature	100(2) K	
Wavelength	0.71073 Å	
Crystal system	Triclinic	
Space group	P1	
Unit cell dimensions	a = 11.6689(7) Å	α = 70.5144(17)°.
	b = 20.0852(12) Å	β = 85.5360(17)°.
	c = 21.5643(13) Å	γ = 78.1792(17)°.
Volume	4663.3(5) $Å^3$	
Z	1	
Density (calculated)	1.263 Mg/m^3	
Absorption coefficient	0.642 mm^{-1}	
F(000)	1847	
Crystal size	0.220 x 0.040 x 0.010 mm^3	
Theta range for data collection	2.191 to 26.450°.	
Index ranges	-14<=h<=14, -25<=k<=25, -26<=l<=26	
Reflections collected	109471	
Independent reflections	36808 [R(int) = 0.0449]	
Completeness to theta = 25.242°	99.9 %	
Refinement method	Full-matrix least-squares on F^2	
Data / restraints / parameters	36808 / 1888 / 2348	
Goodness-of-fit on F^2	1.020	
Final R indices [I>2sigma(I)]	R1 = 0.0461, wR2 = 0.0848	
R indices (all data)	R1 = 0.0795, wR2 = 0.0948	
Absolute structure parameter	-0.033(8)	
Extinction coefficient	n/a	
Largest diff. peak and hole	1.204 and -0.613 $e.Å^{-3}$	

7.5 References and Notes

(1) Johnson, L. K.; Killian, C. M.; Brookhart, M. S. *J. Am. Chem. Soc.* **1995**, *117*, 6414.

(2) Johnson, L. K.; Mecking, S.; Brookhart, M. S. *J. Am. Chem. Soc.* **1996**, *118*, 267.

(3) Ittel, S. D.; Johnson, L. K.; Brookhart, M. S. *Chem. Rev.* **2000**, *100*, 1169.

(4) Guo, L.; Dai, S.; Sui, X.; Chen, C. *ACS Catal.* **2016**, *6*, 428.

(5) Popeney, C. S.; Camacho, D. H.; Guan, Z. *J. Am. Chem. Soc.* **2007**, *129*, 10062.

(6) Allen, K. E.; Campos, J.; Daugulis, O.; Brookhart, M. S. *ACS Catal.* **2014**, 456.

(7) Dai, S.; Sui, X.; Chen, C. *Angew. Chem., Int. Ed.* **2015**, *54*, 9948.

(8) Dai, S.; Chen, C. *Angew. Chem., Int. Ed.* **2016**, *55*, 13281.

(9) Takano, S.; Takeuchi, D.; Osakada, K.; Akamatsu, N.; Shishido, A. *Angew. Chem., Int. Ed.* **2014**, *53*, 9246.

(10) Popeney, C. S.; Guan, Z. *Organometallics* **2005**, *24*, 1145.

(11) Gheewala, C. D.; Collins, B. E.; Lambert, T. H. *Science* **2016**, *351*, 961.

(12) Ho, C.-Y.; Chan, C.-W.; He, L. *Angew. Chem., Int. Ed.* **2015**, *54*, 4512.

(13) Kondakov, D. Y.; Negishi, E.-i. *J. Am. Chem. Soc.* **1995**, *117*, 10771.

(14) Giardello, M. A.; Eisen, M. S.; Stern, C. L.; Marks, T. J. *J. Am. Chem. Soc.* **1993**, *115*, 3326.

(15) Cesarotti, E.; Kagan, H. B.; Goddard, R.; Krüger, C. *J. Organomet. Chem.* **1978**, *162*, 297.

(16) Ota, Y.; Ito, S.; Kuroda, J.-i.; Okumura, Y.; Nozaki, K. *J. Am. Chem. Soc.* **2014**, *136*, 11898.

(17) Beckmann, J.; Dakternieks, D.; Dräger, M.; Duthie, A. *Angew. Chem., Int. Ed.* **2006**, *45*, 6509.

(18) Thaler, T.; Haag, B.; Gavryushin, A.; Schober, K.; Hartmann, E.; Gschwind, R. M.; Zipse, H.; Mayer, P.; Knochel, P. *Nat. Chem.* **2010**, *2*, 125.

(19) Haquette, P.; Dagorne, S.; Welter, R.; Jaouen, G. *J. Organomet. Chem.* **2003**, *682*, 240.

(20) Gasperini, M.; Ragaini, F.; Gazzola, E.; Caselli, A.; Macchi, P. *Dalton Trans.* **2004**, 3376.

(21) The assignment and quantification of **L1-*E,E-anti*** was difficult due to extensive overlapping of NMR signals and low concentration. The resonances of **L1-*Z,E*** were also resolved at -60 °C, however, the exchange process between **L1-*Z,E-anti*** and **L1-*Z,E-syn*** were not studied due to their relatively low concentrations.

(22) Meinhard, D.; Wegner, M. M.; Kipiani, G.; Hearley, A. K.; Reuter, P.; Fischer, S.; Marti, O.; Rieger, B. *J. Am. Chem. Soc.* **2007**, *129*, 9182.

(23) Popeney, C. S.; Rheingold, A. L.; Guan, Z. *Organometallics* **2009**, *28*, 4452.

(24) Popeney, C. S.; Levins, C. M.; Guan, Z. *Organometallics* **2011**, *30*, 2432.

(25) Wagner, J. P.; Schreiner, P. R. *Angew. Chem., Int. Ed.* **2015**, *54*, 12274.

(26) Schreiner, P. R.; Chernish, L. V.; Gunchenko, P. A.; Tikhonchuk, E. Y.; Hausmann, H.; Serafin, M.; Schlecht, S.; Dahl, J. E. P.; Carlson, R. M. K.; Fokin, A. A. *Nature* **2011**, *477*, 308.

(27) Lin, C. Y.; Guo, J.-D.; Fettinger, J. C.; Nagase, S.; Grandjean, F.; Long, G. J.; Chilton, N. F.; Power, P. P. *Inorg. Chem.* **2013**, *52*, 13584.

(28) Guo, J.-D.; Liptrot, D. J.; Nagase, S.; Power, P. P. *Chem. Sci.* **2015**, *6*, 6235.

(29) Liptrot, D. J.; Guo, J.-D.; Nagase, S.; Power, P. P. *Angew. Chem., Int. Ed.* **2016**, *55*, 14766.

(30) Yang, L.; Adam, C.; Nichol, G. S.; Cockroft, S. L. *Nat. Chem.* **2013**, *5*, 1006.

(31) Echeverría, J.; Aullón, G.; Danovich, D.; Shaik, S.; Alvarez, S. *Nat. Chem.* **2011**, *3*, 323.

(32) Zou, H.; Hu, S.; Huang, H.; Zhu, F.; Wu, Q. *Eur. Polym. J.* **2007**, *43*, 3882.

(33) Killian, C. M.; Tempel, D. J.; Johnson, L. K.; Brookhart, M. S. *J. Am. Chem. Soc.* **1996**, *118*, 11664.

(34) Camacho, D. H.; Guan, Z. *Macromolecules* **2005**, *38*, 2544.

(35) Rose, J. M.; Cherian, A. E.; Coates, G. W. *J. Am. Chem. Soc.* **2006**, *128*, 4186.

(36) McCord, E. F.; McLain, S. J.; Nelson, L. T. J.; Ittel, S. D.; Tempel, D. J.; Killian, C. M.; Johnson, L. K.; Brookhart, M. S. *Macromolecules* **2007**, *40*, 410.

(37) Merna, J.; Hošťálek, Z.; Peleška, J.; Roda, J. *Polymer* **2009**, *50*, 5016.

(38) Vaidya, T.; Klimovica, K.; LaPointe, A. M.; Keresztes, I.; Lobkovsky, E. B.; Daugulis, O.; Coates, G. W. *J. Am. Chem. Soc.* **2014**, *136*, 7213.

(39) Senaratne, P. a.; Orihuela, F. M.; Malcolm, A. J.; Anderson, K. G. *Org. Process Res. Dev.* **2003**, *7*, 185.

(40) Voss, T.; Chen, C.; Kehr, G.; Nauha, E.; Erker, G.; Stephan, D. W. *Chem. Eur. J.* **2010**, *16*, 3005.

(41) Korshin, E. E.; Leitus, G.; Shimon, L. J. W.; Konstantinovski, L.; Milstein, D. *Inorg. Chem.* **2008**, *47*, 7177.

(42) Grinshpun, V.; Rudin, A. *Makromol. Chem., Rapid Commun.* **1985**, *6*, 219.

(43) Spek, A. L. *Acta Cryst.* **2015**, *C71*, 9.

(44) van der Sluis, P.; Spek, A. L. *Acta Cryst.* **1990**, *A46*, 194.

(45) Spek, A. L. *Acta Cryst.* **2009**, *D65*, 148.